TRANSPORTATION RESEARCH
RECORD

No. 1260

Pavement Design, Management, and Performance

Measurement of Pavement Surface Condition 1990

A peer-reviewed publication of the Transportation Research Board

TRANSPORTATION RESEARCH BOARD
NATIONAL RESEARCH COUNCIL
WASHINGTON, D.C. 1990

Transportation Research Record 1260
Price: $38.00

Subscriber Category: IIB pavement design, management, and performance

Mode
1 highway transportation

Subject Areas
24 pavement design and performance
51 transportation safety
61 soil exploration and classification

TRB Publications Staff
Director of Publications: Nancy A. Ackerman
Senior Editor: Naomi C. Kassabian
Associate Editor: Alison G. Tobias
Assistant Editors: Luanne Crayton, Norman Solomon
Production Editor: Kieran P. O'Leary
Graphics Coordinator: Karen L. White
Office Manager: Phyllis D. Barber
Production Assistant: Betty L. Hawkins

Printed in the United States of America

Library of Congress Cataloging-in-Publication Data
National Research Council. Transportation Research Board.

Measurement of pavement surface condition.
p. cm.—(Transportation research record, ISSN 0361-1981 ; no. 1260)
Research papers from the 69th Annual Meeting of the Transportation Research Board, Jan. 1990.
Includes bibliographic references.
ISBN 0-309-05013-8
1. Pavements—Testing. 2. Pavements—Design and construction—Management. 3. Surface roughness—Measurement. I. National Research Council (U.S.). Transportation Research Board. Meeting (69th : 1990 : Washington, D.C.) II. Series: Transportation research record ; 1260.
TE7.H5 no. 1260
[TE250]
380 s—dc20
[625.8] 90-6580
CIP

Sponsorship of Transportation Research Record 1260

GROUP 2—DESIGN AND CONSTRUCTION OF TRANSPORTATION FACILITIES
Chairman: Raymond A. Forsyth, Sacramento, California

Pavement Management Section
Chairman: R. G. Hicks, Oregon State University

Committee on Strength and Deformation Characteristics of Pavement Sections
Chairman: J. Brent Rauhut, Brent Rauhut Engineering, Inc.
Mark Anderson, Gilbert Y. Baladi, Richard D. Barksdale, Stephen F. Brown, Albert J. Bush III, Yu T. Chou, George R. Cochran, Billy G. Connor, Mark P. Gardner, Amir N. Hanna, R. G. Hicks, Lynne H. Irwin, William J. Kenis, Thomas W. Kennedy, Robert L. Lytton, Michael S. Mamlouk, Frank Meyer, Lutfi Raad, Richard B. Rogers, Byron E. Ruth, Stephen B. Seeds, Roger E. Smith, R. N. Stubstad, Marshall R. Thompson, Per Ullidtz, Jacob Uzan, Thomas D. White

Committee on Pavement Monitoring, Evaluation, and Data Storage
Chairman: Freddy L. Roberts, Auburn University
Secretary: Don H. Kobi, Paris, Ontario, Canada
A. T. Bergan, Frank V. Botelho, Billy G. Connor, Brian E. Cox, Jerome F. Daleiden, Karl H. Dunn, Wade L. Gramling, Jerry J. Hajek, Amir N. Hanna, Andris A. Jumikis, Scott A. Kutz, Kenneth J. Law, W. N. Lofroos, Kenneth H. McGhee, Amy L. Mueller, Edwin C. Novak, Jr., Dennis G. Richardson, Richard B. Rogers, Ivan F. Scazziga, Mohamed Y. Shahin, Robert M. Smith, Roger E. Smith, Herbert F. Southgate, Elson B. Spangler, John P. Zaniewski

Committee on Surface Properties–Vehicle Interaction
Chairman: John Jewett Henry, Pennsylvania State University
Secretary: James C. Wambold, Pennsylvania State University
James L. Burchett, Gaylord Cumberledge, Kathleen T. Diringer, Stephen W. Forster, Thomas D. Gillespie, Lawrence E. Hart, Carlton M. Hayden, Brian S. Heaton, Walter B. Horne, David L. Huft, Michael S. Janoff, Kenneth J. Law, Jean Lucas, Georg Magnusson, David C. Mahone, James E. McQuirt, Jr., William G. Miley, Thomas H. Morrow, Robert L. Novak, Bobby G. Page, A. Scott Parrish, Jean Reichert, Dennis G. Richardson, Elson B. Spangler, William H. Temple

Evaluations, Systems, and Procedures Section
Chairman: Terry M. Mitchell, Federal Highway Administration, U.S. Department of Transportation

Committee on Applications of Emerging Technology
Chairman: Chris T. Hendrickson, Carnegie-Mellon University
Kenneth R. Agent, Roy E. Benner, William Bowlby, Wiley D. Cunagin, Donald R. Curphey, C. Page Fisher, Thomas A. Fuca, Richard C. Ingberg, Terry M. Mitchell, Justin J. Rennilson, Earl C. Shirley, Simon Slutsky, Walter A. Winter, David C. Wyant

G. P. Jayaprakash, Transportation Research Board staff

Sponsorship is indicated by a footnote at the end of each paper. The organizational units, officers, and members are as of December 31, 1989.

Transportation Research Record 1260

Contents

Foreword

The 22 papers in this Record are concerned with the collection, analysis, and management of data concerning the surface condition and deflection of pavements. The data are intended for use in indicating the present distress level, skid resistance, roughness, and structural capacity of the pavement. With inventory information, the data can be used in pavement management systems. The papers will be of interest to pavement engineers and planners as well as researchers. Some papers will also be of interest to maintenance engineers.

Four of the papers are concerned with pavement management or with the Strategic Highway Research Program (SHRP) long-term pavement performance (LTPP) program. DuBose describes the procedures used by the Illinois Department of Transportation to obtain original design and rehabilitation data for its pavement management system. Many existing files of information designed for other purposes were found to be useful. Haas and McNeil describe the hardware, software, and procedural elements used to acquire, store, process, report, and use pavement distress data; they go on to develop a set of criteria for evaluating pavement imaging systems. Three example systems are used to illustrate combinations of elements.

Goulias et al. outline the types of pavement and environmental data to be collected in the SHRP LTPP program. Inventory items and monitoring of distress are included. Clarke et al. discuss an information management system under development for transferring SHRP LTPP data from SHRP regional office data handling systems to the TRB timesharing VAX system, and include a brief description of the ORACLE data base management program and its potential for access by researchers and others.

Nine papers address the characterization and measurement of pavement surface properties. Five papers are on roughness. Ksaibati et al. provide data that show that pavement profile measurements with the PRORUT laser sensor at 10 and 55 mph corresponded closely to the profile determined with a rod and level survey, except on a chip seal surface. Improvements are suggested for the PRORUT system. Cumbaa describes research on pavement roughness designed to enable Louisiana to satisfy roughness testing and reporting requirements of the Highway Performance Monitoring System. Comparisons of measurements by the K. J. Law 8300 Roughness Surveyor, the Face Dipstick, and the Mays Ride Meter are reported. Sayers shows that the length of the averaging base line is important when applying the moving average filter to obtain a smoothed profile of pavement roughness. Fernando et al. compare profiles measured with the Texas Surface Dynamics Profilometer and with the Siometer. The Siometer is said to be the more economical device. Lu et al. present a canceling model for the speed effect on roughness measurements and illustrate its application to the Automatic Road Analyzer.

Three papers deal with distress modeling. Haas and Hendrickson explain the development of a general model to characterize and represent pavement surfaces. The model supports multiple types of sensor information, provides methods to integrate different sensor data, and incorporates multiple surface characteristics. The model is being demonstrated in automated pavement distress identification and analysis and in automated pavement maintenance. El-Korchi and Wittels' two papers are on the use of luminance (light reflectance) for modeling cracks in pavement imaging systems. Lamm et al. develop what they believe is an objective scale for relating friction factors to speed, based on data from New York State, the Federal Republic of Germany, and other European countries.

Nine papers cover the determination of structural properties of pavements by nondestructive testing. Bush and Bentsen report a study to determine the applicability of seven different nondestructive testing methods to the structural evaluation of airfield pavements. From analysis of the data, they present conclusions on the methods of test, the applicability of each type of equipment, and variability in predicted subgrade moduli. Scullion et al. developed MODULUS, a rapid (5 sec) microcomputer system for the backcalculation of pavement moduli. The computer program and validation of the system are described. Zhou et al. discuss BOUSDEF, a rapid program for the backcalculation of pavement moduli. BOUSDEF

solutions compared well to theory and to other solutions obtained with slower programs. Santha et al. developed a new version of the computer program LOADRATE, which uses data from a Dynaflect or falling weight deflectometer (FWD) to predict rut depth for lighter structure pavements for given traffic load inputs. The program also predicts remaining life and gives a rating of pavement condition. Rada et al. describe a software program to automate the FWD data collection process and a corresponding study to examine data checks in the program. The study also determined that use of the program's digital filtering of high-frequency noise introduced and compounded random errors. Tabatabaee and Sebaaly discuss the state of the art of strain gauges, pressure cells, and deflection, temperature, and transverse location sensors for instrumenting flexible pavements. Yazdani and Scullion describe the installation and use of a multidepth deflectometer for monitoring pavement response to loads. Up to six depth modules can be placed in a single hole for measuring the relative deflection of each layer. The study included an evaluation of anchor movement. Roesset et al. describe a new adaptation of the spectral analysis surface wave (SASW) method for measuring the modulus and thickness of the surface layer of asphalt or portland cement concrete pavements. A piezoelectric shaker is used to generate surface waves. The test requires about 5 min per test site. Hiltunen and Woods describe the further development of the SASW method for determining the elastic modulus of asphalt concrete in situ. They determined that two sizes of sources (a light-weight hammer and a heavy sledge) are adequate for the generation of transient waves over the entire dispersion area.

Abridgment

Collection of Pavement Inventory Data for the Illinois Pavement Feedback System

JAMES B. DUBOSE

Collection of inventory data for a pavement management system requires searching for data from several sources. Often, locations of these sources are not commonly known. Many times, officials of government bureaus or district agencies do not even realize that they have certain pieces of information in their own files. Thorough procedures were used in the Illinois Department of Transportation, Bureau of Materials and Physical Research, to obtain original construction and rehabilitation design information for the Department's pavement management system.

Collection of inventory data for the Illinois Pavement Feedback System (IPFS) has been a long and grueling process. Many problems have hampered collection of these data. Establishing a pavement inventory data base requires plenty of patience and perseverance. Thorough procedures were used in the Illinois Department of Transportation, Bureau of Materials and Physical Research (BMPR), to obtain original construction and rehabilitation design information for the Department's pavement management system.

DATA ELEMENTS

The first step was to decide what data elements were required for the system. Because this step is described in detail in other reports (*1,2*), it is only discussed briefly. It involved forming a team of users to decide what outputs from the system would be desirable. The required data elements were determined on the basis of these output reports. The data elements were then organized into a hierarchy with the contract number of the project as the primary key.

PAVEMENT MANAGEMENT FILE (PMF)

In data collection efforts, the most readily available information was obtained first. The logical starting point was the PMF, which was established before development of the IPFS. The PMF, created by the Office of Planning and Programming in 1983, is now maintained by the Bureau of Design. The PMF contains valuable information, such as the original pavement design, construction sections, subbase type, aggregate sources, previous pavement rehabilitations, and previous shoulder rehabilitations for the Illinois Interstate and supplemental freeway systems. Because the initial scope of the Illinois Pavement Feedback System was the Interstate highway system, the PMF was a good starting point.

Illinois Department of Transportation, Bureau of Materials and Physical Research, Springfield, Ill. 62704–4766.

However, the PMF had some limitations that prevented its direct use. The PMF was divided into management units described by milepost limits that did not necessarily correspond to the limits required for the IPFS. For the IPFS, initial efforts concentrated on determining the milepost limits for the original design contracts. In most cases, the milepost limits in the PMF did not correspond to the original contract limits, for two reasons. First, when analysts for the PMF felt that there were not any significant differences between adjacent contracts, they included two or more contracts in the same management unit. Second, in some instances milepost limits were modified to reflect limits of a rehabilitation contract that were either longer or shorter than those of the original construction contract.

Some information was missing from the PMF. For example, a few sections on the Interstate highway system incorporated parts of existing highways. Approximately 28 mi of I-55 in Grundy and Will counties contains pavement constructed for US 66 and its predecessors. For these sections, the PMF simply listed the construction section as unknown and listed the original pavement type as 10-in. jointed pavement even though there were several stretches of 9–7–9-in. thickened-edge pavement contained in these sections. Another problem was that experimental sections, of great interest for research purposes, were usually not broken out in the PMF either because of their complexity or their short length. Finally, the PMF did not contain contract numbers either for original construction or rehabilitation contracts. Because the contract number was to be the primary key for the data base, it was of paramount importance to obtain these items of information.

MONTHLY CONSTRUCTION REPORTS

The first attempt at obtaining contract information was through the Monthly Construction Report published by the Bureau of Construction. The Monthly Construction Report contains information such as project number, route, section, contract price, date work started, and date work completed. The BMPR has a copy of every year-end summary of the Monthly Construction Report dating from 1944 to the present. This time span covered the construction of all the Illinois Interstate system except for a few sections where older routes were incorporated into the system. Unfortunately, the Monthly Construction Report only contains contract numbers for projects constructed after 1970. More than half of the Illinois Interstate system was constructed before 1970. Nevertheless, the Monthly Construction Report is still the best source for obtaining contract information easily.

The contract information search began by using old Monthly Construction Reports to locate information on the original sections and rehabilitations listed in the PMF. The PMF lists the year each section was originally constructed as well as the years rehabilitations were performed. For these years, the appropriate year-end summaries were located. However, the year listed in the PMF was often incorrect, necessitating that several summaries be searched for years preceding and following the year listed. A minimal amount of information was collected the first time through. During this phase, the contract number, date that contract was awarded, date that work started, and date that work was completed were recorded. For older sections for which the contract number was not listed, the Federal Aid project number was recorded instead.

DISTRICT 1 INPUT

Next, a breakthrough occurred. While in the process of updating the PMF, the Bureau of Design had sent each of Illinois' nine highway districts a copy of the pertinent pavement management sections and asked them to make corrections and updates as necessary. For some districts, this process was relatively easy, but for District 1, located in northeastern Illinois and containing the city of Chicago, it required a great deal of work. Rather than making the updates directly, the District 1 Bureau of Maintenance supplied the BMPR with information needed to make the updates. This information included a summary of the original construction and rehabilitation sections, maintenance team section maps, and copies of typical sections from the construction plans. The summary contained the route number, section number, approximate year originally constructed, type of construction, and microfilm reel number on which the plans were located. The maintenance team section maps listed the original and rehabilitation sections and, most important, provided the station limits for the sections. Of course, the original construction plans were the most valuable pieces of information of all.

Experience with District 1 provided direction for the remainder of the project. Information on the plans considered useful was recorded on notebook paper because the data entry sheets had not yet been finalized. Milepost limits and contract number for each contract still had to be determined.

MILEPOST LIMITS

Two methods for determining the milepost limits were used. In most cases, the survey sheets from the pavement distress survey were sufficient. The BMPR had been conducting a detailed distress survey biennially since 1985. This survey is done on a sample unit basis with 500-ft sample units surveyed at each milepost. Any stationing found in the pavement along with its distance from the start of the unit is recorded. In this manner, the required link between the stationing and the mileposts was established. The one problem with this method was that it could not be applied in areas where the distress survey was not conducted. These areas, all located near Chicago, were skipped because of high traffic levels that made it too dangerous to conduct the survey manually. Therefore, the milepost station link was established by using the maintenance team section maps and the roadway inventory file. The roadway inventory file, maintained by the Office of Planning and Programming, contains the milemarker, to the nearest 0.01 mi, for all structures located along a given route. Because the maintenance team section maps provide the stations for all structures, connections between mileposts and stationing could be established.

CONTRACT NUMBERS

For the jobs constructed after 1970, contract numbers were obtained from the Monthly Construction Report. Many of the older contract numbers were obtained directly from the plans. Usually, the contract number was stamped on the plans. Unfortunately, a large portion of the expressways around Chicago were constructed by Cook County rather than the State of Illinois. As a result, these jobs often did not have state contract numbers. Also, some of the older jobs constructed before the start of the Interstate program did not have contract numbers stamped on the plans. Dummy contract numbers were assigned in these cases.

DOWNSTATE DISTRICTS

Using knowledge gained from the experience with District 1, a search for contract information for the other eight districts was begun. Each district bureau of maintenance was called and a copy of its maintenance team section maps was requested. After the maps were obtained, the milepost limits for the original construction sections could be calculated using pavement distress survey sheets.

MICROFILM

Next, a copy of the cover sheet and typical sections from the construction plans were needed. The plans were on microfilm, but which reels contained the plans was not known. However, the Bureau of Design maintains a card file that contains the microfilm reel numbers for both original construction and rehabilitation contracts. By providing the Bureau of Design with the route number, county, section, and either the contract number or Federal Aid project number, the microfilm reel numbers could be obtained—with a few exceptions for which the cross sections had been contained in the proposal and no formal plans had been prepared. This problem will be discussed later.

DATA ENTRY

After the reel numbers were received, copies of the cover sheet and typical cross sections for each contract were made. By this time, data entry sheets were complete, so entering data could be started. After the original construction design data were entered, the data sheets were proofread. Many errors were found. Contracts that contained more than one design type were not always split up, incorrect assumptions were made regarding materials used, and milepost limits were

often miscalculated or left blank. It was decided that it would be best if one individual, the pavement inventory engineer, maintain control of entering the design data. Inaccurate contracts were corrected and all subsequent data sheets were filled out by the pavement inventory engineer except for sheets containing general contract data from the Monthly Construction Report, which were filled out by others and checked by the pavement inventory engineer.

On completion of the original construction contract phase, information on rehabilitation contracts was collected. The process was virtually identical to the one used for the original construction contracts. Many rehabilitations had proposal plans rather than formal plans. After some searching, it was found that the districts had copies of the job proposals needed in their dead files. Later, it was discovered that the copies of the proposals needed were in the BMPR's own file room. The more recent jobs were in paper files and the older ones were on microfilm. The sheets for these last few rehabilitation contracts were soon due to be completed.

DATA BASE STATUS

Although data for almost all of the Interstate contracts have been entered, the data base is at present far from complete. Most of the original construction contract plans did not contain any design traffic or reinforcement data. Also, in many cases the plans were ambiguous. Usually, three options were shown for the shoulder design with no indication of which design was used. The subbase type was usually described as 4-in. stabilized, without specification whether it was bituminous aggregate mixture (BAM), cement aggregate mixture (CAM I), or Econocrete (CAM II). Underdrains were described by diameter, but the type of material used was not specified.

CONCLUSION

Trying to collect inventory data requires searching for data from several sources. The location of these data is often not commonly known. In many cases, officials of a given bureau or district agency may not even realize that they have certain pieces of information in their own files. The purpose of the IPFS is to give everyone easy access to this type of information through computer terminals. Although this project has required the expenditure of much time, money, and effort, the potential future savings are enormous. It is hoped that this paper will give agency officials of other states a realistic idea of the effort required as they embark on creating their own pavement management systems. To successfully complete this kind of undertaking, it is important to be prepared for potential problems and to persevere.

REFERENCES

1. J. P. Hall, M. E. Dwiggins, M. I. Darter, C. L. Flowers, and J. B. DuBose. Development and Implementation Methodology for the Illinois Pavement Feedback System. *Proc., 2nd North American Conference on Managing Pavements*, 1987.
2. M. E. Dwiggins, J. P. Hall, M. I. Darter, C. L. Flowers, and J. B. DuBose. *Logical and Physical Design of the Illinois Pavement Feedback System*. Report FHWA-IL-UI-219, FHWA, U.S. Department of Transportation, June 1988.

Publication of this paper sponsored by Committee on Pavement Monitoring, Evaluation, and Data Storage.

Pavement Distress Surveys in the Strategic Highway Research Program's Long-Term Pavement Performance Study

DIMITRIOS G. GOULIAS, HUMBERTO CASTEDO, AND W. RONALD HUDSON

The pavement distress data collection of the Long-Term Pavement Performance (LTPP) study is a part of the Strategic Highway Research Program. Pavement distress data are an important component of the international data base that will be developed during the LTPP. The pavement distress information is to be collected on 500-ft (152-m) monitoring sections on a periodic basis to provide a historical data base to show relationships between distress, performance, traffic, axle loads, age, and significant pavement structural variables. Pavement distress measurements will, in most cases, be made every year on about 1,000 pavement sections. Various categories of distress data will be collected for both rigid and flexible LTPP test sections, using manual and automatic survey procedures. Detailed information is given in the contents of survey manuals to be used during this study. The distress identification and field survey manuals have as a primary objective the provision of a uniform basis for collection of distress data. It is expected that the distress identification, definitions, and measurement procedures described in these manuals will be adopted by highway and roadway agencies in this country and abroad, so that the resulting data base may offer broad opportunities for evaluating and understanding pavement performance under different circumstances.

The rapid deterioration of the national highway network is important because the United States spends more than $30 billion every year in maintaining and upgrading highways (*1*). In 1987, the Strategic Highway Research Program (SHRP) undertook major research in six areas, one of which was Long-Term Pavement Performance (LTPP), the study of which had the following specific objectives (*2*):

- Evaluation of existing design methods.
- Development of improved strategies and design procedures for the rehabilitation of existing pavements.
- Development of improved design equations for new and reconstructed pavements.
- Determination of the effects of loading, environment, material properties and variability, construction quality, and maintenance levels on pavement distress and performance.
- Establishment of an international long-term pavement data base to support these objectives and future needs.

The LTPP data base, a major component of this research, will contain a broad range of data elements, described in the Data Collection Guide for Long-Term Pavement Performance studies (*3*). The information will cover approximately 1,000 LTPP test sections in the United States and Canada. However, additional data from other participating countries will be included in the data base to provide international coverage for pavement performance evaluation.

Pavement distress evaluation is a part of the LTPP monitoring data set. Various categories of distress data will be collected periodically in both rigid and flexible LTPP test sections using manual or automatic survey procedures.

The Texas Research and Development Foundation (TRDF), with The University of Texas at Austin as a subcontractor, has been selected for the SHRP–LTPP technical support project P001. The pavement distress-related end products completed thus far by the P001 team include the *Distress Identification Manual* (*4*) and the *Field Manual for Distress Survey of Pavements* (*5*). These manuals will be used during the periodic manual monitoring of the LTPP test sections.

LTPP DATA BASE

The data collection activities for the creation of the LTPP data base have been organized in a systematic way to achieve maximum efficiency in both data collection and analysis. The categories of data included in the LTPP study are summarized in the following paragraphs.

Inventory Data

The inventory data include information necessary to identify the test section and to describe its geometric details, its construction techniques, and the material properties of its structural constituents, among others. All of these data are expected to remain the same throughout the monitoring period, unless the pavement is resurfaced or rehabilitated. The inventory data items to be collected have been described in detail (*3*).

Monitoring Data

The monitoring data include pavement distress information, profile measurements, skid data, and deflection testing results. These measurements will be collected on a 500-ft (152-m) monitoring section on a periodic basis to provide a historical data base for developing relationships between distress,

D. B. Goulias and H. Castedo, Center for Transportation Research, The University of Texas at Austin, Austin, Tex. 78712. W. R. Hudson, Department of Civil Engineering, The University of Texas at Austin, Austin, Tex. 78712.

performance, traffic, axle loads, age, and other significant variables. It is expected that deflection, skid, distress, and serviceability measurements will be made every year on every LTPP section unless otherwise required in relation to the pavement's rate of deterioration.

Traffic Data

Traffic data are to be collected separately for each lane to be monitored. For the LTPP, collection will be done in the outside lane in one direction. The traffic data include average annual daily traffic (AADT), percent heavy trucks, distribution of traffic by vehicle classes, and distribution of axle loads for single, tandem, and tridem axles.

Environmental Data

These data will include information necessary to characterize the environment in which the LTPP pavement test section exists. The environmental data elements to be collected have been described elsewhere (*3*).

Maintenance Data

Maintenance guidelines (*6*) have been developed to allow the application of the same routine maintenance that a study site would have normally received if it had not been selected as a monitoring site, with limitations on treatments that influence the structural response of the pavement.

Rehabilitation Data

The rehabilitation data pertain to rehabilitation that will occur after initiation of test section monitoring. Most procedures, such as recycling or overlay, result in a test section having a modified pavement structure; whereas other procedures, such as undersealing, may be considered to restore without modifying the pavement's structure. Reworking of shoulders and placement of edge drains are other examples of improvements that may be made without changing the original pavement structure; however, any such rehabilitation converts the pavement from an original pavement to a rehabilitated pavement. Data items to be taken during rehabilitation will be similar to the items listed in the inventory data section. Additional detailed information for specific rehabilitation procedures will also be collected.

PAVEMENT DISTRESS DATA COLLECTION

The main objective of the pavement distress data collection is to provide practical, uniform, comprehensive, and reliable pavement condition information. The characteristics described previously must be reflected within all pavement data collection steps, which are

- Identification of LTPP monitoring test sections,
- Identification of pavement distress data to be collected,
- Following field distress survey procedures and data processing, and
- Training of raters and other personnel.

The information collected from such surveys is to be stored in the LTPP data base; it can be used to define the pavement's present condition as well as its condition trend under specific load and environmental conditions to develop pavement performance prediction models. A review of the pavement monitoring literature (*4*) revealed as many techniques and procedures as there are highway agencies involved in this process. Because the object of the LTPP studies is to produce an international pavement data base, preliminary studies were made by TRDF and CTR for recommending and defining a uniform condition survey to be used in the LTPP test sections.

LTPP MONITORING TEST SECTIONS

The LTPP monitoring data will be collected in the outside lane in one direction of traffic of existing highways in North America. These data are to be collected on 500-ft-long test sections of asphalt concrete and asphalt overlay surfaced pavements as well as jointed and continuously reinforced concrete pavements. Approximately 1,000 test sections located on existing pavements (general pavement sections, GPS) will be monitored, including preoverlay and presurface seal coat condition surveys.

IDENTIFICATION AND DEFINITION OF DISTRESS DATA

Pavement distress represents any undesirable manifestation of defects in the pavement surface able to affect pavement serviceability, structural capacity, or appearance. The review of the literature (*4*) revealed a large number of distress identification manuals from state agencies interested in developing such surveys. The distress type, severity levels, and extent descriptions included in these manuals are based on local distress manifestations and pavement conditions. In addition, a lack of uniformity in terminology and classification of pavement's defects has been observed. Because the objective of the LTPP study is to create a national data base for use in all regions of North America, there was a need to

- Standardize defect terminology for defining distress type, severity, and extent to obtain a uniform data base,
- Include distress types that have a significant influence on pavement performance as determined from previous studies,
- Obtain consistency between classification of distresses as well as use detailed measurements to minimize errors, and
- Standardize graphical and visual descriptions of distress types and severity levels to minimize different interpretations between raters.

The distress data to be collected in the LTPP test sections are presented in the *Distress Identification Manual* (*4*). Because asphalt concrete pavement (ACP), jointed (plain and reinforced) concrete pavement (JCP), and continuously reinforced concrete pavement (CRCP) present some noncommon

defect manifestations, the distresses for each pavement type are presented separately.

The distresses for ACP surfaces have been grouped into one of the following general categories:

- Cracking,
- Patching and potholes,
- Surface deformation,
- Surface defects, and
- Miscellaneous distresses.

Table 1 presents a summary of distresses, severity levels, and units of measurement for this type of pavement surface. The cracking defect mode includes alligator (fatigue), block, edge, longitudinal, and transverse cracking, as well as reflection cracking of joints for the overlayed sections. The extent of these distresses must be determined for each severity level, using the corresponding measurement units (*5*). Because, from the examination of the specific distress types present in the pavement section the rater can identify possible pavement deterioration causes, the following possible defects causes have been defined (*7,8*): alligator (fatigue) cracking has been associated with load, moisture, and drainage, whereas block cracking is associated with climate and durability factors. Edge cracking is caused by load, climate, and durability factors, whereas longitudinal and reflection cracking at joints, in addition to climate and durability, are also associated with construction defects.

The second distress group includes the patching and pothole distresses, the extent of which must be monitored within each severity level defined. Patch-patch deterioration has been related to load, climate, and durability for asphalt concrete pavements, whereas potholes, in addition to the previous two causes, have been associated with moisture and drainage factors.

Rutting and shoving constitute the surface defects type. Both of these have no severity levels defined and must be monitored according to the *Distress Identification Manual* (*4*)

TABLE 1 SURFACE DISTRESS TYPES FOR ACP LTPP TEST SECTIONS (*4*)

Distress Type	Severity Levels			Surveying Units	Surveying Technique
Cracking					
1. Alligator (Fatigue) Cracking	L[a]	M[b]	H[c]	Square Feet	P[d]/M[e]
2. Block Cracking	L	M	H	Square Feet	P/M
3. Edge Cracking	L	M	H	Linear Feet	P/M
4. Longitudinal Cracking	L	M	H	Linear Feet	P/M
5. Reflection Cracking at Joints	L	M	H	Number	P/M
6. Transverse Cracking	L	M	H	Number	P/M
Patching and Potholes					
7. Patch/Patch Deterioration	L	M	H	Square Feet, Number	P/M
8. Potholes	L	M	H	Number	P/M
Surface Deformation					
9. Rutting		None		Inches	P/M
10. Shoving		None		Square Feet	P/M
Surface Defects					
11. Bleeding	L	M	H	Square Feet	P/M
12. Polished Aggregate		None		Square Feet	M
13. Raveling and Weathering	L	M	H	Square Feet	M
Miscellaneous Distress					
14. Lane-to-Shoulder Drop-off		None		Inches	M
15. Water Bleeding and Pumping	L	M	H	Number	M

(a) L = Low; (b) M = Moderate; (c) H = High; (d) P=PASCO; (e) M=Manual

descriptions. Rutting is related to load and construction defects (inadequate compaction), whereas shoving is usually the result of heavy loads on unstable asphalt mixtures.

Bleeding, polished aggregate, and raveling and weathering constitute the surface defects type. Bleeding, raveling, and weathering have been related to climatic, durability, and material factors, whereas it is reported that polished aggregate is a load-related distress (*7,8*).

The last category of defects to be monitored in the asphalt-surfaced LTPP test sections is miscellaneous distresses. These include water bleeding and pumping (related to climate and durability), to be recorded in any of three severity levels, and lane-to-shoulder dropoff, which has no severity levels and is caused by factors such as consolidation of subgrade and load applications.

For JCP, the following categories of defects have been considered:

- Cracking,
- Joint deficiencies,
- Surface defects, and
- Miscellaneous distresses.

Table 2 presents a summary of distresses for each one of these categories with corresponding severity levels and units of measurement. As can be seen from this table, corner breaks and durability (*D*) cracks, as well as longitudinal and transverse cracks, are included in the cracking category. The extent of these distresses has to be recorded separately for each severity level using measurement units reported in Table 2

TABLE 2 SURFACE DISTRESS TYPES FOR JCP LTPP TEST SECTIONS (*4*)

Distress Type	Severity Levels			Surveying Units	Surveying Technique
Cracking					
1. Corner Breaks	L[a]	M[b]	H[c]	Number	P[d]/M[e]
2. Durability "D" Cracking	L	M	H	Number	P/M
3. Longitudinal Cracking	L	M	H	Linear Fee	P/M
4. Transverse Cracking	L	M	H	Number	P/M
Joint Deficiencies					
5. Joint Seal Damage of Transv. Joints	L	M	H	Number	P/M
6. Spalling of Longitudinal Joints	L	M	H	Linear Fee	P/M
7. Spalling of Transverse Joints	L	M	H	Number	P/M
Surface Defects					
8. Map Cracking and Scaling	L	M	H	Square Feet	P/M
9. Polished Aggregate		None		Square Feet	SR[f]/M
10. Popouts		None		Number/Square Feet	P/M Total Sq. Feet
Miscellaneous Distress					
11. Blowup		None		Number	P/M
12. Faulting of Transv. Joints/Cracks		None		Inches	M
13. Lane-to-Shoulder Drop-off		None		Inches	M
14. Lane-to-Shoulder Separation		None		Inches	P/M
15. Patch/Patch Deterioration	L	M	H	Square Feet, Number	P/M
16. Water Bleeding and Pumping	L	M	H	Number	P/M

(a) L = Low; (b) M = Moderate; (c) H = High; (d) P=PASCO; (e) M=Manual; (f) SR=Skid Resistance

and defined in the *Distress Identification Manual* (*4*). The causes associated with each distress manifestation are as follows: corner breaks are related to load and moisture and drainage, whereas *D* cracking is related to climate and durability factors; longitudinal and transverse cracking are related to climate, durability, and load (*7,8*).

The joint deficiencies defects category includes joint seal damage of transverse joints (associated with climate and durability causes), and spalling of longitudinal and transverse joints, which in addition to the previous causes are related to load factors as well.

The category surface defects includes map-cracking and scaling, polished aggregate, and popouts. Of these distresses, only map cracking and scaling must be monitored for each severity level defined. Polished aggregate is a load-related distress, whereas map cracking and scaling and popouts are related to climate and durability; however, construction defects can also produce scaling (*7,8*).

Under the last category for JCP, miscellaneous distresses, are included blowups, faulting of transverse joints and cracks, lane-to-shoulder dropoff and separation, patch-patch deterioration, and water bleeding and pumping; only the last two distresses must be monitored by severity levels. These distresses and the possible causes associated with each one are blowups, related to climate and durability; faulting of transverse joints and cracks, related to subgrade erosion and construction defects; lane-to-shoulder dropoff caused by subgrade consolidation and pumping; lane-to-shoulder separation caused by subgrade consolidation and shoulder movement; patch-patch deterioration, caused by load, climate, durability, and moisture and drainage factors; and water bleeding and pumping, related to climate, durability, moisture, and drainage (*7,8*).

For CRCP, the last pavement type considered in the LTPP studies, the following distress groups have been included:

- Cracking,
- Surface defects, and
- Miscellaneous distresses.

Table 3 presents a summary of distresses under each of the above groups, with corresponding severity levels and units of

TABLE 3 SURFACE DISTRESS TYPES FOR CRCP LTPP TEST SECTIONS (*4*)

Distress Type	Severity Levels			Surveying Units	Surveying Technique
Cracking					
1. Durability "D" Cracking	L[a]	M[b]	H[c]	Number	P[d]/M[e]
2. Longitudinal Cracking	L	M	H	Linear Feet	P/M
3. Transverse Cracking	L	M	H	Number	P/M
Surface Defects					
4. Map Cracking and Scaling	L	M	H	Square Feet	P/M
5. Polished Aggregate		None		Square Feet	SR[f]/M
6. Popouts		None		Number/Square Feet	P/M Total Sq. Feet
Miscellaneous Distress					
7. Blowup		None		Number	P/M
8. Construction Joint Deterioration	L	M	H	Number	P/M
9. Lane-to-Shoulder Drop-off		None		Inches	M
10. Lane-to-Shoulder Separation		None		Inches	P/M
11. Patch/Patch Deterioration	L	M	H	Square Feet, Number	P/M
12. Punchouts	L	M	H	Number	P/M
13. Spalling of Longitudinal Joint	L	M	H	Linear Feet	P/M
14. Water Bleeding and Pumping	L	M	H	Number	P/M

(a) L = Low; (b) M = Moderate; (c) H = High; (d) P=PASCO; (e) M=Manual; (f) SR=Skid Resistance

measurement. For this type of pavement, the following defects are included under cracking: *D* cracks and longitudinal and transverse cracks. *D* cracking is related to climate and durability, whereas longitudinal and transverse cracking, in addition to the previous causes, are related to load factors as well (*7,8*).

The second defect category considered for CRCP is surface defects, which includes map cracking and scaling, polished aggregate, and popouts. The considerations related to such distresses are similar to the one reported previously for surface defects of the JCP.

The last distress group is miscellaneous distresses (see Table 3), which includes blowups, construction joint deterioration, lane-to-shoulder dropoff, lane-to-shoulder separation, patch-patch deterioration, punchouts, spalling of longitudinal joint, and water bleeding and pumping. The extent of these defects in the pavement surface must be monitored using one of the three severity levels available, with the exception of blowouts, lane-to-shoulder dropoff, and lane-to-shoulder separation, for which no severity levels have been defined. The causes associated with blowups, lane-to-shoulder dropoff and separation, patch-patch deterioration, and water bleeding and pumping are as described previously for miscellaneous deficiencies of the JCP; construction joint deterioration is a manifestation of construction imperfections; whereas punchouts are related to load and loss of subgrade and subbase support; finally spalling of longitudinal joints is caused by load, climate, and durability causes.

METHODS FOR FIELD SURVEY OF LTPP PAVEMENT SECTIONS

Two pavement distress surveying techniques have been selected for use in the LTPP study: a visual or manual survey procedure and an automatic technique using the PASCO multifunction survey vehicle. The visual surveys are intended for use as a backup at times when it is not possible to schedule a visit by the PASCO vehicle. If PASCO has surveyed the test section within 3 months before maintenance and rehabilitation work, it is not necessary to perform the visual distress survey, which will be performed, however, in remote areas (e.g., Hawaii, Puerto Rico) not directly accessible to PASCO. About 233 GPS test sections have been surveyed to date with the PASCO equipment and it is expected that by the end of the fall of 1989 most of the LTPP test sections will be surveyed.

The *Distress Identification Manual* (*4*) should be used as a standard guide for interpretation, identification, and rating of observed pavement distresses. The *Field Manual for Distress Surveys* (*5*) provides instructions, data forms, and maps for use in visual collection of defect information for pavements with asphalt concrete (Chapter 2), jointed concrete (Chapter 3), and continuously reinforced concrete (Chapter 4) pavements.

Visual or Manual Pavement Distress Survey Procedure

In the visual pavement distress survey, raters walk along the pavement section and manually draw a map showing the type and exact location of all defects present on the pavement surface, similar to the procedure used at the AASHO road test (*9*).

The equipment necessary for performing field condition surveys is as follows:

- *Field Manual for Distress Surveys* (*5*);
- *Distress Identification Manual* (*4*);
- Extra blank data sheets and maps;
- Clipboard, pencils, calculator, 35-mm camera, film, video camera, tapes;
- Two tape measures, one at least 100 ft long, and an engineering scale or ruler;
- Straight edge (4-ft) or rut depth gauge; and
- Hard hat and safety vest.

The severity level of each distress is identified and recorded on the maps and the data sheets included in the *Field Manual for Distress Surveys* (*5*). The field maps (see example shown in Figure 1) provide the exact location of each defect type existing on the test section. Five sheets are used for mapping; each sheet contains two 50-ft maps that represent 100 ft of the LTPP section.

To map the test section, a 100-ft tape measure should be placed on the shoulder adjacent to the test section, from Station 0 to Station 1. Once the tape is in place, the distresses can be mapped and their longitudinal location can be read directly from the tape. The transverse location of the distresses can be recorded using the additional tape measure. Once the first 100-ft subsection is mapped, the tape measure should be moved to Station 1 through Station 2 to map the second 100-ft subsection, and the process is repeated throughout the 500-ft test section.

The defects are drawn on the map at the appropriate locations using the various distress symbols defined in the *Field Manual for Distress Surveys* (*5*). Once the distress is drawn, it is labeled and numbered using the relative symbols and corresponding severity levels (*L*, *M*, or *H*), if applicable. Any distresses that are not described in the manuals should be photographed and videotaped. The location and extent of them should be shown and labeled on the map.

If bleeding, polished aggregate, raveling, or weathering occurs in extended areas over an asphalt concrete surfaced pavement test section, the total extent is not mapped. For jointed concrete pavement sections and continuously reinforced concrete pavements, if map cracking or scaling, polished aggregate, or popouts occur in large areas over the test section, the total extent must not be mapped as well. Instead, the location, extent, and severity level (if applicable) of all the distresses must be noted in the space for comments at the bottom of each map. These distresses should be mapped only if they occur in localized areas.

Lane-to-shoulder dropoff for both CRCP and JCP and lane-to-shoulder separation for CRCP are not mapped but are recorded in the corresponding sheets.

The data sheets or forms included in the *Field Manual for Distress Surveys* (*5*) provide space for recording the state ID number, the SHRP ID (state code plus SHRP Section ID), the survey date, and the results of distress surveys, on different sheets for each pavement type. Except where otherwise indicated, entries have to be made for all distress data

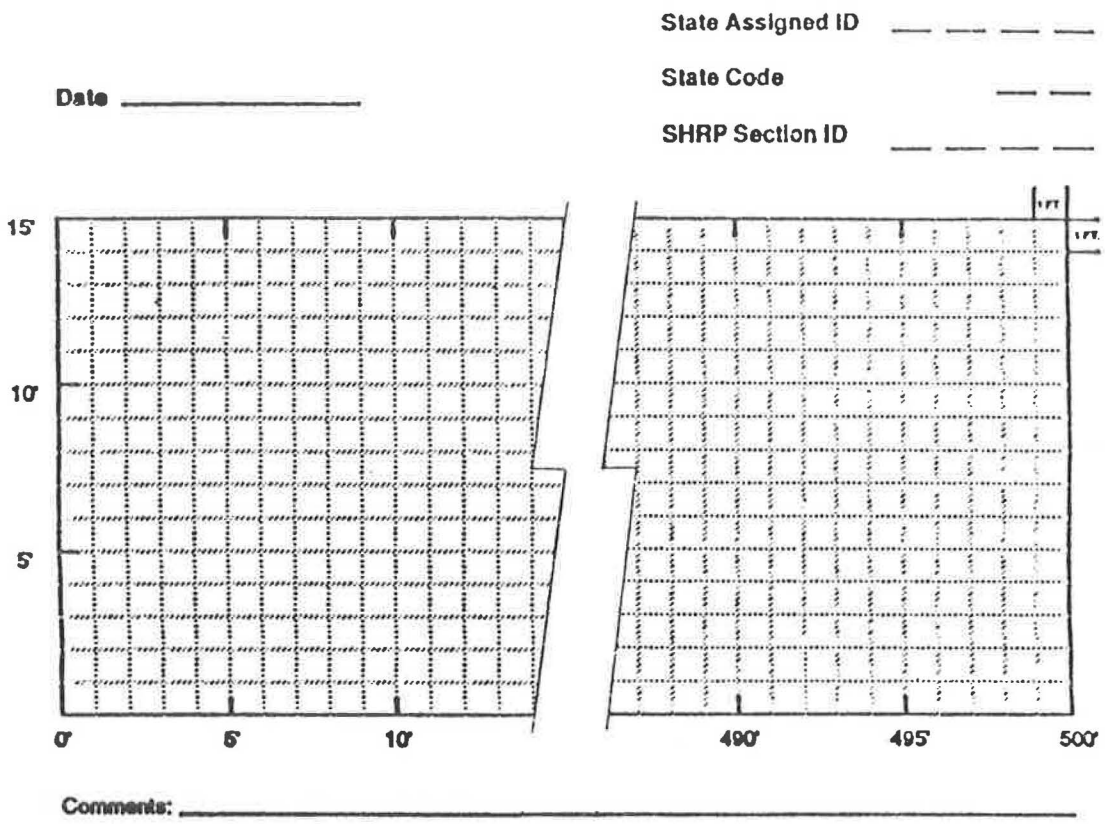

FIGURE 1 LTPP pavement distress map form (5).

elements. If a particular type of distress does not exist, a zero should be entered in the appropriate space. All data sheets and maps are to be completed in the field. Particular attention is required for monitoring the following distresses per pavement type.

In asphalt concrete pavements (ACP), shoving and polished aggregate are recorded only in extent. Rutting is measured as the maximum vertical depression (to the nearest 0.1 in.) of the pavement surface in a wheelpath, from the center of a 4-ft straight edge or rut depth gauge (*9*). Measurements are taken at the beginning of the test section and at 50-ft intervals. There should be a total of 11 measurements in each wheelpath, for a total of 22 measurements on each test section (see Table 4). Lane-to-shoulder dropoff is measured as the difference in elevation (to the nearest 0.1 in.) between the pavement and the adjacent shoulder surface. Measurements are taken at the beginning of the test section and at 100-ft intervals (a total of six measurements) at the lane-shoulder interface or joint. Lane-to-shoulder dropoff typically occurs when the outside shoulder settles. However, heave of the shoulder may occur due to frost action or swelling soil and if it is present, it should be recorded as a negative (−) value. At a point where there is no lane-to-shoulder dropoff, enter zero. In addition, space is provided to list other distress types found on the test section but not listed on the data sheets.

For portland cement concrete pavements, polished aggregate, popouts, and blowups are recorded only by extent. Faulting of transverse joints and cracks is measured as the difference in elevation (to the nearest 0.1 in.) between the pavement surface on either side of a transverse joint or crack. It is measured 1 ft from the outside slab edge. Measurements are taken at every joint and crack that has faulting. If more than 10 joints or cracks have faulting, record the measurements in additional copies of the corresponding data sheets or forms (see Table 5). The distance from the start of the test section to the point where the measurement is taken is recorded. The space to the left of the entry of measured faulting is filled with a positive or negative sign. If the approach slab is higher than the departure slab, a positive sign (+) is entered. If the approach slab is lower, a negative sign (−) is entered.

Lane-to-shoulder dropoff for both JCP and CRCP is recorded in the same way as for ACP. In addition, for both JCP and CRCP, lane-to-shoulder separation is measured as the width of the joint (to the nearest 0.1 in.) between the outside lane and the adjacent shoulder surface (*6*). Measurements (a total of six) are taken at the beginning of the test section and at 100-ft intervals. At each point where there is no lane-to-shoulder separation, a zero must be entered.

Automatic Pavement Distress Survey Procedure

The PASCO multifunction survey vehicle (*10*) has been selected for surveying the LTPP test sections. The photographs and other visual images of the pavement surface collected by this vehicle will be later interpreted in the office. This vehicle is used to speed up the field data collection time and provide a permanent visual record of the actual pavement condition. Cracking, patching, and other distresses are recorded using the ROADRECON-70 system. The vehicle travels at speeds

TABLE 4 MONITORING SHEET FOR RUTTING OF ASPHALT CONCRETE SURFACED PAVEMENTS (*5*)

Inner Wheel Path			Outer Wheel Path		
Point Number	Point Distance[1] (feet)	Rut Depth (inches)	Point Number	Point Distance[1] (feet)	Rut Depth (inches)
1	0.	_._	1	0.	_._
2	50.	_._	2	50.	_._
3	100.	_._	3	100.	_._
4	150.	_._	4	150.	_._
5	200.	_._	5	200.	_._
6	250.	_._	6	250.	_._
7	300.	_._	7	300.	_._
8	350.	_._	8	350.	_._
9	400.	_._	9	400.	_._
10	450.	_._	10	450.	_._
11	500.	_._	11	500.	_._

[1]Point Distance is the distance in feet from the start of the test section to the point where the measurement was made.

between 3 and 53 mph (5 and 85 km/hr). A continuous photographic record of the pavement surface is made using a 35-mm slit camera. The system synchronizes film feed speed and camera aperture with the speed of the vehicle to equalize image density and photographic reduction. Road widths of up to 16 ft (5 m) can be filmed. Photographing is performed at night using on-board lights. The lights are set at an angle to the road surface so that shadows are produced at cracks and other defects in the surface, making interpretation easier. Interpretations of the distresses are made by a technician viewing the developed 35-mm film enlarged 10 times on the ROADRECON Film Digitizer. A grid pattern is overlayed on the film to aid in qualification of the distress for input into a computer data base.

Rut depth surveys can be carried out at speeds up to 50 mph (80 km/hr) using the ROADRECON-75 system (*10*). A pulse camera mounted on the vehicle photographs hairline optical bars projected onto the road. The camera shutter and hairline projector are synchronized according to the distance covered by the projection vehicle, so that the system is able to create a photographic record of rutting at variable distance intervals. The film is projected onto a digitizing table and traced with a computer mouse, enabling the wave patterns to be processed into a transverse profile of the pavement surface.

TRAINING

Training of the raters before a manual field survey is an important aspect of pavement evaluation. Because of the need for fast but reliable estimates of distress, it is necessary to provide a well-organized training program for assigned personnel. This training will involve familiarization with objectives, definitions, and procedures, followed by field observation under controlled conditions.

Determination of extent (density) and severity is essentially subjective, depending on experience and engineering judgment in a particular area. For this reason, the *Distress Identification Manual* (*4*) will be provided to the raters, because it includes descriptions of each distress type and how density and severity are to be identified. Also, information related to procedures for recording distress included in the *Field Manual for Distress Surveys* (*5*) is vital.

Experience indicates that training sessions should be repeated just before rating periods (*11*). If multiple teams are to be

TABLE 5 MONITORING SHEET FOR FAULTING OF TRANSVERSE JOINTS AND CRACKS OF JOINTED CONCRETE PAVEMENTS (5)

Joint Number[1]	Point Distance[2] (feet)	Joint Faulting[3] (inches)	Joint Number[1]	Point Distance[2] (feet)	Joint Faulting[3] (inches)
1	_ _ _.	_._	1	_ _ _.	_._
2	_ _ _.	_._	2	_ _ _.	_._
3	_ _ _.	_._	3	_ _ _.	_._
4	_ _ _.	_._	4	_ _ _.	_._
5	_ _ _.	_._	5	_ _ _.	_._
6	_ _ _.	_._	6	_ _ _.	_._
7	_ _ _.	_._	7	_ _ _.	_._
8	_ _ _.	_._	8	_ _ _.	_._
9	_ _ _.	_._	9	_ _ _.	_._
10	_ _ _.	_._	10	_ _ _.	_._

[1]Numbers represent only transverse joints or cracks measured.

[2]Point Distance is the distance in feet from the start of the test section to the point where the measurement was made.

[3]Enter either a positive or negative sign in the left space, depending on whether the "approach slab" is higher or lower than the "departure slab," respectively.

TABLE 6 MONITORING SHEET FOR LANE-TO-SHOULDER DROPOFF OF ACP, JCP, AND CRCP AND LANE-TO-SHOULDER SEPARATION FOR JCP AND CRCP (5)

Point Number (feet)	Point Distance[1]	Lane-to-Shoulder Separation (inch)	Lane-to-Shoulder Drop-off (inch)
1	0.	_._	_._
2	100.	_._	_._
3	200.	_._	_._
4	300.	_._	_._
5	400.	_._	_._
6	500.	_._	_._

[1]Point Distance is the distance in feet from the start of the test section to the point where the measurement was made.

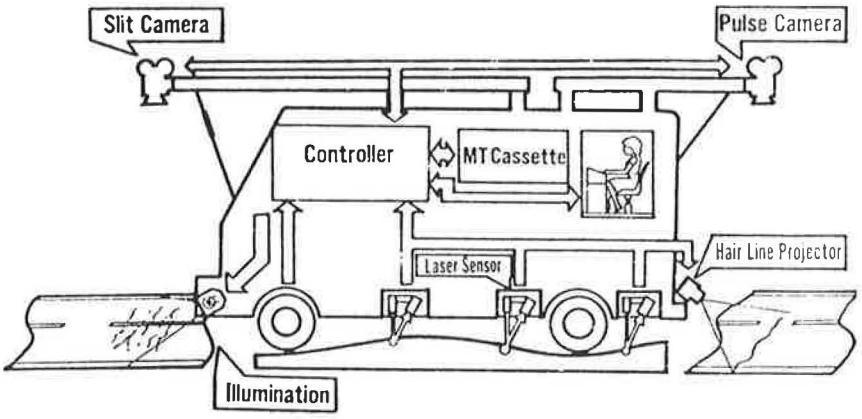

FIGURE 2 PASCO multifunction survey vehicle (*10*).

used, it will be important to calibrate the teams so that consistent ratings are obtained. This can be accomplished by repeatedly rating identical sections by each team until similar results are obtained. Wide variations have been experienced between rating teams on individual projects but when averages for a group of projects are compared between teams, the variation is significantly reduced. Criteria for the training exercise are not available; hence, some judgment must be applied. It is recommended that at least 10 sections be included as the base case (*11*). Each section should have a different amount of distress by type, extent, or severity.

SUMMARY

The distress surveys conducted as part of this long-term study will be used to quantify the condition of a pavement by classifying the amount and extent of distress present annually. The information to be collected from such surveys and to be stored in the LTPP data base is described in this paper and includes categories and types of distress data for both rigid and flexible pavements as well as the possible causes responsible for the manifestation of the defects. The manual and automatic survey procedures are also presented in this paper. Detailed information is given on the contents of survey manuals to be used during this study including identification of the LTPP test sections and monitoring and mapping of distress manifestations in related forms. The distress identification and field survey manuals discussed in this paper have as a primary objective the provision of a uniform basis for collecting distress data and it is expected that the definitions and procedures used in the SHRP LTPP study will be adopted by highway agencies interested in developing condition surveys.

ACKNOWLEDGMENTS

The information included herein is part of an investigation sponsored by the Strategic Highway Research Program (SHRP) for the Long-Term Pavement Performance (LTPP) studies, conducted by the Center for Transportation Research (CTR) of The University of Texas at Austin and the Texas Research and Development Foundation (TRDF) of Austin, Texas. The authors are pleased to acknowledge the support of SHRP, CTR, and TRDF. The assistance of Karen Benson of TRDF and Amir Hanna of SHRP is gratefully acknowledged.

REFERENCES

1. *Research Plans, Strategic Highway Research Program*. Final Report, TRB, National Research Council, Washington, D.C., May 1986.
2. *Special Report 202: America's Highways, Accelerating the Search for Innovation*. TRB, National Research Council, Washington, D.C., 1984.
3. *Data Collection Guide for Long-Term Pavement Performance Studies*. Strategic Highway Research Program, National Research Council, Washington, D.C., June 13, 1988.
4. Texas Research and Development Foundation. *Distress Identification Manual for LTPP Studies*. Strategic Highway Research Program, National Research Council, Washington, D.C., May 1989.
5. Texas Research and Development Foundation. *Field Manual for Distress Surveys*. Strategic Highway Research Program, National Research Council, Washington, D.C., May 1989.
6. *Guidelines for Maintenance of General Pavement Studies (GPS) Test Sections*. Operational Memorandum SHRP-LTPP-001, Strategic Highway Research Program, National Research Council, Washington, D.C., July 1988.
7. M. Y. Shahin and S. D. Kohn. *Pavement Maintenance Management for Roads and Parking Lots*. U.S. Army Corps of Engineers, Construction Engineering Research Laboratory, Oct. 1981.
8. K. D. Smith, M. I. Darter, J. B. Rauhut, and K. T. Hall. *Distress Identification Manual for the LTPP Studies*. Strategic Highway Research Program, National Research Council, Washington, D.C., March 1987.
9. *Special Report 61E: The AASHO Road Test Report 5 Pavement Research*. HRB, National Research Council, Washington, D.C., 1962.
10. *1 for 3, PASCO Road Survey System (PRS-System)—From Theory to Implementation*. PASCO Corporation brochure, c/o MITSUBISHI International Corporation, Project and Development Div., New York, undated.
11. J. A. Epps and C. L. Monismith. *NCHRP Synthesis of Highway Practice 126: Equipment for Obtaining Pavement Condition and Traffic Loading Data*. TRB, National Research Council, Washington, D.C., Sept. 1986.

Publication of this paper sponsored by Committee on Pavement Monitoring, Evaluation, and Data Storage.

Evaluation of the FHWA Profilometer and Rut-Measuring (PRORUT) Device in Indiana

KHALED KSAIBATI, KEITH KERCHER, SEDAT GULEN, AND THOMAS D. WHITE

Purdue University and the Indiana Department of Transportation have evaluated the performance of a profile and rut depth (PRORUT) device developed by the University of Michigan Transportation Research Institute. Several pavement sections with different characteristics were included in the evaluation. Accurate profiles were determined with manual surveying techniques. Subsequently, the PRORUT device was operated over the same pavement sections and an analysis was made to find the variance of the results. The PRORUT profiles agreed closely with the rod and level survey profiles in all cases except for one chip and seal section. Improvements were suggested to enhance the PRORUT operation.

The University of Michigan Transportation Research Institute (UMTRI) under contract to FHWA developed and constructed a highway profiling and rut depth measurement system. This equipment, referred to as the "PRORUT" device, measures profiles of two wheel paths as well as rut depth while operating at highway speeds. The Indiana Department of Transportation (INDOT), Georgia Department of Transportation, and Pennsylvania Department of Transportation were asked to evaluate the equipment within their respective highway systems. The experimental design and findings of the PRORUT evaluation in Indiana are discussed in the following sections, along with detailed explanations of the international roughness index (IRI) and the root mean square vertical acceleration (RMSVA) concepts.

PRORUT: DESCRIPTION AND OPERATION

The PRORUT profilometer system is installed on the 1974 Dodge B300 van. Distance from the mounting position on the vehicle to the road surface can be measured by an interchangeable infrared or laser sensor. However, the infrared sensor proved to be color sensitive, a characteristic that could result in errors in the measured profile. Thus, only the laser sensors are recommended for use with PRORUT.

As shown in Figure 1, the sensors are installed on the van so that measurements can be obtained in both wheel tracks as well as the center of the lane. Rut depth is determined relative to the center of the lane profile. Vertical acceleration of the van in response to the road profile is measured with Sunstrand accelerometers, Model QA–900 servo types, rated at 30 *g* full range, 250 *g* shock, and at 500-Hz natural frequency. The vertical acceleration is integrated to obtain a datum profile from which the sensor readings are subtracted to obtain the relative road profiles. Instantaneous horizontal speed of the van is sensed by a transducer on the right front wheel.

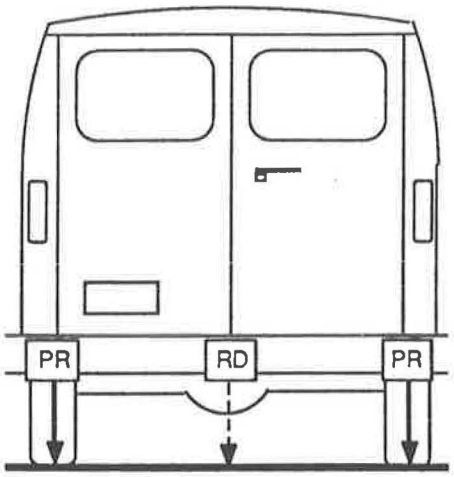

FIGURE 1 The laser sensor locations.

PRORUT is equipped with an onboard IBM XT computer to accomplish the following tasks (*1,2*):

1. User friendly system operation;
2. System calibration;
3. Data collection;
4. Data management and storage;
5. Profile, roughness, and rut depth computations; and
6. Profile plots.

System calibration is done on a daily basis. When selecting the appropriate calibration options, the PRORUT computer

K. Ksaibati, K. Kercher, and S. Gulen, Indiana Department of Transportation, Research Division, P.O. Box 2279, W. Lafayette, Ind. 47906. T. D. White, Purdue University, School of Civil Engineering, W. Lafayette, Ind. 47907.

calibrates the electrical components in the system by supplying voltages at various input points and measuring output voltages. At the same time, the laser sensors are checked to ensure they are at the proper zero and gain settings. This is accomplished by running the vehicle up on blocks and installing a calibration bar under all three sensors. The accelerometers are checked by means of a bounce test. With the vehicle stationary, the operator jumps on the rear bumper to bounce the body up and down while profile measurement is made. If a flat profile is obtained, the accelerometers are correctly calibrated. Finally, the distance sensor can be calibrated by running the PRORUT over a measured distance.

Before start of profile measurement, the operator enters the pavement section and needed system configuration information. Initially, the raw acceleration, height, and distance measurements are stored. Subsequently, the data are transformed to produce longitudinal profiles and rut depth profile by two stages of data processing. Typically, both stages of processing are performed automatically by the system with a first request to view the processed data. The measurements are displayed graphically using plotting routines or printed out in tabular forms.

The PRORUT profilometer was first tested at the Ann Arbor Road Profilometer Meeting. At this meeting, the PRORUT device was operated over several surface types of known profile. An evaluation was made to determine the agreement between the PRORUT and the known profiles. The overall performance is summarized:

1. *Wavelength Range*. The PRORUT profilometer had a demonstrated measurement capability over the wavelength range of 1 to 300 ft.
2. *Roughness Range*. The PRORUT is capable of roughness measurement over the range of 1 to 10 m/km international roughness index (IRI) roughness.
3. *Repeatability*. Results from repeated tests can be characterized as on the order of 0.1 m/km IRI, or better.
4. *Operating Speed Range*. The upper and lower limits of operating speed are 55 and 10 mph, respectively.

APPROACH TO PRORUT EVALUATION

The main objective was to evaluate the PRORUT profilometer operational characteristics and to make comparisons with the INDOT Cox Roadmeter and rod and level surveys for a range of pavement types and roughness. The following tasks were performed:

1. Select pavement types and sites to be tested,
2. Conduct rod and level survey,
3. Survey sections with Cox Roadmeter and PRORUT devices,
4. Process data,
5. Compare rod and level profile with profiles from the Cox Roadmeter and PRORUT device, and
6. Conduct statistical analysis.

The data gathering and the analysis strategies are shown graphically in Figure 2.

SITE SELECTION

Pavement sites tested were selected to represent the range of surface texture and roughness encountered throughout the state. In Indiana, 10 pavement surface types exist in the highway system:

1. Continuously reinforced concrete,
2. Jointed plain concrete,
3. Jointed reinforced concrete,
4. Flexible,
5. Full-depth asphalt,
6. Surface treatments,
7. Restored concrete,
8. Asphalt overlay of CRCP,
9. Asphalt concrete overlay of jointed plain or reinforced concrete, and
10. Asphalt overlay of flexible or full-depth asphalt.

Of the 10 potential pavement surface types, 3 were selected for testing in the study:

1. Asphalt overlay of jointed concrete with no maintenance, reflection cracks, blowups, or extensive patches;
2. Jointed, tied portland cement concrete; and
3. Chip and seal (surface treatment).

Initially, three levels of roughness (low, medium, and high) were considered for each pavement surface type. Because of the significant effort required for the rod and level survey, only six pavement sections were surveyed. Furthermore, it was estimated that 0.1 mi was the longest section that could be profiled by rod and level in 1 day, if elevation was determined at 1-ft increments. To minimize the personnel necessary for traffic control and for the safety of the profile crew, it was decided to limit the sites to 4-lane divided highway sections. As presented in Table 1, all pavements were located on US-52 and I-65 near Lafayette, Indiana. Normally, a chip and seal would not be used on the traveled lanes of a 4-lane divided highway because of the large traffic volumes. In order to satisfy the INDOT safety concerns, a chip and seal shoulder of a newly resurfaced section of I-65 at Lafayette was tested.

INDOT routinely surveys sixty 1-mi sections of pavement each month with the Cox Roadmeter. These surveys are used to monitor the changes in the vehicle suspension in which the Roadmeter is installed. The sections range from very smooth to very rough PCC, flexible, and overlaid PCC pavement. As part of the study, surveys of these sixty 1-mi sections were conducted using the PRORUT device and Cox Roadmeter. Experience was obtained on the operational characteristics of the PRORUT device, and data were collected for a relative evaluation of results of the PRORUT device and Cox Roadmeter.

DATA COLLECTION

On each of the six pavements to be surveyed by rod and level, a section 528 ft long was laid out in one wheelpath using a steel surveying tape. A yellow triangle was painted at each

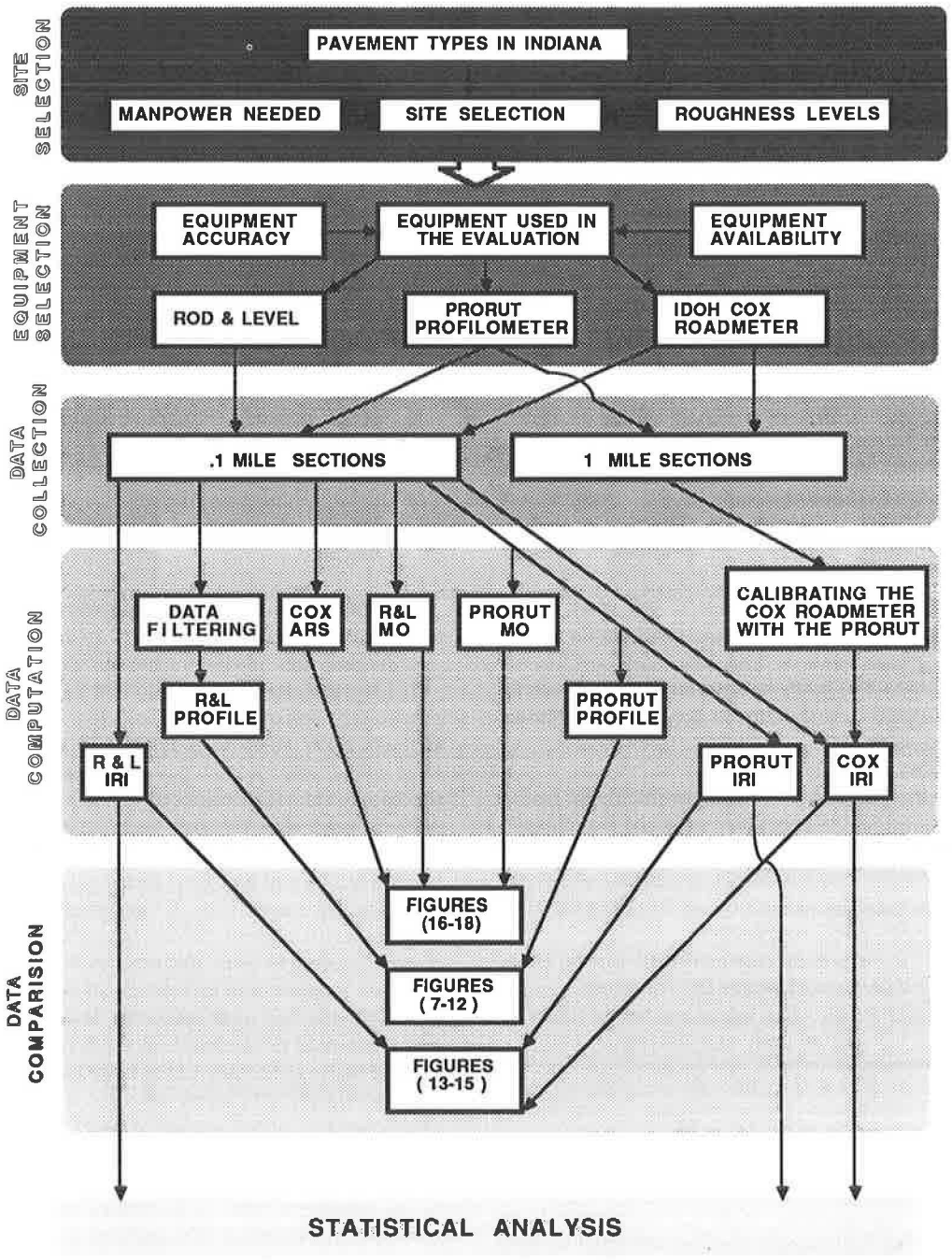

FIGURE 2 Data gathering and analysis strategies.

10-ft increment in the wheel path to maintain alignment when conducting the rod and level profile. PK nails were driven flush with the pavement in the wheel path to be profiled at 132-ft intervals to serve as turning points and temporary bench marks in case profiling of the entire section could not be completed in 1 day.

A Wild N–3 precision level, shown in Figure 3 with a parallel plate micrometer, was used to perform the rod and level surveys. The micrometer for this instrument is graduated to 0.00033 ft (0.1 mm) and the reading can be estimated to the nearest 0.01 mm. The last digit was not estimated, but rounded to the nearest 0.1 mm, because this was already beyond the accuracy of the PRORUT device. The survey crew included an instrument man, note keeper, and rodman. Because of the concentration required to conduct the precision survey, the rodman and the note keeper switched jobs periodically, and the instrument man took a break to rest his eyes at intervals of 132 ft or about every 90 min.

The PRORUT device was driven over the six rod and level survey sites to obtain profiles. In order to thoroughly evaluate

TABLE 1 TEST SECTION DESCRIPTIONS

Site #	Pavement Type	Roughness Level	Location
1	Asphalt Overlay	Low	US-52 West
2	Asphalt Overlay	Medium	US-52 East at Wabash River Bridge
3	Asphalt Overlay	High	US-52 East at Lebanon
4	Asphalt Overlay	Medium	US-52 West at Lebanon
5	Chip & Seal	Low	I-65 North at SR-25 (shoulder)
6	Concrete	Medium	US-52 West at Bypass and Northwestern Avenue

the capabilities of the device, replicate runs were made at various sampling intervals: 1, 2, 3, and 4 samples per foot. Additionally, replicate runs were made at speeds of 30, 40, and 50 mph, as well as while accelerating from 30 to 50 mph on one site. These tests were conducted to evaluate the question of speed independence. The results from all of the PRORUT runs are summarized in Table 2. The INDOT Cox Roadmeter vehicle was also driven on the six 0.1-mi rod and level sites. Table 3 presents the results from three runs at 50 mph made on each site. Both devices were also driven over the sixty 1-mi sections of the correlation loop. The vehicles were operated at 50 mph and the PRORUT sampling rate on these sites was at one sample per foot.

After data had been collected with the PRORUT device on all sixty 1-mi sections and four of the 0.1-mi rod and level sections, it was noticed that the left accelerometer was not passing the bounce test, which was the internal calibration discussed previously. The accelerometer was subsequently replaced with one obtained from the FHWA. In order to be sure that the data included in the analysis were accurate, all of the previously collected data were reobtained. All data were found to be usable, as detailed in the data compilation section of this report.

DATA REDUCTIONS

Road surface elevations were completed using the rod and level readings. These profiles are shown in Figure 4. The plot for Site 1 showed several discrepancies. This site was the smoothest of the six sites and after a field visual survey of the site, it was decided that the rod and level survey was in error. The field notes were reviewed, but the error was not obvious. As a result, the rod and level data for this site were rejected as unusable.

Comparison of the profile produced by the PRORUT with that of the rod and level survey method would have been the most intuitive method to confirm the accuracy of PRORUT. However, the PRORUT profile deviated from the actual profile because not all wavelengths were included. The profile was smoothed by applying the moving average concept over a baselength. The following equation is usually used to perform the calculations:

$$Y_s(i) = Y_s(i-1) + [Y_r(i+K) - Y_r(i-K-1)]/(2K+1) \quad (1)$$

where

$Y_s(i)$ = smoothed profile elevation for sample i,
$Y_r(j)$ = unfiltered profile elevation for sample j,
K = number of samples corresponding to 0.5 of the moving average baselength,
b = $2K^*\Delta K$ = baselength, and
ΔK = distance between samples.

This technique removes short wavelengths. However, pavement profiles are desirable to filter out the long wavelengths, leaving the roughness associated with the short waves. Therefore, the moving average is converted from a low-pass filter to a high-pass filter with the following equation:

$$Y_h(i) = Y_r(i) - Y_s(i) \quad (2)$$

where $Y_h(i)$ is the high-pass filtered elevation for sample i.

Figures 5 through 9 compare the filtered profiles from the PRORUT profilometer and the profiles from the rod and level survey. It appears that the PRORUT captured the basic profile shape for the asphalt overlay and the concrete sections. However, the PRORUT profilometer did not capture the profile details of the chip and seal section. Figure 10 shows the profile obtained by driving the PRORUT at a constant speed of 50 mph and compares it with the profile obtained by driving at varied speeds. It is clear from this figure that speed does not affect the measured profile.

Despite filtering, a direct point-by-point comparison was not a viable means of validation. Alternatively, the independent elevation measurements were analyzed in terms of

FIGURE 3 The instrument used to collect the rod and level data.

summary statistics. The two types of roughness statistics used in this analysis were

1. The international roughness index (IRI).
2. Root-mean-square vertical acceleration (RMSVA).

International Roughness Index (IRI)

The IRI, which is defined as a characteristic of the longitudinal profile of a traveled wheel track, involves controlled measurement of road roughness for a number of roads under a variety of conditions and by a variety of instruments and methods. The IRI is a standardized roughness measurement related to those obtained by response-type road roughness measurement systems (RTRRMS). Because this type of measurement is affected by the speed of the vehicle, a standard speed of 50 mph (80 km/hr) is specified in the definition of IRI. Specifically, the IRI is a measure of the ratio of the accumulated suspension motion of a vehicle to the distance traveled by the vehicle at a speed of 50 mph (80 km/hr) (*3,4*).

The IRI Road Roughness Scale

The roughness scale selected for the IRI satisfied the criteria of being time stable, transportable, relevant, and readily measurable by pavement engineers anywhere in the world. It is a numeric scale that can be correlated not only to roughness measurements obtained through profilometers and response-type road roughness measurement systems (RTRRMSs), but also to subjective public opinion about road roughness. The scale ranges from 0 to 16, with increasing roughness indicated by higher numerical values of the scale. Figure 11 shows the IRI roughness scale, which is based on approximate ranges of roughness for different types of roads.

Computation of IRI from the Rod and Level Survey

Calculation of IRI from rod and level data is accomplished by computing four variables as functions of the measured profile. These four variables simulate the dynamic response of a reference vehicle traveling over the measured profile. The equations for the four variables are solved for each measured elevation point except for the first point. The average slope over the first 34 ft (11 m) is used for initializing the variables by assigning the following values:

$$Z_1' = Z_3' = (Y_a - Y_1)/11 \quad (3)$$

$$Z_2' = Z_4' = 0 \quad (4)$$

$$a = 11/(\Delta x + 1) \quad (5)$$

where

Z_1, Z_2, Z_3, Z_4 = the four variables,
Y_a = ath profile elevation point,
Y_1 = first point, and
Δx = sample interval.

TABLE 2 DATA COLLECTED WITH PRORUT DEVICE

SECTION NO.	PAV. TYPE	SAMPLE PER FT	MICRO TEXT.	MACRO TEXT.	WHEEL PATH	SPEED	PRORUT IRI LEFT	PRORUT IRI RIGHT	PRORUT IRI BOTH
1	1	1	1	1	1	50	48	49	49
1	1	1	1	1	1	50	45	44	45
1	1	1	1	1	1	50	43	43	43
1	1	1	1	1	1	50	58	47	53
1	1	1	1	1	1	40	49	44	47
1	1	1	1	1	1	30	60	49	54
1	1	1	1	1	1	VAR.	59	49	54
1	1	2	1	1	1	50	47	48	47
1	1	2	1	1	1	50	50	46	48
1	1	3	1	1	1	50	50	46	48
1	1	3	1	1	1	50	57	56	57
1	1	4	1	1	1	50	52	52	52
1	1	4	1	1	1	50	45	48	46
1	1	4	1	1	1	50	53	44	49
2	1	1	1	2	2	50	157	119	138
2	1	1	1	2	2	50	120	128	124
2	1	2	1	2	2	50	141	127	134
2	1	2	1	2	2	50	129	122	126
2	1	3	1	2	2	50	138	141	141
2	1	3	1	2	2	50	137	141	139
2	1	4	1	2	2	50	142	130	136
2	1	4	1	2	2	50	139	144	141
3	1	1	1	3	1	50	165	204	184
3	1	1	1	3	1	50	183	203	193
3	1	2	1	3	1	50	170	209	190
3	1	2	1	3	1	50	185	192	188
3	1	3	1	3	1	50	177	218	197
3	1	3	1	3	1	50	195	213	204
3	1	4	1	3	1	50	179	223	201
3	1	4	1	3	1	50	197	216	206
4	1	1	1	2	1	50	171	206	189
4	1	1	1	2	1	50	184	204	194
4	1	2	1	2	1	50	175	214	194
4	1	2	1	2	1	50	208	224	216
4	1	3	1	2	1	50	187	224	206
4	1	3	1	2	1	50	200	216	208
4	1	4	1	2	1	50	188	228	208
4	1	4	1	2	1	50	194	211	203
5	2	1	2	1	2	50	36	34	35
5	2	2	2	1	2	50	39	40	39
5	2	3	2	1	2	50	40	37	39
5	2	4	2	1	2	50	41	36	38
6	3	1	2	2	2	50	149	150	150
6	3	2	2	2	2	50	156	158	157
6	3	3	2	2	2	50	156	161	159
6	3	4	2	2	2	50	156	160	158

PAVEMENT TYPE: #1. OVERLAYED
#2. CHIP & SEAL
#3. CONCRETE

WHEEL PATH: #1. RIGHT
#2. LEFT

MACRO TEXTURE: #1. LOW
#2. MED.
#3. HIGH

MICRO TEXTURE: #1. LOW
#2. HIGH

TABLE 3 COX ROADMETER MEASUREMENTS IN TERMS OF IRI

Site #	Speed	Roadmeter - 3 Runs				IRI
		#1	#2	#3	Average	In/Mile
1	50	15	15	14	14.7	67
2	50	35	33	31	33.0	120
3	50	70	63	69	67.3	203
4	50	55	44	48	49.0	161
5	50	14	12	13	13.0	62
6	50	36	41	31	36.0	128

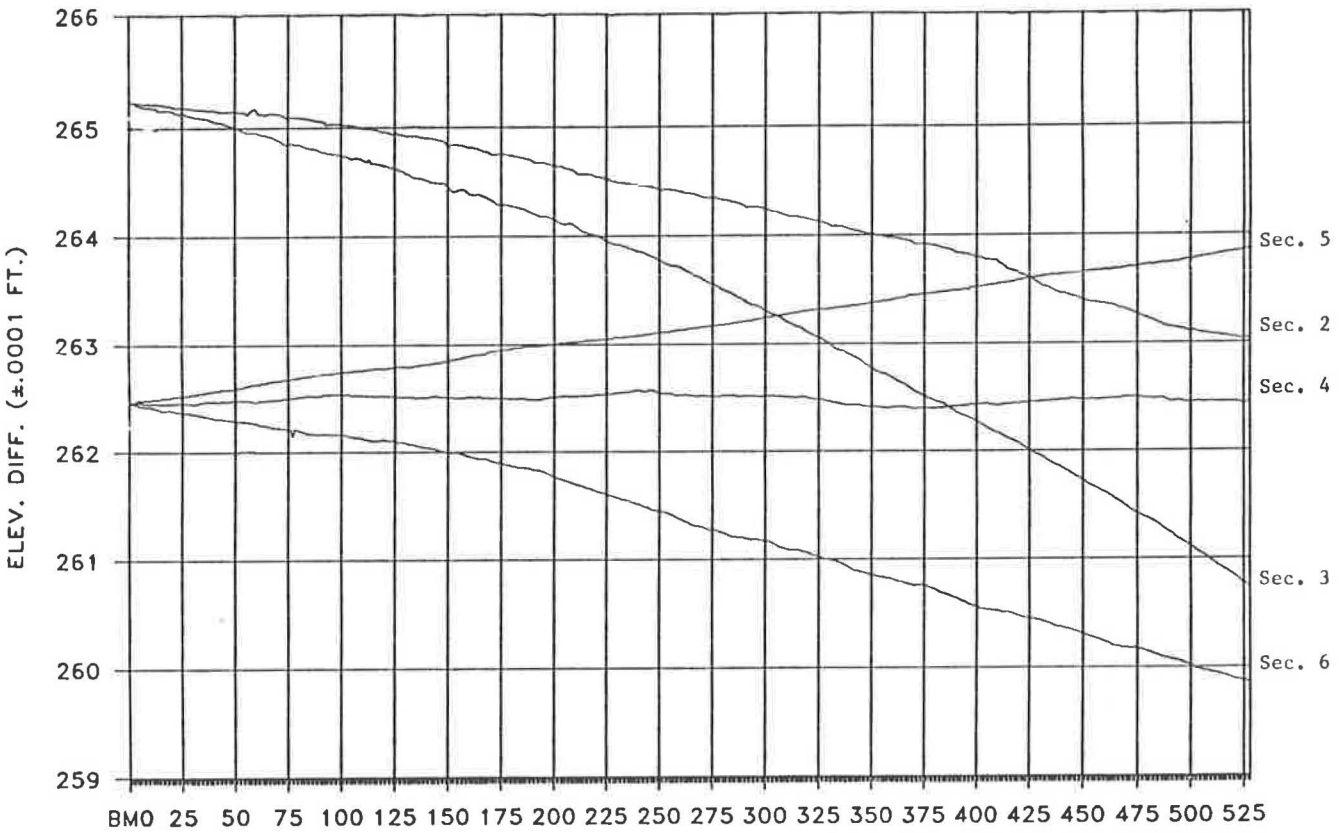

FIGURE 4 Combined rod and level profile plots.

Then for each elevation point from 2 to n, where n = number of elevation measurements, the following four recursive equations are solved:

$$Z_1 = S_{11}{}^*Z_1' + S_{12}{}^*Z_2' + S_{13}{}^*Z_3' + S_{14}{}^*Z_4' + P_1{}^*Y' \quad (6)$$

$$Z_2 = S_{21}{}^*Z_1' + S_{22}{}^*Z_2' + S_{23}{}^*Z_3' + S_{24}{}^*Z_4' + P_1{}^*Y' \quad (7)$$

$$Z_3 = S_{31}{}^*Z_1' + S_{32}{}^*Z_2' + S_{33}{}^*Z_3' + S_{34}{}^*Z_4' + P_1{}^*Y' \quad (8)$$

$$Z_4 = S_{41}{}^*Z_1' + S_{42}{}^*Z_2' + S_{43}{}^*Z_3' + S_{44}{}^*Z_4' + P_1{}^*Y' \quad (9)$$

where

$Y' = (Y_i - Y_{i-1})/\Delta x$ = slope input,
$Z_j' = Z_j$ from previous position, j = 1, 2, 3, 4, and (10)
S_{ij}, P_j = coefficients that are fixed for a given sample interval Δx.

Equations 6–9 are solved for one position along the wheel track and Equation 10 is used to reset the values of Z_1', Z_2', Z_3', and Z_4' for the next position. Subsequently, the equations are solved for each position along the wheel path. Also for each position, the rectified slope RS of the filtered profile is computed as

$$RS_i = |Z_3 - Z_1| \quad (11)$$

After these equations have been solved for all profile points, the IRI is calculated as

$$IRI = \Sigma RS_i/(n - 1) \quad (12)$$

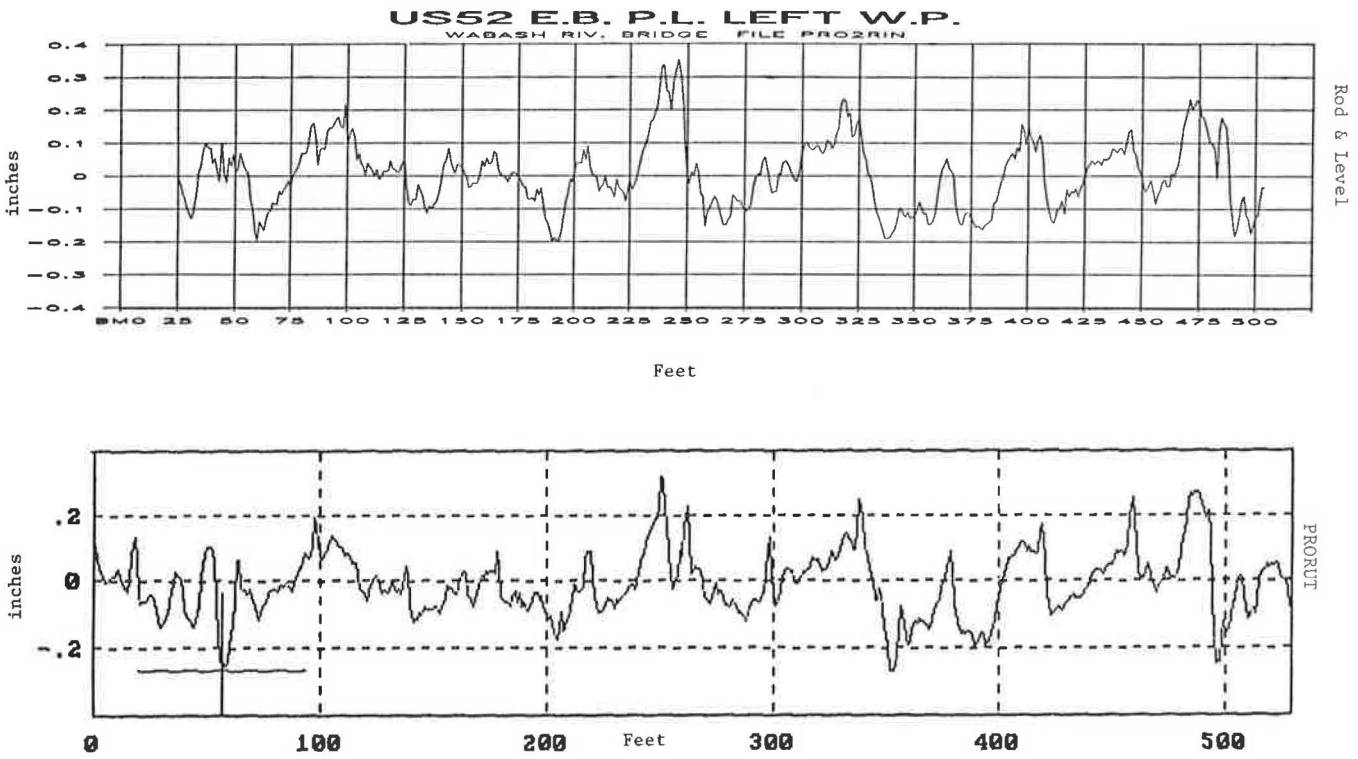

FIGURE 5 Comparison of profiles obtained from PRORUT and rod and level measurements for Section 2.

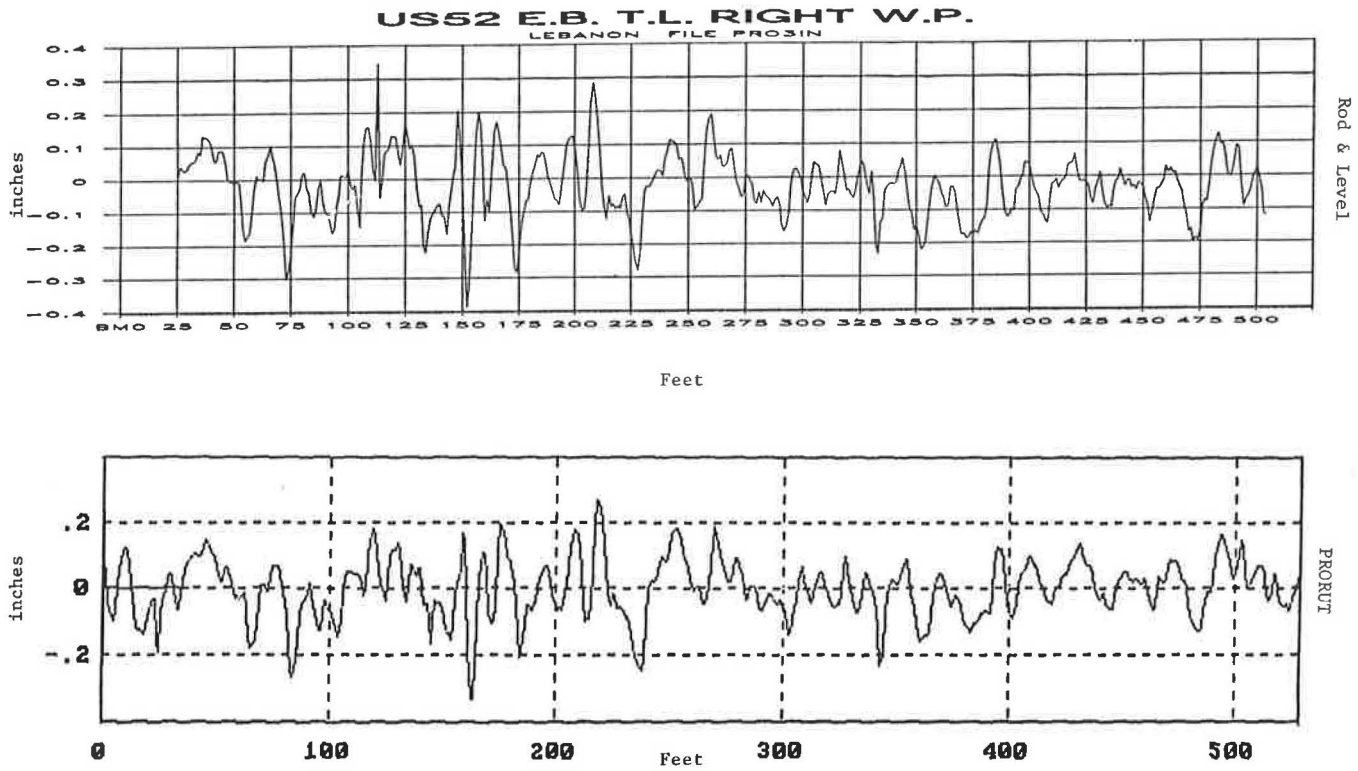

FIGURE 6 Comparison of profiles obtained from PRORUT and rod and level measurements for Section 3.

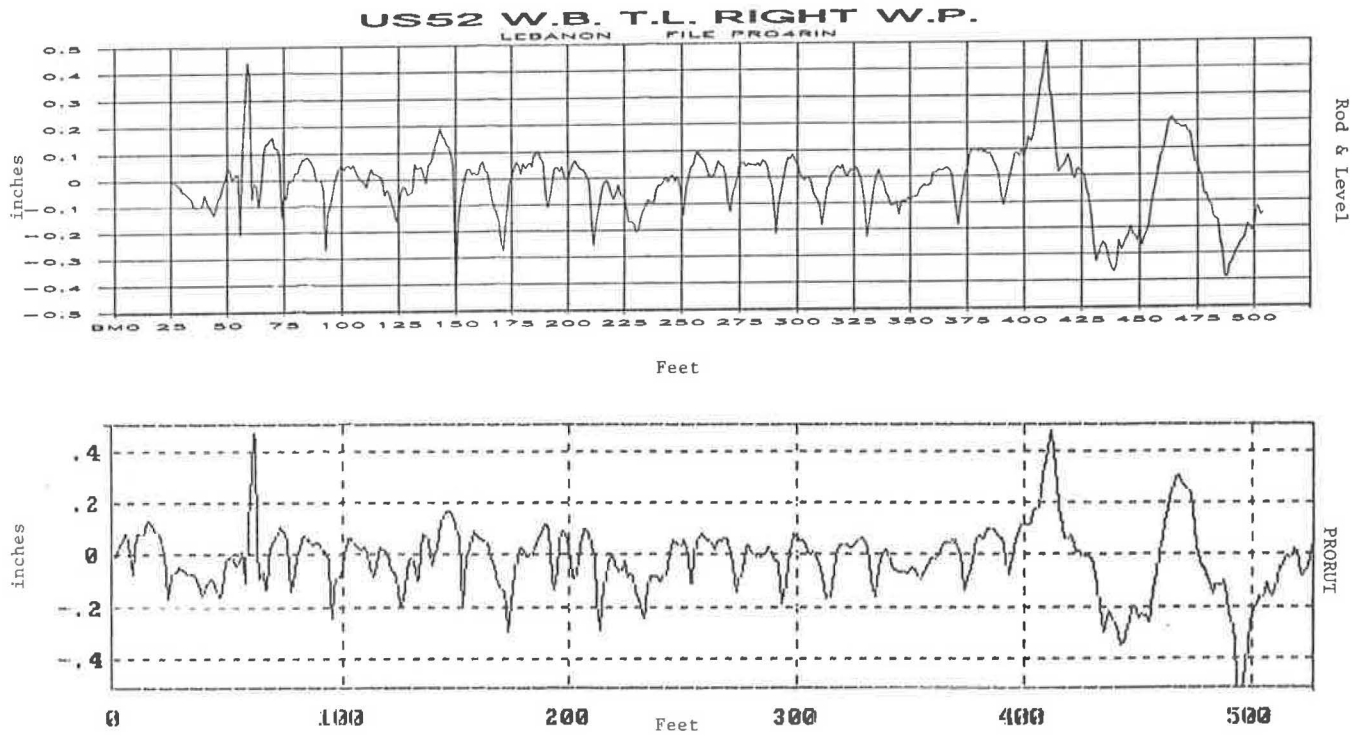

FIGURE 7 Comparison of profiles obtained from PRORUT and rod and level measurements for Section 4.

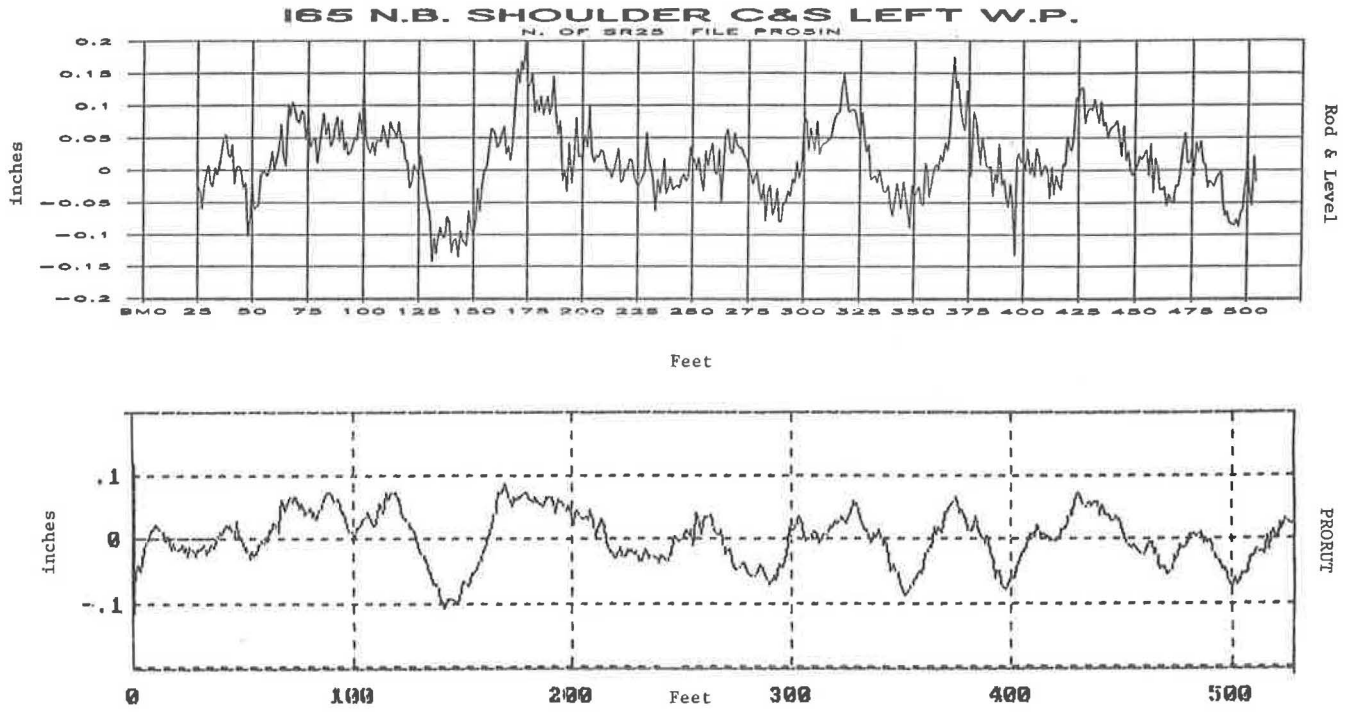

FIGURE 8 Comparison of profiles obtained from PRORUT and rod and level measurements for Section 5.

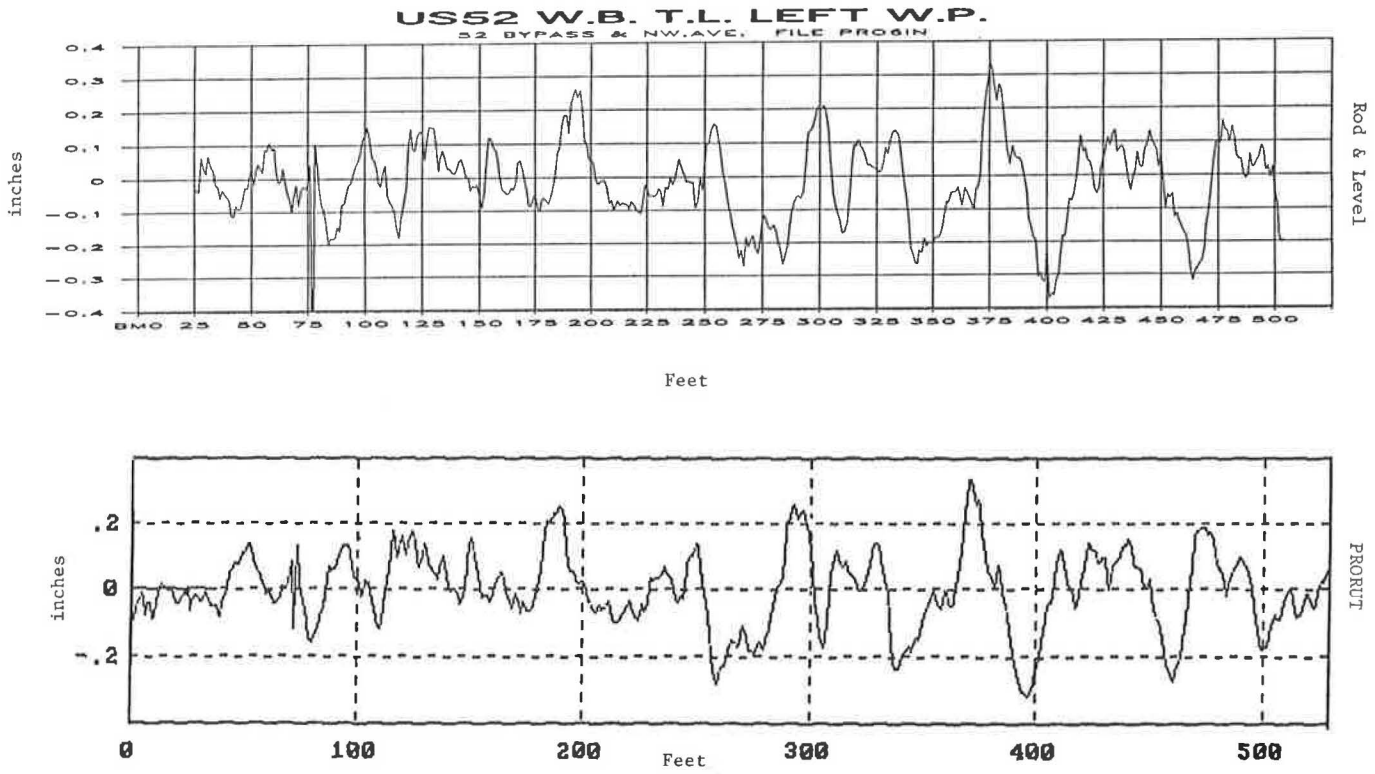

FIGURE 9 Comparison of profiles obtained from PRORUT and rod and level measurements for Section 6.

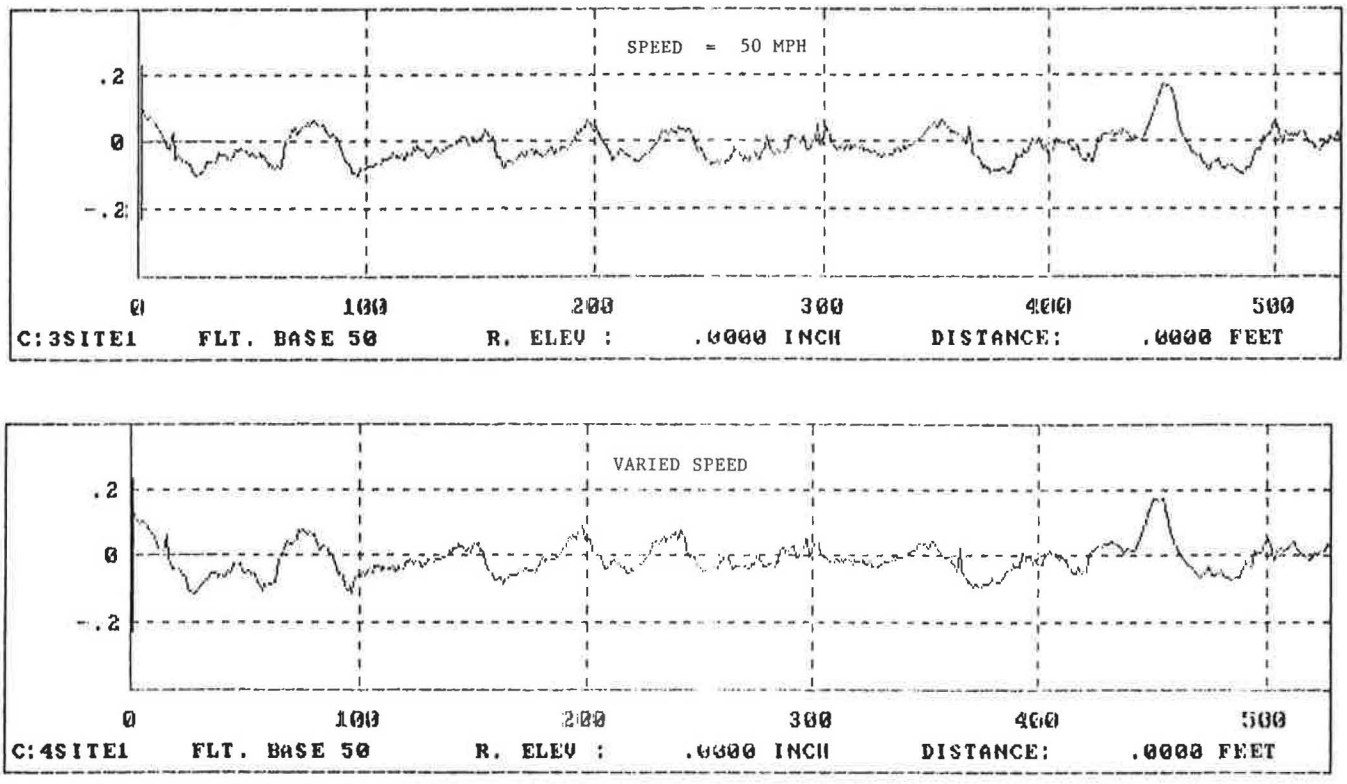

FIGURE 10 The effect of speed on a measured profile.

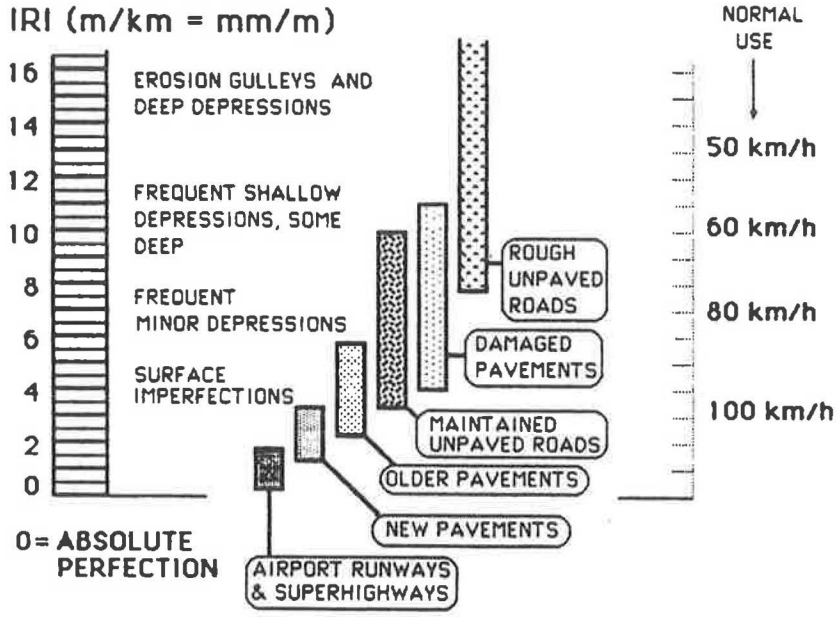

FIGURE 11 The IRI roughness scale (*1*).

The IRI statistic is thus the average of the RS variable over the length of the site.

This procedure is valid for any sample interval between $\Delta x = 0.8$ ft (0.25 m) and $\Delta x = 2.0$ ft (0.61 m). For shorter sample intervals, a moving average is obtained as the average of all points over a baselength of 0.25 m, and the IRI is calculated by solving the equations for each averaged point using coefficients in the equations appropriate for the smaller interval.

Estimation of IRI Using a Calibrated RTRRMS Instrument

A potential problem with RTRRMSs is that any two devices, even of the same make, will respond differently to road roughness. Thus, it is necessary to transform the measures to the standard IRI scale using correlation. Correlation is achieved by obtaining raw measures of average rectified slope (ARS) measured by an RTRRMS on special calibration sites. These sites are sections of road that have known IRI roughness values as determined with a profile device or a rod and level survey. The raw ARS values from the RTRRMS are plotted against the IRI values. A line is fitted to the data points and used to estimate IRI from RTRRMS measurements taken in the field. The accuracy of the calibrated measures can be based on the scatter of the points about the fitted line. The calibration equation for an RTRRMS is

$$E(\text{IRI}) = A + B * \text{ARS} + C * \text{ARS}^2 \tag{13}$$

where

E(IRI) = expected value of the IRI;
ARS = raw measure (e.g., counts/km, in./mi);
A, B, and C = coefficients based on number of calibration sites, ARS measurements on different sites, and roughness of the sites measured.

The computations needed to determine A, B, and C are as follows:

$$\bar{x} = \frac{1}{N}\sum_{i=1}^{N} x_i = (x_1 + x_2 + \ldots + x_N)/N \tag{14}$$

$$\overline{x^2} = \frac{1}{N}\sum_{i=1}^{N} x_i^2 = (x_1^2 + x_2^2 + \ldots + x_N^2)/N \tag{15}$$

$$\overline{x^3} = \frac{1}{N}\sum_{i=1}^{N} x_i^3 = (x_1^3 + x_2^3 + \ldots + x_N^3)/N \tag{16}$$

$$\overline{x^4} = \frac{1}{N}\sum_{i=1}^{N} x_i^4 = (x_1^4 + x_2^4 + \ldots + x_N^4)/N \tag{17}$$

$$\bar{y} = \frac{1}{N}\sum_{i=1}^{N} y_i = (y_1 + y_2 + \ldots + y_N)/N \tag{18}$$

$$\overline{y^2} = \frac{1}{N}\sum_{i=1}^{N} y_i^2 = (y_1^2 + y_2^2 + \ldots + y_N^2)/N \tag{19}$$

$$\overline{xy} = \frac{1}{N}\sum_{i=1}^{N} x_i \cdot y_i = (x_1 \cdot y_1 + x_2 \cdot y_2 + \ldots + x_N \cdot y_N)/N \tag{20}$$

$$\overline{x^2 y} = \frac{1}{N}\sum_{i=1}^{N} x_i^2 \cdot y_i = (x_1^2 \cdot y_1 + x_2^2 \cdot y_2 + \ldots + x_N^2 \cdot y_N)/N \tag{21}$$

$$A = \bar{y} - B \cdot \bar{x} - C \cdot \overline{x^2} \tag{22}$$

$$B = \frac{[\overline{xy} - \bar{x} \cdot \bar{y} + C \cdot (\bar{x} \cdot \overline{x^2} - \overline{x^3})]}{\overline{x^2} - \bar{x} \cdot \bar{x}} \tag{23}$$

$$C = \frac{(\overline{x^2y} - \overline{x^2}\cdot\overline{y})\cdot(\overline{x^2} - \overline{x}\cdot\overline{x}) + (\overline{x}\cdot\overline{x^2} - \overline{x^3})\cdot(\overline{xy} - \overline{x}\cdot\overline{y})}{(\overline{x^4} - \overline{x^2}\cdot\overline{x^2})\cdot(\overline{x^2} - \overline{x}\cdot\overline{x}) - (\overline{x^3} - \overline{x}\cdot\overline{x^2})^2} \quad (24)$$

$$\begin{aligned} SE = {} & \overline{y^2} + A^2 + (B^2 + 2A\cdot C)\cdot\overline{x^2} + C^2\cdot\overline{x^4} \\ & - 2A\cdot\overline{y} - 2B\cdot\overline{xy} - 2C\cdot\overline{x^2y} \\ & + 2A\cdot B\cdot\overline{x} + 2C\cdot\overline{x^3} \end{aligned} \quad (25)$$

where

N = number of calibration sites,
x_i = ARS measurement on Site i,
y_i = $RARS_{80}$ roughness of Site i computed from a measured profile, and
SE = standard error.

The standard error is a measure of the accuracy of E(IRI).

The PRORUT IRI Measurements

A response roughness device was developed by the Bureau of Public Roads (BPR) to measure road roughness at highway speeds. The BPR roughometer is mounted on a single-wheel trailer and is considered to represent the response to road roughness of one-quarter of a car. Since that time, mathematical models that simulate such a response have been developed. In the 1980s, the World Bank adopted the quarter-car simulation (QCS) model, which was distinguished by a unique set of vehicle parameters (*3–5*). The model determines the IRI on the basis of a single wheel track for a simulation speed of 50 mph.

The PRORUT device software computes the IRI automatically from the measured profile. To be able to compare the same roughness index, the computer program shown in Figure 12 was written to determine the IRI from the rod and level survey. To produce the IRI from the Cox Roadmeter data, the correlation previously described was used. Thirteen of the sixty 1-mi sections were used to determine the constants of the correlation equation. The computations shown in Table 4 produced the following correlation equation:

$$E[\text{IRI}] = 19.22 + 3.38 \cdot \text{ARS} - 0.0096 \cdot \text{ARS}^2 \quad (26)$$

where

E[IRI] = Cox estimate of the IRI, and
ARS = Cox raw measure (counts/mi).

This equation was used to convert the Cox readings of the six 0.1-mi sections into an equivalent IRI. Before the conversion to IRI, three Cox readings on the same pavement section were made and then averaged, as presented in Table 3.

The results from the rod and level survey were used as the reference for the PRORUT and Cox Roadmeter. Figure 13 shows the comparison of rod and level survey with the PRORUT. Results from four sections were distributed closely about the line of equality. However, the results from Section 5, containing chip and seal, were not in agreement. Figure 14 shows the rod and level survey and the Cox Roadmeter results. The Cox Roadmeter IRI values agreed closely with the rod and level survey IRI values; however, the Cox values were less in all cases. Good correlation between Cox Roadmeter and PRORUT results is shown in Figure 15.

The Root Mean Square Vertical Acceleration

The RMSVA for a pavement section can be determined by first calculating the variable $VA_b(i)$, defined as

$$VA_b(i) = [Y_{i-K} + Y_{i+K} - 2 * Y_i] * (K * \Delta x)^{-2} \quad (27)$$

where

Y_i = profile elevation at Position i,
i = sample number,
K = an integer used to define baselength,
Δx = distance between samples, and
b = $K * \Delta x$ = baselength.

After calculating $VA_b(i)$ for all positions, the RMSVA at baselength b can be determined by using the following equation:

$$RMSVA_b = C * \left[\sum_{i=K+1}^{n-K} VA_b(i)^2\right]^{0.5} * (n - 2 * K)^{-1} \quad (28)$$

where

$C = V^2$, and
V = speed of the response-type device used (e.g., 50 mph).

The RMSVA produces a midchord deviation from a simulated rolling straightedge (*6*). The RMSVA computation is equivalent to taking the second derivative of the height with respect to time of an object in contact with a profile while moving at a constant horizontal speed. Such computation yields values for the vertical acceleration of the object. In addition, a series of vertical acceleration values results from evaluations at many discrete elevation points; therefore, a root mean square of these values can be computed. No single baselength will produce an RMSVA numeric well matched to the wavelengths seen by roughness-measuring vehicles. Therefore, two RMSVA values for at least two baselengths are used to obtain a summary roughness numeric. The MO index, developed in Texas, is determined by first computing two midchord deviations from a profile, with baselengths of 4 and 16 ft, and combining these by means of the following linear equation:

$$MO = -20 + 23 \cdot RMSVA_4 + 58 \cdot RMSVA_{16} \quad (29)$$

In this analysis, MO indices were calculated for the six 0.1-mi rod and level survey sections. Table 5 presents MO indices from PRORUT and rod and level survey profiles. The MO index for Section 5, which was very smooth, could not be calculated from PRORUT because the MO equation gave a negative value. An MO plot, similar to the plots obtained previously with the IRI, is shown in Figure 16. The MO indices from PRORUT and the rod and level survey were also plotted against the ARS values obtained from the Cox Roadmeter, as shown in Figures 17 and 18.

```
900  * THIS PROGRAM CAN BE USED TO DETERMINE THE INTERNATIONAL
910  * ROUGHNESS INDEX. THE ELEVATIONS , IN THE UNIT METER, SHOULD
920  * BE ADDED TO THE END OF THE PROGRAM. THE THE IRI WILL BE GIVEN
930  * IN THE UNITS IN/MILE.
1000 LPRINT "SECTION 4"
1040 DIM y(26), Z(4), Z1(4), ST(4, 4), PR(4)
1050 READ DX
1060 k = INT(.25 / DX + .5) + 1
1070 IF k < 2 THEN k = 2
1080 BL = (k - 1) * DX
1090 FOR I = 1 TO 4
1100     FOR J = 1 TO 4
1110             READ ST(I, J)
1120             NEXT J
1130             READ PR(I)
1140    NEXT I
1160 INPUT "PROFILE ELEVATION 11 M FROM START:", y(k)
1170 INPUT "X = 0 ELEVATION=", y(1)
1180 Z1(1) = (y(k) - y(1)) / 11
1190 Z1(2) = 0
1200 Z1(3) = Z1(1)
1210 Z1(4) = 0
1220 RS = 0
1230 IX = 1
1240 I = 0
1250 READ N
1260 I = I + 1
1270 LPRINT "X="; IX * DX,
1280 IX = IX + 1
1290 READ y(k)
1310 IF IX < k THEN y(IX) = y(k)
1320 IF IX < k THEN GOTO 1270
1330             YP = (y(k) - y(1)) / BL
1340             FOR J = 2 TO k
1350                 y(J - 1) = y(J)
1360             NEXT J
1380 FOR J = 1 TO 4
1390    Z(J) = PR(J) * YP
1400    FOR JJ = 1 TO 4
1410             Z(J) = Z(J) + ST(J, JJ) * Z1(JJ)
1420    NEXT JJ
1430 NEXT J
1440 FOR J = 1 TO 4
1450    Z1(J) = Z(J)
1460 NEXT J
1470 RS = RS + ABS(Z(1) - Z(3))
1475 LPRINT "IRI="; RS * 63358 / I
1485 IF IX > N THEN GOTO 1500
1490 GOTO 1260
1500 END
1510 DATA .3048
1520 DATA .9951219,.01323022,-.004721649,.0004516408,.009599989
1530 DATA -.6468806,.9338062,-1.319262,.05659404,1.966143
1540 DATA .03018876,.003010939,.6487856,.009129263,.3210257
1550 DATA 3.661957,.3772937,-43.40468,.3016807,39.74273
1555 DATA 529
```

FIGURE 12 IRI computer program.

TABLE 4 COX CALIBRATION EQUATION

Section #	Cox Roughness (x)	PRORUT ROUGHNESS Left	Right	Both (y)
1	14.00	50.00	46.00	48.00
9	16.00	82.00	71.00	76.00
15	15.00	62.00	63.00	62.00
18	32.00	117.00	122.00	120.00
29	22.00	104.00	116.00	110.00
31	36.00	124.00	151.00	138.00
34	31.00	121.00	133.00	127.00
36	69.00	205.00	210.00	207.00
39	59.00	209.00	180.00	195.00
40	91.00	253.00	238.00	246.00
49	33.00	109.00	112.00	111.00
52	48.00	134.00	128.00	131.00
41	87.00	258.00	233.00	245.00

x_2 =	42.54	y_2 =	139.69
x_3 =	2455.92	y^2 =	23422.62
x_4 =	170966.85	y^2*y =	7494.08
x^2*y =	13168006.09	y^3*y =	499875.77

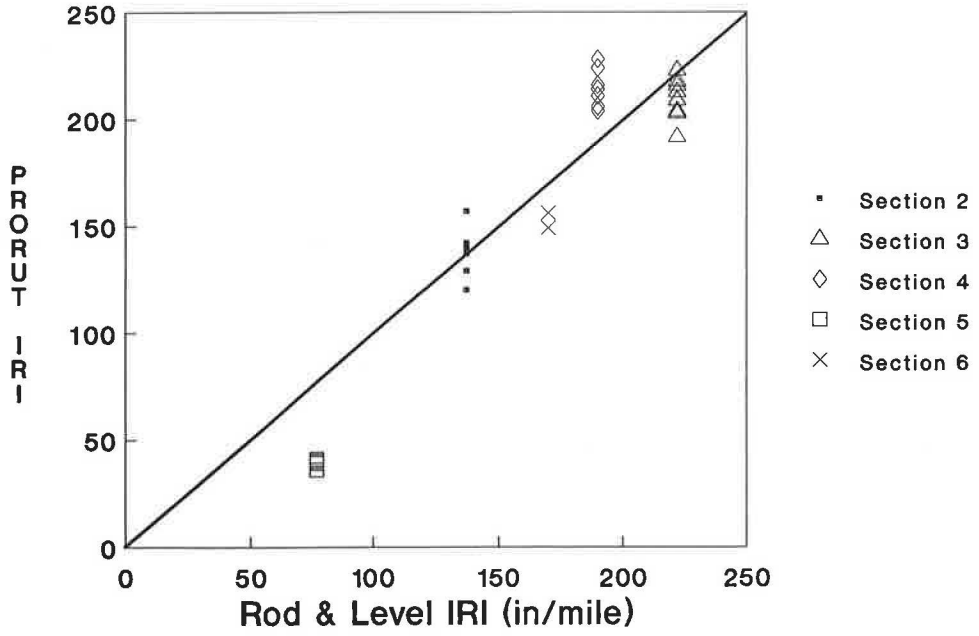

FIGURE 13 Comparison of PRORUT and rod and level measurements.

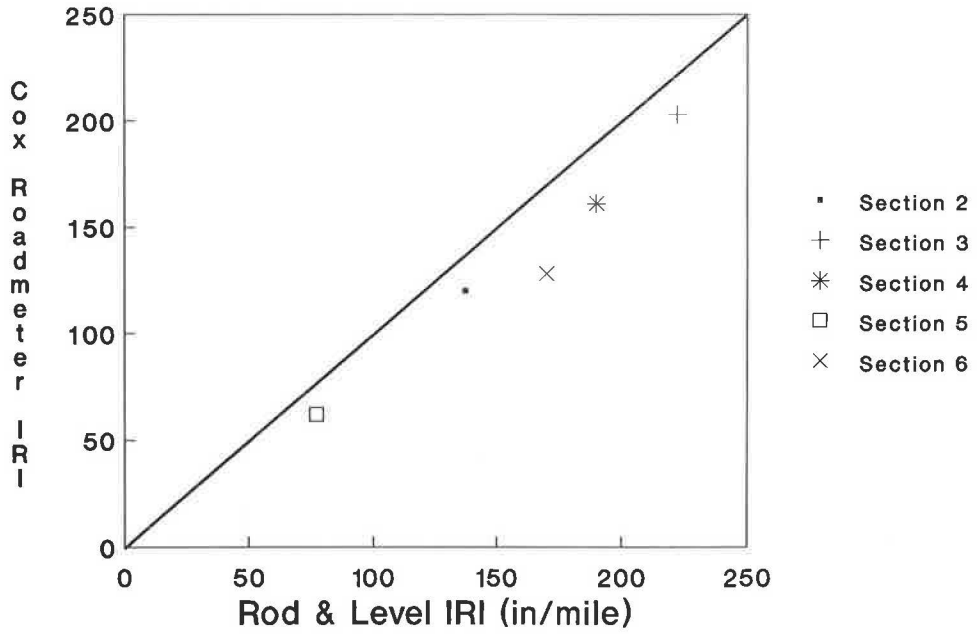

FIGURE 14 Comparison of rod and level and Cox Roadmeter measurements.

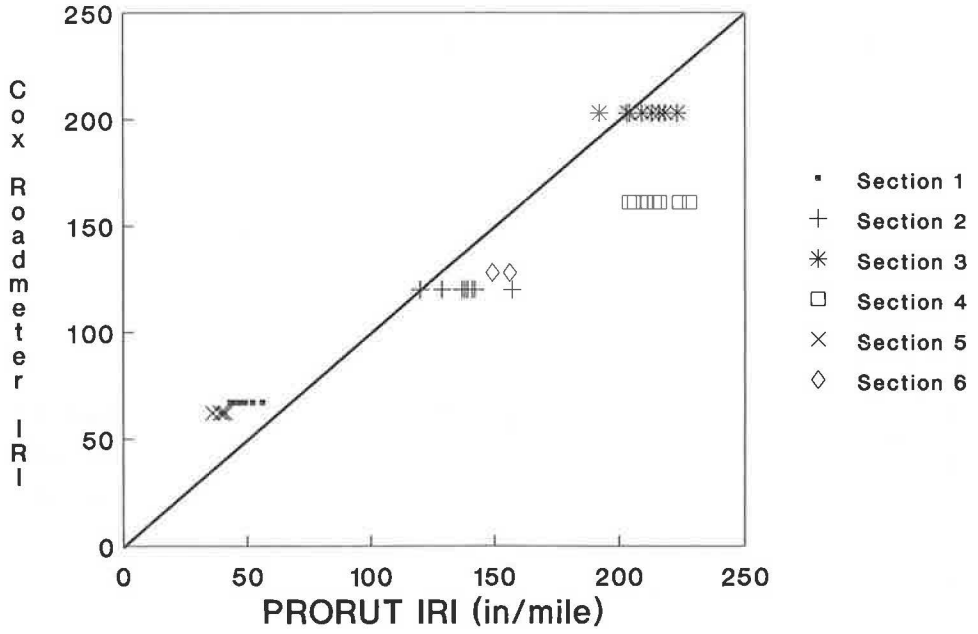

FIGURE 15 Comparison of PRORUT and Cox Roadmeter measurements.

STATISTICAL ANALYSIS

The IRI values produced from PRORUT, rod and level survey, and Cox Roadmeter measurements were statistically analyzed. The data from the PRORUT profilometer were analyzed separately to determine whether the number of samples per foot had any effect on the PRORUT device measurements. The data from all other devices were then used to correlate the measurements. The following factors and dependent variables were included in the analyses:

Statistical factors

1. SMPL is a fixed variable, the number of readings per foot by using the PRORUT profilometer, with the following four levels:

Level 1—one reading per foot,
Level 2—two readings per foot,
Level 3—three readings per foot, and
Level 4—four readings per foot.

TABLE 5 SUMMARY OF RMSVA AND MO INDICES FROM PRORUT AND ROD AND LEVEL SURVEYS

SEC.	PAV. TYPE	ROD & LEVEL RMSVA4	ROD & LEVEL RMSVA16	ROD & LEVEL MO	PRORUT RMSVA4	PRORUT RMSVA16	PRORUT MO	%DIFF.
2	1	1.71	0.27	34.72	2.08	0.25	42.13	21.34
3	1	3.09	0.24	64.62	2.85	0.23	58.73	-9.11
4	1	2.72	0.31	60.71	2.82	0.34	64.30	5.91
5	2	0.99	0.14	10.85	0.38	0.10	**	**
6	3	2.27	0.32	50.80	1.77	0.30	38.30	-24.61

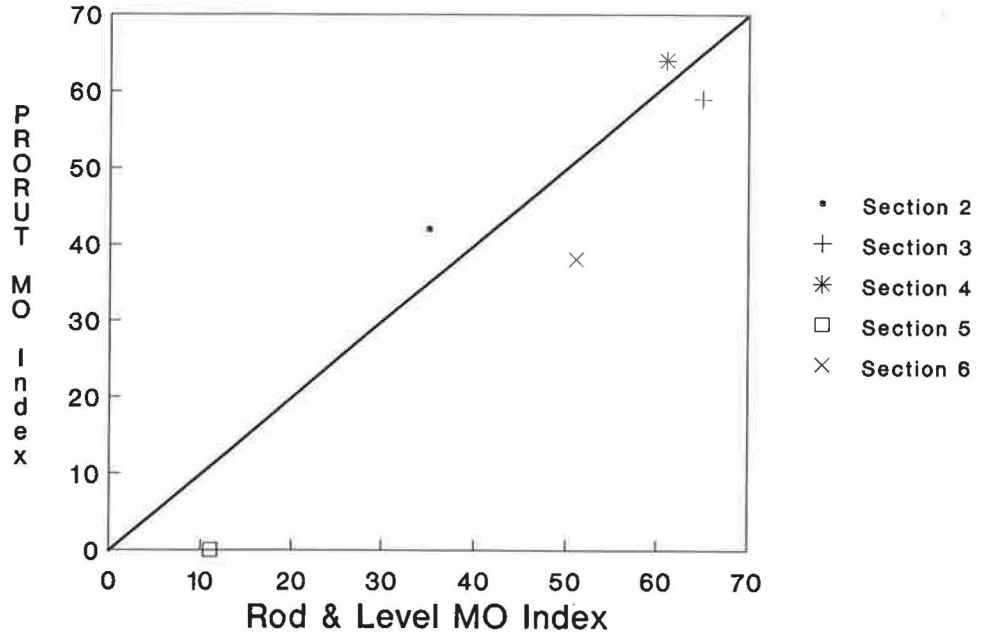

FIGURE 16 Comparison of MO indices obtained from PRORUT and rod and level measurements.

2. PVMT is a fixed variable, the pavement type, with the following three levels:

Level 1—Bituminous overlaid concrete,
Level 2—Chip and seal, and
Level 3—Concrete.

3. SEC is a random variable, the number of a section within a pavement type.
4. SYS is a fixed variable, the type of device, with the following three levels:

Level 1—PRORUT device,
Level 2—Rod and level survey, and
Level 3—Cox Roadmeter.

Dependent variables

1. IRI values from the PRORUT profilometer.
2. IRI values from the rod and level survey.
3. Estimated IRI values from the Cox Roadmeter.

The PRORUT Data Analysis

Because the PRORUT profilometer could collect data at different intervals (e.g., 1, 2, 3, or 4 measurements per foot), it was essential to determine whether the choice of interval had an impact on the IRI values. A preliminary analysis of the data presented in Table 2 indicated the following:

1. Variances for the different rates are homogeneous, based on the Burr-Foster Q-test.
2. Error terms are normally distributed, based on the Shapiro and Wilk test.

An analysis of variance (ANOVA) test was performed to test for the significance of the number of samples per foot. The following model was used:

$$\text{IRI}_{\text{PRORUT}} = A + \text{PVMT} + \text{SEC(PVMT)} + \text{SMPL} + \text{PVMT} * \text{SMPL} + \text{SEC(PVMT)} * \text{SMPL} + \text{ERROR TERM} \quad (30)$$

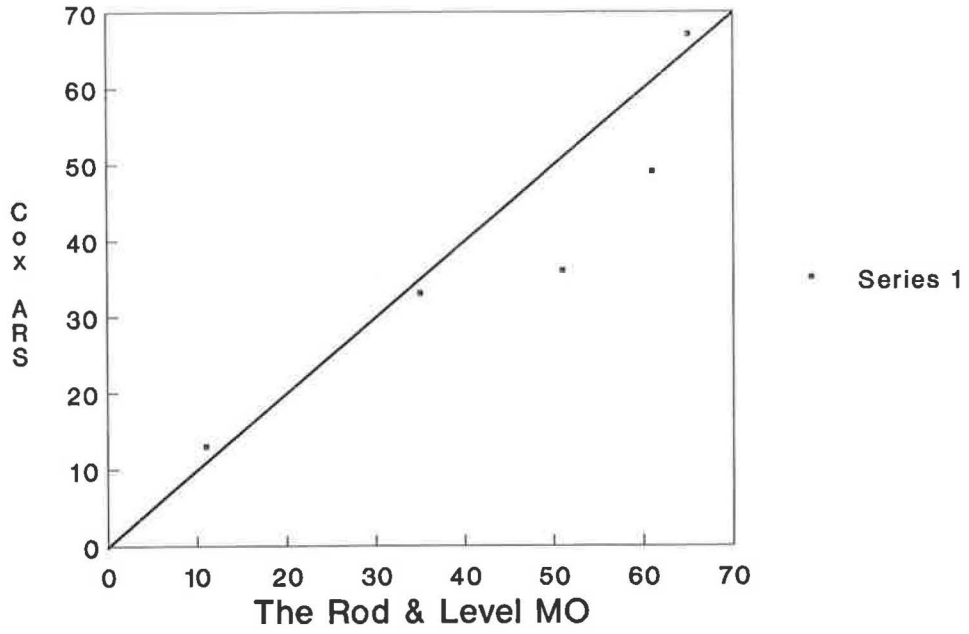

FIGURE 17 Comparison of Cox ARS and rod and level MO indices.

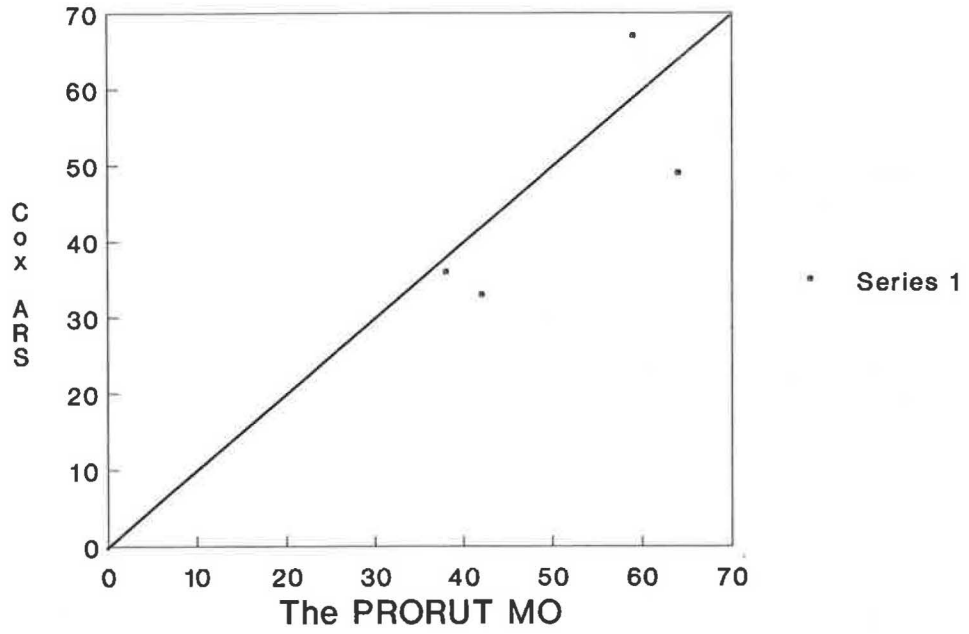

FIGURE 18 Comparison of Cox ARS and PRORUT MO indices.

where

A = regression coefficient, and
IRI_{PRORUT} = IRI value produced from PRORUT.

All other variables are as described earlier.

The ANOVA tests concluded that the rate of sampling is not significant at the $\alpha = 0.10$ level. The sample interaction terms were not significant, either. In addition, Duncan's test at the $\alpha = 0.10$ level was used to rank the sample factor in Sections 1, 2, 3, and 4. The variable SMPL, the number of samples per foot, was insignificant in Sections 1, 2, and 4; however, it was found to be significant in Section 3, which was the roughest site.

Comparisons Among Devices

As presented in Table 6, the three profiling methods did not produce equal results. Consequently, an attempt was made to correlate the results from all three devices. Pavement type

TABLE 6 COMPARISONS OF DATA COLLECTED WITH COX ROADMETER, PRORUT, AND ROD AND LEVEL SURVEYS

SEC. NO.	PAV. TYPE	PRORUT IRI	R&L IRI	COX IRI	% DIFF. PRO/R&L	%DIFF. COX/R&L	%DIFF. COX/PRO
1	1	49		67			
1	1	44		67			
1	1	43		67			
1	1	47		67			
1	1	44		67			
1	1	49		67			
1	1	49		67			
1	1	48		67			
1	1	46		67			
1	1	46		67			
1	1	56		67			
1	1	52		67			
1	1	48		67			
1	1	44		67			
2	1	157	137	120	14.60	-12.41	-23.57
2	1	120	137	120	-12.41	-12.41	0.00
2	1	141	137	120	2.92	-12.41	-14.89
2	1	129	137	120	-5.84	-12.41	-6.98
2	1	138	137	120	0.73	-12.41	-13.04
2	1	137	137	120	0.00	-12.41	-12.41
2	1	142	137	120	3.65	-12.41	-15.49
2	1	139	137	120	1.46	-12.41	-13.67
3	1	204	222	203	-8.11	-8.56	-0.49
3	1	203	222	203	-8.56	-8.56	0.00
3	1	209	222	203	-5.86	-8.56	-2.87
3	1	192	222	203	-13.51	-8.56	5.73
3	1	218	222	203	-1.80	-8.56	-6.88
3	1	213	222	203	-4.05	-8.56	-4.69
3	1	223	222	203	0.45	-8.56	-8.97
3	1	216	222	203	-2.70	-8.56	-6.02
4	1	206	190	161	8.42	-15.26	-21.84
4	1	204	190	161	7.37	-15.26	-21.08
4	1	214	190	161	12.63	-15.26	-24.77
4	1	224	190	161	17.89	-15.26	-28.13
4	1	224	190	161	17.89	-15.26	-28.13
4	1	216	190	161	13.68	-15.26	-25.46
4	1	228	190	161	20.00	-15.26	-29.39
4	1	211	190	161	11.05	-15.26	-23.70
5	2	36	77	62	-53.25	-19.48	72.22
5	2	39	77	62	-49.35	-19.48	58.97
5	2	40	77	62	-48.05	-19.48	55.00
5	2	41	77	62	-46.75	-19.48	51.22
6	3	149	170	128	-12.35	-24.71	-14.09
6	3	156	170	128	-8.24	-24.71	-17.95
6	3	156	170	128	-8.24	-24.71	-17.95
6	3	156	170	128	-8.24	-24.71	-17.95

was found to be significant and hence was included in the model by using an indicator (dummy variable), as follows:

$$Y = A0 + A1 * OL + A2 * CS + B1 * X + B2 * X2 + \text{ERROR TERM} \quad (31)$$

where

Y = system i;
X = system s;
A0, A1, A2, B1, B2 = regression coefficients;
OL = 1 if the pavement is overlay, otherwise OL = 0; and
CS = 1 if the pavement is chip and seal, otherwise CS = 0.

If OL = 0 and CS = 0, the pavement is concrete.

The models developed are presented in the upper part of Table 7. R^2 values near 1.0 indicate the presence of a strong relationship. Because chip and seal sections showed significant variations in the data, the regression models were also developed excluding the chip and seal pavement data. For the two remaining pavement types, regression analysis demonstrated that pavement type was not significant and could be dropped from the model. The lower part of Table 7 presents these models.

TABLE 7 STATISTICAL MODELS CORRELATING THE MEASUREMENT SYSTEMS

Devices Correlated	Pavement Type Considered	Model	R^2
PRORUT versus Cox	All	$IRI_{PRORUT} = -176.7 + 9.9 * OL + 17 * CS + 3.79\ Cox + 0.0094(Cox)^2$	0.97
PRORUT versus R&L	All	$IRI_{PRORUT} = -618.2 + 45.1 * OL + 167.2\ CS + 7.87\ R\&L + 0.196(R\&L)^2$	0.98
PRORUT versus Cox	All but chip & seal	$IRI_{PRORUT} = -159.8 + 3.64 * Cox - 0.0088(Cox)^2$	0.96
PRORUT versus R&L	All but chip & seal	$IRI_{PRORUT} = -304.8 + 4.67 * R\&L - 0.0104(R\&L)^2$	0.79

CONCLUSIONS

The following conclusions are drawn from this analysis:

1. There is close agreement between the PRORUT profiles and the rod and level profiles in all cases except for the chip and seal section.
2. Changes in speed while collecting data did not affect the profile measurement as shown in Figure 10.
3. The IRI values from the PRORUT and the rod and level devices are close, although they are not statistically equal.
4. The estimated IRI values from the calibrated Cox Roadmeter did not fully match the IRI values from the PRORUT.
5. The effect of number of samples per foot appears to be statistically insignificant in all cases except one, in which the pavement roughness was high.
6. The models presented in Table 6 can be used to relate the measurements from the PRORUT and the rod and level devices.
7. Because the center sensor, which provides a basis to measure rutting, did not pass the calibration test, rut depth measurements were not included in the analysis.

RECOMMENDATIONS

In general, evaluation of the PRORUT device indicated that it is a satisfactory profilometer within the capability limitations identified. The following improvements to the PRORUT hardware would increase safety and productivity:

1. A newer host vehicle would ensure a safer and more convenient environment.
2. The computer system (IBM XT) is outdated and should be replaced with a faster system.
3. The laser sensor that measures rut depth should be replaced because it did not pass the calibration tests.
4. The wiring system should be checked because the PRORUT stopped functioning several times while collecting data.

REFERENCES

1. *Reference Manual for the UMTRI/FHWA Road Profiling (PRORUT) System*. Report FHWA/RD-87/042, FHWA, U.S. Department of Transportation, Dec. 1987.
2. Users Manual for the UMTRI/FHWA Road Profiling (PRORUT) System. Report FHWA/RD-87/043, FHWA, U.S. Department of Transportation, Dec. 1987.
3. M. W. Sayers, T. D. Gillespie, and W. D. O. Paterson. *Guidelines for Conducting and Calibrating Road Roughness Measurements*. World Bank, Technical Paper Number 46, Washington, D.C., 1986.
4. M. W. Sayers. *Development, Implementation, and Application of The Reference Quarter-Car Simulation*. STP 884, ASTM, Philadelphia, Pa., 1985.
5. W. R. Hudson, D. Halbach, J. P. Zaniewski, and L. Moser. *Root-Mean-Square Vertical Acceleration As a Summary Roughness Statistic*. STP 884, ASTM, Philadelphia, Pa., 1985.
6. M. W. Sayers, T. D. Gillespie, and C. A. V. Queiroz. *The International Road Roughness Experiment, Establishing Correlation and a Calibration Standard for Measurements*. World Bank Technical Paper Number 45, Washington, D.C., 1986.

Publication of this paper sponsored by Committee on Pavement Monitoring, Evaluation, and Data Storage.

SHRP Long-Term Pavement Performance Information Management System

DAVID B. CLARKE, SANDRA B. HARRIS, ANTHONY C. HEITZMAN, AND RICHARD A. MARGIOTTA

The Long-Term Pavement Performance (LTPP) project is a major component of the Strategic Highway Research Program (SHRP). This 20-year effort is the most intensive evaluation of pavement performance since the AASHO Road Test in the early 1960s. Over 700 in-service general pavement sections throughout the United States and Canada have been selected to date for the LTPP effort. An additional 200 to 300 specific pavement sections will be constructed or modified to evaluate different pavement designs and maintenance treatments. Throughout the life of the project, SHRP will collect data for each section on material properties, environmental conditions, traffic, maintenance and rehabilitation, surface condition, and pavement response. Many of these measurements will use state-of-the-art techniques. On the basis of the AASHO experience, SHRP recognized that LTPP would produce a tremendous volume of data. In order to maintain these data in a form readily accessible to the research community, SHRP is developing a sophisticated information management system (IMS). The IMS is based on the ORACLE relational data base management system. The data base is distributed across several hardware platforms; a VAX computer serves as the primary data retrieval machine. The detailed structure and functions of the LTPP IMS will give potential researchers insight into the nature of this valuable resource.

The Long-Term Pavement Performance (LTPP) project is a major component of the Strategic Highway Research Program (SHRP). This 20-year effort is the most intensive evaluation of pavement performance since the AASHO Road Test in the early 1960s. Over 700 in-service general pavement sections (GPSs) throughout the United States and Canada have been selected to date for the LTPP effort. An additional 200 to 300 specific pavement sections (SPSs) will be constructed or modified to evaluate different pavement designs and maintenance treatments. Throughout the life of the project, SHRP will collect data for each section on material properties, environmental conditions, traffic, maintenance and rehabilitation, surface condition, and pavement response. Many of these measurements will use state-of-the-art techniques.

The information management system (IMS) is now under development for the LTPP program of SHRP. The LTPP objective is to generate data that will allow a more comprehensive understanding of pavement performance under actual operating conditions on in-service highways. Using these data, researchers will be able to improve pavement designs and maintenance methods. SHRP has designed a number of LTPP experiments from which a tremendous volume of data will flow. Under current plans, however, analysis of pavement performance using these data will be conducted by the research community. (SHRP plans to select a contractor to perform some level of data analysis on the data that is collected within the first few years of the program, but the scope of this effort has not been determined.) The IMS will be used to validate and store the data, and to serve as a conduit for its dissemination. Therefore, this paper will provide potential users with an overview of the data stored in the IMS. More detailed descriptions may be found in the technical documentation of the IMS.

In any project, information storage and retrieval is an important consideration. Use of the computer to manage research data is, of course, routine. Techniques for managing these data, however, have been steadily increasing in sophistication. Ten years ago, most data were stored in flat files. Today, powerful data base management systems (DBMSs) are available for personal computers (PCs). As projects increase in size and scope, however, their data management needs often grow beyond the capabilities of a basic DBMS. Large projects may have numerous hardware platforms, complicated data structures, multiple data bases, many types of data, and many sources of data. The relationships between the data may be complex and dynamic.

BACKGROUND

The fundamental relationships used in pavement design were developed nearly 30 years ago at the AASHO Road Test. These relationships have been criticized for failure to account for many exogenous factors, including soil types, maintenance and construction practices, composition of materials, long-term loads, and climatic effects. Such issues can only be addressed with a controlled, in-depth, long-range field experiment using highway segments representing a wide variety of conditions.

The LTPP program of SHRP was designed to rectify the perceived deficiencies of the AASHO Road Test and to improve the current state of knowledge. The stated objectives of the LTPP program are to

1. Evaluate existing design methods;
2. Develop improved design methods and strategies for the rehabilitation of existing pavements;
3. Develop improved design equations for new and reconstructed pavements;

D. B. Clarke and R. A. Margiotta, Transportation Center, The University of Tennessee, Knoxville, Tenn. 37996. S. B. Harris and A. C. Heitzman, Science Applications International Corp., 800 Oak Ridge Turnpike, Oak Ridge, Tenn. 37831.

4. Determine the effects on pavement distress and performance of loading, environment, material properties and their variability, construction quality, and maintenance levels;
5. Determine the effects of specific design features on pavement performance; and
6. Establish a national long-term pavement data base to support these objectives and future research needs.

In order to accomplish these objectives, SHRP has designed two sets of pavement studies: GPS and one for SPS. These studies will collect data on in-service pavement sections throughout the country over a 20-year period. Sections for both sets of studies are 500 ft long by 1 lane in width. Over this time span, some sections may be discarded or may switch to other experimental categories if they are changed substantially so they no longer match the original experimental requirements. For example, major reconstruction may completely change the pavement section so it does not match any of the experimental definitions. Similarly, an asphalt cement (AC) overlay on an original AC pavement would change it from one pavement experiment to another.

The designers of the LTPP project realized early on that the research would generate immense volumes of data. Unlike SHRP, which has a 5-year life, LTPP has a 20-year data collection horizon. After SHRP expires, the state highway agencies (SHAs) will continue to provide data to the system. This long lifetime means that the IMS must be carefully designed, because it will no doubt span significant changes in the state of the art for computer technology, materials testing, and highway instrumentation.

Because it is a key component of LTPP, planning for the IMS was begun during SHRP's interim phase. FHWA sponsored a study to evaluate the LTPP plans and prepare preliminary design criteria for the proposed LTPP IMS. This effort resulted in the implementation plan (*1*), which recommended a basic hardware and software architecture for the IMS, and estimated such parameters as mass storage requirements and required CPU capacity.

On the basis of the recommendations of the Implementation Plan, SHRP decided that each of its four proposed regional offices would serve as data collection nodes for the IMS. Each office would have a small IMS to collect and validate data gathered for the region. These data would then be forwarded periodically to a central IMS node for storage and dissemination to the research community. To provide continuity over the 20-year LTPP data collection process, SHRP selected TRB to operate the central system.

The IMS development project encompasses the following tasks:

1. Implementation of the national IMS and four regional IMS nodes;
2. Installation of the national IMS at TRB;
3. Installation of the four regional nodes;
4. Installation of necessary interface and quality control subsystems between the regional offices and existing SHRP and contractor offices;
5. Provision of documentation and training to allow operation of the complete IMS by SHRP, TRB, and contractor staff;
6. Installation of interfaces between SHRP and contractor offices to allow flexible access to the data for a national analysis program; and
7. Maintenance support following system delivery.

IMS COMPONENTS

The overall IMS consists of five nodes. Each of the four LTPP offices has a regional IMS. The regional machines are primarily used for data collection and validation. Personnel in the regions have a working relationship with all of the data providers and the technical expertise to judge data quality.

The national IMS is located at TRB in Washington, D.C. The IMS computer, which will be used for data storage and retrieval, has the processing power to query large data bases and to perform statistical analysis of large data sets. Data are interchanged between the regional and national machines by means of tape cassette. Direct communications between the machines is possible using modems and telephone connections, but is normally not required, as the data are not time sensitive. In addition, the telephone connection has a low throughput.

Hardware

Hardware selection for the regional and national machines was based on numerous criteria. The basic goals, however, were cost effectiveness, system compatibility, sufficient power for the tasks at hand, and a ready upgrade path. Numerous systems and software packages were examined using these and other criteria before a final selection was made.

It was decided early in the evaluation period that the national and regional systems did not require compatible hardware architectures, because their purposes would differ. Instead, the design philosophy was to use software and media compatibility to link the two systems.

Regional IMS

The regional IMS machines are Compaq personal computers with the following specifications:

1. 25-mHz 80386 microprocessor;
2. 5 megabytes (MB) of random access memory;
3. 300 MB of fixed disk storage;
4. 3½-in. 1.44-MB microfloppy drive;
5. 5¼-in. 1.2-MB floppy drive;
6. High-speed dot matrix printer;
7. 2,400-baud telephone modem;
8. 120-MB streaming tape drive; and
9. Enhanced graphics display adapter and color display.

These machines were chosen after a detailed evaluation of regional requirements revealed that a single user system would be adequate. The SHRP regional centers will only be in place for 5 years, so the long-term upgrade path is not as important for these systems. The 80386 machines are currently the state of the art in personal computing.

The regional machines run version 3.31 of the MS-DOS operating system. The system users liked DOS for two reasons: (a) it is compatible with existing office equipment and software, and (b) they felt most familiar with it. The version has been modified by the vendor to handle files and devices in excess of the normal 32-MB DOS limit. The planned operating system upgrade path is to OS/2 and UNIX should capacity demands require multiprocessing or multiuser operation. The machine was sized for four users in a UNIX configuration.

The regional machines have expansion slots allowing for the addition of additional peripheral device controllers, network adapters, or communications ports should the need be identified.

National IMS

The national machine is a Digital Equipment Corporation MicroVAX 3900 minicomputer. This machine has the following specifications:

1. CMOS implementation of VAX processor architecture,
2. 32-MB random access memory,
3. Hardware floating point processor,
4. Ethernet adapter,
5. 622-MB fixed disk storage,
6. 1600/6250-bpi ½-in. magnetic tape drive,
7. 296-MB cartridge tape drive,
8. Terminal server,
9. 2,400-baud telephone modem,
10. High-speed line printer, and
11. 4-gigabyte program address space using virtual memory.

SHRP required that the national machine support a multiuser, multiprocessing operation, with the capacity for 10 simultaneous timesharing users. The VAX machine was selected because it met these performance criteria and had an excellent upgrade path. The VAX series is common in research settings, and a wide variety of software is available. The IMS VAX will run under the VAX/VMS operating system.

SHRP also decided to purchase an extra regional machine for the national center. The extra computer will be used for regional software development and data exchange between the regions and the national VAX. The VAX and the PC are interconnected using DECnet software and a high-speed Ethernet link.

Support Software

SHRP specified the use of a relational data base management system for the IMS. ORACLE was selected from the group of candidate products after an evaluation that included product capabilities, technical support, vendor stability, hardware support, and market share.

ORACLE uses the industry standard, Structured Query Language (SQL), which offers an extremely powerful command set for data manipulation and data base maintenance. The ORACLE product also includes a host language interface, a form management package, a report writer, and a menu manager. Numerous third-party products are also available for the DBMS.

ORACLE has compatible versions for both hardware platforms chosen for the IMS. This is important because the regional and national systems are integrated using software. Having one software product for both machines simplifies software development and maintenance, ensures data compatibility, and eases training requirements.

Applications developed for the PC are being ported and executed without change on the national minicomputer. Table structures and data are also portable. Some problems with memory management have been observed in the PC software, but a new version of the product promises improvement.

All non-ORACLE applications for the IMS are written in ANSI C programming language. This decision was made to further ensure the portability of the system software. These applications are primarily filters for processing machine-readable data. As of this writing, the number of ORACLE and C language applications may be summarized as follows:

Application	*Number*	*Function*
Forms	160	Data entry/menus
Reports	13	Summarize data
C programs	15	Data transfer/filters
Batch files	20	Software interfaces

IMS DATA STRUCTURE AND COLLECTION

Information to be collected for the LTPP program and included in the IMS may be subdivided into seven basic data types: (a) inventory, (b) maintenance, (c) rehabilitation, (d) traffic, (e) materials testing, (f) environmental aspects, and (g) monitoring. Individual data elements for each data type are defined through a cooperative effort between expert task groups and the LTPP technical assistance contractor. Although these groups have striven for completeness in selecting the data elements for the IMS, financial considerations for data collection have also played a role.

For the most part, the four SHRP regional offices are coordinating the collection of data for the pavement sections. Each of these offices has responsibility for sections in a group of states or provinces. Data providers include SHAs, field sampling and testing contractors, SHRP regional contractor staff, and selected external data systems. The collection cycle for the data types is shown in Figure 1.

DATA TYPE	REPORTING FREQ.	RESPONSIBILITY
HISTORICAL (INV, TRAFFIC, MAINT/REHAB)	ONCE	SHA'S
TRAFFIC	MO./ANNUALLY	SHA'S
MAINT/REHAB	AS THEY OCCUR	SHA'S
MATERIALS TEST.	(NOW; +20 YRS)	CONTRACTORS
MONITORING		CONTRACTORS
FWD	TWICE IN 5 YRS	
PROFILOMETER	ANNUALLY	
DISTRESS	ANNUALLY	
ENVIRONMENTAL	ANNUALLY	NWS

FIGURE 1 IMS data reporting.

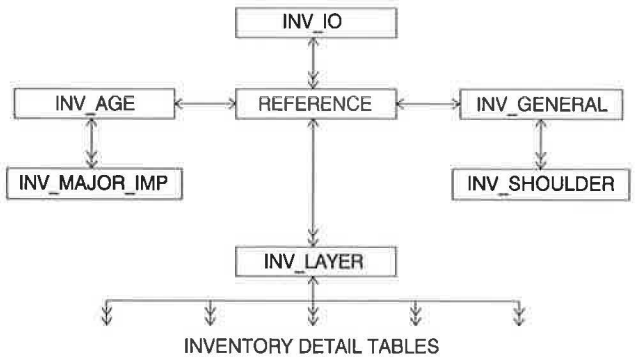

FIGURE 2 IMS relational structure: inventory.

As previously stated, the IMS follows a relational structure. The basic structure of the IMS, using inventory data as an example, is shown in Figure 2. The INV_ID (inventory identification) table contains the information needed to locate the pavement section (e.g., state, route, and geographical coordinates). The reference table is the link with the remaining inventory data tables; this is true for all other data types as well. It contains data on the construction history of the section. Thus, additions are made to the reference table as construction occurred in the past and will occur in the future. To complete the example, INV_GENERAL holds data on the geometric and drainage characteristics. Because two shoulders are normally associated with a roadway section, INV_SHOULDER is linked to INV_GENERAL and has two entries for each entry in INV_SHOULDER; this is the idea behind relational structure. Similar structures used for the remaining data will not be discussed in this paper. (A complete discussion may be found in the IMS technical documentation.)

Inventory

Inventory data consist of information on the history and current status of the pavement section. Included is basic information to identify the section, such as the highway, milepost and station, section type, and responsible agency (Figure 3). Inventory data also describe the geometric details of the section and its materials properties as well as information on the historical costs of construction and maintenance. From a pavement perspective, the most significant data contained in inventory are the layer data (Figure 4). For every pavement layer—from surface to subgrade—detailed data on the original construction are included from SHA records. The data elements vary by the basic type of material from which the layer is constructed.

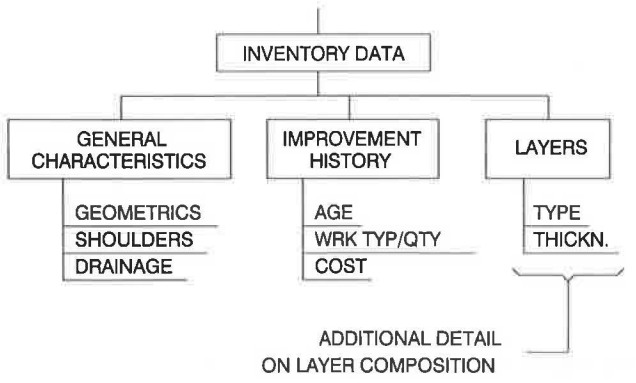

FIGURE 3 IMS inventory data.

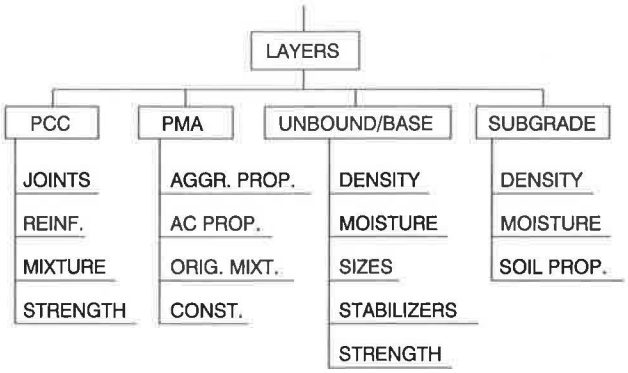

FIGURE 4 IMS layer detail data (part of inventory).

SHAs provide inventory data to the SHRP regional offices. Using their records, the SHAs fill out detailed data collection forms for each of their sections. These forms are submitted to the regional offices, where they are reviewed and entered into the regional IMS. Before delivery of the IMS, arriving inventory data are loaded into an interim data base. After installation of the IMS, the data are transferred from the interim data base to the IMS.

Inventory data collection is still in progress. Experience to date has shown that the quality of inventory data varies widely. Some sections have extensive records, whereas the original construction data for others could not be located by the SHAs. In these cases, the material testing data will help to fill in the void.

Maintenance

Data will be collected for a GPS each time maintenance is performed. These data will consist of detailed information on treatment type and location, application methods, materials properties, and cost (Figure 5). When available, historical maintenance activities for the section will be included. Again, the data vary by the type of material used. The expert task group and the technical assistance contractor are still defining the exact data fields and formats. Because of differences in the practices used by the states, the IMS must be able to accommodate a wide variety of maintenance data.

To help ensure that all maintenance actions are recorded, the states have agreed to control maintenance on the SHRP sections. When maintenance is to be performed, SHRP will be contacted. The regional staff will then coordinate with the state to collect the required data. Current plans are for the maintenance data to be submitted to the regions using data forms.

The maintenance cost effectiveness (MCE) study of the Highway Operations Technical Research Areas is applying specific treatments to SPS sections. This project's objective is to compare the effectiveness and performance of these treatments. MCE will collect extremely detailed information

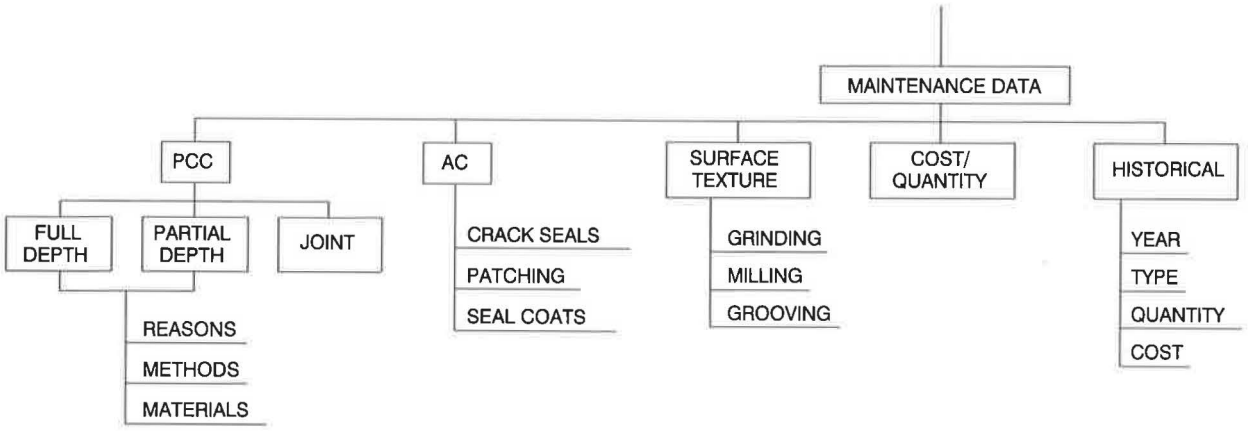

FIGURE 5 IMS maintenance data.

on its test sections. Unlike LTPP, MCE will have a controlled set of maintenance actions, so data formats will be highly standardized. These data will be stored in the IMS.

Rehabilitation

The LTPP will record data on rehabilitation activities that occur after section monitoring begins. Rehabilitation activities are considered to revise the layer structure of the section. The collected data will describe the time and type of rehabilitation, changes to the existing section layer structure, reconstruction methods, material and layer properties, and costs. SHRP is still developing data collection specifications for rehabilitation. Current plans are for the SHAs to record data during rehabilitation activities and to forward these data to the SHRP on collection forms.

Traffic

The LTPP plans to obtain traffic data for all sections (Figure 6). These traffic data will include both the historic activity before section monitoring and the actual traffic during monitoring.

Historical traffic data will be collected from SHA records. Where data are missing, backcasting and other estimation techniques will be used to generate values. The SHAs will provide the data both on paper forms and computer files.

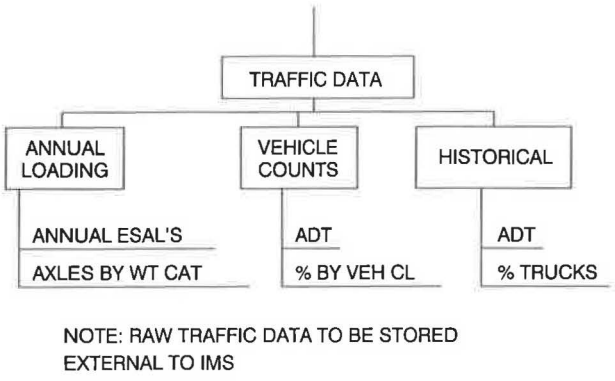

FIGURE 6 IMS traffic data.

The plan for collecting data during the monitoring phase is still being finalized. However, SHRP's goal is to have automated continuous vehicle classification and weigh-in-motion systems at or near each GPS section. The SHAs will collect this information and forward it to SHRP as required for the duration of the LTPP program; the traffic data will thus be used by the SHAs for their own purposes as well as by the LTPP program. Should funding limitations preclude the installation of these devices, regional staff will conduct periodic counts using portable equipment. The sampling plan for these counts will be developed to account for daily and seasonal variations in traffic.

SHRP plans a five-tiered approach to traffic data collection and storage. The top tier consists of the annualized equivalent single-axle loading (ESAL) experienced by the section during the study. The second tier consists of data such as the annual average daily traffic (AADT), truck percentage, and vehicle classifications for each year of the study. The third level is composed of daily records for traffic counts, vehicle classifications, and truck weights. The fourth level of traffic data consists of individual truck weight records and hourly vehicle classifications. All other traffic data—such as the historical data sheets and supporting data supplied by the States—is stored in the fifth level.

All of the traffic data collected will not be stored in the IMS. Current plans call for only the first and third levels to be included in the IMS, providing users with summarized annual loadings as well as daily records to make independent estimates. The remaining tiers of data are voluminous and will be stored externally to the IMS to allow manipulation of the data before the select (first and third levels) data are sent to the IMS.

Materials Testing

LTPP is conducting a field sampling and materials testing campaign that will cover all GPS sections. Figure 7 shows the basic materials testing data to be collected. The purpose of this campaign is to examine the layer structure of the sections and to verify the material properties of the layers. These

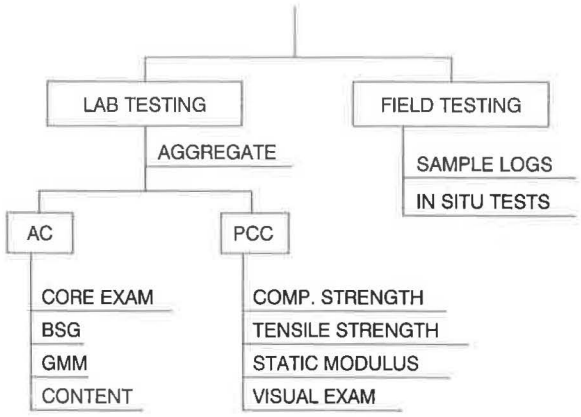

FIGURE 7 IMS materials testing data.

results should provide insight into the performance of the materials since construction.

During the field operation, crews will take various types of samples from the pavement layers immediately before and after the test section. The location, type, and condition of these samples will be recorded in the IMS. The crews will also probe for rock and perform certain in situ tests.

At the laboratory, the samples will be subjected to a variety of tests. Tests are assigned to the extracted samples according to the material (AC or PCC), the layer, the location of sample origin, and other conditions. The layer structure of the pavement section must be agreed on and approved by the laboratory and the regional centers before actual testing begins.

The IMS will store the raw test data and aggregated values for the specific layers. At present, the field sampling and materials test data will be sent to SHRP on paper forms. Once entered into the IMS, summary reports can be used to view the data in a variety of formats.

Environmental Data

Environmental data for sections will include rainfall, temperature, solar radiation, and freeze-thaw characteristics. The data will be summarized on a monthly and an annual basis (Figure 8). Specifics of the environmental data collection program are still being worked out. Various sources specializing in climate information, such as the National Climatic Data Center or the State Climatologist, will most likely provide the data in machine-readable format.

The IMS may be required to calculate a representative value from several weather stations near a section. In this case, it will store both the raw station data and the derived values for the section.

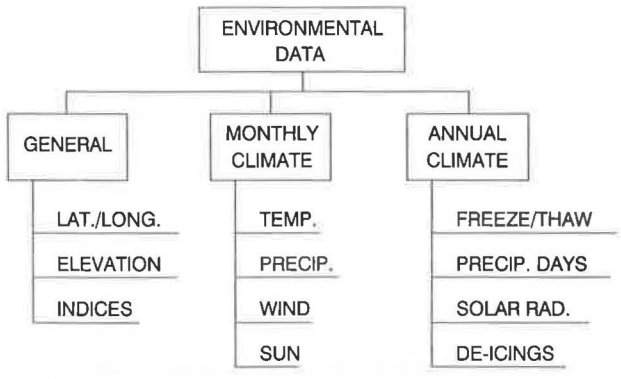

FIGURE 8 IMS environmental data.

Monitoring

The monitoring category is an extensive portion of the LTPP data collection and represents the most important dependent variables for pavement performance research (Figure 9). Detail on the categories follows.

Surface Distress and Transverse Profile

LTPP will use high-speed 35-mm photography to record images of the pavement surface. The equipment, produced by PASCO, USA, also provides transverse profile information. It is also possible in some cases that distress surveys will be conducted manually in the field, specially before maintenance activities. The MCE study is expected to use this procedure exclusively. The PASCO photographs will be reduced using a computerized system. The data reduction specifications call for the user to be able to record distress types and severities for 1-ft-square increments of the test section. The reduced data will be in machine-readable form (Figure 10). The IMS will record all of the localized distress information and will have an aggregate summary for the section. The PASCO equipment also provides transverse profile data in machine-readable format.

Deflection

Deflection data will be obtained using falling weight deflectometers (FWD). SHRP has purchased a fleet of four FWDs from Dynatest Consulting, Inc. Current plans are for FWD equipment to be operated over each GPS section twice during the first 5-year period. State-owned FWDs may be used to provide supplementary information. Deflection measurements will be made at numerous points within a section. At each test location, a number of drops will be conducted using various loading conditions. The exact number of total drops within a section varies according to the pavement type. The

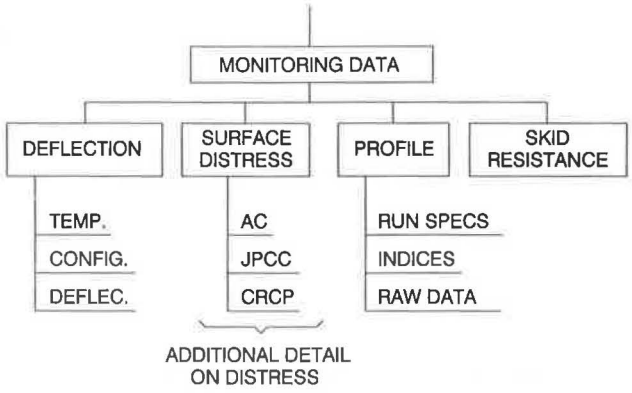

FIGURE 9 IMS monitoring data.

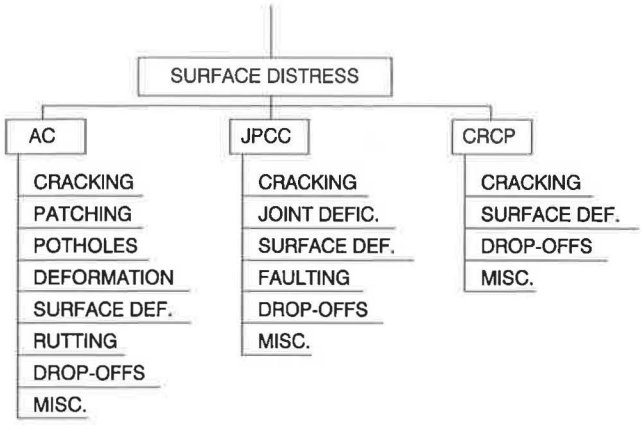

FIGURE 10 IMS surface distress detail data (part of monitoring).

positioning of the deflection sensors may also vary. For each drop site, the FWD will produce data sets containing test parameters, peak response values, and load-deflection time history information. The total amount of raw data for a test section ranges as high as 4.9 million characters. The Dynatest FWD places test data on IBM PC format data diskettes. During the deflection tests, a technician will record pavement layer temperatures at two locations within the section. Temperature sensors will be installed in the pavement for this purpose.

The IMS must take the FWD data files, filter them to extract necessary data, and load these data into tables. Raw time history data will be stored offline. The test parameters, peak data, temperatures, and machine configuration are retained online. Summary data for the deflection tests may also be developed.

Longitudinal Profile

SHRP will record the longitudinal profile of the pavement sections annually for the first 5 years. The main instrument to be used for this is the K. J. Law Profilometer. SHRP has purchased three of these devices. Use of the Face DIPstick is also being considered because of its flexibility.

The current profiling plan is to obtain measurements (elevation versus longitudinal coordinate) at 15.24-cm (6-in.) intervals in both wheel paths. These data would be maintained in the IMS in raw form. Summary statistics such as the International Roughness Index (IRI) would also be maintained for each test.

The K. J. Law profilometers use DEC PDP–11 minicomputers for data collection and reduction. These data can be transferred to the IMS on magnetic tape. The DIPstick stores data internally, but can download it through a serial port to the IMS.

Data Base Table Structure

In DBMSs, tables are groups of related fields. The IMS contains over a hundred data base tables. These consist of several types: administrative, lookup, data, and utility. Administrative tables are the highest level in the IMS data structure. They contain such information as experiment definitions, user access privileges, and valid section identifications. The IMS code uses these tables to direct many of its low level activities. Write access to these tables is only possible at the national center and is strictly controlled.

Lookup tables are lists used to validate data or to translate values. Their contents, too, are controlled by the national center.

Data tables contain the information collected by the study. (Figure 2 shows an example of how tables are defined in the IMS.) These tables are logically related through various key structures. The highest level key in the IMS is the section key, which uniquely identifies an LTPP section. Other keys are added to uniquely identify table records as necessary. Almost all contents of the data tables originate at the regional centers. As of this writing, 2,700 fields have been defined. By the time the IMS is fully specified, a total of nearly 4,000 are expected.

Utility tables are used in various processing steps. Certain reports use utility tables, for example, to store intermediate results. These tables are also used to pass results between applications.

Because much of the data collection plan is incomplete, table specifications are still being developed for the IMS. Even after completion of the plan, many changes will be identified during the course of the program. One of the benefits of the relational data model is the ease with which the data tables can be altered.

IMS OPERATION

Operation of the IMS began in mid-1989. This section discusses some of the major IMS operational activities.

Data Processing and Validation

With the exception of environmental data, all information for the IMS flows into the regional nodes (Figure 11). Before attempting to enter data, the regional center staff conducts numerous checks and attempts to correct obvious errors (Figure 12). The data will then be entered, depending on its type,

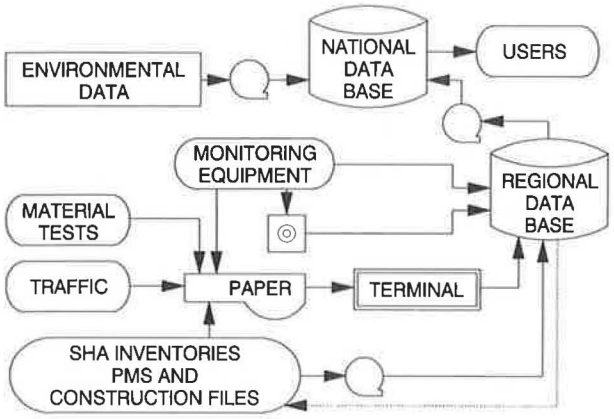

FIGURE 11 IMS overview.

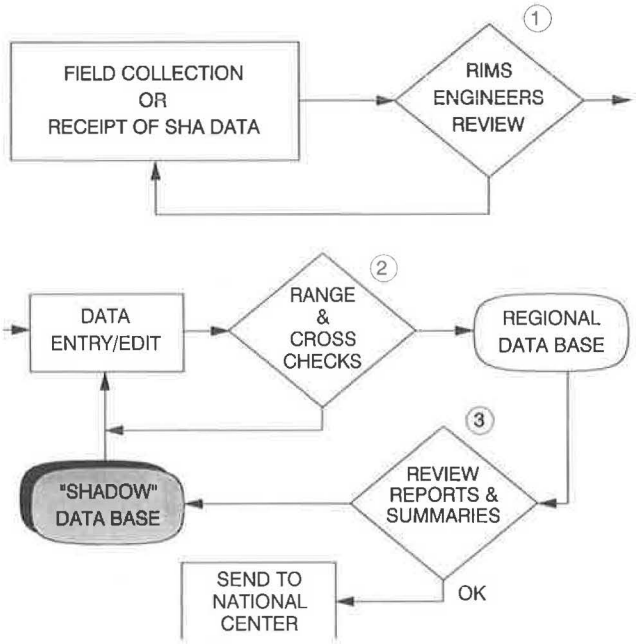

FIGURE 12 IMS data validation: regional level.

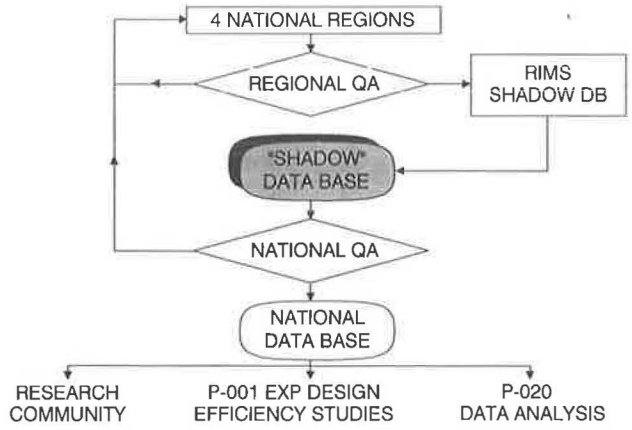

FIGURE 13 IMS data validation: national level.

by means of a form application or a special utility program. These applications perform an extensive number of range and logic checks. Depending on the severity of errors, incoming records may be rejected. The regional center staff reviews these and makes the needed corrections.

After loading batches of data, the regional staff may run various reports to evaluate data trends and perform interrecord consistency checks. The staff again takes action to remedy problems found during these analyses. If certain fields or records are found to be in error, the regional staff will set a flag on these so they are not transmitted to the national center and can be revised; this concept is shown as the shadow data base in Figure 12 and is a mechanism for distinguishing approved and nonapproved data.

At selected intervals, the regional centers transmit their validated data to the national center. Records are selected for transmission via the journaling facility. All transactions since the last data transmission are selected. The data, along with the journal file, are written to cartridge tape and sent to the national center. The regional journal is then reinitialized.

Upon receipt of data from a region, the national center operator uses the journal file to update the national data base. The data are read using the 386 platform and transmitted by means of the communications data link to the VAX. New blocks of data are moved into another shadow data base at the national center, where the LTPP Technical Assistance Contractor will perform interregional quality checks (Figure 13). Any data found to have problems are referred back to the regions for correction. Only after the data pass these tests are they moved into the actual national data base and made available to the research community.

System Updates

The general philosophy behind IMS updates is to keep tight control at the national center. This is necessary to prevent unauthorized changes from rendering data inconsistent or software incompatible.

System table updates are performed under the control of the national system operator. All changes to administrative and lookup tables are made on the national machine. Copies of the tables are then transmitted to the regions. Regional systems lack the utility applications for administrative table maintenance.

Software development and testing will also take place at the national center. Updates will be transmitted to the regions as necessary. The regions do not have the staff necessary for these activities; their primary responsibility is to handle the experiment. SHRP will, however, ensure that the national center operator is an information systems engineer trained in the use of the IMS hardware and software.

Disseminating Data

Requests for data will be served by the national center. The regions may provide selected data to their states as a courtesy, but the research community will only receive cleansed data from the national data base.

The mechanism for initiating requests has not yet been fully developed. It is expected, however, that researchers will contact SHRP or TRB to request information. The request will be turned over to the national center operator, who will select the necessary records and output them in the specified format. SHRP does not envision that requesters of the data will have direct access to the data base. It is possible that users may be allowed dial-in access to the national machine to make requests or download selected data.

The IMS can provide data on ½-in., nine-track magnetic tape and various IBM PC floppy disk formats. The national machine can write 1600/6250-bpi IBM standard label or nonlabeled tapes in ASCII or EBCDIC. The national center uses the captive PC to create floppy disks. Future distribution of data on other media will be considered if demand warrants.

CONCLUSIONS

This paper has presented an overview of the development and structure of the LTPP IMS so that potential researchers will

be aware of the nature of this valuable pavement data resource. Highly detailed specifications on the data base will be available in the technical documentation when it is finalized.

A great deal of planning and investment have gone into the LTPP IMS. SHRP places a high emphasis on the development of the system. They have selected advanced hardware and software and integrated them into a system designed to function for the duration of a long project. It is too early to make any claims about the performance of the system or about the data collected because much of the IMS development lies ahead. Still, it is unlikely that pavement researchers will have cause to complain about their ability to obtain LTPP data. Further, sufficient data quality assurance procedures have been built into the system to ensure usable and accurate data.

ACKNOWLEDGMENT

The project described in this paper was sponsored by the Strategic Highway Research Program of the National Research Council under a nonexclusive license of the National Academy of Sciences, AASHTO, its member states, and FHWA. The authors also gratefully acknowledge the guidance of Chuck Niessner of FHWA and Heikki Jämsä of SHRP on this project.

REFERENCE

1. Coe-Truman Technologies, Inc. *Long-Term Pavement Performance Information Management System—Final Report.* FHWA, U.S. Department of Transportation, 1987.

Publication of this paper sponsored by Committee on Pavement Monitoring, Evaluation, and Data Storage.

Variables Affecting the Testing of Pavements by the Surface Waves Method

DENNIS R. HILTUNEN AND RICHARD D. WOODS

The spectral analysis of surface waves (SASW) method is a nondestructive testing procedure under development for determining the elastic modulus profile of pavement systems in situ. The ultimate objective for practical use of the SASW method is the design of a totally automated, movable test rig for investigating pavement systems. An important step toward this objective would be the development of a multiple-transducer testing procedure in which the source-to-near-receiver distance S and source type are significant variables. Tests conducted on two asphaltic concrete pavements to study the effects of these variables determined that the ratio of S to receiver spacing X should be ≤ 2. In addition, dispersion data were independent of S when wavelengths longer than $2X$ were eliminated from the data. The effect of source type on the ranges of useful frequencies for a given value of X was significant. In general, both the lower and upper cutoff frequencies decreased as the weight of the source increased. The dispersion curves generated with the data were compared with optimum ones using a constant source type. Although no single source type consistently yielded an optimum dispersion curve, combining the data from a 4-oz ball peen hammer and an 8-lb sledge hammer yielded an optimum dispersion curve over all wavelengths.

In pavement engineering, in situ values of elastic moduli are important parameters in the determination of overlay thicknesses and allowable loads for existing pavement structures and for assessment of other rehabilitation needs. Elastic moduli for pavement systems are typically determined in situ by deflection-based measuring devices such as the falling weight deflectometer (FWD). Modulus values are determined from the deflection measurements through use of multilayer elastic analysis. Deflection techniques, however, have well-known limitations. First, the backcalculation of moduli from deflection measurements for pavements with thin surface layers is nearly impossible because of the insensitivity of the deflection basin to the stiffness of the thin surface layer (*1,2*). Second, the deflection procedures must assume values for the thicknesses of the pavement layers or determine the values from cores (*1,3*). Third, the deflection procedures are only capable of determining an average modulus to represent each pavement layer, when in fact the modulus usually varies throughout the layer (*4*). Fourth, the deflection procedures use a static model of the pavement system to backcalculate the moduli, despite the dynamic nature of the test itself (*5–9*). It is seen, therefore, that an improved nondestructive method of determining in situ stiffness profiles of pavement systems is needed.

D. R. Hiltunen, Department of Civil Engineering, Pennsylvania State University, University Park, Pa. 16802. R. D. Woods, Department of Civil Engineering, University of Michigan, Ann Arbor, Mich. 48109.

A new method for measuring in situ elastic modulus profiles, the spectral analysis of surface waves (SASW), has been under continuous development since 1980. The SASW method is based on the generation and detection of Rayleigh waves from the surface of the pavement system. Although the main disadvantage of SASW is that the testing and data reduction are slow, it is felt that with continued research and development the testing and data reduction time can be substantially reduced. Previous work conducted at the University of Michigan to further the development of the SASW method has also been reported (*10*).

THE SASW METHOD

The SASW method is a testing procedure for determining elastic modulus profiles of pavement systems in situ. The test is performed on the pavement surface. Measurements are made at strain levels below 0.001 percent, where elastic properties of pavement materials are considered independent of strain amplitude. The key elements in SASW testing are the generation and measurement of Rayleigh waves.

Several publications (*10–18*) in recent years have described the SASW method in detail. A schematic of the experimental arrangement for SASW tests is shown in Figure 1. Current practice calls for locating two vertical receivers on the pavement surface a known distance apart. Then a transient wave containing a large range of frequencies is generated in the pavement by means of a hammer. The surface waves are detected by the receivers and recorded using a Fourier spectrum analyzer. The analyzer is used to transform the waveforms from the time domain to the frequency domain and then to perform spectral analyses on them. The spectral analysis functions of interest here are the phase information of the cross power spectrum and the coherence function. Knowing the distance and the relative phase shift between the receivers for each frequency, the phase velocity and wavelength associated with that frequency are calculated. The final step is application of an inversion process that constructs the elastic modulus profile from the phase velocity versus wavelength (dispersion curve) information.

The principal advantage of using the SASW method for pavement evaluation is its capabilities for determining

- The elastic modulus of thin pavement surface layers (*15,19*);
- The thicknesses of pavement layers (*13,15,17–19*);
- The variation of elastic modulus within a given pavement layer, i.e., values of the modulus gradient (*13,15–16*); and
- The elastic moduli of the pavement system in the presence of bedrock close to the surface (*15*).

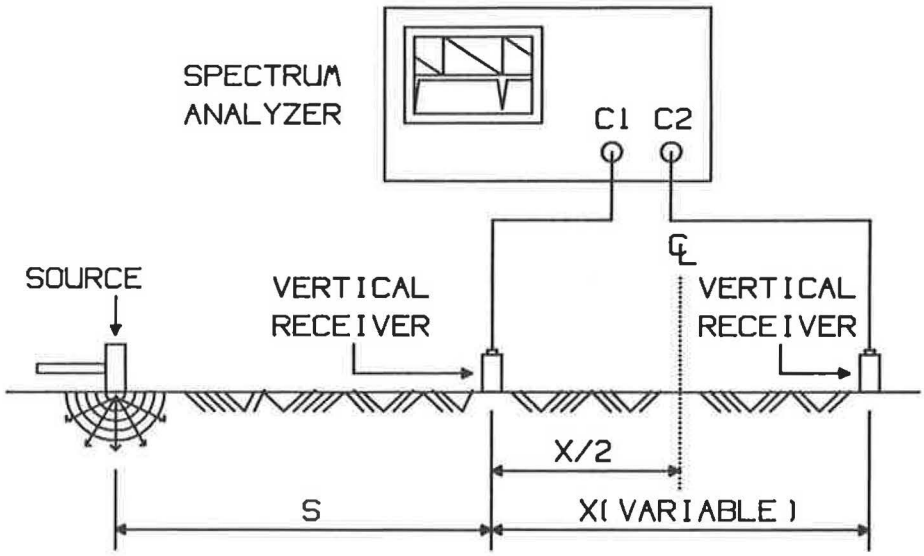

FIGURE 1 Schematic of experimental arrangement for SASW tests [after Nazarian (*12*)].

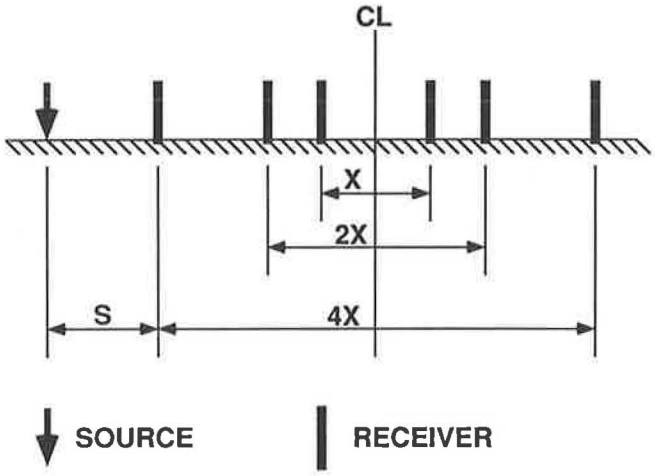

FIGURE 2 Multiple transducer configuration using six transducers and CRMP geometry.

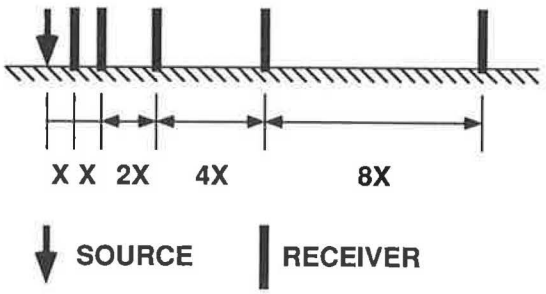

FIGURE 3 Multiple transducer configuration using five transducers and CS geometry.

These capabilities would provide a useful supplement to the deflection-based procedures, specially for cases in which the deflection procedures suffer from the limitations detailed earlier.

The ultimate objective for the SASW method is a totally automated, self-contained, movable test rig for investigating pavement systems. An important step toward this objective is the development of a multiple-transducer testing procedure in which all the data for a given site can be obtained with the least number of source excitations on the test surface as possible. Currently, the SASW method is conducted using only two transducers, primarily because a two-channel spectrum analyzer is a convenient means of collecting and observing the data in the field. This means of data collection requires a good deal of time, because several different receiver spacings are usually required to fully investigate a site. The extension of this procedure to more than two transducers, i.e., to a multiple-transducer testing procedure, thus seems appropriate.

Hiltunen and Woods (*20*) suggested two possible multiple-transducer arrays, one on the basis of the common receivers' midpoint (CRMP) geometry (Figure 2), and the other on the common source (CS) geometry (Figure 3). They further suggested that to implement a multiple-transducer array, the following characteristics of the two-transducer array relative to receiver separation X and source-receiver distance S must be determined:

- The source-receiver scaling geometry most appropriate for testing pavements (by varying X while keeping $S = X$ and varying the position of the receivers' midpoint relative to the source); and
- The best source location (by varying S, while keeping X constant).

Furthermore, the most appropriate source type should be determined.

Hiltunen and Woods (*20*) have presented results from tests conducted at an asphaltic concrete pavement site that suggest that SASW measurements are independent of source-receiver scaling geometry. In the present work, tests were conducted to investigate the effects of S and source type on the measurements. Results from the entire test program are summarized

and a multiple-transducer configuration for pavement testing is suggested.

PREVIOUS RESEARCH

Source-to-Near-Receiver Distance (S)

Nazarian (*12*) has discussed the factors that limit the range of possible values of S. The source should be far enough away from the near receiver that a significant amount of the body wave energy dies out before arriving at the near receiver. However, if the source is too far away from the receivers, the Rayleigh wave energy associated with the frequencies of interest may not be sufficient for detection by the receivers, and background noise may dominate the record.

On the basis of experimental studies, Heisey et al. (*11*) have suggested that $S = X$ is adequate, provided that wavelengths $< 0.5X$ or $> 3X$ are eliminated from the data.

However, theoretical studies conducted by Sanchez-Salinero et al. (*21*) have indicated criteria that are drastically different from the experimental results of Heisey et al. (*11*). For CRMP geometry with $S = X$, and assuming plane Rayleigh waves [as the inversion program INVERT (*12*) does], they suggest that the field data be filtered for wavelengths $> 0.5X$.

The disparity between experimental and theoretical results is evident in this discussion. More important, however, it is evident that little work has been done to systematically study the effects of S by changing its value over a range. Yet, the results of such a study would be vital to the development of a multiple-transducer array using a fixed source location. Therefore, tests were conducted to examine this question.

Source Type

Nearly all previous work on the SASW method has somehow addressed the issue of source selection, particularly sources for impact testing. It has been clearly demonstrated that the choice of source depends on the frequency range of interest. Small, lightweight sources produce high frequencies necessary for sampling shallow depths, while larger, heavier sources produce low frequencies for sampling greater depths. The intent here was not to reaffirm these findings. Rather, the questions that arise when confronted with implementing a multiple-transducer array is how many sources are required and of what size.

Past work has shown that when conducting SASW tests using two receivers it is often necessary to use a different source for each receiver spacing. However, this process often results in overlap in the dispersion curve data for different receiver spacings. This overlap provides some insurance that the data obtained are reliable, but it may be possible to adequately sample a site with fewer sources if some of the overlap in data for different receiver spacings is redundant. Thus, two series of tests were conducted to determine the minimum number of sources necessary for adequately defining the dispersion curve for a site. The sources under investigation were all of the impact type and conclusions obtained were valid for this type of excitation.

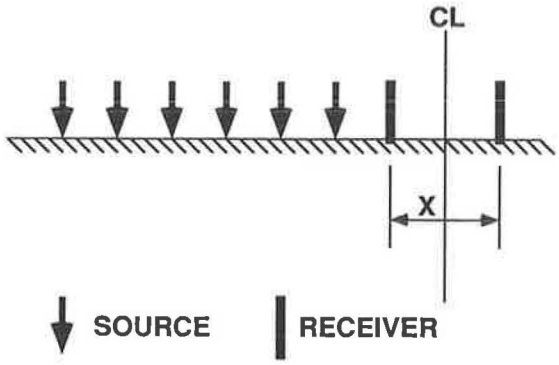

FIGURE 4 Schematic of two-transducer tests using CRMP geometry and various source-to-near-receiver distances.

DISCUSSION OF TESTS

Sites and Geometries Selected

The tests to study the effects of S and source type were conducted at two asphaltic concrete pavement sites. The first series of tests was conducted at the G. G. Brown parking lot site on the University of Michigan campus in August 1986. The second series of tests was conducted at the SEMTA parking lot site in Livonia, Michigan, in June 1987.

A schematic of the two-transducer tests conducted to examine the effects of S is shown in Figure 4. The transducer placement followed the CRMP geometry in that each transducer pair was placed symmetrically about the same imaginary centerline. Transducer spacings of 0.5, 1, 2, 4, and 8 ft were examined. The range of source locations used at each receiver spacing X limited values of the ratio S/X to the range 0.5 to 3. The intent was to determine the optimum value for S/X and to provide guidance in developing the geometry for a multiple-transducer array.

The effects of source type were studied both at the G. G. Brown and SEMTA parking lot sites. During the CS geometry tests at the SEMTA parking lot site (*20*), data were collected using five source types at each receiver spacing. The sources ranged in weight from 4 oz (a ball peen hammer) to 8 lb (a sledge hammer). The effects of source and receiver geometry have been studied by Hiltunen and Woods (*20*) using the optimum source (see Table 1) for each receiver spacing; data for other sources are examined herein. Table 1 presents such data obtained from the tests at the SEMTA parking lot site.

Useful Frequency Ranges

Tables 2–4 present useful frequency ranges from cross power spectrum and coherence function data as functions of S and source type. The cross power spectrum and coherence function data collected in the field have also been used to determine Rayleigh wave dispersion curves (*10,12*). Part of this process requires determining frequency ranges in which useful data exist. Because S and source type affect the ranges of useful frequencies, they ultimately determine how well the dispersion curves are defined. For a given test setup, as more frequencies are eliminated because of poor phase or poor coherence, the less well defined the dispersion curves become.

TABLE 1 TEST PARAMETERS FOR SEMTA PARKING LOT SITE

Receiver Spacing (ft)	Receiver Type	Frequency Span (Hz)	Source Type[a]
0.5	Accel.	10000	4 oz[b]
0.5	Accel.	10000	8 oz
0.5	Accel.	10000	16 oz
0.5	Accel.	10000	40 oz
0.5	Accel.	10000	128 oz
1	Accel.	6250	4 oz[b]
1	Accel.	6250	8 oz
1	Accel.	6250	16 oz
1	Accel.	6250	40 oz
1	Accel.	6250	128 oz
2	Velocity	1000	4 oz
2	Velocity	1000	8 oz
2	Velocity	1000	16 oz[b]
2	Velocity	1000	40 oz
2	Velocity	1000	128 oz
4	Velocity	800	4 oz
4	Velocity	800	8 oz
4	Velocity	800	16 oz
4	Velocity	800	40 oz[b]
4	Velocity	800	128 oz
8	Velocity	250	4 oz
8	Velocity	250	8 oz
8	Velocity	250	16 oz
8	Velocity	250	40 oz
8	Velocity	250	128 oz[b]

[a] Refers to the weight or size rating of hand-held hammer used as impact source.

[b] "Optimum" source for given receiver spacing.

TABLE 2 USEFUL FREQUENCY RANGES FOR 0.5-ft RECEIVER SPACING X AS A FUNCTION OF SOURCE-TO-NEAR-RECEIVER DISTANCE S AT SEMTA PARKING LOT SITE

Source-to-Near-Receiver Distance (S) (ft)	S/X	Lower Cutoff Frequency (Hz)	Upper Cutoff Frequency (Hz)
0.25	0.5	112	5800
0.50	1.0	125	5875
0.75	1.5	887	5900
1.00	2.0	1000	5950
1.25	2.5	1000	5000
1.50	3.0	1050	4100

TABLE 3 USEFUL FREQUENCY RANGES FOR 0.5-ft RECEIVER SPACING X AS A FUNCTION OF SOURCE-TO-NEAR-RECEIVER DISTANCE S AT G. G. BROWN PARKING LOT SITE

Source-to-Near-Receiver Distance (S) (ft)	S/X	Lower Cutoff Frequency (Hz)	Upper Cutoff Frequency (Hz)
0.25	0.5	100	8900
0.50	1.0	125	9250
0.75	1.5	100	8125
1.00	2.0	100	6650
1.50	3.0	125	2800

Tables 2–4 of the useful frequency ranges determined from each cross power spectrum and coherence function pair were developed as a representative example because of the large amount of data collected. The minimum- and maximum-frequency cutoffs for each pair were determined as functions of S and source type. The effects of S and source type were significant.

Source-to-Near-Receiver Distance

Ranges of useful frequencies as functions of S for the 0.5-ft receiver spacing at the SEMTA parking lot site are presented in Table 2; similar data for the G. G. Brown parking lot site are presented in Table 3. Results for the remaining receiver spacings have been provided by Hiltunen (*10*).

The upper cutoff frequency decreases significantly for $S/X > 2$. This decrease in the upper cutoff frequency is specially important for the testing of pavements because high frequencies are required to define the dispersion curve of the shallow portions of the pavement system. Inadequate definition of the high-frequency portion of the dispersion curve would result in an inaccurate modulus profile for all layers in the system. Thus, S/X should be ≤ 2 for SASW testing of pavements. The complete sets of data from both test sites strongly support this conclusion (*10*).

TABLE 4 USEFUL FREQUENCY RANGES FOR 0.5-ft RECEIVER SPACING X AS A FUNCTION OF SOURCE TYPE AT SEMTA PARKING LOT SITE

Source Type	Lower Cutoff Frequency (Hz)	Upper Cutoff Frequency (Hz)
4 oz	100	6375
8 oz	100	6012
16 oz	87	5950
40 oz	75	5300
128 oz	62	5250

Source Type

The ranges of useful frequencies as a function of source type for the 0.5-ft receiver spacing at the SEMTA parking lot site are shown in Table 4. The results for the remaining receiver spacings and for the G. G. Brown parking lot site have been provided by Hiltunen (*10*).

The weight of the source had a dramatic influence on the dispersion curves obtained. In general, both the upper and lower cutoff frequencies decreased as the weight of the source increased. The complete sets of data (*10*) from both test sites strongly support these observations.

Magnitude of the Cross Power Spectrum

The magnitude of the cross power spectrum is defined to be the product of the magnitudes of the two signals. As a measure of the mutual power between two sources, it is thus useful for isolating signals that are common to both. For SASW testing, the cross power spectrum establishes the energy distribution as a function of frequency common to both signals. When the energy is high compared to the background noise, good coherence and thus good data are expected. Conversely, when the energy is low compared with background noise, poor coherence and thus bad data are expected. The magnitude of the cross power spectrum is thus useful for explaining the effects of S and source type on the dispersion curves.

Source-to-Near-Receiver Distance (S)

Examples of magnitudes of the cross power spectra as a function of S for the 0.5-ft receiver spacing at the SEMTA parking lot site are shown in Figures 5 and 6. [Additional plots for the SEMTA and G. G. Brown parking lot sites have been provided by Hiltunen (*10*).] Each plot contains the spectra for S/X = 0.5, 1.0, 1.5, 2.0, 2.5, and 3.0, for the given receiver

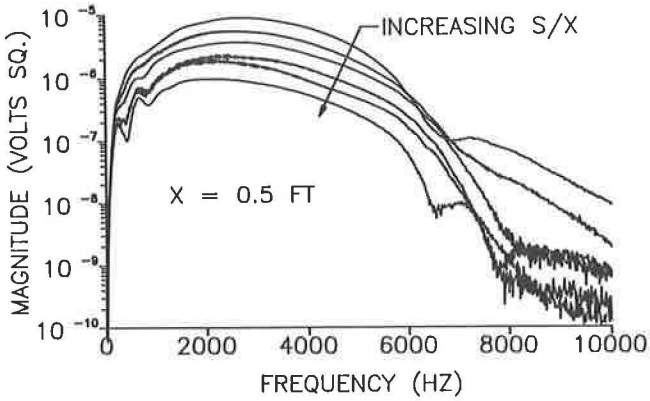

FIGURE 5 Magnitude (absolute) of cross power spectrum as a function of source-to-near-receiver distance S for X = 0.5 ft at SEMTA parking lot site.

spacing. The spectra on each plot are difficult to separate, but it is not necessary that they be individually distinguished. The trend is more important. Therefore, each spectrum is presented in two formats. First (Figure 5), the actual or absolute magnitudes are shown as recorded in the field. The second plot (Figure 6) shows relative magnitudes, defined as the absolute magnitude divided by the peak magnitude for each spectrum. The plot of absolute magnitudes indicates how the actual energy levels change with S for the given value of X. The plot of relative magnitudes indicates how the shape of the energy distribution over frequency varies with S for the given value of X.

The absolute magnitude of the cross power spectrum decreases with increasing S/X, partially because of geometric damping of the signals. This fact alone does not account for the decrease in upper cutoff frequency as S/X increases. For a perfectly elastic system, the shape of the cross power spectrum should be independent of S, because the only damping present in the system is geometric, and therefore does not

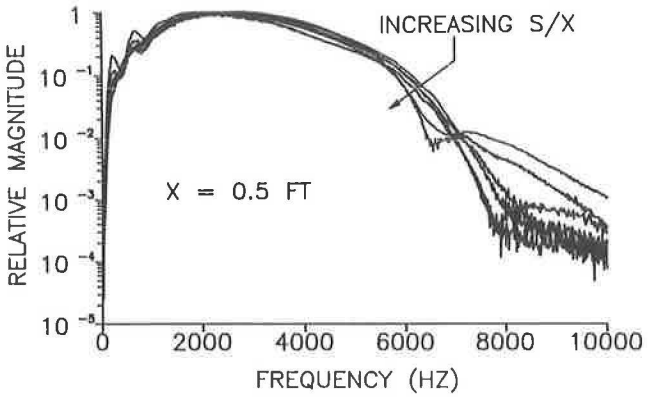

FIGURE 6 Magnitude (relative) of cross power spectrum as a function of source-to-near-receiver distance S for X = 0.5 ft at SEMTA parking lot site.

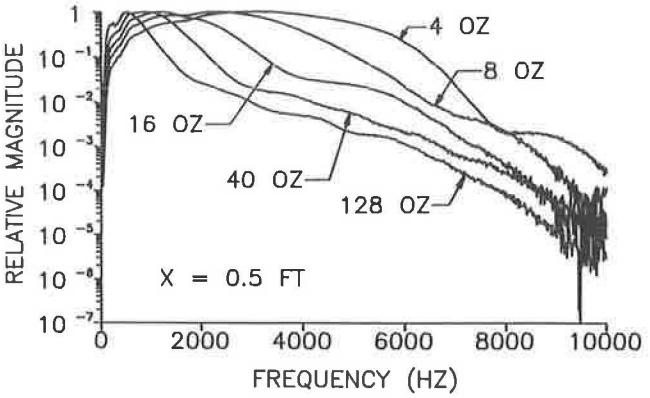

FIGURE 8 Magnitude (relative) of cross power spectrum as a function of source type for X = 0.5 ft at SEMTA parking lot site.

depend on the frequency of the waveform. However, in a real system, e.g., pavement, material damping of the waveform will occur as well. Material damping is frequency dependent. Higher frequency waves attenuate more than lower frequency waves over the same propagation distances in the same pavement because they undergo more cycles of motion. The plots, e.g., in Figure 6, of relative magnitude of the cross power spectrum show this point quite clearly. For the given receiver spacing, the spectra as a function of S/X do not coincide as they would if the system under test was perfectly elastic. In addition, the magnitudes of the high-frequency components dramatically decrease and the upper cutoff frequencies also decrease as S/X increases because of the material damping. For $S/X > 2$, the high-frequency components of the waveforms attenuate excessively and become buried in background noise. Poor phase data and poor coherence data result. [The complete data set (*10*) strongly supports these observations.]

Source Type

Examples of the magnitudes of the cross power spectra as functions of source type for the 0.5-ft receiver spacing at the SEMTA parking lot site are shown in Figures 7 and 8. Each plot contains the spectra for each source type studied at the given receiver spacing. Further, each spectrum is presented in absolute and relative formats. [Again, additional spectra for the SEMTA and G. G. Brown parking lot sites have been provided by Hiltunen (*10*).]

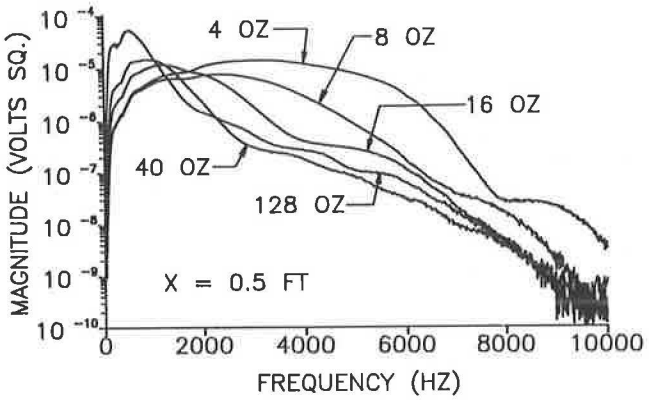

FIGURE 7 Magnitude (absolute) of cross power spectrum as a function of source type for X = 0.5 ft at SEMTA parking lot site.

The effect of source type on the magnitude of the cross power spectrum is similar to that of S. However, the underlying reasons for the observed trends are different. Although material damping explains the effect of S, the mechanics of the source impulse explains the effect of source type.

The time signal of the force created by each hammer is an impulse, i.e., the duration of the force is very small in comparison to the total record length. The energy distribution of an impulse signal in the frequency domain is inversely proportional to the time duration of the impulse. In a short-duration impulse, the energy is spread over a wide frequency band, whereas in a longer duration impulse the energy is concentrated at low frequencies. The impulse duration for a specific source is determined by the elasticity of the materials of the structure and source that are in contact during impact and on the mass of the source. In the present case, the structure (pavement) is the same for all sources. In addition, all of the sources used are steel hammers. Thus, the only remaining factor is the weight of the source. The duration of the impulse is directly proportional to the weight of the source. Thus, light hammers produce a short impulse and distribute the energy over a wide frequency band, whereas heavier hammers produce a longer impulse and concentrate the energy at lower frequencies. Exactly this behavior is observed in the plots of the cross power spectrum magnitudes. In the low-frequency range of the absolute magnitude plots, the energy levels are largest for the heavier hammers. However, the relative magnitude plots reveal that the light hammers distribute the energy over a much wider frequency band.

The cutoff frequencies are the result of poor phase or poor coherence data. The poor data occur at frequencies at which the signals contain a large proportion of background noise. Thus, the lower cutoff frequency decreases with increasing hammer weight because the heavier hammers concentrate more energy at low frequencies. The upper cutoff frequency increases with decreasing hammer weight because the lighter hammers concentrate energy at higher frequencies while distributing the energy over a wider frequency band. [Again, the complete data set (*10*) strongly supports these observations.]

Combined Dispersion Curves for Constant X/L_R, Where L_R Is the Rayleigh Wavelength

The effect of S on the range of useful data collected in the field has been discussed. S also affects the resulting dispersion curve and thus the interpreted stiffness profile.

A criterion for filtering data for wavelengths that are inappropriate for the spacing of the receivers has been given for a test setup for which $S/X = 1$ (*11*). According to this criterion, wavelengths smaller than one-half the receiver spacing and greater than three times the receiver spacing are eliminated. In other words, for a given receiver spacing, waves that have traveled for less than one-third cycle or greater than two cycles are filtered out.

Sanchez-Salinero et al. (*21*) studied the wavelength-receiver spacing filter criterion from a theoretical point of view. In the SASW method, it is assumed that because about two-thirds of the energy generated by the source is transmitted by Rayleigh waves, and because these waves attenuate less than body waves, the wavetrain passing by the receivers is composed primarily of Rayleigh waves. It is further assumed that the Rayleigh waves are plane waves, i.e., generated by a source at infinity.

These assumptions lead to the question of the number of cycles the wave must travel before these assumptions are valid. To examine this question, a series of analytical studies that simulate the testing procedure was performed. Theoretical dispersion curves were generated by two methods, one that assumes plane Rayleigh waves only, and one that includes the Rayleigh and body waves generated by a point source located at a finite distance from the receivers. The studies were performed for test setups such that $S/X = 1$. Further, dispersion curves generated by the method that included the body waves were for constant values of X/L_R, the ratio of the receiver spacing to the wavelength of the Rayleigh wave. In other words, the curves were generated for constant values of the number of cycles the waves traveled. By comparing the dispersion curves for different values of the X/L_R ratio with the curve generated by assuming only plane Rayleigh waves, the number of cycles necessary for the wave to travel before the assumption is valid was established. Sanchez-Salinero et al. (*21*) found that for a test setup in which $S = X$, the field data should be filtered for wavelengths $> 0.5X$. Thus, the assumption that only plane Rayleigh waves exist is best when the wave has traveled two or more cycles.

The disparity between the experimental and theoretical criterion should be observed. Heisey et al. (*11*) suggest that waves traveling more than two cycles will attenuate excessively and thus should be eliminated from the collected data, whereas Sanchez-Salinero et al. (*21*) suggest that the waves must travel at least two cycles to prevent contamination by body waves. Which criterion should be used for analyzing field data from SASW tests? If the entire wavetrain attenuates excessively after two cycles, as the experimental results indicate, after how many cycles do the body waves attenuate to an insignificant level? Some insight into these questions can be gained by examining the data collected as part of this research. If the experimental dispersion curves for constant values of X/L_R are compared as a function of S/X, some indication of the body wave attenuation can be obtained. For a given value of X/L_R, as the source is moved further from the receivers, the wavetrain at the receivers should contain a higher percentage of Rayleigh wave energy. When the body wave energy attenuates to an insignificant level, i.e., the value of X/L_R becomes large enough, the dispersion curves for all values of S/X should be the same because the only energy of significance is from the Rayleigh wave.

Many experimental dispersion curves for constant values of X/L_R as a function of S/X for the G. G. Brown and SEMTA parking lot sites have been provided by Hiltunen (*10*). Two examples of dispersion curves for values of X/L_R between 0.2 and 2 are shown in Figures 9 and 10.

The measured phase velocities are practically independent of S/X for wavelengths > 5 ft for all values of X/L_R. (The data for all values of S/X are nearly the same.) This condition suggests that wavelengths larger than approximately 5 ft are not contaminated with body wave energy. Thus, body wave energy is only significant in the upper layers of the pavement system.

Second, the measured phase velocities are significantly dependent on S/X for small values of X/L_R for wavelengths < 5 ft (Figure 9). In particular, the measured phase velocities generally increase with decreasing S/X for a given value of X/L_R. This relation suggests that body wave energy is present in the signals. The velocities both of compression and shear waves exceed that of the Rayleigh wave. As the source is moved closer to the first receiver, the amount of body wave energy in the signals increases. The expected increase in measured velocity is exactly what has been measured.

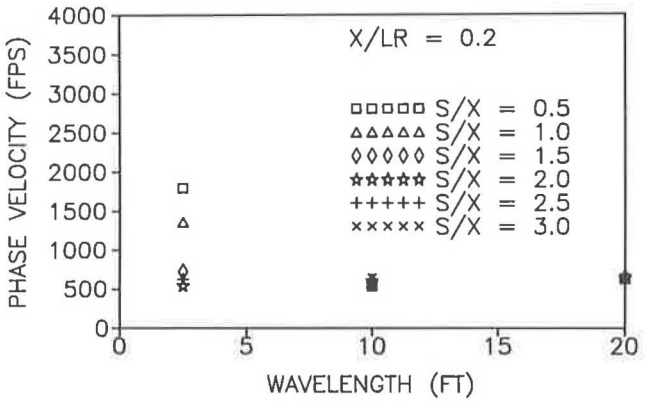

FIGURE 9 Experimental dispersion curves for $X/L_R = 0.2$ at G. G. Brown parking lot site.

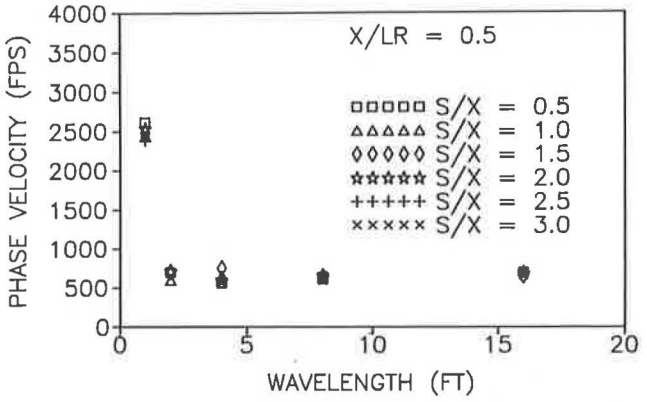

FIGURE 10 Experimental dispersion curves for $X/L_R = 0.5$ at G. G. Brown parking lot site.

Third, the measured phase velocities are practically independent of S/X for values of X/L_R of 0.5 (Figure 10) or greater, for all wavelengths. This condition suggests that body wave energy is insignificant if the wave has traveled at least one-half cycle between the two receivers. Thus, the assumption of plane Rayleigh waves can be made if wavelengths longer than $2X$ are eliminated from the data. [The work of Hiltunen (*10*) supports these observations.]

Combined Dispersion Curves

Effects of Source-to-Near-Receiver Distance (S)

The effects of S on the combined experimental dispersion curves were obtainable from the test data. The dispersion curves resulted from using an averaging algorithm for combining the data obtained for all values of X. They are also the dispersion curves that would be used in the inversion process for determining a stiffness profile. Two curves are shown for each value of X and S. The first curve, shown in Figure 11, is designated as "unfiltered," meaning that it contains data for all frequencies not eliminated from the field data because of poor phase or poor coherence. The second curve, shown in Figure 12, is designated as "filtered," meaning that the wavelength and receiver spacing filter criterion suggested in the previous section has been applied to the data. All wavelengths longer than $2X$ have been eliminated from each individual dispersion curve before processing with the averaging program.

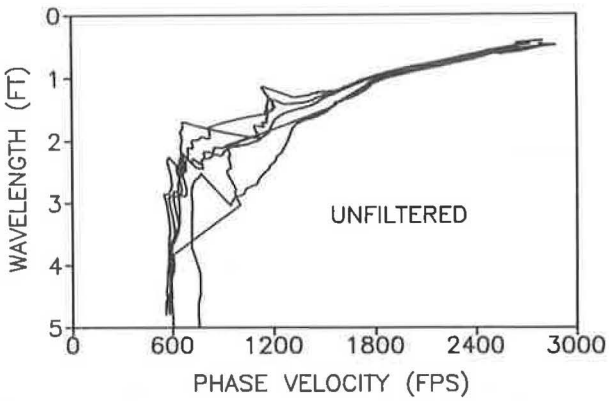

FIGURE 11 Average experimental dispersion curves (unfiltered) as a function of source-to-near-receiver distance S at SEMTA parking lot site.

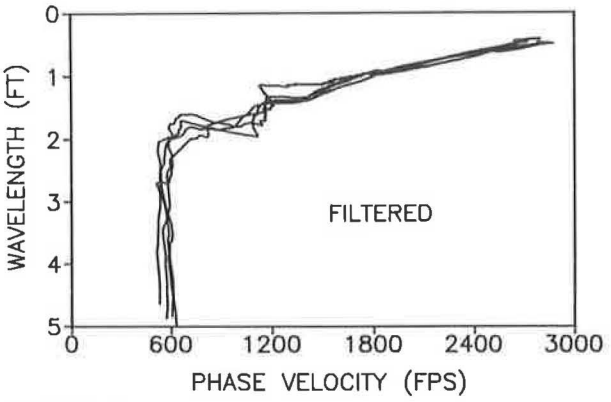

FIGURE 12 Average experimental dispersion curves (filtered) as a function of source-to-near-receiver distance S at SEMTA parking lot site.

The combined dispersion curves for the SEMTA parking lot site are shown in Figures 11 and 12. Only wavelengths from 0 to 5 ft are shown because the data for wavelengths larger than 5 ft essentially coincide, as discussed previously. [Similar plots for the G. G. Brown parking lot site have been provided by Hiltunen (*10*).]

Comparing the unfiltered with the filtered dispersion curves indicates that the recommended filter criterion substantially eliminates the dependence of the results on S. The filtered curves essentially coincide after wavelengths longer than $2X$ are removed. Because body wave energy in the signals is negligible if the waves have traveled a minimum of one-half cycle between the receivers, a new wavelength-receiver spacing filter should be implemented for SASW data analysis of pavement sites, i.e., removal of wavelengths longer than $2X$.

Effects of Source Type

This section examines the effects of source type on the combined experimental dispersion curves generated from the filtered test data, i.e., after all wavelengths longer than $2X$ are eliminated. The two dispersion curves shown on the plots in Figures 13–16 illustrate the effects of source type. First, the combined dispersion curve obtained using the optimum hammers that were identified in Table 1 is shown. By definition, the optimum hammer for a given value of X is the hammer that provides dispersion data of significant energy over the largest frequency range. The corresponding dispersion curve thus determined is the best curve for the given site. The second curve shown on the plots in Figures 13–16 is the combined dispersion curve for a constant source type, i.e., the result of combining the data obtained for all receiver spacings using the same source. The goal was to determine the minimum number of sources required to adequately define the dispersion curve for a given site.

Combined dispersion curves for both the SEMTA and G. G. Brown parking lot sites have been provided by Hiltunen (*10*). Five sources were used at the SEMTA parking lot site and

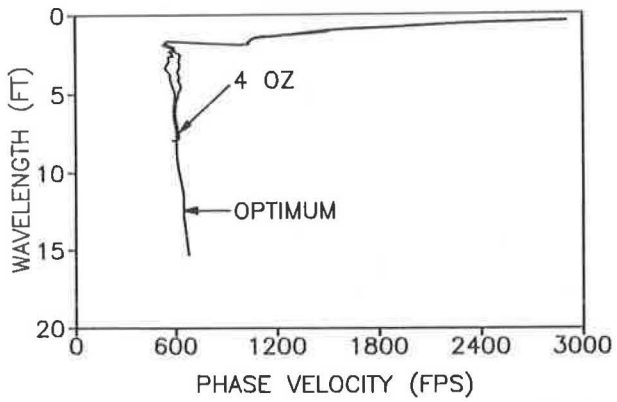

FIGURE 13 Average experimental dispersion curve for 4-oz hammer for SEMTA parking lot site (all wavelengths).

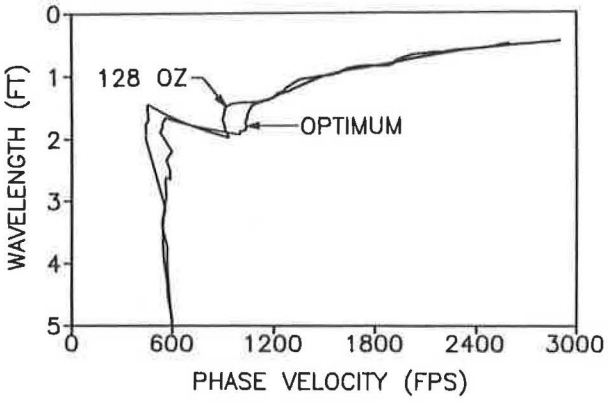

FIGURE 14 Average experimental dispersion curve for 128-oz hammer at SEMTA parking lot site (0- to 5-ft wavelengths).

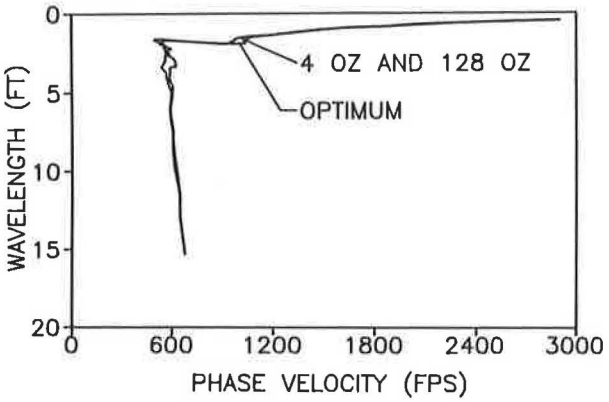

FIGURE 15 Average experimental dispersion curve for 4- and 128-oz hammers at SEMTA parking lot site (all wavelengths).

data were collected with each source at all receiver spacings (see Table 1). Only the results for the 4- and 128-oz hammers are presented here.

Figures 13 and 14 show the optimum results and the dispersion data generated from a single source type. From these plots and results reported by Hiltunen (*10*), no single source consistently duplicated the optimum results over all wavelengths. The light hammers cannot generate low enough frequencies, whereas the heavy hammers cannot generate high enough frequencies. However, in the wavelength ranges at which data exist for a constant source type, the phase velocities are nearly identical to those for the optimum results.

Because single source types fail to consistently duplicate the optimum results, Figures 15 and 16 show a comparison of the optimum results with those obtained from combining the data for the 4-oz and 8-lb hammers. These hammers were the lightest and heaviest hammers tested, respectively, and thus matched the optimum results at the high and low frequencies. The results for the overlap of the frequency ranges were also indistinguishable from the optimum results. Thus, to fully characterize the dispersion curve, only these two sources are required.

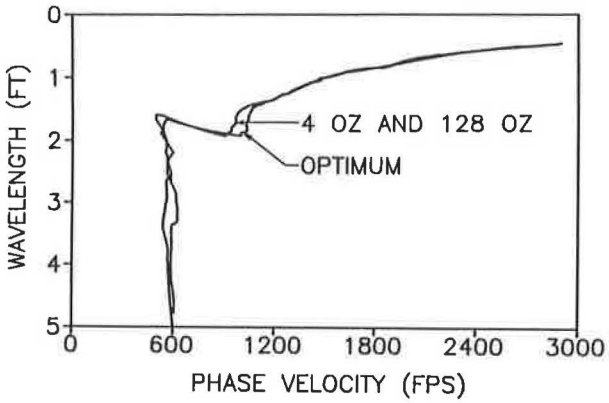

FIGURE 16 Average experimental dispersion curve for 4- and 128-oz hammers at SEMTA parking lot site (0- to 5-ft wavelengths).

SUMMARY AND CONCLUSIONS

The purpose of the research reported herein and in the research program of Hiltunen (*10*) was to further the development of the SASW method toward a practical technique for in situ investigation of pavement systems. Eventually an automated testing procedure will be developed for collecting the necessary data in the field, analogous to the deflection measurement procedures currently used in the pavement industry. The development of a multiple-transducer testing procedure is an important step toward this goal, but poses questions about (a) the source and receiver geometry, (b) location of the source, and (c) source type. A systematic experimental investigation was therefore conducted at two asphaltic concrete pavement sites on the effects of source and receiver geometry, source-to-near-receiver distance S, and source type, in the context of a multiple-transducer testing procedure. The results were independent of source and receiver geometry (*20*). The effects of S were extremely important. The ratio S/X should be ≤ 2. Phase velocity measurements were independent of S when wavelengths longer than $2X$ were filtered from the data. The effects of source type on the ranges of useful frequencies for a given receiver spacing were significant. In general, both the lower and upper cutoff frequencies decreased as the weight of the hammer increased. Single source types failed to consistently duplicate the optimum results at all frequencies. In general, the light hammers could not define the dispersion curve on the low-frequency end, and the heavy hammers could not define the dispersion curve on the high-frequency end. However, dispersion curves generated by combining the data from a 4-oz ball peen hammer and an 8-lb sledge hammer yielded the optimum results over all wavelengths.

Implications of findings [as supported by the complete research program (*10*)] for a multiple-transducer testing procedure are as follows:

- CRMP geometry would not be appropriate for a multiple-transducer testing procedure with a fixed source location because such an array could not meet the requirement that $S/X \leq 2$.
- The CS geometry with $S/X = 1$ is recommended for a multiple-transducer array.

• Use of two impact sources is a means of collecting dispersion curve data for multiple-transducer testing procedures.

ACKNOWLEDGMENT

The research described herein was supported by the Geotechnical Laboratory of the U.S. Army Engineer Waterways Experiment Station, Vicksburg, Mississippi. The authors gratefully acknowledge this support.

REFERENCES

1. D. R. Alexander, S. D. Kohn, and W. P. Grogan. Nondestructive Testing Techniques and Evaluation Procedures for Airfield Pavements. In *Nondestructive Testing of Pavements and Backcalculation of Moduli*, STP 1026, A. J. Bush III and G. Y. Baladi (eds.), ASTM, Philadelphia, Pa., 1989, pp. 502–524.
2. S. W. Lee, J. P. Mahoney, and N. C. Jackson. Verification of Backcalculation of Pavement Moduli. In *Transportation Research Record 1196*, TRB, National Research Council, Washington, D.C., 1988, pp. 85–95.
3. T. Rwebangira, R. G. Hicks, and M. Truebe. Sensitivity Analysis of Selected Backcalculation Procedures. In *Transportation Research Record 1117*, TRB, National Research Council, Washington, D.C., 1987.
4. R. L. Lytton. Backcalculation of Pavement Layer Properties. In *Nondestructive Testing of Pavements and Backcalculation of Moduli*, STP 1026, A. J. Bush III and G. Y. Baladi (eds.), ASTM, Philadelphia, Pa., 1989, pp. 7–38.
5. T. G. Davies and M. S. Mamlouk. Theoretical Response of Multilayer Pavement Systems to Dynamic Nondestructive Testing. In *Transportation Research Record 1022*, TRB, National Research Council, Washington, D.C., 1985, pp. 1–7.
6. M. S. Mamlouk. Use of Dynamic Analysis in Predicting Field Multilayer Pavement Moduli. In *Transportation Research Record 1043*, TRB, National Research Council, Washington, D.C., 1985, pp. 113–119.
7. M. S. Mamlouk and T. G. Davies. Elasto-Dynamic Analysis of Pavement Deflections. *Journal of Transportation Engineering*, ASCE, Vol. 110, No. TE6, Nov. 1984, pp. 536–550.
8. J. M. Roesset and K. Y. Shao. Dynamic Interpretation of Dynaflect and Falling Weight Deflectometer Tests. In *Transportation Research Record 1022*, TRB, National Research Council, Washington, D.C., 1985, pp. 7–16.
9. K. Y. Shao, J. M. Roesset, and K. H. Stokoe, II. *Dynamic Interpretation of Dynaflect and Falling Weight Deflectometer Tests on Pavement Systems*. Research Report 437-1, Center for Transportation Research, The University of Texas at Austin, Aug. 1986, 60 pp.
10. D. R. Hiltunen. *Experimental Evaluation of Variables Affecting the Testing of Pavements by the Spectral-Analysis-of-Surface-Waves Method*. Technical Report GL-88-12, U.S. Army Engineer Waterways Experiment Station, Vicksburg, Miss., Aug. 1988, 303 pp.
11. J. S. Heisey, K. H. Stokoe, II, W. R. Hudson, and A. H. Meyer. Determination of In Situ Shear Wave Velocities from Spectral Analysis of Surface Waves. Research Report No. 256-2, Center for Transportation Research, The University of Texas at Austin, Dec. 1982, 277 pp.
12. S. Nazarian. In Situ Determination of Elastic Moduli of Soil Deposits and Pavement Systems by Spectral-Analysis-of-Surface-Waves Method. Ph.D. dissertation, The University of Texas at Austin, 1984, 453 pp.
13. S. Nazarian and K. H. Stokoe, II. Nondestructive Testing of Pavements Using Surface Waves. In *Transportation Research Record 993*, TRB, National Research Council, Washington, D.C., 1984, pp. 67–79.
14. S. Nazarian and K. H. Stokoe, II. Use of Surface Waves in Pavement Evaluation. In *Transportation Research Record 1070*, TRB, National Research Council, Washington, D.C., 1986, pp. 132–144.
15. S. Nazarian and K. H. Stokoe, II. Nondestructive Evaluation of Pavements by Surface Wave Method. In *Nondestructive Testing of Pavements and Backcalculation of Moduli*, STP 1026, A. J. Bush III and G. Y. Baladi (eds.), ASTM, Philadelphia, Pa., 1989, pp. 119–137.
16. S. Nazarian, K. H. Stokoe, II, and R. C. Briggs. Nondestructively Delineating Changes in Modulus Profiles of Secondary Roads. In *Transportation Research Record 1136*, TRB, National Research Council, Washington, D.C., 1987.
17. S. Nazarian, K. H. Stokoe, II, R. C. Briggs, and R. Rogers. Determination of Pavement Layer Thicknesses and Moduli by SASW Method. In *Transportation Research Record 1196*, TRB, National Research Council, Washington, D.C., 1988.
18. S. Nazarian, K. H. Stokoe, II, and W. R. Hudson. Use of Spectral Analysis of Surface Waves Method for Determination of Moduli and Thicknesses of Pavement Systems. In *Transportation Research Record 930*, TRB, National Research Council, Washington, D.C., 1983, pp. 38–45.
19. J. C. Sheu, G. J. Rix, and K. H. Stokoe, II. Rapid Determination of Modulus and Thickness of Pavement Surface Layer. Presented at 67th Annual Meeting of the Transportation Research Board, Washington, D.C., Jan. 1988.
20. D. R. Hiltunen and R. D. Woods. Influence of Source and Receiver Geometry on the Testing of Pavements by the Surface Waves Method. In *Nondestructive Testing of Pavements and Backcalculation of Moduli*, STP 1026, A. J. Bush III and G. Y. Baladi, eds., ASTM, Philadelphia, Pa., 1989, pp. 138–154.
21. I. Sanchez-Salinero, J. M. Roesset, K. Y. Shao, K. H. Stokoe, II, and G. J. Rix. Analytical Evaluation of Variables Affecting Surface Wave Testing of Pavements. In *Transportation Research Record 1136*, TRB, National Research Council, Washington, D.C., 1987.

Publication of this paper sponsored by Committee on Pavement Monitoring, Evaluation, and Data Storage.

Modulus and Thickness of the Pavement Surface Layer from SASW Tests

JOSE M. ROESSET, DER-WEN CHANG, KENNETH H. STOKOE II, AND MARWAN AOUAD

The spectral analysis of surface waves (SASW) test can be used rapidly in the field to determine the stiffness and thickness of the pavement surface layer. The test is equally applicable to asphalt concrete and portland cement concrete pavements. One of the most important features is that testing can be performed quickly (in approximately 5 min at each location). Values of Young's modulus and thickness of the surface layer are determined using a straightforward procedure. Analytical studies are presented to substantiate this procedure and to optimize its use. Several case studies from asphalt concrete pavements and one Portland cement concrete pavement are presented. The results show that this adaptation of the SASW test provides values of Young's modulus that are sensitive to the elastic stiffness of the surface layer and also provides reasonable estimates of the thickness of the surface layer. In addition, changes in the stiffness of the surface layer with time and temperature are easily monitored in situ.

Reliable measurements of the in situ conditions of pavements are an important aspect in effectively managing pavement systems. Existing nondestructive devices for moduli measurements, such as the Dynaflect or falling weight deflectometer, cannot be used to perform an independent measure of only the surface layer. In addition, these devices can be somewhat insensitive to the modulus of the pavement surface layer, specially for the cases of a thin surface layer on the order of a few inches thick or under those conditions where bedrock is near the surface. Optimum results are also obtained with these tests when the thickness of the layers in the pavement are known a priori. On the other hand, the spectral analysis of surface waves (SASW) test is very sensitive to the value of Young's modulus of the surface layer and bedrock conditions do not affect the near-surface measurements. In addition, the thickness of surface layer is not required to evaluate the measurements but can be estimated from the field data.

As originally proposed, the SASW method (*1–3*) has been a rather complex nondestructive method involving the use of surface waves to evaluate the modulus profile of the entire pavement system. However, if only the stiffness and thickness of the surface layer are required, the SASW test can be greatly simplified so that testing can be performed rapidly and values of moduli and thickness can be determined immediately in the field. This adaptation of the SASW test, originally proposed by Sheu et al. (*4*), is based on a theoretically sound procedure that is simple, easy to implement, and does not require knowledge of any of the layer thicknesses in the pavement profile.

Department of Civil Engineering, University of Texas at Austin, Austin, Tex. 78712.

In the following sections, this adaptation of the SASW test is briefly described along with an analytical study of the dispersive properties of surface waves in the pavement surface layer. Typical test results from several pavements, including one where the Portland cement concrete was curing, are then presented.

GENERAL BACKGROUND

Evolution of SASW Method

The SASW method (*1–3*) is an in situ seismic method that is used for near-surface profiling of pavement sites. The SASW method is a modification of the steady-state Rayleigh wave technique introduced in the 1950s for the measurement of elastic properties of pavements (*5,6*). The original technique involved testing with bulky equipment and analyzing the data with an empirical approach. These two shortcomings resulted in the method's never gaining wide acceptance. In fact, the empirical basis for data analysis resulted in erroneous results under certain conditions that often occur in pavement systems.

Because of the development of portable, sophisticated electronic equipment capable of performing accurate, high-frequency data acquisition and complex mathematical manipulations rapidly in the field, the bulky equipment associated with the steady-state technique is no longer required. In addition, a theoretically sound basis for data analysis has been developed (*7–10*). These two developments have resulted in the application of the SASW method to nondestructive pavement testing. One of the important areas in which the SASW method can easily be used is the rapid determination of the modulus and thickness of the pavement surface layer. This application is possible because of the simplicity of data analysis in a uniform top layer of any layered system.

Equipment and Field Testing

The general arrangement of the source, receivers (accelerometers), and recording equipment in an SASW test is shown schematically in Figure 1. No boreholes are required because both the source and receivers are placed on the pavement surface. A piezoelectric shaker is an effective source for generating a group of surface waves over frequencies ranging from about 1 to 50 kHz. These high frequencies are necessary to sample the surface layer. A digital waveform analyzer

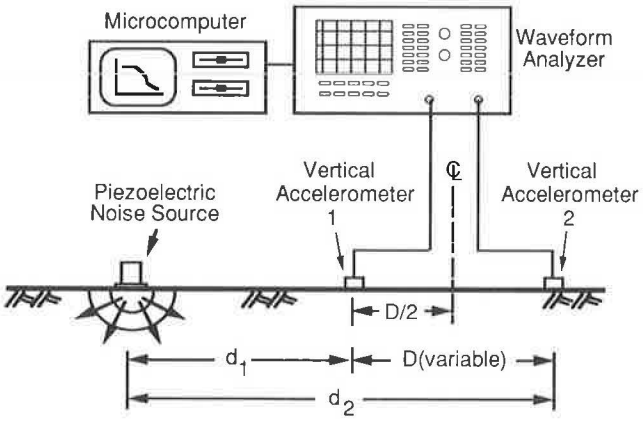

FIGURE 1 General configuration of equipment used to evaluate the surface layer.

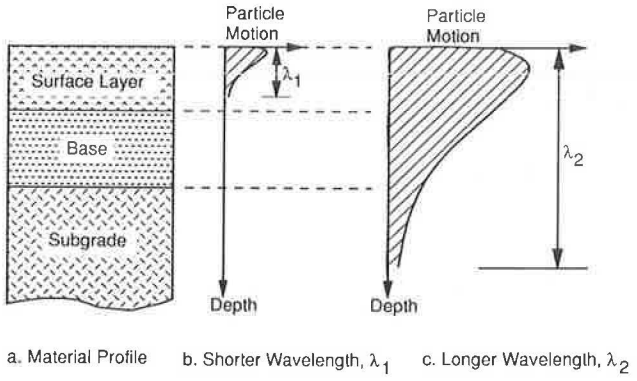

FIGURE 2 Approximate distribution of vertical particle motion with depth for two surface waves of different wavelengths.

coupled with a microcomputer is used to capture and process the outputs from the receivers.

The vertical accelerometers and source are arranged in a linear array. The distance D between receivers (see Figure 1) is usually 6 in. but may be varied by the operator to optimize the test results for a particular site. (Distances of 3 to 12 in. have been used in practice.) The distance d_1 between the source and the first receiver is usually kept equal to D but may also be increased by the operator to minimize destructive interference from body wave reflections. However, d_1/D = 1.0 is normally a good arrangement, as shown in the following analytical studies.

Surface Wave Dispersion

The dispersive property of surface waves permits use of the SASW method. Dispersion refers to the variation of surface wave phase velocity with wavelength (or frequency). Dispersion arises because surface waves of different wavelengths sample different parts of the pavement profile, as shown in Figure 2. As wavelength increases, particle motion extends to greater depths in the profile. The velocities of surface waves are representative of the material stiffness over depths for which there is significant particle motion. For example, the particle motion of a wave that has a wavelength less than the thickness of the pavement surface layer is confined to this layer (Figure 2b). Therefore, the wave velocity is affected by the stiffness of the surface layer and not by the lower layers. The velocity of a wave with a wavelength of several feet is influenced by the properties of the surface layer, base, and subgrade because a significant portion of the particle motion is in these layers (Figure 2c). Thus, by using surface waves over a wide range of wavelengths, it is possible to assess material properties over a range of depths. However, to monitor only the stiffness of a surface layer, only wavelengths less than the thickness of this surface layer need to be generated and measured.

The overall objective in SASW testing is to make field measurements of surface wave dispersion (i.e., measurements of surface wave velocity V_R at various wavelengths L_R) and then to determine the stiffnesses of the layers in the profile. For the case of a uniform surface layer, the surface wave phase velocity V_R is related to the shear wave velocity V_S of the material by Poisson's ratio ν. The ratio of V_R to V_S varies from 0.874 to 0.955 for values of Poisson's ratio ν ranging from 0 to 0.5. Therefore, once the surface wave phase velocity of the uniform surface layer has been measured, it is a simple matter to calculate the shear wave velocity and, hence, Young's modulus of the surface layer using the following relationships:

$$V_S = C \cdot V_R \tag{1}$$

$$G = (\gamma/g) \cdot V_S^2 \tag{2}$$

$$E = 2\,G\,(1 + \nu) \tag{3}$$

where

C = 1.135 − 0.182 · ν (for $\nu \geq 0.1$),
G = shear modulus,
γ = total unit weight,
g = acceleration due to gravity, and
E = Young's modulus.

Because the values of moduli calculated in Equations 1 through 3 are a result of seismic measurements, these values represent the moduli at small strain amplitudes. Moduli measured at these strain levels are maximum values of moduli. Additionally, if the material stiffness is frequency dependent (such as for asphalt concrete), then seismic tests will result in higher values of stiffness than determined by static tests because of the high frequencies used in seismic testing. As a result, the seismically determined values should be adjusted accordingly.

ANALYTICAL STUDIES

To apply the SASW test effectively to measurements of the surface layer, analytical studies of the dispersive characteristic of waves propagating in a uniform layer over a half-space were conducted. Two general cases were studied: (a) dispersion of plane Rayleigh waves, and (b) dispersion of combined Rayleigh and body waves. The theoretical solution involving plane Rayleigh wave propagation forms the basis for the simplest analysis procedure used to interpret SASW field data. However, vertical excitation at a point on the surface of a

layered system creates a group of seismic waves that are composed of body waves [compression (P) and shear (SV) waves] as well as surface (Rayleigh) waves, which propagate radially away from the source. Therefore, simulation of wave dispersion from the combined body and surface waves is important to understanding SASW testing, particularly at distances from the source that are small relative to the wavelength (near-field effect). In the following sections, the dispersion characteristics of both plane Rayleigh wave propagation and combined waves excited by a vertical dynamic load are discussed.

The mathematical model consists in both cases of a horizontally layered half-space with homogeneous properties within each layer. The solution to the differential equations of motion for each layer permits the stresses and displacements at the top of the layer to be related to the stresses and displacements at the bottom of the layer for a given frequency and wave number (or wavelength). The stresses and displacements are given by a system of equations in terms of a matrix **T** called the "transfer" or "propagator" matrix. Expressions for the elements of the matrix **T** can be found in the literature (*7,11*).

Alternatively, the stresses at the top and bottom of a layer can be expressed in terms of the displacements at the top and bottom through a dynamic stiffness matrix, as suggested by Kausel and Roesset (*9*).

Dispersion of Plane Rayleigh Waves

By imposing compatibility of displacements and equilibrium of stresses at the interfaces between two layers, a series of multiplications of the transfer matrices **T** of each layer provides a relationship between the stresses and displacements at the free surface and those at any depth. By assuming no excitation at the top and no waves propagating upward within the underlying half-space, the system of equations can be reduced to a set of homogeneous equations in terms of a 2 $\times$ 2 matrix. To obtain nontrivial solutions, this matrix must be singular. The values of the wave numbers k (for a fixed frequency) that make the determinant of this matrix equal to zero provide the wave numbers of the Rayleigh waves propagating at that frequency through the soil profile. For each value of k, one can then obtain the wavelength $2\pi/k$ and the corresponding propagation velocity V_R.

Using instead the dynamic stiffness matrices of the layers, one can assemble a stiffness matrix for the complete soil profile following the same procedures used in matrix structural analysis. Again to obtain the modes of propagation, the determinant of the global stiffness matrix is set equal to zero. The total stiffness matrix is a tridiagonal matrix in terms of 2 $\times$ 2 submatrices, and therefore the evaluation of the determinant is rather simple.

In the case of a uniform half-space, the zero determinant matrices in both approaches lead to a frequency (or wavelength) independent solution for the characteristic equation. The dispersion curve is thus a straight line as shown in Figure 3. In this special case, propagation velocity is independent of wavelength because the half-space has a uniform stiffness and only plane Rayleigh waves are being considered.

For a layer resting on a half-space with different properties, V_R will vary with frequency. At very low frequencies (long wavelengths), the velocity will tend to the velocity of the half-space. At very high frequencies (short wavelengths), the value of V_R will equal the value of Rayleigh wave velocity in the top layer. Figure 4 shows a typical dispersion curve for a softer layer overlying a stiffer half-space, with stiffness ratio $E_1/E_2 = 0.25$. This system could represent an asphalt concrete (AC) layer over a thick cemented base. Figure 5 shows a similar dispersion curve for a stiffer layer overlying a softer half-space, with $E_1/E_2 = 4$. This system could represent a rather soft surface layer over a stiff uncemented base and subgrade with similar stiffnesses or it could represent a Portland cement concrete (PCC) layer over a thick AC base. In either of the cases shown in Figures 4 and 5, the top layer in the profile appears as though it were a uniform half-space for waves with very short wavelengths (high-frequency waves). In other words, these short-wavelength surface waves sample only the stiffness of the top layer. As such, the shear wave velocity, shear modulus, and Young's modulus of the top layer may be calculated using the relationships in Equations 1 through 3. This important point forms the basis of the application of the SASW method presented herein. In addition, the thickness h of the top layer may be estimated using the critical wavelength L_C, as shown in Figure 6.

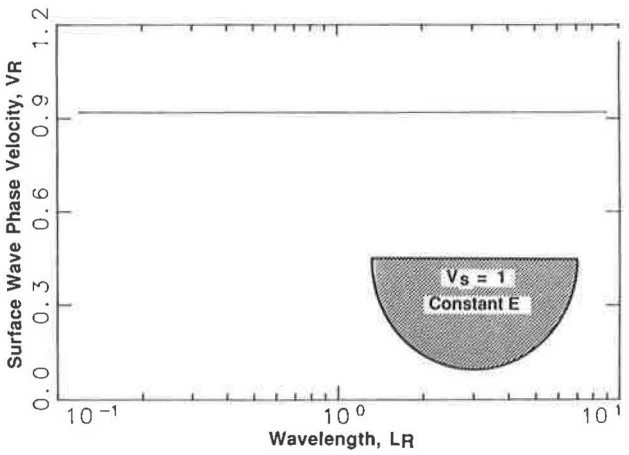

FIGURE 3 Dispersion curve for plane Rayleigh waves propagating in a uniform half-space.

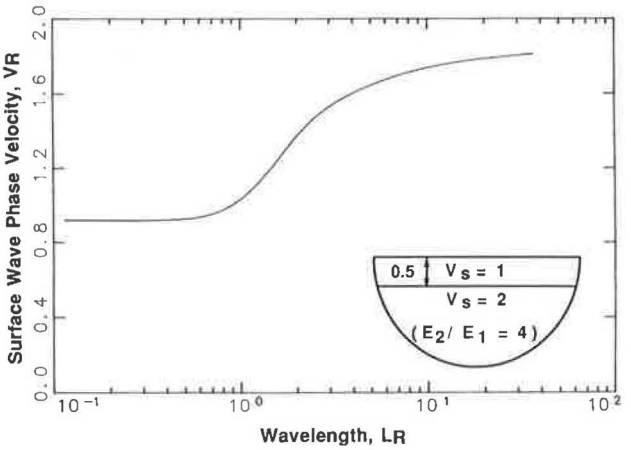

FIGURE 4 Dispersion curve for plane Rayleigh waves propagating in a softer layer over a stiffer half-space.

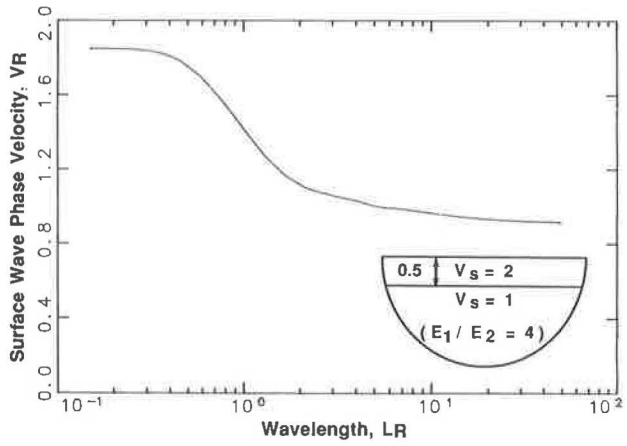

FIGURE 5 Dispersion curve for plane Rayleigh waves propagating in a stiffer layer over a softer half-space.

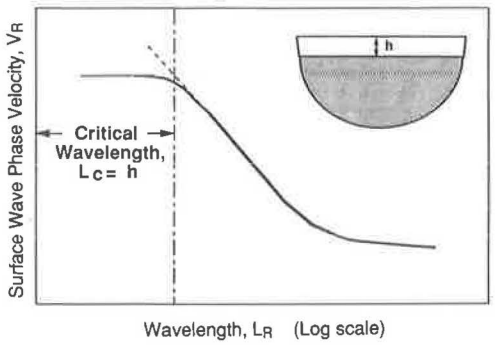

FIGURE 6 Determination of the surface layer thickness from the dispersion curve for plane Rayleigh waves.

Dispersion of Combined Body and Rayleigh Waves

The physical phenomenon is more complicated when applying a vertical impulse at a point on top of a layered system. Waves generated in this case involve both surface waves that propagate radially outward from the source along a cylindrical wave front and body waves that propagate radially outward along a hemispherical wave front. The analytical formulation requires the following processes:

1. Decomposition of the load into a series of cylindrical functions (Bessel functions) in the radial direction. Each term of the series corresponds to a wave number k.
2. Calculation of displacements and stresses for a given frequency and wave number using the global stiffness matrix of the complete layered system. The results are the Green's functions.
3. Determination of total displacements and stresses integrating the product of the Green's functions by the corresponding terms of the load decomposition.

Because the terms of the stiffness matrices of each layer are transcendental functions (complex exponentials), the integrals involved in the calculation of the Green's functions are done normally by numerical integration. Formulations along these lines have been implemented by Gazetas and Roesset (*12*) in Cartesian coordinates and Apsel and Luco (*13*) in cylindrical coordinates. This procedure is particularly convenient when dealing with a uniform half-space or a small number of layers, but expensive when a large number of layers is needed to reproduce the variation of properties with depth. An alternative to this formulation is to use the exact analytical expressions (displacements and stresses) in the two horizontal (or radial and circumferential) directions, and a simpler polynomial expansion in the vertical (z) direction if the thickness of the layers is sufficiently small. The approximation in the z direction leads to much simpler algebraic expressions for the terms of the stiffness matrices of the layers. By expressing the solution in terms of the mode shapes of the waves propagating through the layered system, Kausel (*14*) was able to obtain explicit solutions for the displacements caused by harmonic loads at any point in the system. Using Kausel's formulation with an approximate solution for a half-space at the bottom of a layered stratum (*11*) and with the rule suggested by Shao (*15*) in dividing automatically the physical layers into finer sublayers to provide an appropriate thickness for each sublayer, dispersion data for the SASW test can be evaluated.

For example, the dispersion curve for a uniform half-space with shear wave velocity of 1, Poisson's ratio of 0.25, mass density of 1, and material damping ratio of 0.02 is shown in Figure 7. By applying a vertical load at a point on the surface of the half-space, the response (amplitude and phase) at five other points spaced 1, 1.2, 1.5, 2, and 3 units from the source was computed; then the surface wave phase velocities were obtained from the phase differences and distances between adjacent receivers. This source-receiver configuration was chosen to evaluate the field SASW setup and to verify the near-field effect. The four dispersion curves are similar over the entire range. For relatively high frequencies ($f > 2$ Hz, which corresponds to $L_R < 0.5$), the curves match very well and correspond to the stiffness of the half-space. For values of d_1/L_R less than 2 ($f = 2$ Hz corresponds to $d_1/L_R = 2$, $d_1 = 1$, and $L_R = 0.5$, as calculated from $L_R = V_R/f$), surface

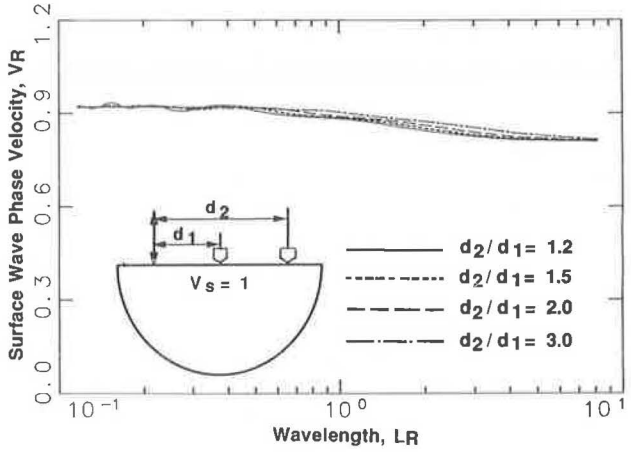

FIGURE 7 Dispersion curve for combined waves propagating in a uniform half-space.

wave phase velocities are smaller (within 10 percent difference) than the phase velocities of the plane Rayleigh wave. This difference is believed to be caused by the coupling effect of body waves and Rayleigh waves in the zone near the source (often called the near-field effect). Slight fluctuations can be seen in the curve corresponding to the smallest distance ratio d_2/d_1. This result indicates that larger values of d_2/d_1 are preferred. In SASW testing, a ratio of two is commonly used.

PARAMETRIC STUDIES

A number of studies were conducted to investigate the appropriate SASW configurations (spacings between source and receivers) to minimize the near-field effect. In considering d_1 and d_2 as the distances from the source to the two receivers, L_R as the wavelength (computed by dividing the phase velocity by the frequency), and h as the thickness of the top layer, the agreement between the dispersion curves corresponding to plane Rayleigh waves and those computed by taking into account all the propagating waves is in general a function of the ratios d_1/L_R, d_2/L_R or $(d_2 - d_1)/L_R$, d_1/h, and d_2/h. The results are also influenced to some extent by the stiffness contrast between the upper layer and the half-space.

To simulate the pavement system, where the top layer is often stiffer than the underlying layers, a set of simplified, two-layer systems consisting of a surface layer with shear wave velocities of 1.414, 2, 3, 5, and 10 overlying a half-space with a shear wave velocity of 1 was studied. These cases correspond to stiffness ratios E_1/E_2 of 2, 4, 9, 25, and 100. (Mass density and Poisson's ratio of both layers were assigned as 1 and 0.25, respectively, in all cases.) For each stiffness ratio, values of the thickness h of the top layer of 0.1, 0.25, 0.5, 1, 2, and 5 were used. Because the distance d_1 from the source to the first receiver remained 1 in all cases, the ratios d_1/h were 10, 4, 2, 1, 0.5, and 0.2. Four values of SASW spacing ratios d_2/d_1 of 1.2, 1.5, 2, and 3 were studied. Linear material damping values of 0 and 2 percent were assumed in the calculation of the plane Rayleigh wave solution and the discrete Green's solutions, respectively, to differentiate the simplified theoretical SASW interpretation from a more complete representation of the field results.

Two sets of results for stiffness ratios of 4 and 25 are shown in Figures 8 through 11. Significant fluctuations in the dispersion curves result from coupling of the body and Rayleigh waves. The parametric studies show that the best results are generally obtained when d_2/d_1 is of the order of 1.5 to 2. The main complication in this case is that, for wavelengths of the order of the layer thickness, there are reflections at the bottom of the layer that result in large oscillations in the complete solution. These oscillations are more pronounced for small values of d_2/d_1 and increase with increasing contrast in stiffnesses between the layer and the half-space. Values of d_1/L_R between 0.5 and 2 generally produce results that are very close to those of the plane Rayleigh waves. When the modulus of the top layer is much larger than that of the underlying material, as would happen with a PCC layer over an uncemented base and subgrade, determination of the dispersion curves in the range of wavelengths around the thickness of the layer is always difficult because of the large fluctuations.

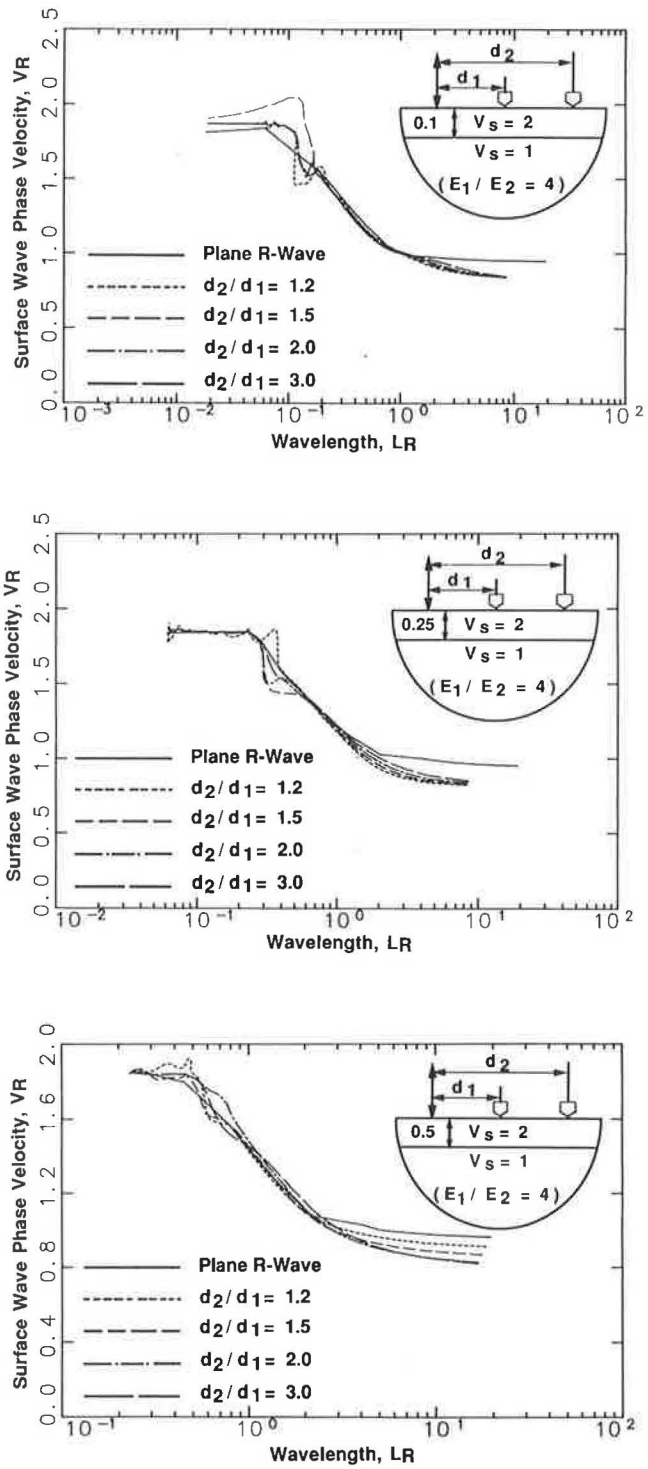

FIGURE 8 Comparison of dispersion curves based on plane Rayleigh waves and combined waves for SASW configurations: $E_1/E_2 = 4$, $d_1 = 1$, and $H = 0.1, 0.25, 0.5$.

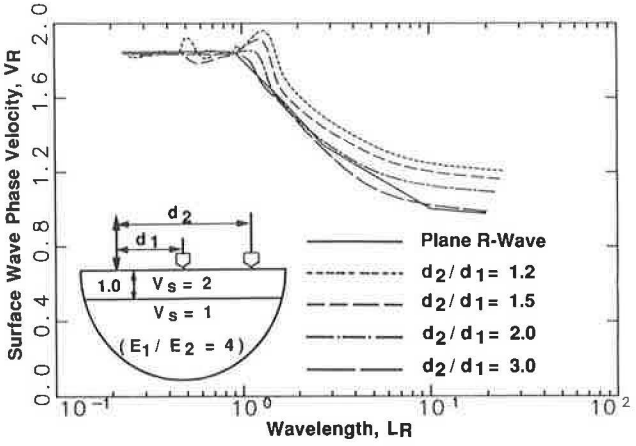

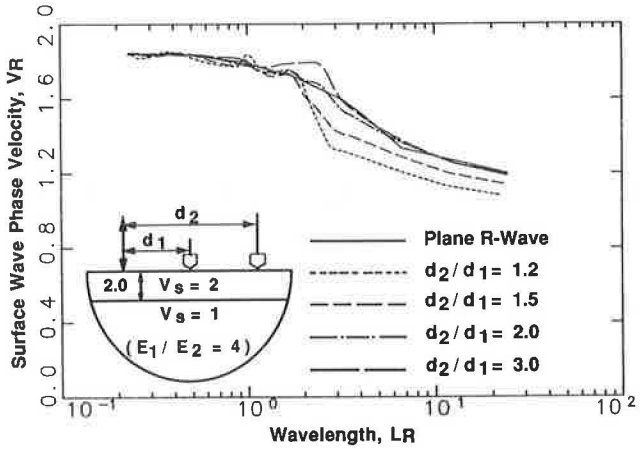

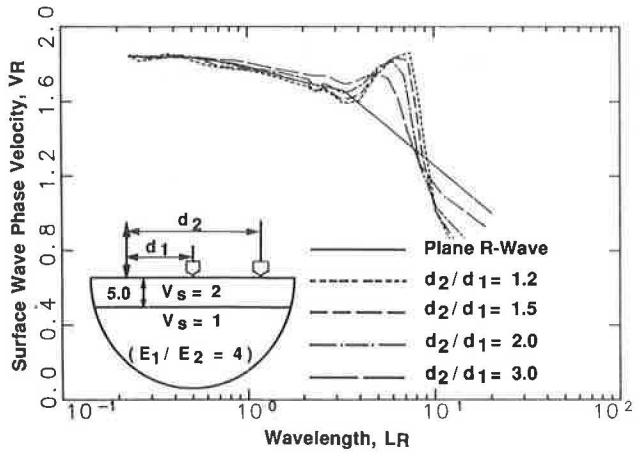

FIGURE 9 Comparison of dispersion curves based on plane Rayleigh waves and combined waves for SASW configurations: $E_1/E_2 = 4$, $d_1 = 1$, and $H = 1.0, 2.0, 5.0$.

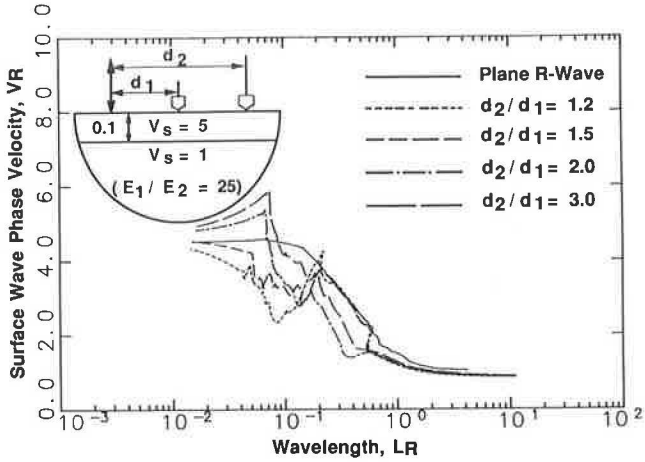

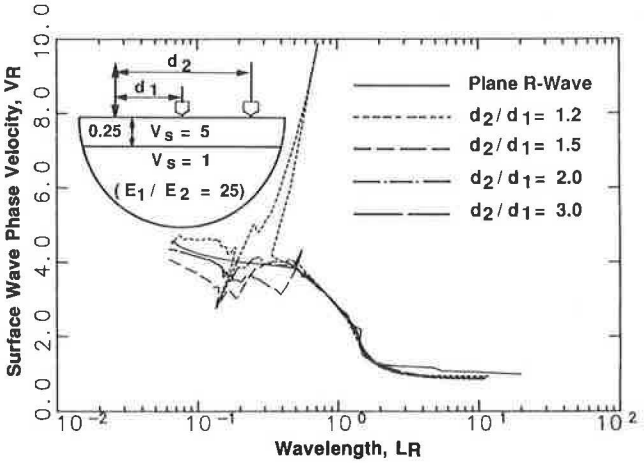

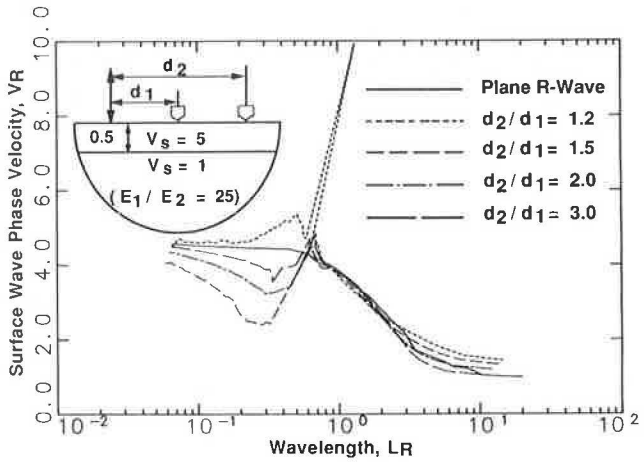

FIGURE 10 Comparison of dispersion curves based on plane Rayleigh waves and combined waves for SASW configurations: $E_1/E_2 = 25$, $d_1 = 1$, and $H = 0.1, 0.25, 0.5$.

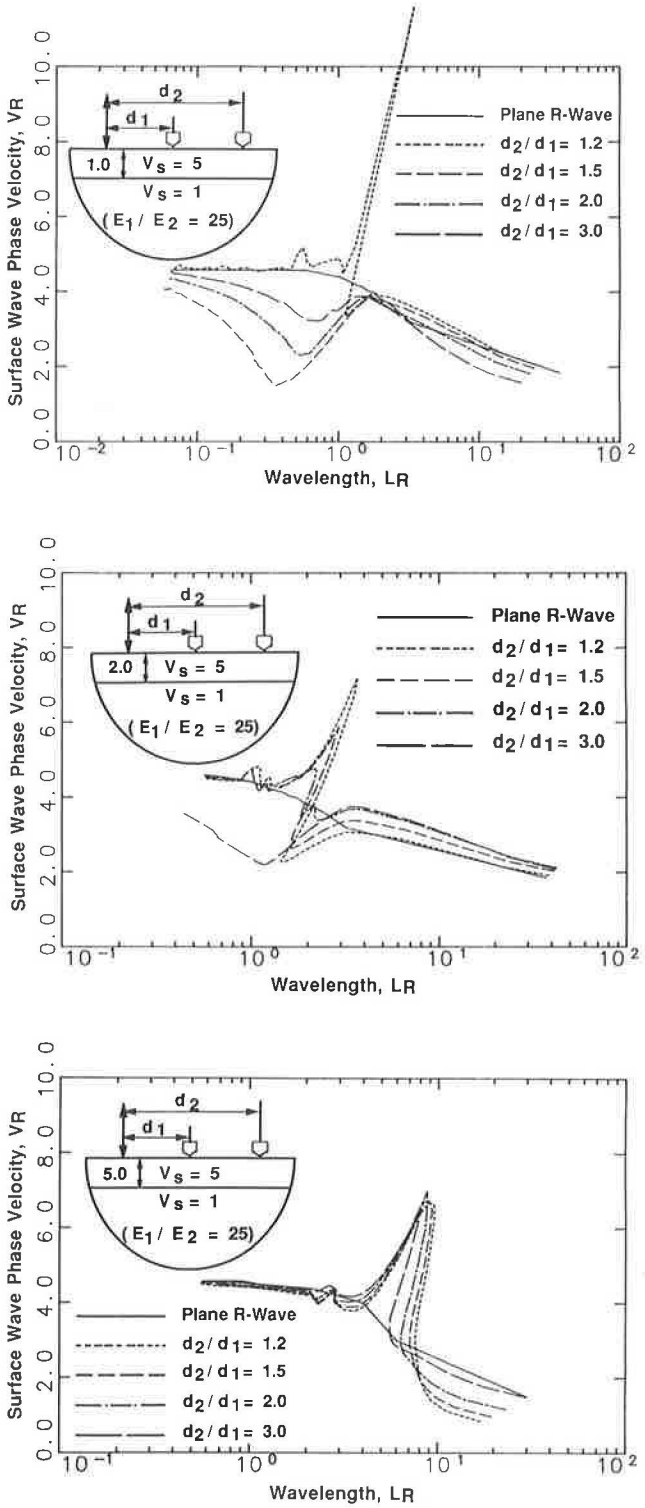

FIGURE 11 Comparison of dispersion curves based on plane Rayleigh waves and combined waves for SASW configurations: $E_1/E_2 = 25$, $d_1 = 1$, and $H = 1.0, 2.0, 5.0$.

The dispersion curve obtained in the field needs to be smoothed if it is going to be assumed to correspond to a plane Rayleigh wave to backfigure the stiffness and thicknesses of the surface layer. However, this smoothing operation is quite straightforward in most cases.

CASE STUDIES

This adaptation of the SASW method for determining the modulus and thickness of the pavement surface layer has been used on many pavement sections in Texas, including 10 sections at the Texas Transportation Institute Annex of Texas A&M University. In all cases, the thicknesses of the pavement surface layer were known. Results from four of these sites are presented in the following sections.

New Highway in Austin, Texas

Tests were performed on a new asphalt concrete pavement about 4 days after placement. The resulting dispersion curve is shown in Figure 12. The surface layer exhibited some frequency dependence as noted by the inclined portion of the initial part of the dispersion curve. The average value of V_R is about 4,500 ft/sec, which results in a Young's modulus of about 2.8×10^8 psf. The thickness was estimated to be 0.51 ft as compared with 0.58 ft measured by cores, a reasonable comparison.

The value of the modulus seems too large in comparison with values determined by conventional laboratory tests. As mentioned earlier, moduli measured at strain levels associated with seismic testing are maximum values. Second, the high frequencies used in the SASW test result in higher values of stiffness for AC material. Tests performed on cores of this material to evaluate the frequency effect are shown in Figure 13. The effect of frequency is significant. If one wanted the modulus at 30 Hz (say to compare with the FWD), then the SASW value would be divided by a factor of about 4; hence the modulus would be 7.0×10^7 psf.

TTI Annex

The experimental dispersion curve calculated from measurements on one test section at the TTI Annex is shown in Figure 14. Using an average value of 5,200 ft/sec for the surface wave phase velocity, a Poisson's ratio of 0.33, and a unit weight equal to 145 pcf, the resulting Young's modulus is determined to be 2.7×10^6 psi for the AC layer. Again, the stiffness of the asphalt concrete is high because of the small strains and high frequencies involved. The thickness of the surface layer is estimated to be 0.42 ft. Cores from the site show the thickness is 0.42 ft, a very good comparison.

Monitoring Changes with Time

To illustrate the usefulness and sensitivity of this approach in testing the surface layer, changes in the stiffness of the layer

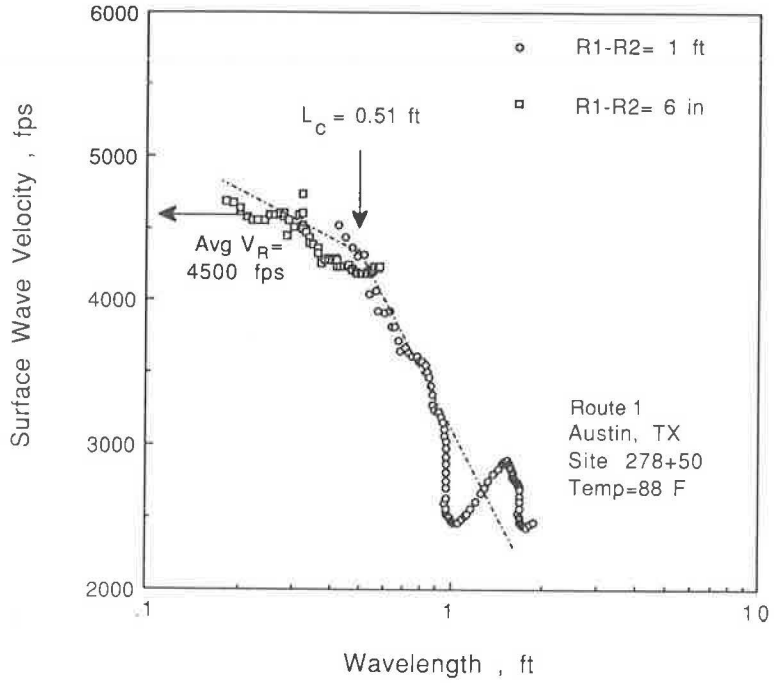

FIGURE 12 Dispersion curve measured on new ACP about 4 days after placement.

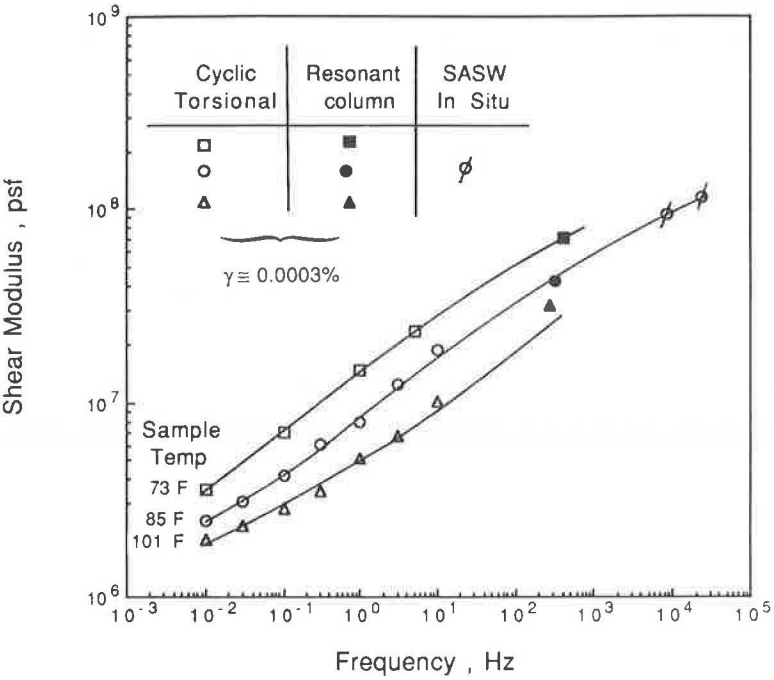

FIGURE 13 Influence of frequency and temperature on the small-strain shear modulus of asphalt concrete: sample cored from a new highway in Austin, Texas.

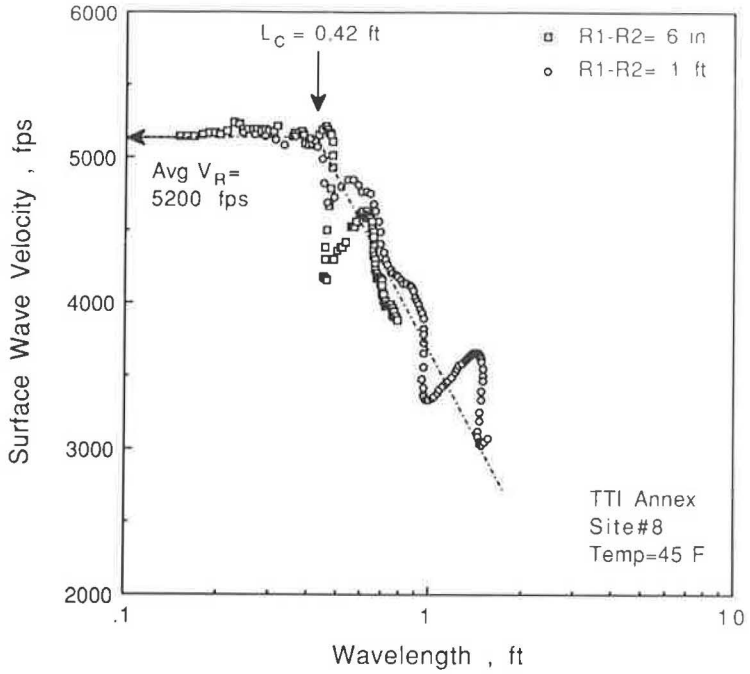

FIGURE 14 Dispersion curve measured on ACP section at the Texas Transportation Institute Annex in College Station.

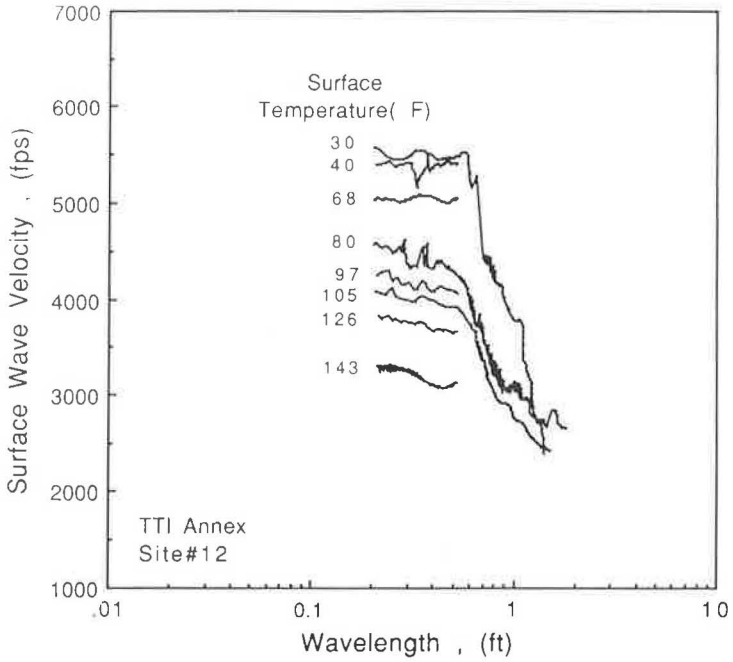

FIGURE 15 In situ measurement of the variation in stiffness of an AC layer with temperature.

with time were measured in situ. The first case, shown in Figure 15, shows the influence of temperature on the stiffness of an AC layer at the TTI Annex. The second case, shown in Figure 16, shows the stiffening of a portland cement concrete layer during curing (*16*). In both cases, the changes in the surface layer were easily measured with a sensitivity unattainable with any other in situ test.

CONCLUSIONS

A new adaptation of the SASW method to determine the moduli of the surface layer of both asphalt concrete and portland cement concrete pavements using surface waves has been developed. This method may also be used to provide a reasonable estimate of the thickness of the pavement surface

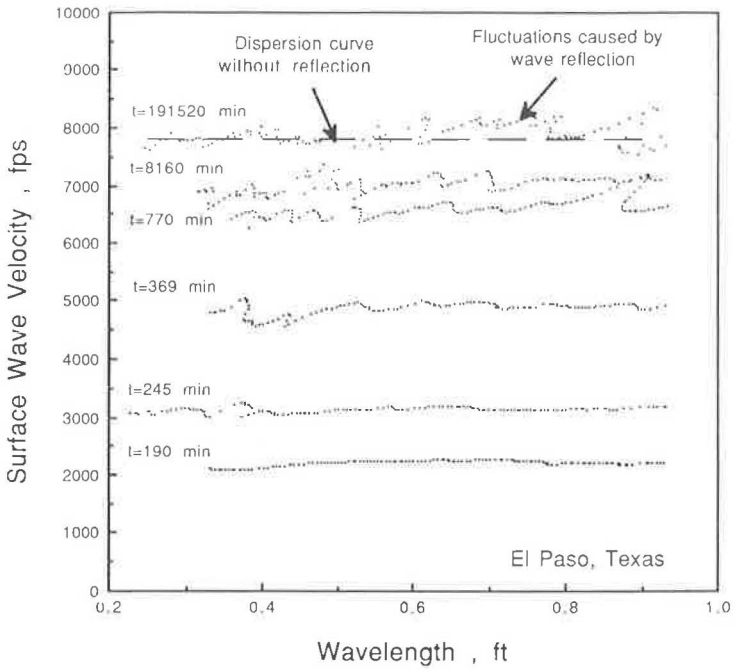

FIGURE 16 Dispersion curves measured on a continuously reinforced PCC pavement section during curing at various times after addition of water to the mix.

layer. The most important features of the technique are the following:

1. Testing can be rapidly performed in the field. At the present time, approximately 5 min is required to perform the test at each location. The time required to conduct the test can be further reduced by automating the placement of the source and receivers.
2. Values of Young's modulus and estimates of the thickness of the pavement surface layer are available immediately in the field. The calculation of these values is based on a simple, straightforward procedure that can be easily implemented.
3. Young's modulus values are calculated using a theoretically sound procedure based on the dispersive property of surface waves. Analytical studies presented herein establish the validity of this approach.
4. Unlike other nondestructive test methods, this technique is very sensitive to the modulus of the pavement surface layer.
5. Because of the small strain levels that exist in seismic testing, measured moduli correspond to maximum values. Also, because of the high frequencies involved, moduli of AC material need to be reduced to compare with moduli evaluated by other nondestructive field tests such as the falling weight deflectometer or Dynaflect.

ACKNOWLEDGMENTS

This work was supported by the Texas State Department of Highways and Public Transportation. The authors wish to express their appreciation for this support.

REFERENCES

1. S. Heisey, K. H. Stokoe, II, and A. H. Meyer. Moduli of Pavement Systems from Spectral Analysis of Surface Waves. In *Transportation Research Record 852*, TRB, National Research Council, Washington, D.C., 1982, pp. 22–31.
2. S. Nazarian, K. H. Stokoe, II, and W. R. Hudson. Use of Spectral Analysis of Surface Waves Method for Determination of Moduli and Thicknesses of Pavement Systems. In *Transportation Research Record 930*, TRB, National Research Council, Washington, D.C., 1983, pp. 38–45.
3. S. Nazarian and K. H. Stokoe, II. Use of Surface Waves in Pavement Evaluation. In *Transportation Research Record 1070*, TRB, National Research Council, Washington, D.C., 1986, pp. 132–144.
4. J.-C. Sheu, G. J. Rix, and K. H. Stokoe, II. Rapid Determination of Modulus and Thickness of Pavement Surface Layer. Paper presented at the 66th Annual Meeting of the Transportation Research Board, Washington, D.C., 1987.
5. R. Jones. Surface Wave Technique for Measuring the Elastic Properties and Thickness of Roads: Theoretical Development. *British Journal of Applied Physics*, Vol. 13, 1962, pp. 21–29.
6. R. Jones. Following Changes in the Properties of Road Bases and Sub-Bases by the Surface Wave Propagation Method. *Civil Engineering and Public Works Review*, May 1963, pp. 613–617.
7. N. A. Haskell. The Dispersion of Surface Waves in Multilayered Media. *Bulletin of the Seismological Society of America*, Vol. 43, 1953, pp. 17–34.
8. S. Nazarian. *In Situ Determination of Elastic Moduli of Soil Deposits and Pavement Systems by Spectral-Analysis-of-Surface-Waves Method (Practical Aspects)*. Research Report 368-1F, Center for Transportation Research, The University of Texas at Austin, May 1986, pp. 27–75.
9. E. Kausel and J. M. Roesset. Stiffness Matrices for Layered Soils. *Bulletin of the Seismological Society of America*, Vol. 71, No. 6, Dec. 1981, pp. 1743–1761.

10. R. J. Apsel. *Dynamic Green's Functions for Layered Media and Applications to Boundary Value Problems.* Ph.D. dissertation, University of California at San Diego, 1979.
11. S. W. Hull and E. Kausel. Dynamic Loads in Layered Half-Spaces. *Proc., 5th Engineering Mechanics Division Specialty Conference*, ASCE, Laramie, Wyo., 1984, pp. 201–204.
12. G. Gazetas and J. M. Roesset. Forced Vibrations of Strip Footings in Layered Soils. *Proc., National Structural Engineering Conference*, ASCE, Madison, Wis., Aug. 1976, pp. 115–131.
13. R. J. Aspel and J. E. Luco. On the Green's Functions for a Layered Half-Space, Part II. *Bulletin of the Seismological Society of America*, Vol. 73, No. 4, Aug. 1983, pp. 931–951.
14. E. Kausel. *An Explicit Solution for the Green Functions for Dynamic Loads in Layered Media.* Research Report R81-13, Massachusetts Institute of Technology, Cambridge, 1981, pp. 5–62.
15. K.-Y. Shao. *Dynamic Interpretation of Dynaflect, Falling Weight Deflectometer and Spectral Analysis of Surface Waves Tests on Pavement Systems.* Research Report 437-1, Center for Transportation Research, The University of Texas at Austin, 1986, pp. 33–49.
16. G. J. Rix, J. A. Bay, and K. H. Stokoe, II. Assessing In Situ Stiffness of Curing Portland Cement Concrete with Seismic Tests. Presented at the 69th Annual Meeting of the Transportation Research Board, Washington, D.C., 1990.

Publication of this paper sponsored by Committee on Pavement Monitoring, Evaluation, and Data Storage.

Criteria for Evaluating Pavement Imaging Systems

CARL HAAS AND SUE MCNEIL

A number of pavement imaging systems have been developed in the last few years. Choosing the system that will best fit an agency's needs and resources is a difficult task, because of the wide variation of alternatives. However, automated pavement imaging systems technology is mature enough to be broken down into a distinct set of elements and activities. Understanding the elements, how they are combined, and the design tradeoffs between them is necessary to develop and understand criteria with which a pavement imaging system can be evaluated. A description is therefore presented of the hardware, software, and procedural elements that are used to acquire, store, process, report, and use pavement distress data. On the basis of this knowledge, a set of criteria is developed for evaluating pavement imaging systems. Three example systems are used to illustrate element combinations, and to illustrate how the criteria can be used to evaluate alternatives in practice.

Interest in automated pavement imaging systems is increasing as system developers are demonstrating that accurate pavement surface distress data can be collected at relatively high speeds. However, the variety of approaches to data collection, processing, and storage is bewildering, making the selection of a particular system a difficult task. In order to assist decision makers, a set of criteria is described that can be appraised for any imaging system to ensure consistent, rational comparisons of systems. Pavement condition data and developments in automated pavement distress data collection bear out the importance of these criteria.

Pavement condition data are widely used in pavement management systems to select maintenance and rehabilitation strategies and to predict future performance (*1*,*2*). A commonly used measure of pavement condition is surface distress (*1*). Many agencies have developed methods for assessment of pavement surface distress on the basis of the density of each distress type and severity of distress (*1*,*3*,*4*). With rare exception, the evaluation of pavement distress has been performed by manual observation of the surface condition. However, there are several compelling reasons for automating the recording and evaluation of pavement distress. These reasons include the need to reduce data collection costs, to improve data quality, and to improve the safety of the data collection effort. Visual surveys are subjective, and almost always lead to inconsistencies in distress detail over space and across evaluations. In addition, they require extensive time and resources for data collection. Given current constraints in time and resources, visual techniques are limited to small sample sizes, simple record keeping procedures, and infrequent data collection. Automated techniques are potentially more consistent and thorough. Furthermore, there is likely to be more emphasis on condition data with the mandate from FHWA for all state highway agencies to develop pavement management systems (PMSs), and more agencies will be looking for fast, efficient ways to collect data.

Automated technologies have already been introduced to replace or complement current data collection methods. Several research and development efforts, both in the United States and abroad, have focused on the development of automated methods for pavement surface distress evaluation. The results of these efforts vary in cost, complexity, and functionality. Examples range from laboratory-based prototypes with automated image processing to streamlined, all-purpose survey vehicles. These efforts include the ADDA system (*5*), the PCES system (*6–8*), the ACM system (*9*), the EKTRON system (*10*), the French GERPHO system (*11*,*12*), the Gulf Research Institute system (*13*), and the Komatsu system (*14*). Though a great deal of effort has recently been applied to this area of research, no one system stands out in terms of overall performance as the results of field tests indicated (*15*).

These new technologies for automated detection of surface distresses are generally faster, more objective, and more consistent than human observations. Although the potential advantages of the new technologies are clear, they may be costly, subject to bias, and their introduction will require additional training. The selection of the best or most appropriate pavement imaging system for a particular organization, such as a state highway agency, is not a clear decision. In addition, because these systems have not been operative for long, and are mostly in the development and testing phase, their accuracy and performance are not fully characterized. This paper develops and describes criteria to assist in the evaluation and comparison of pavement imaging systems. These criteria can then be used to make subjective judgments, or they can be used as input to multiobjective and multiattribute decision making tools such as the analytical hierarchy process (*16*). The criteria are applied to two existing systems and a hypothetical system to demonstrate their use. The elements of pavement imaging systems and the three systems used to demonstrate the application of the criteria are described in the following section.

ELEMENTS OF PAVEMENT IMAGING SYSTEMS

To develop pavement imaging systems evaluation criteria, it is necessary to first understand the systems' parts, what they do, and how they interact. This section discusses how elements

Department of Civil Engineering, Carnegie Mellon University, Pittsburgh, Pa. 15213.

are combined to form a pavement imaging system, and it identifies and describes those elements common to many pavement imaging systems. Design tradeoffs between elements are also discussed. Three system architectures are used to illustrate these concepts. Two of the systems are currently in use, and one is a hypothetical design.

Pavement imaging systems integrate hardware, software, and procedural elements to perform several actions on pavement data. The hardware elements include computer, sensing, illumination, and other components. The software elements are algorithms and processes implemented using high level code or machine language. The procedural elements represent particular approaches to the design and operation of the pavement imaging system, as well as the output of the system.

The actions performed by the hardware, software, and procedural elements are (a) sensor data acquisition, (b) sensor and processed data storage, (c) data processing, (d) reporting distress condition data, and (e) using the data for various applications. For most actions, various combinations of hardware, software, and procedural elements can be used (Figure 1). As indicated in the figure, the pavement imaging system hardware is used for data acquisition, storage, processing, and reporting. Examples of devices that could be used for these actions are a line scan camera, a video cassette, a workstation type computer, and a printer, respectively. Although software is used in almost all activities, configuration choices primarily exist in processing, such as coding of image processing algorithms, and reporting, such as graphical presentation of results. Finally, procedural elements are inherent in all the actions. They include decisions such as the sampling strategy for data acquisition, the processing sequence for storage, the device location and speed of processing, the level of aggregation of the data for reporting, and the type of data produced for an intended use.

SAMPLE ARCHITECTURES

Three sample architectures are presented to illustrate the use of the criteria for evaluation. Two architectures, the PCES and the Komatsu systems, continue to be under development. The third architecture is a hypothetical system.

PCES System Architecture

The PCES Pavement Distress Imager I (*8*) (Figure 2) is an on-board, real time pavement imaging system. It uses intense illumination and 27-μsec exposure CCD line cameras to acquire image data line by line, and completely process it as the vehicle moves down the road at speeds up to 50 or 60 mph. It uses a feedback image processing control strategy, by selecting binarization thresholds based on histograms accumulated from the last eight frames processed. The processing hardware is arranged in a pipeline architecture with a 32-bit controller. The hardware, which requires environmental control for operation, uses dynamic threshold selection and 4- × 4-ft area thresholding. Possible gross changes in surface texture and color are flagged automatically, whereas manual flagging is used for other artifacts such as patching. The system covers 33 percent of a 4-m-wide pavement surface, so it will not observe progressive edge cracking. However, the system can

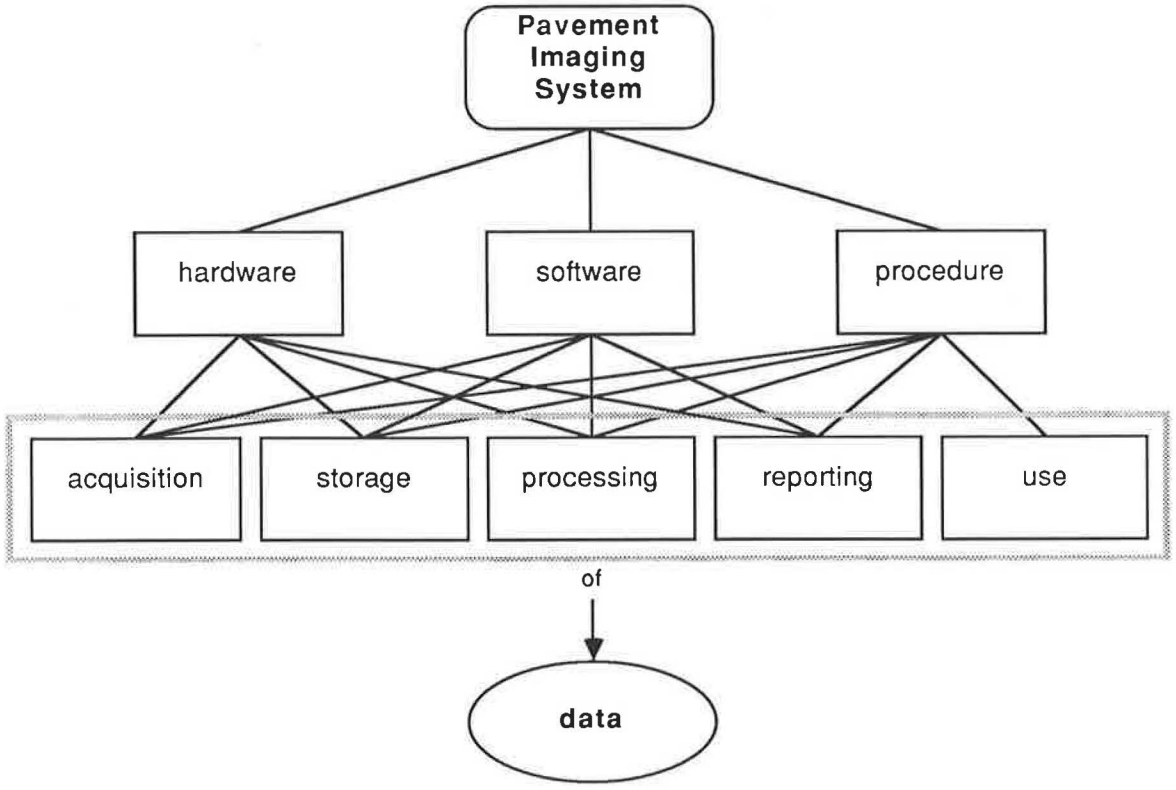

FIGURE 1 Elements and actions of pavement imaging systems.

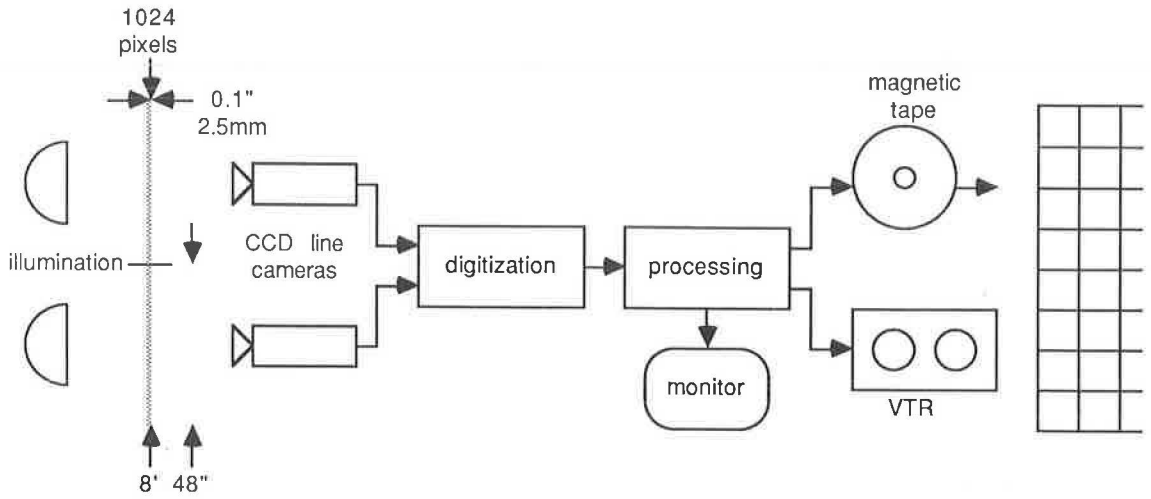

FIGURE 2 PCES system architecture.

produce an estimate of the extent of cracking in each 1-ft-square section covered, on the basis of a count of the number of black pixels left in the square after thresholding. Identification of type of cracking is suggested using spatial reasoning on the results. Although the threshold selection is responsive to surface conditions, it is unclear how the cracking magnitude estimates that are the results will be calibrated between pavement sections and with manual observations.

Komatsu System Architecture

The Komatsu Automatic Pavement Distress Survey System (*14*) shown in Figure 3 acquires cracking, rutting, and longitudinal profile data concurrently at up to 40 km/hr. The rutting and longitudinal profile data are processed in real time, on board the survey vehicle. The image data analysis subsystem, which is discussed here, processes image data at a rate up to 450 m/hr or about ¼ mph, and can process the data on board. The system uses argon laser irradiation of a strip in front of the vehicle, 4 m wide. The strip is scanned for imaging information using a photomultiplier tube and the image data are stored on a high-density video tape recorder device for later analysis. The processing system uses a parallel-processing architecture with a variable number of processors to implement a sophisticated processing algorithm that is potentially capable of identifying width, length, and direction of cracks, and of identifying type of cracking within 0.5-m-square

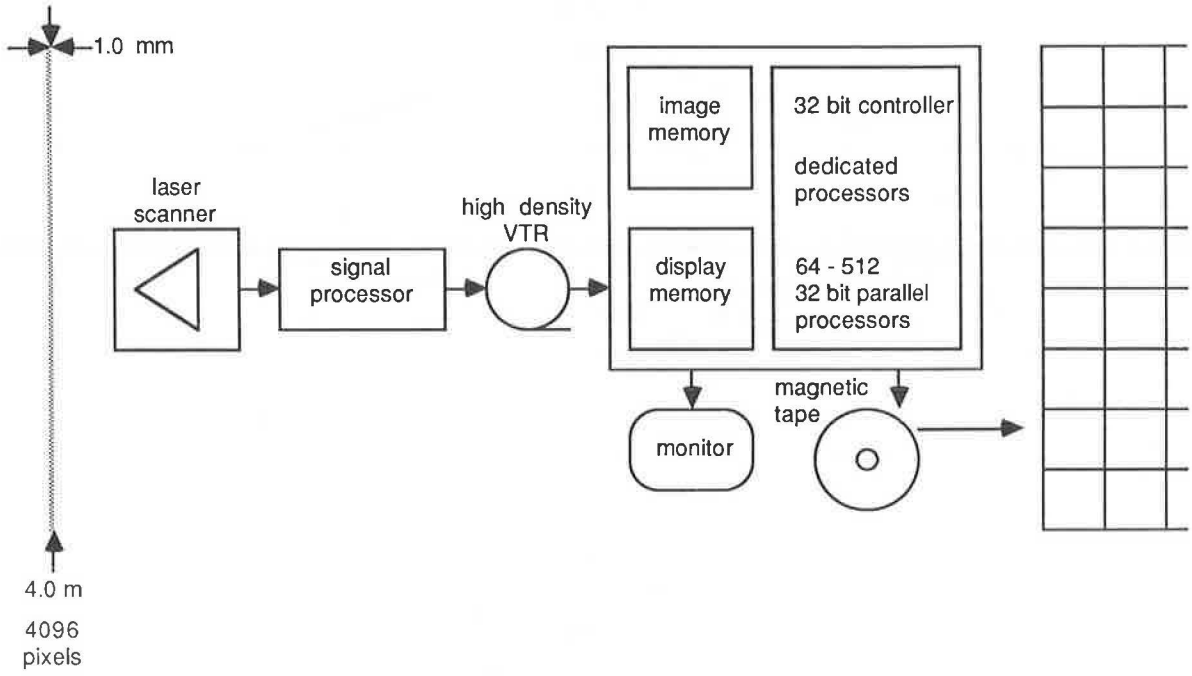

FIGURE 3 Komatsu system architecture.

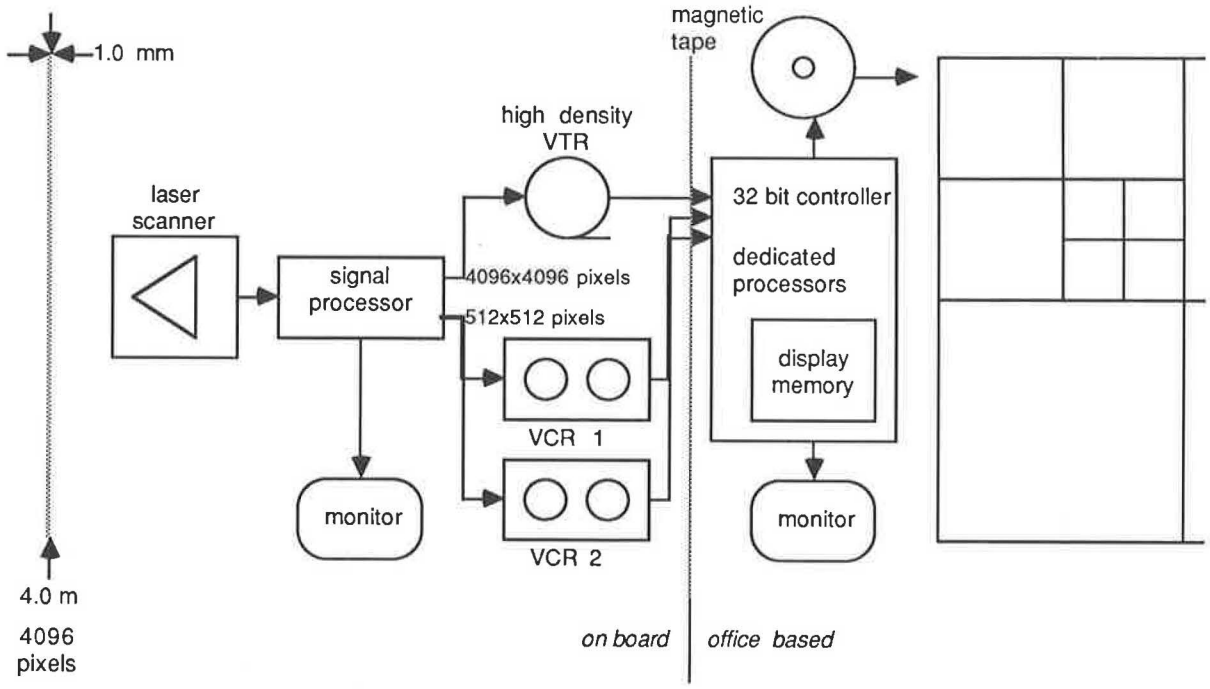

FIGURE 4 Hypothetical system architecture.

sections. The system is estimated to perform at 80 percent of the accuracy of manual identification with hand digitization of cracks on a view screen.

Hypothetical System Architecture

The hypothetical system (Figure 4) uses the Komatsu image data acquisition and storage technologies. Samples consisting of 5 percent of the road length are siphoned off the high-density raw image data stream. The remaining data are digitally compressed by a factor of four in each dimension and stored on two standard density, addressable VCR systems. Compression and storage are performed on board in order to extend the Komatsu data acquisition system's current range of 10 km by several times. [A feasible alternative is a photographic image acquisition and storage system such as the Pasco (*17*) or the GERPHO (*12*) system coupled with an office-based projection imaging configuration.] Crack width and length distributions are derived from the high-density data sample for every 100 m section. The standard-density data for each section are processed to yield cracking location and type using a simple edge vector based classification algorithm (*5*). This is possible in near-real time using dedicated convolution processors. The distributions from the high-density sample are used to further characterize the low-density results (*18*), for a maximum amount of information with a minimal amount of processing. The results are stored in a strip quadtree format (as described by Haas and Hendrickson in another paper in this Record), which includes type location and density information, and then integrated with other condition data for presentation and further processing at various levels of aggregation.

CRITERIA

The three system configurations described in the previous section illustrate combinations of hardware, software, and procedural elements. The evaluation of any system is complicated for several reasons. First, tradeoffs between the design elements make direct comparison of actions difficult. Second, the interrelationships between the actions vary, because particular actions occur at different points in the system. Finally, the system output differs in form, quantity, and quality. Because of these complicating factors, well-defined criteria for evaluating imaging systems are needed so potential users of these systems can make consistent, rational decisions.

Six criteria have been identified. The criteria are not mutually exclusive or collectively exhaustive but were chosen to capture the important features of systems that should be considered in the evaluation. They are economic costs, system reliability, quality of data, survey rate, manufacturer support, and system flexibility. These criteria are described in the following paragraphs.

Economic Costs

Economic costs include all costs incurred in acquiring, operating, and maintaining the system over its life. For this one criterion alone, tradeoffs are present because the more automated the system the less the operating costs but the higher the acquisition costs. A general discussion of these costs is given by Kaimakamidis (*19*). Because systems may be acquired through purchase, annual contract, licensing agreements, or leasing, the different components of costs may be included in different ways. For example, some costs included in the

economic analysis may be annualized costs rather than initial costs. The selection of a financing approach and contractual agreements is independent of the economic analysis. Because the economic costs differ over the life of the system, a planning horizon and minimum attractive rate of return must be selected, and the economic analysis must consider the effect of assumptions regarding these parameters as well as the life of the system. Therefore, acquisition costs include initial costs, purchase costs, financing or leasing costs, and personnel training costs. Purchase costs not only reflect system development cost and material acquisition and assembly, but options for system operation as well. For example, the system may include a custom-engineered survey vehicle or may be added to an existing vehicle.

Operating costs include personnel, energy, and expendable hardware. Personnel are required to navigate the system, and to control processing and interpret the results. These costs vary with the extent of automation, and the required frequency and procedures for recalibration of the equipment. Vehicular and energy costs and the type, cost, and rate of usage of storage media are also important operating costs. Large survey vehicles with extensive on-board computing may be heavy fuel users. High-density, reusable storage media are expensive but possibly better economic value than lower cost, low-density media.

Maintenance costs include maintenance of physical equipment (vehicle, power supply, computing equipment, and sensors), software, and storage media. These elements may be covered under an annual service contract. Physical equipment maintenance ranges from routine cleaning and preventive maintenance, such as oil changes, to component replacement. Software maintenance includes implementing software improvements and updates, ensuring compatibility of hardware and software, updating documentation, and supporting user applications. Storage media maintenance involves removal of incorrect and out-of-date data. The time required for this maintenance varies with the approach used for storing data, the amount and type of data stored, and the ultimate use for the data.

Economic costs are measured in discounted constant dollar amounts over a planning horizon using a figure of merit such as the net present value (*20*). The evaluation of the economic costs of using a new technology for condition data collection based on net present value analysis is presented by Kaimakamidis (*19*).

System Reliability

The reliability of the system is a function of the quality of the manufactured system, and operation and maintenance of the system over its life. This criterion should be evaluated in terms of the expected frequency and duration of downtime, and the implications of downtime. For example, systems with low expected frequency of downtime but with a long expected duration of downtime may be preferable to a system with frequent but short downtime, if downtime can be used efficiently. The implications of downtime may be measured as the costs of other equipment or personnel that are idle when the system is not functioning or the cost to rent similar equipment.

Quality of Data

The quality of data must be assessed in two different ways. The first way is from the perspective of the intended use of the data. The second way is in terms of the accuracy of the data. Each approach is considered in the following paragraphs.

The form of the data directly affects the quality of data for the user in terms of whether or not the data meet the user's needs. Form may be defined as

- Type of measurement, such as the linear foot of cracking or extent of cracking. Therefore, the types of measurements vary from the recognition of the presence of distress to measures of distress type, extent, and severity.
- Coverage of the system in terms of the fraction of the area surveyed. This fraction is determined by field of view (that is, the width observed during one pass of the system), the area of pavement observed as the system moves along, and the data collection strategy used to obtain transverse coverage. Because most systems operate with the traffic stream, they are constrained to operate in the center of a lane and only one pass is made in each lane.
- Representation of the data. The data collected may be presented at various levels of aggregation. For example, data may be averaged over a pavement section, or disaggregate data can include the location, orientation, width, and length of individual cracks.

Because most agencies have experience with visual assessments of pavement surface distress, if the form of the data is not compatible with existing procedures, then adoption of the system will require changes in other procedures within the organization. For example, manual visual surveys may inspect 100 percent of the pavement, whereas an automated system (or survey) may observe only parts of the pavement. Alternatively, cracks may be measured by severity (width) and extent rather than total length. Different forms of data may require revision of decision criteria used for rehabilitation and maintenance strategy selection.

The accuracy of the data is an extremely important component of quality, because inaccurate data may be biased or show great variability and result in poor management decisions. The implications of inaccurate data include premature rehabilitation, increased user costs due to deferred maintenance and rehabilitation, and inadequate budgets for necessary projects (*19*). Errors enter the data collection process in each of the elements shown in Figure 1 and because of the interrelationships between the elements, the errors are propagated throughout. The accuracy of the final measurement depends on the hardware, the software, and the procedures used for calibration and registration. The procedures may be automated, operator assisted, or manual. The accuracy of the data is difficult to assess without extensive validation. Because experience with these systems is relatively limited, experiments need to be conducted. Accuracy may be specified for various elements in terms of resolution, but overall system accuracy should include error bounds with confidence intervals. It is important to realize that high levels of accuracy are not necessary for all applications. For example, planning for rehabilitation of a network does not require accurate measurements of the width of each crack.

Survey Rate

Although the survey rate has already been considered in determining operating costs, the survey rate is important for determining the impact of the vehicle on traffic and the number of units required to cover the required area at a reasonable frequency. Survey rates are commonly measured in lane-miles per hour and should also note any operating limitations, such as being restricted to night time operation.

Manufacturer Support

The availability of manufacturer support is important, because most organizations are unlikely to have sufficient technical expertise to independently use, operate, and maintain these systems. Manufacturer support can include upgrades, availability of training and service contracts, and easily accessible technical support.

Flexibility of the System

Both sensing and computing software and hardware have undergone rapid technological change. Although this technology is maturing and stabilizing, systems need to be sufficiently flexible to embrace changes that will make the system more efficient, more accurate, or decrease costs. Similarly, if additional data are required or data are needed in a different form, the ideal system can be modified to provide the data.

The set of criteria just described is summarized in Table 1. The table also indicates the type and units of possible measures that may be used and the optimal levels for each of the criteria. These levels cannot be achieved for all criteria together because there are clear tradeoffs between them. Although several other criteria can be identified, they are generally captured in those listed. For example, a criterion for ease of use has not been included because this attribute should be captured in the operating and maintenance costs and the evaluation of the form of data.

EVALUATION EXAMPLES

The evaluation of a system through the use of these criteria in itself will not ensure the best alternative. The specification of alternatives including assessing the value of the information gained, comparison with the null alternative and the status quo, various configurations of a system, and financing alternatives are all important components of the final evaluation. The examples chosen for this evaluation are not intended to be exhaustive but to demonstrate the use of the criteria.

Much of the information required for a full evaluation of the pavement imaging system examples described here is not available at this time. No pricing data have been published by the manufacturers; however, some approximate, comparative economic cost estimates based on system component costs are possible. Lack of experience with any of the systems makes evaluating system reliability and manufacturer support difficult, but data quality, survey rate, and system flexibility are largely dependent on the system design, so they can be evaluated more accurately. Although some criteria are qualitative, the set of criteria offered provides a consistent basis on which to evaluate and compare different systems. The ultimate choice depends on the user's needs, resources, and intended applications.

TABLE 1 CRITERIA FOR EVALUATION

System Criteria	Measurement Type	Measurement Units	Optimum
Economic Cost	Discounted Net Present Value	$	Minimum Cost
Reliability	Frequency Downtime Duration of Downtime Implications	Rate\Year Hours $	Minimum Frequency Minimum Time Minimum Cost
Quality - Form	Qualitative Assessment of Appropriateness	Not Applicable	Compatible with Existing Approaches
Quality - Accuracy	Error Bound Confidence Interval	%	Minimum Error Maximum Confidence
Survey Rate	Speed Restrictions	Lane Miles per hour Not Applicable	Maximum Speed None
Manufacturer support	Qualitative Assessment of Availability	Not Applicable	Readily Accessible
Flexibility	Qualitative Assessment	Not Applicable	Very Flexible

TABLE 2 SUMMARY OF EXAMPLE EVALUATIONS

System Criteria	PCES	Komatsu	Hypothetical
Economic Cost	Moderate	High	Moderate
Reliability	Unknown	Unknown	Unknown
Quality - Form			
o Coverage	30%	100%	100%
o Type	Extent and location	Location, Type, Severity Extent or Density	Location, Type, Severity Extent or Density
o Representation	Simple	Measures per 0.5 sq meter	Measures at any level of aggregation
Quality - Accuracy	Moderate	Moderate	Good
Survey Rate	Up to 60 mph	Up to 40 mph	Up to 40 mph
Manufacturer support	Unknown	Unknown	Unknown
Flexibility	Poor	Poor, but has potential	Very good

Evaluations of the three example systems are summarized in Table 2. The pavement imaging subsystem of the Komatsu system is likely the most costly in terms of component costs because of its advanced scanning mechanism, the high-density VCR storage device, and the large number of expensive processors in the processing system. However, the system collects several measures of pavement condition, and hardware costs cannot be simply allocated to vision. The PCES system is likely less costly because it has fewer and generally simpler components. The hypothetical system will cost significantly less than the Komatsu system, because it has far fewer processing components. If a photographic film data acquisition system is used, costs may be reduced even more, but at the possible expense of image quality.

The PCES system reliability is unknown, but should be good because of the relative simplicity of the system. The Komatsu system reliability is unknown, but it is being used in practice. The hypothetical system may be the most reliable because of the office-based location of critical system components, and its relative simplicity.

The quality of data for each system is summarized in Table 2. The Komatsu system accuracy is highest in terms of resolution, and its overall quality of data is the greatest. The qualitative evaluation presented in the table should be replaced by actual performance data when they become available. The PCES system survey rate is excellent, whereas the Komatsu system survey rate is poor. The hypothetical system's survey rate would probably be close to but less than the PCES rate. Manufacturer support is unknown at this time, but it will become a significant factor as the technologies mature and enter the market place.

The flexibility of the PCES system is poor because the processing algorithms are implemented as hardware. The method of code development is not known, however. Because of the Komatsu system's interim, recognized crack segments representation, its potential flexibility is good. The hypothetical system's flexibility is very good, because of the dual raw data storage format, and the office-based general processing system that would be coded in a high-level language.

In summary, the Komatsu system is probably most appropriate for small-scale, intensive, and detailed surface characterization activities. The PCES system would be most appropriate for surveying large networks to acquire condition information for simple network pavement management systems. The hypothetical design should be appropriate for both those types of applications and more, depending on the current need.

CONCLUSIONS

Pavement imaging systems are formed from hardware, software, and procedural elements in order to perform several actions on pavement data (Figure 1). The actions include (a) sensor data acquisition, (b) sensor and processed data storage, (c) data processing, (d) reporting distress condition data, and (e) using the data for various applications. Each action may consist of various combinations of hardware, software, and procedural elements. On the basis of this understanding of pavement imaging systems, criteria can be developed for evaluating and comparing system alternatives.

The set of criteria proposed includes

1. Economic costs,
2. System reliability,
3. Quality of data,
4. Survey rate,
5. Manufacturer support, and
6. System flexibility.

Three systems that were used as example alternatives for evaluation included the PCES Pavement Distress Imager I, the Komatsu Automatic Pavement Distress Survey System, and a hypothetical system design. The results of the evaluations were that the Komatsu system is probably most appropriate for small-scale, intensive, and detailed surface characterization activities. The PCES system would be most appropriate for surveying large networks to acquire condition information for simple network pavement management systems. The hypothetical design should be appropriate for both those types of applications and more, depending on current need.

In conclusion, a set of criteria has been developed and illustrated here that can be used to consistently evaluate pavement imaging systems.

APPENDIX—PAVEMENT IMAGING SYSTEM ACTIONS

This appendix considers each of the actions performed by a pavement imaging system in terms of hardware, software, and procedural elements. Only elements involving choices are discussed in detail. For example, software for data storage is not discussed because it almost entirely depends on and is integrated into the type of storage device. The order in which the elements are considered for each action reflects the way design decisions are likely to be made. For example, data acquisition options for sensor hardware are described first, because this is the most fundamental choice.

Data Acquisition

Hardware for data acquisition includes the choice of sensor and illumination. Typical sensors include laser, video, 35-mm film, line scan camera, and slit integrator. Illumination may be natural or artificial. Artificial illumination can come from a variety of sources, such as single-frequency-band or high-candle lamps. Sensor and illumination hardware may be characterized in terms of the following attributes:

- Motion blur—due to vehicle speed and sensor exposure duration; exposure duration can be reduced with intense lighting produced by artificial illumination.
- Dynamic range—the range of combined surface luminance and reflectance (real grey levels) that the sensor can detect.
- Resolution—depends on type, positioning, and number of sensors; the higher the resolution per unit area, the greater the processing requirements.
- Environmental conditioning—relates the external conditions that the sensor hardware can endure and the internal operating conditions (such as cooling) required.

Sampling is the procedural element that determines the following characteristics of the data acquisition activity:

- Scanning—its density per unit area directly affects processing requirements.
- Overall surface coverage—different patterns that may be derived for local, project, and network level analysis also affect processing requirements.

Storage

Devices store data in one or both of the following forms:

- Analog—images may be stored as analog signals on videotape or compact discs; they can then be played back for visual inspection or for digitization and processing; image addressing is possible on both these mediums, allowing the possibility of advanced feedback control methods for processing.
- Digital—image data processed through to pavement condition index (PCI) data can be stored in digital format; image data are usually managed frame by frame in RAM, because it is impractical to store many frames of image data in digital format, even on magnetic tape or compact discs [one existing system (*14*) would require 400 MB of storage for 100 m of pavement image data]; therefore, digital storage in the form of RAM frame buffers and system memory is used to store image frames and intermediate processing results, whereas hard disc and magnetic tape devices are used to store general surface representations and final processing results.

The storage hardware elements are characterized by the following attributes:

- Reuse—although most storage media can be written to and read from many times, most compact discs are WORM (Write Once Read Many times) type devices; compact discs are also expensive, but their advantage is quick image addressing and access.
- Access speed—pavement image processing systems require large amounts of RAM, because moving image data back and forth between a hard disc and RAM creates a data processing bottleneck, making real time or close to real time image analysis impossible.
- Capacity—analog storage devices have tremendous capacity for image data and are used to store raw image data; hard disc and tapes can be used to store sample images and processing results; RAM is used for dynamic storage of image frames and process data.

The processing sequence used for data storage has significant impacts on other activities, such as the demands on memory and choice of memory device to meet those demands. For example, real time, on-board (a vehicle) processing will require large amounts of RAM for frame data, may not require any analog storage, and may require a common magnetic tape device for storage of survey results.

Processing

Several fundamental procedural choices affect the choices of hardware and software elements and the tradeoffs between these elements:

- Real time processing—processing of raw sensor data at the rate that it is acquired (not necessarily at the same time); however, it does necessitate the use of special computing hardware.
- On-board processing—processing of image data on the survey vehicle; advantages include immediate verification of results, and quick access for subsequent analysis; disadvantages include the necessity of real time processing, very little

flexibility of sampling and processing procedures, and commitment of hardware and software resources to restricted daily and annual use; of course, the data need not be fully processed on board, but this is the practice in current systems.

- Office processing—processing of data in the office; the advantages include the necessity of less hardware because the computers can work 24 hours per day (including days that a survey vehicle would be in transit or on vacation), the requirement of less robust hardware components, flexible sampling and processing, continuity between image data processing and pavement management software, and use of general computing resources for other purposes during off time; the disadvantages include delayed and less reliable manual verification (from relatively low resolution video records), and the costs that bad data would incur.
- Process control—represents the options for feedback control of image processing and depends on the choice of office-based or on-board processing and the sequence in which data are acquired, stored, and processed. For example, if the image data are stored on addressable video tape, a computationally efficient sampler could move ahead of the main image processor in the image sequence and guide application of subsequent analysis; the result would be the potential for increased sophistication and reliability of analysis with less processing and therefore fewer hardware resources.

These choices influence the nature and the required speed of processing and therefore necessitate the subsequent choice of processing hardware before software.

Whereas general-purpose processors are required to some extent in any pavement imaging system, there is a direct tradeoff or exchange between dedicated or special-purpose processors and software. The special-purpose processors can implement functions in real time that would take magnitudes more time if implemented in a high-level language on a general-purpose processor. The cost of such processor hardware, however, is far higher than functionally equivalent software, but if the software is too slow, at a certain point, time costs and practical considerations outweigh the hardware costs. Dedicated and special purpose hardware can be configured in various ways such as multiprocessor, pipeline, and array architectures.

- General-purpose processors—these include workstation computers and minicomputers that can be used to process raw image data, but are more often used for higher level analysis, and to control other hardware in the pavement imaging system.
- Dedicated processors—these are computers designed to perform a limited range of tasks such as convolution processing or histogram computation and look-up table operations.
- Special-purpose processors—these include computers designed to implement specific algorithms in hardware; they can be powerful but inflexible.

Several choices have to be made with respect to the software implementation of the processing including the environment, design approach, algorithms, and control of the system, as follows:

- Language—C and FORTRAN are usually used, because they are portable, and they provide high-level abstraction capabilities while at the same time allowing hardware level control; also most software toolkits are written in these two languages. Although assembly code may be used for embedded system software, the software is much more portable if it is developed on a host system and cross compiled for the target processors; portability permits future hardware upgrades with minimal software development cost.
- Design and mutability—software may be designed for specific hardware and for a specific purpose, or it may be designed to be easily modified as new hardware becomes available and new ideas emerge; the advantage of the former is usually speed of operation, whereas the advantage of the latter is flexibility, which can be important given the pace of technological advancement.
- Algorithms—algorithms for pavement image analysis have been extensively treated in the literature (e.g., *5*, *8*, *13*, *14*, *21*, *22*); they have been implemented in prototype and field systems. Many can be implemented in hardware or software, and they can be grouped into several distinct steps that can be combined and included or excluded in any number of ways, but usually in the approximate order of (a) image enhancement, (b) filtering, (c) data reduction, (d) feature extraction, (e) classification, (f) analysis, and (g) interpretation.
- System control—treated as a separate issue, because it is unlikely that any system can treat all pavement types and combinations of surface distress equally without some sort of calibration; the calibration may include selected intensive analysis and manual intervention, and usually results in adjusted filtering and classification parameters.

Reporting

Procedural choices for reporting the results of data acquisition and processing include the selection of the level of aggregation of the results, the delay time, and format. The impacts of these decisions are as follows:

- Level—network level analysis of pavement condition data is usually based on aggregate measures of section condition. Thus, a pavement imaging system should include the capability of reporting some form of PCI for each section of road surveyed. Alternatively, at the project level, detailed surface characteristics over a particular section are reported. Project level reporting may be included in a pavement imaging system for a cost greater than that of network level reporting, because more memory, computing power, and software are required.
- Delay time—the choice of on-board or office-based processing is only one factor affecting the choice of delay time between pavement data acquisition and reporting of analysis results; other factors include organizational procedure, which may allow a significant delay time; significant allowable delay time may create feasible conditions for cheaper office based processing.
- Format—a flexible reporting format may be included at some extra cost.

Software is required to implement the procedural elements listed as well as the following system options, if they are included:

- Data base integration—the imaging system software may be directly linked with a pavement condition data base to

enable data selection options for inspection and reporting, and for vertical integration with pavement management systems.

- Graphics—it is possible to represent pavement surface distress information at various levels of aggregation and in various formats for reporting purposes.

Output devices such as printers, plotters, and display screens, and computer hardware to provide access to the results have to be selected. A wide variety of off-the-shelf and special-purpose hardware is available.

Use

The intended use of the pavement imaging system's surface condition assessment reports imposes criteria and constraints on the other elements of the system.

- Maintenance selection and project level design—integrated with other condition data, the system output could be used by an automated pavement maintenance selection system, or for project level design once maintenance or rehabilitation action has been selected; of course, project level reporting is required.
- Resource allocation—the detail and significance of the condition data produced (surface distress) by a pavement imaging system may make accurate resource allocation possible; again, project level reporting capability is required.
- Deterioration modeling—detailed surface distress data along with other condition data may facilitate more accurate deterioration modeling; project level reporting is required.
- Network level pavement management—network level reporting is required.
- Maintenance operation—real time control is required.

REFERENCES

1. *NCHRP Synthesis of Highway Practice 76: Collection and Use of Pavement Condition Data.* TRB, National Research Council, Washington, D.C., 1981.
2. W. R. Hudson and R. Haas. *Pavement Management Systems.* McGraw-Hill, New York, 1978.
3. M. I. Darter, J. M. Becker, M. B. Snyder, and R. E. Smith. *NCHRP Report 277: Portland Cement Concrete Pavement Evaluation System.* TRB, National Research Council, Washington, D.C., 1985.
4. M. Shahin and S. Kohn. *Pavement Maintenance for Roads and Parking Lots.* Technical Report M-294, Construction Engineering Research Laboratory, U.S. Army Corps of Engineers, Dec. 1981.
5. C. Haas, H. Shen, and R. Haas. *ADDA System 1 (Automated Distress Data Acquisition and Evaluation System).* Final Report, OJTCRP Project 21156, Ontario Ministry of Transport, Aug. 1985.
6. D. Curphey, G. Cox, D. Fronek, and J. Wilson. Highway Pavement Surface Remote Sensing Using Video Image Processing. Presented at the ASCE Spring Convention, 1985.
7. G. Cox, D. Curphey, D. Fronek, and J. Wilson. *Remote Video Sensing of Highway Pavements at Road Speed.* Elsevier, 1986.
8. B. C. Butler, Jr. Pavement Surface Distress Segmentation Using Real Time Imaging. *Proc., 1st International Conference on Applications of Advanced Technology to Transportation*, C. T. Hendrickson and K. Sinha (eds.), ASCE, Feb. 1989.
9. D. Mahler. *Final Design of Automated Pavement Crack Measurement Instrumentation from a Survey Vehicle.* Final Report DTFH 61-86-C-001, FHWA, U.S. Department of Transportation, May 1985.
10. D. H. Mendelsohn. *Automated Pavement Crack Detection: An Assessment of Leading Technologies.* Development Paper for FHWA DTFH61-84-C-00077, EKTRON Applied Imaging, Bedford, Mass., 1984.
11. G. Caroff, P. Joubert, F. Prudhomme, and G. Soussain. Classification of Pavement Distresses by Image Processing (MACADAM SUYTEM). *Proc., 1st International Conference on Applications of Advanced Technologies in Transportation Engineering*, C. T. Hendrickson and K. Sinha (eds.), ASCE, Feb. 1989.
12. W. R. Hudson, G. E. Elkins, W. Uddin, and K. T. Reilley. *Improved Methods and Equipment to Conduct Pavement Distress Surveys.* FHWA-TS-87-213, ARE, Inc., Austin, Tex., April 1987.
13. L. C. Bomar, W. F. Horne, D. R. Brown, P. E. Smart, and J. L. Smart. *NCHRP Report 304: Determining Deteriorated Areas in Portland Cement Concrete Pavements Using Radar and Video Imaging.* TRB, National Research Council, Washington, D.C., Dec. 1988.
14. T. Fukuhara, K. Terada, M. Nagao, S. Kasahara, and S. Ichihashi. Automatic Pavement Distress Survey System. *Proc., 1st International Conference on Applications of Advanced Technology to Transportation*, C. T. Hendrickson and K. Sinha (eds.), ASCE, Feb. 1989.
15. K. R. Benson, G. E. Elkins, W. Uddin, and W. R. Hudson. Comparison of Methods and Equipment to Conduct Pavement Distress Surveys. In *Transportation Research Record 1196*, TRB, National Research Council, Washington, D.C., 1988.
16. T. L. Saaty. *Decision Making for Leaders.* Lifetime Learning Publications, Belmont, Calif., 1982.
17. PASCO Inc. USA. *PASCO Road Survey System.* Product Literature, 1988.
18. S. McNeil and F. Humplick. Evaluation of Errors in Pavement Surface Distress Data Acquisition. *Proc., 1st International Conference on Applications of Advanced Technology to Transportation*, C. T. Hendrickson and K. Sinha (eds.), ASCE, Feb. 1989.
19. I. Kaimakamidis. *Economic Evaluation of New Technologies for Construction.* Master's thesis, Carnegie Mellon University, Pittsburgh, Pa., Aug. 1989.
20. T. Au and T. P. Au. *Engineering Economics for Capital Investment Analysis.* Allyn and Bacon, Inc., Boston, 1983.
21. K. R. Maser and J. Schott. *Automated Visual Imaging for High Speed Inspection of Large Structures.* Final Report, National Science Foundation, Washington, D.C., July 1981.
22. M. Wigan and M. C. Cullinan. *Image Processing Applied to Roads: Surface Texture, Mensuration, Vehicle Shape and Number Detection.* Special Report 145, Australian Road Research Board, Nunawading, Victoria, Jan. 1987.

Publication of this paper sponsored by Committee on Pavement Monitoring, Evaluation, and Data Storage.

Visual Appearance of Surface Distress in PCC Pavements: I. Crack Luminance

TAHAR EL-KORCHI AND NORMAN WITTELS

Visual examination is widely used for evaluating the extent and severity of pavement distress. The visually assessed pavement surface condition is combined with structural information to rate the pavement on the basis of scoring systems that have been developed by the state transportation agencies to evaluate which pavement sections require regular maintenance, overlay, or complete reconstruction. Although scoring is often computerized, the raw data are usually collected by slow, laborious manual and visual methods during site inspections by trained field personnel and they are input into the computer manually. These methods are expensive and prone to subjectivity, error, and nonrepeatability. Automated surface distress evaluation has not developed rapidly because the accuracy of automated systems has not been sufficient to inspire confidence among the pavement engineers who have to rely on the evaluation results. System accuracy can be enhanced by using better engineering methods and data in designing the image acquisition and image processing portions of automated inspection systems. The visual signal—the apparent luminance of cracks in portland cement concrete (PCC) pavements and the contrast that they exhibit compared to surrounding pavement surfaces—is the input to the automated inspection system. The luminance depends on the reflectivities of the paving materials. Reflectivity measurement methods are specified and data are tabulated. In a companion paper in this Record computer modeling methods for determining and analyzing crack luminance are reported. The methods and data presented in these papers are useful for designing automated pavement inspection systems.

The deterioration of transportation systems in the United States is a problem of major concern to local, state, and federal agencies and to the public. Highways in the United States are deteriorating at an alarming rate due to normal aging processes and to traffic loads that exceed design limits. The nation's economic growth is critically dependent on a sound highway pavement system. The projected cost for maintenance through the year 2000 is estimated to be hundreds of billions of dollars, a problem compounded by decreases in available funding for restoration of this vital element of the infrastructure. Financial improvements are not expected, as maintenance and construction costs increase due to inflation in material and labor costs and as revenues decline.

This discouraging picture has prompted development and utilization of more efficient and systematic procedures to assist transportation agencies with their pavement management systems (PMSs) (*1*). An increasing number of state transportation agencies are utilizing PMSs to provide current and accurate assessment of the condition of highway pavements and to allocate available funds efficiently for pavement restoration (*2–6*). A PMS is generally used for evaluation of statewide pavement surface condition, analysis and evaluation of structural adequacy, development of alternative maintenance and construction strategies, and selection of an optimal pavement management strategy. Surface evaluation provides the data necessary to judge the service adequacy of existing pavement, to determine if structural evaluation is necessary, to determine the probable causes of surface distress, and to estimate needs and priorities for preventative and corrective maintenance (*3*).

Evaluating the extent and severity of surface distress requires the acquisition of large amounts of visual data, typically obtained by on-site inspection. The pavement surface condition is rated using a pavement distress index based on scoring systems that have been developed by the state transportation agencies to determine if a pavement section requires maintenance, overlay, or reconstruction. The scoring systems are customized for the different pavement construction and maintenance practices used by the respective agencies. Although the computation process is usually computerized, the raw data are still input manually, a laborious and expensive task, in addition to the slow and laborious manual and visual data collection during site inspections by trained field personnel. These methods are inefficient and can lead to a high degree of subjectivity, error, and nonrepeatability in the measurements.

Thus, the need for an automated visual pavement surface distress system is increasingly evident. A number of research and development projects have been carried out by national and state transportation agencies and private companies; to date, these projects have displayed only limited success. However, the effort to understand the nature of the problems and to develop pertinent research and engineering methods and data will make future attempts more successful.

BACKGROUND

There are two major steps in automated pavement inspection—an image acquisition system obtains images of pavements, and an image processing system evaluates those images to assess the severity and extent of surface distress. In this section, the approaches that have been attempted, the difficulties encountered, and the engineering methods and data that can facilitate further automated inspection efforts are discussed.

Image Acquisition

The image acquisition system that looks at the pavement comprises the camera, the lens, and the computer hardware. Distinguishing between distressed and sound pavement surfaces

T. El-Korchi, Civil Engineering Department, N. Wittels, Electrical Engineering Department, Worcester Polytechnic Institute, Worcester, Mass. 01609.

is easy for a human but difficult for a machine vision system. Whereas the human retina contains nerve tissue specifically dedicated to the task of detecting thin, discontinuous features such as cracks in images, a machine vision camera contains no such specialized receptors. Its output, a voltage proportional to the amount of light falling on the sensor, is sampled by a frame grabber to produce a digital image made of picture elements (pixels) that are laid out in a grid-like pattern across the image of the pavement. The digital image is just a matrix of numbers, each of which represents the amount of light from a discrete area on the pavement surface that is imaged into the corresponding pixel. These numbers are called "gray levels"; the higher a number, the lighter the corresponding shade of gray in a pixel. The goal of the image processing system is to identify various types of surface distress from the matrices of gray level numbers that represent images of pavement surfaces. Finding cracks in digital images happens during the image processing step.

The image acquisition system must acquire information that is adequate to meet highway maintenance needs. A reasonable acquisition specification is that the system observe 100 percent of the road surface and that it be able to detect cracks 1/16 in. (1.5 mm) wide within a 12-ft (3.7-m) lane from a vehicle traveling at 55 mph (90 km/h). Successful detection means that the probability that crack gray levels are distinguishable from surface gray levels is acceptably high—an acceptable percentage of false positives, apparent cracks that are only artifacts of the image acquisition system, and false negatives, cracks that escape detection, are usually included in the acquisition specification. There are two problems with designing an acquisition system capable of meeting such a specification—resolution and data bandwidth.

The specification implies the ability to resolve cracks only 1/2,400 of the lane width. Although such resolution is comparable to the capabilities of the human eye (*7*), it greatly exceeds the resolution of commercially available television cameras, which typically have only about 500 pixels per line. Even that number is an overestimate of the camera's resolution. When the image of a crack is less than two pixels in width, the image contrast (the relative difference in the video signal between the light and dark image areas) is greatly reduced. The only way to ensure that small cracks do not escape detection is to ensure that the image acquisition system has an equivalent pixel count of at least 4,800 in the direction transverse to the lane. The actual pixel count may have to be higher because the apparent crack width can be foreshortened by perspective projection through the camera lens and a crack can appear as much as 30 percent narrower than it actually is, depending on how close it lies to the edges of the lane and the camera's height above the pavement surface.

The bandwidth problem concerns the rate at which image data are generated. The acquisition specification under discussion requires a video bandwidth of greater than 30 MHz. If video signals are stored digitally, this rate corresponds to greater than 240 Mbaud, assuming 8-bit gray levels. Commercial video cameras and recorders typically have bandwidths in the 4- to 6-MHz range, a factor by at least five too low. Thus, image acquisition systems based on the RS–170 (*8*) commercial video standard generally have insufficient signal bandwidth for pavement inspection, unless multiple cameras are used or unless one or more of the constraints on speed, coverage, or minimum crack size are reduced.

Several approaches have been used in the past to acquire video images for automated pavement inspection. The system developed at the University of Waterloo (*9*) uses an RS–170 camera and has a resolution of only about ¼ in. (6.5 mm). Even systems with multiple cameras have not yet achieved sufficient resolution and coverage (*10*). Nonstandard systems with line-scanning arrays (*11–13*) can solve the resolution problem, but still require the processing of enormous amounts of data, also true for pavement inspection systems that analyze films exposed to photologging equipment. One technique for solving the data rate problem is real-time data analysis: only summaries of the data are retained. The system built by Ektron for FHWA uses analog signal processing to identify pavement distress signatures in signals obtained with custom cameras. That system has reduced data rates but it may not be sufficiently reliable for general pavement evaluation use. Another disadvantage is that it destroys the raw video data, which can be important to a pavement engineer assessing the nature of the distress in making maintenance decisions. Finally, image compression is a useful technique for greatly reducing the amount of visual data that must be processed or stored (*14,15*); however, developing compression algorithms suitable for pavement images would require a better understanding of the nature of the visual information than is now available. No digital image acquisition system that is capable of meeting the acquisition specification under discussion is presently known.

What information would allow the designer of image acquisition systems to meet the specification? Cracks are visible because they are darker or lighter than the surrounding pavement surface. The image contrast depends on the depth and width of the crack, the reflectivity of the paving materials, the alignment of the crack with the light source, and the viewing direction. Carefully matching the image contrast, camera optics, and the camera sensor characteristics can ensure that there is sufficient image contrast for the image processing system to meet its specification reliably (*16,17*). Therefore, understanding and characterizing the inherent crack contrast in pavement images is a first engineering step in designing an image acquisition system. That understanding, which is also necessary to the design of image analysis and compression algorithms, is universally applicable to the design and analysis of all automated pavement inspection systems.

Image Processing

Once supplied with images of sufficient contrast to assure that cracks are detectable, the next step is to use image processing, a sequence of mathematical operations or algorithms performed on a digital image, to detect those cracks. There are hundreds of image processing algorithms available to the vision system engineer (*18–27*). Traditionally, image processing algorithm selection has been a heuristic process with few numerical measures of success; algorithm effectiveness is often demonstrated by before and after images. Successful pavement surface distress detection requires selecting a sequence of algorithms that reliably locates pavement distress and that fits within the available computing assets. (Some algorithms take considerably more computing power than others.) The methods and data presented in this paper can provide a basis for evaluating the algorithms objectively on the basis of the probability of detection.

The rows and columns of the digital image are typically aligned with the transverse and longitudinal directions of the lane; the initial image processing algorithms are intended to determine which row and column intersections contain gray levels that indicate cracks or patch edges at the corresponding points on the pavement. These algorithms are local operators because they operate locally to determine whether or not each pixel is part of a crack. A second class of algorithms, global operators, string together adjacent pixels of the same type to determine the size and orientation of each crack or patch. These are the algorithms that classify and measure pavement surface distress from the locations of crack and patch edge pixels. Global algorithms fail if the local algorithms do not provide the correct information. Hence, in this paper the nature of the data that the local algorithms analyze is emphasized.

Many factors contribute in making the data difficult for local algorithms to interpret correctly. Lighting on the pavement changes with the time of day, amount of cloud cover, and presence of shadows of fixed and moving objects on or near the road. Aggregate in the paving material makes up a much larger portion of the information in a pavement image than does surface distress. (The characterization of aggregate appearance on the pavement surface is beyond the scope of this paper, but it is required for a complete understanding of the visual appearance of distressed pavement.) The reflectivity characteristics of the pavement surface change with wear and with weather conditions. Other markings or objects on the road, such as oil stains, skid marks, lane markings, dirt, and debris can confuse the distress detection and classification process. Understanding and characterizing of all of these effects is a necessary prelude to algorithm selection.

A class of local algorithms that is very useful for detecting surface distress is the edge finder. These algorithms locate edge pixels by searching for distinguishing characteristics in the digital image. One typical algorithm, the thresholding algorithm, labels any pixel darker than some preset value or that has a gradient higher than some preset value as belonging to a crack. Because they are fast and easy to implement, thresholding algorithms are frequently used for locating pavement cracks (*9–12,28,29*).

Unfortunately, thresholding algorithms are not particularly reliable edge finders. Figure 1 shows a photograph taken in direct sunlight of alligator cracking in an asphaltic concrete pavement. The resolution of the 35-mm film used to produce this photograph exceeds that of any commercially available machine vision camera and the film's usable contrast range is greater than that of a camera's sensor. In a digital image of distress acquired on a sunny day with a commercial, solid state, RS–170 video camera (Figure 2), camera limitations reduce crack sharpness and contrast. The top half of the figure shows a photograph of the digital image. The white horizontal line denotes a typical pixel row in the image. In the bottom half of the figure, a graph of the gray levels in a typical matrix row indicates the difficulty in designing an edge finder suitable for detecting pavement distress. (High values in the graph correspond to light pixels; low values are dark.) Extrema in both the gray-level signal and in its derivative can be found at the edges of both cracks and aggregate, making it difficult to distinguish between them. In other words, some pieces of aggregate are as dark as the cracks, and some aggregate edges are as sharp as the edges of cracks.

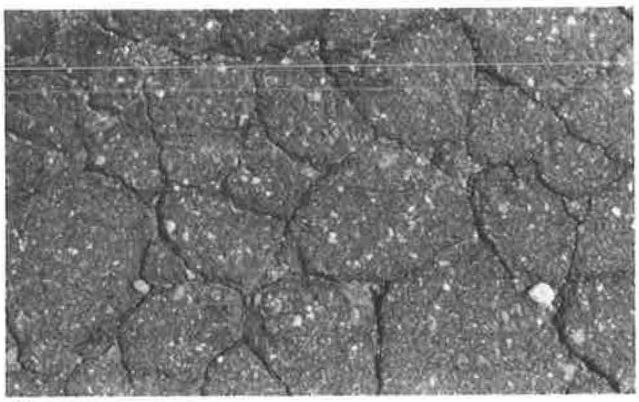

FIGURE 1 Photograph of alligator cracking in an asphaltic concrete taken with a 35-mm camera.

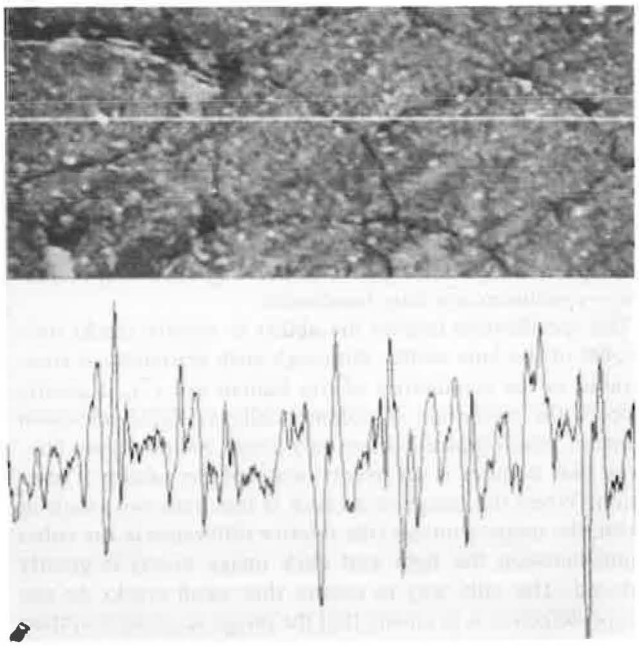

FIGURE 2 Digital image of alligator cracking.

Other edge finding algorithms also have difficulty with pavement images (*10*). No edge finding algorithms are known that can reliably detect cracks in images of this quality nor is any way known to design acquisition systems in whose digital images cracks can always be distinguished from aggregate by simple edge finders.

These figures also show the differences in the way cracks appear to humans and to machine vision cameras. In the photograph (Figure 1), narrow cracks are as dark as wide cracks. In the digital image (Figure 2), the narrow cracks have significantly reduced contrast and can even disappear completely. The fact that a crack is readily apparent to the eye is no guarantee that a camera can see it; the human eye is a poor substitute for objective measurement in evaluating image processing algorithms.

Probability of Detection

What are objective measures for evaluating image acquisition systems and image processing algorithms? How are crack luminances used in these evaluations? One criterion is crack detection probability. To meet a minimum crack detectability contrast specification, the gray level of a crack pixel, in combination with the gray levels of surrounding pixels, must be different enough from the gray levels of sound pavement pixels for the crack to be detected. Although the methods for calculating this minimum gray level difference for any specific machine vision system are beyond the scope of this paper, such a value exists and forms the upper bound to actual system performance; any real edge finder will degrade this value and hence produce more errors than the theoretically calculated error rate.

In judging whether a machine vision system, in principle, can reliably detect cracks, the machine vision system design engineer calculates the minimum acceptable image crack contrast using crack luminance values, camera models, and other system design parameters. This parameter must exceed the minimum crack detectability contrast, which is calculated from minimum crack size and detectability values in the image acquisition specification. In testing algorithms, digital images can be altered to replace crack pixel gray levels by the minimum detectability values to create worst case images. These images can be used to ensure that the algorithms operate effectively. Crack luminance values are useful because they characterize pavement images during both design and testing of both parts of the image acquisition system. In the next section, why cracks appear to have the luminances they do is explained.

CRACK LUMINANCE

In the last section, it was established that the crack luminance (the fraction of light reflected into the camera from each portion along the bottom and side walls of a crack) determines the apparent crack contrast, which is used in the design of image acquisition and image processing systems. In this section, the factors that determine crack luminance are discussed.

Reflectivities of Paving Materials

Pavements are visible because they reflect light. The luminance of each visible surface, including crack sidewalls and bottom, is proportional to the total amount of illuminance they receive and their reflectivities. In this section, the results of reflectivity measurements made on paving materials and the conclusions that can be drawn for crack detection are discussed. In a later section on reflectivity measurements, details of light reflection from paving materials are described and the equipment and techniques used to make measurements of the reflectivity are outlined. It is this reflectivity value that is used to characterize a surface.

The reflectivities of mortar, isolated aggregates, and portland cement concretes are measured using the equipment and methods described in a later section. Mortar has a reflectivity of 0.30 to 0.35 for both freshly prepared surfaces and for cut or fractured surfaces; that means between 30 and 35 percent of all of the incident light is reflected back from its surface. Although the aggregate materials measured were chosen with mindful regard that their availability, price, and structural properties be compatible with their use in PCC pavements, a primary selection criterion was that materials were wanted with as wide a range of reflectivities as possible. Figure 3 shows a photograph of some of the aggregate samples measured. The materials, clockwise from top left, are schist, feldspar, chert, marble, basalt diabase, basalt, and organic shale. As shown in Figure 4, the least reflective materials (organic shales and magnetites) have reflectivities as low as 0.05, and the most reflective material (marble) has reflectivity above 0.65 and as high as 0.90. These values are only representative; measurements should be made on the specific aggregates used in any pavement being analyzed. The reflectivity range shown in Figure 4 is enormous—it is comparable to the range spanned

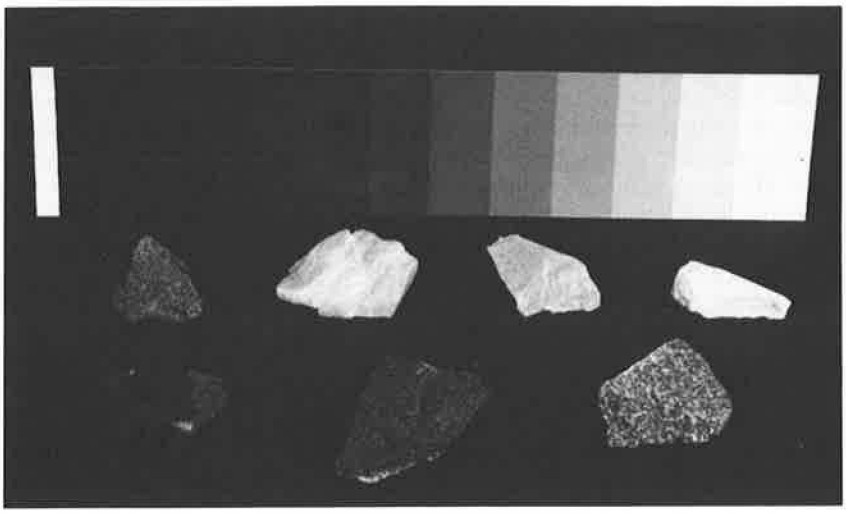

FIGURE 3 Photograph of typical aggregate samples used in the reflectivity measurements and a step wedge reflectance standard (with reflectivity ratio between adjacent steps of $\sqrt{2} = 1.414$).

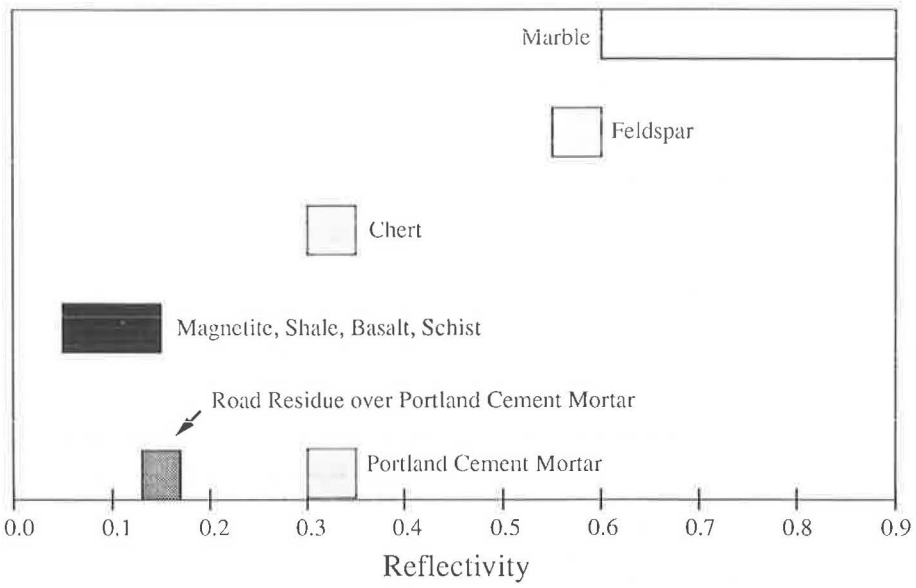

FIGURE 4 Reflectivities of some aggregate materials chosen for the maximum reflectivity range.

by the least and most highly reflective household materials, black velvet and white paper, and it exceeds the contrast ranges of almost all commercially available cameras.

It was also of concern that weathered and worn PCC pavements might differ in appearance from the freshly prepared pavement samples measured. On material removed from old PCC pavements, the reflectivity of the road surfaces and of both cracked and cut cross sections was measured. The cut and cracked surfaces have reflectivities almost identical to those of freshly prepared portland cement mortar. In general, the worn pavement surface is visually similar to freshly prepared pavement except that the reflectivities of all materials, mortar and aggregate alike, are reduced by a factor of about two (see Figure 4). The most significant difference is that worn pavements exhibit more specular reflection than freshly prepared pavements at glancing angles of illumination and observation, conditions that are unattractive for automated inspection purposes. Thus, the effects of wear and residue can be simulated by viewing a freshly prepared pavement sample through a neutral-density filter or by applying a low-gloss varnish of the appropriate darkness to the sample surface; both methods have been used with success, although the results obtained with varnishes have been less consistent. The ability to simulate the visual effects of wear and aging on pavements is important if the results of laboratory measurements on new samples are to be applicable to analyzing images obtained from old highway pavements.

Luminance Measurements

Luminance of reflecting objects is usually measured by means of a spot photometer, a type of imaging light meter with better spatial resolution and light measurement accuracy than the vision system camera. In measuring the luminance of pavement surfaces, two questions were addressed. First, were the reflectivities measured on laboratory samples of mortar and aggregates adequate to explain the luminance of those materials in PCC pavements? Second, can luminance values that are calculated from material reflectivities adequately explain and predict the luminance of both sound and distressed pavements under all conditions of lighting?

To answer the first question, PCC samples were prepared using a 3:1 weight ratio of uniform quartz sand and portland cement with a water-cement ratio of 0.3. Course aggregate was hand-selected from batches of material whose reflectivities had been characterized. Using simulated sunlight, the luminance was measured on mortar and aggregate on both the prepared pavement surface and on cut and cracked cross sections through the samples. In summary, the luminance values of the mortar and the aggregates in concrete are identical to the values predicted from reflectivity measurements on the parent materials, within the measurement errors of about ± 5 percent. In other words, reflectivity measurements on the components of a pavement can be used to predict the appearance of the pavement surface. The reflectivities of other materials found on pavement surfaces—paint, lane markers, patch materials, joint fillers, debris, etc.—have not been measured, but including them in calculations of the luminance of pavement surfaces should be straightforward.

Unfortunately, it is not so easy to predict or explain the luminance of internal crack surfaces, for four reasons. First, the crack bottom and sides can be made of mortar or aggregate, which often have different reflectivities. Cracks usually propagate through the mortar or along the interface between mortar and aggregate (*30*). Therefore, as shown in Figure 5, aggregate can form at most one sidewall or the crack bottom, so the effective reflectivity, and hence the apparent luminance, of the crack will depend on the observation direction. When the crack involves only mortar, the surfaces are homogeneous. In cracks that propagate along the surface of aggregate, one sidewall or the crack bottom can have reflectivity different from the rest of the crack surface. Cracks with aggregate along two sidewalls are unlikely because they would have

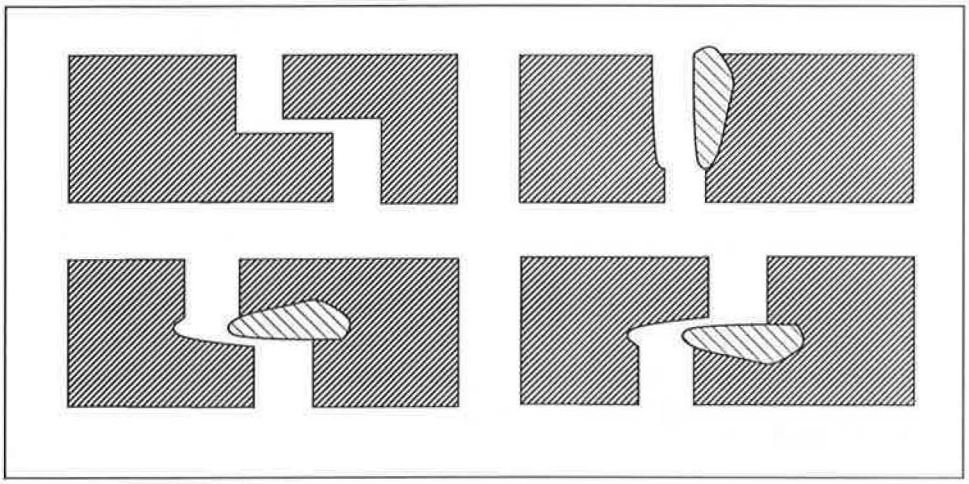

FIGURE 5 Schematic diagrams of cracks in PCC pavements.

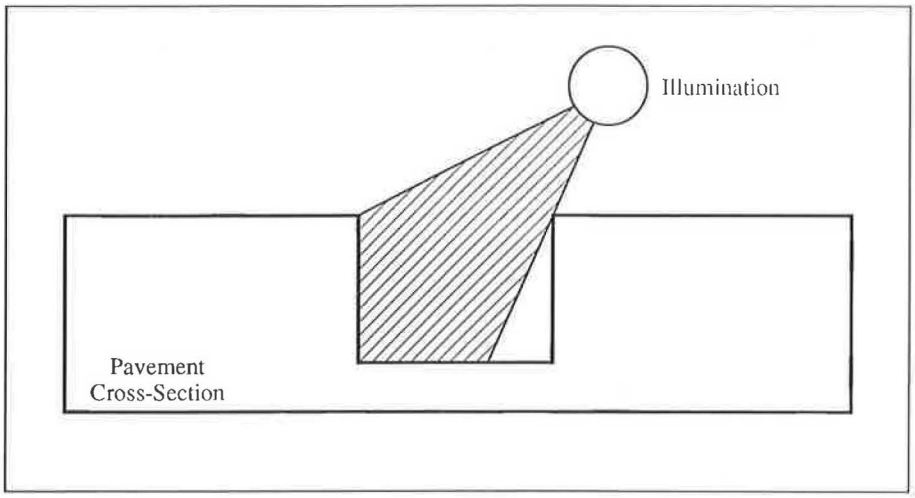

FIGURE 6 Cross-sectional view of an idealized pavement crack.

to result from directly touching aggregate pieces that had not been wet by the paste or from cracks that propagated through aggregate; in properly prepared concrete neither case should obtain. The second problem has to do with the direction of incidence. When the light comes from a small source such as the sun or a lamp, one sidewall, at least part of the bottom, and possibly part of the second wall will be shadowed so they will appear to be less luminous. A detailed description of the lighting is necessary to calculate the effects of this shadowing. This shadowing is shown in Figure 6, which also shows the third problem—different angles of light incidence on the crack bottom and sides. The effective illumination from a small source varies as the cosine of the angle of incidence. The crack sidewalls are roughly perpendicular to the surface and bottom so they may receive the illumination at different angles of incidence. Therefore, unshadowed crack surfaces with the same reflectance as the surface may have different apparent luminances. The fourth problem is also shown in Figure 6. The unshadowed portion of the crack bottom is illuminated not only by direct illumination from the source, but also from indirect illumination received from light reflected off other nearby crack surfaces. In the example illustrated, the crack bottom luminance should be greater than the surface luminance because of this interreflected light.

Examples of these four difficulties are also shown in Figures 7 and 8. A sample of PCC made with selected granite aggregates was cracked and placed on a mechanical slide to allow varying the crack width [set to 3 mm (0.12 in.) in this case]. Figure 7 shows a side view of the sample; the lighting has been adjusted so that the granite aggregate can be seen clearly on the cut side surface. Figure 8a shows a digital image of the top surface of the sample with crack width set to 1.5 mm (0.06 in.). The sample is illuminated crosswise to the crack by simulated bright sunlight at 60 degrees above the horizon. The crack is clearly darker than the surface, because of shadowing. Figure 8b shows the same crack illuminated from the same elevation but along the crack direction, which eliminates shadowing on most of the bottom surface. Interreflection has now caused portions of the crack bottom to be more luminous than the pavement surface. (The brightest pixels in the image are

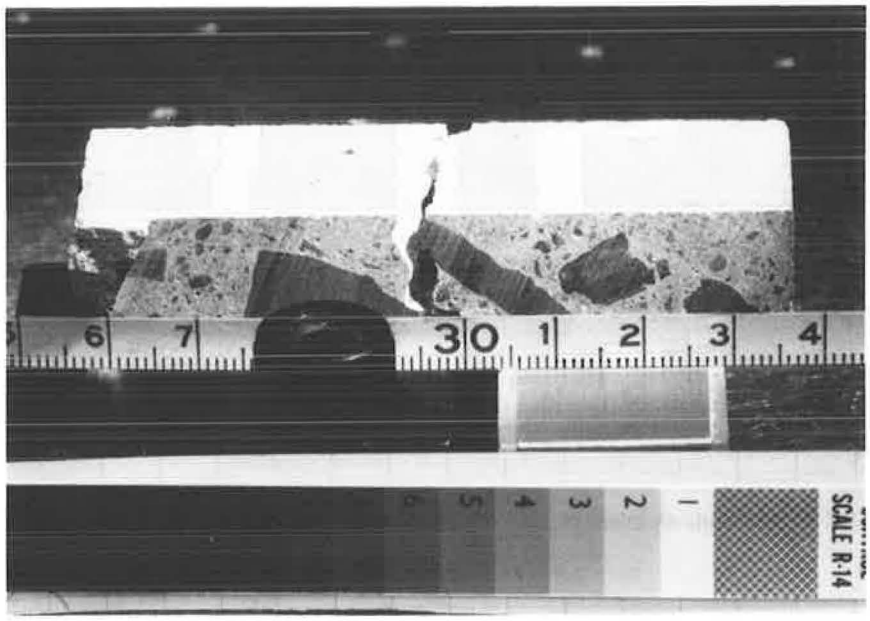

FIGURE 7 Photograph of a cracked PCC sample made with granite aggregate.

inside the crack in the center of the figure.) Where the crack bottom is formed by aggregate, which is less reflective than the mortar, the crack bottom is less luminous than the surface, despite interreflection. The digital images of Figure 8 were used for luminance measurements so the resolution is much better than an automated pavement inspection system would display. In that case, the crack in Figure 8a would be easily detectable but the crack in Figure 8b would appear as discontinuous pixels, some with gray levels higher than the surrounding pavement and some with lower values. Designing an image processing algorithm that can reliably detect the crack in Figure 8b is most challenging.

Figures 8a and 8b show the same physical crack, only the lighting has changed. Because cracks come in all orientations, the same crack can have different detectability at different times of the day; or, some lighting conditions emphasize transverse over longitudinal cracks.

In summary, the surface luminance of pavements is easy to understand and to predict but the crack luminance is a complicated function of many parameters—the reflectivities of all of the paving materials, illumination direction and intensity, and crack size and orientation.

DISCUSSION

In the last section, the factors that affect apparent pavement luminance, material reflectivities, illumination conditions, and crack geometry were discussed. Understanding digital images of PCC pavement surfaces is straightforward—contrast depends only on the ratios of reflectivities of the aggregate materials and the mortar. The values may have to be adjusted to account for wear and weathering of the pavement surface. Understanding crack luminance, however, is much more difficult—small changes in crack geometry or lighting can cause major changes in crack contrast.

In testing automated pavement inspection systems, it is traditional to rely on field tests of the system and to compare with the results obtained by human observers. From looking at digital images of distressed PCC pavements and attempting to generalize luminance measurements based on them, much of the difficulties in past approaches to automated distress evaluation was understood. The fact that under some lighting conditions cracks are more luminous than the surrounding pavement was unexpected; careful measurements of gray levels in digital images of PCC pavements confirmed that cracks illuminated by small bright light sources can appear brighter than, darker than, or identical to the pavement surface. This result violates the basic human intuition that cracks are always dark and demonstrates why image processing algorithms designed for automated pavement inspection must be based on measured video signal values rather than on human notions of crack appearance. That fact leads into the second difficulty with generalizing digital pavement images—the variabilities due to material reflectivities, crack geometry, and lighting make it difficult to characterize crack luminance by merely collecting a large number of crack images. For example, the actual lighting situation is even more complicated than was suggested in the last section in which only a single, small illumination source such as the sun or a lamp was considered. In addition to this direct illumination, cracks usually receive omnidirectional ambient illumination, such as skylight. The ratio of ambient to direct sunlight directly affects the crack luminance. Multiple direct light sources, such as a bank of lamps, will produce even different luminance values. There are many other factors that can alter the crack luminance. It is difficult to imagine that a collection of pavement images, however extensive, can include all of the contrast cases that an inspection system will encounter on the highways. It is not even clear how to select, from a collection of images, the worst case images with which to test automated pavement inspection systems. In other words, exclusive use of unstruc-

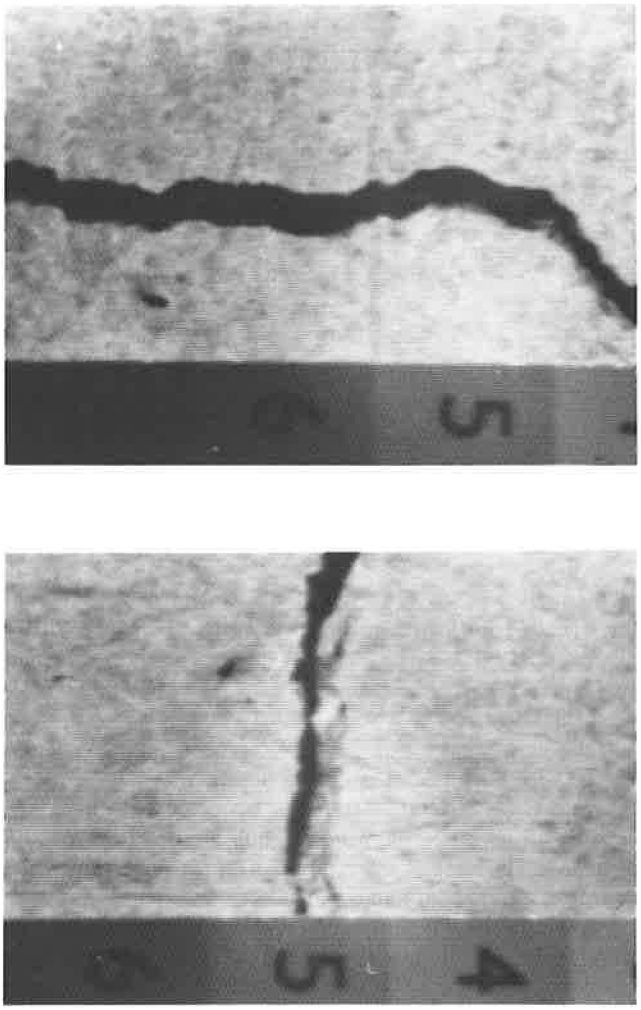

FIGURE 8 Digital images of the pavement sample shown in Figure 7 except that the crack width is 1.5 mm (0.06 in.) (top) illumination crosswise to the crack and (bottom) illumination along the crack.

tured field testing of vision systems is not a good way to validate that the system will work reliably.

In addition to the difficulty of validating system performance, the other problem with using collections of digital pavement images is that it is difficult to generalize an understanding of how to design image acquisition and image processing systems to optimize crack detection. For example, even if the considerable expense and difficulty of obtaining and documenting an exhaustive library of pavement distress images were incurred, the effort would have to be duplicated for all combinations of cameras and other major system components that the system designer might consider using. Similarly, in deciding between natural and artificial lighting, the designer would need images acquired under all possible lighting conditions. This is clearly infeasible.

In this paper, the importance of detailed understanding of crack luminance in designing automated systems for evaluating pavement surface distress has been shown. Although reflectivity measurements of pavement materials can be used to understand the appearance of pavement surfaces, the complexity of the light incidence and reflection that produces luminance inside the cracks defies attempts to generalize an understanding from measuring highway pavement images. As a way around this problem, Wittels and El-Korchi in a companion paper discuss the combination of computer simulations of crack luminance with pavement images as a step in designing and testing automated pavement distress inspection systems.

REFLECTIVITY MEASUREMENTS

This section contains detailed information about the reflectivity measurements. It is presented for the benefit of those requiring detailed knowledge of the methods, but it is placed at the end of the paper so as not to impede the reader who does not need this level of detail.

Pavements are visible because they reflect part of the light they receive. That can be light received directly from the sun or lamps or it can be sun- or lamplight that is reflected by other surfaces. When the surface is a diffuse (or matte) reflector, it obeys Lambert's Law—the luminance of the reflected light is independent of illumination direction and varies cosinusoidally with the viewing angle, measured from the surface normal. This results in an apparent luminance that is independent of viewing angle. The opposite extreme is specular (mirror-like) reflection in which the angle of reflection is equal but opposite to the angle of incidence, relative to the surface normal. Most materials have reflection characteristics between these two extremes and characterizing them can be quite complicated (*31*). Diffuse reflection is the simplest case to model because the surface can be characterized completely by a single reflectivity, a number equal to the ratio of the total light out divided by the total light in, and because the apparent luminance is independent of the viewing angle.

A material's reflectivity can be measured using the reflectometer shown schematically in Figure 9. In this configuration, the light source produces controlled surface illumination and two cameras are used to measure the light reflected. Camera 1 is in line with the illumination and at the same polar angle with respect to the surface normal; it receives both specularly and diffusely reflected light. Camera 2 is at the same polar angle as the illumination, but 90 degrees away in azimuthal angle; it receives only diffusely reflected light. The camera signals are compared during sequential observations of a sample and a diffuse reflectivity standard, MgO; the ratio of the reflectivities is the same as the ratio of the camera signals. This same instrument can be used to verify that a sample reflects diffusely. If the sample is a diffuse reflector, the signals from Camera 1 and Camera 2 will be equal. If it has a specular reflectivity component, Camera 1 will receive substantially more light than Camera 2.

In calculating crack luminances, it is useful to assume that paving materials reflect light diffusely and it is important to validate that assumption. Using the equivalent of a two-camera measurement technique, it was found, with very few exceptions, that the nondiffuse component of reflectivity is less than 0.05 (less than 5 percent of the incident light is reflected specularly) for most paving materials, which is less than the natural variation in total material reflectivities. The most notable exception was feldspar. When used as an aggregate material, the specular reflection from feldspar samples can overwhelm the diffuse reflection under some lighting

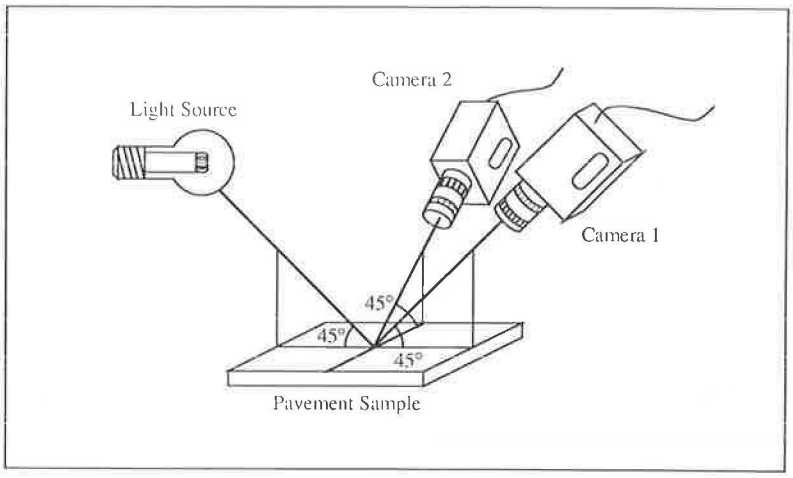

FIGURE 9 Schematic representation of a reflectometer.

conditions. The assumption of diffuse reflection is invalid for wet pavements. It also breaks down on weathered pavements at glancing angles of illumination, as evidenced by the road glare when driving into the sun. That illumination condition produces images that emphasize unimportant variations in surface texture so it would not normally be used for pavement inspection. Therefore, the measurements support the diffuse reflection assumption for most paving materials and most observing conditions.

Figure 9 contains only a schematic representation of a reflectometer. Reflectometer design is beyond the scope of this paper (*17*,*32*), but there are several important design features that should be incorporated into a reflectometer intended for measuring paving materials. They include the following:

- Illumination and observation angles should match the actual conditions under which the pavement will be viewed by an automated surface distress evaluation system. The solid angle that the camera lens aperture subtends should match that of the automated system's lens. If directed illumination is used, the illumination solid angle should be matched in the reflectometer. These precautions ensure that both systems will measure comparable quantities and will react similarly to pavement materials that produce small specular glints, such as asphaltic pavements.
- The reflectometer light source and sensor should have the same color temperature and spectral sensitivity, respectively, as the automated distress evaluation system. This is to prevent inaccuracies when using the equipment with highly colored paving materials.
- The size of the measured area should be comparable to the minimum crack width to be detected. This ensures that the reflectometer measures local reflectivity variations with size scale comparable to the image acquisition system.

The reflectivity measurements in Figure 4 were made under the following conditions:

- The illumination cone angle was about 0.5 degree, comparable to sunlight. The observation cone angle was about 0.05 degree, comparable to observation with an f/2.8, 5-mm lens. That is the lens that images a 12-ft (3.7-m) wide lane on to a standard 0.35-in. (8.8-mm) video camera sensor when the camera is suspended about 6.8 ft (2 m) above the pavement surface.
- The light source was a 3,200°K tungsten-halogen lamp filtered with a Kodak 80A filter to approximate sunlight and the sensor was a United Detector Corporation model 248 silicon barrier detector with a photometric filter having approximately the spectral response of typical photometrically corrected commercial video cameras.
- A sample area on the order of 0.4 in. (10 mm) in diameter was illuminated and the reflected light measurement was made a spot of diameter 0.08 in. (2 mm) centered in the illuminated area.

ACKNOWLEDGMENTS

The authors gratefully acknowledge the help and encouragement of many people who contributed to this work. Their colleagues M. Ward and M. Gennert aided in developing the technical strategy and some of the analyses used in the work, including the graph in Figure 2. M. Turo of the Massachusetts Department of Public Works helped them understand the operational and technical requirements of automated pavement evaluation systems. J. Sage aided in selecting the aggregate materials used. A. Bielund, S. Annecharico, and J. LeBlanc assisted in the calculations and experiments. This work was supported by the Research Development Council of the Worcester Polytechnic Institute.

REFERENCES

1. R. Haas and W. R. Hudson. *Pavement Management Systems*. McGraw-Hill, New York, 1978.
2. S. G. Ritchie, C.-I. Yeh, J. P. Mahoney, and N. C. Jackson. Development of an Expert System for Pavement Rehabilitation Decision Making. In *Transportation Research Record 1070*, 1986, pp. 96–103.
3. S. G. Ritchie. Expert Systems in Pavement Management. *Transportation Research*, Vol. 21A, 1987, pp. 145–152.

4. G. Schoenberger. A Pavement Management Information System for Evaluating Pavements and Setting Priorities for Maintenance. In *Transportation Research Record 951*, 1984, pp. 60–63.
5. D. S. Turner, J. V. Walters, T. C. Glover, and E. R. Mansfield. An Asphalt Pavement Rating System Based on Highway Maintenance Engineers' Experience. In *Transportation Research Record 1060*, 1986, pp. 9–16.
6. R. Uzarski. Managing Better with PAVER. In *Transportation Research Record 951*, 1984, pp. 41–51.
7. I. Overington. *Vision and Acquisition*. Pentech Press, London, 1976.
8. *EIA Standard RS–170*. Electronic Industries Association, Washington, D.C., Nov. 1957 (and later editions).
9. C. Haas, H. Shen, W. A. Phang, and R. Haas. An Expert System for Automation of Pavement Condition Inventory Data. *Proc., North American Pavement Management Conference*, 1985, pp. 4.46–4.57.
10. D. S. Mahler. Final Design of Automated Pavement Crack Measurement Instrumentation from a Survey Vehicle. Report FHWA/RD-85/077, KLO Associates, Huntington Station, N.Y., 1985.
11. G. Cox, D. Curphey, D. Fronek, and J. Wilson. Remote Video Sensing of Highway Pavements at Road Speeds. In *Microcomputers in Civil Engineering*, Vol. 1, 1986, pp. 1–13.
12. G. Cox, R. Merrill, and D. Fronek. Pavement Management System with Real Time Microprocessor-Based Computation. In *Microcomputers in Civil Engineering*, Vol. 1, 1986, pp. 95–105.
13. D. R. Curphey, D. K. Fronek, W. J. Shan, and J. E. Wilson. Pavement Evaluation Using Image Processing. *Proc., ISA International Conference*, 1984, pp. 1043–1052.
14. A. K. Jain. *Fundamentals of Digital Image Processing*. Prentice-Hall, Englewood Cliffs, N.J., 1989.
15. W. F. Schreiber. *Fundamentals of Electronic Imaging Systems*. Springer-Verlag, 1986.
16. N. Wittels and S. H. Zisk. Lighting Design for Industrial Machine Vision. *Proc., Society of Photooptical Instrumentation Engineers*, Vol. 728, Bellingham, Wash., 1986, pp. 47–56.
17. N. Wittels, R. A. Beiler, and A. P. Irwin. How to Design Inspection Systems for Electronic Components. *Proc., Society of Photooptical Instrumentation Engineers*, Vol. 850, Bellingham, Wash., 1987, pp. 81–87.
18. D. H. Ballard and C. M. Brown. *Computer Vision*. Prentice-Hall, Englewood Cliffs, N.J., 1982.
19. K. R. Castleman. *Digital Image Processing*. Prentice-Hall, Englewood Cliffs, N.J., 1979.
20. R. Chellappa and A. A. Sawchuck (eds.). *Digital Image Processing and Analysis*, 2 Vols., IEEE Computer Science Press, Washington, D.C., 1985.
21. R. O. Duda and P. E. Hart. *Pattern Classification and Scene Analysis*. John Wiley, New York, 1973.
22. R. C. Gonzales and P. Wintz. *Digital Image Processing*. Addison-Wesley, Reading, Mass., 1987.
23. B. K. P. Horn. *Robot Vision*. MIT Press, Cambridge, Mass., 1986.
24. T. Pavlidis. *Algorithms for Graphics and Image Processing*. IEEE Computer Science Press, 1982.
25. W. Pratt. *Digital Image Processing*. John Wiley, New York, 1978.
26. A. Rosenfeld and A. C. Kak. *Digital Picture Processing*. Academic Press, New York, 1982.
27. J. Serra. *Image Analysis and Mathematical Morphology*. Academic Press, New York, 1982.
28. L. C. Bomar, W. F. Horne, D. R. Brown, and J. L. Smart. *NCHRP Report 304: Determining Deteriorated Areas in Portland Cement Concrete Pavements using Radar and Video Imaging*. TRB, National Research Council, Washington, D.C., Dec. 1988.
29. C. H. Chien, W. N. Martin, A. H. Meyer, and J. K. Aggarwal. *Detection of Cracks on Highway Pavements*. Report FHWA/TX-83/7+256-3, University of Texas at Austin, 1983.
30. P. K. Mehta. *Concrete: Structure, Properties, and Materials*. Prentice-Hall, Englewood Cliffs, N.J., 1986.
31. A. K. Stenius. Nomenclature and Definitions Applicable to Radiometric and Photometric Characteristics of Matter. STP 475, ASTM, Philadelphia, Pa., 1970.
32. J. R. McClellan et al. Reflectometer for Industrial Machine Vision. *Proc., Society of Photooptical Instrumentation Engineers*, Vol. 1194, Bellingham, Wash., 1989.

Publication of this paper sponsored by Committee on Pavement Monitoring, Evaluation, and Data Storage.

Visual Appearance of Surface Distress in PCC Pavements: II. Crack Modeling

NORMAN WITTELS AND TAHAR EL-KORCHI

In the previous paper in this Record, the fundamental engineering data required to design automated pavement surface distress evaluation systems were discussed; in particular, luminance values along the crack sidewalls and bottom were used to calculate the visual contrast between the crack and surrounding pavement. Image contrast is an important parameter in machine vision design. Computer modeling of light reflection in portland cement concrete (PCC) pavement cracks can be used to simulate the luminance values in pavement images. Such a model, presented for the luminance of long rectangular slots in homogeneous pavements, is experimentally validated, extended, and applied to pavement surface distress. The model and resulting data are useful for the design of image acquisition and image processing systems and in the simulation of worst case images for testing pavement evaluation systems.

Automated pavement surface distress evaluation systems are an important ingredient in the computerized pavement management systems (PMS) being constructed by many transportation agencies. Although a number of experimental and developmental evaluation systems have been built, they have not demonstrated a consistently high degree of reliability in use. In the previous paper in this Record, the technical challenges associated with building reliable pavement inspection systems were examined and a detailed understanding of the luminance values along the sidewalls and bottoms of cracks was shown to help design image acquisition and image processing systems. Although it is easy to measure the crack luminance values for any given crack and lighting arrangement, it is difficult to predict the luminance values. Without some way to make such predictions, one cannot easily select worst case images for testing systems, nor can one gain the understanding that aids in system design. Computer simulations of cracks in portland cement concrete (PCC) pavements can be used for making such predictions and simulation results can be used for designing automated pavement inspection systems.

SIMULATION

There are three steps in developing a satisfactory computer simulation of crack luminance values: producing a mathematical model of a crack, validating the model by comparing simulated with actual luminance values, and showing how to apply the model to problems of automated pavement inspection. These steps will be discussed in that order.

N. Wittels, Electrical Engineering Department, T. El-Korchi, Civil Engineering Department, Worcester Polytechnic Institute, Worcester, Mass. 01609.

Simulation Model

There are many possible physical models of pavement distress from which to build a mathematical model of crack luminance values. The simplest is to assume that the pavement is a homogeneous material and that a crack is a straight rectangular slot in the pavement. The later section on interreflection calculation contains a detailed description of the model and its implementation. Because this model is a gross oversimplification of real pavements and real pavement surface distress, it is first shown that the model accurately simulates the appearance of rectangular slots in homogeneous pavements. In the following discussion, the results from the simple model are related to characterization of actual pavement distress.

The key physical parameters of the model are the material reflectivities, the ratio of directed to ambient illumination, the incidence direction of the directed illumination, and the crack geometry. The ranges of possible values for most of these parameters are bounded; the applicable values are discussed in the following paragraphs.

In the previous paper in this Record, reflectivity values were measured on typical PCC pavement materials. Mortar has a reflectivity of 0.30 to 0.35 for both freshly prepared surfaces and for cut or fractured surfaces, implying that between 30 and 35 percent of all of the incident light is diffusely reflected back from its surface. The surface reflectivity of old pavements is about half as large. Aggregate materials have reflectivities between 0.05 and 0.90; the most commonly used materials have reflectivities between 0.15 and 0.60. At most one of the crack sidewalls or the crack bottom can be a piece of aggregate. In summary, the pavement surface has a reflectivity of roughly 0.15, two of the crack surfaces have reflectivity about 0.30, and the third crack surface has reflectivity between 0.15 and 0.60, depending on the aggregate material.

There are two types of lighting used in automated pavement surface distress evaluation, natural and artificial. Natural lighting is a mixture of skylight and sunlight (*1*,*2*). Skylight is omnidirectional or ambient lighting and is assumed to arrive with equal intensity from the entire hemisphere of sky. An artificial lighting system that surrounds the pavement with omnidirectional lighting (*3*) can be considered to be skylight. The inside surfaces of cracks illuminated by skylight receive somewhat less illuminance than the pavement surface because less of the sky is seen (the sidewalls occlude part of the hemisphere of illumination). Sunlight can be considered to be perfectly collimated light (as from a distant point source) because the shadow unsharpness in a crack image caused by the sun's finite size is much smaller than the resolution limit of an automated pavement evaluation system. Spotlight illumination can be

modeled in the same way as sunlight but artificial illumination using multiple sources or extended sources may require modifications to the model, as discussed in a later section. Absolute object luminances are not usually used in machine vision because the best system operation requires that the camera aperture (or illumination intensity) be adjusted to place the sensor illuminance in the most luminous portion of the scene just below the camera's saturation level (*4*). Therefore, only the ratio of the components of surface illuminance caused by skylight and sunlight is important in the calculation. The skylight-sunlight ratio can have values between 1:0 (a totally overcast day) and 1:8 (noon on a bright sunlit day) or 0:1 (a spotlight at night with no other indirect illumination). With artificial illumination, this system can be designed to produce almost any value of this ratio.

Skylight is omnidirectional, but sunlight has a definite direction of incidence. Two angles are required to specify the sunlight direction. The polar angle (angle from the zenith) can have values between a low value of approximately the local latitude minus 23° (the minimum is 0° for those latitudes where the sun passes through zenith) to 90° (horizon), although angles greater than about 70°—corresponding to the sun low on the horizon—overly emphasize the pavement surface texture and are usually inappropriate for surface distress evaluation. The azimuthal angle can have any value between 0° (perpendicular to the crack sidewall) and 90° (directed along the crack).

For purposes of the simple model, crack geometry is specified by a width and a depth. In general, other information about the local crookedness of the crack may also be important in determining its luminance values. In the later section on interreflection, two physical dimensions are used in the model, crack depth and width. However, because dimensionless distances are used in the model there is only one independent variable, the ratio of crack depth to width. Wide, shallow cracks have depth-width ratios less than 1 and deep cracks have ratios greater than 1.

Using the parameters summarized, it is straightforward to calculate the sidewall, crack bottom, and pavement surface luminances for the simplified crack. Before applying the results it is appropriate to validate the model.

Model Validation

To validate the model, the luminances of pavements that matched the simple geometry were measured. Mortar samples were prepared using uniform quartz sand and portland cement with a 3:1 weight proportion and a water-cement ratio of 0.3. The samples were cured for 3 days and rectangular slots were cut with depth-width ratios between 0.4 and 4.0 (Figure 1, top). The slots were illuminated with mixtures of ambient and directed lighting and were observed perpendicular to the surface (the preferred observation direction for an automated inspection system because it minimizes the perspective distortion of the imaging optics and maintains constant resolution across the image). Illumination was provided by 3,200°K quartz halogen lamps. Color temperature correction was not required because the color of the samples is neutral. The directed illumination was provided by a collimating optical system to simulate sunlight, and the ambient illumination was produced by surrounding the sample with a cone of translucent material uniformly illuminated by multiple light sources (Figure 1, bottom). Illumination uniformity was verified using the method proposed by Goodman (*5*). Digital images were made with a Schneider 50-mm Companon-S lens and a CIDTEC 2505A solid-state camera whose output was sampled by a Data Translation DT2851 frame grabber. The camera output voltage levels were converted to sensor illuminances (*6–8*), which are proportional to crack luminances. The measured luminances along the bottom of the slots were compared with the surface luminances.

There are two ways to compare measured with calculated luminance values: they can either be compared directly, pixel by pixel, or average values can be compared. Figure 2 shows a direct comparison of simulated and measured luminances for a representative slot. In this case, the ratio of direct to indirect illumination was 1:1 and the direct illumination was incident at the angles $\Phi = 45$ degrees, $\Theta = 0$ degrees, where the angles are defined in Figure 6. The values have been normalized to the average pavement surface luminance. The ripple in the measured data is an inherent part of the electronic signal and has a typical peak-to-peak value of about 5 percent of the maximum signal level. The measured and simulated values agree well, within about 10 percent at all locations within the crack. The unsharpness of the measured values at the crack edges is inherent in solid state video cameras (*6,7*). Other cases tested produce comparable agreement.

Although direct pixel-by-pixel comparison between simulated and actual luminance values across the slot is an important step in validating the model, detailed luminance values are not the most useful measure of image contrast for automated inspection system design. The large field of view of an automated pavement evaluation system, up to a 12-ft (3.6-m) highway lane width, and the relatively poor resolution limits of machine vision cameras, typically less than 1/500 of the field of view, result in digital images in which small cracks, the hardest to see, are rarely more than one or two pixels wide. A camera's output is a measure of the average image illuminance across each pixel, so a better measure of image contrast is the average luminance value along the bottom of the crack (or the imaged sidewall, if the crack is observed obliquely). Figure 3 shows measured and calculated average bottom luminances, normalized to the pavement surface luminance, for several representative slot geometries and two lighting conditions. The values agree well, to within $\pm(5–10)$ percent of maximum value, for cracks with depth-width ratios in the range 0.8 to 2.0. For smaller ratios (wide, shallow cracks), the samples were too narrow so the luminances were higher than predicted by the model, which assumes that slots are infinitely long. For higher ratios (thin, deep cracks), the luminances were too low to be measured accurately by the experimental arrangement used. In the one measurement where a spot photometer was substituted for the video camera, the bottom luminance agreed with the predicted value. The tests have not been exhaustive but they give a preliminary indication that the model provides accurate simulations of the luminance of rectangular slots in portland cement mortar samples. Further testing of the model is planned and will be reported in later publications. In the next section, the applicability of this model to digital images of pavement distress is discussed.

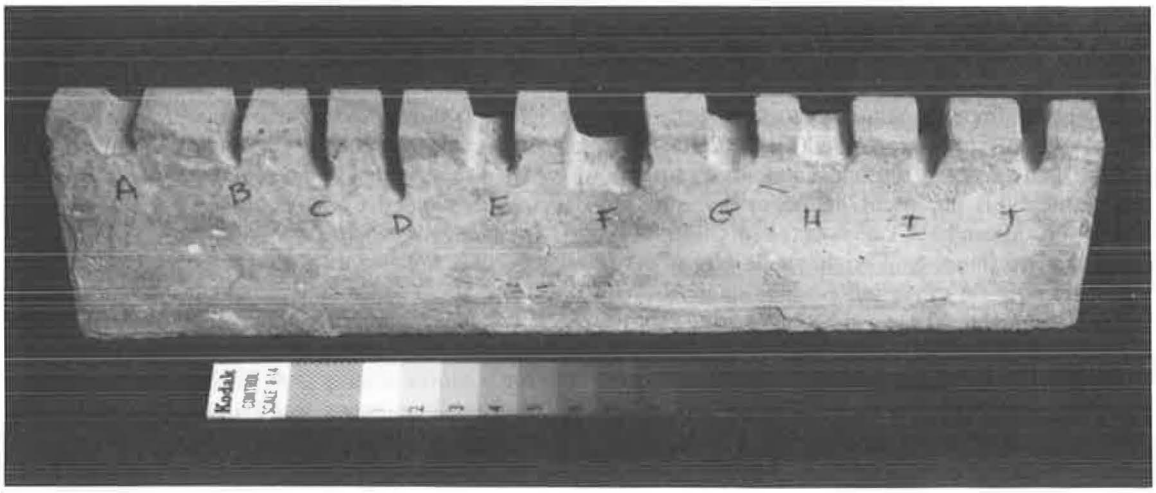

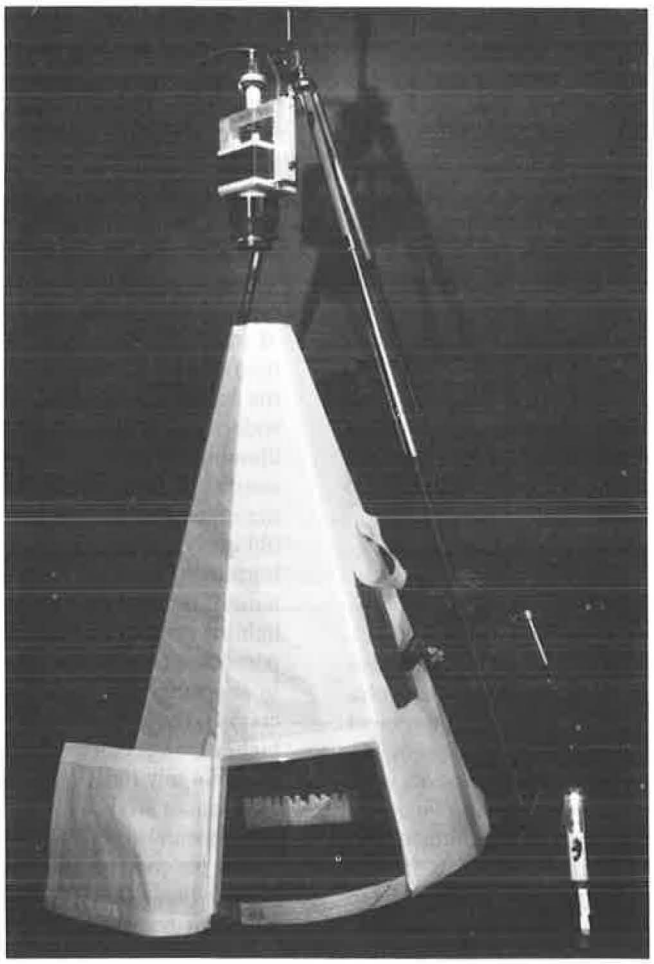

FIGURE 1 Photographs of the simulation validation experiment: top, portland cement mortar sample showing cut rectangular slots of varying depths and widths; bottom, experimental arrangement showing sample, lighting, and camera.

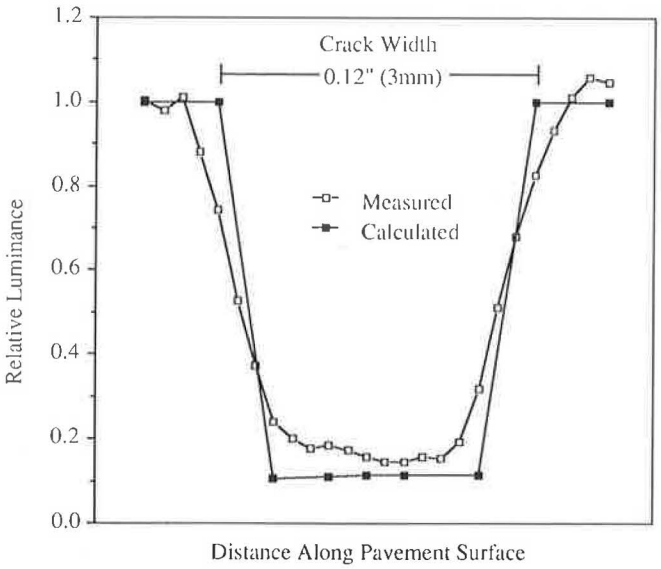

FIGURE 2 Comparison of crack luminances simulated by a computer and measured using a 0.12-in. (3-mm) wide and 0.20-in. (5-mm) deep slot cut in a prepared mortar sample.

DISCUSSION

In this section, the limitations of the simple luminance simulation model when used to characterize pavement distress are discussed. Also, future work that leads toward a complete characterization of the visual appearance of pavement surface distress is outlined.

Limitations of the Model

There are two concerns about using the simulation model to simulate PCC pavement surface distress: pavement cracks are not rectangular slots and PCC pavements are not homogeneous because they contain aggregate in addition to mortar. In this subsection, these concerns are discussed.

The first model limitation concerns crack geometry: cracks are generally neither straight nor perpendicular to the pavement surface, nor are their depths and widths constant along their lengths. The model, which is a two-dimensional interreflection model, does not allow geometry changes along the crack length. From three-dimensional extensions of this model, calculations show that light reflected from a region on a crack sidewall or bottom can only significantly affect the luminances of other crack regions that lie within a few crack widths distance. Thus, except for small (distances less than the crack width) transition regions where abrupt geometric changes occur, the crack can be modeled as line segments along which the model is valid. The crack illuminance is relatively insensitive to small changes in illumination angle; to first order, it varies as the cosine of the angle at which the light strikes the illuminated surfaces. Thus, straight line segments can be used to model most crack geometries. More work needs to be done to characterize the crack luminance in the transition regions.

In order to test the statement that a straight line model can be applied to pavement distress, a sample was prepared using the same mortar as the samples for the model validation pre-

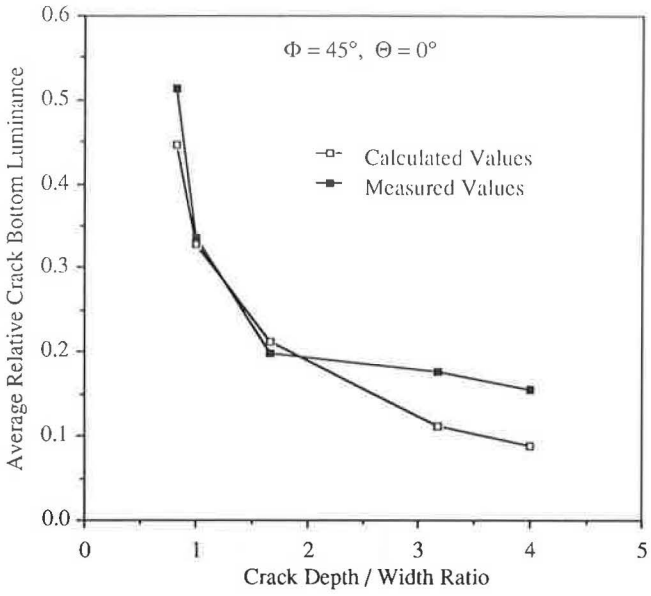

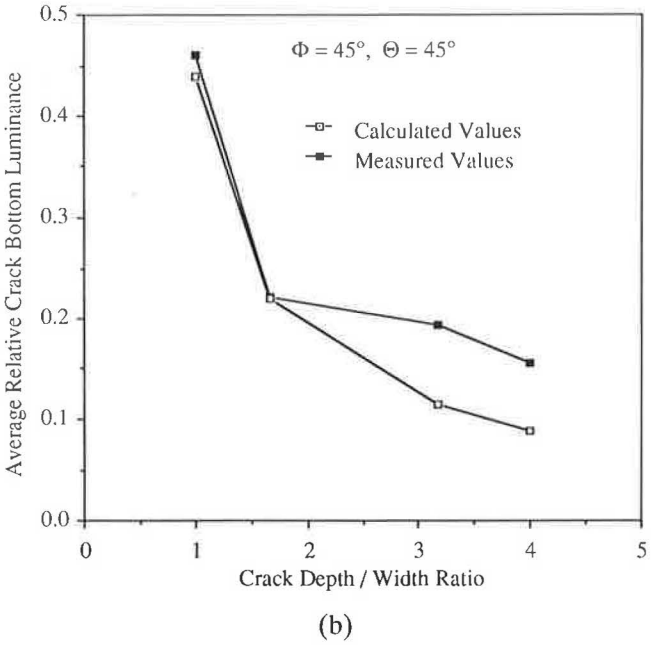

FIGURE 3 Comparison of simulated and measured average crack bottom luminances, normalized to the average pavement surface luminance, for cracks with several depth/width ratios (a) for illumination conditions as in Figure 2, Φ = 0 degrees and (b) for illumination conditions as in Figure 2, Θ = 45 degrees.

viously. It was cracked and mounted on a mechanical slide to make the crack width adjustable; the same configuration but with a different sample was shown in Figure 7 of El-Korchi and Wittels (*1*). The average crack bottom luminance was measured for several illumination conditions and crack widths. The bottom values were typically within ±(5–10) percent of the average value. Most of that variation is attributable to noise in the image acquisition system. Only a few tests were performed, but no major variations in bottom luminance were

found, so it is reasonably certain that a straight slot model is useful for understanding and simulating the luminance of cracks in distressed portland cement mortar samples.

The second limitation concerns reflectivity changes. In an image of a PCC pavement, the luminances of the mortar and aggregate are proportional to their respective reflectivities; visible contrast is caused by reflectivity differences between coarse aggregate and mortar. As pointed out earlier, the crack surfaces will all have the reflectivity of mortar except for at most one of the sidewalls or the bottom, which will have the reflectivity of aggregate. In the simulation model, the reflectivities of the crack surface, sidewalls, and bottom can be specified independently, allowing representation of all of the crack cases although it does not account for reflectivity changes along the crack length.

Unlike the effects of geometric changes just discussed, reflectivity changes are abrupt at the aggregate-mortar boundaries. Because material reflectivity difference is a major cause of image contrast, understanding the exact luminance values in these boundary regions is important in specifying and evaluating image processing algorithms that distinguish distressed from sound pavement. The simple model can simulate crack contrast in the region adjacent to a piece of aggregate but it cannot give detailed information about how the contrast varies at the aggregate boundaries. Figure 8 in El-Korchi and Wittels, the previous paper in this Record, shows digital images of a 0.06-in. (1.5-mm) crack in a prepared PCC sample containing hand-selected course granite aggregate with a maximum size of ⅜ in. (10 mm). The most luminous portion of Figure 8b in El-Korchi and Wittels is a shelf of mortar-covered aggregate about 1/16 in. (1.5 mm) below the pavement surface. The measured luminance on the shelf, relative to the average surface luminance, is 1.08, and the luminance calculated for a rectangular slot with the same dimensions and reflectivities is 1.02; the agreement between the modeled and measured luminance values is about at the limit of the experimental errors. The calculation provides luminance values when the crack bottom is mortar or when it is aggregate, but does not provide detailed information about how the luminance varies between them in the transition region at the ends of the aggregate. Enhancements to the model may provide a tool for future studies of the image contrast in these transition regions.

Total Characterization of the Pavement Images

In this section, limitations of the simulation model have been discussed, and simple arguments and measurements have been used to show that the model can be applied to understanding surface distress in PCC pavements. More testing and analysis need to be done to determine whether the model can be applied universally. That work is in progress and will be reported later. On the assumption that the model, or some modification of it, can be applied to most pavement conditions, it is useful to speculate on future directions that the work can take. First, the model can be applied to the problem of designing image acquisition and illumination systems. For example, an exhaustive search of crack contrasts calculated for a wide range of illuminating conditions may provide insights in how to optimize the illumination for crack detection. Or, calculated crack contrast can be used to write the video noise specification that will enable the image acquisition equipment to meet the system specification regarding probability of crack detection.

The second major use for computer models of pavement distress is in aiding development and testing of image processing algorithms. The pavement image contains signals from cracks and from aggregate on the concrete surface. In this paper, the visual appearance of cracks was described; comparable work remains to characterize the visual appearance of aggregate. Also, only PCC pavements were discussed; extension of the modeling to include surface distress in overlays and asphaltic concretes would be useful.

INTERREFLECTION CALCULATION

This section contains detailed information about the interreflection calculation model. It is presented for the benefit of those requiring detailed knowledge of the methods but it is placed at the end of the paper so as not to impede the reader who does not need this level of detail. Note that photometric units for light are used throughout this work. Originally designed to measure the response of the human eye to broadband natural illumination (sunlight), they are well suited to working with solid state cameras whose sensors are spectrally matched to the sensitivity of the human eye.

Cracks are jagged, irregular gaps in the pavement. For modeling purposes, they are considered to be rectangular slots of infinite length. The key parameters in the model are shown in Figure 4. Ambient lighting is omnidirectional and represents skylight; it is characterized by its apparent luminance. Directed lighting represents sunlight or the illumination from a spotlight directed at the pavement; it is characterized by an illuminance and a direction. The surfaces are assumed to be diffuse reflectors with four distinct reflectivities: pavement surface, crack sidewalls (the sides lit and unlit by the directed illumination), and crack bottom.

The crack is illuminated by one of two sources, ambient or direct illumination, as shown in Figure 5. In the model for ambient illumination (left), a uniformly diffuse emitter with luminance L_0 covers the top of the crack. In the model for directed illumination (right), a perfectly collimated beam with illuminance E_0 illuminates all surfaces except where shadowed by crack edges. The total illuminance at each point is the sum of two components. Using the incidence angles shown in Figure 6 (Φ is the polar angle relative to the pavement surface normal and Θ is the azimuthal angle relative to the crack sidewall normal), the illuminances at a point P_1 on the sidewall and a point P_2 on the crack bottom due to directed illumination are given by

$$E_{1,D} = E_0 \sin \Phi \cos \Theta$$

$$E_{2,D} = E_0 \cos \Phi \tag{1}$$

Note that the direct illuminance equations only apply to those portions of the crack walls and floor that are not shadowed by the crack edge. The shadow edge falls either on the crack bottom at $x = D \tan \Phi \cos \Theta$ or on the crack sidewall at $z = W/(\tan \Phi \cos \Theta)$, where the coordinate axes and dimensions are shown in Figure 5. The illuminances of the

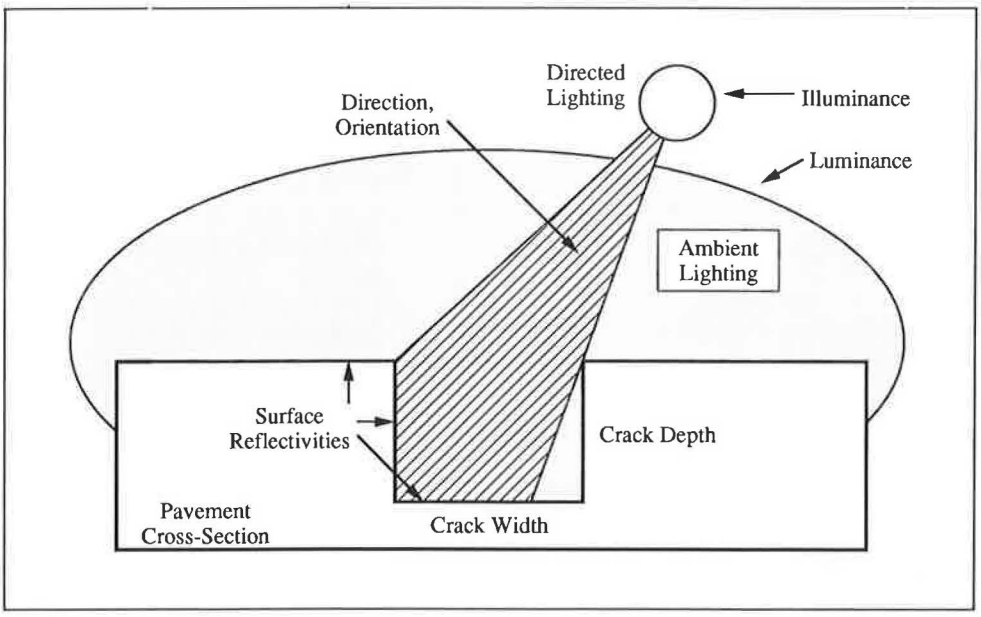

FIGURE 4 Cross-sectional view of an ideal pavement crack showing the adjustable parameters in the mathematical model.

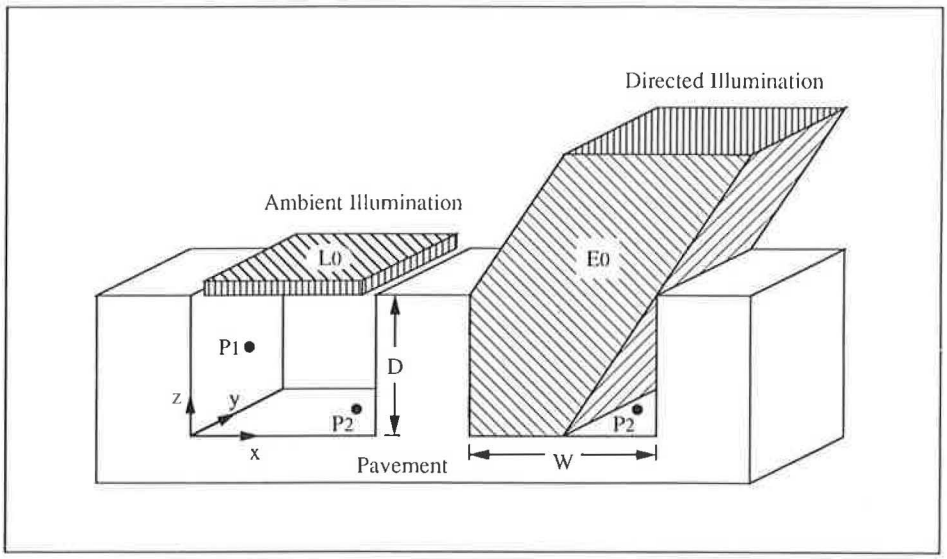

FIGURE 5 Thin slice through an infinitely long ideal crack showing definitions of the coordinate system, the symbols used for crack width and depth, and ideal illumination models for ambient illumination (left) and directed illumination (right).

same two points due to ambient illumination are given by the following equations:

$$E_{1,A} = \frac{\pi L_0}{2}\left(1 - \frac{z}{\sqrt{z^2 + W^2}}\right)$$

$$E_{2,A} = \frac{\pi L_0}{2}\left(\frac{x}{\sqrt{x^2 + D^2}} + \frac{(W - x)}{\sqrt{(W - x)^2 + D^2}}\right) \quad (2)$$

The total incident illuminance is the sum of two terms:

$$E_1 = E_{1,A} + E_{1,D};\ E_2 = E_{2,A} + E_{2,D}$$

A portion of the incident light is reflected back into the camera and on to all surrounding surfaces, including other parts of the crack. This interreflection between crack surfaces can significantly alter the apparent crack luminances and must be included in the calculation.

Divide the surface inside the crack into N infinitely long strips as shown in Figure 6, and assume that all surfaces reflect diffusely and that the reflectivities are as defined. If the total (incident plus interreflected) illuminance falling on the ith strip is E_i then the luminance of that strip is $L_i = R_i E_i/\pi$, where R_i is the strip's reflectance. In addition to the direct and ambient incident illuminances, there is a contri-

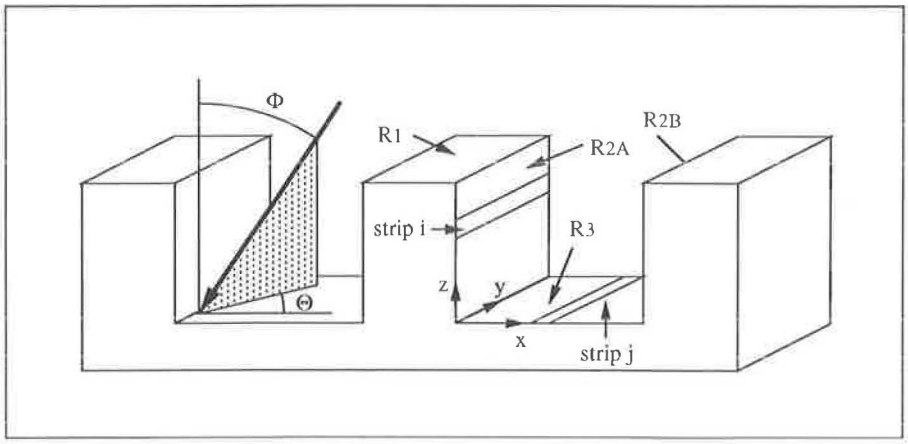

FIGURE 6 Polar coordinates used to define orientation of direct illumination (left) and two interreflecting strips (right).

bution from the light reflected by each of the other strips (except those lying on the same crack face as the ith strip). The contribution to E_i caused by L_j is

$$E_i = \frac{\pi L_j}{2}\left(\frac{z}{\sqrt{x_{jL}^2 + z^2}} - \frac{z}{\sqrt{x_{jR}^2 + z^2}}\right) = A_{ij}E_j \tag{3}$$

where x_{jL} is the left edge of the jth strip and x_{jL} is the right edge. This equation applies for the case illustrated—i is on a sidewall and j is on the crack bottom. Similar expressions apply to the other cases. The illuminances are thus related by a set of N linear equations:

$$E_i - \sum_{j \neq i}^{N} A_{ij}E_j = E_{i,D} + E_{i,A} \tag{4}$$

These equations are solved simultaneously to calculate the illuminance, and hence the luminance values, of each strip. If a further goal is to simulate the visual appearance of the crack, it can be calculated from the luminance values by using the perspective transformation techniques of computer graphics (*9*,*10*).

Note, the two-source model is satisfactory for simulating cracks illuminated by all possible combinations of skylight and sunlight. Because artificial illumination systems can be designed to produce arbitrary spatial and angular illuminance variations, this model may require modification. The right side of the last set of equations would be replaced by the strip illuminances caused by the light sources. The method of solution will otherwise remain the same as that discussed previously.

ACKNOWLEDGMENTS

The authors gratefully acknowledge the help and encouragement of many people who contributed to this work. Their colleagues M. Ward and M. Gennert aided in developing the technical strategy and some of the analyses used in the work. M. Turo of the Massachusetts Department of Public Works helped them understand the operational and technical requirements of automated pavement evaluation systems. J. Sage of the WPI CE Department aided in selecting the aggregate materials used. B. Bian contributed ideas on interreflection calculation methods. A. Bielund, S. Annecharico, and J. LeBlanc assisted in the calculations and experiments. This work was supported by the Research Development Council of the Worcester Polytechnic Institute.

REFERENCES

1. J. E. Kaufman (ed.). *IES Lighting Handbook*. Illuminating Engineering Society of North America, New York, 1981.
2. W. Thomas, Jr. (ed.). *SPSE Handbook of Photographic Science and Engineering*. John Wiley, New York, 1973.
3. J. Baker, B. Dahlstrom, K. Longenecker, and T. Buu. Video Image Distress Analysis Technique for Idaho Transportation Department Pavement Management System. In *Transportation Research Record 1117*, TRB, National Research Council, Washington, D.C., 1987, pp. 159–163.
4. N. Wittels and S. H. Zisk. Lighting Design for Industrial Machine Vision. *Proc., Society of Photooptical Instrumentation Engineers*, Vol. 728, 1986, pp. 47–56.
5. D. S. Goodman. Illumination Analysis with a Reflecting Sphere. *Applied Optics*, Vol. 24, 1985, pp. 1217–1219.
6. J. R. McClellan. Characterization and Correction of Image Acquisition System Response for Machine Vision. Master's thesis, Worcester Polytechnic Institute, Worcester, Mass., 1989.
7. J. R. McClellan et al. Characterization and Correction of Image Acquisition System Response for Machine Vision. *Proc., Society of Photooptical Instrumentation Engineers*, Vol. 1194, 1989.
8. N. Wittels et al. Lighting Design for Industrial Machine Vision. *Proc., Society of Photooptical Instrumentation Engineers*, Vol. 1005, 1988, pp. 47–56.
9. R. M. Haralick. Using Perspective Transformations in Scene Analysis. *Computer Graphics and Image Processing*, Vol. 13, 1980, pp. 191–221.
10. L. G. Roberts. Homogeneous Matrix Representation and Manipulation of *N*-Dimensional Constructs. Report MS-1405, MIT Lincoln Laboratory, Cambridge, Mass., 1966.

Publication of this paper sponsored by Committee on Pavement Monitoring, Evaluation, and Data Storage.

Computer-Based Model of Pavement Surfaces

CARL HAAS AND CHRIS HENDRICKSON

In order to facilitate the effective monitoring, testing, maintenance, and rehabilitation of pavement surfaces, a general model of pavement surface characteristics suitable for a wide range of applications is being developed. The surface model can include multiple types of sensor information, provides methods to integrate differing sensor data, incorporates multiple surface characteristics, supports automatic extraction of characteristics, provides different levels of surface model abstraction, and represents characteristics at different levels of spatial aggregation. With such a representation model, the development, implementation, and integration of improved sensors, management aids, and robot effectors could be considerably simplified. Although the primary applications of the model are to pavements, the model could be used for other constructed surfaces.

Maintenance and rehabilitation of pavements in the United States alone requires over $17 billion a year (*1*). This money is spent on a cycle of condition data acquisition, management, and work activities. The substantial resource costs involved have motivated the development of automated methods for acquisition of surface information, and for using surface characterizations for management or for automated maintenance and rehabilitation. Automated data acquisition can provide better quality data at less cost than conventional methods, and superior data can be used to improve management decision making. However, the manipulation of surface observations and the representation of surfaces to date are typically ad hoc and narrowly focused. Competing firms and agencies have developed separate and incompatible representation schemes. It is the premise of this work that a general standardized surface model could be extremely beneficial to the development of automated systems for characterization, management, and surface work. In effect, deriving a general standardized surface representation using the model would be the function of data acquisition, and the model would then be available for a multitude of purposes including management decision making and robot control across a wide range of applications.

Standardized representation models have been found to be useful in a broad range of computer based applications. For example, IBM's mathematical programming system (MPS) format has been widely used to represent and communicate linear programming problems among different computers and applications programs. In computer science, numerous standard representations are used, such as the instruction set processor notation language (ISPS) for central processors or the processor memory switch (PMS) notation to describe hardware architectures (*2*). In electrical engineering, standardized descriptive models exist that provide machine-readable representations of applications such as the layout of large scale integrated circuits; an example is the Caltech Intermediate Form to describe graphic items of very large scale integrated (VLSI) circuits (*3*). A recent example of a useful two-dimensional standardized representation model is the PostScript language to describe documents (*4*). Numerous document production and word processing programs will produce files in PostScript; and, similarly, numerous printers will accept files formatted in PostScript. In each of these cases, a standardized representation language has greatly aided the development of application modules and hardware.

The model described here is intended to serve as a general, standardized way to characterize and represent pavement surfaces. It could significantly improve data quality and process productivity through its surface representation and the unification and automation of key characterization procedures. For management applications, the improved data quality can result in more effective maintenance and rehabilitation strategies, thus decreasing life cycle costs. The model could also be useful for automatic substance recognition and its representation will be useful for planning machine actions; both are useful functions for tasks such as crack filling, patching, and grinding.

The recent introduction and improved availability and capability of new sensing technologies, such as laser distance sensors and video image analysis, has increased the range and magnitude of surface data available. It is clear that new methods are required to process and store this data. Representations and methods of analysis to date have been hampered by severe computing restrictions. The data structure size and the processing required by the model described here can be handled with the advent of affordable, large-memory, and multiprocessor desktop systems. Engineering workstations now exist with several megabytes of dynamic memory and the capability of adding additional processing boards for special functions. An additional factor motivating development of the model is the requirement imposed by several prototype systems for improved surface representation. For example, several prototype knowledge-based systems that have been developed for condition diagnosis (*5–7*) and project level rehabilitation and maintenance design (*8,9*) require the detailed information contained in the representation model.

The general pavement surfaces model and its implementation are discussed, then to illustrate its use one key application of the model is described. Before the model is described, the requirements of the model are considered. In essence, the model must produce a better description of pavement surfaces than what is currently available. In doing so, it must exceed the levels of efficiency and usefulness exhibited by existing

Department of Civil Engineering, Carnegie Mellon University, Pittsburgh, Pa. 15213–3890.

alternatives. Functionally, the model should meet the following requirements:

- Integrate information from multiple sources;
- Represent the surface using descriptive, accurate, and useful characterizations;
- Support representations at different levels of abstraction;
- Support different levels of spatial aggregation and characterization;
- Maintain well-defined spatial relationships among surface characteristics;
- Support quick access to surface characteristics;
- Store data efficiently;
- Support efficient and effective feature extraction; and
- Be easy to understand and apply.

This model has been implemented in the form of a software kernel, or tool kit. The implementation language is C++, an object-oriented language that is well suited to the purpose. The development environment has been UNIX. The kernel includes an interface to a relational data base management system (DBMS) that can be used for management of the large amounts of information. The kernel includes data manipulation, graphics, and basic interface software. Applications software for specific demonstrations is built using the kernel and application specific routines. The use of a software kernel establishes the general applicability of the model. The kernel should also be available and will be useful for other applications projects.

OVERVIEW

The general pavement surfaces model shown in Figure 1 is the combination of a surface representation and the process of deriving it. The surface representation includes characteristics at various levels of abstraction and aggregation. On the basis of this definition, derivation of the representation is termed "characterization." Characterization consists of two basic operations—data fusion and data structuring. Common data structures support characterization and facilitate the surface representation, and in this way unify the elements of the model.

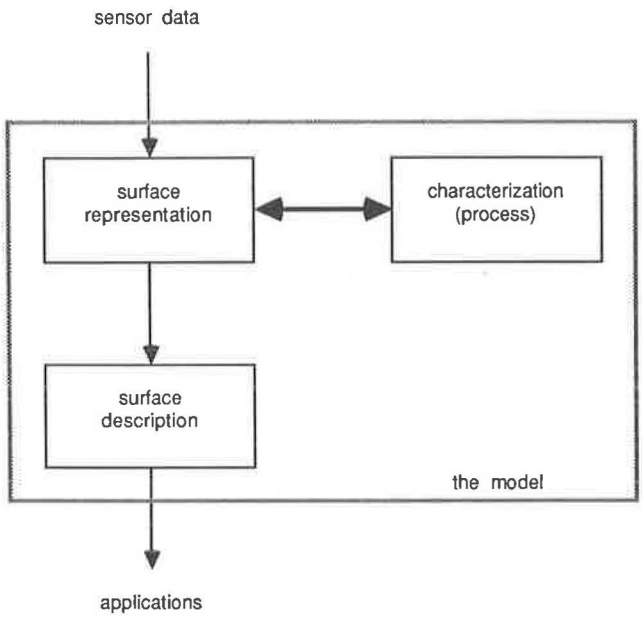

FIGURE 1 Standardized pavement surfaces model.

The model assumes that pavement surfaces are of two and one-half dimensions, so that pavement depth and deflection information can be included. This assumption implies that all significant parts of the surface are visible from directly above and therefore pavement surfaces can be described spatially with depth as a scalar component. Surfaces are represented by characteristics at different levels of aggregation or spatial extent. Three levels of characteristics are defined as follows:

- Properties—measured directly or derived from other properties,
- Features—derived from properties and other features, and
- Regions—aggregations of sets of features and properties.

The two basic operations in characterization can be defined as (a) data fusion, which is the process of combining existing data into a new datum, and (b) data structuring, which is the process of linking and integrating existing data. As an example, feature extraction implements fusion and structuring at the higher levels of abstraction and aggregation. Property and feature information including gray level, texture, and range data can be fused and then structured using feature extraction algorithms into features distinguishing new from filled pavement cracks.

The fusion and structuring procedures forming the characterization process are unified through a common data representation that also serves to describe the surface. The representation contains primarily two data structures, a grid, which supports sensor data structuring and early fusion processes, and a multilayer surface quadtree, which is used to relate properties and features in a framework useful for feature extraction and for applications. The multilayer surface quadtree has advantages over other surface descriptions. It is compact because of its hierarchical structure and is unified because its nodes create a useful parallelism among surface characteristics. Each node is a data structure, with slots for each property and feature in a quadrant and with values for each slot. Descriptions of features or unchanging properties spanning a wide area of the surface may be contained in higher nodes and propagated down the tree to access information at any level, including points. For example, Figure 2 shows a hierarchical representation of pavement depression and cracking information. In their final state, each quadrant encompasses an area in which the property or feature value is relatively constant.

A fundamental assumption of the model is that sensor data measurements can be mapped to points in a common two-dimensional grid pattern in cartesian coordinates. Measurements from different sensors can be referenced to a common point and thereby be related to each other. The grid thus becomes the most basic common structure by which the data are unified. The grid also serves another purpose. Each point in the grid has properties associated with it. Through processing, these properties give rise to more abstract surface characteristics stored in the quadtree, as described in the following paragraphs.

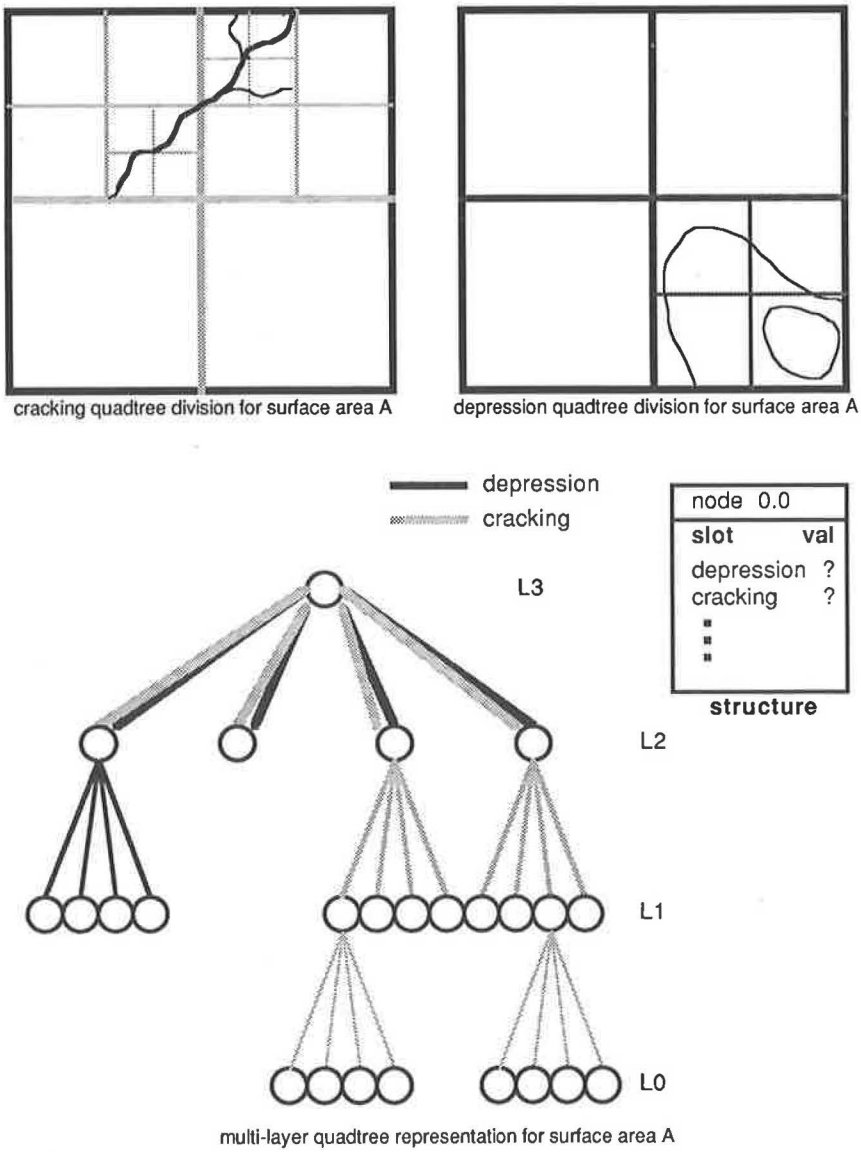

FIGURE 2 Multilayer surface quadtree.

SURFACE CHARACTERISTICS

Data are stored at different levels of surface aggregation and abstraction in the model. The levels defined include regions, features, and properties.

Properties

Properties are values associated directly with a grid point. A point property is defined as the value of a phenomena measured or calculated at a point in the *xy* grid. Point properties may include

- Elevation—the depth (i.e., distance in the negative z direction) of a point with respect to an *xy* reference plane above the surface.
- Color—the intensity of the red, green, and blue spectrums of light sampled at a point on the surface.
- Gray level—the intensity of a pixel in a monochrome video image.
- Infrared level—the degree of infrared radiation detected at a position on the surface.
- Electromagnetic potential—the magnitude and direction measured at a point on or just above the surface (useful for detecting subsurface reinforcing bars, for example).

A local property is defined as a value measured or calculated about and centered on a point in the *xy* grid. Examples of useful local properties include

- Gradient—calculated for elevation, gray level, color, or even other local properties.
- Texture—the phenomena of globally repetitive surface elements.
- Edges—an edge is the boundary between two different areas. Points on the grid can be identified as edges through simple gradient thresholding operations or by more complex means.

- Friction—measured using regular rubber tires, for example.

Features

A feature is defined as a spatial attribute of the surface that helps to characterize it. Features are associated with areas of the surface. In the model, they form the primary descriptions of the surface though they can be grouped or formed into regions for specific applications. A representative list of possible features includes

- Material type—such as asphalt mixtures and concrete types.
- Cracking—an area with one or more cracks identified can be described as cracked.
- Rutting—a longitudinally depressed area in the path of the wheel track.
- Raveling—the loss of surface aggregate in an area.
- Flushing—where excess asphalt has been flushed to the surface.
- Shoving and rippling—areas shoved by slowing or accelerating vehicles.
- Patching—an area that has been covered over or filled, usually with asphalt.
- Potholing—an area has this feature if it is part of the hole.
- Depression and swelling—a downward or upward bulge, respectively, in the pavement surface.
- Strength—derived from deflection.
- Histogram distribution—a function giving the frequency of occurrence of property values.
- Frequency spectrum—can be calculated for elevation or gray level across an area.

This is by no means a comprehensive list. Also, it should be noted that road distress features are often classed by severity and density. These two factors can be easily integrated in the model. For a thorough definition of pavement characterizing features, see the AASHTO pavement design guide (*10*).

Regions

A region is defined as a continuous area of a set of features and/or properties. Regions can be areas of hypothetical condition and cause pairs, areas of a particular condition, or areas where a set of features is relatively constant, such as areas of a type of material or substance. Regions can be derived using manual, algorithmic, or knowledge-based processes.

THE GRID REPRESENTATION

The grid is the basic common structure by which sensor data are unified. It is an array of points laid out in a rectangular pattern in an xy reference plane. The plane is normally located above the surface and its orientation is arbitrary. The space between the points along either axis is the same, but the number of points along either axis is variable as well as the magnitude of the space between the points. The dimensions of the grid should be chosen so that all sensor data can be associated in a one-to-one mapping with points on the grid—so that no two datums from one sensor can be mapped to the same grid point. This condition is satisfied if the data type with the highest spatial resolution is used as a basis for the grid dimensions. The highest will often be digitized image data.

The definition of the grid ignores sensor performance in terms of spatial resolution, range resolution, scanner position accuracy, and dynamic range. Instead, these factors are considered in the measure of variance associated with each sensor that may be used for sensor fusion. Spatial and range resolutions should be considered when configuring a sensing system for the task at hand. The grid model is concerned only with the fact that sensor measurements are centered on points and that these points can be related to a common rectangular grid.

THE MULTILAYER SURFACE QUADTREE

Quadtrees are a regular, symmetric, recursive decomposition of a plane into homogeneous areas. Their focus on interesting subsets of the plane results in efficient representation. This efficiency and their hierarchical nature facilitate efficient processing for image data processing, including set operations. The fusion and feature extraction operations included in the pavement surfaces model are in a large degree composed of set operations. The major applications of quadtree technology to date have been cartographic data systems, VLSI circuit layout, and image compression (*11*). Although many of the fundamental objects and algorithms developed for cartographic applications in particular are useful for the pavement surfaces model, the multilayer quadtree is a significant departure from practice.

The single quadtree for a binary valued feature such as material type can be visualized as an upside-down tree shaped like a pyramid with branch nodes which are black, white, or gray. At any level on the tree, if all of the areas below the level contain (or do not contain) the feature, then the node at that level is black or white; that is, it does or does not contain the feature, correspondingly. If the areas below are both black and white, then the node at that level is gray; that is, areas below may contain the feature. At the grid point level, a point and the area about it either are associated with the feature or are not. Construction of the quadtree may proceed from the grid point level upward if features have been derived at that level, or it may proceed from the highest aggregate level of the grid on downward if features are recursively detected within quadrants. In practice, construction may be a hybrid depending on the feature extraction control strategy. Extensions to discrete valued variables are possible.

To permit efficient characterization of pavement surfaces and to provide a useful representation for applications, it is necessary to closely relate features and properties spatially and to access related characteristics quickly. This is a requirement for both the data fusion and data structuring operations that form feature extraction, and it is required for applications such as pavement condition diagnosis where features must be compared and related spatially in order to draw conclusions.

The solution is to merge the single quadtrees into one multilayer quadtree (Figure 2).

In order to understand the relationship between the multilayer quadtree and feature extraction, an example may be useful. To extract the feature "fatigue cracking," the characteristics rutting, strength, and cracking might be used. These characteristics may be found in the multilayer quadtree as slot values (numeric values rather than the gray or black slots described earlier) in a quadrant's node. The slot values are datums that are combined by the feature extraction algorithm into a new datum that represents fatigue cracking. This process is data fusion. Relating the new feature, fatigue cracking, to an area of the surface is achieved by inserting its value into a new feature slot. The structure of the multilayer quadtree relates the fatigue cracking feature spatially to the other characteristics. The insertion of the value "fatigue cracking" is data structuring. The process of feature extraction is made more efficient by permitting quick access of comparative datums because of the tree structure and because the fusion process is achieved at the highest level of aggregation possible (i.e., where the values of both characteristic datums are black and white). This condition is used to make applications such as local diagnosis more efficient also.

THE STRIP QUADTREE

The quadtree representation of the pavement surface must be functionally continuous. In practice, functional continuity means that for a section of road perhaps as much as 1 km long, its representation should consist of a single unified data structure, a data indexing scheme, or a combination of these two. Also, quadtree algorithms should work without modification over the entirety of the structure. For a square area such as that selected for automated surface work (or even for a large rectangular area like a building wall or parking lot), the structure would be a standard multilayer quadtree with a single root. For a pavement section, or an area shaped like a strip, when individual quadtrees grow to fill the width of the pavement section they may be linked to a larger quadtree having many blank nodes, or through a transition mechanism into a binary type tree along the length of the section with a single root for the section. Alternatively, the top quadtree nodes can be overlapped so that each quadrant can have one parent but two root nodes (Figure 3). The root nodes, their substructures, and their position on the grid along the section can then be stored in a table for subsequent access to the condition data. This latter approach to linking the quadtree quadrants along the pavement section is used to implement functional continuity. The resulting structure is called the strip quadtree.

An implementation issue of key concern is information management. This issue includes management of raw sensor data files and the permanent storage and retrieval of quadtree surface representations. To achieve the latter, the structure of the quadtree must be retained in memory. To do this, quadtree representations can be broken up and stored in regular files. Access to section data by area and by level of aggregation is facilitated by this stored structure and a table of index and address information. Quadrant files can be ordered by their grid addresses. Each quadrant data file will have its section address, section, file name, and other associated data

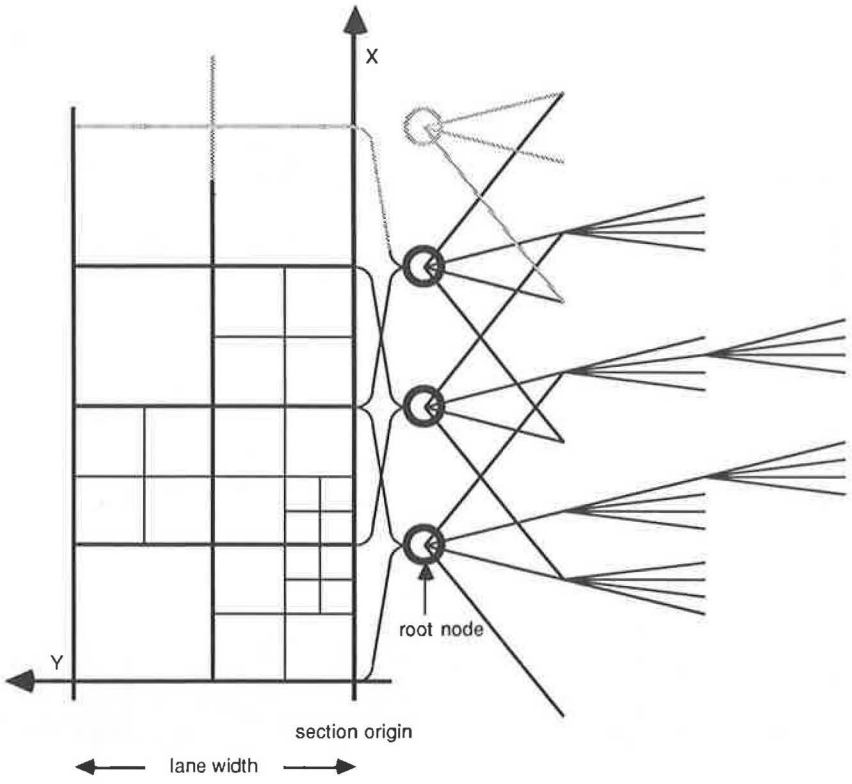

FIGURE 3 The strip quadtree.

stored in a table. This table, and a table for sensor data arranged into files with associated addresses, can be implemented in a relational DBMS (*12*) (Figure 4). In the first relation, the grid coordinates are the key. In the second, the sensor data view file name is the key. Grid coordinates link the tables as they do other components of the model. Access to information concerning a section of road that has been characterized using the multilayer quadtree representation is thus made possible at various levels of aggregation and by area. Automated applications such as condition assessment and maintenance selection can be constructed on top of this kernel facility. Direct user requests for information are possible, too. This facility could also be implemented within an existing pavement management data base system, so that condition estimates and maintenance and rehabilitation activities can be related as well.

sensor data DBMS table

sensor_data filename	x_start	x_end	y_start	y_end	section name

multi-layer quadtree data DBMS table

quad_data filename	x_start	x_end	y_start	y_end	section name

FIGURE 4 Information access tables.

EXAMPLE APPLICATION

Pavement management systems are a typical application relying on surface characterizations. Although numerous examples of pavement management systems exist (*13,14*), no general surface representation exists that provides a vertical, automated, common link between data acquisition systems and pavement condition reporting systems for maintenance and rehabilitation prioritization. The general pavement surfaces model can act as this link. Surface features like cracking, rutting, roughness, and strength can be derived using the model and reported at any degree of aggregation. Using the strip quadtree, the model can even be used to calculate aggregate pavement condition indexes for whole sections of pavement.

A simple demonstration of this type of application is to use the model for information integration, surface characterization, and condition reporting. For example, correlated data are available from the Komatsu Automatic Pavement Distress Survey System (*15*), among others. The data are based on an approximately 1-mm-square grid. Digital image data are provided in a 4-m scan width across the pavement (Figure 5). Automatically recognized crack data derived from the image data are provided in vector format based on the grid. Roughness data are provided approximately every 10 cm, and rutting data approximately every 5 cm. Some road use data are also provided. Although the data available are sufficient for demonstration purposes, it would be desirable also to have friction, deflection, and detailed road use data.

A representative set of the data described is being integrated using the pavement surfaces model, and the model's representation is being used to characterize and assess the condition of the pavement sections concerned. The representation bounds are presented in Figure 6. The lowest level of aggregation is 0.5 m^2 for the cracking data. This corresponds to the fourth level of the quadtree from the top. The

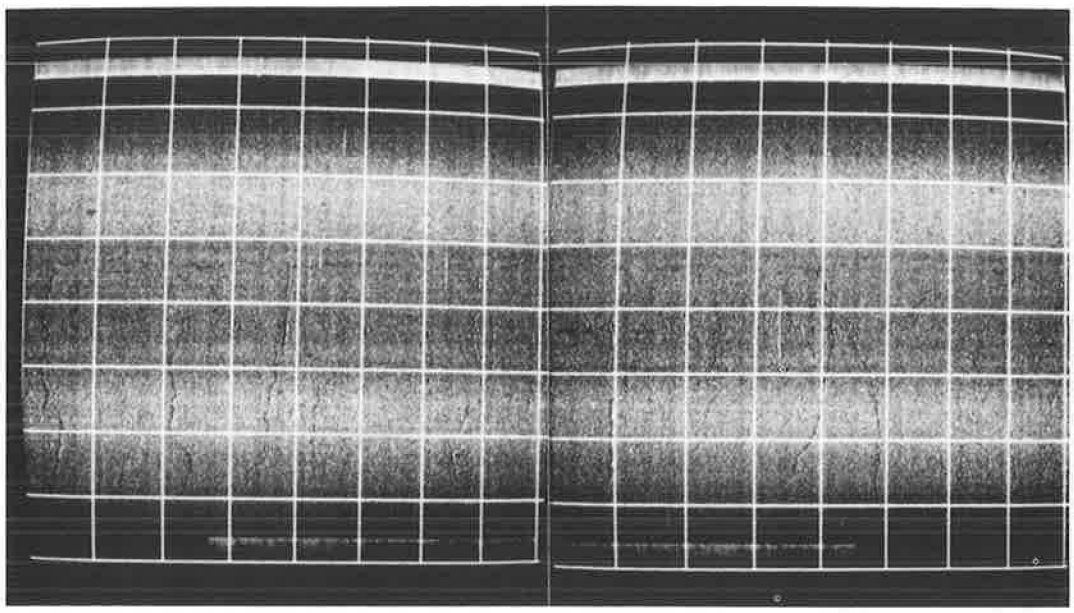

FIGURE 5 Pavement image data.

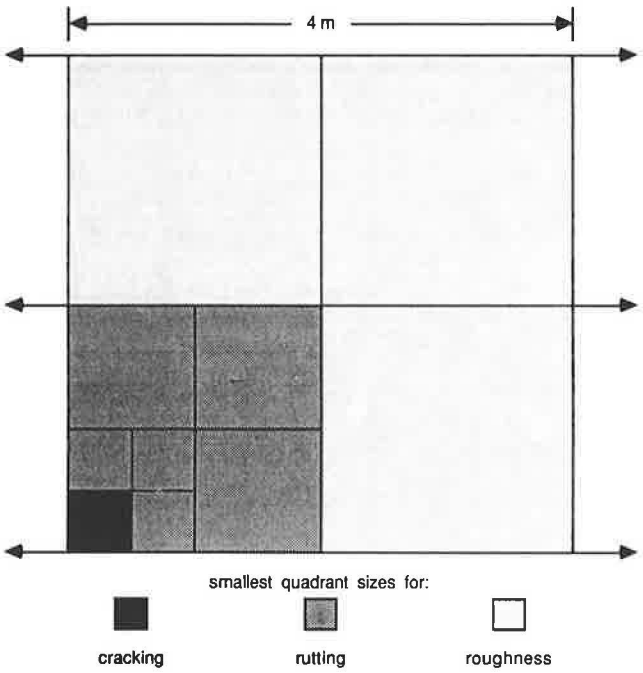

FIGURE 6 Pavement surface representation.

rutting data are averaged and at their lowest level represented for every 2.0 m square, or the second level of the quadtree from the top. The roughness data are derived for every 4.0-m square, or for each root of the strip quadtree. These three surface characteristics could be represented in more detail with the strip quadtree structure. However, the low bounds of aggregation chosen seem reasonable. Extension down to the basic grid level of 1 mm square is possible if more detailed modeling is required. Road use data can be stored in a global context structure. Surface conditions such as fatigue cracking can be derived from the spatial intersection recorded in the quadtree of the characteristics described. After including such derived surface conditions in the representation, maintenance actions can be selected automatically. Accurate pavement condition index values can also be derived using this representation, and for sophisticated applications such as deterioration modeling, the percent of road surface covered by a condition can be calculated.

CONCLUSIONS

A general model of pavement surfaces has been described. The model can include multiple types of sensor information, provides methods to integrate differing sensor data, incorporates multiple surface characteristics, supports automatic extraction of characteristics, provides different levels of surface model abstraction, and represents characteristics at different levels of spatial aggregation. Surface characteristics are represented as properties, features, and regions. They are unified through a common grid structure. A multilayer quadtree is constructed on top of the grid. It supports information integration and automated surface characterization, and it provides surface descriptions suitable for a wide range of applications. A unique strip quadtree construct is used to represent nonsquare pavement surface areas for functional continuity.

A software kernel implements the pavement surfaces model and is closely linked with a relational DBMS. Applications software can be produced using the kernel as a tool kit. The model is being applied to several problems for demonstration and evaluation including (a) automated pavement distress identification and analysis, and (b) automated pavement maintenance (*16*). The model's advantages in data integration, data compression and processing, data storage and retrieval, and automated work planning are being investigated in these applications.

With the pavement surfaces model, the development, implementation, and integration of improved sensors, management aids, and robot effectors should be considerably simplified.

ACKNOWLEDGMENTS

The research on which this paper is based has been supported in part by the CMU Department of Civil Engineering, the Natural Sciences and Engineering Research Council of Canada, and the Roads and Transportation Association of Canada. The research has also become the basis for subsequent research support from the Strategic Highway Research Program of the National Research Council, National Academy of Sciences. The authors would like to express their sincere appreciation for this support.

REFERENCES

1. *Our Nation's Highways: Selected Facts and Figures*. Report 7558-106, FHWA, U.S. Department of Transportation, Jan. 1987.
2. C. G. Bell, J. C. Mudge, and J. E. McNamara. *Computer Engineering*. Digital Press, 1978.
3. C. Mead and L. Conway. *Introduction to VLSI Systems*. Addison-Wesley, Reading, Mass., 1980.
4. Adobe Systems Incorporated. *PostScript Language Reference Manual*. Addison-Wesley, Reading, Mass., 1985.
5. R. Littlefield, B. Brademeyer, and K. Maser. Pavement Condition Diagnosis Based on Multisensor Data. In *Knowledge Based Expert Systems for Engineering*, Computational Mechanics Publications, Southampton, U.K., 1987, pp. 55–70.
6. K. R. Maser. Automated Interpretation for Sensing In Situ Conditions. *Journal of Computing in Civil Engineering*, Vol. 2, No. 3, July 1988, pp. 215–238.
7. J. Hajek and C. Haas. Applications of Artificial Intelligence in Highway Pavement Maintenance. *Proc., 3rd International Conference on Applications of Artificial Intelligence in Engineering, Stanford, California*, Computational Mechanics International Ltd., Aug. 1988.
8. C. Haas and H. Shen. Preserver: A Knowledge Based Pavement Maintenance Consulting Program. *Proc., 2nd North American Conference on Managing Pavements*, Ministry of Transportation and Communications, Ontario, Nov. 1987, pp. 2.327–2.338.
9. S. G. Ritchie. Applications of Expert Systems for Managing Pavements. *Proc., 2nd North American Conference on Managing Pavements*, Ministry of Transportation and Communications, Ontario, Nov. 1987, pp. 2.277–2.287.
10. *AASHTO Guide for Design of Pavement Structures*. AASHTO, Washington, D.C., 1986.
11. H. Samet. The Quadtree and Related Hierarchical Data

Structures. *Computing Surveys*, Vol. 16, No. 2, June 1984, pp. 187–260.
12. C. J. Date. *An Introduction to Database Systems*. In *The Addison-Wesley System Programming Series, Volume 1, 3rd Edition*, Addison-Wesley, Reading, Mass., 1982.
13. W. R. Hudson and R. Haas. *Pavement Management Systems*. McGraw-Hill, New York, 1978.
14. M. Shahin and S. Kohn. *Pavement Maintenance for Roads and Parking Lots*. Technical Report M-294, Construction Engineering Research Laboratory, U.S. Army Corps of Engineers, Champaign, Ill., Dec. 1981.
15. T. Fukuhara, K. Terada, M. Nagao, A. Kasahara, and S. Ichihashi. Automatic Pavement Distress Survey System. *Proc., 1st International Conference on Applications of Advanced Technologies in Transportation Engineering*, Sinha and Hendrickson (eds.), Purdue University, W. Lafayette, Ind., Feb. 1989.
16. C. Haas, C. Hendrickson, and S. McNeil. *A Design for Automated Pavement Crack Filling*. Technical Report, Department of Civil Engineering, Carnegie Mellon University, Pittsburgh, Pa., Feb. 1990.

None of the supporting parties may be held responsible for the analysis or conclusions stated herein.

Publication of this paper sponsored by Committee on Pavement Monitoring, Evaluation, and Data Storage.

Correlation of Profile-Based and Response-Type Roughness Devices for Louisiana's Highway Performance Monitoring System

STEVEN L. CUMBAA

Relationships were developed to meet and facilitate roughness reporting and calibration requirements of the Highway Performance Monitoring System (HPMS) in Louisiana. Pavement roughness statistics obtained from a Face Dipstick, K. J. Law Model 8300 Roughness Surveyor, and Mays Ride Meter equipment were correlated to enable Louisiana to satisfy these requirements. On the basis of the results of this research and previously established relationships between the Mays Ride Meter and the AASHO serviceability index (SI), comparisons of the international roughness index (IRI) and SI were then drawn for flexible and rigid pavements. A correlation was established between the IRI values obtained with the Face Dipstick and those obtained with the Model 8300 Roughness Surveyor for 5 flexible and 4 rigid pavement test sections. Correlations from field testing of the Model 8300 Roughness Surveyor and Mays Ride Meter on 20 flexible and 19 rigid test sections resulted in a distinct relational equation for each pavement type. However, results relating IRI and SI indicated that this relationship was the same for all pavement types. This methodology can be developed so that Louisiana can satisfy HPMS roughness testing and reporting requirements.

Recent changes in reporting requirements for the Highway Performance Monitoring System (HPMS) require each state to report roughness in the form of the international roughness index (IRI). The IRI summary roughness statistic resulted from work conducted at the International Road Roughness Experiment in Brazil in 1982, as documented in World Bank Technical Paper No. 45 (*1*). IRI values for each HPMS section may be determined with any of a number of calibrated roughness measuring devices. In general, all commonly used roughness measuring devices may be used as long as the selected device is calibrated against a known-profile reference statistic, which for HPMS requirements is the IRI as computed from a direct measure of the longitudinal profile.

Direct measures of the longitudinal profile are obtained from Class I devices (and methods), which include longitudinal survey by rod and level and Face Dipstick, or Class II devices, which include the 690 DNC Profilometer, APL Longitudinal Profile Analyzer, and Automatic Road Analyzer (ARAN), among others. The accuracy of Class II devices must be validated by means of comparisons with Class I devices to satisfy HPMS reporting requirements.

Indirect measures of the longitudinal profile are those obtained from response-type road roughness meters (RTRRM) systems such as the Mays Ride Meter. RTRRM systems are referred to as Class III devices by HPMS.

In an effort to facilitate and fulfill calibration requirements, Louisiana Transportation Research Center recently purchased a Face Dipstick, a Class I device that replaces the traditional rod and level type of survey.

Correlations of a Class II device to a Class I device and additionally a Class III device to the Class II device were obtained for both flexible and rigid test sections. Relationships were also developed that linked the IRI obtained from a Class I and Class II device to a Class III device and the AASHO serviceability index (SI) or ride rating.

The correlations and relationships indicated in this paper are considered relevant only to normally constructed flexible and jointed (rigid) pavements. Highly textured pavements, such as an open graded friction course or a heavily tined rigid pavement, and pavements with atypical characteristic roughness, may not produce an equivalent response or measure from some of the devices as did the pavements tested in this study.

Roughness data collected and evaluated during this study are presented in Table 1.

CORRELATION: CLASS II TO CLASS I

The IRI is a summary roughness statistic—the accumulated suspension motion divided by the distance traveled—as obtained from a mathematical model of a simulated quarter-car traversing a measured profile at 50 mph (*1*).

The K. J. Law Model 8300 Roughness Surveyor (Class II) is attached to a vehicle and uses an ultrasonic probe and accelerometer to measure the longitudinal roadway profile in one wheel path. One of the data outputs of the device is called the Mays Index. The Mays Index has units of inches per mile and is equivalent to the IRI in the same units (*2*). The Roughness Surveyor was correlated to the Face Dipstick (Class I) by means of testing a 0.2-mi portion of five flexible and four rigid project test sections in the outside wheel path.

The Face Dipstick is a manually operated device that is walked along the test path on two so-called "feet" spaced 1 ft apart. This device automatically records each individual change in elevation, and thereby the profile, as it is incrementally walked through the test path. Using an on-board

Louisiana Transportation Research Center, 4101 Gourrier Ave., Baton Rouge, La. 70808.

TABLE 1 ROUGHNESS DATA

Section Number	Face Dipstick IRI(in./mi)	LA. MRM. (in./mi)	Louisiana Predicted SI	K.J.Law 8300 8300 IRI (in./mi)	World Bank Recommended IRI(in./mi)
Rigid Test Sections					
21	N/A	192	2.30	268	271
22	N/A	51	4.10	109	69
24	N/A	48	4.20	98	61
31	N/A	128	3.00	210	178
32	N/A	106	3.20	187	156
33	N/A	93	3.40	142	134
35	N/A	80	3.60	120	114
37	N/A	138	2.80	193	202
39	N/A	80	3.60	118	114
71	N/A	112	3.10	192	167
82	N/A	64	3.90	108	87
83	N/A	109	3.20	153	156
84	N/A	45	4.20	92	61
85	N/A	38	4.40	86	45
86	N/A	35	4.50	84	37
87	N/A	38	4.40	72	45
88	N/A	35	4.50	81	37
89	N/A	243	1.90	314	337
90	N/A	176	2.50	240	242
97	110	N/A	N/A	26	N/A
98	89	N/A	N/A	96	N/A
99	168	N/A	N/A	174	N/A
100	284	N/A	N/A	322	N/A
Flexible Test Sections					
1	N/A	26	4.40	74	45
2	N/A	22	4.50	75	37
3	N/A	13	4.80	76	14
4	N/A	16	4.70	77	22
7	N/A	147	1.80	293	356
8	N/A	138	1.90	284	337
9	N/A	99	2.50	212	242
10	N/A	42	3.90	113	87
11	N/A	45	3.80	110	96
12	N/A	192	1.40	512	444
13	N/A	54	3.50	167	124
14	N/A	70	3.10	172	167
15	N/A	77	3.00	185	178
16	N/A	51	3.60	142	114
17	N/A	67	3.20	162	156
18	N/A	19	4.60	87	29
19	N/A	35	4.10	90	69
20	N/A	35	4.10	95	69
91	N/A	170	1.60	492	N/A
92	120	N/A	N/A	34	N/A
93	45	N/A	N/A	47	N/A
94	147	N/A	N/A	175	N/A
95	298	N/A	N/A	330	N/A
96	293	N/A	N/A	335	N/A

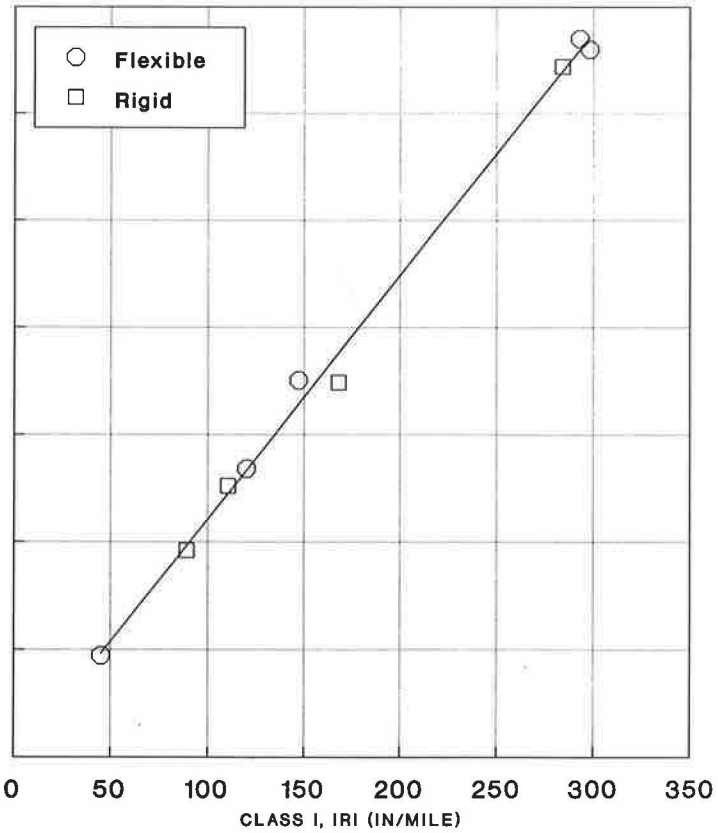

FIGURE 1 Correlation of the K. J. Law Model 8300 Roughness Surveyor (IRI) and the Face Dipstick (IRI).

computer system, the Dipstick computes the IRI of the tested section from the measured profile in units of inches per mile.

The correlation of the Roughness Surveyor to the Dipstick is shown in Figure 1. The derived relationship between the two devices is expressed in Equation 1, in units of inches per mile. This correlation should only be considered as valid within the range of roughness sampled.

$$(\text{IRI, Class II}) = 1.14(\text{IRI, Class I}) - 3.10 \quad (1)$$
$$R^2 = 0.99$$

Previous research (yet to be published) conducted by Louisiana Transportation Research Center with the Roughness Surveyor has indicated that this instrument has a significant ability to obtain repeatable measurements on both flexible and rigid pavements across a wide range of roughness levels. This research has indicated that the Roughness Surveyor might have less repeatability when testing open-textured pavements. Although the Dipstick appears to be repeatable, to date this aspect has not been fully evaluated in Louisiana.

CORRELATION: CLASS III TO CLASS II

Due to fundamental differences in materials and construction techniques, characteristic profiles are significantly different between flexible and rigid pavements (*3–5*). Previous research has indicated that the RTRRM response is specific to the vehicle, meter, pavement type, and roughness level combination under consideration. In other words, a particular RTRRM system may or may not (generally will not) respond equally to equivalent roughness contents contained within a typical flexible and rigid pavement. Additionally, nonlinearities and other detrimental effects inherent within each system and between individual units further hamper or distort the abilities of RTRRM systems to ideally quantify a pavement's roughness. It has been widely reported that separate correlations (unique to pavement type) are needed when relationships are developed using RTRRMs (*1,3–7*).

Correlations were developed by comparing the data obtained by Louisiana's Mays Ride Meter (Class III) in units of inches per mile to that of the Roughness Surveyor in IRI units, which are also inches per mile. Twenty flexible and 19 rigid test sections were tested repeatedly over a period of several months with both devices. The correlation of the Class III device to the Class II device for both the flexible and rigid test sections is shown in Figure 2. This correlation is for a particular Mays Ride Meter and vehicle combination during a particular period of time.

The derived relationship between the two devices for flexible pavements is expressed in Equation 2. The relationship for rigid pavements is expressed in Equation 3.

Flexible Pavement

$$(\text{in./mi, Class III}) = 0.40(\text{IRI, Class II}) - 2.89 \quad (2)$$
$$R^2 = 0.93$$

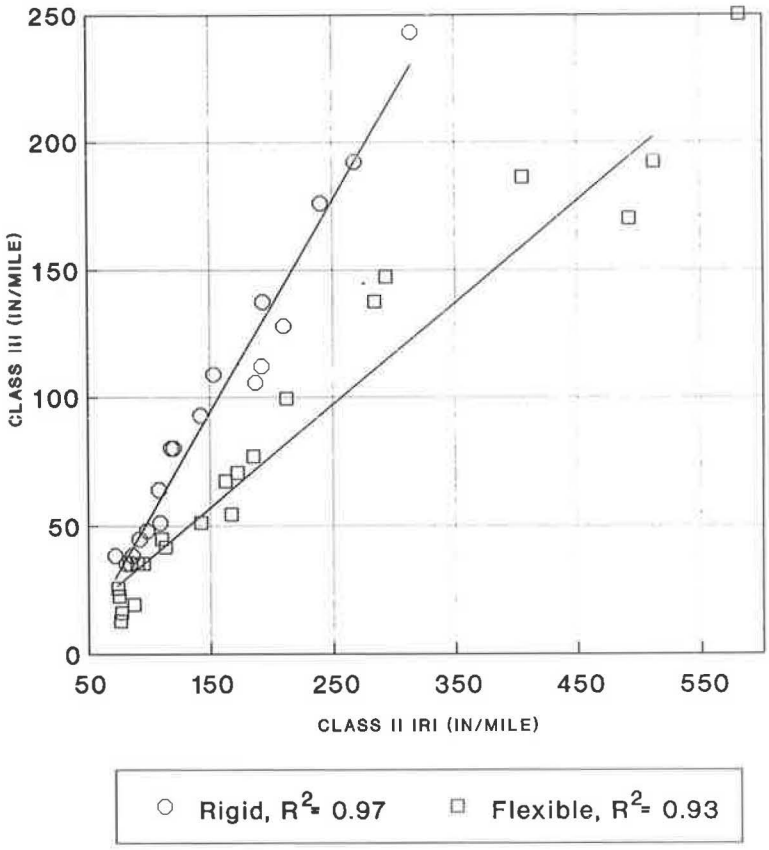

FIGURE 2 Correlation of Louisiana's Mays Ride Meter (Model 259–526) (in./mi) and the K. J. Law Model 8300 Roughness Surveyor (IRI).

Rigid Pavement

$$\text{(in./mi, Class III)} = 0.83(\text{IRI, Class II}) - 30.30 \quad (3)$$

$R^2 = 0.97$

RELATIONSHIP: CLASS III TO CLASS I

Substituting Equation 1 into Equations 2 and 3 yields relationships between the Dipstick and Louisiana's Mays Ride Meter for flexible and rigid pavements. The relationships derived in this manner are shown in Figure 3. The resulting equations are expressed as Equation 4 for flexible pavements and Equation 5 for rigid pavements. Equations 4 and 5 should only be considered as valid within the range of roughness sampled with the Class I device.

Flexible Pavements

$$\text{(in./mi, Class III)} = 0.46(\text{IRI, Class I}) - 4.26 \quad (4)$$

Rigid Pavements

$$\text{(in./mi, Class III)} = 0.95(\text{IRI, Class I}) - 32.87 \quad (5)$$

RELATIONSHIP: AASHO SERVICEABILITY INDEX TO CLASS II IRI

Through the years, numerous roughness measuring devices, profile analysis techniques, and tools have been developed in an effort to characterize a pavement's roughness to such a degree that it would equate to a subjective panel rating. Without a link to SI or a ride rating, all summary roughness statistics are only relative indicators of roughness.

At the AASHO Road Test, the panel reacted (rated rideability) differently depending on pavement type when measured levels of roughness (AASHO profilometer) were the same (*8*). This anomaly resulted in the formulation of separate equations to relate measured roughness to serviceability rating.

Louisiana currently uses a dual system to relate Mays Ride Meter inches-per-mile statistics to the serviceability index (SI). These relationships were developed through correlations with a Surface Dynamics and Chloe profilometers and verified by a recent panel rating (*6*). The equations developed from these relationships for the particular Mays Ride Meter used in this research are presented as Equations 6 and 7 for flexible and rigid pavements, respectively.

Flexible Pavements

$$SI = 5.01e^{-[\ln(\text{in./mi, Class III})/4.977]^{4.738}} \quad (6)$$

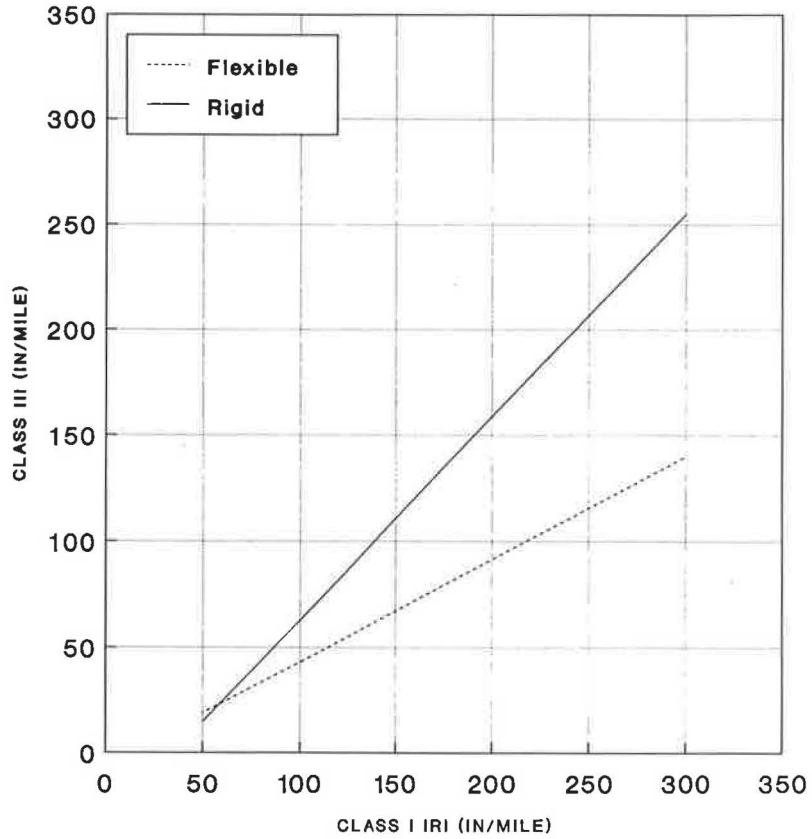

FIGURE 3 Relationship between Louisiana's Mays Ride Meter (Model 259–526) (in./mi) and the Face Dipstick (IRI).

Rigid Pavements

$$SI = 5.16e^{-[\ln(\text{in./mi, Class III})/5.521]^{4.423}} \quad (7)$$

Figure 4 shows a plot of the relational data trend between an IRI as measured by the 8300 Roughness Surveyor (Class II) and the SI (or ride rating) for the 20 flexible and 19 rigid test sections. In this plot, the SI of each of the tested sections is the serviceability as estimated on these sections by the previously established relationships between Louisiana's Mays Ride Meter and SI for flexible and rigid pavements. As shown in Figure 4, the relationship indicated between IRI and SI is the same regardless of pavement type.

Shown in Figure 4 for comparison is the relation between IRI and SI for the tested sections as determined through a predictive equation recommended by D. O. Paterson (*9*) from his work at the International Roughness Experiment sponsored by the World Bank. Generally, there is close agreement indicated in the relationships of IRI and SI as estimated in this report, and as predicted by Paterson (*9*).

RELATIONSHIP: CLASS I TO SERVICEABILITY

Figure 5 is similar to Figure 4, except that in this case the IRI values for the tested sections were not measured, but calculated from the relationship between Classes I and II expressed in Equation 1. A unique relationship is again indicated, with even fewer discernible differences between pavement types or the relationship recommended by the World Bank (*1*).

ADDITIONAL RESEARCH NEEDED

If it is true that the IRI uniquely relates to a subjective rating by a panel and is not pavement-type specific, then the following question arises: "Are the historical (AASHO) Chloe profilometer relationships between slope variance and panel rating unique to pavement type due to the panel's subjective judgment that equivalent slope variance measures on flexible and rigid pavements feel different, or is slope variance combined with the (AASHO) Chloe profilometer not able to adequately quantify or measure equivalent roughness between pavement type?"

To answer this question, it would be interesting to determine the IRI relationship to panel rating for those pavement profiles on which the slope variance and serviceability rating relationships were developed for the AASHTO Road Test.

The International Road Roughness Experiment was conducted in Brazil in 1982 on sites that were asphaltic concrete, surface treatment, gravel, and earth (*1*). Research that provides information verifying the IRI-SI relationship, including that obtained on continuously reinforced concrete, jointed concrete, and asphaltic concrete overlays of the same, is also needed.

Another area of research that would be of benefit would be a correlation of the IRI obtained through a precise rod and level survey and that obtained with the Face Dipstick on a variety of pavement surfaces. Due to its accuracy and relative ease of operation, the Dipstick in many ways can be considered superior to the conventional rod and level survey.

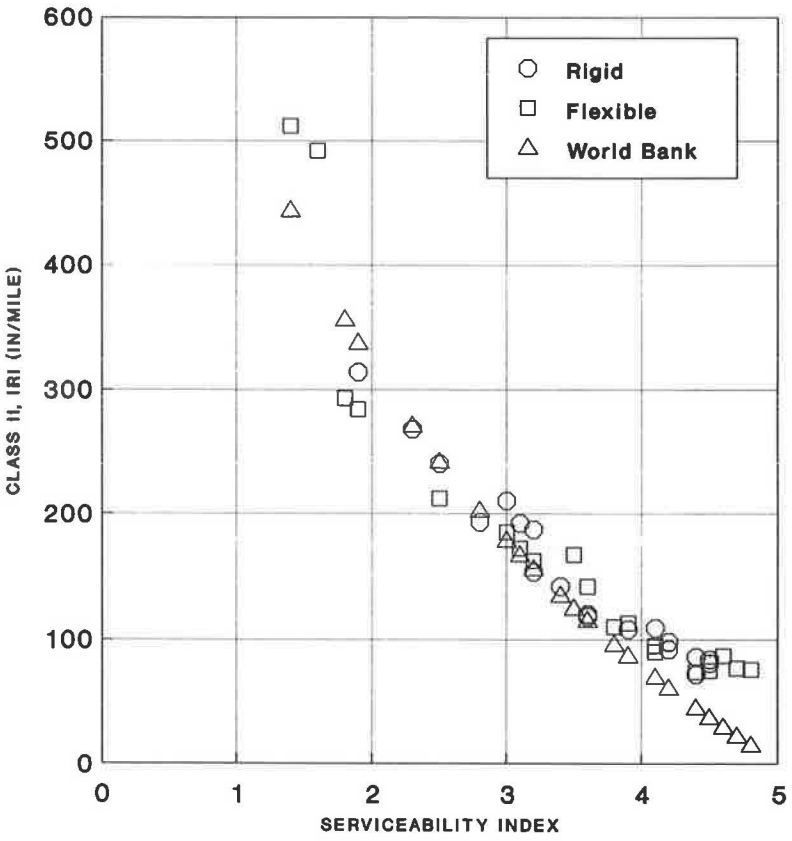

FIGURE 4 Relationship between the K. J. Law Model 8300 Roughness Surveyor (IRI) and SI.

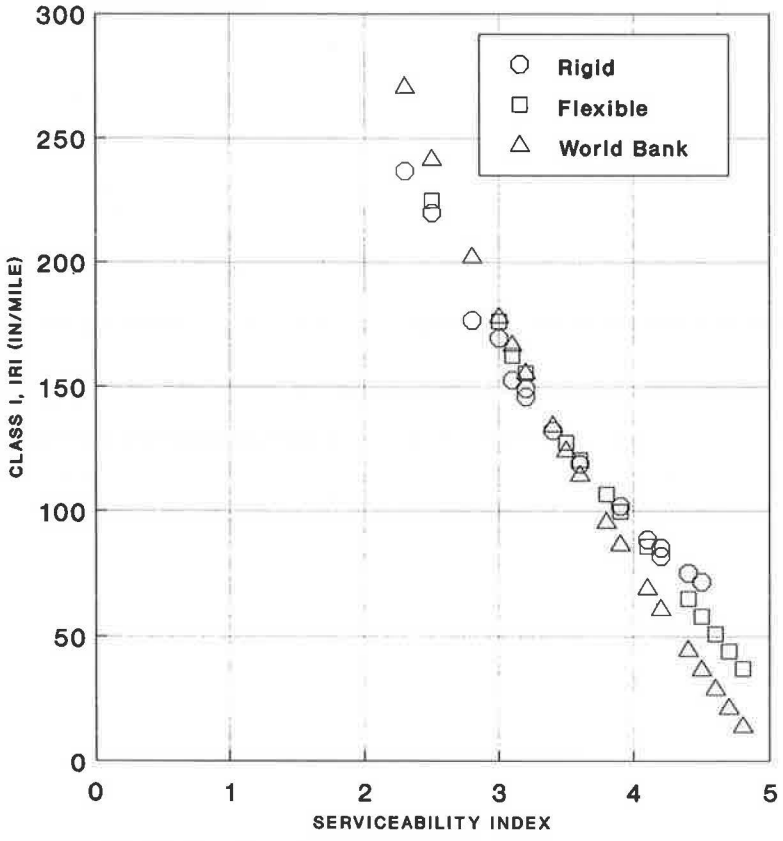

FIGURE 5 Relationship between the Face Dipstick (IRI) and SI.

CONCLUSIONS

1. A linear relationship exists between the IRI as measured and computed by the Face Dipstick and the K. J. Law Model 8300 Roughness Surveyor. Test results to date indicate that the Face Dipstick is an acceptable tool against which other devices that measure the pavement profile and calculate the IRI can be calibrated.
2. The K. J. Law Model 8300 Roughness Surveyor is suitable for conducting the HPMS survey by using the Class I and Class II correlation equation developed through this research.
3. A calibrated Mays Ride Meter is suitable for conducting an HPMS survey by using specific Class I, Class II, and Class III relationships developed for the particular meter, vehicle, and pavement type.
4. The IRI appears to be a useful tool for the identification of relative roughness levels between pavements and for predicting the rideability rating that a panel might provide irrespective of pavement type.

REFERENCES

1. T. D. Gillespie, M. W. Sayers, and C. A. V. Queiroz. *The International Road Roughness Experiment, Establishing Correlation and a Calibration Standard for Measurements*. World Bank Technical Paper 45, Washington, D.C., Jan. 1986.
2. M. W. Sayers and T. D. Gillespie. *The Ann Arbor Road Profilometer Meeting*. Transportation Research Institute, The University of Michigan, Report FHWA/RD-86/100, Ann Arbor, July 1986.
3. T. D. Gillespie, M. W. Sayers, and L. Segel. *NCHRP Report 228: Calibration of Response-Type Road Roughness Measuring Systems*. TRB, National Research Council, Washington, D.C., Dec. 1980.
4. M. S. Janoff, J. B. Nick, and P. S. Davit. *NCHRP Report 275: Pavement Roughness and Rideability*. TRB, National Research Council, Washington, D.C., Sept. 1985.
5. M. S. Janoff. *NCHRP Report 308: Pavement Roughness and Rideability Field Evaluation*. TRB, National Research Council, Washington, D.C., July 1988.
6. W. H. Temple and S. L. Cumbaa. Serviceability Index Base for Acceptance of Jointed Concrete Pavements. In *Transportation Research Record 1196*, TRB, National Research Council, Washington, D.C., 1988.
7. S. K. Nair, R. W. Hudson, and C. E. Lee. *Realistic Pavement Serviceability Equations Using the 690D Surface Dynamics Profilometer*. Center for Transportation Research, The University of Texas at Austin, Aug. 1985.
8. *Special Report 61E: The AASHO Road Test—Report 5 Pavement Research*. HRB, National Research Council, Washington, D.C., 1962.
9. W. D. O. Paterson. International Roughness Index: Relationship to Other Measures of Roughness and Riding Quality. In *Transportation Research Record 1084*, TRB, National Research Council, Washington, D.C., 1986.

Publication of this paper sponsored by Committee on Surface Properties–Vehicle Interaction.

Profiles of Roughness

MICHAEL W. SAYERS

Road roughness is normally characterized by a summary index that applies over a length of road. Summary index measures are obtained most directly by measuring the longitudinal profile and then applying a mathematical analysis to reduce the profile to the roughness statistic. The moving average smoothing filter can be used to obtain a profile of one such roughness measure—the international roughness index (IRI). The roughness profile provides another dimension to the description of roughness, showing with maximum detail how the roughness is distributed over the length of the road. The baselength used for the IRI averaging must be considered. Specifying the baselength becomes particularly important when specifications for road quality are formulated, or when profiling accuracy is prescribed. That the variation in IRI found over the length of a road is more extreme when the baselength is short should be taken into account when reporting instrument accuracy or writing roughness specifications. Specifically, the accuracy of high-speed profiling systems should be specified according to baselength.

Road roughness is measured in many ways, for a multitude of purposes. The bulk of the data collected in the United States to date has been obtained with instrumented vehicles called "response-type road roughness measuring systems" (RTRRMSs). The RTRRMS involves instrumentation that is inexpensive, simple to install, and simple to operate. Roughness measures from such systems are routinely normalized by the distance traveled, and can usually be scaled to provide roughness as a measure of slope, with units such as inches per mile or meters per kilometer (*1,2*). The length of road used for an individual measurement varies among users, but is generally between 0.1 and 2 mi.

Because the RTRRMS relies on the vehicle as a critical element of the overall system, it is difficult to calibrate in a meaningful sense. Without a valid calibration, the measurements are neither reproducible nor stable with time (even with the same RTRRMS). A valid calibration is obtained only by correlating the measures from an RTRRMS with reference measures obtained by a method that is reproducible and stable with time (*2*). The reference methods involve a direct measure of the road profile, either by static means (rod and level or equivalent) or with a high-speed profiling system. With the profiling approach, the roughness is nearly always obtained in two steps. First, the profile is measured. The measurement provides elevation or slope of the road as a function of distance along the road. Second, the profile is processed by computer to calculate a summary roughness statistic. (Although these two steps generally exist separately, they often take place in the same computer program, giving the appearance that they occur together.)

The University of Michigan, Transportation Research Institute, Ann Arbor, Mich. 48109.

A standardized roughness measurement called the international roughness index (IRI) can be measured by either approach. The IRI was originally developed for the World Bank (*3,4*), on the basis of continuation of research that was begun in an NCHRP project (*2*). It is the only existing roughness index that has been demonstrated to be reproducible with a wide variety of equipment, including single- and two-track profiling systems, rod and level, and RTRRMSs. Since the World Bank published guidelines for conducting and calibrating roughness measurements, the IRI has been adopted as a standard for the FHWA Highway Performance Monitoring System (HPMS) data base (*5*), and is becoming a de facto standard in several countries, including the United States and Canada.

In the original World Bank guidelines, IRI roughness measuring methods were organized into the following four classifications:

Class 4—a roughness measure is not reproducible or stable with time, and can only be compared to IRI by subjective estimation. This class covers panel ratings and measures made with uncalibrated RTRRMSs.

Class 3—a measure obtained from an RTRRMS is calibrated to the IRI scale by correlation with reference measures from a Class 1 or 2 system.

Class 2—a profile-based method is used that is reproducible and stable with time, and that is calibrated independently of other roughness measuring instruments.

Class 1—a profile-based method similar to Class 2 is used. A profile-based measurement qualifies as a Class 1 measure if it is so accurate that further improvements in accuracy would not be apparent.

This classification was made to emphasize that different methods of measuring roughness on the same scale would have different levels of accuracy, where accuracy is quantified by the variation of a measure of IRI from the measure that would be obtained with a Class 1 method. The concepts of Classes 1 through 3 are repeated in the HPMS definitions (*5*).

Profile measuring equipment has been first viewed by many as a calibration reference for response-type systems. In fact, a primary consideration in designing the IRI was to devise a roughness index that showed maximum correlation with the RTRRMSs in use. (Other considerations, which are becoming more significant today, were that the IRI be a measure relevant to vehicle response, and measurable by existing and future profiling instruments.) However, as the profiling equipment grows more robust and becomes easier to operate, the RTRRMS is being dropped by some users due to the accuracy limitations and the great effort needed to obtain a valid

calibration. Profiling instruments are used to directly measure IRI over the road networks.

With the capabilities of profiling systems in mind, IRI can be used to quantify roughness of specific pavement events, such as intersections, railroad crossings, bridge approaches, and slab faulting. When analyzing such events, it is necessary to consider roughness over fairly short intervals, such as 50 ft or less. It will be shown that normal variations in roughness increase as the length of road being considered is reduced.

When profiling equipment is used to measure IRI, it is possible to view a profile of roughness, rather than a single index. For example, the PRORUT system owned by FHWA has this capability built in to its software (*6,7*). The roughness profile is particularly relevant when roughness is used to specify (a) the quality of pavements after construction or repair, and (b) the accuracy of profiling equipment.

Using the concept of the roughness profile, this paper explores ways of dealing with the variation in roughness that exists in the road itself, over its length. The nature of these variations must be recognized and understood to specify roughness limits in roads and roughness instruments. For example, the distinction between Class 1 and 2 instruments is primarily that a single Class 1 measurement provides the right answer with negligible potential for improvement by making repeated measures. When determining if a system is Class 1 or 2, it is necessary to understand how the length of the typical test contributes to the reproducibility.

ROUGHNESS PROFILES

Consider a roughness analysis of a single longitudinal profile of a traveled wheeltrack. Roughness is necessarily defined over an interval of profile. It is meaningless to talk of the roughness of a point. Instead, one must always consider roughness as a summary description of deviations that occur over an interval between two points.

Many of the basic techniques for reducing a profile to a single summary roughness have the following three steps in common (*8*):

Step 1. The profile is filtered spatially to remove wavelengths outside of a band of interest. Wavelengths within the band of interest are weighted by the mathematical properties of the roughness analysis algorithm. For the IRI and many other roughness analyses that have been used, this step is a linear transformation.

Step 2. The filtered profile is transformed to eliminate negative values. In most analyses, this transformation is accomplished either by squaring or taking the absolute values of the individual values.

Step 3. The processed profile is averaged to provide a summary index. If the transformation in Step 2 was squaring, a root-mean-square (RMS) value is obtained; if the transformation was absolute value, an average rectified (AR) value is obtained. (The IRI uses the latter method.)

The filtering of Step 1 is needed to remove influences of the profile measuring equipment. Without filtering, the true average elevation variance is generally determined by the length of the profile and whether it includes a hill. The true variance of slope and spatial acceleration is infinite. (A tiny crack, with a vertical wall, has an infinite slope. Infinity, of course, takes a long time to average out.)

After the processing of Step 2, the result is a profile that can be scaled with the units per length convention needed for the IRI and other roughness indices. When this scaling is done, the result is a rudimentary roughness profile that shows how the roughness is distributed over the length of the road.

There are three profiles that are relevant to the IRI scale. The first is the elevation profile, measured by most Class 1 and 2 systems. An example profile of this sort is shown in Figure 1. This particular profile was measured by the PRORUT instrument (*6*) on a badly damaged portland cement concrete (PCC) road as part of the 1984 Ann Arbor Road Profilometer Meeting (*9*). The visual appearance of the profile shape is dominated by long wavelengths that do not contribute much to vehicle vibrations. For example, the 2-in. change in elevation over 200 ft is almost imperceptible when traveling over the road. However, the spikes in the plot that occur every 80 ft or so are due to open gaps between PCC slabs, and these are apparent to traversing vehicles (and their occupants).

The IRI is a measure of slope. In the United States, it is common to apply units of in./mi to slope when it is used as a roughness numeric. The profile from Figure 1 is shown again as a slope profile in Figure 2. The conversion of the elevation profile to a slope profile is performed simply by taking the differences between adjacent elevation measures (in.), dividing by the sample interval (ft), and then converting to the desired units (multiplying by 5,280 ft/mi). As noted earlier, the true slope profile includes occurrences of infinite slope. The appearance of a measured profile of the sort shown here

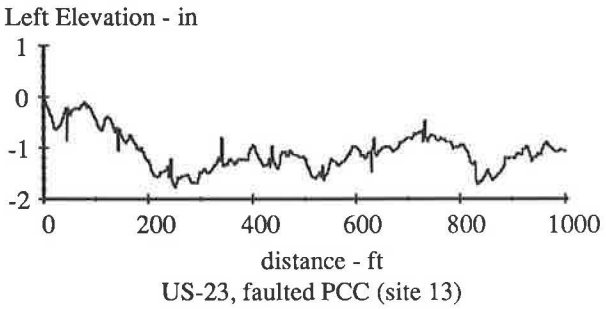

FIGURE 1 Elevation profile for faulted PCC, measured with PRORUT.

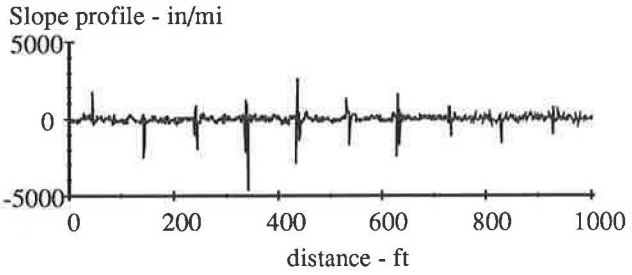

FIGURE 2 Slope profile for same road.

is strongly influenced by the properties of the method used to obtain the measurement. This particular measurement was obtained using the PRORUT with a sample interval of about 3 in., and a low-pass (smoothing) antialiasing filter set at about a 1-ft wavelength. Thus, the amplitudes of the profile in Figure 2, which reach 5,000 in./mi, reflect a 1-ft wavelength limit. Higher amplitudes would be seen for the same road if the PRORUT had been run using a finer sample interval. (The cutoff wavelength of the PRORUT is always set automatically to about four times the sample interval.) Conversely, smaller amplitudes would be seen if the PRORUT had been run using a coarser interval.

The same slope profile was then filtered using the quarter-car analysis of the IRI. The filter has the spatial transfer function shown in Figure 3. After this filtering, the influence of the profiling system has been removed (assuming that the original measurement was valid over the range of wavelengths shown, covering about 3-ft waves to about 80-ft waves with good fidelity.) The resulting filtered profile is shown in Figure 4.

At this stage, the plotted profile amplitude differs from IRI only because it includes negative values. After the profile is rectified, the result is a plot of IRI at about 1-ft intervals down the road. Values range from 0 to 2,000 in./mi, depending on exactly which 1-ft interval is being considered.

IRI would never be reported over such small intervals. As noted earlier, the typical length associated with a single IRI numeric (and virtually all other roughness indices that have been used in the past decades) ranges from 0.1 mi to several miles. In nearly all past uses before the PRORUT system, roughness statistics such as IRI were used to reduce a profile to a single numeric. However, a different method will be used now. Instead of reducing the profile, a moving average smoothing filter is used to obtain the same averaging, while retaining the representation of roughness as a continuous function of distance.

A moving average filter is applied to a point in a profile by averaging elevation over a baselength centered at the longitudinal location of the point of interest, as shown in Figure 5.

For example, consider a moving average of 100 ft, applied to a profile measured at intervals of 0.25 ft. The averaging covers 401 points. The first filtered value is the average of the first 401 profile values. The second filtered value is the average of the values going from number 2 to number 402. Each new point in the filtered profile is obtained by moving the start of the average by one sample.

Figure 6 shows how the roughness profile is smoothed by applying a moving average. The figure overlays four plots, each prepared using a moving average with a different baselength. As the baselength increases from 20 to 528 ft, the smoothing has a greater effect.

Because the moving average applies a simple unweighted average, every point shown in the plot is a valid IRI value for some interval of profile. For example, the first point for

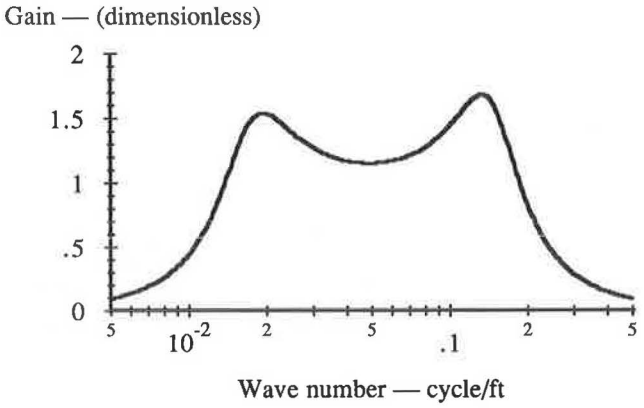

FIGURE 3 Spatial transfer function of quarter-car filter of IRI.

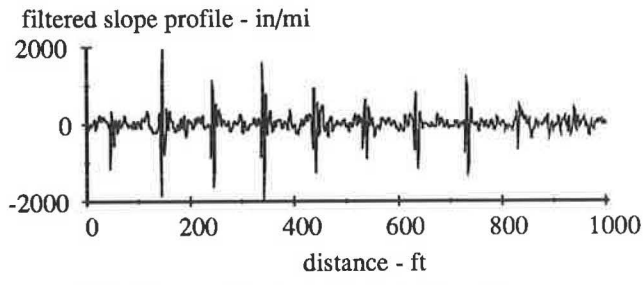

FIGURE 4 Slope profile for same road, filtered by quarter-car analysis.

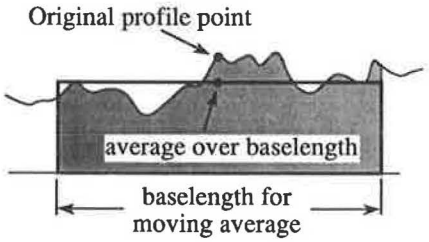

FIGURE 5 Moving average filter.

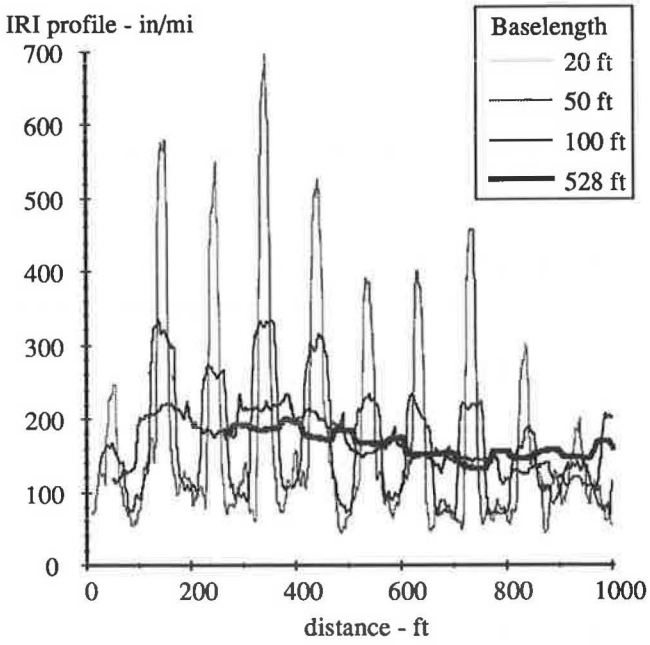

FIGURE 6 Roughness profiles for faulted PCC road.

the 528-ft average, shown at a location 264 ft into the profile, is the IRI for the interval going from 0 to 528 ft.

Note that with increasing baselength, some of the original profile is lost. Specifically, a length equal to the baselength of the moving average is lost. Figure 6 was prepared by plotting each point of the smoothed profile at the center of the averaging interval. Thus, the first value for the 528-ft average appears 264 ft from the beginning of the test site. Although not shown, the last plotted point appears 264 ft from the end of the test site. That is, half of the baselength is lost at each end.

Figure 6 shows directly how a choice of baselength influences the variation in roughness seen over a section of this road. Using a 528-ft average, the roughness ranges from 140 to 200 in./mi for 528-ft intervals lying in the first 1,268 ft of the test site. However, using a 20-ft average, the range covers about 50 to 700 in./mi. Also, when the baselength is 20 or 50 ft, the profile shows clearly that the road alternates between smooth and rough sections, with the smooth sections having a roughness level of about 100 in./mi.

This example is obviously one in which the roughness is localized and occurs mostly at the openings between the slabs of PCC. A similar plot is shown in Figure 7 for a much newer PCC road, in which the roughness is both lower and more uniformly distributed over length. In this figure, the entire measured length is included. Note that the longer averages cause the roughness profile to be shortened at the end also. Although a longer length is included in the plot than in Figure 6, the range of IRI is much less.

Roughness profiles can also be made for statistics that use the RMS averaging, although the processing and interpretation are more complicated. If a roughness profile is obtained for an RMS statistic, a choice must be made either to apply the simple moving average to the squared variable of interest and plot the profile of the squared index, or to apply the moving average to the squared variable and then plot the square root of each point.

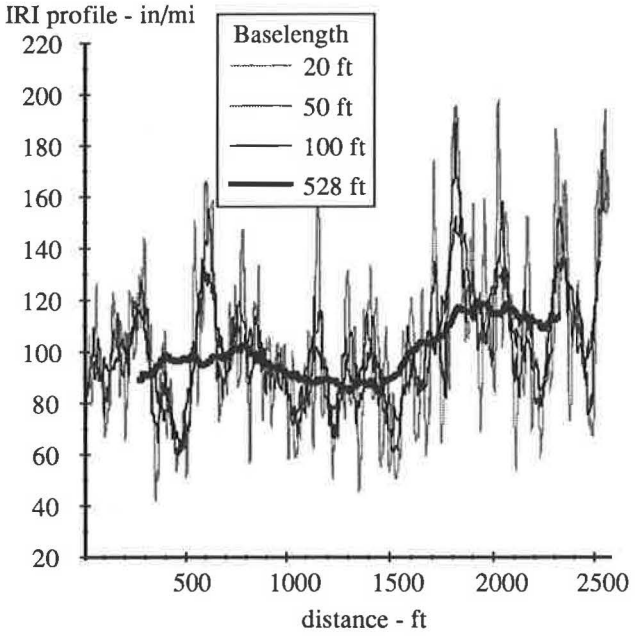

FIGURE 7 Roughness profiles for new PCC road.

CHOOSING AN APPROPRIATE BASELENGTH

From the two examples shown in Figures 6 and 7, it is clear that different pictures of the road roughness are revealed by choosing different baselengths to prepare roughness profiles, even though all measures are on the same IRI roughness scale. Without averaging, IRI ranges from zero to about 2,000 in./mi for the faulted PCC (Figure 4) whose average over the 0.5-mi test site is about 170 in./mi. As the baselength increases (Figure 6), the IRI numbers approach the average for the entire site.

By choosing an appropriate baselength, the IRI can be used to either reveal or hide the variation in roughness over the length of the road.

When only averages of IRI numerics over long distances are considered, the detail provided by roughness profiles may not be required. However, when considering limit specifications of IRI, the choice of baselengths becomes critical. The previous examples show that the range of IRI values encountered over a length of profile increases as the baselength decreases. That is, a specification involving a specific value of IRI generally becomes more stringent when the baselength is decreased. This effect will be discussed for specifications of the pavement and for the equipment used to measure profile.

Pavement Descriptions

In determining what baselength to use, it is helpful to consider that the IRI analysis is a quarter-car analysis based on a simulated travel speed of 80 km/hr (49.7 mph = 73 ft/sec). The IRI filter responds to a bump after encountering it, just as a vehicle does. A singular event, such as a pothole, affects the vehicle vibration strongly for a few 10ths of a second. Lingering oscillations last about 1 sec. A baselength of 20 ft is suggested as a minimum for use with the IRI. (At the simulated speed, 20 ft corresponds to 0.27 sec.)

Ideally, the baselength used to prepare a roughness profile should correspond to the source of roughness that is of interest. If the concern is to obtain simply an average roughness over the miles of the network, a baselength of 528 ft or more is appropriate. However, if there is a need to discern specific events, a much shorter baselength is desirable. Ideally, the baselength should be smaller than the minimum distance between events, so that each event can be distinguished.

Table 1 presents the maximum roughness anywhere in the sites used for the two previous examples. For baselengths of 50 ft and longer, the measures from the site of Figure 7 are about 70 percent rougher than those from the site of Figure 6. However, for the 20-ft baselength, the maximum IRI from the faulted site jumps to being 344 percent higher.

Pavement Specifications

If roughness is used as a specification for pavement, the associated baselength is a major factor. Table 1 shows that (a) the maximum roughness expected in a site increases as the baselength is shortened, and (b) short baselengths can reveal highly localized roughness that might otherwise be lost in the averaging. One way to control both the overall quality of a

TABLE 1 SUMMARY OF MAXIMUM IRI FOR TWO EXAMPLE TEST SITES

Baselength (ft)	Maximum IRI (in./mi)	
	Faulted PCC (Figure 6)	New PCC (Figure 7)
528	200	120
100	240	150
50	335	190
20	670	195
Site average	170	100

road and the roughness of short events is to specify roughness using two baselengths. For example, a 528-ft baselength would be used to set the overall quality (say, a maximum limit of 60 in./mi over 528 ft for new construction), and a 20-ft baselength would be used to guard against any sudden surprises (say, a maximum limit of 90 in./mi over 20 ft).

Profile Measurement Specifications

Profile measurements are subject to error in the capabilities of the instrument and the operator. A direct way of specifying the accuracy of a profiling system is to perform the routine analyses of the profiles, and compare the results with reference measures. For example, if the profiles are mainly used to obtain IRI, then the overall accuracy of the system can be determined by comparing the IRI numerics obtained with the candidate system to those obtained by a reference.

The main difference between Classes 1 and 2 in the World Bank guidelines is in the reproducibility of a single measure of IRI. If the measure of IRI cannot be significantly improved, then the method is considered to fall in Class 1. Generally, this has been taken to mean high-precision static measurements. Profiles taken with high-speed profiling systems are not as repeatable and are considered Class 2. Also, profiles obtained statically with less precise specifications are considered Class 2.

In the 1984 Ann Arbor Profilometer Meeting, various profiling systems were compared, based on their abilities to measure IRI over 0.1-mi sections. For some of the systems, the limiting factor was the ability of the driver to follow exactly the same path in repeated tests. Even with experienced drivers operating under controlled conditions, it was common to find differences in the starting position of 50 to 100 ft longitudinally, and about 2 ft laterally. (Generally, each driver was repeatable to within 20 ft. However, when comparing driver A's idea of the start to driver B's idea, the 50 to 100 ft differences were observed.) The significance of this error can be viewed directly in the roughness profiles. In Figure 6, even a delay of 20 ft in the starting position causes a change in the IRI of up to 30 in./mi for certain 528-ft sections. (Compare the 528-ft section centered at 760 ft with that centered at 780 ft into the test site.)

When dealing with baselengths of 528 ft and less, any high-speed profiling system should be considered a Class 2 system because of the limits of the operator.

The baselength is a factor when considering the reproducibility of a roughness measurement. In past work (by this author, as well as others), comparisons are made by summary values tabulated for a number of test sites. The roughness profile provides a much better means for comparing two systems. The roughness profiles from two systems can be overlaid. If there is an offset in the starting point, it is immediately obvious. After adjusting the longitudinal positions to eliminate that source of error, the average and maximum differences observed between roughness profiles can be computed and used to define the accuracy limits of the system being validated.

There is presently not much data showing how accurate profiling systems are, or how the accuracy is influenced by measurement length. In future studies, the roughness profile should prove useful for better characterizing the performance of such systems.

RECOMMENDATIONS

The roughness profile provides a detailed view of how roughness is distributed over the length of a road. Although a profiling system such as the PRORUT is needed to obtain a roughness profile, the profile is fully compatible with IRI numerics obtained from RTRRMSs, and can be used to extend the information available about the road as new equipment becomes available. By overlaying roughness profiles for various baselengths, extra dimensions are added to the knowledge about the roughness state of a road.

When considering roughness specifications for contractors, the baselength should be considered and included explicitly in the specification. Short baselengths result in the specifications being more stringent.

When evaluating new profiling systems, or when characterizing the performance of existing systems, the roughness profile can show the reproducibility much more concisely than the methods of comparison used in the past. Also, operator error in starting the beginning of a test site is easily detected and corrected.

When baselengths of 528 ft and shorter are used to obtain IRI measurements, all high-speed profiling systems should be considered as Class 2 devices, due to limitations of the ability of the driver and the operator to cover exactly the same profile in repeated runs. With longer baselengths, it is possible that some high-speed systems could be considered as Class 1 devices.

REFERENCES

1. *Standard Test Method for Measurement of Vehicular Response to Traveled Surface Roughness*. ASTM E 1082. American Society for Testing and Materials, Philadelphia, Pa., 1987.
2. T. D. Gillespie, M. W. Sayers, and L. Segel. *NCHRP Report 228: Calibration of Response-Type Road Roughness Measuring Systems*. TRB, National Research Council, Washington, D.C., Dec. 1980, 88 pp.
3. M. W. Sayers, T. D. Gillespie, and C. Queiroz. *International Experiment to Establish Correlations and Standard Calibration Methods for Road Roughness Measurements*. World Bank Technical Paper 45, The World Bank, Washington, D.C., 1986, 464 pp.
4. M. W. Sayers, T. D. Gillespie, and W. D. Paterson. *Guidelines for the Conduct and Calibration of Road Roughness Measurements*. World Bank Technical Paper 46, The World Bank, Washington, D.C., 1986, 99 pp.

5. *Highway Performance Monitoring System Field Manual for the Continuing Analytical and Statistical Database*, Appendix J. FHWA Order M5600.1A, OMB No. 2125-0028, FHWA, U.S. Department of Transportation, Dec. 1987.
6. T. D. Gillespie and M. W. Sayers. *Methodology of Road Roughness Profiling and Rut Depth Measurement*. Report FHWA/RD-87/042, FHWA, U.S. Department of Transportation, July 1987, 50 pp.
7. M. W. Sayers and T. D. Gillespie. *User's Manual for UMTRI/FHWA Road Profiling (PRORUT) System*. Report FHWA/RD-87/043, FHWA, U.S. Department of Transportation, July 1987, 66 pp.
8. M. W. Sayers, T. D. Gillespie, and C. Queiroz. The International Road Roughness Experiment: A Basis for Establishing a Standard Scale for Road Roughness Measurements. In *Transportation Research Record 1084*, TRB, National Research Council, Washington, D.C., 1986, pp. 76–85.
9. M. W. Sayers and T. D. Gillespie. *The Ann Arbor Road Profilometer Meeting*. Report FHWA/RD-86/100, FHWA, U.S. Department of Transportation, July 1986, 237 pp.

Publication of this paper sponsored by Committee on Surface Properties–Vehicle Interaction.

Evaluation of the Siometer as a Device for Measurement of Pavement Profiles

EMMANUEL G. FERNANDO, ROGER S. WALKER, AND ROBERT L. LYTTON

Highway engineers have always been concerned with providing pavements of acceptable serviceability. The serviceability of a highway segment, which is largely a function of pavement roughness, is a widely used criterion for deciding when pavements are in need of rehabilitation. For this application, various statistics are currently used as indicators of pavement serviceability, the most common being the present serviceability index. These statistics are largely determined from measurements of pavement roughness. Various devices and procedures have been developed for accomplishing these measurements. Of practical necessity, devices for measuring pavement roughness must be capable of providing repeatable measurements at normal highway speeds. In addition, devices that do not require difficult calibration procedures, that possess the capability for field processing of the data collected, and that are relatively inexpensive to own, operate, and maintain are most desirable. The Siometer, which is currently used by the Texas State Department of Highways and Public Transportation (SDHPT) for evaluation of pavement riding quality, holds promise as an instrument for the routine collection of profile data on a network-wide scale. The Texas SDHPT has recently begun investigating the profile-measuring capability of the Siometer. A unique feature of this device is the statistical modeling procedure for characterizing the vehicle on which it is installed, which lends portability to the Siometer. In it, the parameters of the statistical model are determined in a self-calibration procedure that is run before profile data are collected. To evaluate the applicability of the Siometer as a device for profile measurements, profile measurements with the Siometer were compared with those from a profilometer.

Pavement roughness is the principal determinant of riding quality as perceived by the road user. In order to provide roads that offer a smooth and comfortable ride, a transportation agency requires measurement techniques for quantifying pavement surface roughness. An evaluation was made of a profile-measuring device known as the Siometer. This device, developed by Dr. Roger Walker of the University of Texas at Arlington, is used by the Texas State Department of Highways and Public Transportation (SDHPT) for evaluating the riding quality of pavement sections in the state.

Pavement surface profiles measured with the Siometer were compared with those determined from the surface dynamics profilometer (SDP). Over the years, the SDP has gained wide acceptance as a device for evaluating pavement profiles. It is classified as a Class 2 instrument by the World Bank (*1*) for the measurement of the international roughness index (IRI).

The SDP was designed by General Motors and built by K. J. Law Engineers in 1967. Originally, it had as primary sensors two accelerometers and two linear potentiometers, connected to road-following wheels. The accelerometers determine the amount and direction of vertical acceleration experienced by the vehicle, whereas the potentiometers and wheels measure the distance from the vehicle body to the road surface. A profile measurement is calculated by summing the double integral of the accelerometer signal and the displacement signal from the potentiometer (*2*). In the latest version of this device, the potentiometers and road-following wheels have been replaced by noncontact sensors.

The SDP is capable of measuring profiles of considerable accuracy and consistency at normal highway speeds without the need for calibration. It has been used as a reference device for measurement of present serviceability index (PSI) within the Texas SDHPT. The principal statistic currently used by the Department in computing PSI from profile data is the root-mean-square vertical acceleration (*3*).

Although the SDP provides a fairly rapid and accurate method of determining pavement profiles from which various roughness statistics can be computed, it requires a large initial capital outlay and is relatively expensive to operate. Consequently, many state transportation agencies generally use response-type road roughness measuring devices, such as the Mays meter, for collecting roughness data on a network-wide basis. However, such devices require periodic calibration, which often entails significant effort. What is clearly needed is a device that can be used to collect fairly accurate and consistent profile data at normal highway speeds, that is relatively inexpensive to own and operate, and that does not require difficult calibration procedures. A device that has the potential of offering all of these advantages is the Siometer. The applicability of this device for measuring pavement profiles is evaluated in the following sections.

THE SIOMETER

The development of the Siometer was initiated by Walker during the early 1970s. A unique feature of this device is the statistical modeling procedure for characterizing the vehicle on which it is installed. Through this procedure, the influence of the vehicle on the measurement process is identified and removed (*4,5*). The statistical model is parameterized with the Siometer's on-board microcomputer using vertical accelerations of the vehicle measured at fixed distances as the vehicle is driven down the road. Vertical accelerations are obtained from an accelerometer that is housed in a small case and installed in the trunk of the vehicle. Once the parameters of the vehicle are determined, the Siometer is calibrated and

E. G. Fernando and R. L. Lytton, Texas Transportation Institute, Texas A&M University, College Station, Tex. 77843. R. S. Walker, Department of Computer Science Engineering, The University of Texas at Arlington, Arlington, Tex. 76019-0015.

ready for profile measurements. The vehicle is then driven over the roadway sections for which profiles are to be determined and the resulting accelerations are measured. The differences between the actual measurements and those predicted from the statistical model are used to estimate the road profile by integrating the acceleration differences with the time between successive samples.

The primary application of the Siometer within the Texas SDHPT is for evaluation of riding quality. Thus, the device became known as the Siometer because its primary output is the serviceability index (SI) for a particular pavement section, even though the SI is calculated using statistics derived from the predicted road profile. The device is portable and can be easily transferred from one vehicle to another. Furthermore, because it implements a self-calibration procedure, the device, in theory, can be installed in any vehicle because the effect of the vehicle is modeled in the same process.

The current version of the Siometer used by the Texas SDHPT is the R680 system manufactured by Micro-sher Incorporated. The R680 system consists of three components, namely (a) a sensor unit, (b) a main control module, and (c) a laptop computer for storing the results. The system computes and displays SI and predicts the pavement profile. The sensor unit and the main control module currently cost $20,000. The laptop computer can be purchased separately by the user from any other vendor.

The sensor unit includes the accelerometer and a distance-measuring signal. The accelerometer is housed in a small case that is weighed down with a sandbag and mounted vertically inside the trunk of the vehicle, where it measures the vertical acceleration. The signal from the accelerometer is transmitted to the main control module where it is digitized in accordance with the distance signal and processed.

The main control module contains two Motorola 68000 microprocessors working in parallel. One performs input-output operations and the other performs numerical computations.

The data storage component is a portable laptop computer. A communications program provides the interface between the control module and the laptop computer. This program and the personal computer provide the means of obtaining continuous SI or profile measurements. The entire Siometer system is portable and can be easily installed in most standard vehicles.

An enhanced version has also been developed that implements the South Dakota method of measuring longitudinal profiles. The South Dakota profiler, currently considered by many to be a Class 2 instrument, is becoming a popular device for measuring pavement profiles. This device measures pavement profile elevations by the use of an accelerometer and acoustic sensors, which perform the same function as the laser probes in the SDP. The South Dakota profiler differs from the SDP in this respect and also in the procedure used for integrating the accelerometer signal. The current version of the device measures longitudinal profile elevations at the inner wheelpath and also provides estimates of pavement rutting using data from the acoustic sensors. At present, the roll of the vehicle is not considered in the determination of pavement rutting although numerous tests indicate reasonable agreement between rut depth data obtained manually and rut depth estimates from the profiler. Because the Siometer can easily implement the South Dakota profiler concept by the simple installation of acoustic sensors in the test vehicle, it has recently been upgraded for this purpose and is undergoing evaluation by the Texas SDHPT. In addition, to identify the influence of vehicle roll, the possibility of using additional accelerometers in conjunction with up to five acoustic sensors is being considered. This improvement will require modifications to the Siometer hardware, but consideration of vehicle roll will provide the Texas SDHPT with the capability of measuring transverse pavement profiles in addition to longitudinal profiles.

EVALUATION OF PAVEMENT PROFILES MEASURED FROM THE SIOMETER

The Texas SDHPT has recently begun investigating the profile-measuring capability of the Siometer. The findings presented herein are based on results obtained thus far. In order to evaluate the applicability of the Siometer for profile measurements, the SDP was used as a reference.

In this evaluation, nine bituminous test sections were selected on which profile measurements using the SDP and the Siometer were made. Three of the test sections were smooth, three were rough, and the other three were intermediate. All sections were 0.2 mi in length. The serviceability indices calculated from the SDP profiles on the nine selected sections are shown in Table 1. All sections, with the exception of TC7 in Tarrant County, are located within the general vicinity of Austin, Texas.

The pavement profiles of the nine sections were measured using the SDP and Siometer of the Texas SDHPT. The SDHPT's SDP is similar in design to that originally built by K. J. Law except that the potentiometer and road-following wheel combination has been replaced with two noncontact Selcom laser probes. This feature has reduced maintenance problems associated with the mechanical road-following wheels and has allowed profile measurements to be conducted at faster highway speeds. In addition, data acquisition and processing capability was upgraded to take advantage of improvements in hardware technology and thus allow data reduction to be conducted in the field. Consequently, roughness statistics and profile data can now be obtained as soon as a run is completed on a particular highway segment.

For each test section selected, two profile measurements were obtained from each device. Profile elevations were taken at 0.50-ft intervals along each 0.2-mi section. Because the Siometer was portable, the device could be installed inside the SDP van. This allowed profile measurements to be made simultaneously on both devices for any given run, thus eliminating errors associated with run-to-run variations, such as differences in wheelpaths tracked between runs, differences in vehicle track widths, and differences in starting times between profile measurements. All measurements were taken at 20 mph in an attempt to traverse the same wheelpaths each time a run was made on a particular section. On two of the rough sections (Sections 1 and 4), yellow dots painted at regular intervals on the wheelpaths were used to guide the direction of travel between runs.

In order to establish a benchmark for evaluating Siometer profiles, a comparison of the profiles from repeat runs of the SDP was initially made. Figure 1 shows a comparison of

TABLE 1 TEST SECTIONS WHERE PROFILE MEASUREMENTS WERE COLLECTED

Section	Location	Present Serviceability Index (PSI)*
1	Decker Lake Road West, approximately 0.2 miles west of FM 973	1.87
4	Decker Lake Road East, approximately 0.3 miles west of FM 973	1.30
7	U.S. 183 South, 1.5 miles north of Burleson Road	4.24
12	U.S. 183 North, 1.1 miles north of Burleson Road at one-way sign at cross-over north of creek	4.57
21	Pearce Lane West, approximately 0.9 miles east of FM 973	1.69
31	FM 685 North, approximately 0.2 miles north of Phillips 66 gas station	2.55
40	FM 973 South, 0.56 miles south of Schmidt Lane	3.06
42	FM 3177 South, at Texas Heritage Center sign	4.01
TC7	U.S. 183 frontage road, west bound, near intersection with U.S. 157, in Tarrant county, north of Arlington	3.36

* average PSI from 2 SDP runs on section

measured left wheelpath profile elevations from repeat runs of the SDP on Section 1. The correlation coefficient r between the measured profile elevations was determined to be 0.985 (as shown in Figure 1) with a standard error of the estimate of approximately 91 mils. Similarly, standard errors of estimate and correlation coefficients between measured profile elevations from repeat runs of the SDP on the other test sections were calculated. The results are presented in Table 2.

The correlation coefficients and standard errors of estimate shown in Table 2 were compared with the corresponding statistics calculated using Siometer and SDP profile elevations measured during a given run (Table 3). In general, the correlation coefficients between SDP and Siometer profiles taken during the same run are comparable with the correlation coefficients between corresponding SDP replicate runs. In addition, for six of the nine test sections (i.e., Sections 1, 7, 12, 40, 42, and TC7), the standard errors of estimate calculated using SDP and Siometer profiles are somewhat better than those calculated using SDP replicate profiles. Figures 2, 3, and 4 show the generally favorable agreement obtained between SDP and Siometer profiles for data measured from the left wheelpaths of Sections 1, 7, and 40, respectively.

An overall measure of the agreement between Siometer and SDP profile elevations was obtained by calculating the overall correlation coefficient between measured profile elevations from the two devices. Figure 5 shows a comparison of all measured profile elevations from the Siometer with the corresponding profile elevations from the SDP. The overall correlation coefficient between measured profiles taken during the same run from the two devices was determined to be 0.971, as shown in Figure 5. This is slightly greater than the overall correlation coefficient of 0.960 between profile

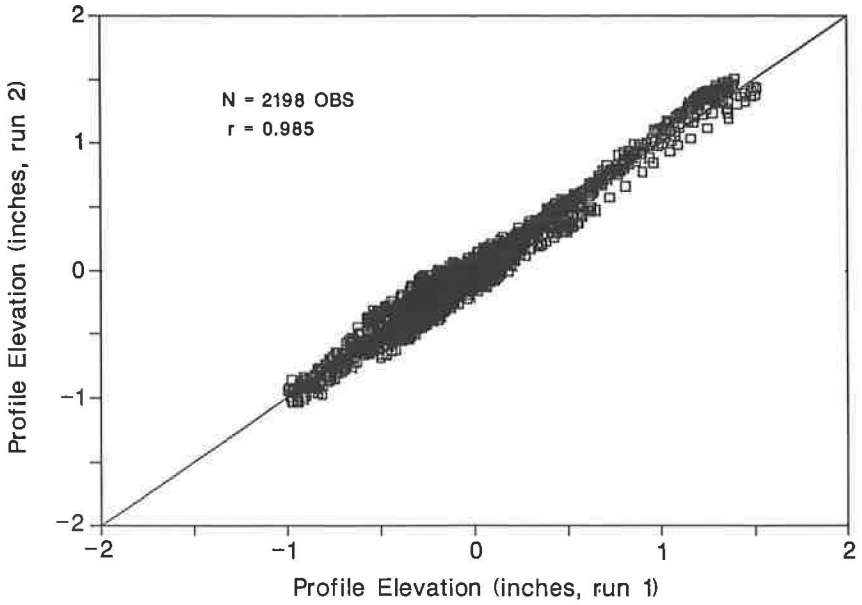

FIGURE 1 Comparison of left wheelpath profile elevations from repeat runs of the SDP on Section 1.

TABLE 2 CORRELATION COEFFICIENTS AND STANDARD ERRORS OF ESTIMATE BETWEEN REPEAT PROFILOMETER MEASUREMENTS

Section	Wheelpath	Correlation Coefficient	Standard Error of Estimate (mils)
1	left	0.985	91
1	right	0.967	125
4	left	0.983	94
4	right	0.976	122
7	left	0.936	70
7	right	0.936	70
12	left	0.890	92
12	right	0.866	99
21	left	0.987	73
21	right	0.952	121
31	left	0.973	55
31	right	0.980	80
40	left	0.961	117
40	right	0.969	137
42	left	0.956	67
42	right	0.935	80
TC7	left	0.833	168
TC7	right	0.869	168

elevations from repeat runs of the SDP. In addition, the overall standard error of the estimate between corresponding profile elevations from the Siometer and the SDP was calculated to be approximately 90 mils. The same statistic calculated using corresponding profile elevations from repeat SDP runs was determined to be approximately 107 mils.

The slightly lower correlation coefficient between profile elevations from repeat SDP runs and the higher standard error of the estimate obtained are largely attributed to variations in wheelpaths tracked between runs of the instrument. It is also likely that differences in starting times between repeat runs would have contributed to the slightly higher variation

TABLE 3 CORRELATION COEFFICIENTS AND STANDARD ERRORS OF ESTIMATE BETWEEN PROFILOMETER AND SIOMETER MEASUREMENTS TAKEN DURING THE SAME RUN

Section	Run Number	Wheelpath	Correlation Coefficient	Standard Error of Estimate (mils)
1	1	left	0.986	83
1	1	right	0.974	102
1	2	left	0.987	82
1	2	right	0.975	107
4	1	left	0.967	126
4	1	right	0.972	136
4	2	left	0.968	124
4	2	right	0.963	147
7	1	left	0.977	39
7	1	right	0.974	44
7	2	left	0.980	39
7	2	right	0.971	49
12	1	left	0.989	31
12	1	right	0.966	44
12	2	left	0.985	35
12	2	right	0.974	47
21	1	left	0.970	128
21	1	right	0.944	141
21	2	left	0.964	119
21	2	right	0.927	146
31	1	left	0.951	78
31	1	right	0.942	127
31	2	left	0.946	82
31	2	right	0.937	130
40	1	left	0.990	64
40	1	right	0.987	94
40	2	left	0.987	67
40	2	right	0.986	93
42	1	left	0.978	43
42	1	right	0.973	51
42	2	left	0.980	44
42	2	right	0.965	58
TC7	1	left	0.979	51
TC7	1	right	0.979	56
TC7	2	left	0.986	48
TC7	2	right	0.986	55

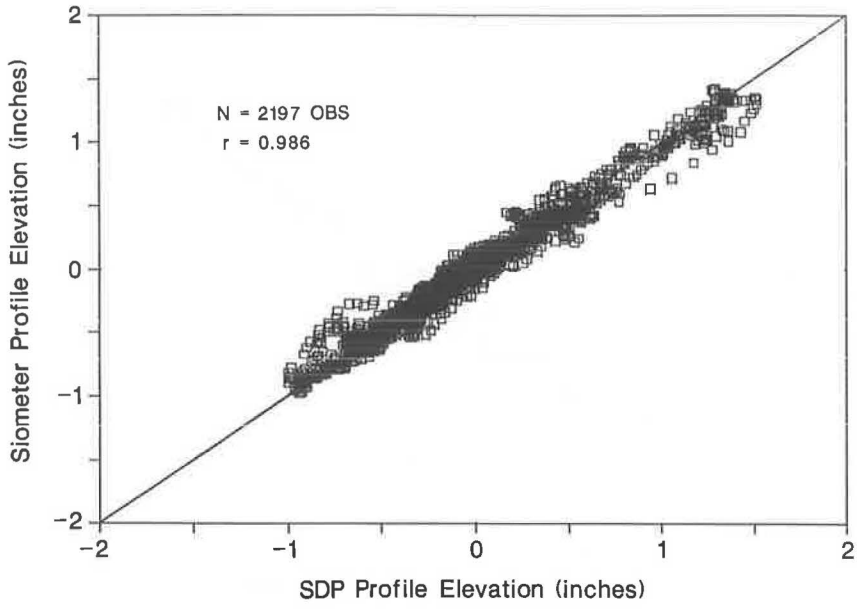

FIGURE 2 Comparison of profile elevations measured with the SDP and Siometer for the left wheelpath of Section 1 (Run 1).

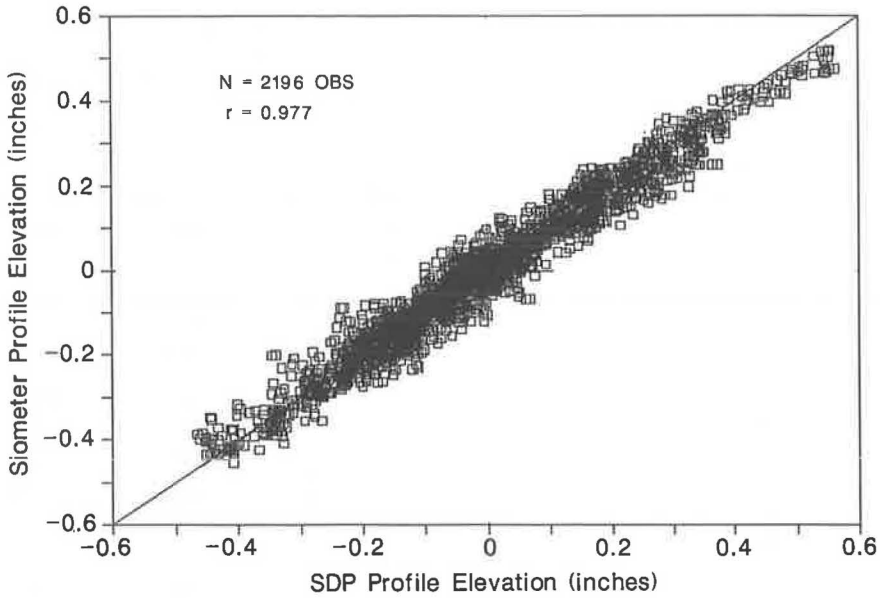

FIGURE 3 Comparison of profile elevations measured with the SDP and Siometer for the left wheelpath of Section 7 (Run 1).

between corresponding profile elevations from the SDP. However, to compensate for the effect of this factor, the SDP profiles from repeat runs were initially lined up before calculation of the statistics presented. This was done by means of cross-correlation analysis wherein profiles from repeat SDP runs were shifted relative to each other until a maximum cross correlation was obtained.

The close agreement between Siometer and SDP profiles taken under identical operating conditions lends credibility to the Siometer's approach for estimating pavement profiles. The essential element of this technique is the self-calibration scheme for parameterizing the statistical model of the vehicle on which the device is installed. The calibrated statistical model provides a way of separating the vehicle's contribution to the measured vertical accelerations from the input attributable to the road profile. In essence, the road profile is estimated from integration of the differences between measured accelerations and those predicted from the statistical model. For this study, the right and left sides of the SDP van were modeled differently so that the statistical models for the right and left wheelpaths were different.

In estimating pavement profiles with the Siometer, measured accelerations from the accelerometers mounted inside the SDP van were used in the computations. Thus, the

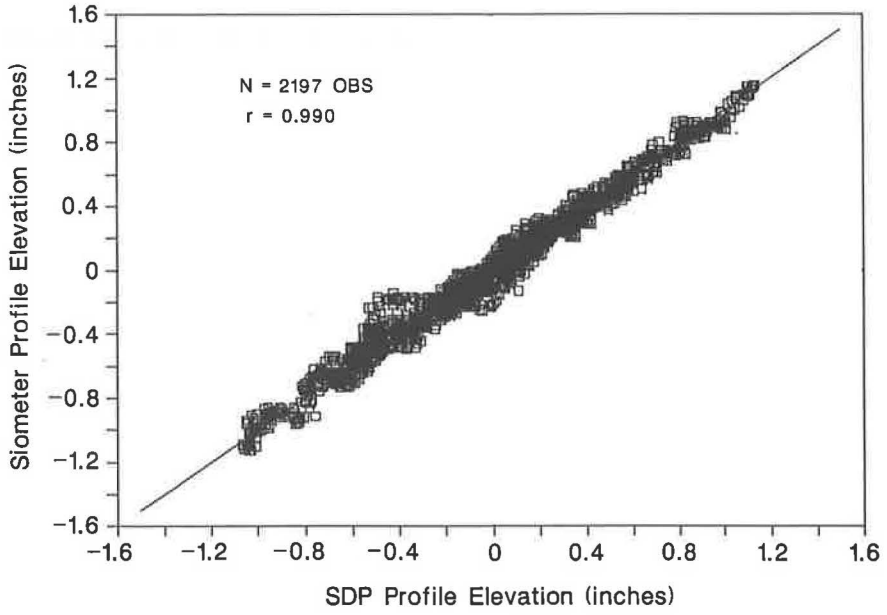

FIGURE 4 Comparison of profile elevations measured with the SDP and Siometer for the left wheelpath of Section 40 (Run 1).

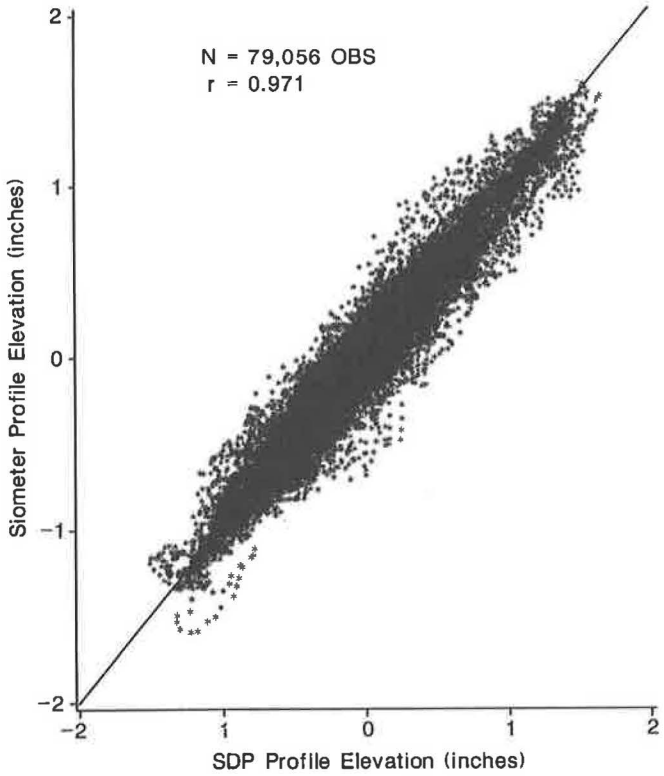

FIGURE 5 Comparison of Siometer profile elevations with SDP profile elevations.

operating conditions under which the SDP and Siometer profiles were taken were as close to being completely identical as can be arranged. In this way, the comparisons between the SDP and Siometer profiles clearly demonstrate the degree of capability of the Siometer's method of measuring pavement profiles. Judging from the results obtained, the Siometer's approach, based on measured vertical accelerations coupled with a statistical model of the vehicle, leads to profiles that are comparable to those obtained from the SDP, which is based on measured vertical accelerations and the use of noncontact probes (lasers) for determining the distance between the vehicle and the ground at any given time.

EVALUATION OF PROFILE POWER SPECTRA

The comparison of measured profiles between the SDP and the Siometer forms a basis for evaluating the applicability of the Siometer as a device for measuring pavement profiles. However, the evaluation should not stop here because differences in the frequency content of two pavement profiles may exist that are not readily apparent from a visual examination of the measured profiles. One can picture pavement profiles as consisting of the sum of a variety of waveforms of different frequencies and amplitudes. Waveforms of low frequencies or long wavelengths may be identifiable from a visual examination of a particular pavement profile. However, the high-frequency components will in all likelihood be masked because of the scales involved. Consequently, to obtain complete information on the frequency content of a particular pavement profile, its power spectrum must be evaluated by means of spectral analysis. A power spectrum is a graph of the frequency (as the abscissa) versus the power, which is the square of the amplitude of each frequency. In this way, the dominant frequencies or wavelengths within the profile can be identified. In addition, by comparing the characteristics of two profiles in the frequency domain, the similarity in the waveform composition of the two profiles can be evaluated.

A spectral analysis was conducted to determine the power spectra of the measured SDP and Siometer profile elevations. Figures 6 and 7 show the power spectra for the left wheelpath profiles of Sections 1 and 7, respectively. The higher the power at a given frequency, the more dominant are the waveforms of that particular frequency within a given pavement profile.

The results shown in Figures 6 and 7, which are typical of those that were obtained for all of the other profiles, illustrate the reasonable agreement between the power spectral densities of corresponding SDP and Siometer profile elevations. In these figures, the power spectral density (PSD) is expressed in dB units, defined herein as $10^*\log_{10}$ (amplitude squared per cycle per foot). In order to evaluate the agreement between SDP and Siometer power spectral densities, the overall correlation coefficient between the PSDs was determined. Figure 8 shows the PSDs of Siometer profile elevations and the corresponding PSDs of SDP profile elevations. Power spectral densities determined from SDP and Siometer profiles taken during the same run were compared.

The overall correlation coefficient between SDP and Siometer power spectral densities was determined to be 0.990. This value compares favorably with the overall correlation coefficient of 0.993 between the PSDs of profile elevations from repeat SDP runs.

In addition, a root-mean-square statistic that provides an overall measure of the match between the amplitudes of SDP and Siometer power spectra was calculated from the following expression:

$$\text{RMSD} = \sqrt{\frac{\sum_{i=1}^{n} (Y_i - Y_i')^2}{n}} \tag{1}$$

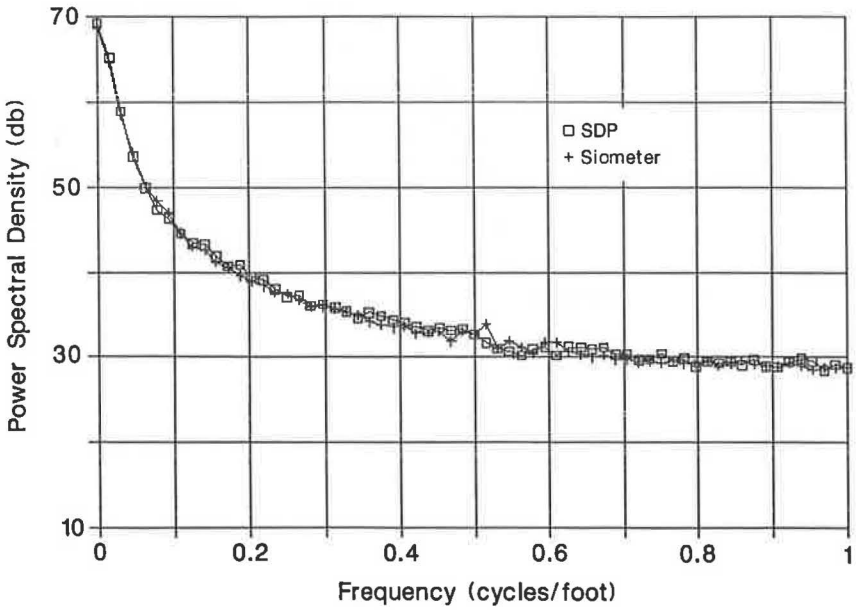

FIGURE 6 Power spectra of pavement profiles measured with the SDP and Siometer for the left wheelpath of Section 1 (Run 1).

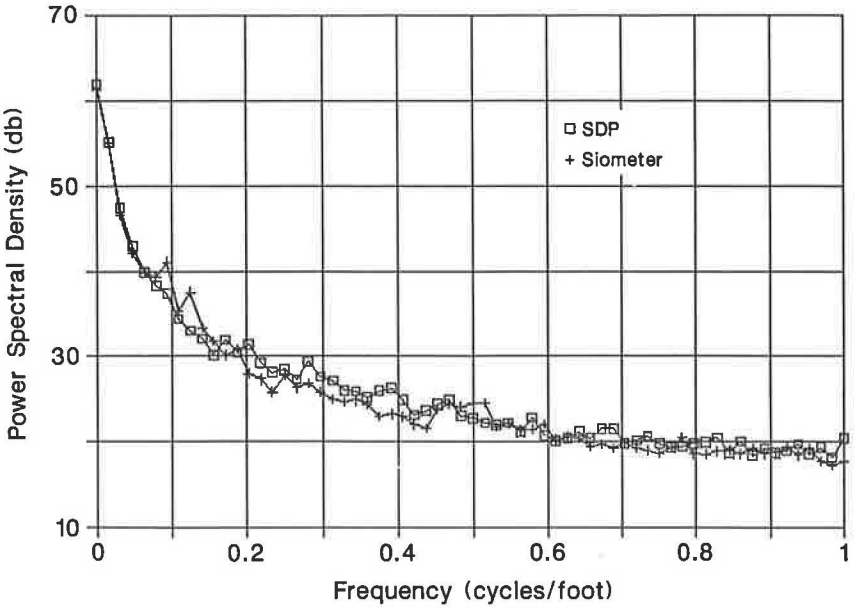

FIGURE 7 Power spectra of pavement profiles measured with the SDP and Siometer for the left wheelpath of Section 7 (Run 1).

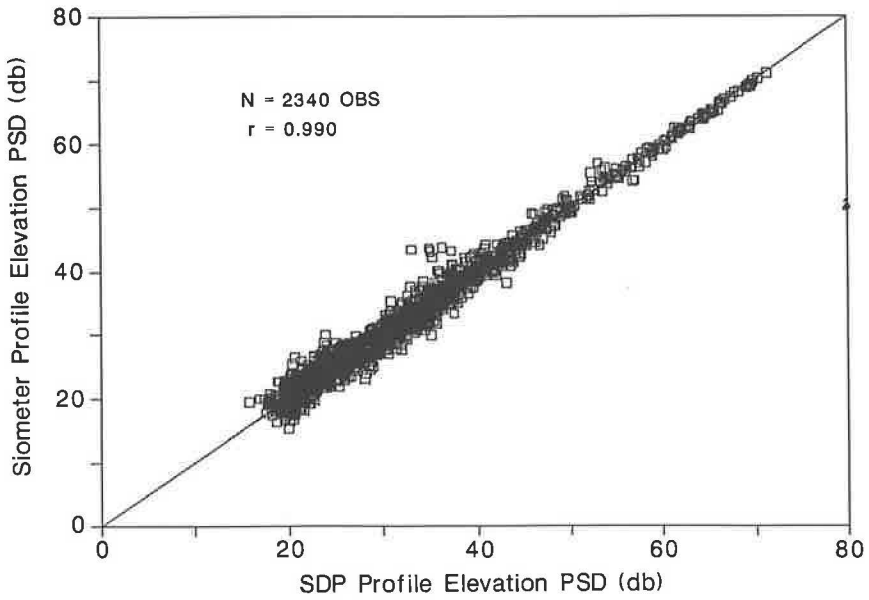

FIGURE 8 Comparison of power spectral densities of Siometer profile elevations with power spectral densities of SDP profile elevations.

where

RMSD = root-mean-square deviation, mils;
Y_i = SDP amplitude, mils;
Y_i' = Siometer amplitude, mils; and
n = number of observations.

Using Equation 1, the RMSD associated with the Siometer power spectra was determined to be 2.46 mils with 2,340 observations. A similar statistic calculated from the power spectra between repeat SDP runs was found to equal 3.87 mils with 1,170 observations. On the average, therefore, the amplitudes of the waveforms associated with Siometer profile elevations deviated from the amplitudes of the corresponding SDP waveforms by approximately 2.5 mils. Similarly, the amplitudes of the waveforms from repeat runs of the SDP differed, on the average, by about 4 mils. The higher RMSD obtained between amplitudes of power spectra from repeat SDP runs is again indicative of the effects of variations in wheelpaths tracked between runs of the instrument. Judging from the statistics presented, it is evident that the Siometer power spectra compare favorably with the corresponding SDP power spectra.

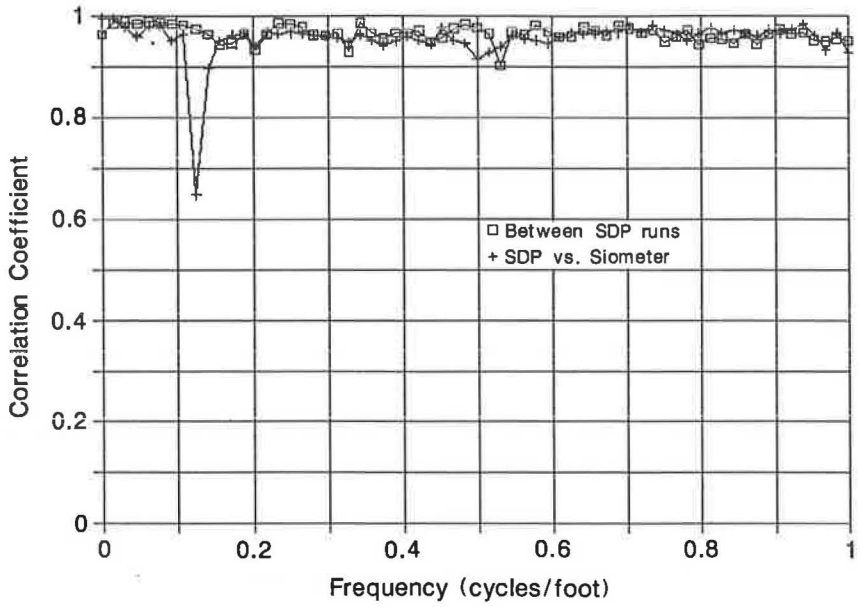

FIGURE 9 Correlation coefficients between roughness power spectral densities across the frequency domain.

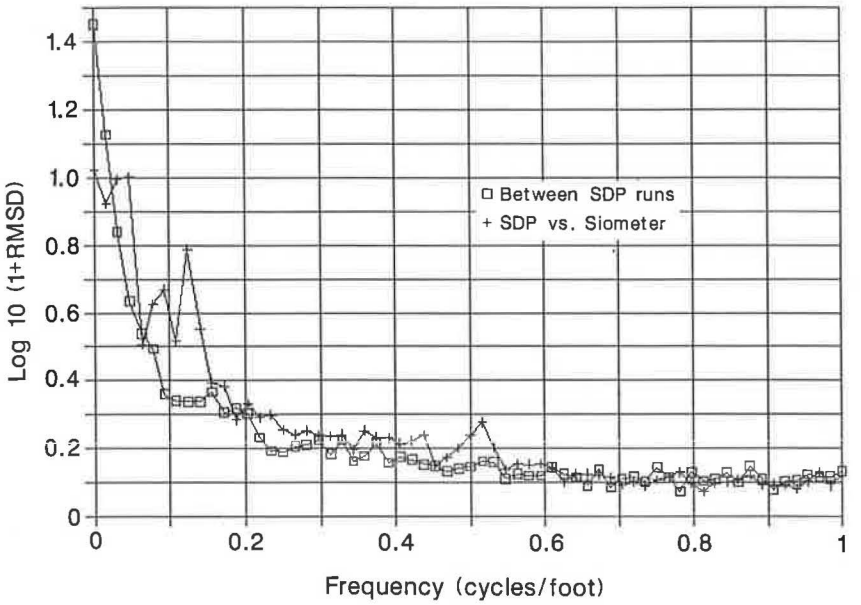

FIGURE 10 Root-mean-square deviations between amplitudes of profile spectra across the frequency domain.

However, while this may be true, the statistics presented only provide an overall measure of the agreement between SDP and Siometer profiles. It is also important to evaluate the agreement between profiles frequency by frequency. Consequently, the correlation coefficients and RMSD values were also compared frequency by frequency.

Figure 9 shows the correlation coefficients across the frequency domain, between PSD values from repeat SDP runs, and between PSD values from corresponding Siometer and SDP runs. Figure 10 shows the RMSD values. It is generally observed that the Siometer power spectra compare favorably with the SDP power spectra. However, at a frequency of 0.125 cycles/ft (about 3.7 Hz at 20 mph), the agreement is not as good compared with the other frequencies. At 0.125 cycles/ft, the correlation coefficient between Siometer and profilometer PSD values drops to about 0.65 as shown by Figure 9. This result suggests that a fundamental response frequency of the vehicle has not been removed and that a need exists for fine-tuning the procedure to parameterize the statistical model of the vehicle so that better agreement between the power spectra of Siometer and SDP profile elevations may be achieved within the entire frequency range.

EVALUATION OF LOAD PROFILES PREDICTED FROM SIOMETER ROAD PROFILES

Pavement surface roughness affects the vehicle dynamic loadings that are imparted to the pavement. Consequently, it is also appropriate to compare the load profiles associated with SDP and Siometer pavement profiles. After all, the dynamic loadings produced will affect pavement service life, and it is of value to know how the predicted dynamic load profiles differ from each other. This would provide another basis for judging the acceptability of the Siometer as a device for profile measurements.

A vehicle simulation program developed at Texas A&M University was used to predict the dynamic loadings produced by a given vehicle running over the measured SDP and Siometer profiles. The vehicle modeled was a tractor-semitrailer (3–S2) combination with a 12,000-lb steering axle load and a 34,000-lb tandem axle on each of the drive and trailer axles. The measured profiles for Sections 1 and 7 were used in the analysis. Two different vehicle speeds, 45 and 27 mph, were used in the simulation.

Figure 11 shows axle loads predicted using profiles from repeat SDP runs on Sections 1 and 7. In the simulation, dynamic axle loads were evaluated at 0.50-ft intervals along a given section for all five axles of the tractor-semitrailer combination. The overall correlation coefficient between axle loads associated with profiles from repeat SDP measurements was 0.990.

Similarly, dynamic axle loads predicted using Siometer profiles were compared with those predicted using corresponding SDP profiles. Figure 12 shows the axle loads evaluated using profiles from the two devices. The overall correlation coefficient between dynamic axle loads was 0.952. This value compared favorably with the overall correlation coefficient of 0.990 between axle loads associated with profiles from repeat SDP measurements. In addition, the root-mean-square deviations between dynamic axle loads predicted from SDP and Siometer profile elevations was 986 lb for 82,160 observations. This statistic was determined using Equation 1 with Y_i being the dynamic axle load predicted using SDP profile elevations and Y_i' the dynamic axle load associated with Siometer profiles. A similar statistic calculated between dynamic axle loads predicted using replicate SDP profiles was 446 lb for 41,080 observations. On the average, therefore, the dynamic axle loads associated with Siometer profiles differed from the corresponding axle loads associated with SDP profiles by 986 lb. This value is 8.2 percent of the nominal static axle load of 12,000 lb on the steering axle of the vehicle used in the simulation, and approximately 5.8 percent of the nominal static axle load of 17,000 lb on each axle of the drive and trailer tandems. The results therefore indicate reasonable agreement between SDP-based and Siometer-based dynamic axle loads.

The power spectra of the predicted dynamic loads were also evaluated to check the degree of similarity in the frequency content of the SDP and Siometer load profiles. Figures 13 and 14 show the load power spectral densities associated with the two devices for profile measurements made on Section 1. The load power spectral densities were determined using the predicted dynamic axle loads for the lead axles of the drive and trailer tandems, at a simulation speed of 45 mph. As seen from the figures, there is good agreement between the load PSD values associated with SDP and Siometer profiles.

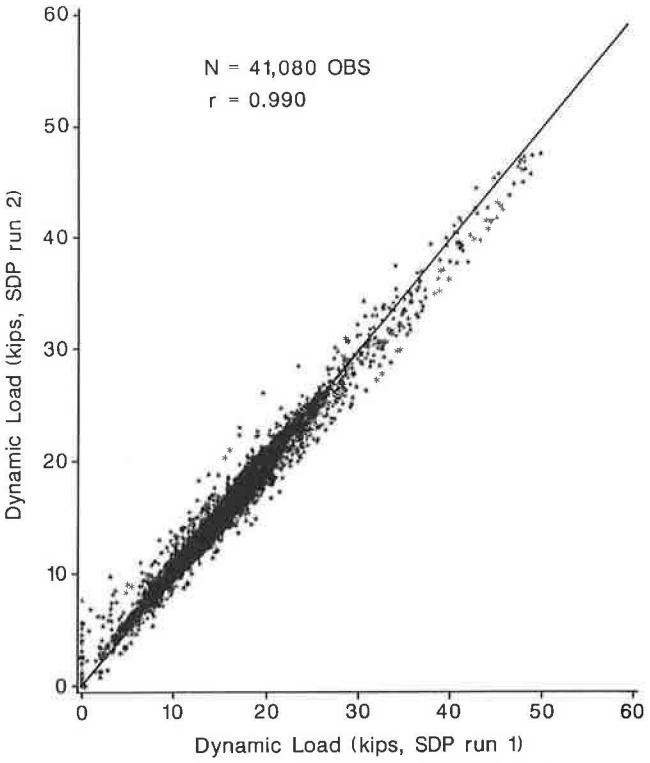

FIGURE 11 Comparison of dynamic axle loads predicted using replicate SDP profile measurements.

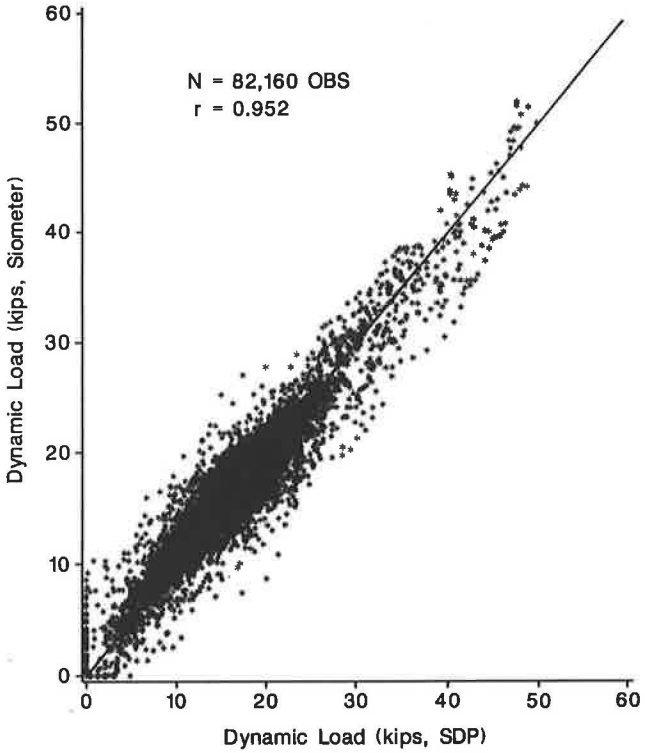

FIGURE 12 Comparison of dynamic axle loads predicted using Siometer profiles with dynamic axle loads predicted using SDP profiles.

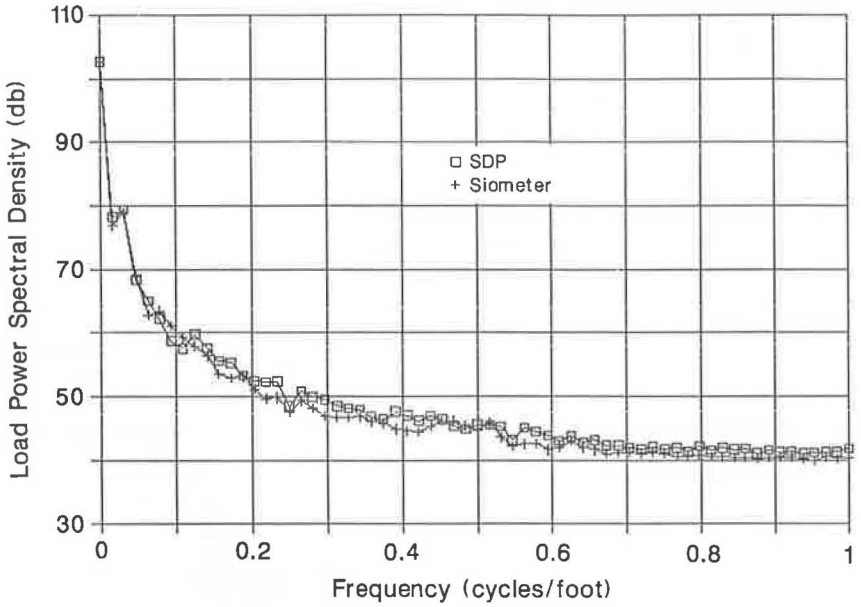

FIGURE 13 Power spectra of dynamic axle loads associated with profiles measured with the SDP and Siometer on Section 1 (Run 1), for the leading axle of the tractor drive tandem assembly.

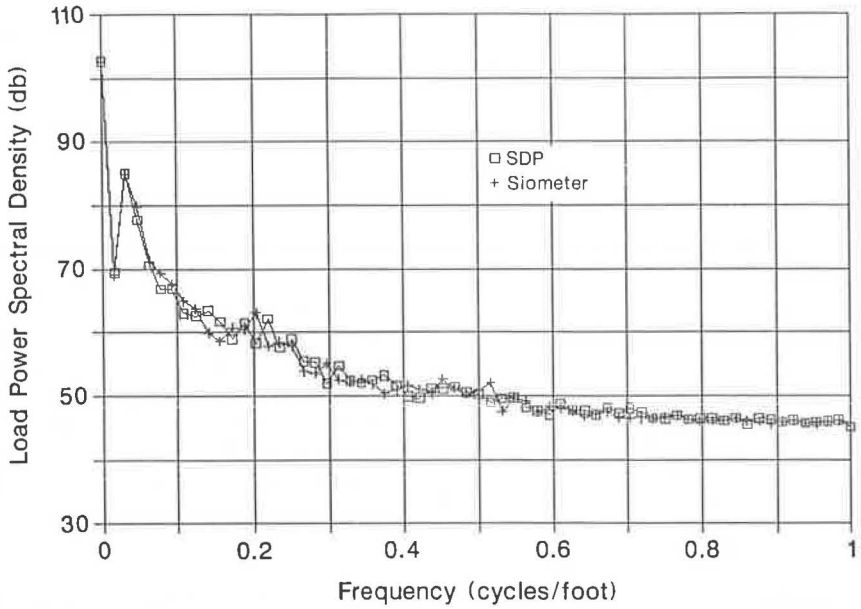

FIGURE 14 Power spectra of dynamic axle loads associated with profiles measured with the SDP and Siometer on Section 1 (Run 1), for the leading axle of the trailer tandem assembly.

In order to evaluate the agreement between SDP and Siometer load power spectral densities, the overall correlation coefficient between PSD values was determined. Figure 15 shows the load power spectral densities associated with SDP and Siometer profiles. An overall correlation coefficient of 0.982 was determined, as indicated in the figure. This value compares favorably with the overall correlation coefficient of 0.997 between power spectral densities associated with repeat SDP profile measurements.

In addition, the root-mean-square deviation between the amplitudes of SDP and Siometer load spectra was determined to be 29.58 lb for 2,600 observations. A similar statistic between the amplitudes of load spectra associated with repeat SDP profile measurements was found to equal 12.68 lb with 1,300 observations. Consequently, the amplitudes of the waveforms associated with the Siometer and SDP load power spectra differ on the average by about 30 lb. Similarly, the amplitudes of the waveforms associated with load power spectra from

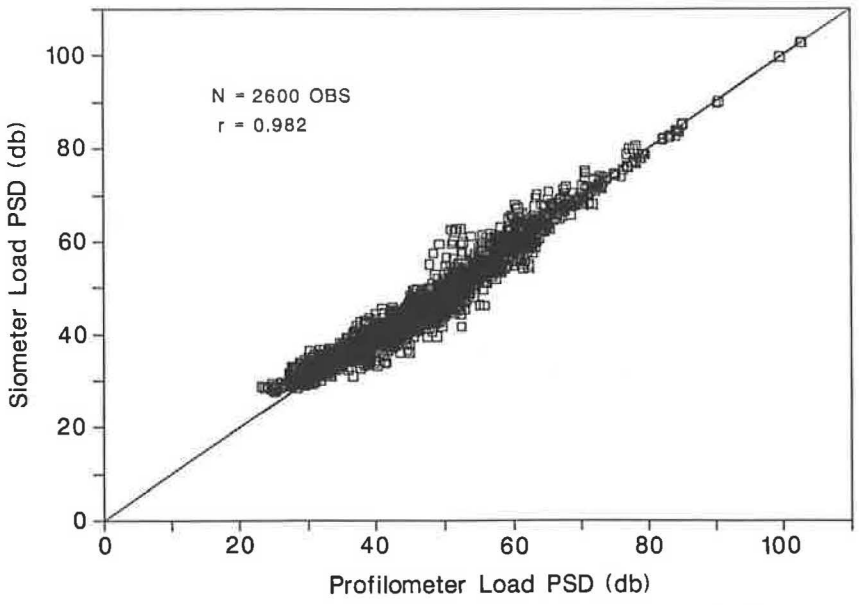

FIGURE 15 Comparison of load power spectral densities associated with Siometer and SDP profiles.

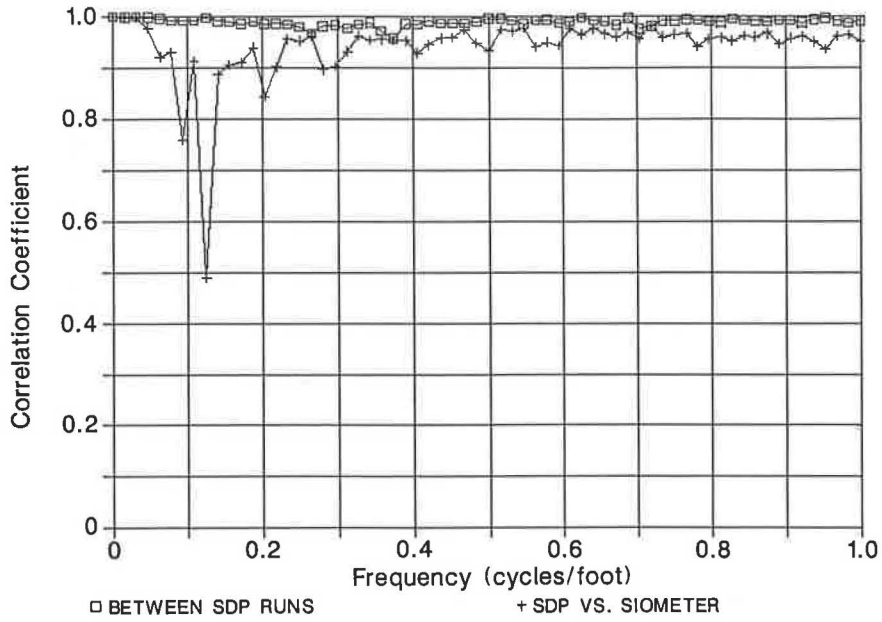

FIGURE 16 Correlation coefficients between load power spectral densities across the frequency domain.

replicate SDP profiles differ on the average by about 13 lb. These values suggest that the Siometer-based load power spectra matches fairly with the corresponding SDP-based load spectra.

The similarity in the load spectra associated with SDP and Siometer profile measurements was also evaluated frequency by frequency. Figure 16 shows the correlation coefficients between replicate load PSD values associated with repeat SDP runs and the correlation coefficients between load PSD values associated with Siometer and SDP roughness measurements. The trends observed are similar to those shown in Figure 9 of the correlation coefficients between power spectral densities of SDP and Siometer profile elevations across the frequency domain. The correlation coefficients across the frequency domain between SDP and Siometer load power spectral densities are generally acceptable. However, at a frequency of 0.125 cycles/ft, the correlation coefficient decreases to slightly less than 0.50. This decrease coincides with the decrease at this same frequency in the correlation coefficient between PSD values of SDP and Siometer profile elevations (see Figure 9). This result again points to a need for refining the vehicle modeling procedure on which the Siometer is based.

CONCLUSIONS

From the results of the evaluation conducted, the following findings are noted:

1. From an examination of the pavement profiles obtained from the same run, there is close agreement between SDP and Siometer profiles. This finding suggests that for practical purposes, the Siometer can show just as well as the SDP can, where the rough spots are on a particular stretch of highway.
2. From a comparison of predicted load profiles, Siometer profiles can reasonably be used in conjunction with a vehicle simulation program for identifying those portions of a given highway segment that are likely to be subjected to severe dynamic loadings.
3. From the spectral analysis of SDP and Siometer profile elevations, the Siometer power spectra compared favorably with the SDP power spectra. However, at a frequency of 0.125 cycles/ft, the correlation coefficient between power spectral densities of SDP and Siometer profile elevations decreased to approximately 0.65, indicating a need for fine tuning the vehicle modeling procedure on which the Siometer is based.
4. From the spectral analysis of dynamic axle loads associated with SDP and Siometer profiles, reasonable agreement between computed load PSD values was observed. The results also suggest that improving the correlation between power spectral densities of SDP and Siometer profile elevations at 0.125 cycles/ft will lead to better agreement between SDP and Siometer load PSD values within the entire frequency spectrum.

Overall, the results obtained are promising and show the potential of the Siometer as an economical, practical, and useful device for collecting profile data on a network-wide scale. Future measurements using the Siometer and the SDP are planned to get more data to further verify the acceptability of the Siometer as a device for profile measurements. Plans include measurements on portland cement pavement sections and reevaluation of the parameterization procedure for modeling the vehicle in the measurement process.

ACKNOWLEDGMENTS

This paper is based on results of a project funded by the Texas SDHPT.

REFERENCES

1. M. W. Sayers, T. D. Gillespie, and C. A. V. Queiroz. *The International Road Roughness Experiment—Establishing Correlation and a Calibration Standard for Measurements*. World Bank Technical Paper 45, The World Bank, Washington, D.C., 1986.
2. E. B. Spangler and W. J. Kelly. *GMR Road Profilometer—A Method for Measuring Road Profiles*. Research Publication GMR-452, Engineering Mechanics Department, General Motors Corporation, Detroit, Mich., Dec. 1964.
3. D. W. McKenzie, W. R. Hudson, and C. E. Lee. *The Use of Road Profile Statistics for Mays Meter Calibration*. Cooperative Research Program, Texas State Department of Highways and Public Transportation, Research Report 251-1, Austin, Tex., Feb. 1982.
4. R. S. Walker. *A Self-Calibrating Roughness Measuring Process*. Research Report 279-1, Texas State Department of Highways and Public Transportation, Austin, Tex., Aug. 1982.
5. R. S. Walker and T. P. Luat. *The Walker Roughness Device for Roughness Measurements*. Research Report 479-1F, The University of Texas at Arlington, July 1987.

Publication of this paper sponsored by Committee on Surface Properties–Vehicle Interaction.

Speed Effect Analysis and Canceling Model of a Response-Type Road Roughness Measuring System

JIAN LU, CARL BERTRAND, AND W. R. HUDSON

Response-type road roughness measuring (RTRRM) systems have been widely used in the United States and internationally in the evaluation of pavement surface roughness. One of the major problems associated with the calibration and operation of RTRRM systems has been the speed dependence of the systems. A reporting statistic from an RTRRM system has to be reported and qualified with speed of operation before the statistic has a meaningful relationship with surface roughness. Because the frequency pass band of an RTRRM system is limited, the outputs of the instruments are also affected by the frequencies of the surface profile. The Center for Transportation Research (CTR) of The University of Texas at Austin has been in the process of calibrating Highway Product International's Automatic Road Analyzer (ARAN) unit for the Texas State Department of Highways and Public Transportation (SDHPT). During the process, a statistical model was developed to cancel the speed effect from the ARAN output. The methodology for generating this model can be applied to any of the various types of RTRRM instruments. The research effort concerning the model being conducted by CTR is introduced. The testing speed effect is analyzed by use of the transfer function of a simulation model of an RTRRM system [i.e., the reference quarter-car simulation (RQCS)]. The amplitude-frequency characteristics of the vehicle axle's vertical acceleration due to changing profile elevations are obtained. In order to quantitatively see the effect of the testing speed on the RTRRM system, it was necessary to simulate the RQCS by the digital difference equation approach with a sine function as the simulation input. A speed effect canceling model unit was generated, and also applied to the ARAN unit. The resulting model will be used to standardize the roughness outputs of the RTRRM system and eliminate the operational speed effect from the output statistics. The methodology is explained and can be applied to other types of RTRRM instruments.

The roughness of paved road surfaces has been explored and monitored by various highway agencies in the United States and throughout the world for many years. In the early 1960s, both static and dynamic instrumentation was being developed to monitor the pavement surface roughness. The surface roughness of paved roads has the following two main areas of concern for the highway design engineers and the riding public: (a) whether smoother road surfaces last longer than rougher roads, and (b) the user's perception of the roadway's ride quality.

Many different types of instrumentation have been developed over the years to monitor the surface roughness of the nation's roadways. These various types of instruments have been categorized broadly by whether they are static (manual) or dynamic in nature. Recently, the World Bank (*1*) has further classified these instruments according to their measurement intervals and the maximum error associated with their operation. FHWA has recently adopted this classification scheme (*2*) and has mandated its use to the individual states. The roughness monitoring instrumentation is divided into three categories:

Class I—Manually operated instruments, which accurately measure short-wavelength profiles of the roads. The measurement interval is less than or equal to 1 ft and the maximum error is 1.5 percent bias, or 19 in./mi. Examples of such instruments are the rod and level, the Face Dipstick, and the Transportation and Road Research Laboratory (TRRL) Beam.

Class II—Dynamic direct profiling instruments, which use a variety of methods to produce elevation data from the road surface. The measurement interval is less than or equal to 2 ft and the maximum error is 5 percent bias, or 44 in./mi. Examples of these instruments include the Longitudinal Profile Analyzer (APL) Trailer, GM profilometer, K. J. Law profilometer, and South Dakota profilometer.

Class III—Response-type road roughness measuring (RTRRM) systems that accumulate suspension deflections (axle to body or acceleration values) from the roadway surfaces. The maximum error associated with the operation of these instruments is 10 percent, or 32 to 63 in./mi, and the measurement interval is the test section length. Examples of these instruments include the Mays Ride Meter, Cox Roadmeter, Bureau of Public Roads (BPR) roughometer, and Automatic Road Analyzer (ARAN) unit.

The basic concept of Class I and II systems is the measurement of pavement surface profiles with limited wavelengths. Obviously, the shortest and the longest wavelengths these instruments can monitor are limited to the sampling interval of the system and the length of the body equipped with this kind of system. Class I instruments do not give information about how vehicles and their passengers will react or perceive the ride quality of the surface being monitored. Class II systems usually use filtering (hardware or software) to limit the influence of the longer wavelengths. They also use filtering or data averaging techniques to limit the short wavelengths and smooth the incoming elevation data. These two classifications give good indications of the true profile of the surfaces being monitored but may not relate to the user's perception of the surface profile.

Center for Transportation Research, The University of Texas at Austin, Austin, Tex. 78712.

The pavement surface ride quality can be directly related to the passenger's perception of the vehicle vibration, or the vehicle's response to certain frequencies. Class III instruments attempt to give an indication of the user's perception to the road's surface profile by monitoring the dynamic response of a mechanical device as it travels over the surface at a constant speed. These RTRRM systems use a variety of techniques, such as axle and body displacement transducers and accelerometers, to measure vehicle response. Class III instruments are the most widely used high-speed roughness monitoring devices in use today because they are relatively inexpensive, high-speed instruments that give good indications of the user's perception to the surface roughness. However, the RTRRM system outputs are speed dependent. That is, the reporting statistics will be different on the same road surface if the speed of travel is different. The different suspension system characteristics of each RTRRM vehicle make each response to a surface profile unique. These facts make it necessary to calibrate and standardize the outputs so that the reporting statistics from one vehicle can accurately be related to those of another vehicle.

To cancel the effect of speed dependence theoretically, two methods could be used, i.e., the system identification method and the statistical modeling method. The system identification method is carried out by conducting a series of dynamic tests on each RTRRM system. A set of parameters for each suspension system is estimated by means of these tests. The dynamic response characteristics of the suspension system can then be approximated by describing an abstracted dynamic response model in the time domain, or a transfer function in the frequency domain. Usually, these mathematical models need to be linearized and the corresponding dimensional degree should be as small as possible to simplify the model. Linearization of mathematical models also simplifies the solution to complex mathematical relationships. After the dynamic response model is identified, the speed dependence of the RTRRM system can be canceled mathematically. But, in practice, different vehicles have different dynamic response characteristics, and, therefore, the models should be different. Under normal circumstances, it is not worthwhile to test the dynamic parameters for each RTRRM system because the test procedure is complicated and expensive. Generally, it is not practical to use the system identification method to cancel the effect of speed dependence.

The basic concept of the statistical modeling method is to correlate the outputs of an RTRRM system collected from field tests, with their outputs at different testing speeds. The statistical relationships between the roughness outputs and the corresponding speeds can largely cancel the effect of speed dependence. The basic speed effect canceling model that results from the statistical method is relatively simple, and the methodology for the modeling can be used for practically all RTRRM system vehicles. The RTRRM systems must have relatively repeatable response for the same surface roughness characteristics before this approach is valid. But the coefficients in the speed effect canceling model should be estimated for each individual RTRRM system so that the corresponding speed effect canceling model can be generated.

The researchers have chosen the statistical method for modeling and canceling the RTRRM system speed effects because it is simpler and more practical than the dynamic response method. This paper describes how the speed effect canceling model was derived by the statistical modeling method. This model is applied to the ARAN unit and the result is a specific speed effect canceling model generated for the ARAN unit.

In order to explain how the testing speed affects the outputs of RTRRM systems, the reference quarter-car simulation [RQCS (*3*)] of an RTRRM system is introduced. The transfer function of the axle vertical acceleration to the pavement profile elevation is derived. Then, the amplitude frequency characteristics of the transfer function are used to explain the testing speed effect.

A quantitative simulating analysis is presented with an explanation of the testing speed effect using amplitude frequency characteristics of the transfer function of RQCS. The transfer function of RQCS is transformed into a digital difference equation corresponding to RQCS. The pavement profiles are then simulated by a sine function. The sine wave is input into the digital difference equation with different testing speeds. In this way, the simulated relationship between the output of RQCS and the testing speed is obtained.

The Center for Transportation Research (CTR) at The University of Texas at Austin has been evaluating and calibrating different subsystems of the Highway Product International (HPI) ARAN unit for the Texas State Department of Highways and Public Transportation (SDHPT). One of these subsystems involves the one that reports surface roughness statistics. During this evaluation and calibration effort, a mathematical model was developed for modeling the dynamic response of the suspension system. A statistical model has been generated for canceling the speed effect from the reported statistics.

SPEED EFFECT ANALYSIS BY TRANSFER FUNCTION AND SIMULATING MODEL

Reference Quarter-Car Simulation

The outputs obtained by an RTRRM system are based on the response of the vehicle to pavement surface profiles or slopes. Accurate modeling of the suspension system of the vehicle equipped with a measuring system is very complicated and expensive. RQCS, a simplified reference simulation of an RTRRM system, can be used in the analysis of the dynamic characteristics of an RTRRM system with certain boundary conditions. Figure 1 shows RQCS with the following parameters:

$$K_1 = \frac{K_t}{M_s} = 653 \text{ sec}^{-2}$$

$$K_2 = \frac{K_s}{M_s} = 63.3 \text{ sec}^{-2}$$

$$U = \frac{M_u}{M_s} = 0.15$$

$$C = \frac{C_s}{M_s} = 6.00 \text{ sec}^{-1}$$

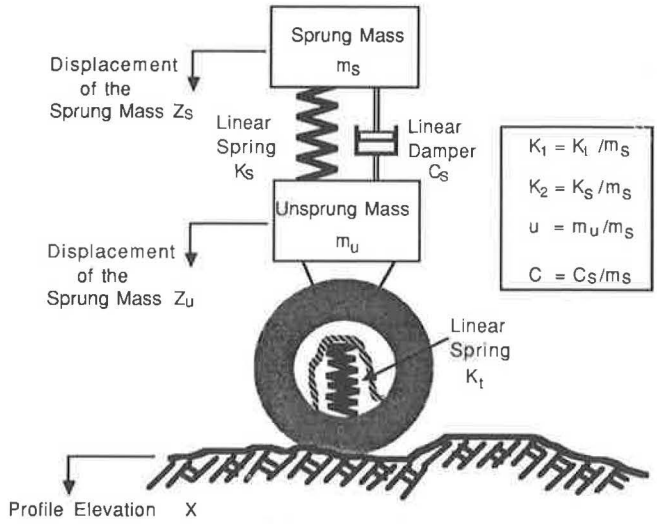

FIGURE 1 The reference quarter-car simulation (2).

The dynamic mathematical model shown in Figure 1 is defined mathematically by two second-order differential equations:

$$\frac{d^2Z_s}{dt^2} + C\left(\frac{dZ_s}{dt} - \frac{dZ_u}{dt}\right) + K_2(Z_s - Z_u) = 0 \tag{1}$$

and

$$\frac{d^2Z_s}{dt^2} + U\frac{d^2Z_u}{dt^2} + K_1Z_u = K_1X \tag{2}$$

where X, Z_s, and Z_u are defined as shown in Figure 1. Clearly, because Equations 1 and 2 are linear and constant equations, these two equations can be used only in a relatively narrow range because the linearization process is valid only within the given limits.

Amplitude-Frequency Characteristic of RQCS

Equations 1 and 2 describe the dynamic relationship of the displacements (Z_s and Z_u) and profile elevation X. Some RTRRM systems measure vehicle vertical acceleration instead of displacement. Therefore, to consider the amplitude-frequency characteristics with vehicle axle vertical acceleration as output, Equations 1 and 2 need to be changed using the following substitutions:

$$a_s = \frac{d^2Z_s}{dt^2} \tag{3}$$

and

$$a_u = \frac{d^2Z_u}{dt^2} \tag{4}$$

where a_s is the vehicle body vertical acceleration, and a_u is the vehicle axle vertical acceleration.

One of the best methods for frequency characteristics analysis is the Laplace transform method (*4*). By taking the Laplace transform of both sides of Equations 1, 2, 3, and 4, the following equations in the frequency domain can be obtained:

$$S^2Z_s(S) + CS[Z_s(S) - Z_u(S)] + K_2[Z_s(S) - Z_u(S)] = 0 \tag{5}$$

$$S^2Z_s(S) + US^2Z_u(S) + K_1Z_u(S) = K_1X(S) \tag{6}$$

$$A_s(S) = S^2Z_s(S) \tag{7}$$

$$A_u(S) = S^2Z_u(S) \tag{8}$$

where S is the independent variable of the Laplace transform, and $Z_s(S)$, $Z_u(S)$, $A_s(S)$, $A_u(S)$, and $X(S)$ are the Laplace transforms of Z_s, Z_u, a_s, a_u, and X, respectively. From these equations, the transfer function $H(S)$ of axle vertical acceleration a_u to profile elevation X is expressed

$$H(S) = \frac{A_u(S)}{X(S)} \tag{9}$$

$$= \frac{K_1S^4 + K_1CS^3 + K_1K_2S^2}{US^4 + (UC + C)S^3 + (UK_2 + K_2 + K_1)S^2 + K_1CS + K_1K_2}$$

or

$$H(S) = \frac{A_1S^4 + A_2S^2 + A_3S^2}{B_1S^4 + B_2S^3 + B_3S^2 + B_4S + B_5} \tag{10}$$

where

$H(S)$ = the transfer function,
$A_1 = K_1$,
$A_2 = K_1C$,
$A_3 = K_1K_2$,
$B_1 = U$,
$B_2 = UC + C$,
$B_3 = UK_2 + K_2 + K_1$,
$B_4 = K_1C$, and
$B_5 = K_1K_2$.

The amplitude-frequency characteristics of RQCS (for which a_u is the output, X the input) are expressed by the following equation:

$$|H(j\omega)| = \left|\frac{A_u(j\omega)}{X(j\omega)}\right| = \sqrt{\frac{(A_1\omega^4 - A_3\omega^2)^2 + A_2^2\omega^6}{(B_1\omega^4 - B_3\omega^2 + B_5)^2 + (B_4\omega - B_2\omega^3)^2}} \tag{11}$$

where

$\omega = -Sj$ = angular frequency (rad/sec), and
$j = \sqrt{-1}$.

Figure 2 shows the relative amplitude-frequency characteristic with the maximum value of $|H(j2\pi f)|$ (Max$|H(j2\pi f)|$) as the reference value, and the independent variable is frequency f(Hz) with the transformation $f = \omega/2\pi$. From Figure 2, it can be seen that RQCS behaves like a bandpass filter, and,

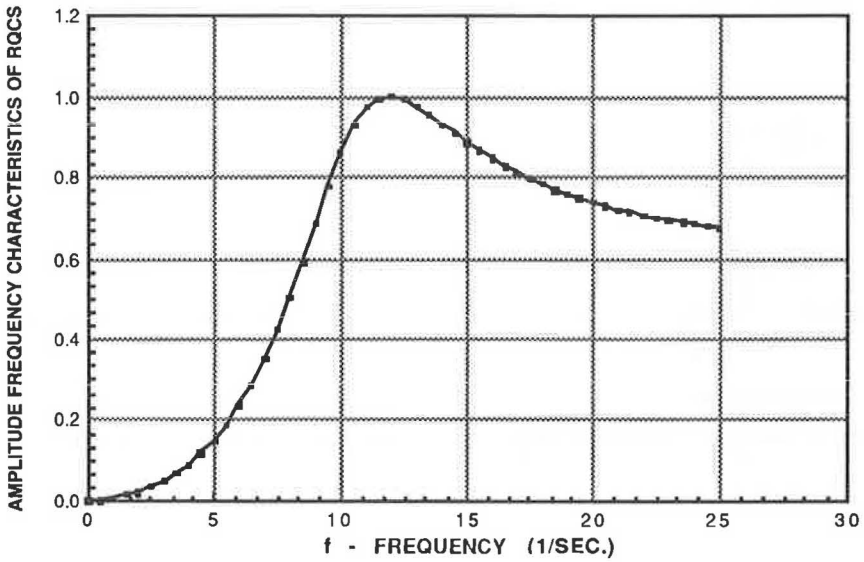

FIGURE 2 RQCS transfer function—amplitude-frequency characteristic of axle acceleration response to elevation profile.

when the frequency reaches approximately 12 Hz, the RQCS has maximum sensitivity.

A comprehensive subjective ride research study on the relative importance of pavement profile frequency on ride comfort was conducted by the Michigan Department of Transportation (*5*). The results indicated that the roughness contained at frequencies ranging from 1.5 to 37 Hz at 50 mph correlated the strongest with the subjective ratings. Further, human body sensitivity to vertical vibration is at a maximum in the range of 5 to 6 Hz. This frequency band for human body sensitivity is, unfortunately, contained in the passband of RQCS. In other words, if an RTRRM system fits the RQCS well, the system will respond to the roughness that includes the frequencies to which passengers are sensitive.

SIMULATING ANALYSIS OF RQCS WITH PROFILE OF A SINE FUNCTION

If the wavelength λ of a given pavement profile is fixed, then the changing of speed is equivalent to the changing of the frequency of the profiles. Roughness results from an RTRRM system are definitely affected by operational speed because the process is dynamic. How are these results affected by the factor of speed? As seen in Figure 2, if frequency f is less than 12 Hz, the sensitivity (gain) of RQCS increases as f increases. Suppose a pavement profile is described by a sine function:

$$X(K) = A \sin \frac{2\pi}{\lambda} vKT \tag{12}$$

where

A = constant,
λ = wavelength (ft),
v = speed (mph),
T = sampling interval (sec), and
K = sample sequence index (K = 0, 1, 2, . . .).

It can be understood that the frequency of this function is

$$f = \frac{5{,}280\, v}{3{,}600\, \lambda} (\text{Hz}) \tag{13}$$

Therefore, if λ is assumed to be 6.5 ft, as speed v increases from 0 to 53 mph, the sensitivity (gain) of RQCS increases, i.e., the acceleration of the axle vertical vibration increases.

A simulating analysis can be conducted using the approximate difference equation solution of RQCS. As shown in Equation 10, RQCS can be described by a Laplace transfer function. In order to obtain the approximate difference equation solution of RQCS, the transfer function needs to be changed by a bilinear transformation (*6*),

$$S = \frac{2}{T} \frac{Z - 1}{Z + 1} \tag{14}$$

where Z is the Z transform factor.

Consequently, the Laplace transfer function is changed into a Z transform transfer function:

$$\frac{A_u(Z)}{X(Z)} = H(Z) = \frac{C_1 + C_2 Z^{-1} + C_3 Z^{-2} + C_4 Z^{-3} + C_5 Z^{-4}}{D_1 + D_2 Z^{-1} + D_3 Z^{-2} + D_4 Z^{-3} + D_5 Z^{-4}} \tag{15}$$

where

$A_u(Z)$ = Z transform of A_u,
$X(Z)$ = Z transform of X,
$C_1 = 16A_1 + 8TA_2 + 4T^2A_3$,
$C_2 = -64A_1 - 16TA_2$,
$C_3 = 96A_1 - 8T^2A_3$,
$C_4 = -64A_1 + 16TA_2$,
$D_1 = 16B_1 + 8TB_2 + 4T^2B_3 + 2T^3B_4 + T^4B_5$,
$D_2 = 64B_1 - 16TB_2 + 4T^3B_4 + 4T^4B_5$,

$$D_3 = 96B_1 - 8T^2B_3 + 6T^4B_5,$$
$$D_4 = -64B_1 + 16TB_2 - 4T^3B_4 + 4T^4B_5,$$
$$D_5 = 16B_1 - 8TB_2 + 4T^2B_3 - 2T^3B_4 + T^4B_5, \text{ and}$$
$$Z^{-1} = \text{one-step delay factor.}$$

Further, Equation 15 can be changed into

$$\begin{aligned} &D_1A_u(Z) + D_2Z^{-1}A_u(Z) + D_3Z^{-2}A_u(Z) \\ &\quad + D_4Z^{-3}A_u(Z) + D_5Z^{-4}A_u(Z) \\ &= C_1X(z) + C_2Z^{-1}X(Z) + C_3Z^{-2}X(Z) \\ &\quad + C_4Z^{-3}X(Z) + C_5Z^{-4}X(Z) \end{aligned} \tag{16}$$

Taking the inverse Z transform of both sides of Equation 16 results in

$$\begin{aligned} &D_1a_u(K) + D_2a_u(K-1) + D_3a_u(K-2) \\ &\quad + D_4a_u(K-3) + D_5a_u(K-4) \\ &= C_1X(K) + C_2X(K-1) + C_3X(K-2) \\ &\quad + C_4X(K-3) + C_5X(K-4) \end{aligned}$$

or

$$\begin{aligned} a_u(K) = &-\frac{D_2}{D_1}a_u(K-1) - \frac{D_3}{D_1}a_u(K-2) \\ &- \frac{D_4}{D_1}a_u(K-3) - \frac{D_5}{D_1}a_u(K-4) \\ &+ \frac{C_1}{D_1}X(K) + \frac{C_2}{D_1}X(K-1) \\ &+ \frac{C_3}{D_1}X(K-2) + \frac{C_4}{D_1}X(K-3) \\ &+ \frac{C_5}{D_1}X(K-4) \end{aligned} \tag{17}$$

Equation 17 is the approximate difference (digital) equation solution of RQCS; $a_u(K)$ is the Kth digital value of the axle vertical acceleration sequence and $X(K)$ is the Kth digital value of the pavement profile elevation sequence.

Suppose the profile elevation sequence $X(K)$ is a sine function described in Equation 12, or

$$X(K) = A\sin\frac{2\pi}{\lambda}vKT = A\sin\frac{2\pi}{\lambda}K\Delta X \tag{18}$$

where ΔX is the sample interval in distance.

If the roughness index root-mean-square vertical acceleration (RMSVA) (*7*) is defined

$$\text{RMSVA} = \sqrt{\frac{1}{N}\sum_{K=1}^{N}[a_u(K)]^2} \tag{19}$$

where N is the sample length, then the simulated results can be obtained by Equations 17, 18, and 19, with the following parameters, variable v (mph), and initial values:

$A = 1$

$\lambda = 6.5$ ft

$\Delta X = 0.5$ ft

$T = \dfrac{21{,}600}{63{,}360v}$ (sec), and

Initial values = 0.

RMSVA should be a function of speed v determined by the profile elevation sequence $X(K)$. From the amplitude-frequency characteristics of RQCS (Figure 2), it can be expected that as v increases from 0 to 50 mph, RMSVA should increase monotonically. Figure 3 shows the simulated results of relative RMSVA versus speed v, where relative RMSVA is defined by

$$\text{Relative RMSVA} = \frac{\text{RMSVA (at } v)}{\text{RMSVA (at 50 mph)}} \tag{20}$$

The simulated results indicate how the factor of speed affects the roughness index.

Figure 4 shows the curve of relative RMSVA versus speed v, obtained from a research study on the evaluation of the ARAN unit conducted by CTR. The data were collected by

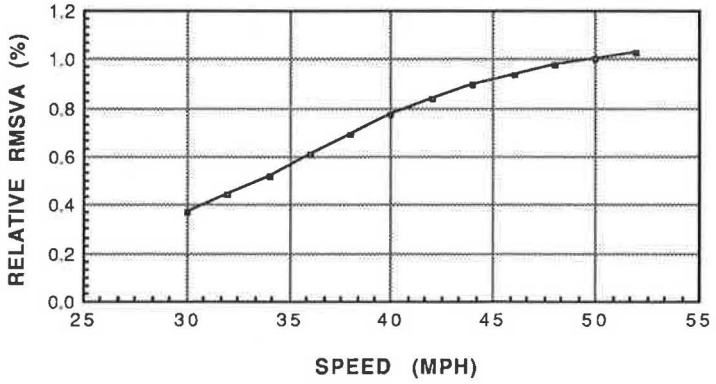

FIGURE 3 Simulation analysis of RQCS response to speed (the output is RMSVA, the input is a sine function).

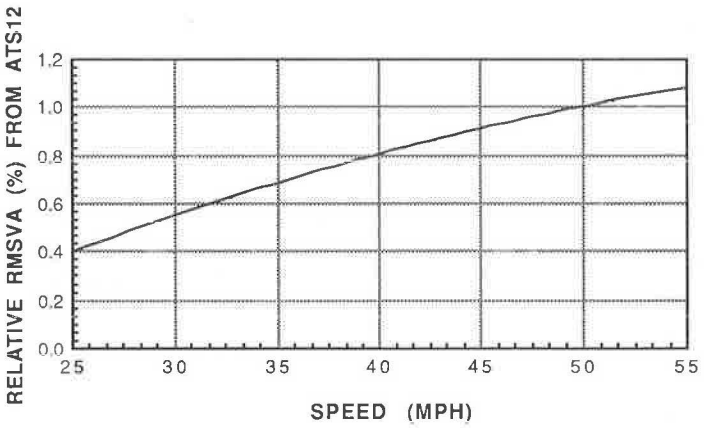

FIGURE 4 Relative RMSVA (percent) versus speed (mph) measured by the ARAN unit at ATS12.

the ARAN unit from a test section named ATS12. The effect of speed on RMSVA can be seen to be similar to that simulated by RQCS.

SPEED EFFECT CANCELING MODEL

The statistical method is more practical for canceling speed effect of the roughness output as measured by an RTRRM system than the system identification method as has been previously stated. The basic idea of implementing the statistical method is to run RTRRM vehicles in the field and obtain the statistical relationship of the roughness output to the testing speed. The roughness output measured at a testing speed V_t can then be referenced to the roughness output at a standard speed V_s.

The roughness output measured at a testing speed V_t can be defined as $\mathrm{RO}(V_t)$. For a given test section, $\mathrm{RO}(V_t)$ is the following function of V_t:

$$\mathrm{RO}(V_t) = f(V_t) \tag{21}$$

where $f(*)$ is a continuous function and $f(*)$ can be obtained by curve-fitting techniques. For example, to demonstrate the methodology, assume $f(*)$ is a second-order function. It should be recognized that this $f(*)$ can be defined in different forms depending on the instrument to be described. Then

$$f(V_t) = A + BV_t + CV_t^2 \tag{22}$$

where A, B, and C are the coefficients that must be estimated. To estimate these coefficients, a certain number of test sections are run at different speeds. For each test section, the coefficients A, B, and C, and the value of $\mathrm{RO}(V_s)$ can then be obtained. The following matrix can be generated from the test section data:

Test Section	$RO(V_s)$	A	B	C
1	x	x	x	x
2	x	x	x	x
3	x	x	x	x
. . .	. . .	. . .	. . .	. . .
M	x	x	x	x

where M is the number of the test sections run by the RTRRM system during field tests, and $\mathrm{RO}(V_s)$ is the standard roughness output for a given test section, because V_s is defined as the standard testing speed. If it is assumed that the coefficients A, B, and C can be related to $\mathrm{RO}(V_s)$ by the linear regression method or the curve-fitting technique, then

$$\begin{aligned} A &= G_A[\mathrm{RO}(V_s)] \\ B &= G_B[\mathrm{RO}(V_s)] \\ C &= G_C[\mathrm{RO}(V_s)] \end{aligned} \tag{23}$$

where $G_A[\mathrm{RO}(V_s)]$, $G_B[\mathrm{RO}(V_s)]$, and $G_C[\mathrm{RO}(V_s)]$ are continuous functions of $\mathrm{RO}(V_s)$. From Equation 22, the following equation can be obtained:

$$\begin{aligned} \mathrm{RO}(V_t) &= G_A[\mathrm{RO}(V_s)] + G_B[\mathrm{RO}(V_s)]V_t + G_C[\mathrm{RO}(V_s)]V_t^2 \\ &= \mathrm{G}[V_t, \mathrm{RO}(V_s)] \end{aligned} \tag{24}$$

where $G(*,*)$ is a two-dimensional continuous function of V_t and $\mathrm{RO}(V_s)$. If $G(*,*)$ is reversible in terms of V_s, then

$$\mathrm{RO}(V_s) = R[V_t, \mathrm{RO}(V_t)] \tag{25}$$

where $R(*,*)$ is the inverse function of $G(*,*)$ in terms of V_s.

Equation 25 is the speed effect canceling model. That is, whatever the testing speed V_t for a particular test section, the standard roughness output can be obtained through Equation 25. For example, if $G_A(*)$, $G_B(*)$, and $G_C(*)$ are the first-order functions, i.e.,

$$\begin{aligned} A &= a_1 + a_2\mathrm{RO}(V_s) \\ B &= b_1 + b_2\mathrm{RO}(V_s) \\ C &= c_1 + c_2\mathrm{RO}(V_s) \end{aligned} \tag{26}$$

then Equation 24 is

$$\begin{aligned} \mathrm{RO}(V_t) &= a_1 + a_2\mathrm{RO}(V_s) + [b_1 + b_2\mathrm{RO}(V_s)]V_t \\ &\quad + [c_1 + c_2\mathrm{RO}(V_s)]V_t^2 \\ &= a_1 + b_1V_t + c_1V_t^2 \\ &\quad + (a_2 + b_2V_t + c_2V_t^2)\mathrm{RO}(V_s) \end{aligned} \tag{27}$$

or

$$\mathrm{RO}(V_s) = \frac{\mathrm{RO}(V_t) - (a_1 + b_1 V_t + c_1 V_t^2)}{a_2 + b_2 V_t + c_2 V_t^2} \tag{28}$$

The canceling model just described can also be completed by a family of curves. The procedure for canceling the speed effect can be completed by referring to the corresponding curves. An example for the development and use of this model is contained in the following section.

APPLICATION OF THE SPEED EFFECT CANCELING MODEL TO RMSVA OF THE ARAN UNIT

In order to obtain the canceling model for the ARAN unit, 30 typical test sections were chosen around the Austin area. This study was sponsored by the Texas State Department of Highways and Public Transportation (SDHPT). The surface roughness statistics, as measured by the ARAN unit on these sections is root-mean-square vertical acceleration (RMSVA). The curves of RMSVA versus V_t are shown in Figure 5. From these curves, Equation 21 has the following form:

$$\mathrm{RMSVA}(V_t) = A + BV_t + (V_t - 25) \tag{29}$$

Table 1 was obtained by curve fitting, interpolation, and letting $V_s = 50$ mph. Figures 6 and 7 show the curves of coefficients A and B, respectively, versus RMSVA(V_s). The data points on the figures can be fitted by the first-order functions. Equation 26 can be used for the curve fitting to obtain the coefficients A and B. The coefficients a_1, a_2, b_1, and b_2 and the corresponding correlation coefficients are shown in Figures 6 and 7. By applying Equation 28 with $C_1 = 0$, $C_2 = 0$, the mathematical model for canceling the speed effect is

$$\mathrm{RMSVA}(V_s) = \frac{\mathrm{RMSVA}(V_t) - [-36.758 + 1.403(V_t - 25)]}{0.44407 + 0.022237(V_t - 25)} \tag{30}$$

The measured RMSVA can be referred to the standard output RMSVA(V_s) through Equation 30 regardless of the operational speed V_t. Figure 8 shows a family of curves for canceling speed effect for the Texas ARAN unit. These curves were obtained by using the following procedure.

From Equation 30, for a given RMSVA(V_s), RMSVA(V_t) is a function of V_t. Therefore, a curve of RMSVA(V_t) versus V_t can be obtained. By changing RMSVA(V_s), another curve of RMSVA(V_t) versus V_t can be obtained, and so on.

It is easy to use Figure 8. For instance, if the ARAN unit measures roughness data at speed V_t, the measured RMSVA(V_t) must be converted to the standard roughness output RMSVA(V_s) according to V_t and RMSVA(V_t). The corresponding RMSVA(V_s) curve can be found at the intersection of the V_t and RMSVA(V_t).

For example, if the ARAN unit is operated at 40 mph ($V_t = 40$ mph) and the obtained RMSVA at 40 mph is 400 milligravities (mg), then by substituting RMSVA(V_t) and V_t into Equation 30, the resulting standard RMSVA at 50 mph [RMSVA(V_s)] should be 533.3 mg. Figure 9 shows how to obtain RMSVA(V_s) using the family of curves presented in Figure 8. The resulting RMSVA(V_s) from Figure 9 is the same as that calculated using Equation 30.

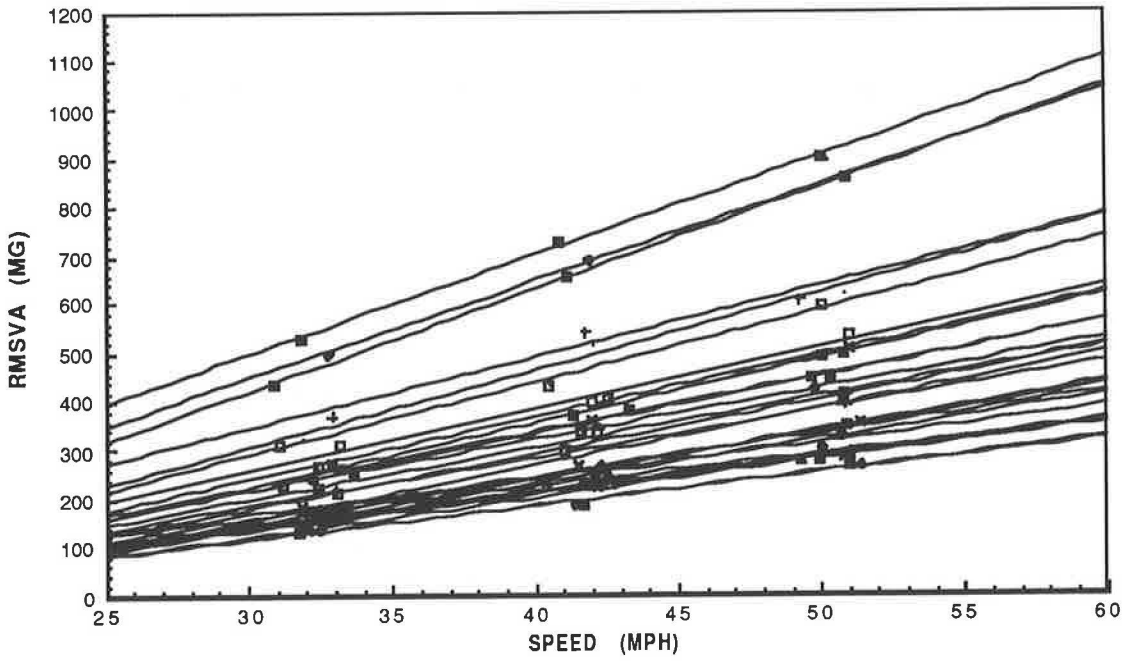

FIGURE 5 Raw RMSVA (mg) versus speed (mph).

TABLE 1 COEFFICIENTS AND RMSVA(V_s) FOR EACH TEST SECTION

Section	RMSVA (V_s), V_s = 50 mph	A	B
ATS01	585.820	215.415	14.813
ATS03	424.729	164.904	10.393
ATS07	313.286	129.496	7.352
ATS08	286.207	108.022	7.127
ATS09	408.910	145.485	10.537
ATS12	331.970	112.270	8.708
ATS15	290.449	125.986	6.578
ATS16	837.530	314.855	20.907
ATS18	449.250	254.775	11.779
ATS19	280.405	79.452	8.038
ATS20	336.395	100.222	9.447
ATS21	901.280	394.455	20.273
ATS22	280.408	97.466	7.318
ATS24	620.310	225.160	15.806
ATS25	494.440	175.765	12.747
ATS27	251.743	82.058	6.787
ATS28	253.799	79.962	6.953
ATS30	842.510	348.735	19.751
ATS31	450.680	165.480	11.408
ATS36	512.680	196.430	12.650
ATS41	320.335	92.898	9.098
ATS42	283.194	105.864	7.093
ATS43	281.258	99.765	7.260
ATS55	634.536	270.711	14.553
IHI-1	338-220	86.370	10.074
IHI-2	381.200	134.185	9.881
IHI-3	401.520	123.045	11.139
IHO-1	382.910	94.610	11.532
IHO-2	485.940	156.390	13.182
IHO-3	487.120	155.970	13.246

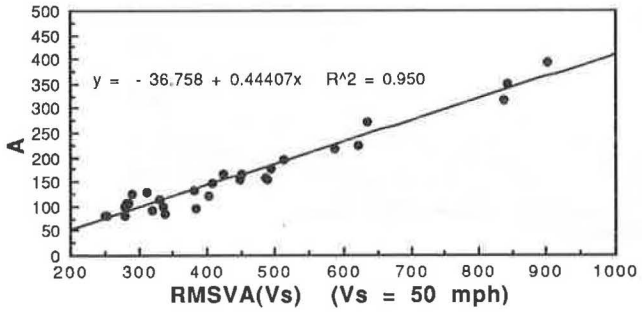

FIGURE 6 Coefficient A versus RMSVA(V_s) at V_s = 50 mph.

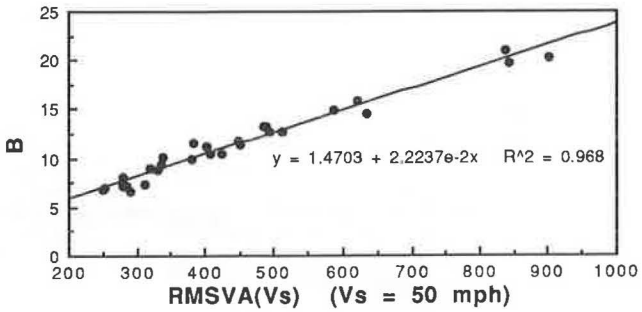

FIGURE 7 Coefficient B versus RMSVA(V_s) at V_s = 50 mph.

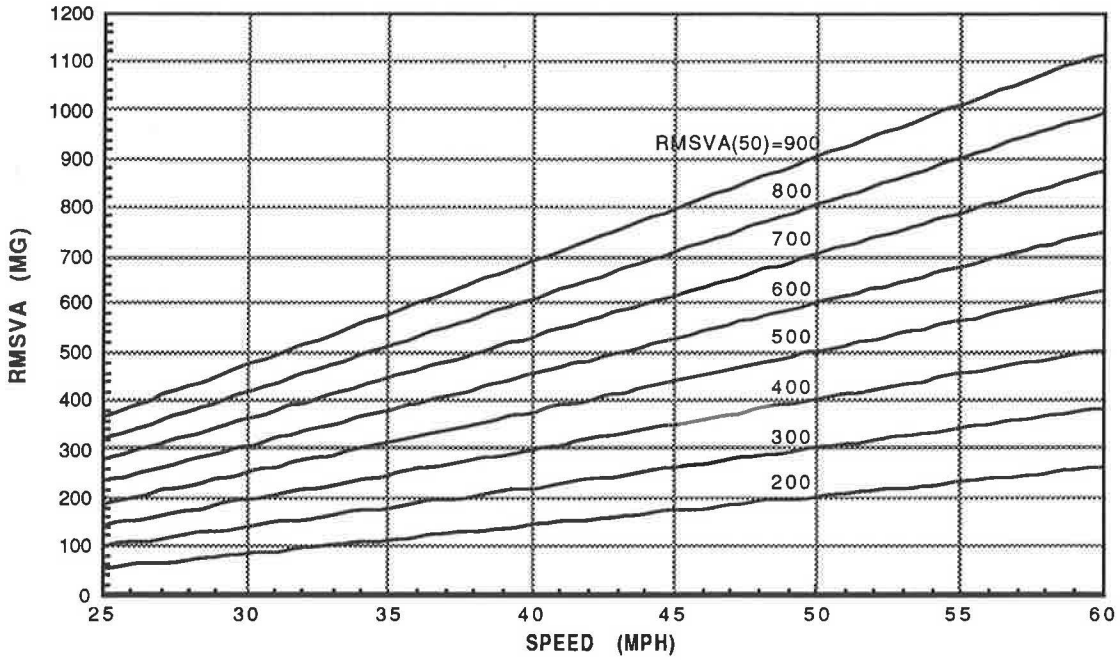

FIGURE 8 Transformation of RMSVA at V_t to the standard RMSVA(V_s) at V_s = 50 mph by the speed effect canceling model.

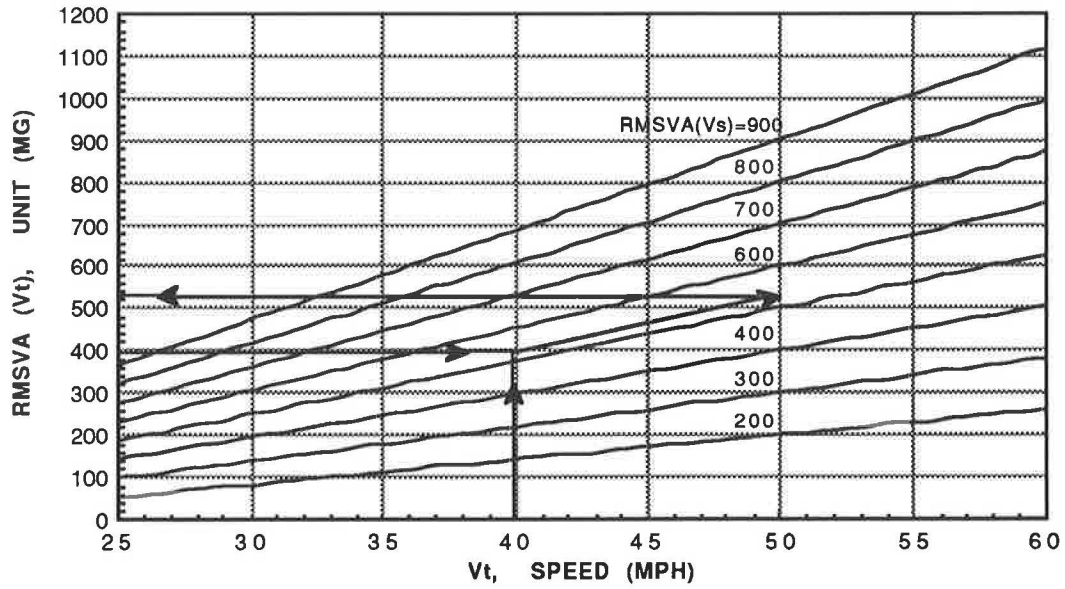

FIGURE 9 Transformation of RMSVA at V_t to the standard RMSVA(V_s) at V_s = 50 mph by the speed effect canceling model.

CONCLUSION

The roughness output for a given roadway measured by an RTRRM system increases as testing speed increases as shown by the simulation analysis of RQCS. In fact, as the speed increases, the feeling of the passenger's comfort to the ride becomes worse because the gain of the suspension systems transfer function increases.

The speed effect canceling methodology of the RTRRM system presented in this paper may be suitable for all types of RTRRM systems, but, in order to set up a model for a specific RTRRM system, a series of field tests should be run so that some adequate function of Equations 21 and 23 and corresponding coefficients can be obtained. As stated in this paper, the method of obtaining the speed effect canceling model is a statistical method. It is hard to totally cancel the effect of speed on the outputs of an RTRRM system, but statistically, the model presented in this paper does significantly cancel the effect of speed.

It should be mentioned here that there are some limitations for this kind of speed effect canceling model. In order to apply the methodology presented in this paper to other RTRRM

systems, relatively good repeatability of the output roughness statistics is required. In addition, the output of the instrument using this speed effect canceling model should include information regarding the operating speed. Further research will be conducted to check the accuracy of this model. This research will include collection of actual profile data to use as inputs to the model presented.

REFERENCES

1. M. W. Sayers, T. D. Gillespie, and W. D. O. Paterson. *Guidelines for the Conduct and Calibration of Road Roughness Measurements*. World Bank Technical Paper 46, The World Bank, Washington, D.C., 1986.
2. *Highway Performance Monitoring Field Manual*. Publication 5600.1A, Appendix J, FHWA, U.S. Department of Transportation, Dec. 1, 1987.
3. M. W. Sayers, T. D. Gillespie, and C. A. V. Queiroz. *The International Road Roughness Experiment—Establishing Correlation and a Calibration Standard for Measurements*. World Bank Technical Paper 45, The World Bank, Washington, D.C., 1986.
4. T. F. Bogart, Jr. *Laplace Transforms and Control Systems Theory for Technology*. John Wiley, New York, 1982.
5. J. R. Darlington. *A Roughness Wavelength Band Determined by Subjective Response*. Michigan Department of State Highway and Transportation, Ann Arbor, Feb. 1976.
6. C.-T. Chen. *One-Dimensional Digital Signal Processing*, Marcel Dekker, Inc., 1979.
7. W. R. Hudson, D. Halbach, J. P. Zaniewski, and L. Moser. *Root-Mean-Square Vertical Acceleration as a Summary Roughness Statistic*. STP 884, ASTM, Philadelphia, Pa., 1985.

Publication of this paper sponsored by Committee on Surface Properties–Vehicle Interaction.

Design Friction Factors of Different Countries Versus Actual Pavement Friction Inventories

RUEDIGER LAMM, ELIAS M. CHOUEIRI, PREM B. GOYAL, AND THEODOR MAILAENDER

A fundamental scale is presented for evaluating appropriate levels of tangential and side friction factors with respect to design speed for new designs, redesigns, and rehabilitation strategies. The friction data used were obtained from the geometric highway design guidelines of the United States and several Western European countries, and from actual pavement friction inventories in New York State and in the Federal Republic of Germany (FRG). From the friction data of the countries in this study, relationships were developed between tangential or side friction factors and speed. The curves resulting from these relationships were then compared with percentile level distribution curves obtained from the actual pavement friction inventories. Analyses indicated that (a) the friction factors produced by the overall regression curves coincided with those obtained from the 90th-percentile level distribution curve of New York State, and with those derived from the 80th-percentile level distribution curve of the FRG; and (b) the friction factors derived from the 95th-percentile level distribution curve of New York State coincided with the friction factors derived from the 95th-percentile level distribution curve of the FRG. On the basis of these results, recommendations are provided for highway design for minimum stopping sight distances and minimum radii of curve. It is estimated that in applying the proposed friction factors for design, redesign, and rehabilitation strategies 95 percent of wet pavements will be covered in the United States and Europe. The recommendations provided should not be regarded as a final solution, but perhaps an international discussion of a larger dynamic safety supply for driving may be useful in reducing accidents on 2-lane rural highways. Because there are often inadequate safety factors in tire-road friction, friction demand often exceeds friction supply, causing more accidents than necessary.

An international review of existing design guidelines (*1–7*) has shown that European countries directly or indirectly address three design issues in their guidelines much more explicitly than United States agencies to gain safety advantages. For example, German, Swedish, and Swiss designers are provided with geometric design criteria that direct them toward

1. Achieving consistency in horizontal alignment,
2. Harmonizing design speed and operating speed on wet pavements, and
3. Providing adequate dynamic safety of driving.

R. Lamm, Institute of Highway and Railroad Engineering, University of Karlsruhe, D–7500 Karlsruhe 1, Kaiserstrasse 12, Federal Republic of Germany. E. M. Choueiri, North Country Community College, Sarnac Lake, Route 1, Box 12, Potsdam, N.Y. 13676. P. B. Goyal, 10 Hunter Lane, Elmsford, N.Y. 10523. T. Mailaender, Mailaender Ingenieur Consult, D–7500 Karlsruhe 1, Mathystrasse 13, Federal Republic of Germany.

Criteria 1 and 2 were the subject of several reports, publications, and presentations by the authors. For example, for the National Science Foundation (*8*), for the New York State Governor's Traffic Safety Committee (*9, 10*), for the Transportation Research Board (*11–14*), for the Ohio Transportation Engineering Conference (*15–18*), for the International Road Federation (*1, 19*), for the Swedish Road and Traffic Research Institute (*20*), for the International Road and Traffic Conference in Berlin (*21*), and for the German research community (*22*). These investigations included (a) processes for evaluating horizontal design consistency and inconsistency; (b) processes for evaluating design speed and operating speed differences; (c) relationships between geometric design parameters, operating speeds, and accident rates; (d) recommendations for achieving good and fair design practices, as well as recommendations for detecting poor designs, provided (*9–11, 19*) on the basis of changes in degrees of curve and operating speeds between successive design elements.

For example, Figure 1 shows the relationships between degree of curve and operating speeds and accident rates for individual lane widths, derived from the analysis of data of 322 two-lane rural highway sections in New York State. The research has demonstrated that (a) the most successful parameter in explaining much of the variability in operating speeds and accident rates was degree of curve, and (b) the relationship between degree of curve and operating speed is valid for both dry and wet pavements so long as visibility is not appreciably affected by heavy rain (*23*).

This paper is primarily concerned with the geometric design Criterion 3, providing adequate dynamic safety of driving.

Recent skid research investigations by Mason and Peterson (*24*) have indicated that sufficient friction supply is to be regarded as an important safety issue. Brinkman (*25*) found that resurfacing alone did not have a significant effect on the mean skid number. He indicated that skid resistance should be regarded as a main safety issue when resurfacing roadways. Glennon et al. (*26*) indicated that the probability that a highway curve may become a frequent accident site increases with decreasing pavement skid resistance.

The primary objective of this study is to develop an objective scale for relating skid resistance—described by coefficient of friction, skid number, or friction number—to speed. In order to achieve this goal, a comparative analysis of tangential and side friction factors in the highway design guidelines of the United States and four Western European

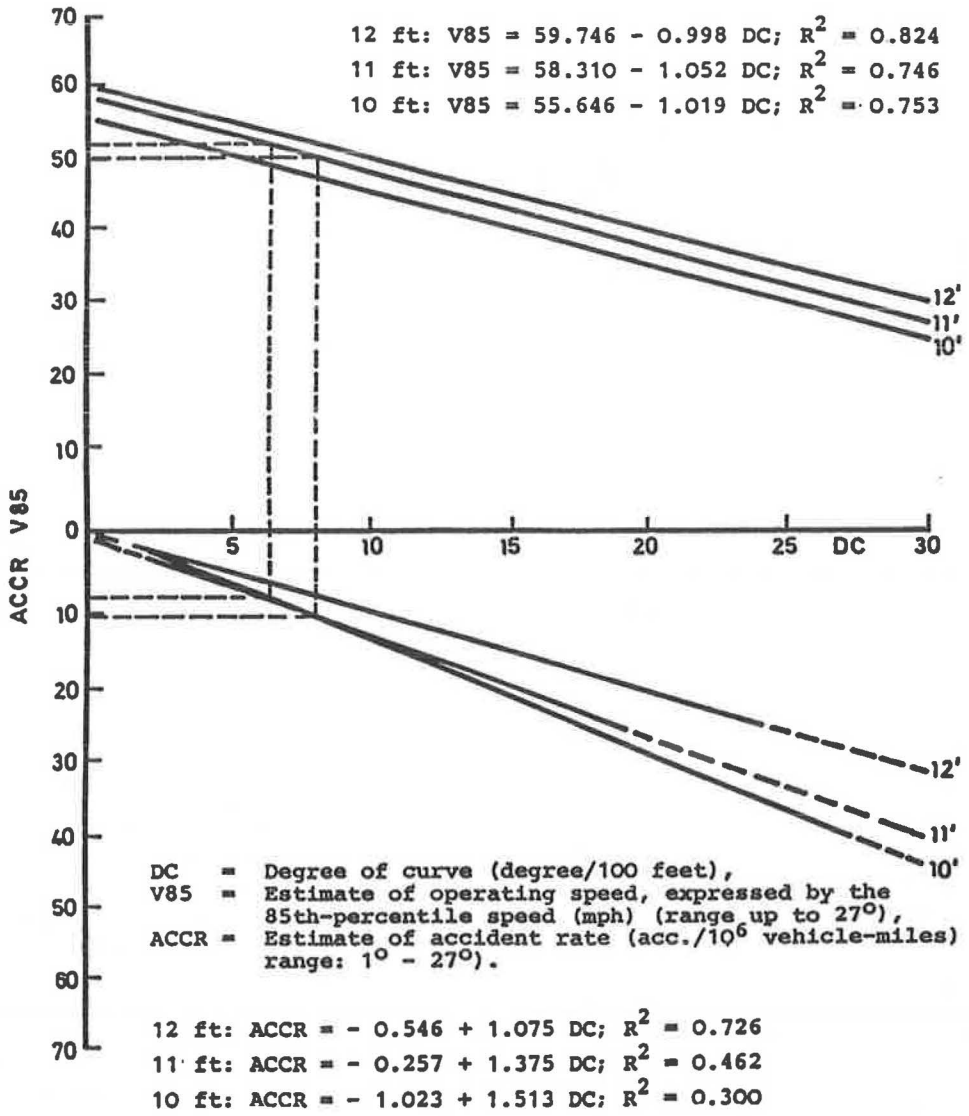

FIGURE 1 Nomogram for evaluating operating speeds and accident rates as related to degree of curve for individual lane widths (*10, 12*).

countries was carried out to determine the type of relationships that exist between friction factors and design speed, and consequently the development of overall relationships between friction and design speed. These overall relationships will then be compared to actual pavement friction inventories in the United States and in the Federal Republic of Germany (FRG), to determine the percentage of wet pavements that could be covered by such relationships.

COMPARATIVE ANALYSES OF FRICTION FACTORS IN DIFFERENT COUNTRIES

How the issue of friction, and equally important the issue of speed in relation to geometric design, are being applied in the United States and several European countries will be subject for discussion later in this section.

Because of the lower coefficients of friction on wet pavements as compared with dry, the wet condition governs in determining stopping sight distances and radii of curve, as revealed in the studied design guidelines. Furthermore, the countries in this study assume that the coefficients of friction used for design criteria should represent not only wet pavements in good condition but also surfaces approaching the end of their useful lives. The values should encompass nearly all significant pavement surface types and the likely field conditions, as it is expressed, for example, in AASHTO 1984 (*7*).

Contacts with responsible transportation agencies in the countries under study revealed that friction data measurements are conducted using an apparatus similar to that of ASTM E 274 (*27*). The apparatus normally consists of the following:

1. An automotive vehicle with one or more test wheels incorporated into it or forming part of a suitable trailer towed by a vehicle.

2. A transducer, instrumentation, water supply, and a proper dispensing system and actuation controls for the brake of the test wheel. The test wheel is equipped with a standard test tire, which is different in different countries.

3. The test apparatus is brought to a desired test speed. The test speeds are different in different countries as they are different in different states of the United States. For example, in the FRG a road section is tested at speeds of 25, 37.5, and 50 mph (40, 60, and 80 km/hr). For evaluating skid resistance, the standard procedure is to compare the measured values with recommended values (*28*): 0.42 for $V = 25$ mph, 0.33 for $V = 37.5$ mph, and 0.26 for $V = 50$ mph. These recommended values represent the skid resistance values that can be reached on 90 percent of road surfaces in the FRG. Similar recommendations exist in several other European countries.

4. Water is delivered ahead of the test tire and the braking system is actuated to lock the test tire. For the test, a water-film thickness of 1 mm is widely used (*29*).

5. The resulting friction force acting between the test tire and the pavement surface, and the speed of the test vehicle are recorded with the proper instrumentation. The skid resistance of the paved surface is determined from the resulting force torque record and reported as the coefficient of friction, the skid number, or the friction number. These values are determined from the force required to slide the locked tire at a stated speed, divided by the effective wheel load. The wheel load depends on the weight of the test trailers used in the different countries.

Because of some variations in testing procedures, the friction data used in this study may be biased. But, the fact remains that the basic method used to measure skid resistance is, to a certain extent, comparable between the countries.

With the exception of the FRG (*2*) and Switzerland (*3, 30, 31*), the rest of the countries in this study do not clearly show how the design friction factors used in their guidelines are obtained from the measured skid resistance values. Despite this lack, the authors still attempted to determine how the friction data used in the guidelines of the subject countries would compare to percentile level distribution curves developed from actual pavement friction inventories in the United States and in the FRG.

Such a comparison should be allowed from a research standpoint because in reality there exist differences in every research field, e.g., medicine and engineering, in testing, as well as in reporting procedures. In performing comparative analyses of data in different countries, there always exists the possibility that the data may be biased.

TANGENTIAL FRICTION FACTOR

The data in Table 1 represent the maximum allowable tangential friction factors for wet pavements with respect to the design speed applied in the highway design guidelines of the United States (USA), Federal Republic of Germany (FRG), France (F), Sweden (S), and Switzerland (CH).

Figure 2 shows an overview of the maximum allowable tangential friction factors of the studied European guidelines and for highway design in the United States with respect to design speed. Note that, with the exception of France, all relationships in Figure 2 are quadratic. The European countries in this study were considered typical European countries by Hayward et al. (*1*). In Figure 2, all speeds have been converted to miles per hour for comparison purposes.

TABLE 1 MAXIMUM ALLOWABLE TANGENTIAL FRICTION FACTORS FOR DIFFERENT DESIGN SPEEDS IN DIFFERENT COUNTRIES (*34*)

Design Speed (mph)	Tangential Friction Factor (f_T) - rounded				
	USA	FRG	F	S	CH
19				.46	
20	.40	.43			.54
25	.38	.39	.37	.44	.50
30	.35	.36			.45
31				.41	
35	.34	.32			.40
38			.37	.39	
40	.32	.29			.37
44				.36	
45	.31	.27			.35
50	.30	.24	.33	.34	.32
55	.30	.22			.30
60	.29	.20			.29
63			.30		
65	.29	.18			.27
70	.28	.17			.26
75		.16	.27		.25

Figure 2 shows that (a) as design speeds increase, friction factors decrease; (b) the friction-speed curves for Switzerland and FRG are nearly parallel, with the friction values of Switzerland higher by about 0.1; (c) the tangential friction values of Sweden are limited because of a maximum design speed of 50 mph on 2-lane rural roads in this country; (d) the American values intersect the German curve at a design speed of about 30 mph and the Swiss curve at a design speed of about 60 mph.

In comparison to the other countries, the United States has the lowest differences in friction values (see Table 1). For example, between design speeds of 30 and 70 mph the difference in the American tangential friction values is 0.07 (0.35 to 0.28), whereas for Germany and Switzerland the difference is 0.19. In the higher, more critical design speed ranges, for example, between 55 and 70 mph, the difference in the American values is only 0.02, whereas for Germany the difference is 0.05, and for Switzerland, 0.04. These small differences in the American friction values, or these low speed gradients of tangential friction, clearly contradict the worldwide research experience that shows that friction values should substantially decrease with increasing speeds (see Figure 2). If this experience is not met, critical driving maneuvers may occur, specially when operating speed exceeds design speed by considerable amounts under wet pavement conditions (*9–11, 19*).

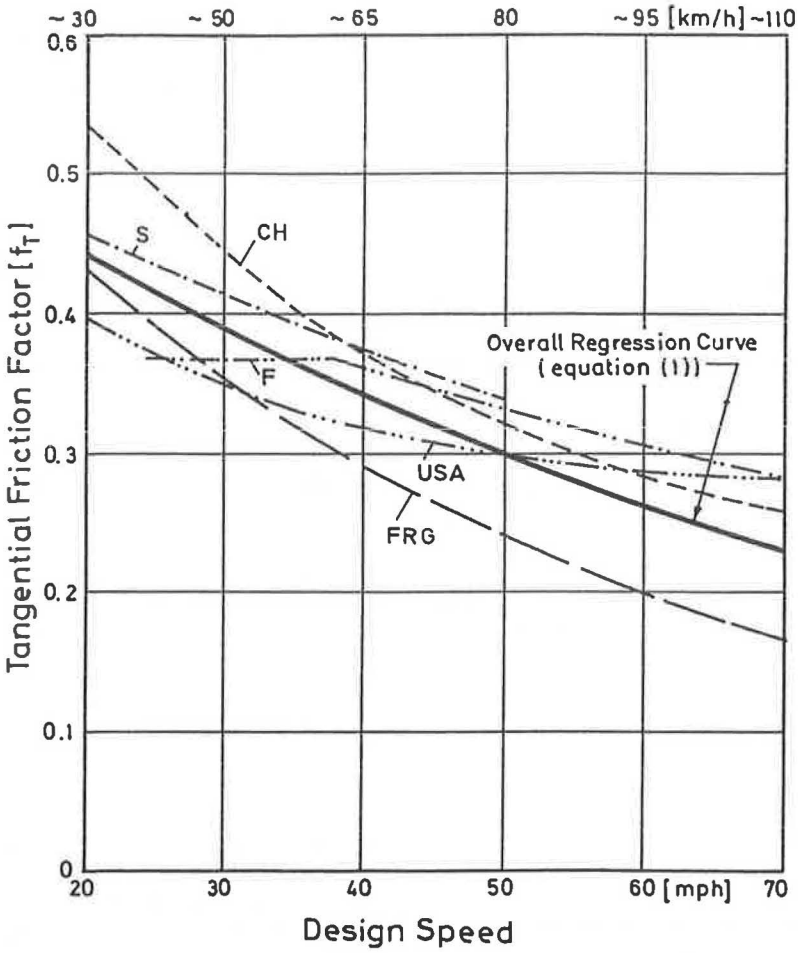

FIGURE 2 Relationships between maximum allowable tangential friction factor and design speed for different countries, along with the overall regression curve.

On the basis of the data of the five studied countries, the following overall regression equation was developed relating tangential friction factor f_T and design speed V_d:

$$f_T = 0.591 - 7.81*10^{-3}V_d + 3.9*10^{-5}(V_d)^2 \quad (1)$$

$$R^2 = 0.731$$

$$\text{SEE} = 0.044$$

where

f_T = tangential friction factor,
V_d = design speed (mph),
R^2 = coefficient of determination, and
SEE = standard error of estimate.

The high value of R^2 and low value of SEE of Equation 1 indicate that the relationship between tangential friction and design speed is a strong one.

Figure 2 shows the calculated values of the tangential friction factor (Equation 1) as a solid line superimposed on the curves of the countries in this study. This figure indicates that (a) the Swiss and Swedish tangential friction values are higher than the tangential friction values of the overall regression curve; (b) for design speeds greater than 35 mph, the French values are higher; (c) the FRG values are lower; and (d) the U.S. tangential friction values intersect the overall regression curve at a design speed of about 50 mph. For design speeds greater than 60 mph, the French and U.S. tangential friction values are higher than the tangential friction values of the other countries.

SIDE FRICTION FACTOR

The data presented in Table 2 give the maximum allowable side friction factors for wet pavements with respect to the design speed applied in the highway design guidelines of the same five countries.

Figure 3 shows an overview of the maximum allowable side friction factors of the European guidelines and for highway design in the United States with respect to design speed. Note that, with the exception of the United States, all relationships in Figure 3 are quadratic. In Figure 3, all speeds have been converted to miles per hour for comparison purposes.

On the basis of the data of the five countries in Table 2, the following overall regression equation was developed relating side friction factor f_R and design speed V_d:

$$f_R = 0.269 - 3.53*10^{-3}V_d + 1.5*10^{-5}(V_d)^2 \quad (2)$$

$$R^2 = 0.799$$

$$\text{SEE} = 0.018$$

TABLE 2 MAXIMUM ALLOWABLE SIDE FRICTION FACTORS FOR DIFFERENT DESIGN SPEEDS IN DIFFERENT COUNTRIES (*34*)

Design Speed (mph)	Side Friction Factor (f_R) - rounded				
	USA	FRG	F	S	CH
19				.210	
20	.170	.200			
25	.165	.180	.250	.190	.220
30	.160	.170			.200
31				.170	
35	.155	.150			.180
38			.160	.160	
40	.150	.130			.160
44				.150	
45	.145	.120			.150
50	.140	.110	.130	.140	.140
55	.130	.100			.130
60	.120	.090			.130
63			.110		
65	.110	.080			.120
70	.100	.075			.110
75		.070	.100		.110

where

f_R = side friction factor, and
V_d = design speed (mph).

The high value of R^2 and the low value of SEE for Equation 2 indicate that the relationship between side friction and design speed is a strong one.

Figure 3 shows the calculated values of the side friction factor from Equation 2 as a solid line superimposed on the curves for the countries in this study. For speeds greater than 40 mph, this figure indicates that the U.S. side friction values are slightly higher than the values of the overall regression curve and the friction values of the European countries in this study, with the exception of Switzerland.

ADDITIONAL INFORMATION FOR DESIGN PURPOSES

In the guidelines of the United States and Europe, maximum allowable tangential friction factors are used to calculate minimum stopping sight distances, whereas side friction factors are used to calculate minimum radii of curve (*1–7*).

For calculating minimum stopping sight distances, the United States uses a perception-reaction time of 2.5 sec, whereas the European countries use 2.0 sec. Both values were found to be adequate in recent papers presented at the 68th Annual Meeting of the TRB, January 1989. Taoka (*32*), for instance, concluded the following: "It appears that the AASHTO design value of 2.5 seconds may correspond to the response time of the 95th-percentile driver. The stopping sight distance design driver assumption is satisfactory at the present time." In contrast, Wilson et al. (*33*) came to the following conclusion: "The current design standard for perception and reaction time is 2.5 seconds. This value compares with the study

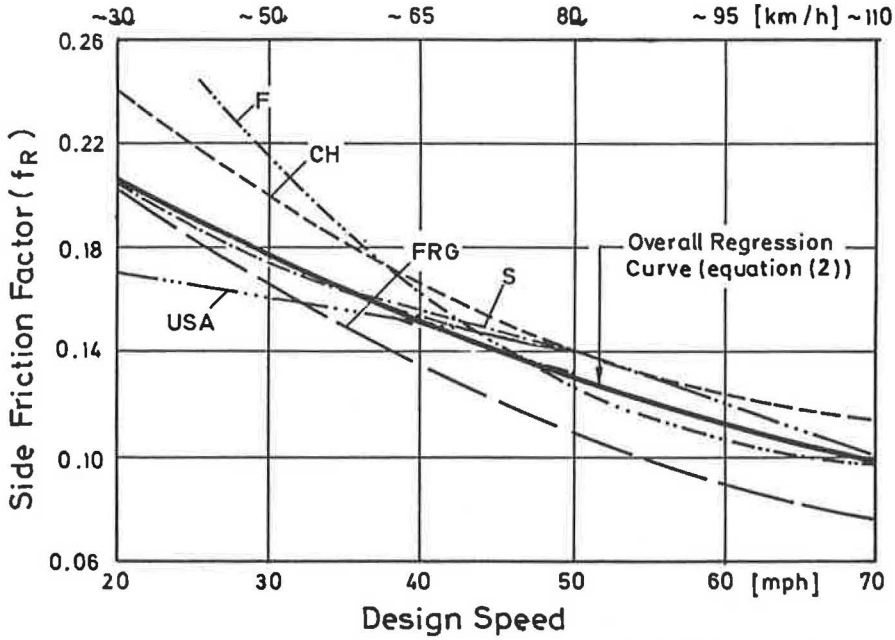

FIGURE 3 Relationships between maximum allowable side friction factor and design speed for different countries, along with the overall regression curve.

findings at the 99th-percentile of 1.60 seconds indicating that the current design standards are conservative."

The maximum superelevation rates used in the different countries for calculating minimum radii of curve can be seen in the following table. The applied superelevation rates range from 5.5 percent in Sweden to 8 percent in the United States.

Country	Perception-Reaction Time (sec)	Superelevation Rate (%)	Superelevation Rate Qualification
United States	2.5	8	Maximum under snow and ice conditions
Federal Republic of Germany	2.0	7 8	Desirable Exception
Switzerland	2.0	7	Unqualified
Great Britain	N/A	5 7	Desirable Absolute
France	2.0	5 7	Desirable Absolute
Sweden	2.0	5.5	Maximum

COMPARATIVE ANALYSES OF THE OVERALL REGRESSION CURVE VERSUS ACTUAL PAVEMENT FRICTION INVENTORIES

In addition to the data in this paper, other studies (*34–38*) were used to determine how the overall regression curve (Equation 1) developed from the data of the countries in this study compares to actual pavement friction inventories. The investigations were based on one friction inventory from New York State (NYS), developed by Goyal (*34*) (see Figure 4), and one inventory from the FRG developed by Wehner and Schulze (e.g., *37, 38*) (see Figure 5). Equations that correspond to the curves in Figures 4 and 5 are given in Table 3, in which V is given in units of miles per hour. The friction values produced by the percentile level distribution curves in Figures 4 and 5 are representative of 60 to 95 percent of wet pavements in the investigated state or country.

The relationships in Figure 4 indicate that the overall regression curve (Equation 1) clearly coincides with the 90th-percentile level distribution curve of NYS. That means that 90 percent of wet pavements could be covered by using the overall regression curve as a driving dynamic basis for design purposes. Figure 5 shows that the overall regression curve could cover about 80 percent or more of wet pavements in the FRG.

Figure 6 shows the results more clearly. This figure shows that the 95th-percentile level distribution curve for NYS nearly coincides with the 95th-percentile level distribution curve for FRG. Furthermore, this figure suggests that AASHTO maximum allowable tangential friction factors (*7*) represent (a) up to a design speed of about 50 mph, 90 percent or more of wet pavements in NYS; (b) up to a design speed of about 60 mph, 80 percent of wet pavements in NYS; and (c) up to a design speed of about 70 mph, only about 65 percent of wet pavements in NYS.

For design speeds greater than 50 mph, AASHTO allows higher tangential friction factors, as compared to the tangential friction factors of the overall regression curve of Equation 1 developed from the data of the countries in this study.

Related to the 95th-percentile level distribution curve for NYS and FRG, these statements would already be true for design speeds greater than 30 mph. The tangential friction factors applied in the German geometric design standards are based on the 95th-percentile level distribution curve for wet pavements, and have been in use in the FRG since 1973 (*39*).

RECOMMENDATIONS FOR HIGHWAY DESIGN

In order not to be too conservative, it is recommended that at least the tangential friction factors produced by the overall regression curve (Equation 1) shall be used for highway design. However, in order to secure the condition that friction supply should most of the time exceed friction demand (*2,35,40*), it may be more appropriate for new design, redesign, and rehabilitation strategies to apply tangential friction factors that correspond to the 95th-percentile level distribution curves developed from actual pavement friction inventories in NYS and FRG.

TANGENTIAL FRICTION FACTOR AND STOPPING SIGHT DISTANCE

The minimum stopping sight distance is defined in most of the geometric design standards studied as follows:

> The minimum stopping sight distance (SSD) is the sum of two distances: (a) the distance traversed by a vehicle from the instant the driver sights an object for which a stop is necessary to the instant the brakes are applied (perception-reaction time), and (b) the distance required to stop the vehicle after the brake application begins (braking distance). The former is primarily a function of speed and perception-reaction time, the latter a function of speed and frictional resistance between the pavement surface and tires.

SSD on level roadway, therefore, may be computed by the formula

$$SSD_{min} = 1.47V_d t + (V_d)^2/30f_{T_{max}} \quad (3)$$

where

SSD_{min} = minimum stopping sight distance (ft);
V_d = design speed (mph);
$f_{T_{max}}$ = maximum allowable tangential friction factor; and
t = perception-reaction time (sec).

In using a 2.0-sec perception-reaction time as generally recommended in Europe, or 2.5 sec currently in use in the United States, Equation 3 then becomes

$$SSD_{min} = 2.94V_d + (V_d)^2/30f_{T_{max}} \quad (4a)$$

or

$$SSD_{min} = 3.67V_d + (V_d)^2/30f_{T_{max}} \quad (4b)$$

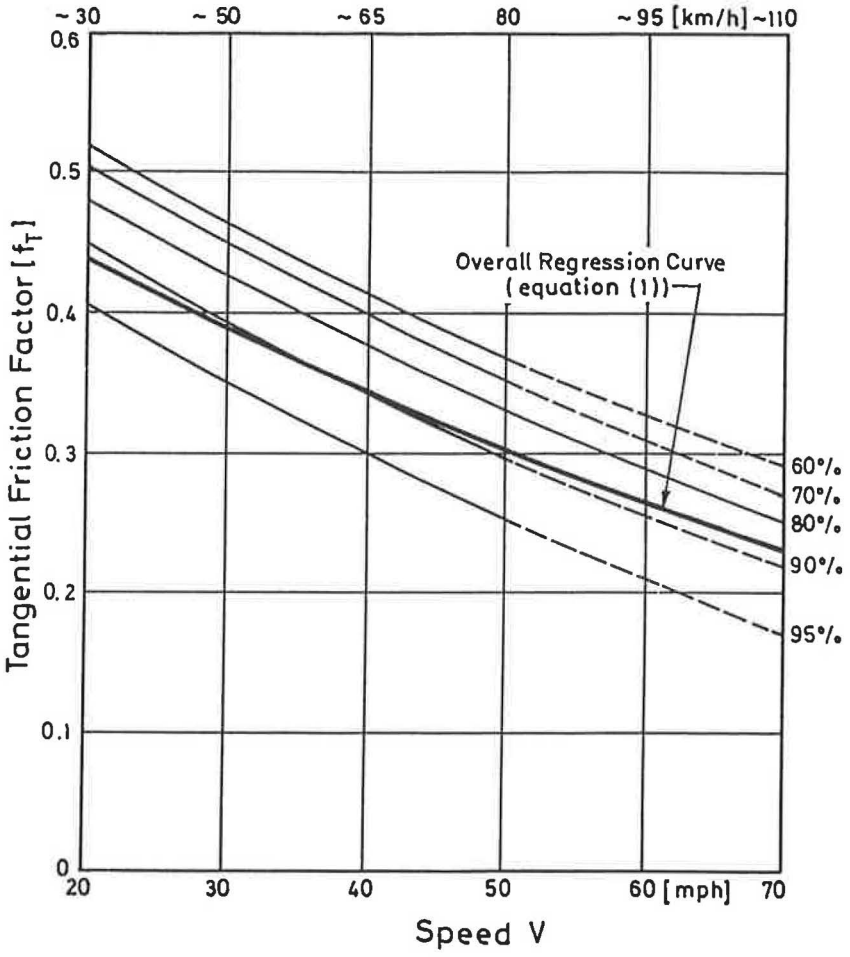

FIGURE 4 Percentile distribution curves for the relationship between tangential friction factor and speed for 93 wet pavements in NYS (*34*).

The data in Table 4 present the computed SSD values from Equations 4a and 4b by using the tangential friction factors produced by the overall regression curve (Equation 1), by the 95th-percentile level distribution curves of NYS and FRG, and by perception-reaction times of 2.0 and 2.5 sec, respectively. For comparative reasons, AASHTO maximum allowable tangential friction factors and ranges of stopping sight distances (*7*) are also presented in Table 4.

Data in Table 4 indicate that (a) for design speeds greater than 55 mph, AASHTO tangential friction factors are higher than the tangential friction factors produced by the overall regression curve ($0.30 > 0.28$); (b) for design speeds greater than 35 mph, AASHTO tangential friction factors are higher than the tangential friction factors produced by the 95th-percentile level distribution curves ($0.34 > 0.32$); and (c) between design speeds of 50 and 70 mph, the difference in the recommended tangential friction factors is between 0.06 (0.30 to 0.24) and 0.08 (0.25 to 0.17), whereas the difference in AASHTO tangential friction factors is only 0.02 (0.30 to 0.28).

For the perception-reaction time of 2.5 sec currently in use by AASHTO, note that (a) the computed stopping sight distances, based on the overall regression curve (Equation 1), exceed the upper limit ranges of AASHTO at speeds of 55 mph (560 ft > 550 ft); whereas (b) the computed stopping sight distances, based on the 95th-percentile level distribution curves, exceed the upper limit ranges of AASHTO values already at speeds of 45 mph (410 ft > 400 ft).

Table 4 was developed only to present, in comparison to AASHTO, the significant differences that exist between the computed stopping sight distances from Equation 3 by using different perception-reaction times and by including different tangential friction factors according to the overall regression curve and the 95th-percentile level distribution curves of NYS and FRG. The computed stopping sight distances in Columns 3, 4, 6, and 7 of Table 4 will have to be modified additionally when taking into consideration the effect of air resistance, as has been done, for example, in the FRG (*2, 35, 40*), and in the *Swedish Standard Specifications for Geometric Design* (*4*). Consequently, different minimum stopping sight distances could result from the application of different models, different perception-reaction times, and different tangential friction factors.

These findings clearly indicate that AASHTO officials, in collaboration with the TRB Committee on Geometric Design (A2A02), should consider the following steps, for example,

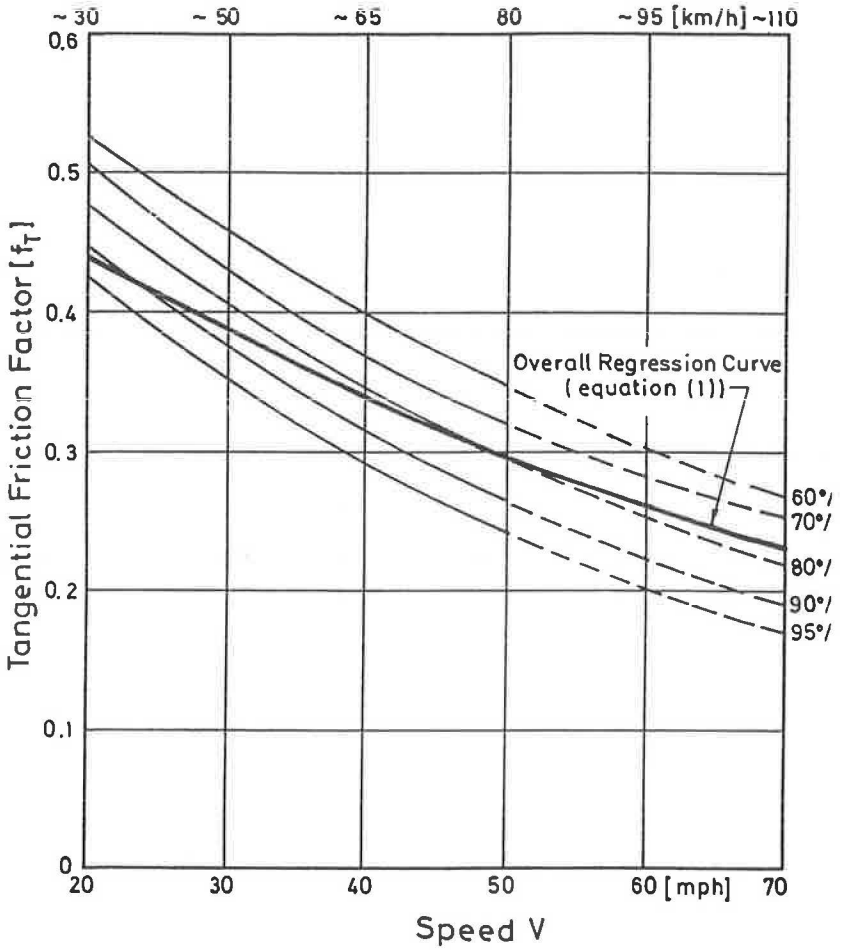

FIGURE 5 Percentile distribution curves for the relationship between tangential friction factor and speed for 600 wet pavements in FRG.

TABLE 3 REGRESSION EQUATIONS FOR TANGENTIAL FRICTION FACTOR VERSUS SPEED FOR PERCENTILE DISTRIBUTION CURVES CORRESPONDING TO FIGURES 4 AND 5 (*34*)

Percentile Level	New York State
60 %	$f_T = 0.6411 - 6.4143 \cdot 10^{-3}\ V + 2.00 \cdot 10^{-5} V^2$
70 %	$f_T = 0.6231 - 6.4143 \cdot 10^{-3}\ V + 2.00 \cdot 10^{-5} V^2$
80 %	$f_T = 0.6040 - 6.4143 \cdot 10^{-3}\ V + 2.00 \cdot 10^{-5} V^2$
90 %	$f_T = 0.5684 - 6.4143 \cdot 10^{-3}\ V + 2.00 \cdot 10^{-5} V^2$
95 %	$f_T = 0.5244 - 6.4143 \cdot 10^{-3}\ V + 2.00 \cdot 10^{-5} V^2$

Percentile Level	Federal Republic of Germany
60 %	$f_T = 0.7063 - 9.7043 \cdot 10^{-3}\ V + 5.1006 \cdot 10^{-5} V^2$
70 %	$f_T = 0.6813 - 9.7043 \cdot 10^{-3}\ V + 5.1006 \cdot 10^{-5} V^2$
80 %	$f_T = 0.6563 - 9.7043 \cdot 10^{-3}\ V + 5.1006 \cdot 10^{-5} V^2$
90 %	$f_T = 0.6263 - 9.7043 \cdot 10^{-3}\ V + 5.1006 \cdot 10^{-5} V^2$
95 %	$f_T = 0.6013 - 9.7043 \cdot 10^{-3}\ V + 5.1006 \cdot 10^{-5} V^2$

in any future plans for achieving well-founded and reliable stopping sight distances:

1. Selection of a model including or not including air resistance. (A model that includes air resistance is recommended.)
2. Selection of perception-reaction time. (A perception-reaction time of 2.0 sec is sufficient.)
3. Selection of reliable maximum allowable tangential friction factors. [At least the values computed from Equation 1 (see Column 2 of Table 4), but preferably the values produced by the 95th-percentile level distribution curves (see Column 5 of Table 4), are recommended.]

SIDE FRICTION FACTOR AND MINIMUM RADIUS OF CURVE

In the *German Design Guidelines* (*2*), the maximum allowable side friction factors are defined as 46 percent of the maximum allowable tangential friction factors for rural highways. In the *Swiss Design Norms* (*3, 30, 31*) and in the *Swedish Specifications* (*4*), the maximum allowable side friction factors are defined as 44 percent of the maximum allowable tangential friction values for rural highways. All three guidelines indicate

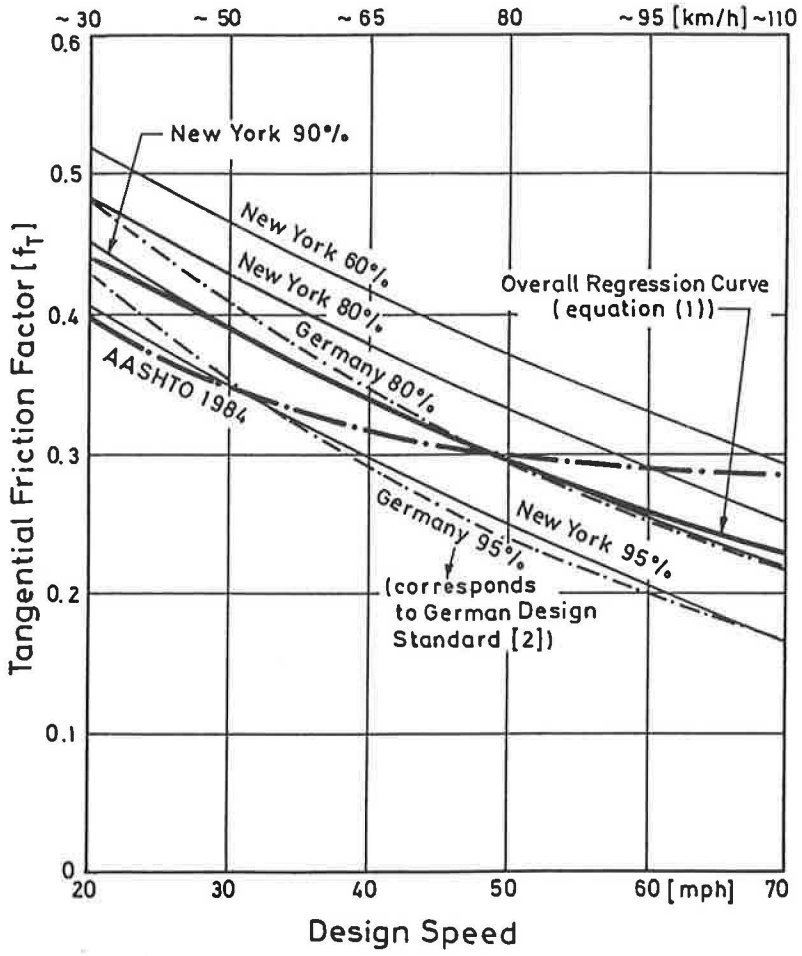

FIGURE 6 Relationships between maximum allowable tangential friction factors and design speed for AASHTO 1984, FRG (80th and 95th percentiles) and NYS (60th, 80th, 90th, and 95th percentiles) along with the overall regression curve.

TABLE 4 RECOMMENDED MAXIMUM ALLOWABLE TANGENTIAL FRICTION FACTORS AND COMPUTED STOPPING SIGHT DISTANCES VERSUS DESIGN SPEEDS

Design Speed (mph)	Stopping Sight Distances based on the Overall Regression Curve (equation (1))			Stopping Sight Distances based on the 95th-Percentile Level Curves of New York State and FRG			Stopping Sight Distances AASHTO 1984	
V_d	f_{Tmax}*	SSD (ft) t = 2,0 s	SSD (ft) t = 2,5 s	f_{Tmax}*	SSD (ft) t = 2,0 s	SSD (ft) t = 2,5 s	f_{Tmax}	SSD (ft) t = 2,5 s
1	2	3	4	5	6	7	8	9
30	.39	165	185	.35	175	195	.35	200-200
35	.37	215	240	.32	230	255	.34	225-250
40	.34	275	305	.30	295	325	.32	275-325
45	.32	345	375	.28	375	410	.31	325-400
50	.30	425	465	.25	475	510	.30	400-475
55	.28	520	560	.23	595	635	.30	450-550
60	.26	635	675	.21	745	785	.29	525-650
65	.25	760	805	.19	925	970	.29	550-725
70	.24	900	950	.17	1145	1200	.28	625-850

*Rounded Values

that by using these percentages of side friction there is still between 80 and 90 percent available for friction in the tangential direction when driving through curves (*35,40*). By this procedure, considerable dynamic safety reserves are still available in the tangential direction in spite of using the maximum allowable side friction factors.

In this study, the maximum allowable side friction factor is defined as 45 percent of the maximum allowable tangential friction factor. This should guarantee that there will be about 90 percent of friction available in the tangential direction for acceleration, deceleration, braking, or evasive maneuvers when driving through curves (*34,35*).

Thus, the equation for the maximum allowable side friction factor for rural highways is

$$f_{R\max} = 0.45 * f_{T\max} \tag{5}$$

Consequently, the equation for the maximum allowable side friction factor for NYS at the 90th-percentile level is (see Table 3):

$$f_{R\max} = 0.2558 - 2.886 * 10^{-3} V + 0.90 * 10^{-5} V^2 \tag{6}$$

and the equation for the maximum allowable side friction factor for NYS at the 95th-percentile level is (see Table 3):

$$f_{R\max} = 0.2360 - 2.886 * 10^{-3} V + 0.90 * 10^{-5} V^2 \tag{7}$$

Equations 6 and 7 are schematically shown in Figure 7. In addition, this figure includes the overall regression curve (Equation 2) between side friction and design speed, based on the data of the five countries in this study, as well as the maximum allowable side friction factors of *AASHTO 1984* (*7*).

Figure 7 indicates that (a) the side friction factors produced by the 90th-percentile level distribution curve of NYS clearly coincide with the friction factors produced by the overall regression curve (Equation 2); (b) the side friction factors produced by the 95th-percentile level distribution curve of NYS clearly coincide again with the side friction factors produced by the 95th-percentile level distribution curve of the FRG; and (c) AASHTO side friction factors intersect the overall regression curve at a design speed of about 40 mph.

A reliable estimate of curve radius may be obtained from the standard centripetal force equation (*7*):

$$R_{\min} = (V_d)^2/[15(e + f_{R\max})] \tag{8}$$

where

$R_{\min}$ = minimum radius of curve (ft);
V_d = design speed (mph);
$f_{R\max}$ = maximum allowable side friction factor; and
e = maximum superelevation rate (ft/ft).

Because Equation 8 is commonly applied in the geometric design guidelines of the countries in this study, recommendations for minimum radii of curve will be easier to make here. The difficulties encountered with the assumptions used to calculate minimum stopping sight distances do not apply here.

To conform with the findings of the countries in this study, typical superelevation rates of 0.05 and 0.07 were selected. Maximum allowable side friction factors and computed minimum radii of curve with respect to design speed are presented in Table 5. The values in this table are again based on the side friction factors produced by the overall regression curve (Equation 2) and by the 95th-percentile level distribution curves of NYS and FRG. For comparative reasons, AASHTO minimum radii of curve are also shown with respect to design speed in the table.

Table 5 indicates that, for design speeds between 50 and 70 mph and superelevation rates of 0.05 and 0.07, AASHTO

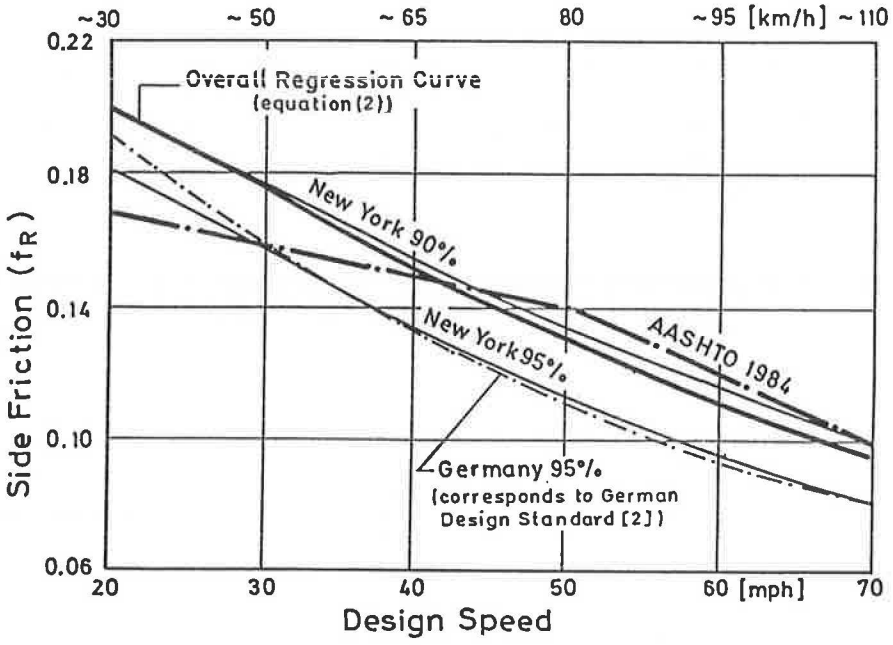

FIGURE 7 Relationships between maximum allowable side friction factors and design speed for AASHTO 1984, FRG (95th percentile), and NYS (90th and 95th percentile), along with the overall regression curve.

TABLE 5 RECOMMENDED MAXIMUM ALLOWABLE SIDE FRICTION FACTORS AND RECOMMENDED MINIMUM RADII OF CURVE VERSUS DESIGN SPEEDS

Design Speed	Superelevation Rate	The least Recommended Minimum Radii of Curve Overall Regression Curve (equation (2))		Recommended Minimum Radii of Curve 95th-Percentile Level Curve of New York State and FRG		Minimum Radii AASHTO 1984	
V_d (mph)	e	f_{Rmax}*	R_{min} (ft)	f_{Rmax}*	R_{min} (ft)	f_{Rmax}	R_{min} (ft)
1	2	3	4	5	6	7	8
30	.05	.18	265	.16	290	.16	286
40	.05	.15	530	.13	575	.15	533
50	.05	.13	925	.11	1015	.14	877
60	.05	.11	1490	.10	1650	.12	1412
65	.05	.105	1840	.09	2065	.11	1760
70	.05	.10	2245	.08	2550	.10	2178
30	.07	.18	245	.16	265	.16	261
40	.07	.15	480	.13	520	.15	485
50	.07	.13	835	.11	905	.14	794
60	.07	.11	1325	.10	1450	.12	1263
65	.07	.105	1630	.09	1800	.11	1564
70	.07	.10	1975	.08	2205	.10	1922

* Rounded Values

minimum radii of curve are 2 to 6 percent lower than those corresponding to the side friction factors produced by the overall regression curve (Equation 2), and about 13 percent lower than those corresponding to the side friction values produced by the 95th-percentile level distribution curves.

It is recommended that at least the side friction factors produced by the overall regression curve (Equation 2) should be regarded in highway design. However, for safety reasons it may be more appropriate to relate minimum radii of curve to the side friction factors produced by the 95th-percentile level distribution curves of NYS and FRG to cover 95 percent of wet pavements, as has been already done in several Western European countries.

CONCLUSIONS

It is difficult to decide where the critical margins for tangential and side friction factors and, derived from them, for minimum stopping sight distances and radii of curve shall be assigned. This is a crucial consideration for engineers concerned with both cost and safety. But using lower maximum allowable friction factors will certainly lead to a higher driving dynamic safety supply, and could reduce the number and severity of accidents. It will also support maintenance personnel by easing the problems of maintaining high tangential and side friction factors for higher design speed classes. Therefore, it is recommended for new designs, redesigns, and rehabilitation strategies to relate minimum stopping sight distances and minimum radii of curve to the proposed tangential and side friction factors that cover 95 percent of wet pavements in this study.

The recommendations provided in this paper should not be regarded as a final solution, but perhaps an international discussion of a larger dynamic safety supply for driving may be useful in reducing accidents on two-lane rural highways. Because there are often inadequate safety factors in tire-road friction, friction demand often exceeds friction supply, causing more accidents than necessary.

One of the most important tasks in modern highway design requires that responsible national and international agencies develop reliable inventories of friction data. If the recommendations about the design criteria mentioned in the introduction are regarded—(a) achieving consistency in horizontal alignment, (b) harmonizing design speed and operating speed on wet pavements, and (c) providing adequate dynamic safety of driving—decisive safety advantages may be expected in future geometric highway design of two-lane rural roads.

REFERENCES

1. J. Hayward, R. Lamm, and A. Lyng. *Survey of Current Geometric and Pavement Design Practices in Europe: Geometric Design.* International Road Federation, Washington, D.C., July 1985.
2. Geometric Design Standards. In *Guidelines for the Design of Roads.* RAS-L-1, German Road and Transportation Research Association, Committee 2.3, 1984.
3. Swiss Association of Road Specialists (VSS), Swiss Norm SN 640080a. *Highway Design, Fundamentals, Speed as a Design Element.* 1981.
4. National Swedish Road Administration. *Standard Specifications for Geometric Design of Rural Roads.* Borlenge, Sweden, 1982.
5. Ministere de l'Equipement et du Logement. *Instruction sur les Conditions Techniques D'Amenagement des Routes Nationales.* Paris, 1975.

6. Department of Transport. *Highway Link Design, Geometric Alignment Standards*. Departmental Standard TD9/81, London, 1981.
7. *A Policy on Geometric Design of Highways and Streets*. AASHTO, Washington, D.C., 1984.
8. R. Lamm and E. M. Choueiri. *A Design Procedure to Determine Critical Dissimilarities in Horizontal Alignment and Enhance Traffic Safety by Appropriate Low-Cost or High-Cost Projects*. Final Report for the National Science Foundation, Washington, D.C., March 1987.
9. E. M. Choueiri and R. Lamm. Operating Speeds and Accident Rates on Two-Lane Rural Highway Curved Sections—Investigations about Consistency and Inconsistency in Horizontal Alignment. Part I of *Rural Roads Speed Inconsistencies Design Methods*, State University of New York Research Foundation, Albany, N.Y., July 1987.
10. R. Lamm, E. M. Choueiri, and A. Paluri. A Design Method to Determine Critical Operating Speed Inconsistencies on Two-Lane Rural Roads in the State of New York. Part II of *Rural Roads Speed Inconsistencies Design Methods*, State University of New York Research Foundation, Albany, N.Y., Oct. 1987.
11. R. Lamm, E. M. Choueiri, J. C. Hayward, and A. Paluri. Possible Design Procedure to Promote Design Consistency in Highway Geometric Design on Two-Lane Rural Roads. In *Transportation Research Record 1195*, TRB, National Research Council, Washington, D.C., 1988.
12. R. Lamm, E. M. Choueiri, and J. C. Hayward. Tangent as an Independent Design Element. In *Transportation Research Record 1195*, TRB, National Research Council, Washington, D.C., 1988.
13. R. Lamm, J. C. Hayward, and J. G. Cargin. Comparison of Different Procedures for Evaluating Speed Consistency. In *Transportation Research Record 1100*, TRB, National Research Council, Washington, D.C., 1986, pp. 10–20.
14. R. Lamm and E. M. Choueiri. Recommendations for Evaluating Horizontal Design Consistency Based on Investigations in the State of New York. In *Transportation Research Record 1122*, TRB, National Research Council, Washington, D.C., 1987, pp. 68–78.
15. R. Lamm. New Developments in Highway Design with Special Consideration of Traffic Safety. *Proc., 36th Annual Ohio Transportation Engineering Conference*, Department of Civil Engineering, Ohio State University, Columbus, 1982, pp. 107–119.
16. R. Lamm and J. G. Cargin. Identifying Operating Speed Inconsistencies on Two-Lane Rural Roads. *Proc., 39th Annual Ohio Transportation Engineering Conference*, Department of Civil Engineering, Ohio State University, Columbus, 1985, pp. 13–22.
17. R. Lamm and E. M. Choueiri. Relationship Between Design, Driving Behavior and Accident Risk on Curves. *Proc., 40th Annual Ohio Transportation Engineering Conference*, Department of Civil Engineering, Ohio State University, Columbus, 1986, pp. 87–100.
18. R. Lamm and E. M. Choueiri. The Impact of Traffic Warning Devices on Operating Speeds and Accident Rates on Two-Lane Rural Highway Curves. *Proc., 41st Annual Ohio Transportation Engineering Conference*, Department of Civil Engineering, Ohio State University, Columbus, 1987, pp. 171–192.
19. R. Lamm, E. M. Choueiri, T. Mailaender, and A. Paluri. A Logical Approach to Geometric Design Consistency of Two-Lane Rural Roads in the U.S.A. *Proc., 11th IRF (International Road Federation) World Meeting*, Vol. II, Seoul, Korea, April 16–21, 1989, pp. 8–11.
20. R. Lamm, E. M. Choueiri, and T. Mailaender. Accident Rates on Curves as Influenced by Highway Design Elements—An International Review and an In-Depth Study. *Proc., Road Safety in Europe*, Gothenburg, Sweden, VTIrapport 344A, Swedish Road and Traffic Research Institute, Linkoeping, Sweden, 1989, pp. 33–54.
21. R. Lamm and E. M. Choueiri. Investigations about Driver Behavior and Accident Experiences at Curved Sites (Including Black Spots) of Two-Lane Rural Highways in the U.S.A. *Proc., Roads and Traffic 2000*, Vol. 4/2, Traffic Engineering and Safety, Berlin, Federal Republic of Germany, Sept. 6–9, 1988, pp. 153–158.
22. R. Lamm, T. Mailaender, and E. M. Choueiri. New Ideas for the Design of Two-Lane Rural Roads in the U.S.A. *International Technical Journal: Road and Construction*, Federal Republic of Germany, Vol. 5, pp. 18–25, May 1989, and Vol. 6, pp. 13–18, June 1989.
23. R. Lamm, E. M. Choueiri, and T. Mailaender. Comparison of Operating Speeds on Dry and Wet Pavements of Two-Lane Rural Highways. In *Transportation Research Record*, TRB, National Research Council, Washington, D.C., 1990 (forthcoming).
24. J. M. Mason and H. C. Peterson. Survey of States' R-R-R Practices and Safety Considerations. In *Transportation Research Record 960*, TRB, National Research Council, Washington, D.C., 1984.
25. C. P. Brinkman. Safety Studies Related to RRR Projects. *Transportation Journal of ASCE*, Vol. 108, July 1983.
26. J. C. Glennon, T. R. Neuman, and J. R. Leisch. Safety and Operational Considerations for Design of Rural Highway Curves. Final Report, Aug. 1983.
27. H. W. Kummer and W. E. Meyer. *NCHRP Report 37: Tentative Skid-Resistance Requirements for Main Rural Highways*. HRB, National Research Council, Washington, D.C., 1967.
28. R. Lamm and H. E. Herring. The Side-Friction Factor in Relation to Speed. *Technical Journal: Road and Autobahn*, Vol. 11, Federal Republic of Germany, Nov. 1970, pp. 435–443.
29. R. Lamm, A. Taubmann, and J. Zoellmer. Comprehensive Study on the Term 'Critical Water' Film Thickness. *Technical Journal: Research Road Construction and Traffic Technique*, Vol. 436, Minister of Transportation, Federal Republic of Germany, 1985.
30. Swiss Association of Road Specialists (VSS). *Sight Distances*. Swiss Norm SNV640090, 1974.
31. Swiss Association of Road Specialists (VSS). *Superelevation Rate in Tangents and Circular Curves*. Swiss Norm SNV640123, 1969.
32. G. T. Taoka. An Analytical Model for Driver Response. In *Transportation Research Record 1213*, TRB, National Research Council, Washington, D.C., 1989, pp. 1–3.
33. F. R. Wilson, J. A. Sinclair, and B. G. Bisson. Evaluation of Driver/Vehicle Accident Reaction Times. Paper Presented at the Transportation Research Board 68th Annual Meeting, TRB, National Research Council, Washington, D.C., Jan. 1989.
34. P. B. Goyal. *Friction Factors for Highway Design Regarding Driving Dynamic Safety Concerns in the State of New York*. Master's thesis, Clarkson University, Potsdam, N.Y., Dec. 1987.
35. R. Lamm. Driving Dynamic Considerations: A Comparison of German and American Friction Coefficients for Highway Design. In *Transportation Research Record 960*, TRB, National Research Council, Washington, D.C., 1984.
36. N. J. Rowan, D. L. Woods, V. G. Stover, D. A. Anderson, and J. H. Dozier. *Safety Design and Operational Practices for Streets and Highways*. Texas Transportation Institute, Texas A&M University, College Station, 1980.
37. Wehner. Results of Skid-Resistance Measurements and Traffic Safety. *Road and Autobahn*, Vol. 8, 1965.
38. K. H. Schulze and L. Beckmann. Friction Properties of Pavements at Different Speeds, ASTM Special Technical Publication, No. 326, Philadelphia, Pa., Dec. 1962.
39. Geometric Design Standards. In *Guidelines for the Design of Rural Roads*. RAL-L-1, German Road and Transportation Research Association, Committee 2.3, 1973.
40. R. Lamm. *Driving Dynamics and Road Characteristics—A Contribution for Highway Design under Special Consideration of Operating Speeds*. Publications of the Institute of Highway and Railroad Engineering, University of Karlsruhe, Vol. 11, Karlsruhe, Federal Republic of Germany, 1973.

Publication of this paper sponsored by Committee on Surface Properties–Vehicle Interaction.

Impact of Digital Filtering on FWD Load Cell and Deflection Sensor Responses

GONZALO R. RADA, SCOTT D. RABINOW, CHERYL ALLEN RICHTER, AND MATTHEW W. WITCZAK

The deflection response of pavements under an applied load will be studied in the Strategic Highway Research Program's (SHRP's) Long-Term Pavement Performance (LTPP) study using a falling weight deflectometer (FWD). The SHRP computer software system for the collection of data also possesses the capability to filter the data by means of a digital low-pass filter. SHRP decided to assess the effects of digital filtering of FWD data before implementation of the software in the field. Comparative analyses of noise were performed using the results of an FWD pilot study conducted in Greensboro, North Carolina, as well as other test sections throughout the United States. The results show that filtering of FWD data introduces significant random errors, particularly for rigid pavements tested under heavy loads. These errors tend to compound each other when the filtered deflections are normalized by the filtered load data. Also, the use of filtered load and deflection data may yield normalized deflection responses that exceed current normalized deflection tolerance limits, particularly for heavy loads on rigid pavements. Accordingly, it has been recommended that all FWD data be collected by SHRP with the filter off. However, because some unknown level of noise is contained within FWD data, it is also recommended that additional load- and deflection-time histories be collected and stored. Thus, if advances occur in the filtering process, the data can be reanalyzed to obtain more accurate peak load and deflection values for use in the backcalculation of layer moduli.

The Strategic Highway Research Program's (SHRP's) Long-Term Pavement Performance (LTPP) study is based on the collection both of inventory and monitoring data for numerous pavement sections located throughout the United States. Within the monitoring data, one of the most significant items that will be collected is the deflection response of these pavement sections under an applied load. This response is an important indicator of structural capacity, material properties, and subsequent pavement performance.

In order to measure this response, SHRP is using a nondestructive testing device called the falling weight deflectometer (FWD). The four FWD units purchased by SHRP, one for each SHRP region, are manufactured by Dynatest and are capable of measuring deflections under an impulse load varying from approximately 2,500 to 27,000 lb (11 to 120 kN).

Because the accurate measurement of deflections is a key element in the success of the LTPP study, SHRP has established guidelines to provide for a uniform and standardized field testing procedure (*1*). This procedure relies on a computer software system for test set-up, data collection, data storage, and a limited amount of data checking.

Although the main purpose of the software is to automate the data collection process, it also possesses the capability of filtering data by means of a digital low-pass (60 or 120 Hz) filter. This filter is intended to screen out high-frequency noise from both the load and deflection signals. Figure 1a provides an example of negative noise, whereas Figure 1b provides an example of positive noise. The noise itself is a high-frequency signal separately imposed on the normal load and deflection signals. When this noise is removed, the expected shape (approximately half-sine) of the signal is present. The unfiltered data are recordings of load and deflection time histories, an inherent capability of these FWDs. The filtering is imposed on these time histories to yield filtered peaks.

At the onset of the FWD testing of the SHRP general pavement sections (GPSs), limited information on the effects of digital filtering on FWD load and deflection response was available. As a result, a study was undertaken by SHRP to assess the impact of data filtering on the SHRP FWD data before routine implementation in the field (*2*). In this study, a comparative investigation of noise, defined as the difference between filtered (X_f) and unfiltered (X_{uf}) data, was performed.

Whereas noise is generally compared to a baseline signal in order to determine its significance, knowledge may be gained from information regarding its absolute magnitude. Accordingly, two variables describing noise were introduced in this study to quantify and define its properties. They are

$$\text{Absolute Noise} = X_f - X_{uf} \quad (1)$$

$$\text{Relative Noise} = \frac{X_f - X_{uf}}{X_{uf}} \times 100 \quad (2)$$

A summary of the SHRP FWD digital filtering study, including results and conclusions, is presented in this paper. The next section provides a brief summary of the FWD data used in the study. The detailed analysis results and conclusions are presented in later sections, and the implications of the findings are discussed in the final section.

SOURCE OF DATA

Analyses and conclusions contained herein are based on the test results of an FWD pilot study conducted in Greensboro,

G. R. Rada and S. D. Rabinow, Pavement Consultancy Services Division, Law Engineering, 12240 Indian Creek Court, Suite 120, Beltsville, Md. 20705. C. A. Richter, Strategic Highway Research Program, 818 Connecticut Avenue, N.W., 4th Floor, Washington, D.C. 20006. M. W. Witczak, Department of Civil Engineering, University of Maryland, College Park, Md. 20740.

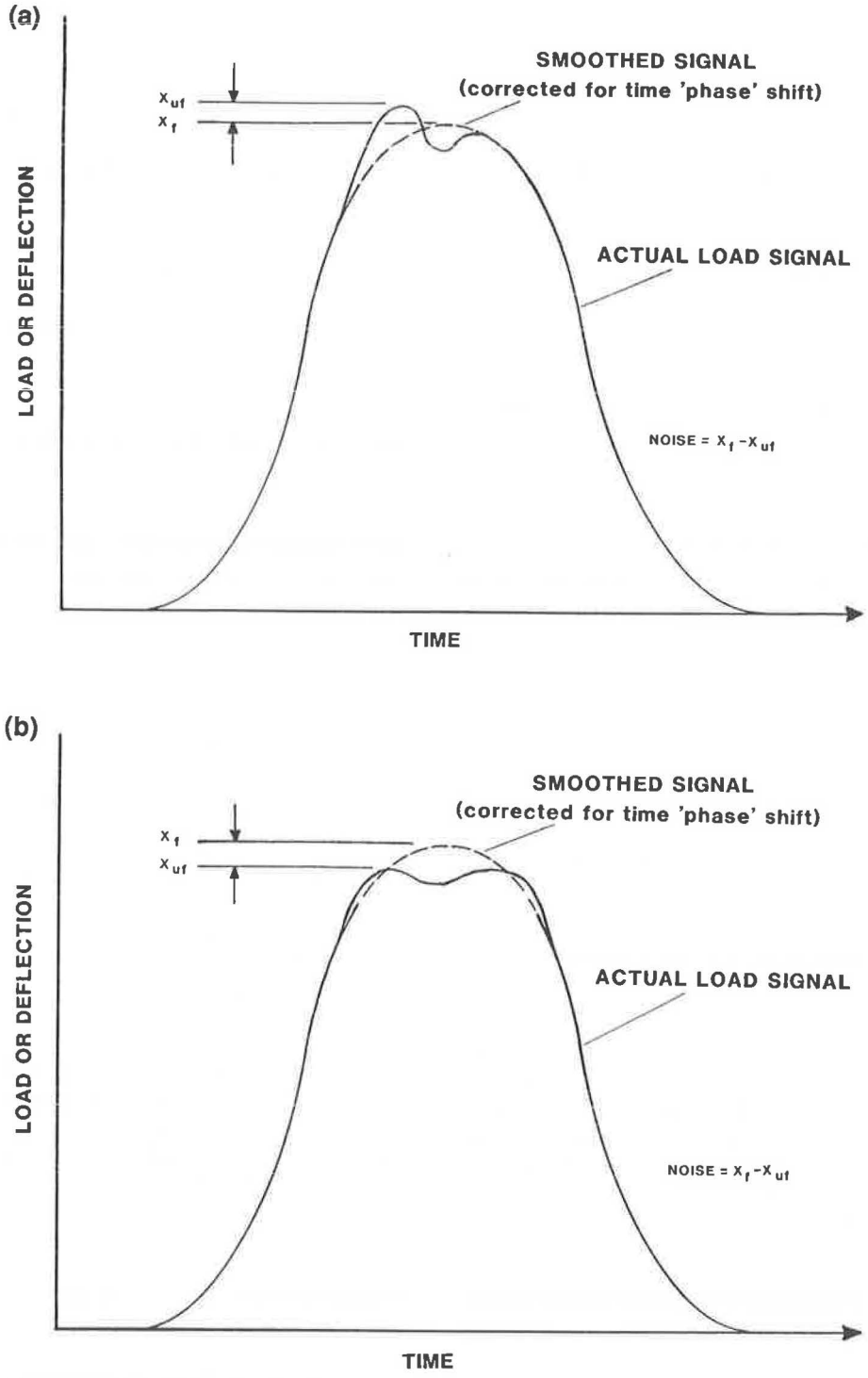

FIGURE 1 Load signal and noise.

North Carolina, in December 1988. Three pavement sections were tested in this pilot study: (a) a 4.5-in. asphalt concrete (AC) over 12-in. crushed-stone flexible pavement, (b) an 8-in. jointed plain concrete (JPCP) over 4-in. lean concrete subbase rigid pavement, and (c) an 8-in. continuously reinforced concrete (CRC) over 4-in. crushed-stone subbase pavement.

A total of 44 locations were tested on the flexible pavement: 23 locations along the midlane (SHRP Test Point Identifier F0–F1) and 21 outer-wheel path (F3) locations. Testing of the rigid pavement included 122 separate locations: 26 midlane, midpanel locations (J0–J1); 24 pavement edge, slab corner locations (J2); 24 pavement edge, midpanel locations (J3); 24 location pairs at joints along the outer-wheel path, on the approach side (J4) and leave side (J5). In the case of the CRC pavement, tests were conducted at 99 separate locations as follows: 23 midlane, midpanel locations (C0–C1); 19 pavement edge locations centered on the crack (C2); 19 pavement edge, midpanel locations (C3); 19 location pairs at cracks

along the outer-wheel path, on the approach side (C4) and leave side (C5).

Although temperature effects were not being ignored during testing, they were also not specifically addressed. However, the order in which tests were performed may mitigate some concerns as to the source of the noise. Center-of-slab testing was performed early in the day and edge testing of slabs was generally performed in the afternoons to ensure that the slab areas at the test locations were in contact with the subbase.

Because four load levels were used for the flexible pavement and three load levels were used for the rigid and CRC pavements, the North Carolina FWD pilot study yielded a total of 839 load and 5,873 deflection measurements. (Each of the seven individual geophones on the FWD is considered a measurement.) More important, this pilot study provided an excellent data base for assessing the impact of FWD data filtering on a wide range of pavement types, load levels, and test locations.

ANALYSES AND RESULTS

On completion of the field data collection phase, an analysis of the data was undertaken to quantify the effects of the digital filtering. Both absolute and relative noise values were first computed from Equations 1 and 2, for all of the load and deflection measurements contained in the North Carolina FWD data files.

Various statistics were then calculated for each data set, including minimums, maximums, means, standard deviations, and coefficients of variation as well as other key distribution statistics associated with noise. Histograms and cumulative frequency distributions were also developed using the computed standard deviation and coefficient of variation values.

On the basis of this information, numerous observations were made and are summarized in the ensuing sections. The initial discussion describes the effect of data filtering on the load cell response output; the effect of filtering on deflection response is presented in the following section of the report.

Load Analysis

The analysis of load signal filtering was performed according to drop height, test location, and pavement type to assess the impact of each factor on the magnitude of both the absolute and relative noise. Statistical summaries of the analysis results are presented in Tables 1 through 3. Table 1 presents average absolute and relative noise values as well as other key distribution statistics for all test location and drop height combinations associated with the flexible pavement. Tables 2 and 3 present similar statistics for the rigid and CRC pavements, respectively. All statistical results generated for this study are contained in the North Carolina Pilot Study (*2*).

Drop Height

Load-related noise for the flexible pavement appears to depend on the drop height (i.e., load level). As presented in Table 1, the magnitudes both of the absolute and relative noise

TABLE 1 STATISTICAL SUMMARY OF LOAD-ASSOCIATED NOISE—FLEXIBLE PAVEMENT

Test Location	Drop Height	Average Absolute Noise (kPa)	Relative Noise (%)		
			Average	Positive Noise (%)	Noise Greater than "±" 5%
F0,F1	1	-5.9	-1.4	12.5	0.0
	2	-5.7	-1.0	20.9	0.0
	3	2.0	0.2	58.3	0.0
	4	1.3	0.2	66.7	0.0
	All	-2.1	-0.5	39.6	0.0
F3	1	-9.6	-2.5	0.0	0.0
	2	-14.5	-2.7	0.0	0.0
	3	-8.5	-1.2	19.1	0.0
	4	-1.0	-0.1	61.9	0.0
	All	-8.4	-1.6	20.3	0.0
ALL	1	-7.7	-2.0	6.8	0.0
	2	-9.9	-1.8	11.4	0.0
	3	-3.0	-0.4	40.9	0.0
	4	0.2	0.0	65.9	0.0
	All	-5.1	-1.0	31.2	0.0

Note: Nominal load levels are as follows: Ht 1, 6000 lbs.
Ht 2, 9000 lbs.
Ht 3, 12000 lbs.
Ht 4, 16000 lbs.

TABLE 2 STATISTICAL SUMMARY OF LOAD-ASSOCIATED NOISE—RIGID PAVEMENT

Test Location	Drop Height	Average Absolute Noise (kPa)	Relative Noise (%)		
			Average	Positive Noise (%)	Noise Greater than "±" 5%
J0,J1	1	-16.0	-4.4	100.0	11.4
	2	-22.2	-4.2	100.0	3.8
	3	-28.7	-2.7	100.0	0.0
	All	-22.3	-3.7	100.0	5.1
J2	1	-24.2	-4.2	100.0	16.8
	2	-20.6	-3.6	100.0	8.4
	3	-18.7	-3.4	100.0	8.4
	All	-21.1	-3.8	100.0	11.2
J3	1	-19.5	-5.5	100.0	37.6
	2	-25.8	-5.1	100.0	22.0
	3	-32.5	-3.1	100.0	12.6
	All	-25.9	-4.6	100.0	24.1
J4	1	-14.5	-4.1	100.0	8.3
	2	-21.1	-4.1	100.0	0.0
	3	-30.8	-2.9	100.0	0.0
	All	-22.1	-3.7	100.0	2.8
J5	1	-14.2	-4.0	100.0	0.0
	2	-20.3	-4.0	100.0	0.0
	3	-28.1	-2.7	100.0	0.0
	All	-20.9	-3.6	100.0	0.0
ALL	1	-15.8	-4.5	100.0	14.8
	2	-22.2	-4.3	100.0	6.8
	3	-29.4	-2.8	100.0	4.2
	All	-22.5	-3.9	100.0	8.5

generally decrease as the drop height increases. Whereas this trend was anticipated for the relative noise because of the increase in load magnitude, it was somewhat unexpected for the absolute noise. However, a closer look at the data reveals that as the load level increases, there is a significant shift in the overall distribution of noise values from negative to positive, causing the average absolute value to decrease. For the first drop height, 12.5 percent of the noise at location F0–F1 and 0.0 percent at location F3 is positive and increases to more than 60 percent for the fourth drop height.

As for flexible pavement, rigid-pavement load-related noise also appears to depend on drop height. As presented in Table 2, absolute noise levels increase and relative noise levels decrease as the drop height increases. Unlike the flexible pavement, there is no shift in the noise distribution from negative to positive with increasing drop height and there are no positive noise values. There is, however, a definite trend regarding the distribution of large noise values. In all cases, the distribution of relative noise values exceeding 5 percent (the so-called "large noise") decreases as the load level increases.

Unlike the previous pavement types, the results presented in Table 3 show no clear trends between noise level and drop height for the CRC pavement. At some locations, noise levels decrease as the load increases, whereas at other locations maximum noise levels occur at the second drop height. A possible explanation for this lack of trend is the shift in the noise distribution from negative to positive with increasing drop height. Also, the percentage of large noise decreases as the drop height increases.

Test Location

Although only two locations were tested, noise levels associated with the flexible pavement appear to depend on the test location also. As presented in Table 1, average absolute and relative noise values in the wheel path (F3) are much larger than those at midlane (F0–F1). However, much of this difference may be due to the distribution of positive and negative values at each location.

Unlike the flexible pavement, load-related noise for the rigid pavement does not appear to depend on the test location. Although noise levels vary from one location to another, the values presented in Table 2 show that these differences are small. The largest difference in average absolute noise occurs between locations J5 and J3 and is equal to 5.0 kPa (0.7 psi). The maximum average relative noise difference also occurs

TABLE 3 STATISTICAL SUMMARY OF LOAD-ASSOCIATED NOISE—CRC PAVEMENT

Test Location	Drop Height	Average Absolute Noise (kPa)	Relative Noise (%)		
			Average	Positive Noise (%)	Noise Greater than "±" 5%
C0,C1	1	-5.1	-1.3	25.9	0.0
	2	-2.1	-0.4	39.0	0.0
	3	-1.7	-0.1	47.8	0.0
	All	-3.0	-0.6	37.6	0.0
C2	1	-12.6	-3.0	0.0	15.9
	2	-11.8	-2.0	26.3	10.5
	3	-6.3	-0.6	26.4	0.0
	All	-10.2	-1.9	17.6	8.8
C3	1	-13.9	-3.4	0.0	0.0
	2	-15.3	-2.7	0.0	0.0
	3	-7.3	-0.8	15.8	0.0
	All	-12.2	-2.3	5.3	0.0
C4	1	-11.7	-3.0	0.0	5.3
	2	-21.6	-3.9	0.0	0.0
	3	-9.6	-1.0	0.0	0.0
	All	-14.3	-2.6	0.0	1.8
C5	1	-11.8	-3.0	0.0	10.6
	2	-20.8	-3.8	0.0	0.0
	3	-7.9	-0.8	5.3	0.0
	All	-13.5	-2.5	1.8	3.5
ALL	1	-10.8	-2.7	5.2	6.4
	2	-13.8	-2.5	13.1	2.1
	3	-6.4	-0.6	19.0	0.0
	All	-10.3	-1.9	12.5	2.8

between locations J5 and J3 and is equal to −1 percent. There are, however, significant differences in the amount of large noise between test locations.

Load-related noise levels on CRC pavements also do not appear to depend on test location. With the exception of location C0–C1, both absolute and relative noise values vary little from one location to another. Aside from location C0–C1, the largest average absolute and relative noise differences occur between locations C2 and C4. However, there are significant differences in the amount of positive noise as well as large noise between test locations.

Pavement Type

In order to assess the effects of pavement type on load-related noise, the analysis results generated in previous sections were combined to develop Figure 2, which shows noise as a function of pavement type and drop height. Note that average values for all test locations were combined to produce those values.

On the basis of the information provided in this figure, there is a definite increase in the average relative noise level as the rigidity of the pavement increases (i.e., from flexible to CRC to rigid). The overall average noise values for each pavement type are −1.0, −1.9, and −3.9 percent, respectively. No trends of relative noise variability (standard deviation) due to pavement type are apparent. The CRC pavement has the highest standard deviation; however, all are within 0.4 percent of each other.

There are also a definite increase in the amount of positive noise and a decrease in the amount of large noise as pavement flexibility increases. Overall, 0.0 percent of the rigid pavement noise data has positive values, compared with 12.5 percent of CRC pavement and 31.2 percent of flexible pavement. In addition, 0.0 percent of flexible pavement noise data is large noise, compared with 2.8 percent of CRC pavement and 8.5 percent of rigid pavement.

Overall Discussion

The major objective of the load signal analysis was to assess the impact of data filtering on the load cell response output. Thus, FWD test results were analyzed to determine the influence of drop height, test location, and pavement type on the load signal. Figures 3 and 4 show the effects of pavement type

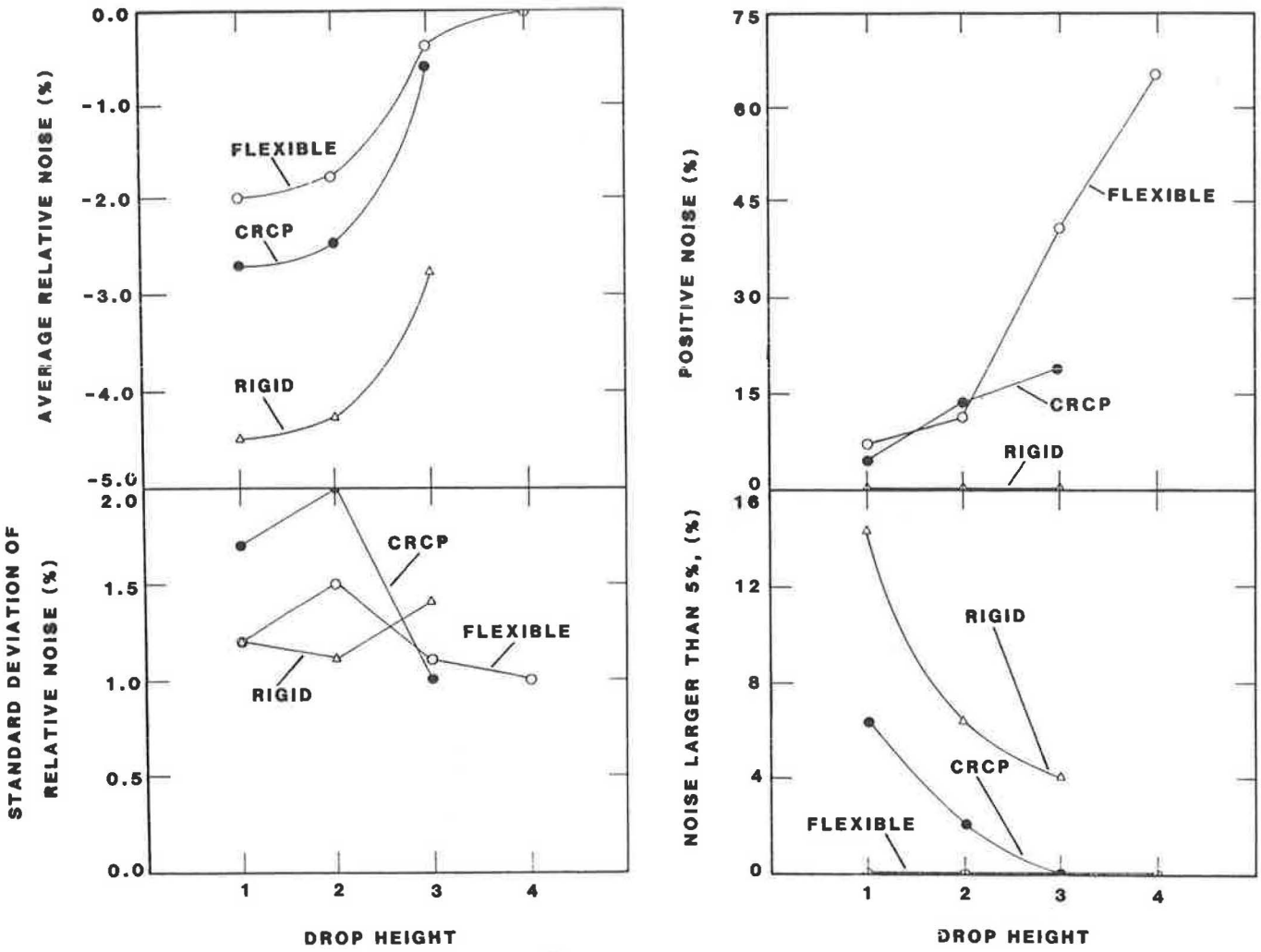

FIGURE 2 Effect of drop height and pavement type.

and FWD drop height on the absolute and relative noise magnitudes, respectively. From this study, the following major conclusions for load signal filtering were developed:

1. Both the absolute and relative noise values appear to be functions of pavement type and load magnitude. Test location does not appear to be as significant an influence on the magnitude of noise.
2. Both absolute and relative average noise values increase with increasing pavement rigidity (i.e., from a flexible to a CRC to a rigid pavement system).
3. Average noise levels were found to be negative for all pavement type and drop height combinations studied, implying that the noise magnitude is not purely random and that filtered load response data are, on average, always less than the unfiltered response.
4. The magnitude of the absolute noise is surprisingly large, especially when viewed through the statistical distribution results. The most severe case is associated with heavy loads on rigid pavements. For this condition, an average noise of −425 lb, with $\bar{X} \pm 2SD$ (average ±2 standard deviations) limits of 0 to −850 lb were computed.
5. The random component of the load filtering process had a coefficient of variation in the 1.3 to 1.5 percent range (*3*). In contrast, load repeatability errors on unfiltered load data, because of replicate drops at a given point and drop height, were approximately CV = 0.4 percent. It could therefore be concluded that the introduction of a load filter procedure introduced an additional variability to load response that was approximately 3 to 4 times as large as the replicate error on unfiltered load response.

Deflection Analysis

The analysis of deflection signal filtering was performed according to geophone number (radial offset), drop height, test location, and pavement type to assess the impact of these factors on noise level. Unlike the load signal, however, no analysis of positive noise or large noise distributions was conducted; only 0.5 percent of all 5,873 deflection values collected were found to have positive noise characteristics, whereas only 1.4 percent of the values exhibited large noise.

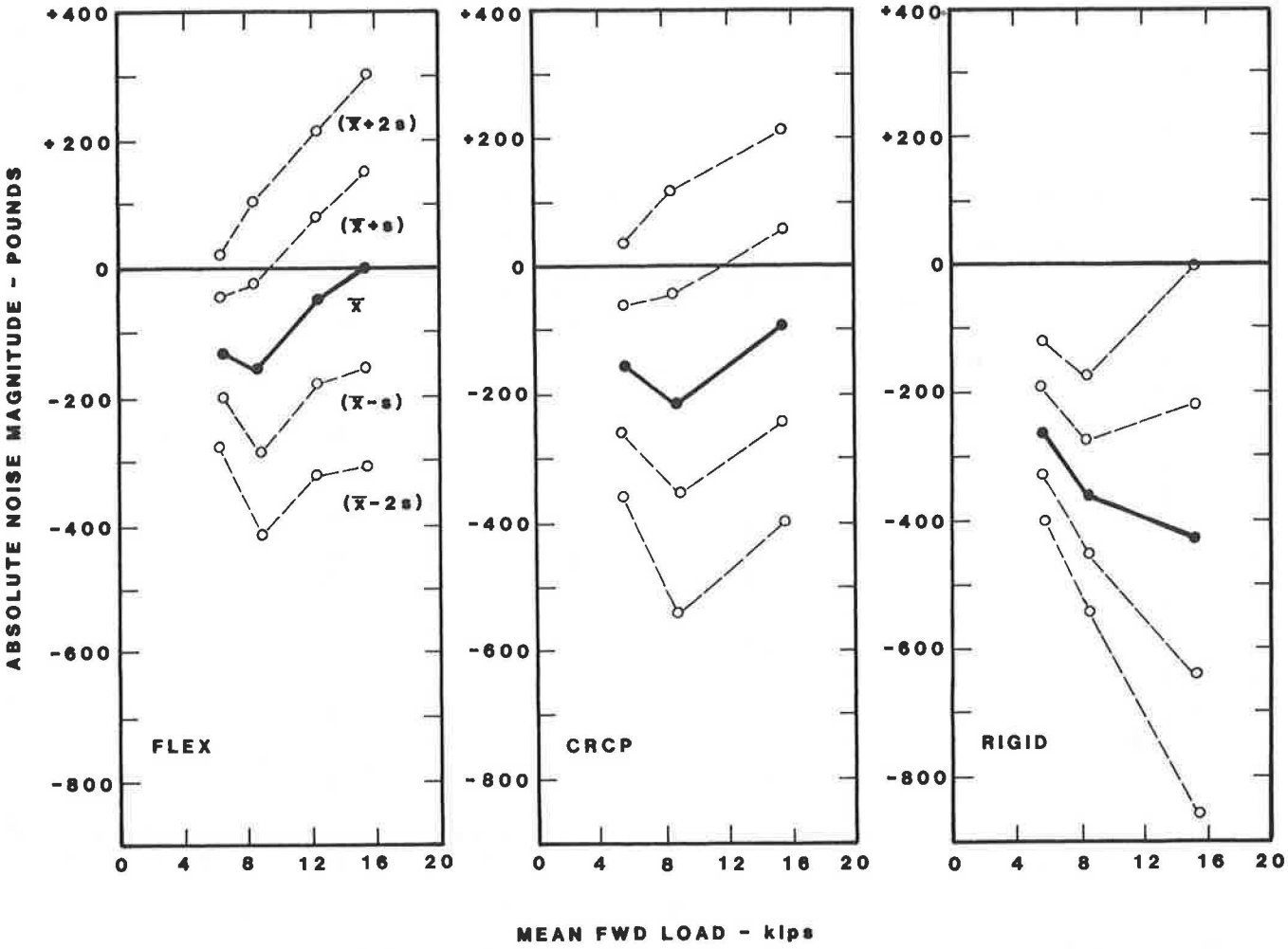

FIGURE 3 Absolute noise magnitude as a function of pavement type and FWD drop height (load).

Results of this analysis are presented in Tables 4 through 6. Table 4 presents average absolute and relative deflection noise for all combinations of test location, drop height, and geophone number on flexible pavement. Similar statistics for rigid and CRC pavements are presented in Tables 5 and 6, respectively.

Geophone Number

The deflection noise associated with the flexible pavement appears to heavily depend on the geophone number. With few exceptions, absolute noise levels decrease whereas relative noise levels increase as the radial distance increases. As presented in Table 4, the overall average absolute value decreases from -1.1 μm (0.043 mils) at Geophone 1 to -0.3 μm (0.012 mils) at Geophone 7, whereas the average relative value increases from -0.2 percent at Geophone 1 to -0.9 percent at Geophone 7.

Like the flexible pavement, rigid pavement deflection noise also appears to depend on the geophone number. In general, absolute noise levels decrease, whereas relative noise levels decrease as the radial distance increases. As presented in Table 5, the overall average absolute noise value decreases from -1.1 μm (0.043 mils) at Geophone 1 to -0.5 μm (0.020 mils) at Geophone 7, and the average relative value increases from -0.8 percent at Geophone 1 to -1.6 percent at Geophone 7.

CRC pavement deflection noise also appears to depend on the geophone number, particularly when compared to that of drop height and test location. Although no clear trend between absolute noise and radial distance is apparent, there is a definite increase in the relative noise levels with radial distance, particularly for the outer geophones. As presented in Table 6, the overall average relative noise varies from -0.2 percent at Geophone 1 to -0.9 percent at Geophone 7.

Drop Height

Deflection noise levels associated with flexible pavement also appear to depend on drop height, but to a lesser degree when compared to geophone location. Although no clear trends in the absolute noise values can be observed, relative noise

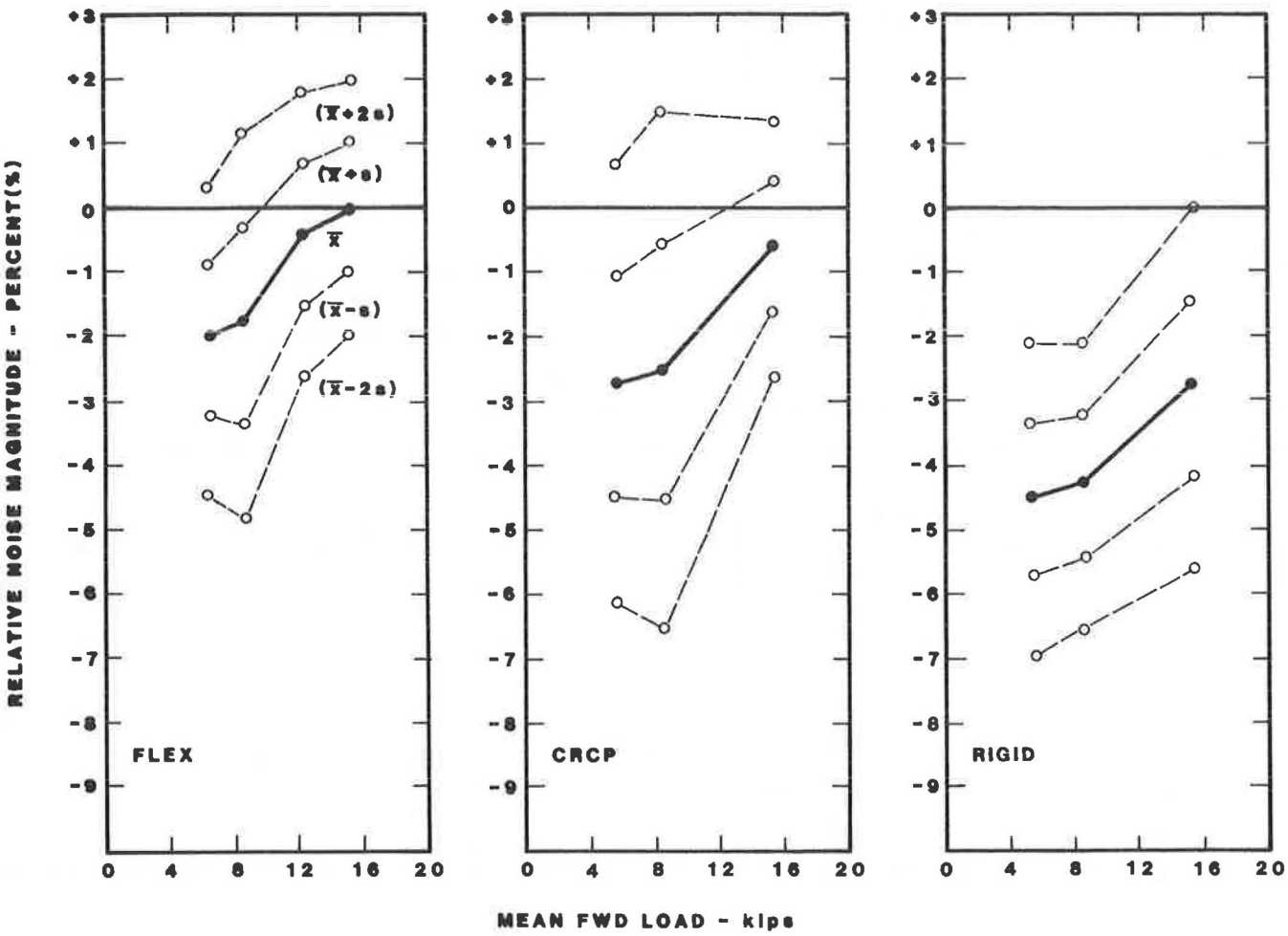

FIGURE 4 Relative noise magnitude as a function of pavement type and FWD drop height (load).

definitely decreases as the drop height increases. As presented in Table 4, the overall average relative noise value for Geophone 1 decreases from −0.4 percent at the first drop height to −0.1 percent at the fourth drop height and from −1.2 to −0.7 percent at Geophone 7.

For the rigid pavement, deflection-related noise also depends on drop height, particularly when compared to the flexible pavement. Although no clear trends in the absolute noise are apparent (see Table 5), the magnitude of the relative noise definitely decreases as the drop height increases. As presented in Table 5, the overall average relative value at Geophone 1 decreases from −1.2 percent at the first drop height to −0.7 percent at the fourth drop height, whereas that at Geophone 7 decreases from −2.5 to −1.6 percent.

Deflection noise in CRC pavement does not appear to be as sensitive to drop height as that for rigid and flexible pavements, specially when compared to geophone location. No general trend between absolute noise and drop height is apparent. Also, no definitive trend is apparent for the relative noise, particularly for the first four geophones. For the last three geophones, as presented in Table 6, the relative noise clearly decreases with increasing load level.

Test Location

From a practical viewpoint, flexible pavement deflection noise does not appear to depend on test location. Although significant differences in the average absolute values are apparent between locations F0–F1 and F3 at the first two geophones, the overall average absolute and relative noise values are similar at both locations (see Table 4). This similarity is particularly true for the relative noise at Geophone 7, where the largest difference, 0.3 percent, occurs.

Unlike the flexible pavement, deflection noise for the rigid pavement does appear to depend on the geophone location but to a lesser degree when compared to the test location. In general, absolute noise differences between test locations appear to decrease, whereas relative noise differences increase as the radial distance increases. Overall, average values are similar, specially when isolated data points are eliminated from the comparison (see Table 5).

Like the flexible pavement, the effects of test location on CRC pavement deflection noise are not significant. Absolute noise differences between test locations decrease as radial distance increases. As presented in Table 6, the maximum

TABLE 4 AVERAGE ABSOLUTE AND RELATIVE DEFLECTION NOISE VALUES—FLEXIBLE PAVEMENT

Test Location	Drop Height	Average Absolute Noise (Microns)							Average Relative Noise (%)						
		Geophone Number							Geophone Number						
		1	2	3	4	5	6	7	1	2	3	4	5	6	7
F1	1	-0.8	-0.7	-0.7	-0.5	-0.6	-0.4	-0.4	-0.4	-0.4	-0.4	-0.4	-0.6	-0.9	-1.8
	2	-1.1	-1.0	-0.9	-0.9	-0.7	-0.6	-0.3	-0.4	-0.4	-0.4	-0.4	-0.5	-1.0	-0.8
	3	-1.0	-0.8	-0.8	-0.5	-0.7	-0.7	-0.5	-0.2	-0.2	-0.2	-0.2	-0.3	-0.7	-1.1
	4	-0.7	-0.5	-0.4	-0.4	-0.2	-0.4	-0.3	-0.1	-0.1	-0.1	-0.1	-0.1	-0.3	-0.5
	All	-0.9	-0.7	-0.7	-0.6	-0.5	-0.5	-0.4	-0.3	-0.3	-0.3	-0.3	-0.4	-0.8	-1.1
F3	1	-1.0	-1.1	-0.6	-0.9	-0.8	-0.3	-0.1	-0.3	-0.4	-0.3	-0.5	-0.7	-0.9	-0.7
	2	-1.1	-1.3	-1.1	-0.7	-0.8	-0.5	-0.3	-0.2	-0.3	-0.3	-0.3	-0.4	-0.8	-1.1
	3	-1.5	-1.5	-1.2	-0.8	-0.7	-0.4	-0.3	-0.2	-0.2	-0.2	-0.2	-0.2	-0.4	-0.7
	4	-1.5	-1.0	-0.8	-0.8	-0.4	-0.3	-0.5	-0.1	-0.1	-0.1	-0.1	-0.1	-0.2	-0.8
	All	-1.3	-1.3	-0.9	-0.8	-0.7	-0.4	-0.3	-0.2	-0.3	-0.2	-0.3	-0.3	-0.6	-0.8
ALL	1	-0.9	-0.9	-0.6	-0.7	-0.7	-0.4	-0.3	-0.4	-0.4	-0.3	-0.5	-0.6	-0.9	-1.2
	2	-1.1	-1.1	-1.0	-0.8	-0.8	-0.5	-0.3	-0.3	-0.3	-0.4	-0.4	-0.4	-0.9	-1.0
	3	-1.3	-1.1	-1.0	-0.6	-0.7	-0.5	-0.4	-0.2	-0.2	-0.2	-0.2	-0.3	-0.6	-0.9
	4	-1.1	-0.8	-0.6	-0.6	-0.3	-0.4	-0.4	-0.1	-0.1	-0.1	-0.1	-0.1	-0.3	-0.7
	All	-1.1	-1.0	-0.8	-0.7	-0.6	-0.5	-0.3	-0.2	-0.3	-0.3	-0.3	-0.3	-0.7	-0.9

TABLE 5 AVERAGE ABSOLUTE AND RELATIVE DEFLECTION NOISE VALUES—RIGID PAVEMENT

Test Location	Drop Height	Average Absolute Noise (Microns)							Average Relative Noise (%)						
		Geophone Number							Geophone Number						
		1	2	3	4	5	6	7	1	2	3	4	5	6	7
J0,J1	1	-0.4	-0.5	-0.6	-0.6	-0.6	-0.5	-0.4	-1.1	-1.3	-1.7	-1.7	-1.8	-2.0	-2.6
	2	-0.6	-0.5	-0.4	-0.4	-0.5	-0.5	-0.6	-1.0	-0.9	-0.7	-0.7	-1.0	-1.3	-2.5
	3	-1.4	-1.0	-1.2	-1.0	-0.7	-0.5	-0.5	-1.0	-0.7	-0.9	-0.8	-0.6	-0.6	-0.9
	All	-0.8	-0.7	-0.7	-0.7	-0.6	-0.5	-0.5	-1.0	-1.0	-1.1	-1.1	-1.2	-1.3	-2.0
J2	1	-1.5	-1.5	-1.1	-1.0	-0.9	-0.5	-0.5	-0.8	-0.9	-0.8	-0.7	-0.8	-0.9	-1.3
	2	-2.2	-1.2	-1.0	-0.7	-1.0	-0.6	-0.3	-1.0	-0.8	-0.6	-0.5	-1.0	-1.1	-0.8
	3	-2.1	-1.4	-1.2	-0.9	-1.0	-0.8	-0.6	-0.9	-0.7	-0.8	-0.7	-0.6	-1.3	-1.6
	All	-1.9	-1.3	-1.1	-0.8	-1.0	-0.6	-0.5	-0.9	-0.8	-0.7	-0.6	-0.8	-1.1	-1.2
J3	1	-0.6	-0.7	-0.6	-0.4	-0.6	-0.3	-0.3	-1.1	-1.2	-1.1	-0.9	-1.4	-1.1	-1.6
	2	-0.4	-0.5	-0.5	-0.6	-0.4	-0.4	-0.5	-0.5	-0.5	-0.6	-0.8	-0.5	-0.8	-1.7
	3	-1.8	-1.4	-1.1	-1.0	-0.8	-0.5	-0.6	-0.9	-0.7	-0.6	-0.6	-0.5	-0.4	-0.8
	All	-0.9	-0.9	-0.7	-0.7	-0.6	-0.4	-0.5	-0.8	-0.8	-0.7	-0.7	-0.8	-0.8	-1.4
J4	1	-1.2	-0.3	-0.5	-0.8	-0.5	-0.8	-0.4	-1.3	-0.8	-1.5	-1.1	-1.6	-3.6	-2.8
	2	-0.7	-0.5	-0.4	-0.4	-0.4	-0.3	-0.5	-0.4	-1.0	-0.9	-0.4	-1.0	-0.9	-2.2
	3	-1.5	-0.5	-0.4	-1.3	-0.5	-0.5	-0.3	-0.5	-0.3	-0.3	-0.5	-0.6	-0.6	-0.5
	All	-1.1	-0.4	-0.4	-0.8	-0.5	-0.5	-0.4	-0.7	-0.7	-0.9	-0.6	-1.0	-1.7	-1.8
J5	1	-0.8	-0.5	-0.5	-0.5	-0.3	-0.5	-0.6	-1.0	-0.7	-0.9	-1.5	-0.6	-1.6	-3.4
	2	-0.4	-0.2	-0.3	-0.5	-0.3	-0.5	-0.5	-0.4	-0.2	-0.3	-0.9	-0.4	-1.1	-1.8
	3	-1.6	-1.0	-1.0	-0.4	-0.6	-0.5	-0.2	-0.6	-0.5	-0.5	-0.3	-0.4	-0.4	-0.3
	All	-0.9	-0.6	-0.6	-0.4	-0.4	-0.5	-0.4	-0.7	-0.5	-0.6	-0.9	-0.5	-1.1	-1.8
ALL	1	-0.9	-0.7	-0.7	-0.6	-0.5	-0.5	-0.5	-1.2	-1.1	-1.3	-1.2	-1.3	-2.0	-2.5
	2	-0.7	-0.6	-0.5	-0.5	-0.5	-0.5	-0.5	-0.8	-0.8	-0.8	-0.8	-0.9	-1.2	-1.6
	3	-1.7	-1.1	-1.0	-0.9	-0.8	-0.5	-0.4	-0.6	-0.7	-0.6	-0.7	-0.8	-1.1	-1.8
	All	-1.1	-0.8	-0.7	-0.7	-0.6	-0.5	-0.5	-0.7	-0.5	-0.5	-0.5	-0.5	-0.5	-0.6

TABLE 6 AVERAGE ABSOLUTE AND RELATIVE DEFLECTION NOISE VALUES—CRC PAVEMENT

Test Location	Drop Height	Average Absolute Noise (Microns)							Average Relative Noise (%)						
		Geophone Number							Geophone Number						
		1	2	3	4	5	6	7	1	2	3	4	5	6	7
C0,C1	1	-0.4	-0.5	-0.7	-0.4	-0.5	-0.6	-0.6	-0.4	-0.4	-0.7	-0.4	-0.6	-1.2	-2.0
	2	-0.6	-0.2	-0.4	-0.5	-0.5	-0.4	-0.5	-0.3	-0.1	-0.3	-0.4	-0.4	-0.5	-1.0
	3	-0.8	-0.4	-0.5	-0.5	-0.3	-0.3	-0.4	-0.3	-0.2	-0.2	-0.2	-0.2	-0.3	-0.5
	All	-0.6	-0.4	-0.5	-0.5	-0.4	-0.5	-0.5	-0.3	-0.2	-0.4	-0.3	-0.4	-0.6	-1.2
C2	1	-0.8	-0.9	-0.6	-0.6	-0.7	-0.8	-0.7	-0.3	-0.4	-0.3	-0.3	-0.4	-0.8	-1.4
	2	-1.0	-0.9	-0.7	-0.8	-0.7	-0.5	-0.4	-0.3	-0.3	-0.2	-0.3	-0.3	-0.3	-0.5
	3	-1.4	-1.2	-1.1	-0.9	-0.9	-0.8	-0.3	-0.3	-0.2	-0.2	-0.2	-0.2	-0.4	-0.2
	All	-1.1	-1.0	-0.8	-0.8	-0.8	-0.7	-0.5	-0.3	-0.3	-0.3	-0.3	-0.3	-0.5	-0.7
C3	1	-0.6	-0.8	-0.7	-0.7	-0.6	-0.5	-0.5	-0.3	-0.5	-0.4	-0.4	-0.4	-0.5	-0.9
	2	-0.7	-0.8	-0.8	-0.8	-0.6	-0.2	-0.5	-0.2	-0.3	-0.3	-0.3	-0.3	-0.2	-0.6
	3	-1.1	-1.1	-1.0	-1.2	-1.0	-0.9	-0.6	-0.2	-0.3	-0.2	-0.3	-0.3	-0.4	-0.5
	All	-0.8	-0.9	-0.8	-0.9	-0.7	-0.6	-0.5	-0.3	-0.3	-0.3	-0.3	-0.3	-0.4	-0.7
C4	1	-0.3	-0.1	-0.2	-0.5	-0.5	-0.7	-0.4	-0.2	-0.1	-0.1	-0.5	-0.6	-1.2	-1.0
	2	-0.2	0.0	-0.1	-0.2	-0.5	-0.5	-0.6	-0.1	0.0	-0.1	-0.1	-0.3	-0.5	-1.1
	3	-0.6	-0.4	-0.6	-0.5	-0.4	-0.4	-0.5	-0.2	-0.1	-0.2	-0.2	-0.1	-0.2	-0.4
	All	-0.4	-0.1	-0.3	-0.4	-0.5	-0.5	-0.5	-0.2	-0.1	-0.1	-0.2	-0.3	-0.6	-0.8
C5	1	-0.2	-0.3	-0.3	-0.4	-0.4	-0.6	-0.5	-0.1	-0.3	-0.2	-0.3	-0.4	-1.0	-1.2
	2	-0.1	0.0	-0.2	-0.2	-0.4	-0.7	-0.4	-0.0	0.0	-0.1	-0.1	-0.3	-0.7	-0.8
	3	-0.5	-0.3	-0.2	-0.4	-0.5	-0.4	-0.5	-0.1	-0.1	-0.1	-0.1	-0.2	-0.2	-0.5
	All	-0.2	-0.2	-0.2	-0.3	-0.4	-0.6	-0.5	-0.1	-0.1	-0.1	-0.2	-0.3	-0.6	-0.8
ALL	1	-0.5	-0.5	-0.5	-0.5	-0.5	-0.6	-0.5	-0.3	-0.3	-0.4	-0.4	-0.5	-0.9	-1.3
	2	-0.5	-0.4	-0.5	-0.5	-0.5	-0.5	-0.5	-0.2	-0.1	-0.2	-0.2	-0.3	-0.4	-0.8
	3	-0.9	-0.7	-0.7	-0.7	-0.6	-0.6	-0.5	-0.2	-0.2	-0.2	-0.2	-0.2	-0.3	-0.4
	All	-0.6	-0.5	-0.5	-0.6	-0.6	-0.6	-0.5	-0.2	-0.2	-0.3	-0.3	-0.3	-0.6	-0.9

absolute average noise difference between locations at Geophone 1 is 0.9 μm and decreases to 0.0 μm at Geophone 7. Unlike the absolute noise, relative noise values appear to be independent of the test location.

Pavement Type

In order to assess the effects of pavement type on deflection-related noise, the analysis results contained in Tables 4 through 6 were used to develop a series of figures that summarize noise as a function of pavement type and other key variables.

Figure 5 shows the cumulative frequency diagrams for absolute deflection noise as a function of the three pavement type categories investigated. As can be observed, although there are small differences between pavement types, their difference from a practical viewpoint is quite insignificant. In addition, unlike the load analysis, there appears to be no significant and observable trend in the absolute noise magnitude relative to the overall flexibility of the pavement structure. In general, average absolute noise levels are quite similar for both flexible and rigid pavements, whereas CRC pavement had the lowest absolute noise level, particularly at geophones near the load plate. Because of this, average relative noise levels are generally the same for flexible and CRC pavements, whereas the rigid pavement average relative noise levels are about 2 to 4 times as great. Therefore, although minor differences between pavement types are noticeable, they are quite insignificant from a practical viewpoint, and it is concluded that the absolute noise distribution is generally independent of pavement type.

Figure 6 shows the effects of drop height on the average deflection noise levels for the three pavement types studied. There is no clear trend for absolute noise level between pavement types and drop heights, with average values ranging between -0.6 and -0.7 μm. In contrast, the average relative noise shows a decreasing trend in noise level with increasing load. However, it can also be observed that there is no unique trend in noise for all pavement types. This indirectly justifies the statement that the best parameter to describe deflection noise is the absolute noise, which appears to be independent of deflection magnitude. Figure 7 shows the absolute noise frequency distribution patterns by drop height and pavement type. It can be observed for all cases that the largest percentage of noise is within the 0 to -2 μm range.

As noted earlier, the one variable that appears to have the most significant impact on deflection noise was geophone location. Figure 8 shows the effects of this variable on the deflection noise values. As shown, there is a general decrease in the average absolute noise level as distance from the load plate increases. From a relative noise viewpoint, the noise is nearly constant for a particular pavement type, specially for

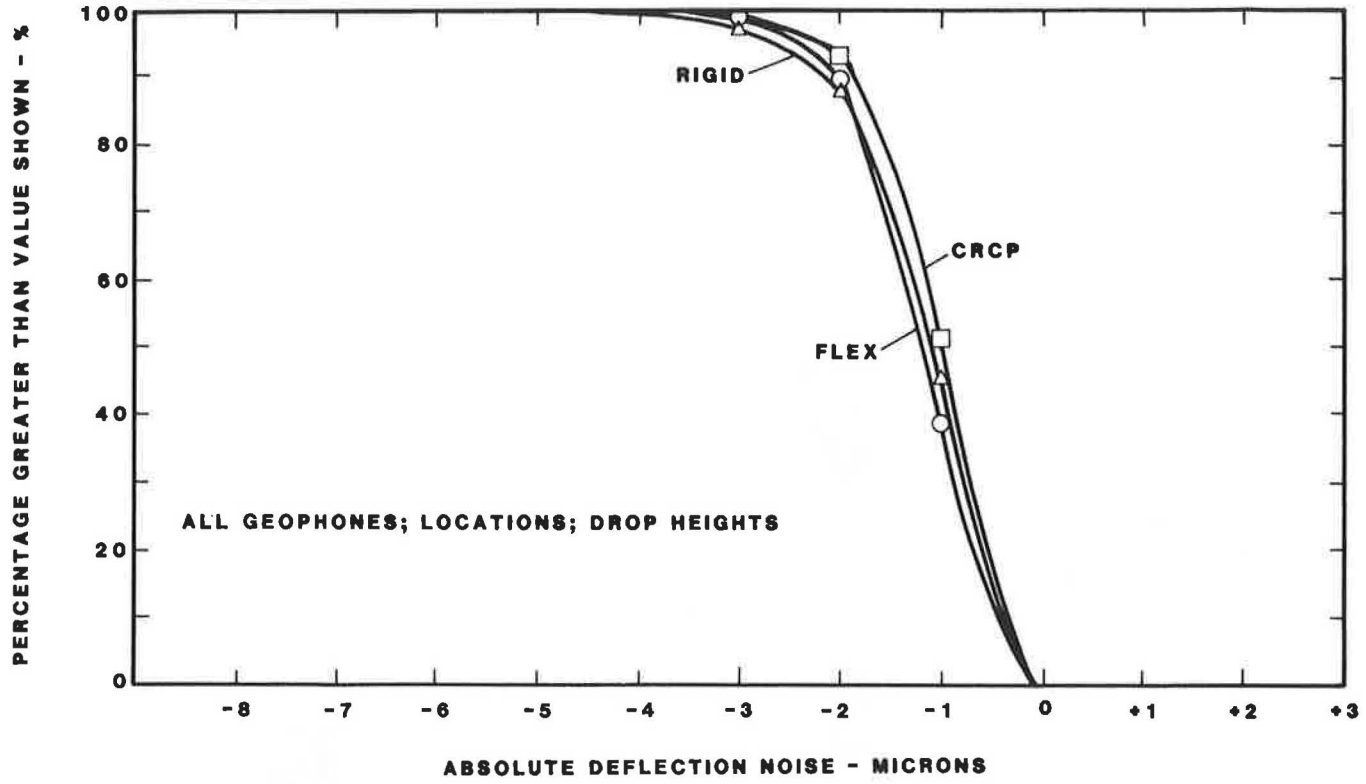

FIGURE 5 Cumulative frequency plot of absolute deflection noise by pavement type.

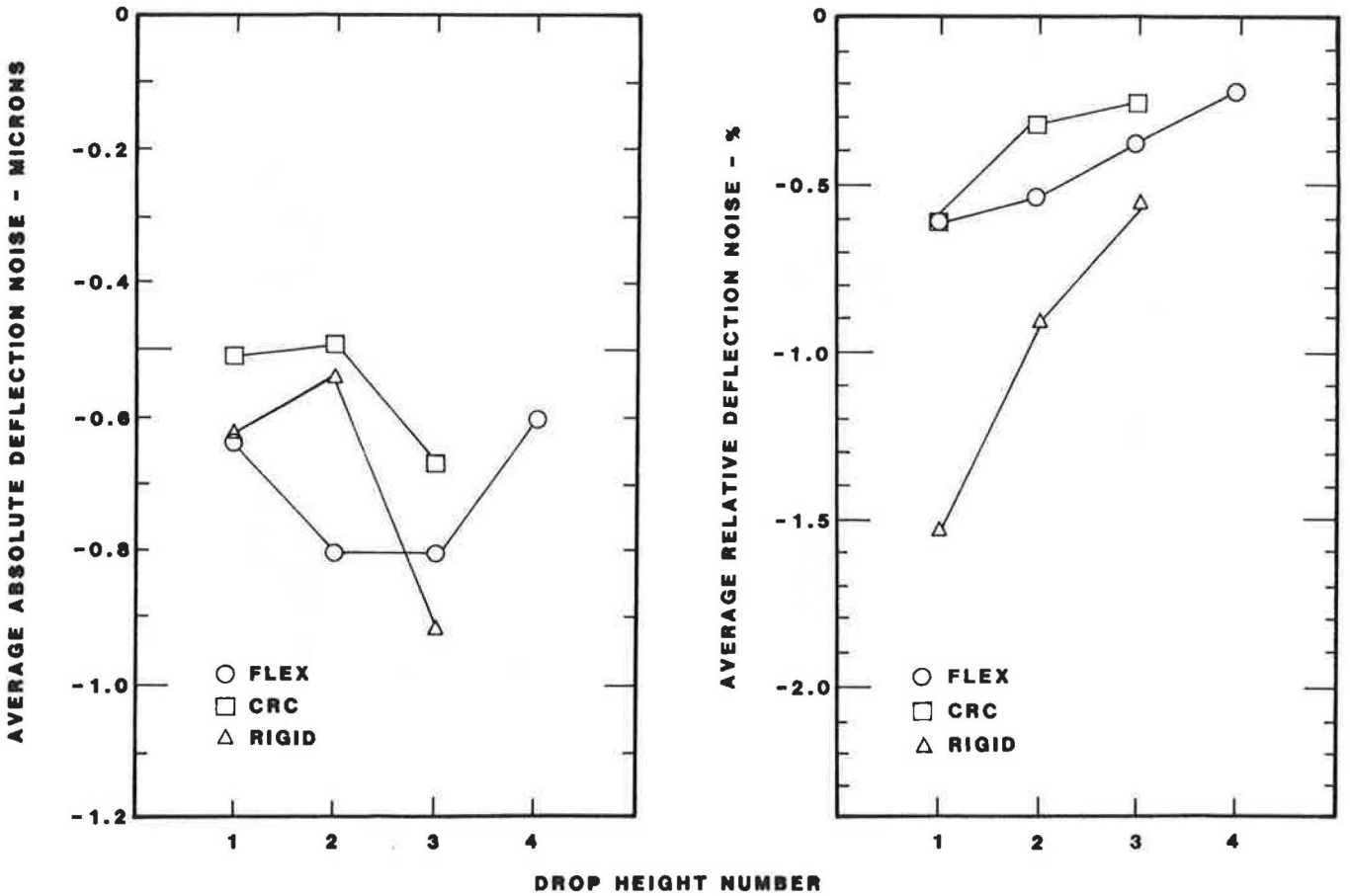

FIGURE 6 Effect of drop height on deflection noise as a function of pavement type.

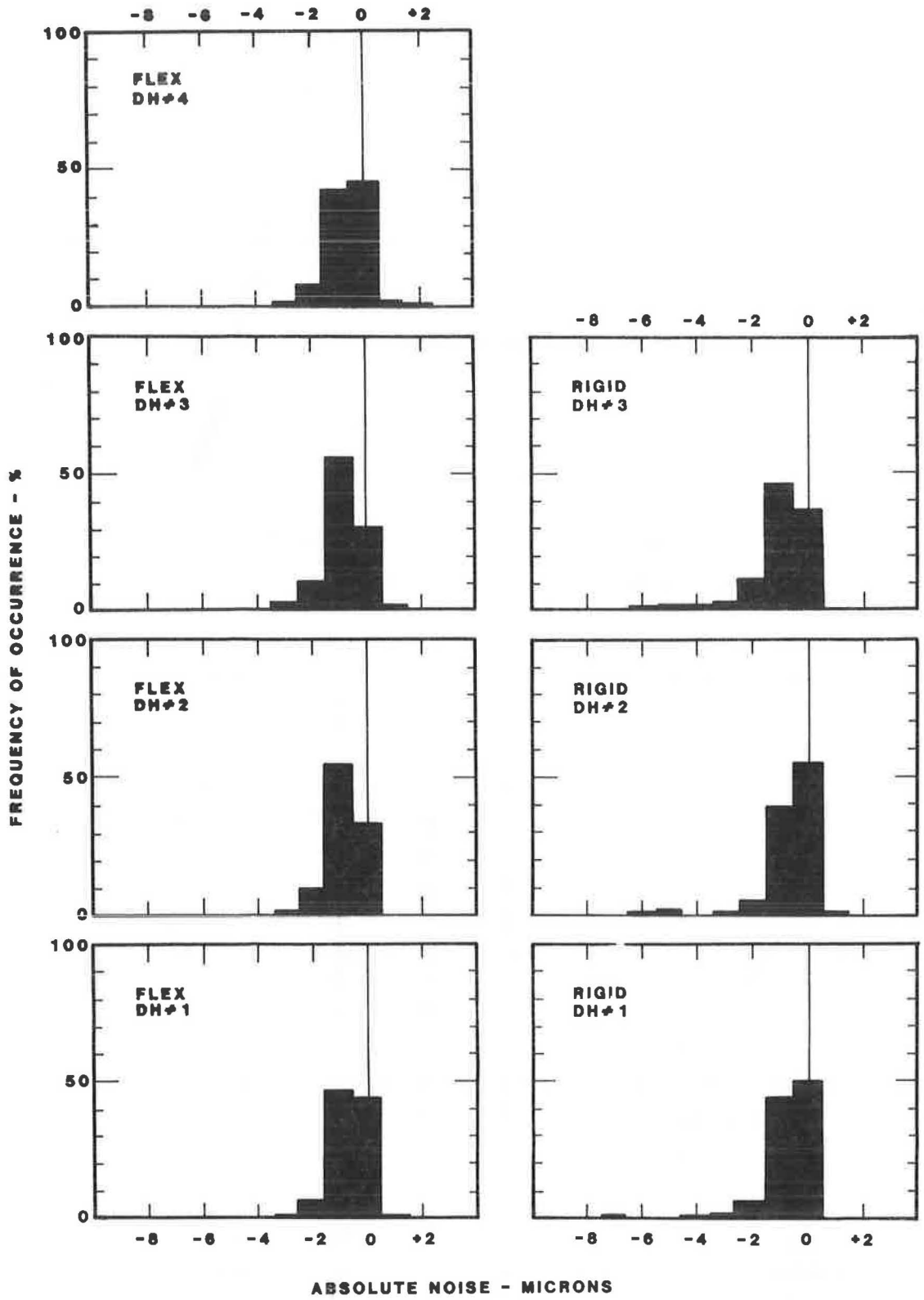

FIGURE 7 Absolute deflection noise frequency distributions as a function of pavement type and drop height.

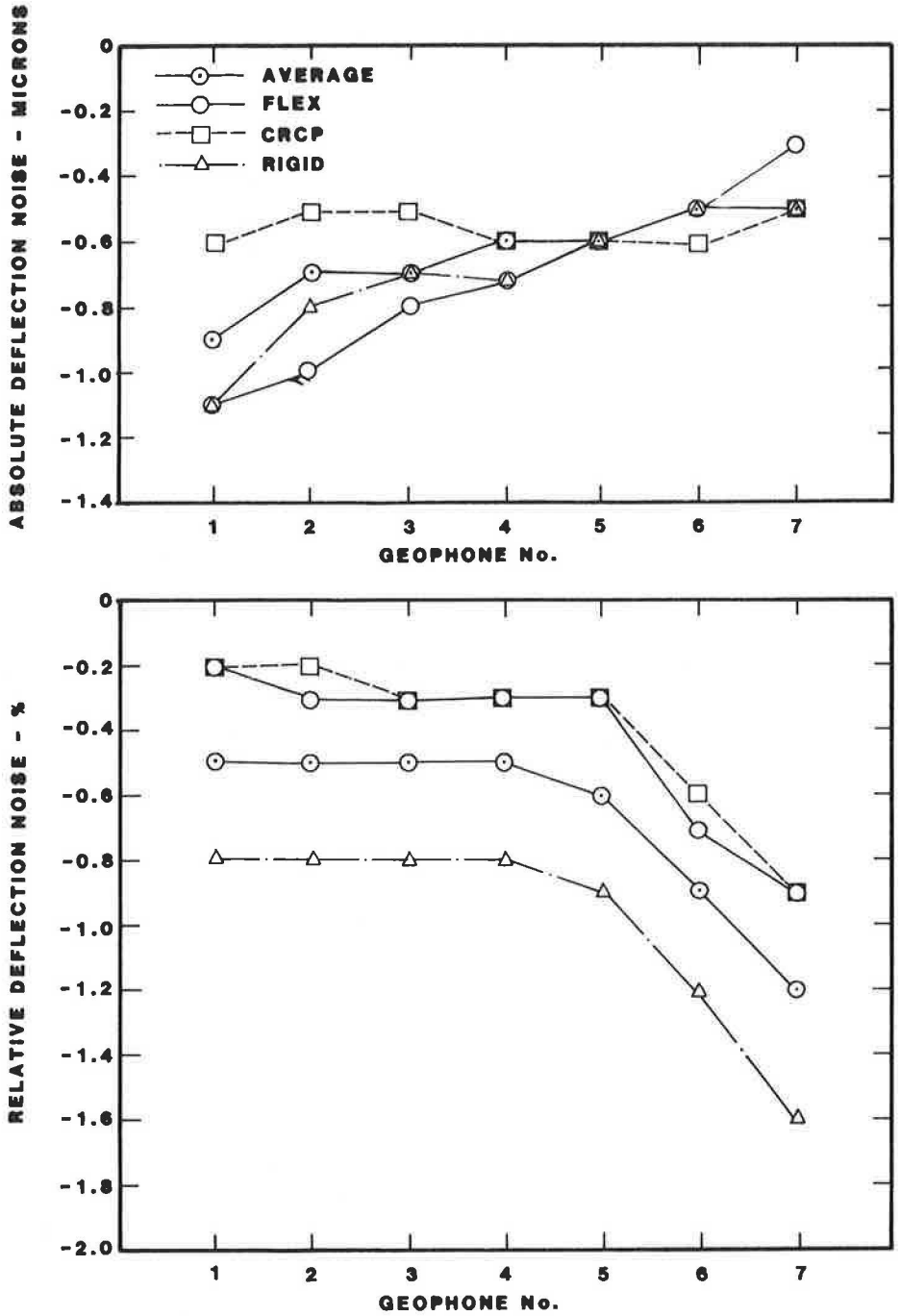

FIGURE 8 Effect of geophone location on deflection noise as a function of pavement type.

the first five geophone locations. Beyond the fifth geophone, the relative noise percentage rapidly increases. Figure 9 similarly supports this conclusion by showing the continuous shift in the cumulative frequency distributions of the absolute noise with increasing geophone number. Although this difference is noticeable by geophone, the overall difference between geophones is quite small.

Overall Discussion

The major objective of the deflection signal analysis was to assess the impact of filtering on the deflection data. Using 5,873 individual test results, the effects of pavement type, test location, drop height, and geophone number were investigated. From this analysis, the following major conclusions were developed:

1. In general, the deflection noise is almost exclusively negative in nature; i.e., filtered deflections are smaller than unfiltered deflections, consistent with expectations.
2. In comparing absolute noise to relative noise parameters, absolute noise is a better descriptor. Using this variable, it appears that pavement type, drop height, and test location do not affect the distribution of absolute deflection noise. The

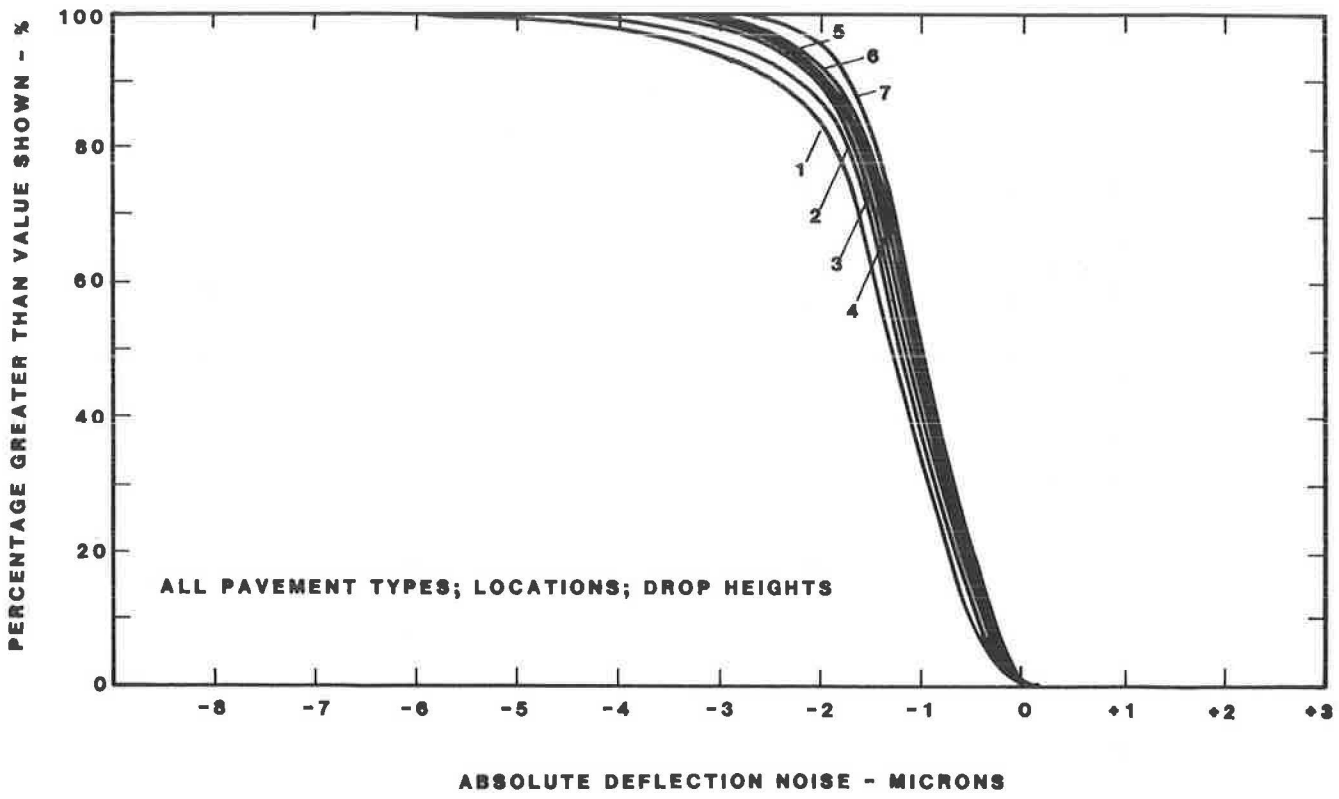

FIGURE 9 Cumulative frequency plot of absolute deflection noise by geophone.

only variable slightly influencing noise was found to be geophone location.

3. Although the geophone location affects the absolute noise level, the practical implication of its effect is considered quite small. Figure 10 shows the statistical distribution effects of both absolute and relative noise as a function of geophone number. For all data analyzed, the average absolute noise is approximately -0.9 μm, with $x \pm 2s$ range of $+1.1$ to -2.9 μm for the geophone directly under the load plate. Similar values for Geophone 7 are -0.5 μm and $+0.7$ to -1.4 μm, respectively.

4. Based on all observations, the overall average absolute deflection noise was -0.65 μm with a standard deviation (s) of 0.73 μm (*2*). This value of s is of the same order of magnitude found for the raw deflection repeatability error (s = 0.6 μm) for repeat drops (*3*). Thus, for filtered raw deflection responses, the random error is approximately twice as large as that for unfiltered data.

SUPPLEMENTAL STUDY

Because of the surprisingly large noise magnitudes found in the original study, specially for the rigid pavement, an additional filtering study was conducted to substantiate these results. In this study, five additional rigid pavements were evaluated: one in Nevada, one in North Carolina, and three in Georgia. Overall, an additional 1,482 load and 10,374 deflection measurements were evaluated.

Like the original study, a comparative statistical analysis of the data was conducted to quantify the effects of the digital filtering process. A complete summary of the analysis results is contained in the North Carolina study (*4*). Figure 11 shows the average absolute and relative load noise as a function of drop height for all pavements investigated. Similar to the North Carolina study, the average absolute noise increases with drop height, whereas no unique trend is apparent for the average relative noise. Also, almost 100 percent of the results are negative, indicating that filtering reduces the peak load. More important, the load signal analysis results confirm the original report results in that the noise level is of significant magnitude. In fact, the average noise of the additional sections is larger than that reported for the North Carolina pilot section. At the maximum drop height, absolute noise levels for the original section varied from 0 to -850 lb (-7.8 psi plate pressure) and from 0 to $-1{,}100$ lb (-10.0 psi) for the additional sections.

Average absolute and relative deflection noise levels as a function of drop height and geophone number are shown in Figures 12 and 13. As in the original study, absolute deflection noise appears to be independent of drop height but is related to the geophone location. Also, the relative noise level decreases with increasing drop height, but is essentially independent of geophone location, specially for the first five or six geophones. In summary, the results of the additional study support the conclusions regarding deflection noise found in the original study. From an absolute deflection viewpoint, the additional sections have noise levels generally greater than that found

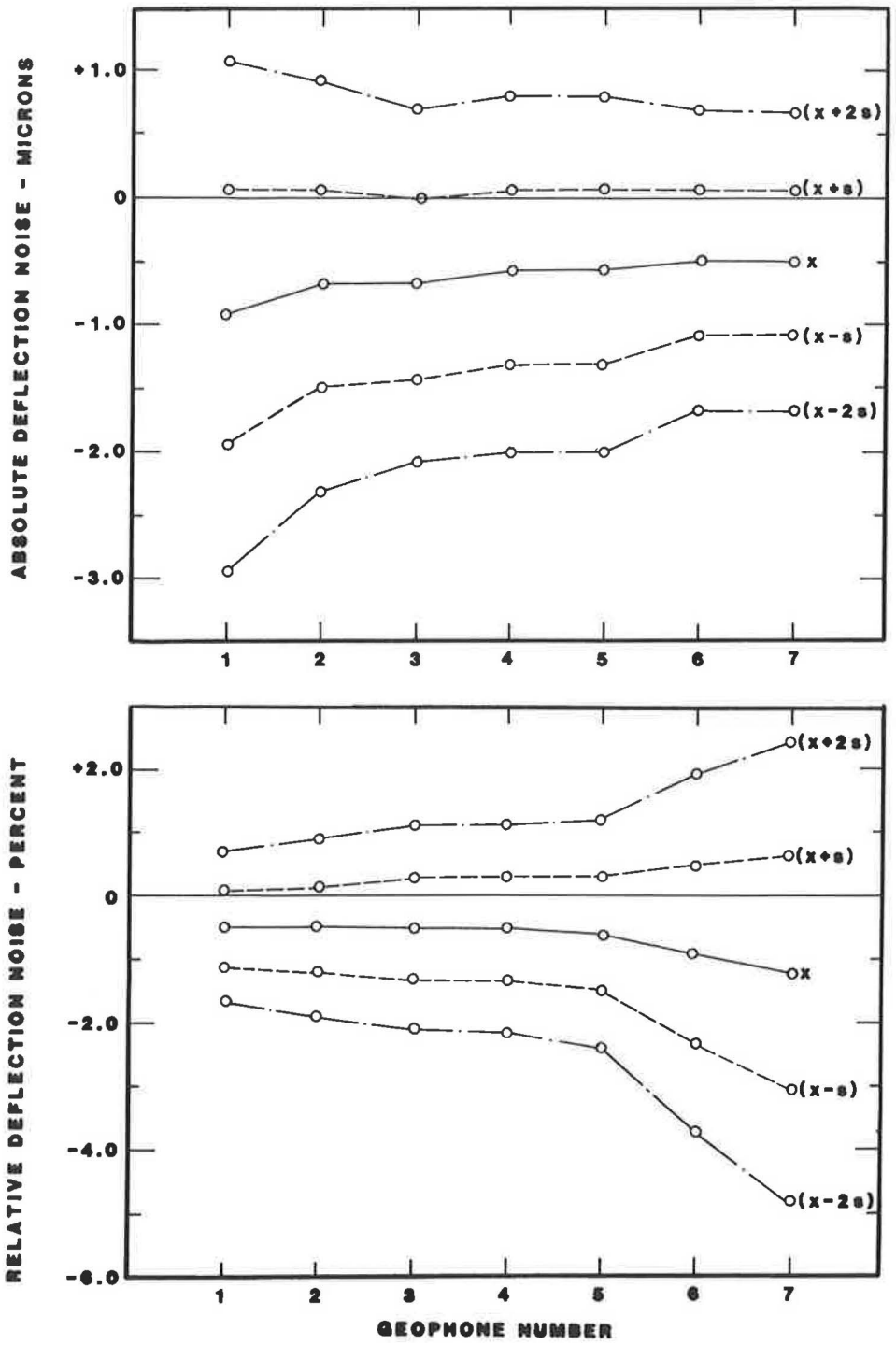

FIGURE 10 Absolute and relative deflection noise limits by geophone location.

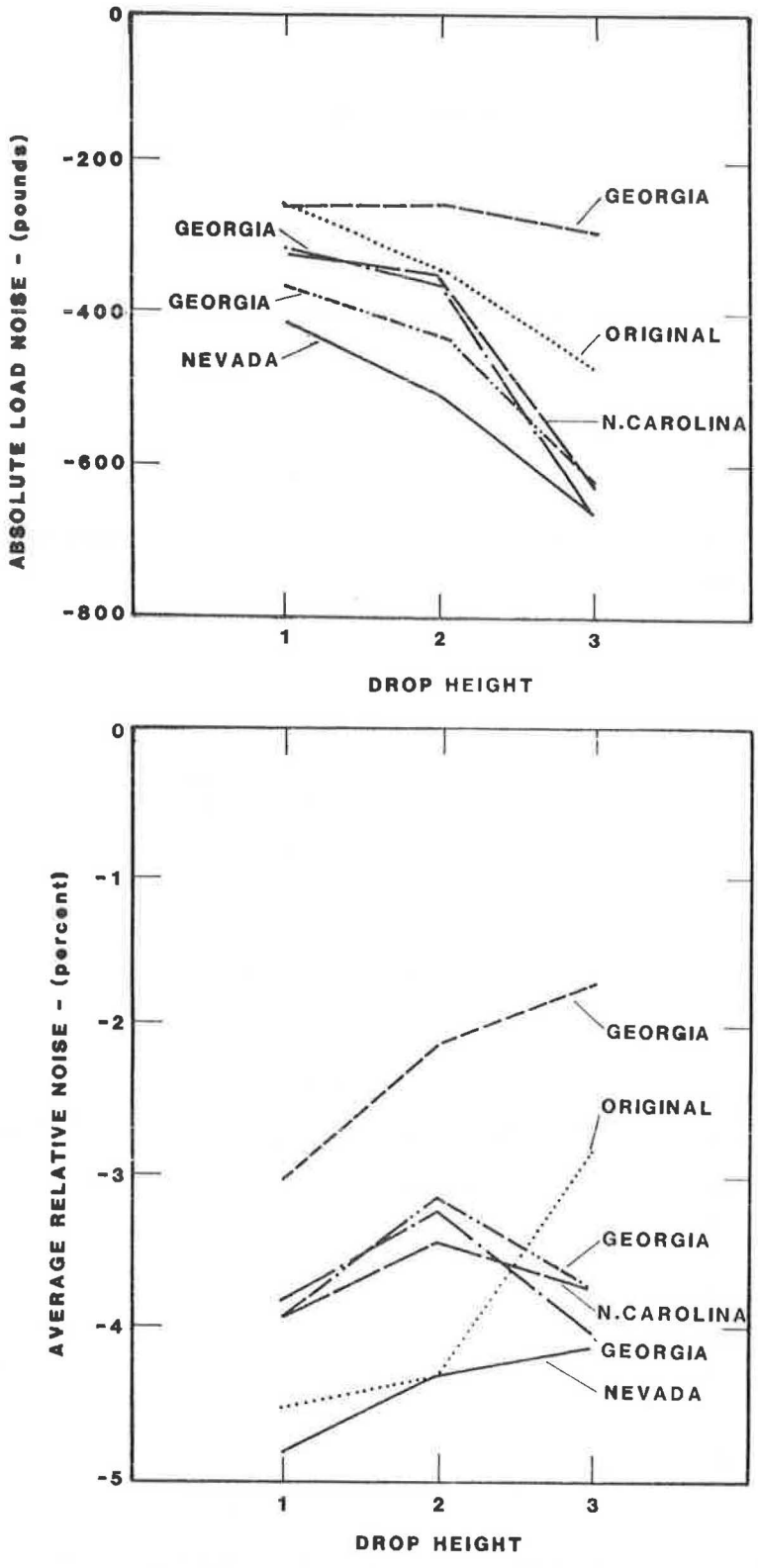

FIGURE 11 Effect of drop height and pavement section on load noise—supplemental study.

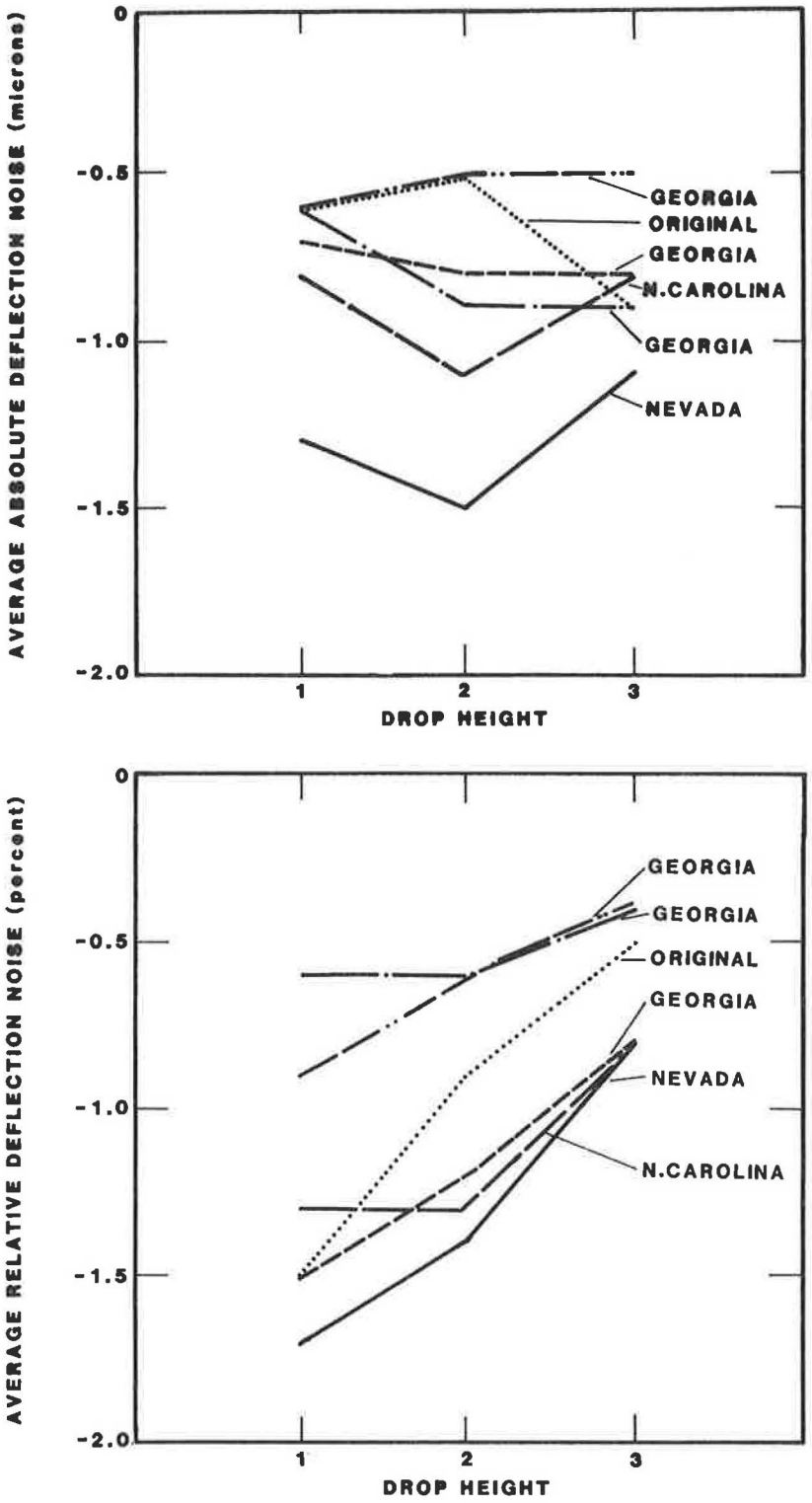

FIGURE 12 Effect of drop height and pavement section on deflection noise—supplemental study.

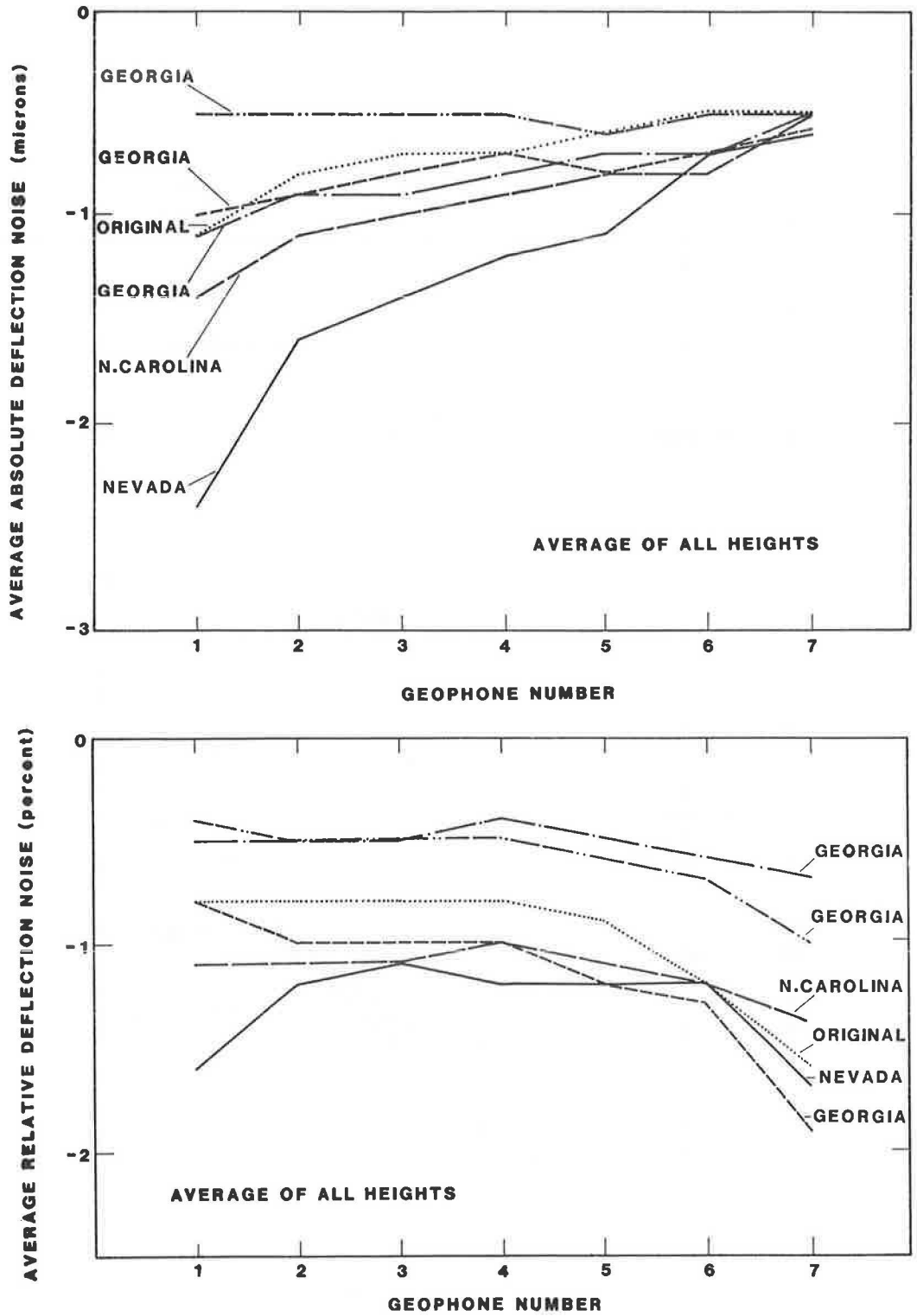

FIGURE 13 Effect of geophone number and pavement section on deflection noise—supplemental study.

in North Carolina. Typical values from -0.5 μm to as large as -1.5 μm were observed.

IMPLICATIONS OF FINDINGS

The findings of both the original and supplemental data filtering studies impact in a small, but significant, manner on SHRP FWD operational field guide procedures. It has been shown that filtering of load data increases the drop-to-drop variability in the peak values, particularly for rigid pavements tested under heavy loads. In addition, the filtering process on deflection data similarly causes an increase in random deflection measurement error (variability) between replicate drops.

Although these two filtering effects are significant in themselves, they tend to compound each other, when the filtered raw deflections are normalized by the filtered load data. It is therefore hypothesized that the use of filtered data yields normalized deflection responses that more than likely exceed current normalized deflection tolerance limits, particularly for rigid pavement and heavy FWD load conditions. Also, although not yet investigated, it can be confidently hypothesized that the use of filtered data will lead to significantly different backcalculated layer moduli than would unfiltered FWD data.

Although large noise magnitudes have been found, the best load-deflection value between filtered and unfiltered data is unknown. Because of the complexity of the problem, the final resolution of this question can only be accomplished through further research and time. It has been recommended that all current and near-future FWD data collected by SHRP be accomplished with the filter off; unfiltered peaks should be used in the data collection process until conclusive research regarding digital filtering is developed.

Because some unknown level of noise is contained within SHRP FWDs, it has also been recommended that additional load- and deflection-time histories be collected and stored. Thus, if future research advances do occur with regard to the filtering process, all unfiltered data can be reanalyzed to obtain the most accurate estimates of peak load-deflection values for use in the backcalculation of layer moduli.

ACKNOWLEDGMENT

The study presented herein was performed under the general terms of the SHRP Technical Assistance contract. The support of SHRP in performing this study is gratefully acknowledged.

REFERENCES

1. SHRP P-001 Technical Advisory Staff. *SHRP-LTPP Manual for FWD Testing and Operational Field Guidelines*. Technical Manual, Strategic Highway Research Program, National Research Council, Washington, D.C., Jan. 1989.
2. SHRP P-001 Technical Advisory Staff. *Analysis of Data Filtering Results from the North Carolina Pilot Study*. Technical Report, Strategic Highway Research Program, National Research Council, Washington, D.C., March 1989.
3. SHRP P-001 Technical Advisory Staff. *Analysis of Within Drop (Replicate) Error of Load Cell and Sensor Responses of the FWD*. Technical Report, Strategic Highway Research Program, National Research Council, Washington, D.C., Jan. 1989.
4. SHRP P-001 Technical Advisory Staff. *Addendum To Analysis of Data Filtering Results from the North Carolina Pilot Study*. Technical Report, Strategic Highway Research Program, National Research Council, Washington, D.C., April 1989.

The views expressed in this paper are exclusively those of the writers and do not reflect the official policy of SHRP.

Publication of this paper sponsored by Committee on Pavement Monitoring, Evaluation, and Data Storage.

BOUSDEF: A Backcalculation Program for Determining Moduli of a Pavement Structure

HAIPING ZHOU, R. G. HICKS, AND C. A. BELL

Highway and transportation agencies have an increasing responsibility for the maintenance, rehabilitation, and management of highways, particularly with regard to asphaltic concrete pavements. Efficient and economical methods are required for determining the structural properties of existing flexible pavements. Nondestructive testing (NDT) of pavements is one of the most useful and cost-effective methods for evaluating the structural adequacy of pavements. With the wide use of NDT, in particular the deflection test, a large amount of test data can be obtained. One common use of deflection data is to determine the pavement layer moduli through backcalculation. The microcomputer program BOUSDEF for backcalculating the moduli of a pavement structure using deflection basin data is presented. The solution techniques for use in developing the program are described, including the use of the method of equivalent thicknesses, Boussinesq theory, consideration of nonlinearity of pavement materials, and consideration of overburden pressure on stress calculation. Evaluation of the program was performed by two approaches: (a) comparing the backcalculated moduli with theoretical moduli, and (b) comparing the backcalculated moduli with results from other developed backcalculation programs. The evaluation shows that the moduli backcalculated using the BOUSDEF program compare well with the theoretical moduli and also are compatible with those from other developed programs. The BOUSDEF program runs fast compared with other backcalculation programs; therefore, the program can be effectively used as a tool to make initial evaluations of deflection testing data for determining pavement layer moduli.

Highway and transportation agencies have increasing responsibility for maintenance, rehabilitation, and management of highways, particularly with regard to asphaltic concrete (AC) pavements. Efficient and economical methods are required for determining structural properties of existing flexible pavements.

Pavement structural properties may be generally stated in terms of the resilient modulus, which is a key element in mechanistic pavement analysis and evaluation procedures. For a multilayer pavement structure, the resilient modulus of each pavement layer may be determined by two possible methods—destructive testing and nondestructive testing (NDT). Destructive testing is generally done by obtaining cores from an existing pavement and testing them using laboratory equipment. NDT, on the other hand, uses deflection basin data generated from an NDT device to quantify the response of a pavement structure due to a known load. The known response is then used in a backcalculation procedure, which generally means using the deflection basin data to determine the pavement layer moduli. The NDT method has certain advantages over the destructive method, such as no physical damage to the pavement structure, and requiring no laboratory tests.

NDT of AC pavements is one of the most useful and cost-effective methods developed by engineers to assist in the management of pavements. With the increased responsibility that highway agencies have for effectively apportioning funds and efficiently designing major rehabilitation projects, the use of NDT methods has become, or in some cases, can become, an invaluable aid in determining the actual condition of pavement sections in a highway network (*1*). The emphasis in the *1986 AASHTO Guide for Design of Pavement Structures* (*2*) on use of the resilient moduli of pavement materials in pavement design and on use of NDT in overlay design also suggests that these methods will have increased usage in the future.

The analysis of NDT data to determine pavement layer properties requires use of mechanistic methods. The principal objective of mechanistic analysis of NDT data is to produce moduli of pavement layers for in-service temperatures at various load levels. These mechanistic methods assume that stresses, strains, and deformations in pavements can be modeled as multilayered linear or nonlinear elastic structures, resting on linear or nonlinear elastic foundations, as shown in Figure 1. This capability makes it possible to use a trial-and-error procedure to assume the layer properties, calculate the surface deflections, compare these with the measured deflections, and repeat the procedure until the calculated and measured deflections are acceptably close. Several such backcalculation methods of analysis have been developed using different assumptions or algorithms concerning the layer material properties, all of which have the trial-and-error procedure as their basis. One drawback of all the available programs is computing efficiency, which seriously impacts their use in routine design work.

BOUSDEF is a much faster backcalculation program. The program is based on the method of equivalent thicknesses and modified Boussinesq equations. The solution technique, development of the program, and comparison with other backcalculation programs are described in the following sections.

H. Zhou, Oregon Department of Transportation, Highway Materials Laboratory, 800 Airport Road, S.E., Salem, Oreg. 97310. R. G. Hicks and C. A. Bell, Department of Civil Engineering, Oregon State University, Corvallis, Oreg. 97331.

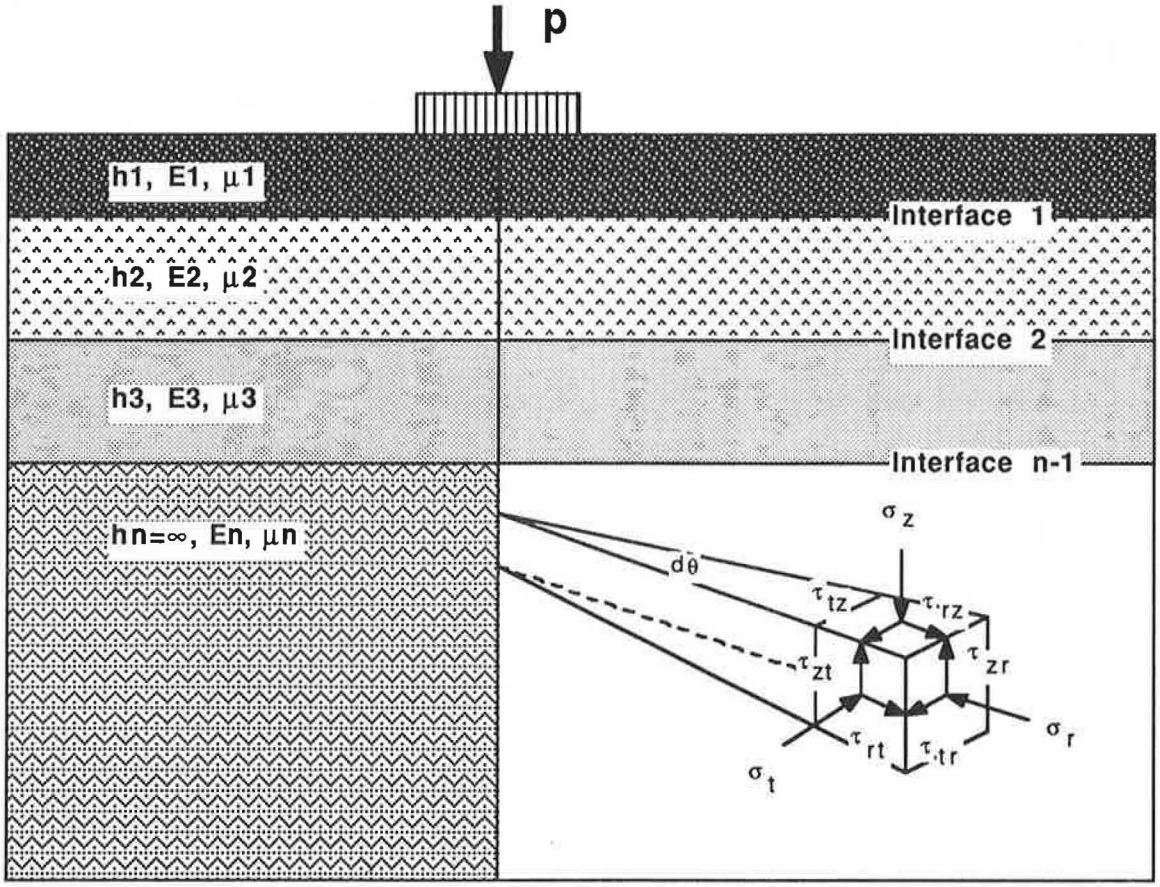

FIGURE 1 Generalized multilayered elastic system.

SOLUTION TECHNIQUE

The BOUSDEF program includes the following techniques:

1. Use of the method of equivalent thicknesses,
2. Use of Boussinesq theory,
3. Consideration of nonlinearity of pavement materials, and
4. Consideration of overburden pressure.

The following paragraphs briefly describe these techniques.

Method of Equivalent Thicknesses

The method of equivalent thicknesses (*3*) assumes that any two layers with similar structural stiffness will distribute loading in the same way. According to this assumption, all layers in a multilayered structure can be converted to one layer with equivalent stiffness by using the following relationship:

$$D = \frac{Eh^3}{12(1 - \mu^2)} \tag{1}$$

where

D = stiffness,
h = layer thickness,
E = modulus of elasticity, and
μ = Poisson's ratio.

For a two-layer system, the equivalent thickness of a layer with modulus E_2 and Poisson's ratio μ_2 relative to a layer of thickness h_1, modulus E_1, and Poisson's ratio μ_1, may be expressed by equating the stiffness of both layers, that is,

$$D_1 = D_2,$$

or,

$$\frac{E_1 h_1^3}{12(1 - \mu_1^2)} = \frac{E_2 h_2^3}{12(1 - \mu_2^2)} \tag{2}$$

Rearranging the equation,

$$h_2 = h_1 \left[\frac{E_1}{E_2}\frac{(1 - \mu_2^2)}{(1 - \mu_1^2)}\right]^{1/3}$$

By expanding this concept for a multilayer system as shown in Figure 2, a general form of the equation may be written

$$h_{ei} = \sum_{i=1}^{n-1} h_i \left[\frac{E_i}{E_n}\frac{(1 - \mu_n^2)}{(1 - \mu_i^2)}\right]^{1/3} \tag{3}$$

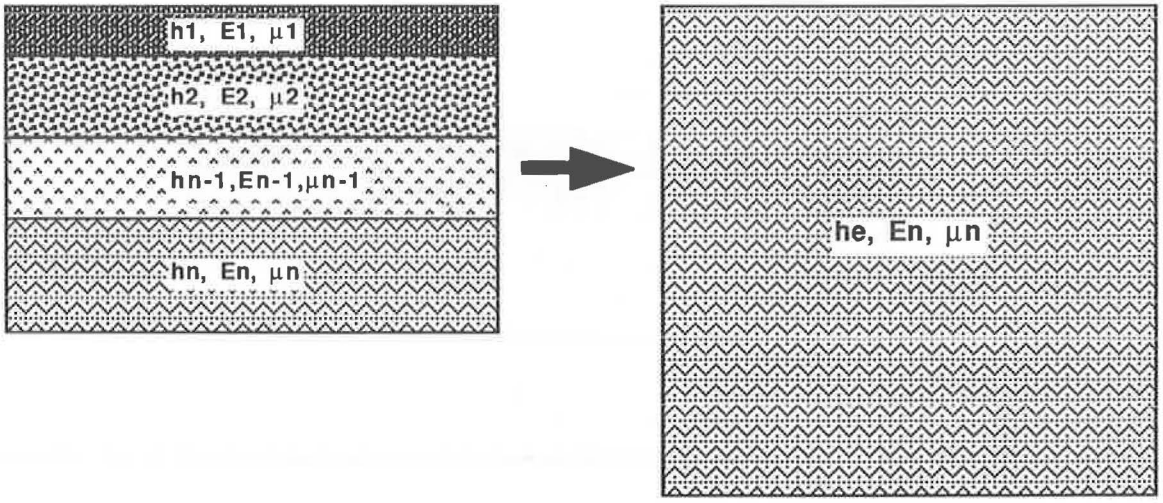

FIGURE 2 Conceptual representation of method of equivalent thicknesses.

where

h_{ei} = equivalent thickness for ith layer,
h_i = thickness of ith layer,
E_i = modulus of ith layer,
E_n = modulus of nth layer,
μ_i = Poisson's ratio for ith layer, and
μ_n = Poisson's ratio for nth layer.

Limitations of the Method of Equivalent Thicknesses

There are a number of limitations with regard to the use of the method of equivalent thicknesses. One is that the pavement layer moduli should decrease with depth, preferably by a factor of at least two between consecutive layers. Another is that the equivalent thickness of a layer should preferably be larger than the radius of the loaded area (*4*).

Boussinesq Equations for Deflections

With the use of the equivalent thicknesses method, the Boussinesq equation for calculating deflection at a depth z and radius r in an elastic half-space can be applied to a multilayer elastic system (*3*). The general equation for deflection due to a point load, as shown in Figure 3a, is,

$$d_{z,r} = \frac{(1 + \mu)P}{2\pi RE}[2(1 - \mu) + \cos^2\Theta] \quad (4)$$

where

$d_{z,r}$ = deflection at depth z and radius r,
P = point load,
R = distance from point load to the location where deformation occurs,
E = modulus of elasticity, and
Θ = angle between centerline of load and location of analysis (see Figure 3a).

For a uniformly distributed load (Figure 3b), integration of Equation 4 yields

$$d_z = \frac{(1 + \mu)\sigma_0 a}{E} \cdot \left[\frac{1}{[1 + (a/z)]^{1/2}} + (1 - 2\mu)\left\{[1 + (z/a)^2]^{1/2} - \frac{z}{a}\right\}\right] \quad (5)$$

where

d_z = deflection on the load axis,
σ_0 = stress under the loading plate,
a = radius of the loading plate, and
z = depth where deformation occurs.

Equation 5 for the uniformly distributed load is valid only for calculation of deflections on the load axis. For points off the axis of the load, the integration cannot be carried out analytically, but for layered systems with a stiff top layer, Boussinesq's equation for a point load, Equation 4, will usually give satisfactory results (*3*).

Boussinesq Equations for Stresses

Boussinesq also formulated equations for calculating stresses for a homogeneous, isotropic, linear, elastic semi-infinite space. The use of the method of equivalent thicknesses allows these equations to be used for a multilayer pavement system. For a load uniformly distributed over a certain area as shown in Figure 3b, the normal stresses can be determined using the following equations:

$$\sigma_z = \sigma_0\left\{1 - \frac{1}{[1 + (a/z)^2]^{3/2}}\right\} \quad (6)$$

$$\sigma_r = \sigma_t = \sigma_0\left\{\frac{1 + 2\mu}{2} - \frac{1 + \mu}{[1 + (a/z)^2]^{1/2}} + \frac{1}{2[1 + (a/z)^2]^{3/2}}\right\} \quad (7)$$

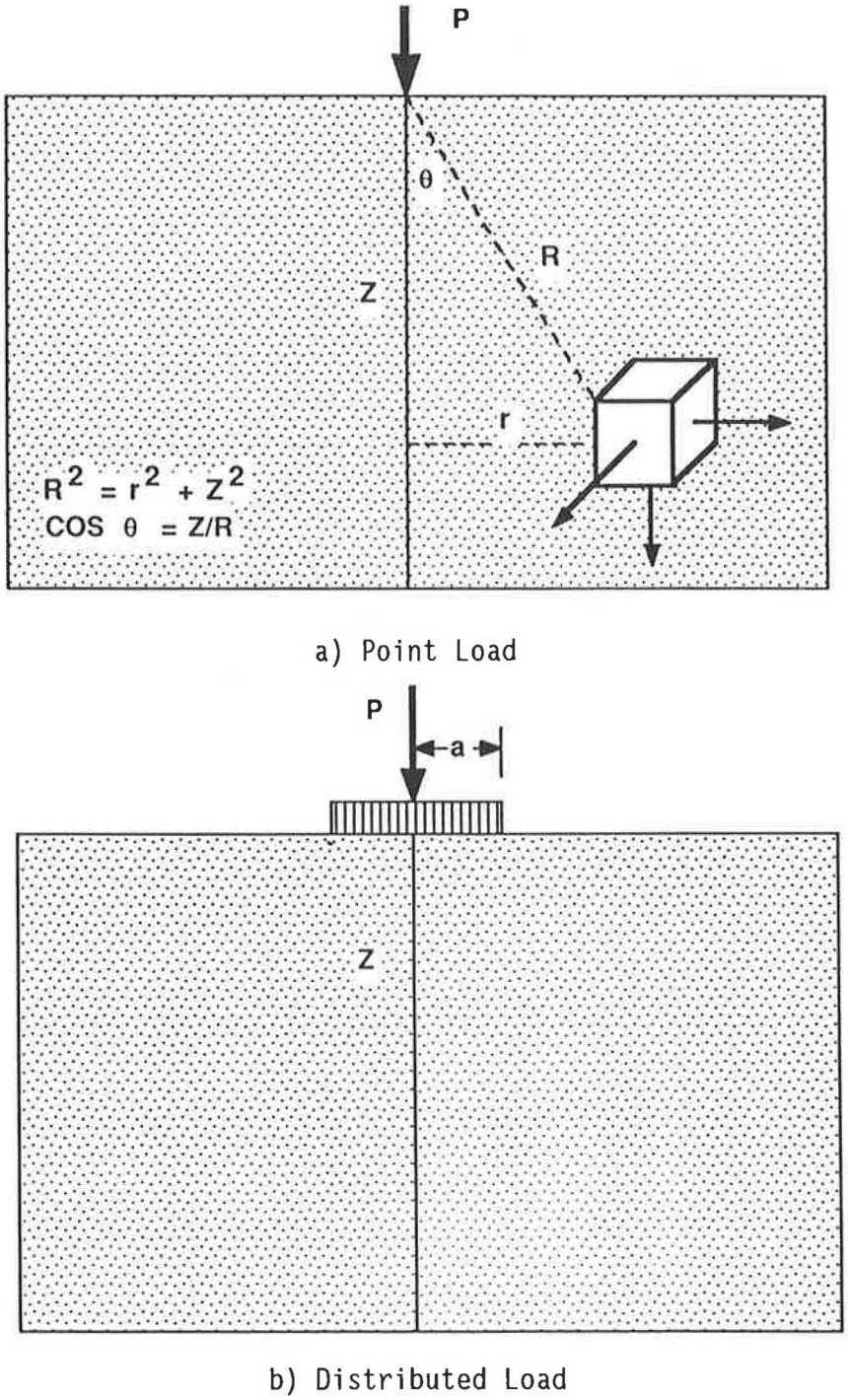

FIGURE 3 Conceptual representation of Boussinesq's half-space loading condition.

where

σ_z = vertical stress, and
$\sigma_r = \sigma_t$ = horizontal stresses.

These equations will be used to calculate stresses induced by loadings.

Correction Factors for Boussinesq Method

The use of the method of equivalent thicknesses allows the Boussinesq theory to be applied in a multilayer system. Stresses, strains, and deformation at any point in an elastic half-space can be determined by using corresponding Boussinesq equations. In order to obtain good agreement between the stresses,

strains, and deflection calculated by the Boussinesq approach and by exact elastic theory, Ullidtz and Peattie (*3*) suggest that correction factors should be applied to the equivalent thicknesses. For the simple case of calculations on the axis of a uniformly distributed load, Equation 3 is modified as follows:

$$h'_{ei} = f \sum_{i=1}^{n-1} h_i \left[\frac{E_i (1 - \mu_n^2)}{E_n (1 - \mu_i^2)} \right]^{1/3} \tag{8}$$

where f is a correction factor; for a two-layer system, $f = 0.9$; for a multilayer system (>2 layers), $f = 1.0$ for the first layer, 0.8 for the rest of the layers.

Additional correction factors are required when using Equation 4 for the point load for more general analysis of deflection, because the assumption that the uniformly distributed load can be approximated by a point load produces inaccuracies near the surface of the pavement. These corrections are as follows (*5*):

$$Z'_i = \frac{1.5a}{2(1 - \mu_i) - [2(1 - \mu_i) - 0.7](Z_i/2a)} \quad Z_i < a \tag{9a}$$

$$Z'_i = Z_i + 0.6 \frac{a^2}{Z_i} \quad Z_i \geq a \tag{9b}$$

where

Z'_i = corrected equivalent thickness for ith layer,
Z_i = h'_{ei}, modified equivalent thickness for ith layer, and
a = load radius.

Consideration of Nonlinearity of Lower Layer Materials

The resilient properties of pavement materials, specially those coarse grained and fine grained, are generally stress dependent. The resilient moduli of the these materials vary according to the stress state within the layers. The moduli of these materials are usually approximated by the following relationships:

$$M_R = k_1 \theta^{k_2} \quad \text{for coarse-grained materials, or} \tag{10a}$$

$$M_R = k_1 \sigma_d^{k_2} \quad \text{for fine-grained materials.} \tag{10b}$$

where

M_R = resilient modulus (psi),
θ = bulk stresses (psi),
σ_d = deviator stress (psi), and
k_1, k_2 = regression coefficients that depend on materials properties.

Most often, these coefficients are determined through laboratory tests.

Consideration of Overburden Stresses

Actual stresses in a pavement structure consist of two parts—load-induced and overburden stresses. For vertical stresses, the overburden pressure is calculated by multiplying the layer thicknesses by their respective densities and summing these to the desired depth. The total vertical stress σ_{vt} is the sum of the load-induced stress σ_{vl} and overburden pressure,

$$\sigma_{vt} = \sigma_{vl} + \sum_{i=1}^{n} h_i \gamma_i \tag{11}$$

where

h_i = thickness of ith layer, and
γ_i = density of ith layer.

The total horizontal stress σ_{ht} is a function of the load-induced horizontal stress σ_{hl} plus horizontal stress due to overburden pressure,

$$\sigma_{ht} = \sigma_{hl} + K_0 \sum_{i=1}^{n} h_i \gamma_i \tag{12}$$

where K_0 is the coefficient of at-rest earth pressure.

These expressions do not include a term for pore water pressure, because pore water pressure is a function of ground water table depth. The assumption is made that the ground water table is at depth below the top of the subgrade and therefore does not affect the results.

The coefficient of at-rest earth pressure K_0 is a function of the angle of friction ϕ for a given soil as determined by a triaxial compression test. For granular soils,

$$K_0 = 1 - \sin \phi \tag{13a}$$

and for fine-grained soils (*6*),

$$K_0 = 0.95 - \sin \phi \tag{13b}$$

Das (*7*) reported an approximate range of ϕ from 25 to 38 degrees for normally consolidated clays and from 26 to 46 degrees for sands. Overall, this represents a range of K_0 from 0.28 to 0.56. For most geotechnical work, when triaxial compression test data are not available, a value of 0.5 is assumed for K_0 (*8*).

DEVELOPMENT OF THE BOUSDEF COMPUTER PROGRAM

Program Flowchart

The BOUSDEF program is developed for determining in situ moduli of a pavement structure using deflection data through a backcalculation technique. Figure 4 shows a flow diagram of the program.

To start with, the program first reads input data sets that include NDT load force and load radius, pavement layer thicknesses, Poisson's ratio, minimum, maximum, and initial modulus, density of pavement materials, deflection data (up to seven sensor readings), percent tolerance to stop the deflection matching process, and number of iterations. By calling the subroutine DEFLECTION, which uses the solution techniques described earlier, the initial modulus and layer thickness information are used to determine the equivalent thick-

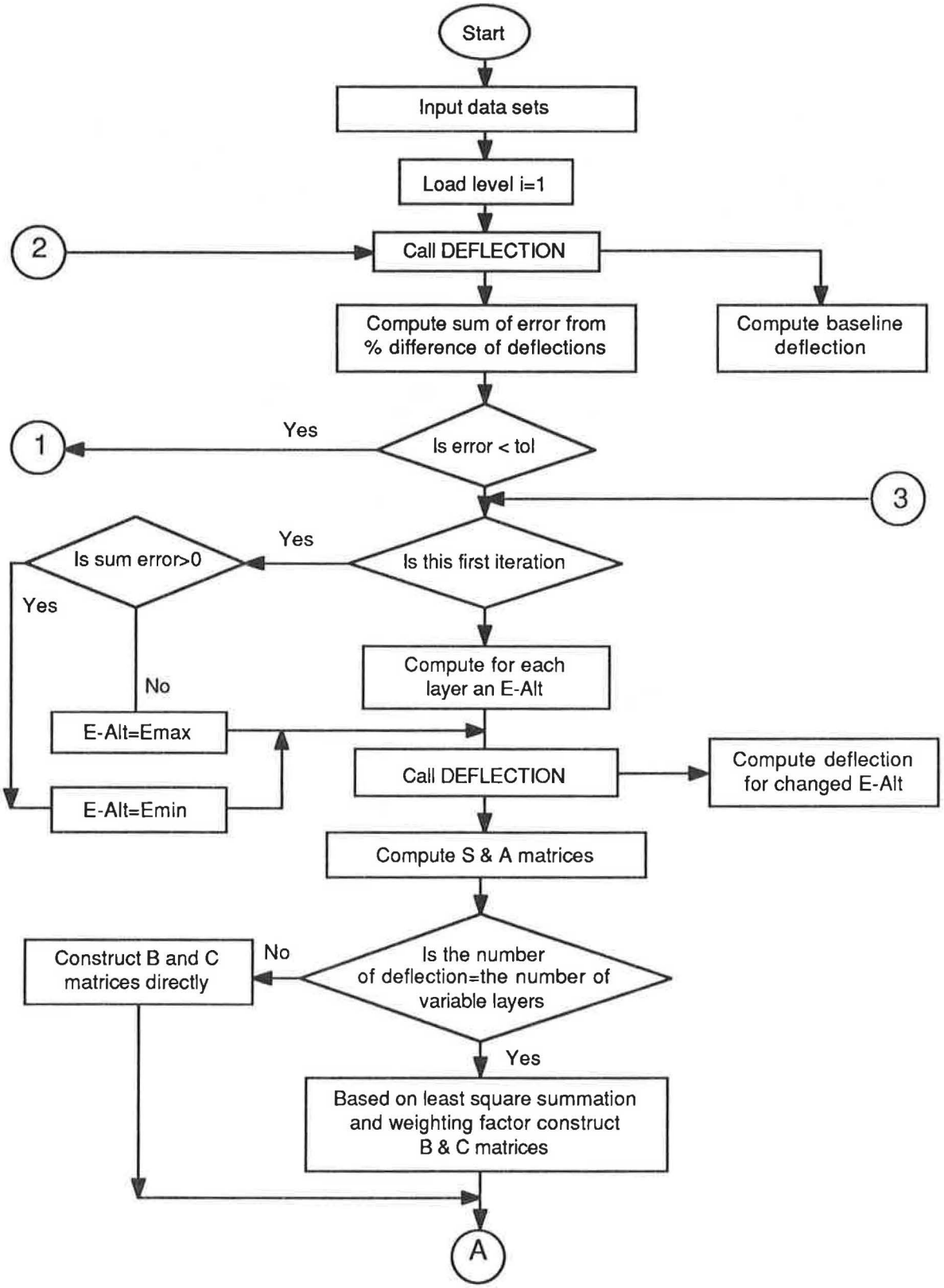

FIGURE 4 Flowchart of BOUSDEF program (*continued on next page*).

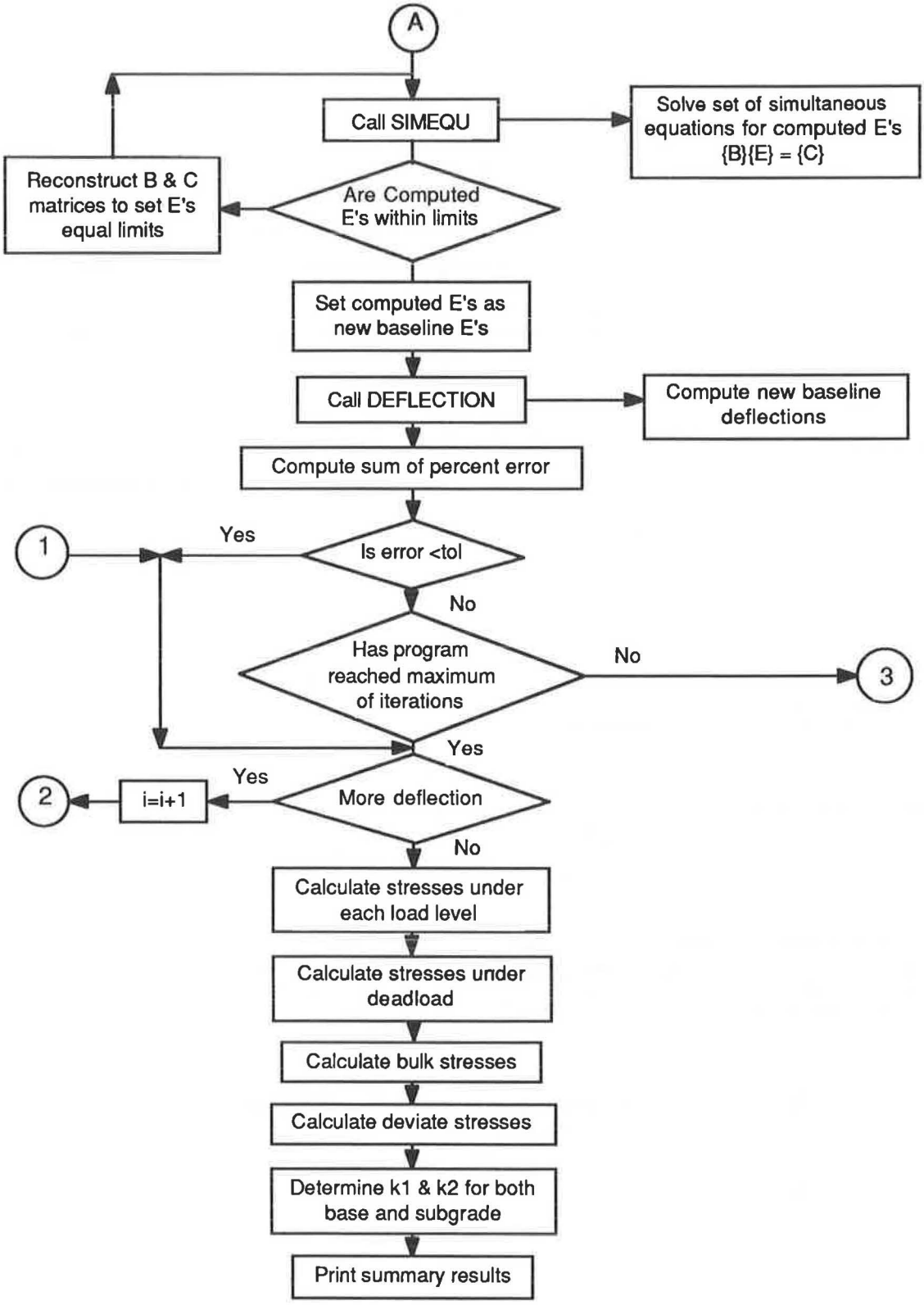

FIGURE 4 *(continued)*

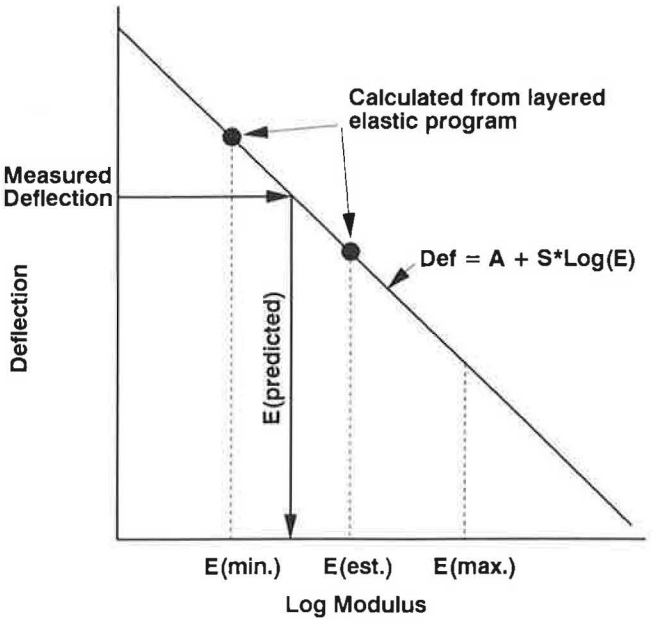

FIGURE 5 Simplified description of deflection matching procedure.

nesses. Deflections for the given NDT load and load radius are then calculated. The calculated deflections are compared to measured deflections. If the sum of the differences is greater than the tolerance specified by the user, the program will start iterations by changing the moduli to compute a new set of deflections.

A simplified description of the deflection matching procedure is shown in Figure 5. This process repeats until the sum of the differences is less than the tolerance or the maximum number of iterations has been reached. This procedure is repeated for each load level until all deflection data are used.

The moduli determined from each set of deflection basin data are used to calculate normal stresses induced by load. Stresses under the deadload of the upper pavement materials are also determined. For the base layer, bulk stresses in the middle of the layer are calculated. For the subgrade, deviator stresses on the top of subgrade are determined. These stress values and moduli are then regressed to find coefficients k_1 and k_2 for both base layer and subgrade.

The backcalculated modulus corresponds to an average condition in the pavement material, whereas the bulk and deviator stresses are calculated under the load at the middle of the base layer and the top of the subgrade rather than through the entire body of the base and subgrade. Therefore, the nonlinear analysis is limited to the stress condition at a specific location rather than at different depths of base and subgrade. Also, the method of equivalent thicknesses or Boussinesq approach is least reliable in predicting horizontal stresses (*3*).

Program Output

The program has the capability of determining the following:

1. Resilient modulus for each pavement layer.
2. Bulk stresses and deviator stresses induced by both load and deadload of upper-layer pavement materials.
3. Coefficients k_1 and k_2 for base and subgrade layers, appearing in Equations 10a and 10b.

Example

An example is provided to illustrate the use of the program. Table 1 presents the pavement and deflection test data for the example. The pavement is a conventional flexible structure with 8-in. asphalt concrete surface, 12-in. aggregate base, and infinite depth of subgrade. Deflection testing was performed using a falling weight deflectometer (FWD) on one short section of a road.

By using the BOUSDEF program, resilient modulus for each pavement layer was determined and presented in Table 2. Bulk stresses in the middle of the base layer and deviator stresses on the top of subgrade are calculated. Regression coefficients k_1 and k_2 for both base and subgrade are also determined. As can be seen in Table 2, both base and subgrade materials appear to have a nonlinear property with $k_2 = 0.58$ for base and -0.13 for subgrade. The results are plotted in Figure 6.

Sensitivity to the User Input

The initial moduli specified by the user seem to have minor effect on the final backcalculated moduli. This feature

TABLE 1 PAVEMENT AND DEFLECTION DATA FOR THE EXAMPLE

Pavement Data

Layer	Thickness	Poisson's ratio	Density (pcf)
AC	8"	0.35	144
Agg. Base	12"	0.40	120
Subgrade	∞	0.40	100

Deflection Data

Load	Sensor 0"	8"	18"	36"	58"
(lbs)	Deflection Readings (mils)				
2789	6.07	4.04	2.41	1.25	0.91
3035	6.59	4.02	2.41	1.37	0.94
3055	6.55	3.89	2.28	1.50	0.94
6521	12.92	8.26	6.47	3.19	1.82
6644	13.18	8.81	7.23	3.53	1.82
6562	13.82	9.57	6.47	3.88	1.72
6521	13.31	8.26	7.10	3.53	1.94
6480	13.05	8.48	5.58	3.65	1.93
6480	13.44	12.72	7.48	5.59	3.50
11442	22.09	14.35	11.92	5.81	3.76
11770	22.48	15.44	13.19	6.38	3.96
11606	23.77	16.74	11.79	6.84	3.83
11442	22.99	14.78	12.68	6.84	3.97
11770	22.35	14.78	10.65	6.84	3.91

Note: Load radius is 5.9 inches

TABLE 2 SUMMARY OF BACKCALCULATION RESULTS FOR THE EXAMPLE

Summary of Non-linear Characteristics of Lower Layers

For base layer: k1= 8069 k2= 0.58
For subgrade: k1= 18687 k2= -0.13

Summary of Moduli and Stresses *

Load (lb)	E(1)	E(2)	E(3)	BSTRS	DSTRS
2,789	106,432	26,911	16,377	7.29	5.59
3,035	83,362	38,107	16,870	8.99	5.76
3,055	74,978	49,985	16,606	9.88	5.59
6,480	104,087	48,343	14,961	16.81	7.75
6,480	399,359	17,074	9,462	7.74	5.96
6,521	117,982	39,666	15,393	15.41	8.01
6,521	99,314	54,258	13,863	17,67	7.44
6,562	142,581	24,546	15,015	12.58	8.40
6,644	158,740	29,287	14,770	13.00	7.96
11,442	117,180	53,092	14,045	27.83	10.55
11,442	100,939	69,773	12,518	31.35	9.65
11,606	136,673	35,135	13,533	23.61	11.16
11,770	156,599	41,680	13,376	24.18	10.46
11,770	105,657	69,787	13,774	31.79	10.18
Average	135,994	42,689	14,326		

* Moduli and stresses are in psi.

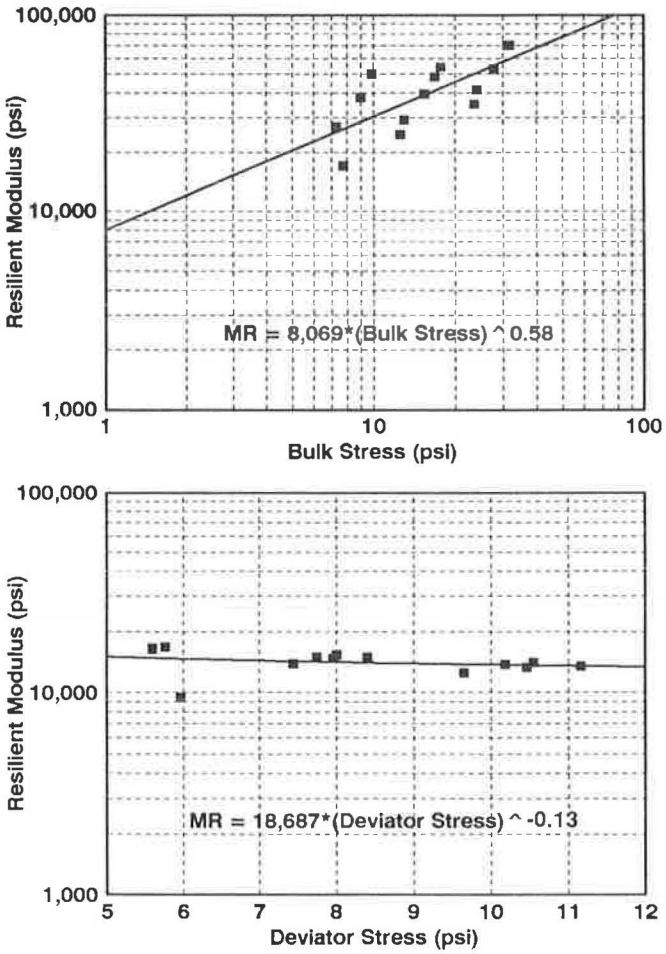

FIGURE 6 Plot of example output.

minimizes the variation in the final moduli caused by the user's input and gives a more reliable solution. An initial evaluation was performed using data presented in Table 3.

Measured deflections for a load of 14,696 lb at loading radius 9.0 in. using the WES Vibrator device were as follows (*1*):

Distance from Load (in.)	*Deflection (mils)*
0.0	6.47
18.0	4.27
36.0	2.34
60.0	1.47

Calculated moduli are presented in Table 4. Apparently, the program provides similar results regardless of what the initial modulus values are.

EVALUATION OF THE BOUSDEF PROGRAM

To evaluate the BOUSDEF program, two approaches were used, (a) comparing backcalculated moduli with theoretical values, and (b) comparing backcalculated moduli with results from other developed programs. The process is described in the following paragraphs.

TABLE 3 DATA USED FOR EVALUATING SENSITIVITY ON INITIAL MODULUS (*1*)

Layer	Thickness	Poisson's Ratio
1	11.0''	0.30
2	15.0''	0.35
3	∞	0.45

Comparison with Theoretical Values

The BOUSDEF program was evaluated by comparing the backcalculated results with hypothesized theoretical values. This comparison is done by assuming a set of pavement structures with different combination of layer thicknesses and different resilient modulus. Among the evaluated pavement structures, as shown in Figure 7, five are conventional pavement systems, with three 3-layer structures and two 4-layer structures. Two pavement systems have a cement-treated base (CTB). Three are portland cement concrete (PCC) pavement structures. To represent typical field conditions, resilient modulus for flexible pavement ranges from 100 to 1,500 ksi. For PCC pavements, typical design values are also used. Poisson's ratio was 0.35 for the AC, 0.4 for the base and subgrade, and 0.15 for the CTB and PCC. Surface deflections for the

TABLE 4 EFFECT OF INITIAL MODULI ON CALCULATED MODULI

Initial Moduli (psi)			Calculated Moduli (psi)		
Surface	Base	Subgrade	Surface	Base	Subgrade
Variation of surface modulus					
200,000	50,000	25,000	768,422	57,228	46,810
300,000	50,000	25,000	768,455	57,248	46,803
400,000	50,000	25,000	768,485	57,248	46,803
500,000	50,000	25,000	764,142	57,702	46,766
600,000	50,000	25,000	764,203	57,693	46,768
700,000	50,000	25,000	764,250	57,689	46,769
800,000	50,000	25,000	772,642	56,432	46,914
900,000	50,000	25,000	769,176	56,987	46,835
1,000,000	50,000	25,000	764,989	57,592	46,791
Variation of base modulus					
500,000	10,000	10,000	728,648	56,086	46,783
500,000	20,000	10,000	739,009	54,808	46,863
500,000	30,000	10,000	738,916	54,843	46,837
500,000	40,000	10,000	738,827	54,860	46,830
500,000	50,000	10,000	738,859	54,845	46,842
500,000	60,000	10,000	738,985	54,813	46,861
500,000	70,000	10,000	728,289	56,131	46,770
500,000	80,000	10,000	735,888	54,997	47,021
500,000	90,000	10,000	740,119	54,560	47,021
500,000	100,000	10,000	739,447	54,540	46,980
Variation of subgrade modulus					
500,000	30,000	10,000	738,916	54,843	46,837
500,000	30,000	20,000	735,079	55,446	46,847
500,000	30,000	30,000	728,013	56,166	46,759
500,000	30,000	40,000	743,267	54,092	46,998
500,000	30,000	50,000	733,450	55,287	47,091
500,000	30,000	60,000	736,109	53,809	48,243
500,000	30,000	70,000	735,286	54,468	47,642
500,000	30,000	80,000	735,390	54,333	47,767
500,000	30,000	90,000	735,356	54,292	47,814
500,000	30,000	100,000	739,984	53,871	47,754

assumed pavement structures were calculated using the method of equivalent thicknesses together with Boussinesq equations. Initial comparison on surface deflections calculated using Boussinesq equations, ELSYM5, and BISAR was made beforehand. The comparison showed that deflections calculated from Boussinesq equations, ELSMY5, and BISAR were similar for conventional and PCC pavements, but not as good for pavements with a stiff base. Thus, Boussinesq equations are valid for computing the surface deflections for the conventional and PCC pavements. Deflections at six radial distances (0, 8, 12, 24, 36, and 58 in.) were calculated for the flexible pavements. For PCC pavements, deflections at seven locations (0, 12, 24, 36, 48, 60, and 84 in.) were computed. The calculated deflection basins were then used as inputs to backcalculate the layer moduli.

Table 5 presents the calculation results. The backcalculated moduli for all structures are close to the theoretical values, indicating the BOUSDEF program has the capability of backcalculating the layer moduli from known deflections, layer thicknesses, and load data. However, the method of equivalent thicknesses is not recommended for pavements with base layers that are stiff compared to the surface (*4*), as mentioned earlier. Pavements with CTB layers were included here to illustrate that BOUSDEF is capable of providing an initial evaluation for such pavements. Alternative means of backcalculation should also be carried out to improve this evaluation.

Comparison with Other Developed Programs

The BOUSDEF program was also compared with four developed programs, BISDEF (*9*), CHEVDEF (*10*), ELSDEF (*1*), and MODCOMP2 (*11*). Pavement data and deflection test data used for the comparison were obtained from a real pavement. Deflections were measured using a KUAB falling weight deflectometer. These data are presented in Tables 6 and 7, respectively. The computed layer moduli for the various programs are presented in Table 8. Results from BOUSDEF are close to those from the other developed programs.

One major advantage of the BOUSDEF program over the other programs is its computational speed. In using a deflection data set presented in Table 3, the BOUSDEF program takes only 3 sec to find the solution, using an IBM AT microcomputer with a math coprocessor. The same data would take significantly longer time using the other programs, as can be seen in Table 9. This feature renders easy the use of the program for evaluating a large amount of deflection data. Furthermore, BOUSDEF is a user-friendly program. The program has a built-in data file creating and editing routine;

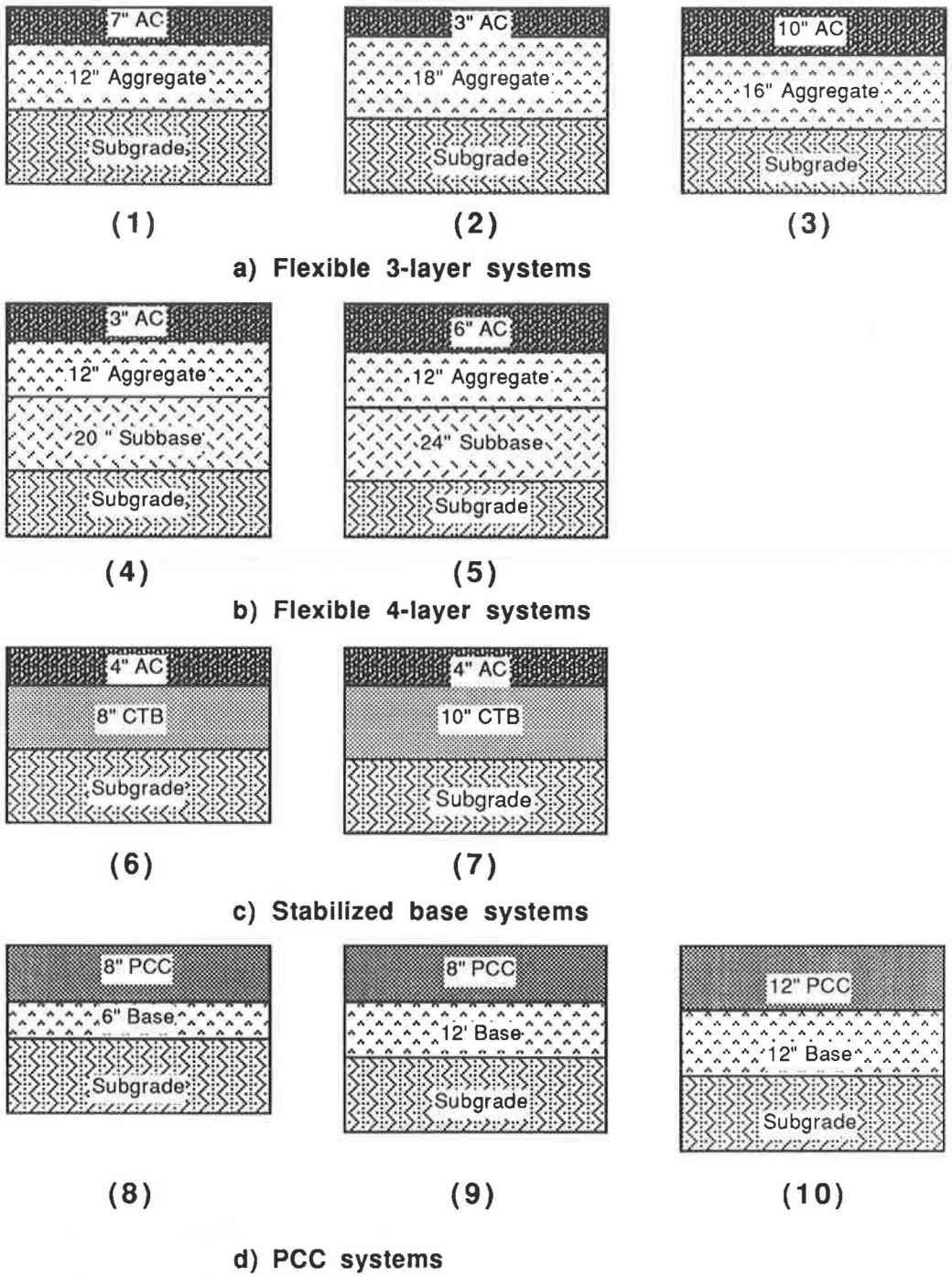

FIGURE 7 Pavement structures used for deflection calculation.

this significantly eases the data input and edit process and avoids possible calculation errors due to improper data entry.

SUMMARY

This paper has presented a microcomputer program for backcalculating the moduli of a pavement structure using deflection basin data. The solution techniques for use in developing the program are described, including use of the method of equivalent thicknesses, Boussinesq theory, consideration of nonlinearity of pavement materials, and consideration of overburden pressure on stress calculation. Evaluation of the program was performed using two approaches: (a) comparing backcalculated moduli with hypothesized theoretical moduli, and (b) comparing backcalculated moduli with those from other developed backcalculation programs. The evaluation shows that the moduli backcalculated using the BOUSDEF program compare well with the theoretical moduli and also are compatible with other developed programs used for comparison.

TABLE 5 COMPARISON BETWEEN THEORETICAL AND BACKCALCULATED VALUES

Pavement Structure	Theoretical Values * 1	2	3	4	5	Backcalculated 1	2	3	4	5
Three-Layer Conventional										
7" AC	100.0	300.0	600.0	1000.0	1500.0	101.9	289.9	602.7	1022.1	1551.1
12" Agg.	25.0	25.0	25.0	25.0	25.0	24.7	25.0	25.1	24.6	24.4
Subgrade	10.0	10.0	10.0	10.0	10.0	10.0	10.1	9.9	9.9	9.9
3" AC	100.0	300.0	600.0	1000.0	1500.0	100.7	310.1	594.3	1017.2	1538.2
18" Agg.	20.0	20.0	20.0	20.0	20.0	20.0	19.8	20.1	19.9	19.8
Subgrade	10.0	10.0	10.0	10.0	10.0	10.0	9.9	9.9	9.9	9.9
10" AC	200.0	600.0	1000.0	1500.0		202.6	615.5	1017.5	1566.5	
16" Agg.	25.0	25.0	25.0	25.0		31.1	31.9	31.6	30.8	
Subgrade	10.0	10.0	10.0	10.0		10.0	9.9	10.1	9.9	
Four-Layer Conventional										
3" AC	300.0	600.0	1000.0	1500.0		357.3	638.8	1024.9	1493.5	
12" Base	25.0	25.0	25.0	25.0		23.6	24.3	24.6	25.0	
20" Subbs	10.0	10.0	10.0	10.0		9.7	10.0	10.0	10.0	
Subgrade	7.0	7.0	7.0	7.0		7.2	7.0	7.0	7.0	
6" AC	100.0	300.0	600.0	1000.0		101.3	298.5	615.6	1027.3	
12" Base	25.0	25.0	25.0	25.0		24.9	25.1	24.0	23.9	
24" Subbs	12.0	12.0	12.0	12.0		12.0	12.0	12.1	12.1	
Subgrade	8.0	8.0	8.0	8.0		8.0	8.0	8.0	8.0	
Cement Treated Base										
4" AC	300.0	600.0	1000.0			294.8	588.3	1158.5		
8" CTB	1200.0	1200.0	1200.0			1216.1	1205.4	1107.7		
Subgrade	10.0	10.0	10.0			10.0	10.0	10.0		
4" AC	300.0	600.0	1000.0			292.7	584.0	1081.8		
10" CTB	1200.0	1200.0	1200.0			1215.0	1225.8	1081.8		
Subgrade	10.0	10.0	10.0			10.0	10.0	10.0		
PCC										
8" PCC	4000.0					4172.8				
6" Base	20.0					21.2				
Subgrade	10.0					9.9				
8" PCC	4000.0					4028.6				
12" Base	20.0					19.8				
Subgrade	10.0					9.9				
12" PCC	4000.0					4015.5				
12" Base	20.0					20.0				
Subgrade	10.0					10.0				

* Moduli are in ksi.

TABLE 6 PAVEMENT DATA USED FOR BACKCALCULATION

Pavement Layer	Material	Thickness (inch)	Poisson's Ratio
1	Asphalt Concrete	9.0	0.35
2	Aggregate Base	16.0	0.40
3	Soil Subgrade	∞	0.40

TABLE 7 DEFLECTION DATA USED FOR BACKCALCULATION

Test Site	FWD Load (lb)	Deflection @ Sensor Location 0"	8"	18"	30"	60"
1	11,729	22.99	16.74	12.81	9.81	4.57
2	11,647	27.39	21.68	14.96	11.06	5.33
3	11,442	20.54	17.28	12.30	9.69	4.90
4	11,073	24.16	20.33	14.08	10.83	5.77
5	11,688	16.28	13.70	8.88	6.95	3.92

Note: FWD Load Radius is 5.9 inches.

TABLE 8 SUMMARY OF BACKCALCULATION RESULTS*

Test Site	Program	AC Surface	Aggregate Base	Subgrade
1	BISDEF	194.0	25.1	11.5
	BOUSDEF	163.0	25.7	11.2
	CHEVDEF	175.8	24.7	12.1
	ELSDEF	200.0	23.6	11.7
	MODCOMP2	162.8	33.4	10.5
2	BISDEF	173.7	15.4	10.5
	BOUSDEF	157.7	15.2	9.9
	CHEVDEF	150.7	16.6	10.5
	ELSDEF	174.0	15.2	10.4
	MODCOMP2	131.5	27.1	9.3
3	BISDEF	288.3	20.1	11.2
	BOUSDEF	262.2	19.3	10.9
	CHEVDEF	257.8	23.3	11.3
	ELSDEF	286.9	20.0	11.3
	MODCOMP2	184.0	50.6	9.3
4	BISDEF	206.4	19.0	9.4
	BOUSDEF	196.5	17.0	9.2
	CHEVDEF	182.3	21.7	9.2
	ELSDEF	205.7	18.9	9.4
	MODCOMP2	431.8	1.0	N/S**
5	BISDEF	259.1	37.7	14.8
	BOUSDEF	266.0	30.5	14.8
	CHEVDEF	260.9	36.4	15.0
	ELSDEF	258.2	37.2	14.8
	MODCOMP2	165.8	89.7	12.9

* Moduli are in ksi.
** N/S = No Solution.

TABLE 9 COMPARISON ON COMPUTING TIME AND BACKCALCULATED RESULTS

PROGRAM	COMPUTED LAYER MODULI (KSI) LAYER 1	LAYER 2	LAYER 3	COMPUTING TIME (SECONDS)
BISDEF*	685.7	55.4	48.8	285
BOUSDEF	764.1	57.7	46.8	3
CHEVDEF	527.8	28.6	29.9	327
ELSDEF	632.1	84.7	34.2	485
MODCOMP2	772.5	35.9	53.0	495

*Contains proprietary BISAR program

The BOUSDEF program runs fast in comparison with other backcalculation programs. Therefore, the program can be effectively used as a tool to make initial evaluation of deflection testing data for determining pavement layer moduli that may further be used for mechanistic analysis of pavement structure and overlay design.

REFERENCES

1. R. L. Lytton, F. L. Roberts, and S. Stoffels. *Determination of Asphaltic Concrete Pavement Structural Properties by Nondestructive Testing*. Final Report, Texas Transportation Institute, College Station, April 1986.
2. *Guide for the Design of Pavement Structures*. AASHTO, Washington, D.C., 1986.
3. P. Ullidtz and K. R. Peattie. Pavement Analysis by Programmable Calculators. *Journal of Transportation Engineering*, ASCE, Sept. 1980.
4. P. Ullidtz. *Pavement Analysis*. Elsevier, 1987.
5. P. Ullidtz. *A Fundamental Method for Prediction of Roughness, Rutting and Cracking of Pavements*. Association of Asphalt Paving Technologists, Vol. 48, 1979, pp. 557–586.
6. E. W. Brooker and H. O. Ireland. Earth Pressure at Rest Related to Stress History. *Canadian Geotechnical Journal*, Vol. 2, No. 1, 1965, pp. 1–15.
7. B. M. Das. *Principles of Foundation Engineering*. Brooks/Cole Engineering Division, Wadsworth, Inc., Monterey, Calif., 1984.
8. D. E. Newcomb. *Development and Evaluation of A Regression Method to Interpret Dynamic Pavement Deflections*. Ph.D. dissertation, University of Washington, Seattle, 1986.
9. A. J. Bush. *Computer Program BISDEF*. U.S. Army, Corps of Engineers, Waterways Experiment Station, Vicksburg, Miss., Nov. 1985.
10. A. J. Bush. *Nondestructive Testing of Light Aircraft Pavements, Phase II, Development of the Nondestructive Evaluation Methodology*. Final Report FAA-RD-80-9-II, FAA, U.S. Department of Transportation, Washington, D.C., Nov. 1980.
11. L. H. Irwin. *User's Guide to MODCOMP2*. Report 83-8, Cornell University Local Roads Program, Ithaca, N.Y., Nov. 1983.

Publication of this paper sponsored by Committee on Strength and Deformation Characteristics of Pavement Sections.

MODULUS: A Microcomputer-Based Backcalculation System

T. SCULLION, J. UZAN, AND M. PAREDES

MODULUS is a microcomputer-based backcalculation system that can be used on 2-, 3-, or 4-layer pavement systems with or without rigid bedrock layers. It uses a linear elastic program to generate a data base of deflection bowls. Once generated, a pattern search routine is used to fit measured and calculated bowls; error minimization is rapid, less than 5 sec per bowl on a 386 type microcomputer. The system is general purpose and can process data from any nondestructive testing device. The user has several options when performing backcalculations, including specifying the depth to bedrock or using existing default data bases for common pavement structures. Outputs include a summary listing showing the mean and variances of moduli values and also a graphical output that plots moduli values along a project and automatically performs subsectioning according to the recommended AASHTO procedure. The MODULUS system is described together with discussion on continuing efforts to validate the moduli values. These validations include (a) comparison of laboratory and field moduli values, and (b) the use of multidepth deflectometers to monitor deflections within the pavement system. The results of monthly deflection measurements on experimental pavements around the state of Texas are also described. Finally, current efforts to improve the MODULUS system are described. These attempts include automatically estimating the depth to bedrock using either the error minimization or zero deflection approach.

In order to assist the engineer in the pavement analysis process, an efficient procedure must be developed that permits modulus backcalculation from surface deflection data and allows review of the data to determine if subsectioning is required. One such microcomputer-based procedure is called "MODULUS" (*1*,*2*). MODULUS uses a linear elastic program to generate a data base of computed deflection bowls, before fitting the measured bowls. Once the data base is generated for a particular pavement, the linear elastic program is not called again, no matter how many bowls are to be analyzed. Therefore, the data base can be generated before testing, and the measured bowls can be processed in real time. The procedure as described in later sections makes use of the properties of the linear elastic solution by working in terms of modular ratios. It can handle a 2-, 3-, or 4-layer problem; in the case of a 4-layer problem, the elastic layer program is automatically run at least 27 times (3 surface × 3 base × 3 subbase modular ratios) to generate the required data base. A pattern search routine is used to fit the measured and calculated bowls.

The data base concept has an advantage over existing programs such as CHEVDEF (*3*), which calls the linear elastic deflection program (NLAYER + 1) * ITER + 1 times for each bowl, where NLAYER is the total number of layers and ITER is the user-specified number of convergence iterations. In the case of a 4-layer system, the CHEVDEF program with ITER = 3 would require 16 runs of the linear elastic program per bowl, whereas the MODULUS program would require only 27 runs independent of the number of bowls to be analyzed. MODULUS has been designed for the highway environment for which many deflection bowls are measured at regular intervals along a project.

A review of the theoretical background to the MODULUS backcalculation procedure is contained in the following section; the next section contains an overview of the system itself, including options available to the user in inputting data, performing backcalculations, and displaying results; the next section contains some case studies conducted in Texas with comparison of field and laboratory E values; the last section describes attempts to validate backcalculated values using instruments buried in pavements. (Multidepth deflectometers were used for this purpose and this approach looks extremely promising. Current activities to automatically locate bedrock are also presented in this section.)

THEORETICAL BACKGROUND

The theoretical background includes the following formulation of the objective function and convexity test. [More details may be found in the literature (*1*,*2*).]

Formulation of the Objective Function

The procedure is to find the set of parameters that corresponds to the best fit of the measured deflection bowl. The best fit is achieved by minimizing the error between the measured and calculated deflection bowl. The objective function to be minimized is therefore written as

$$\varepsilon^2 = \sum_{i=1}^{s} \left(\frac{W_i^m - W_i^c}{W_i^m} \right)^2 \mathrm{We}_i \qquad (1)$$

where

ε^2 = squared error,
W_i^m = measured deflection at sensor i,
W_i^c = computed deflection at sensor i,
s = number of sensors, and
We_i = user-supplied weighing factor for sensor i.

T. Scullion and M. Paredes, Texas Transportation Institute, College Station, Tex. 77843. J. Uzan, Technion, Israel Institute of Technology, Haifa, Israel 32000.

Equation 1 can also be written as

$$\varepsilon^2 = \sum_{i=1}^{s} \left(1 - \frac{W_i^c}{W_i^m}\right)^2 \mathrm{We}_i \quad (2)$$

The unknown variables are those required to compute the surface deflections W_i^c, i.e.,

$$W_i^c = F_i(X_j) \qquad j = 1, 2, 3, \ldots n \quad (3)$$

where X_j are n unknown variables.

Any solution to Equation 2 calls for a solution of Equation 3, which is obtained numerically in most cases by running a separate program (such as BISAR and CHEVRON in the case of linear elasticity and ILLI-PAVE in the case of nonlinear elasticity). The number of calls depends on the minimization algorithm used. In the case of linear elasticity, the computed deflection W_i^c at sensor i (or radial distance r_i) can be expressed as follows:

$$W_i^c = f_i(E_k, \nu_k, h_k, r_i, O)$$

$$i = 1, 2, \ldots s; \qquad k = 1, 2, \ldots n. \quad (4)$$

where

E_k = modulus of elasticity for layer k,
n = number of layers,
ν_k = Poisson's ratio for layer k,
h_k = thickness of layer k, and
O = other variables, such as pressure, contact area, radius, interface conditions.

In backcalculation, all variables except E_k are either assumed or known, and the moduli are the only variables to be determined.

In the case of linear elasticity and a circular contact area, Equation 4 can be written as

$$W_i^c = \frac{p}{E_{sg}} f^i\left(\frac{E^1}{E_{sg}}, \ldots, \frac{E^k}{E_{sg}}, \ldots, \frac{E^n}{E_{sg}}\right) \quad (5)$$

where

p = pressure (psi), and
E_{sg} = subgrade modulus of elasticity (ksi).

Equation 5 represents a unique property of linear elasticity in that the deflection is (a) linearly related to load level, (b) inversely proportional to subgrade modulus, and (c) a function of the modular ratios.

From Equations 2 and 5, it is possible to obtain a direct solution for the subgrade modulus E_{sg}, by taking derivatives of Equation 2 with respect to E_{sg} and equating them to zero to minimize the squared error. Details of the derivation are given in the literature (*1*,*2*), and the calculated solution for E_{sg} is shown in Equation 6.

$$E_{sg} = \frac{pf_1 \sum_{i=1}^{s} f_i^2 \mathrm{We}_i / f_1^2 (W_i^m)^2}{\sum_{i=1}^{s} f_i \mathrm{We}_i / f_1 W_i^m} \quad (6)$$

Although Equation 6 can be simplified, this normalized form is preferred for data processing. Equation 6 provides a direct method for estimating subgrade modulus E_{sg} from the data base of normalized f_i/f_1 deflection values. This data base is built from multiple runs of the linear elastic program. Each run corresponds to a set of modular ratios E_k/E_{sg}. Therefore, an E_{sg} can be calculated for each set of $f_i(E_k/E_{sg})$. In order to decide which solution minimizes the error, it is necessary to calculate the squared error associated with each set of modular ratios using an expanded version of Equation 2.

$$\varepsilon^2 = \sum_{i=1}^{s} \left(1 - \frac{pf_i}{E_{sg} W_i^m}\right)^2 \mathrm{We}_i \quad (7)$$

where E_{sg} is the particular solution of Equation 6 corresponding to the given modular ratio, and p is the actual pressure under which the W_i^c values were calculated. By locating the minimum squared error from Equation 7, a seed value of E_{sg} is selected, and the corresponding seed values of E_{BASE} and $E_{SURFACE}$ are calculated. These seed values are used as input to the pattern search routine.

In the MODULUS system, the Hookes-Jeeves pattern search algorithm is used to find the set of moduli values that minimize error (*4*). This algorithm is known always to converge (sometimes to a local minimum), unlike other algorithms, which may not converge. The possibility of a local minimum is evaluated by a convexity test as described in the next subsection.

Convexity Test

This test involves evaluating the shape of the error surface through the minimum error solution. This test is illustrated with the aid of an example. Table 1 shows the calculated E_{sg} and ε^2 values from Equations 6 and 7, for a range of modular ratios for a particular pavement and input deflection bowl. Figure 1 shows a three-dimensional representation of the error surface. The minimum error occurs at modular ratios $E_1/E_{sg} = 30$, $E_2/E_{sg} = 3$, $E_{sg} = 35.7$ ksi. (These values are used as input seed values for the pattern search routine.) The two-dimensional plot of the error surfaces through the minima are shown in Figure 2. In both cases, the surface is convex and the solution passes the convexity test.

Figure 3 shows an error surface that fails the convexity test. If the slope of the error surface changes, then the error surface

TABLE 1 CALCULATED E_{sg} AND ε^2 FOR EACH MODULAR RATIO FOR A PARTICULAR PAVEMENT TYPE AND INPUT FWD DEFLECTION BOWL

E_1/E_{sg}	E_2/E_{sg}	[a]E_{sg} (ksi)	[b]ε^2
10	1	43.2	0.4496
30	1	39.7	0.1902
100	1	36.9	0.0367
10	3	36.8	0.0230
30	3	35.7	0.0213
100	3	34.7	0.0269
10	10	34.9	0.0866
30	10	34.4	0.153
100	10	33.9	0.231

[a]From Equation 6.
[b]From Equation 7.

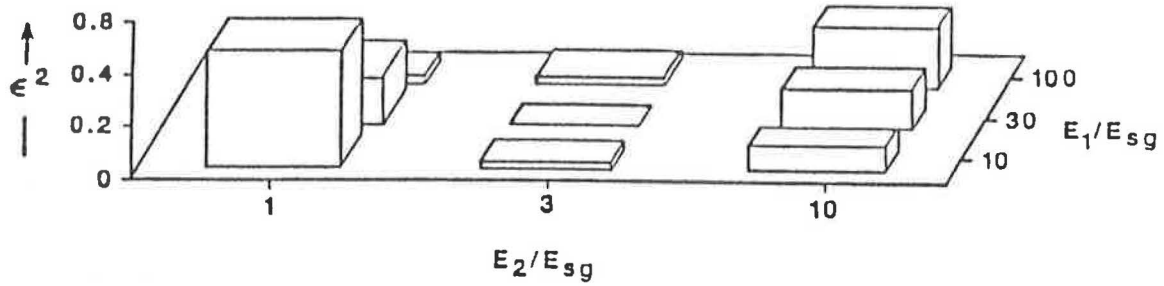

FIGURE 1 Three-dimensional representation of the error surface from Table 1.

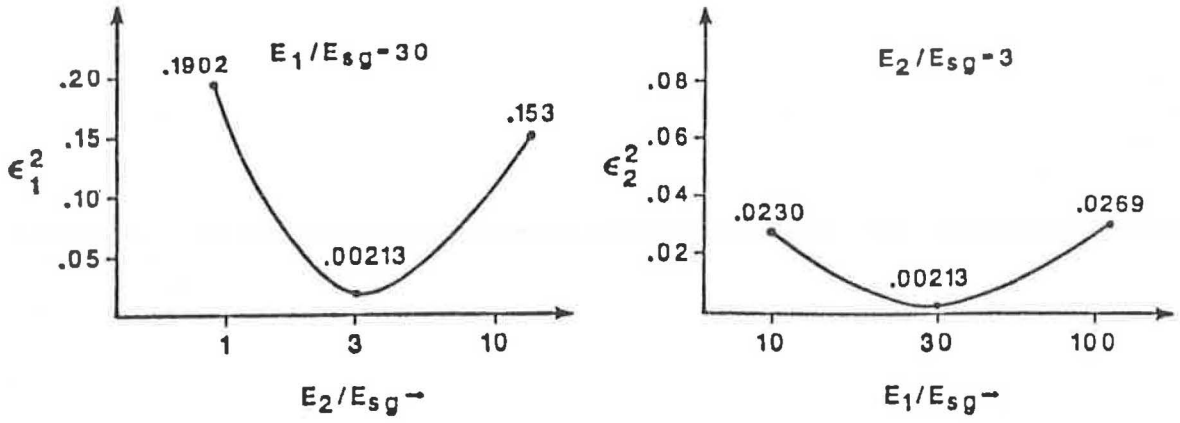

FIGURE 2 Two-dimensional representation of error surface through minimum.

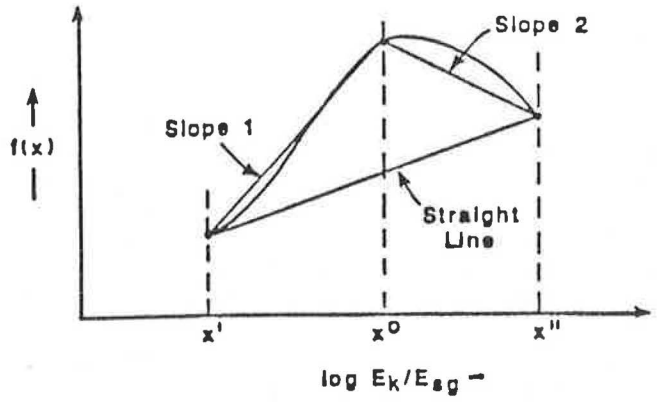

FIGURE 3 Error surface that fails convexity test.

is not convex and MODULUS prints the warning message "failed convexity test." This message implies that increasing the range of acceptable moduli values will possibly result in a lower minimum error.

DESCRIPTION OF THE MODULUS SYSTEM

The MODULUS system is shown schematically in Figure 4. The system has three major subsystems, which are described in the following paragraphs. When running MODULUS, the Main Menu shown in Figure 5 prompts the user to select one of them.

Subsystems

Subsystem 1: Convert FWD Data to Input Data. This subsystem inputs the field diskette from a Dynatest FWD and converts it into a format compatible with the backcalculation subsystem (the .OUT file). Typically during testing, between 1 and 4 drops are made at regular intervals along the highway. The drops may be at a fixed load or at increasing loads. This subsystem requires the user to specify which of these drops are to be included in the analysis. For example, all drop number 2s may be extracted for analysis. For any other NDT device, the .OUT file must be input manually into the required file format.

Subsystem 2: Run MODULUS Backcalculation. The user has the following three options for doing the backcalculation:

- *Option 1—Use an Existing Fixed Design.* The system has built into it 24 default data bases of commonly found pavement types (12 types × 2 depths to a rigid layer), as shown in Figure 6. The users have the option of replacing these default data bases with their own (created using Option 3). In Option 1, the linear elastic program is not run. Only the search routine is used to match the calculated deflections in the data base with the input field deflections.
- *Option 2—Input Material Types.* This option was developed for the inexperienced user who is unfamiliar with backcalculation procedures. The user simply inputs material types, thicknesses, and test temperature, as shown in Figure 7, for example. The system then selects ranges of acceptable moduli values and reasonable Poisson's ratios. In Option 2, the linear

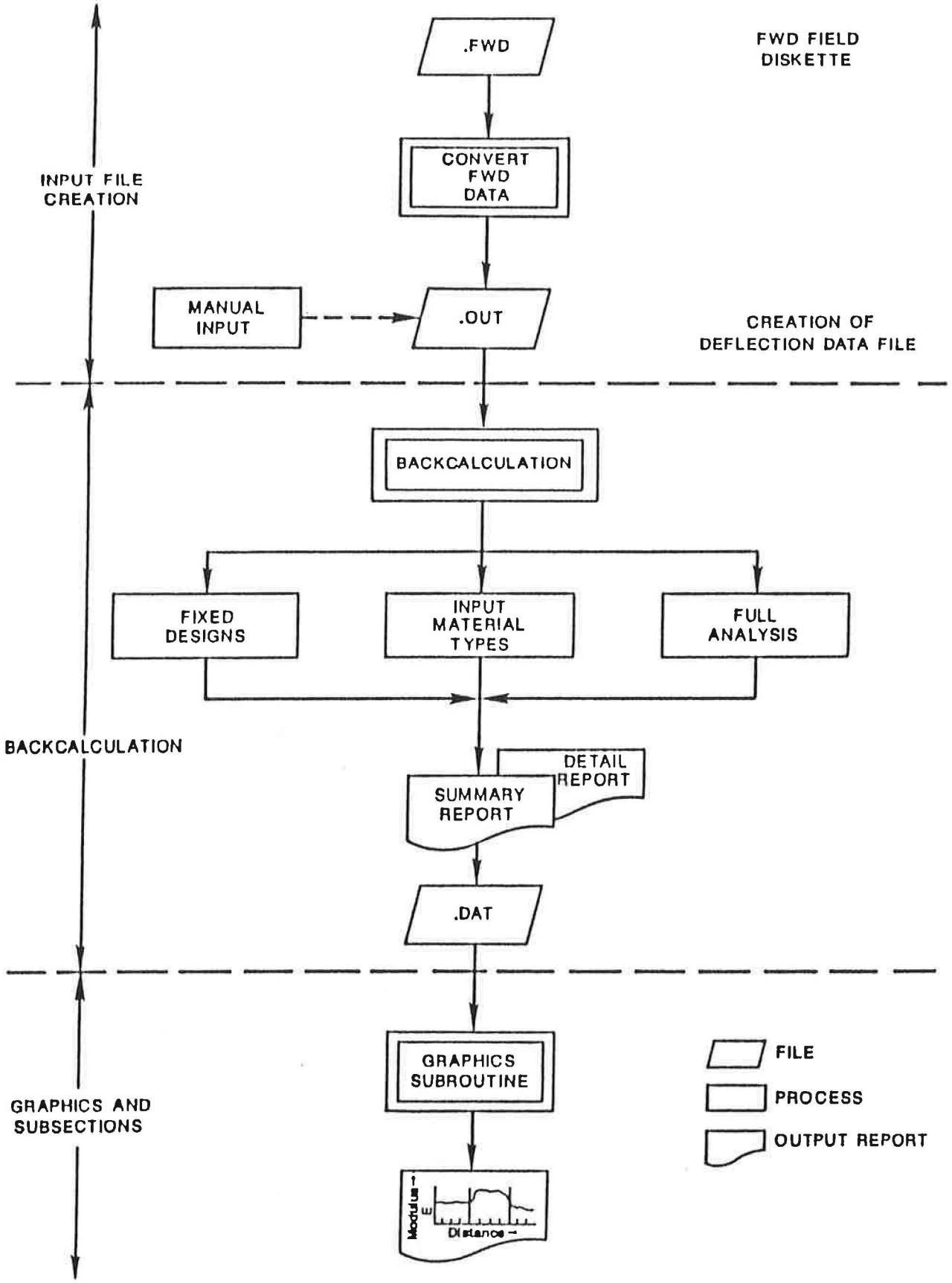

FIGURE 4 MODULUS system flowchart.

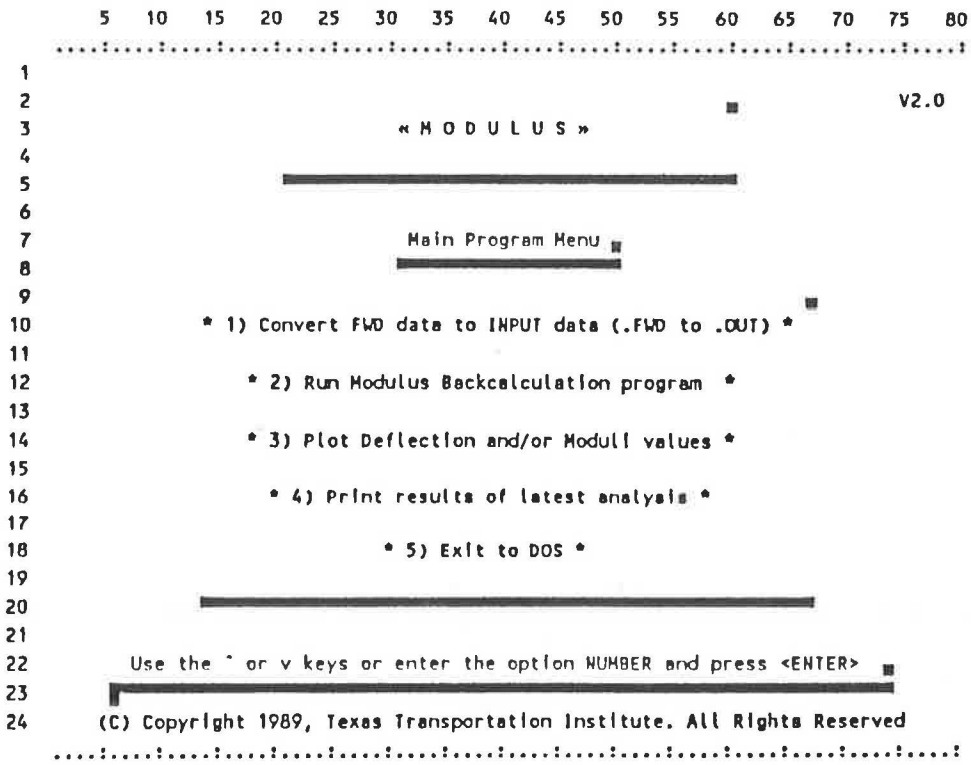

FIGURE 5 Main menu screen from MODULUS.

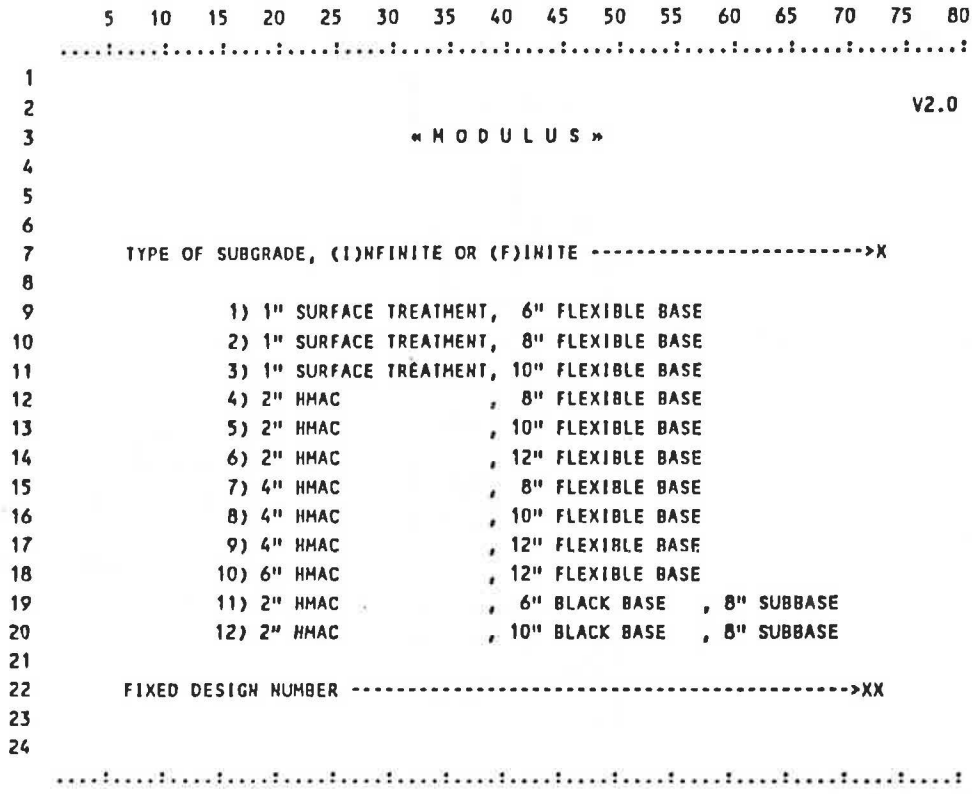

FIGURE 6 Existing data bases within MODULUS backcalculation Option 1.

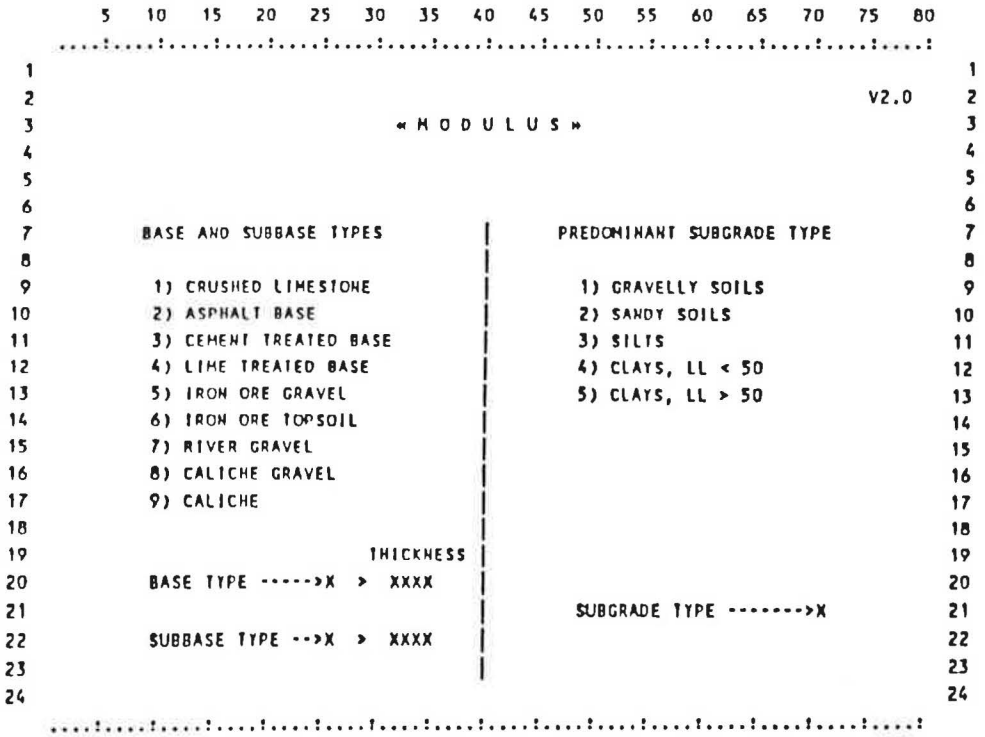

FIGURE 7 A MODULUS input screen for backcalculation Option 2.

elastic program is run to generate a deflection data base before the pattern search routine.

- *Option 3—Run a Full Analysis.* This option is for the experienced user. As shown in Figure 8, the user supplies all the layer thicknesses including depth to bedrock (H4), sensor spacing, and the acceptable ranges of layer moduli.

Once the analysis is complete, a summary or detailed listing of the backcalculated E values is produced. A typical summary listing is presented in Table 2. This table presents the results of the analysis of multiple drops taken at the same spot. The last column in this table is the average error between measured and computed deflection bowls. The percentage error calculation, convexity test results, and other items are available on request in a detail output.

Subsystem 3. Plot Deflection and Moduli Values. The results of the backcalculation process are displayed graphically in this subsystem. An example is shown in Figure 9. MODULUS also uses the cumulative difference method of the *AASHTO Design Guide* (*5*) to perform subsectioning. Mean and standard deviation of moduli values are produced for each subsection identified.

System Requirements

MODULUS occupies approximately 300 kB and minimum system requirements are as follows:

- IBM AT or compatible microcomputer
- 640 kB RAM
- DOS 3.0 or later
- Math co-processor chip 80287 (or equivalent)
- A hard disk
- EGA graphics card with 256 kB of screen memory and a compatible RGB monitor

It is recommended that an advanced microcomputer (286 or 386) be used to minimize execution time. Time estimates for running a simple 3-layer system (surface, base, and semi-infinite subgrade) are shown below:

Machine	*Generate Deflection Data Base (sec)*	*Search Routine (sec/bowl)*
286/12 MHz	258	6.5
386/20 MHz	57	1.8

The time to generate the data base increases as the number of layers and range of acceptable moduli values increase.

CASE STUDIES USING MODULUS

In this section, the following four applications of the MODULUS backcalculation system are presented:

1. Comparison with BISDEF.
2. Analysis of multiple drops at the same location.
3. Effects of depth to rigid layer.
4. Seasonal variations in backcalculated moduli.

All of the deflection data used were collected with a Dynatest FWD.

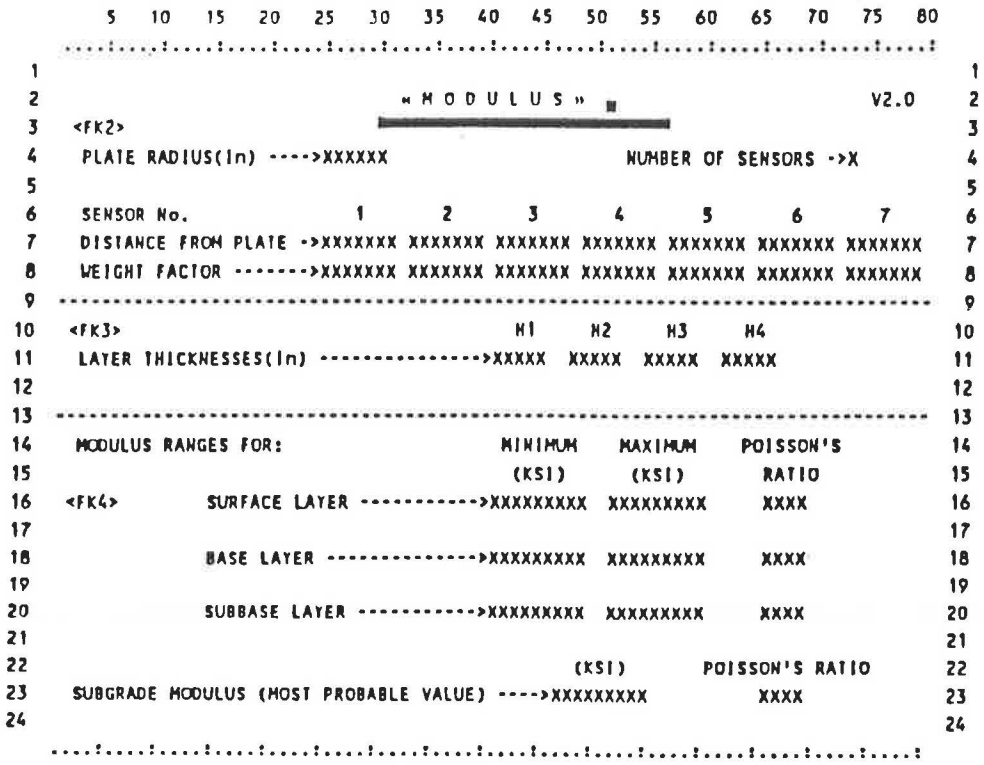

FIGURE 8 A MODULUS input screen for the full analysis option.

TABLE 2 MODULUS OUTPUT FROM MULTIPLE DROPS AT THE SAME LOCATION

TTI DEFLECTION ANALYSIS SYSTEM

District: 17
County: 21
Highway/Road: TTIAMI

	Thickness(in)	MODULI RANGE(psi) Minimum	Maximum
Pavement:	5.00	200,000	800,000
Base:	8.00	30,000	200,000
Subbase:	0.00	0	0
Subgrade:	INFINITY	30,000	

Station	Load (lbs)	Measured Deflection (mils): R1	R2	R3	R4	R5	R6	R7	Calculated Moduli values (psi): SURFACE(E1)	BASE(E2)	SUBBASE(E3)	SUBGRADE(E4)	Absolute I ERROR/Sensor
9.010	9,167	9.34	5.49	3.08	2.08	1.71	1.26	0.83	484,287	71,425	0	35,045	4.31
9.020	8,815	8.85	5.40	3.08	2.12	1.63	1.30	1.05	461,041	89,276	0	32,408	1.93
9.030	8,791	8.73	5.36	3.08	2.12	1.63	1.26	1.01	511,722	83,816	0	32,739	1.66
9.040	8,775	8.69	5.40	3.08	2.08	1.63	1.26	1.01	547,717	79,214	0	32,772	2.00
9.050	8,751	8.73	5.40	3.08	2.12	1.63	1.26	1.01	529,906	80,526	0	32,566	1.74
9.060	8,679	8.61	5.36	3.04	2.08	1.63	1.26	1.01	528,668	82,394	0	32,503	2.16
9.070	8,695	8.61	5.40	3.08	2.08	1.59	1.26	1.05	558,059	79,195	0	32,380	1.84
9.080	8,719	8.61	5.36	3.08	2.08	1.63	1.26	1.01	548,575	81,009	0	32,576	1.96
9.090	8,871	8.90	5.45	3.12	2.12	1.63	1.30	1.05	491,264	84,334	0	32,507	1.76
9.100	8,735	8.73	5.40	3.08	2.12	1.67	1.22	0.93	604,100	69,802	0	33,149	2.97
9.110	8,719	8.73	5.40	3.08	2.12	1.67	1.26	0.97	534,908	78,841	0	32,584	2.63
9.120	8,663	8.65	5.40	3.08	2.12	1.63	1.26	0.97	576,865	75,029	0	32,485	2.27
Mean:		8.77	5.40	3.08	2.10	1.64	1.26	1.00	531,426	79,572	0	32,810	2.27
Std. Dev:		0.20	0.04	0.02	0.02	0.03	0.02	0.05	40,243	5,469	0	734	0.75
Var Coeff(%):		2.31	0.69	0.55	0.98	1.84	1.63	4.94	7.57	6.87	0.00	2.24	33.08

TABLE 5 TYPICAL DEFLECTION DATA FROM ONE SITE IN TTI STUDY 1123

DISTRICT: 21 SITE: 5 HIGHWAY: FM 1425 SOUTH MP 3

MONTH	TIME		LOAD	W1	W2	W3	W4	W5	W6	W7	M1	M2	TS	T1	T2
OCT	AM	LOW	9664	21.33	13.98	7.96	5.20	3.93	3.12	2.57	0.000	-0.131	0.0	87.0	87.0
		HIGH	9552	24.52	16.71	9.57	5.92	4.25	3.28	2.69					
		NORM	9000	22.10	14.87	8.61	5.44	4.03	3.12	2.56					
OCT	PM	LOW	9344	26.80	15.13	8.12	5.36	4.13	3.28	2.69	0.000	-0.131	0.0	98.0	89.0
		HIGH	9336	30.89	18.46	9.77	5.96	4.33	3.40	2.69					
		NORM	9000	27.15	16.60	8.95	5.67	4.16	3.25	2.62					
NOV	AM	LOW	9672	20.66	14.57	8.80	5.56	4.29	3.16	2.77	-0.136	-0.195	98.0	83.0	83.0
		HIGH	9608	24.12	16.83	9.97	6.24	4.41	3.40	2.69					
		NORM	9000	21.56	15.19	9.08	5.72	4.09	3.17	2.56					
NOV	PM	LOW	9472	23.93	14.61	8.20	5.36	4.09	3.20	2.65	0.000	-0.195	104.0	94.0	85.0
		HIGH	9352	27.43	17.23	9.57	5.96	4.37	3.40	2.77					
		NORM	9000	25.47	16.28	9.14	5.71	4.17	3.23	2.61					
DEC	AM	LOW	9808	20.34	15.09	9.77	6.32	4.41	3.40	2.65	0.000	-0.109	92.0	77.0	76.0
		HIGH	9776	23.41	17.03	10.53	6.55	4.53	3.48	2.77					
		NORM	9000	19.67	14.34	9.04	5.80	4.12	3.16	2.50					
DEC	PM	LOW	9600	20.23	13.47	8.04	5.36	4.05	3.20	2.61	-0.111	-0.109	89.0	92.0	90.0
		HIGH	9576	24.00	16.32	9.69	6.12	4.41	3.44	2.73					
		NORM	9000	20.90	14.57	8.99	5.80	4.19	3.22	2.57					
JAN	AM	LOW	7728	9.29	7.53	5.59	4.01	3.02	2.32	1.82	-0.847	-0.045	55.0	55.0	60.0
		HIGH	7728	10.15	8.32	6.15	4.49	3.22	2.48	1.94					
		NORM	9000	11.56	9.57	7.13	5.10	3.77	2.86	2.25					
JAN	PM	LOW	10288	13.42	10.89	8.00	5.68	4.21	3.24	2.57	-1.584	-0.066	58.0	57.0	60.0
		HIGH	10392	14.84	12.32	9.25	6.59	4.85	3.64	2.81					
		NORM	9000	12.47	10.29	7.65	5.48	3.97	3.00	2.32					
FEB	PM	LOW	10096	16.53	12.63	8.64	5.88	4.29	3.28	2.65	-1.355	-0.023	75.0	63.0	63.0
		HIGH	10056	18.61	14.73	10.33	6.95	4.93	3.60	2.89					
		NORM	9000	15.85	12.57	8.81	5.97	4.24	3.15	2.51					
MAR	AM	LOW	9656	24.75	17.66	10.61	6.63	4.65	3.52	2.85	-0.822	0.000	109.0	82.0	78.0
		HIGH	9464	26.99	18.81	10.97	6.71	4.73	3.60	2.89					
		NORM	9000	24.91	17.36	10.28	6.36	4.51	3.44	2.78					
MAR	PM	LOW	9488	25.58	16.36	9.41	5.96	4.41	3.40	2.73	0.000	0.000	108.0	92.0	80.0
		HIGH	9376	29.28	18.93	10.85	6.79	4.93	3.76	3.04					
		NORM	9000	27.05	17.90	10.22	6.33	4.50	3.43	2.73					

NOTE: M=moisture sensors (in bars), TS=surface temperature, T=thermocouples (°F) at bottom of asphalt and base.

tests on the asphalt and triaxial tests on the base and subgrade. The base samples were remolded to approximately the same moisture content and density as found in the field.

A summary of the first 6 months' deflection data collected on this site is presented in Table 5. On average, eight drops at four different load levels were made per site per visit. This table shows the high, low, and normalized average deflection bowls for the drop closest to 9,000 lb. These normalized deflections for this site were processed through the MODULUS system with results as shown in Figures 11 and 12.

Figure 11 shows the backcalculated E value of the asphalt layer plotted against the temperature at the bottom of the asphalt at the time of testing. Also included on this figure are the laboratory determined stiffness values from Figure 10. The laboratory data were collected with the diametrical resilient modulus device, at loading times of 50 and 100 ms. The FWD loading time is approximately 28 ms. There appears to be good agreement between measured and calculated surface moduli for this site.

The variation in calculated subgrade modulus throughout the year is shown in Figure 12. The peak value corresponds to the January data when the pavement was at its coldest.

CURRENT ACTIVITIES TO IMPROVE SYSTEM

The current activities are focused on (a) using pavement instrumentation to validate backcalculated moduli values, and

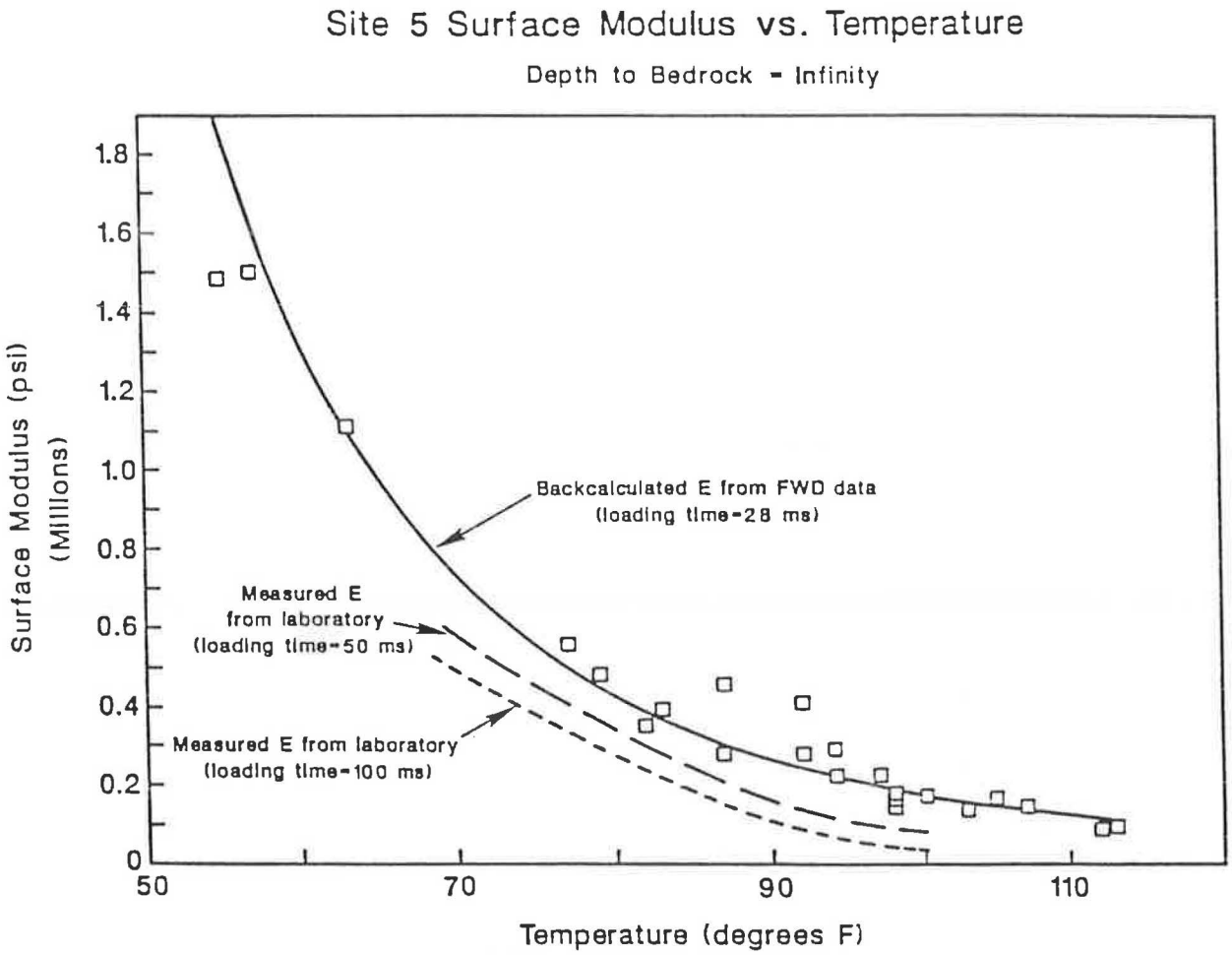

FIGURE 11 Comparison of backcalculated and measured moduli for asphalt surfacing on Site 5.

(b) efforts to automatically locate depth to bedrock. Both of these are discussed in the following paragraphs.

Instrumentation

The best procedure for validating backcalculation results is by using pavement instrumentation. Because it is impossible to replicate field conditions in the laboratory, it is unlikely that any correspondence exists between laboratory- and field-derived E values. The Texas Transportation Institute has been evaluating a multidepth deflectometer (*6*,*7*). By simultaneously taking surface and depth deflections, it is possible to validate backcalculated E values. On thick pavements (5 in. of asphalt over 24 in. of granular base), good agreement was found (*7*) on moduli values calculated independently from surface and depth deflections. Work in this area is continuing.

Depth to Bedrock

Table 4 highlighted the significant influence bedrock has on the backcalculated E values. Two approaches are being evaluated to automatically detect bedrock from the deflection data:

1. Plotting outer sensor deflections (Sensors 5, 6, 7) against the inverse of the radial distance and extrapolating the line to the zero deflection point. Assuming the outer sensors are only affected by the subgrade, then a point of zero surface deflection could indicate the depth of a rigid layer.
2. By rerunning MODULUS using different depths to bedrock and searching for the minimum error condition.

Field tests are under way to evaluate if either of these improve the estimation of layered elastic properties.

CONCLUSIONS

MODULUS is a user-friendly backcalculation system that should assist engineers in their pavement analysis studies. The system has already been prereleased to several state departments of transportation and some consultants. Their recommendations were included in the final system that is ready for release by NCHRP. The system produces results similar to those of existing programs, such as CHEVDEF, but has several additional features that should benefit, such as graphic outputs and subsectioning.

More work is required in the area of correlating laboratory results and field backcalculations. The preliminary subgrade correlations are poor. It is thought that the current triaxial test is only a limited simulation of the stress conditions that

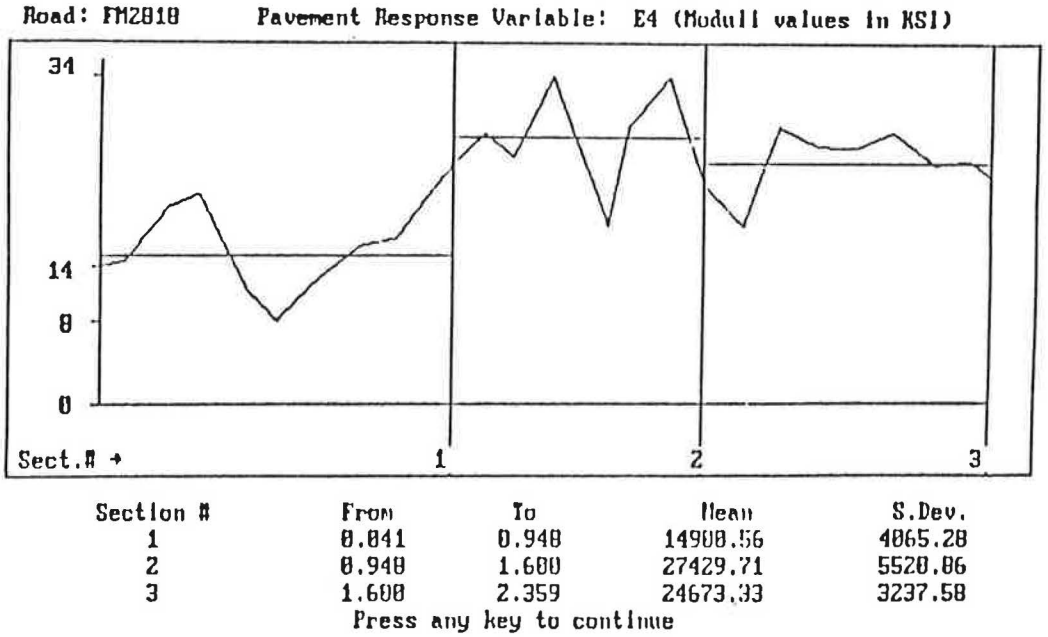

FIGURE 9 Graphical output of backcalculated *E* values, including subsectioning.

Comparison with BISDEF

The output of MODULUS was compared with that of BISDEF, which is the BISAR version of the backcalculation program developed by the Corps of Engineers (*3*,*8*). In this analysis, FWD data were collected on an experimental pavement (at the Texas A&M Research Annex) consisting of 5 in. of asphalt over an 8-in. granular base over a sandy gravel subgrade. The backcalculated moduli values are presented in Table 3. Both procedures give similar *E* values, particularly for the subgrade layer.

Multiple Drops at the Same Location

In order to evaluate the repeatability of MODULUS, 12 drops of the FWD were made at the same location on Section 9 at the TTI Research Annex. The deflection bowls and backcalculated *E* values are presented in Table 2. The purpose of this and other tests (*2*) was to determine the number of readings to be taken at an individual site to characterize the pavement to a specified level of confidence. However, the first deflections taken were significantly higher than the following readings. In Table 3, the maximum deflection of the first drop is 2.85 standard deviations greater than the mean; all subsequent drops are within one standard deviation.

For FWD testing, at a minimum an agency should take two drops at each location and the second should be used for data analysis.

Effects of Rigid Layer

The placement of a rigid layer within the subgrade has considerable effect on the backcalculated moduli values. The Corps of Engineers recommends a layer placed at 20 ft (*3*). The existing MODULUS program allows the placement of a rigid layer at any depth in the subgrade. To illustrate, the same data set was rerun using several depths to a rigid layer. The resulting effect on the backcalculated subgrade modulus and fitting error between measured and calculated deflections is presented in Table 4.

TABLE 3 COMPARISON OF *E* VALUES BACKCALCULATED USING BISDEF AND MODULUS ON SECTION 9 AT THE TTI RESEARCH ANNEX

	MODULUS				BISDEF			
Load	Asphalt	Base	Subgrade	Error	Asphalt	Base	Subgrade	Error
8,711	423.2	65.0	32.7	1.76	476.1	59.9	32.8	1.53
8,527	488.1	55.8	33.3	2.37	522.1	54.0	33.2	2.25
8,551	399.2	69.4	31.5	2.27	457.8	62.9	31.7	2.21
16,743	437.6	50.6	33.5	1.22	467.4	48.7	33.5	1.06
16,711	416.9	60.1	32.9	1.77	476.6	54.9	33.1	1.66
16,751	406.4	60.3	33.1	1.91	462.4	55.0	33.2	1.81

NOTE: Error is the absolute percent error per sensor.

TABLE 4 EFFECT OF PLACING A RIGID LAYER AT VARYING DEPTHS

Depth to Rigid Layer (inches)	Backcalculated Subgrade Modulus (ksi)	Absolute % Error/Sensor
-	21.9	5.72
360	17.6	3.76
300	16.8	3.65
240	15.8	3.96
180	14.3	5.61
120	11.8	10.53
60	7.3	25.12

The best fit between measured and calculated bowls occurred with a rigid layer placed at approximately 300 in. below the surface. Clearly, the subgrade E value obtained is a function of the specified depth to a rigid layer. The implication is that if the depth of the bedrock layer is unknown then the MODULUS system should be rerun with different depth to rigid layers to minimize absolute error.

Seasonal Variations in Backcalculated Moduli

TTI is currently completing a major study of deflection patterns of highway pavements around the state of Texas. Twenty-two experimental pavements have been instrumented with temperature and moisture sensors. These sites are all on in-service pavements and each site is 100 ft in length. Deflections have been measured both in the morning and afternoon, on 1 day per month over a 12-month period. Samples of surfacing, base, and subgrade were taken and returned to the laboratory for stiffness testing. Triaxial tests were performed on base and subgrade samples using the AASHTO T274–82 procedure, and diametrical resilient moduli tests were conducted on the asphalt surfacings.

The laboratory test data for a particular site are shown in Figure 10. This site consists of a 6-in. asphalt layer over a 6-in. granular base over a sandy clay subgrade. The water table was encountered at a depth of 8.5 ft. Thermocouples were installed at the bottom of the surfacing and base, and moisture sensors were placed in the middle of the base and 6 in. into the subgrade. The laboratory test results included diametrical

LABORATORY DATA

ASPHALT

$M_R \times 10^6$ psi

Hz \ °F	0	32	77	100
10	2.04	0.96	0.32	0.06
20	2.22	1.49	0.36	0.09

Hz \ °F	0	32	77	100
10				
20				

BASE

$M_R \times 10^3$ psi

σ_3	σ_D	M_R
1	4.9	12.9
5	4.8	69.9
1	9.6	8.7
5	9.6	23.3
10	9.8	54.0
15	9.8	84.3
1	14.9	8.3

σ_3	σ_D	M_R
5	14.6	13.9
10	14.7	26.1
15	14.8	45.0
25	14.9	77.6
10	24.4	19.2
15	24.6	26.9
25	24.6	41.4

σ_3	σ_D	M_R
15	39.2	21.6
25	39.2	30.3
25	47.8	28.4

$M_R = k_1 \theta^{k2} \sigma_D^{k3}$ $k_1 = 8.80$ $k_2 = 1.49$ $k_3 = -1.53$ $R^2 = 0.96$

SUBGRADE

$M_R \times 10^3$ psi

σ_3	σ_D	M_R
0	1.99	7.5
3	2.06	8.6
6	1.96	9.6
0	3.73	5.7

σ_3	σ_D	M_R
3	3.86	7.1
6	3.86	7.9
0	7.60	3.7
3	7.63	4.4

σ_3	σ_D	M_R
6	7.82	5.0
0	9.61	2.7
3	9.84	3.2
6	9.97	4.2

$M_R = k_1 \theta^{k2} \sigma_D^{k3}$ $k_1 = 9.23$ $k_2 = 0.17$ $k_3 = -.67$ $R^2 = 0.92$

FIGURE 10 Material test results for Site 5.

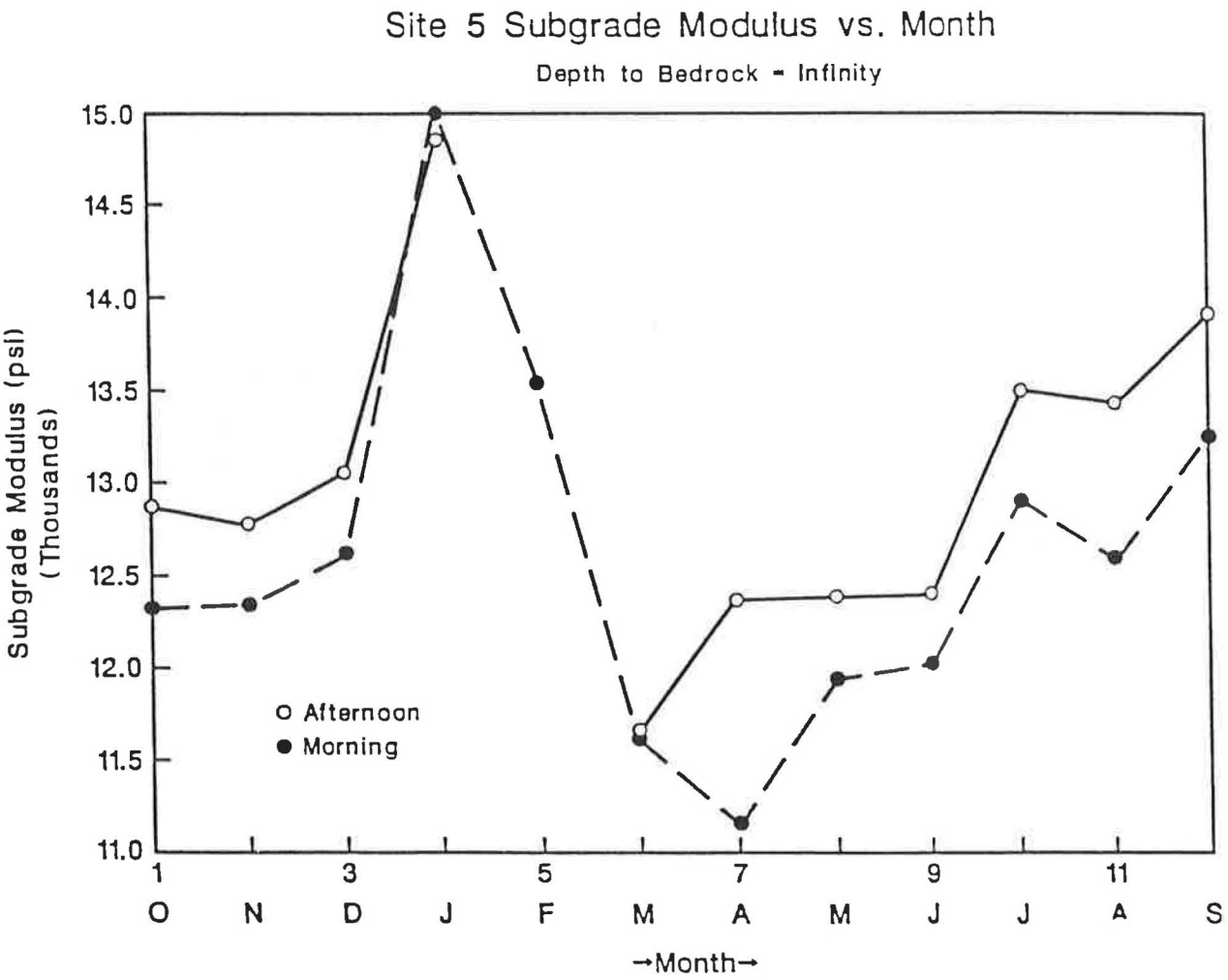

FIGURE 12 Monthly variations in backcalculated subgrade MODULUS.

exist under the FWD. Other factors such as soil suction and disturbances during sampling are major concerns.

ACKNOWLEDGMENTS

The MODULUS system was developed on research studies funded by the Texas State Department of Highways and Public Transportation and the FHWA on an HP&R study and the NCHRP in Study 10–27. Several state departments of transportation, including those of Texas, Colorado, Florida, and Arizona, reviewed the system and made recommendations for improvements. A final version of the system has been completed and will be distributed by NCHRP in the near future.

REFERENCES

1. J. Uzan, R. L. Lytton, and F. P. Germann. General Procedures for Backcalculating Layer Moduli. *Proc., 1st Symposium on NDT of Pavements and Backcalculation of Moduli*, ASTM, Philadelphia, Pa., July 1988.
2. J. Uzan, T. Scullion, C. H. Michalek, M. Paredes, and R. L. Lytton. *A Microcomputer Based Procedure for Backcalculating Layer Moduli from FWD Data*. Research Report 1123-1, Texas Transportation Institute, College Station, July 1988.
3. A. J. Bush. *Nondestructive Testing of Light Aircraft Pavements, Phase II, Development of the Nondestructive Evaluation Methodology*. Report FHWA-RD-80-9-11, FHWA, U.S. Department of Transportation, Washington, D.C., 1980.
4. A. R. Letto. *A Computer Program for Function Optimization Using Pattern Search and Gradient Simulation Techniques*. Master's thesis, Texas A&M University, College Station, Tex., 1968.
5. *AASHTO Guide for Design of Pavement Structures*. Ch. 5, AASHTO, Washington, D.C., 1986.
6. T. Scullion, T. Uzan, J. I. Yazdani, and P. Chan. *Field Evaluation of the Multidepth Deflectometer*. Texas Transportation Institute, Report 1123-2, College Station, Sept. 1988.
7. T. Scullion and A. J. Bush. Use of the Multidepth Deflectometer for Deflection Measurements. *Proc., Symposium—State of the Art of Pavement Response Monitoring Systems for Roads and Airfields*, CRREL Special Report 89-23, Cold Regions Research Laboratory, Hanover, N.H., Sept. 1989.
8. A. J. Bush, III, and D. R. Alexander. Pavement Evaluation Using Deflection Basin Measurements and Layered Theory. In *Transportation Research Record 1022*, TRB, National Research Council, Washington, D.C., pp. 16–29.

Publication of this paper sponsored by Committee on Strength and Deformation Characteristics of Pavement Sections.

Nondestructive Evaluation Equipment for Airfield Pavements

ALBERT J. BUSH III AND ROSS A. BENTSEN

Nondestructive testing (NDT) has provided a rapid means of assessing the structural capacity of airfield pavements during periods of increasing traffic and loadings. A wide range of test equipment is available for airport owners to select from. Various commercially available NDT equipments were applied to the structural evaluation of airfield pavements using a layered elastic method of analysis. Seven different NDT devices were evaluated. Three of the devices imparted vibratory loads to the pavement, whereas four devices applied impulse or falling-weight loads. NDT data were collected on 12 pavements that included thick and thin flexible, rigid, and composite structures over fine- and coarse-grain subgrades. Backcalculated subgrade moduli from the devices were compared. These data were used for estimating the allowable load and overlay requirements for a selected aircraft to demonstrate the variability that could be obtained using different devices.

During the past 10 to 15 years, much effort has been devoted to the development of nondestructive structural evaluation of pavements; as a result, several test devices and analytical procedures have been developed. The work has been sponsored by such federal agencies as the Navy, Army, Air Force, FAA, and FHWA, as well as many state departments of transportation, port authorities, and others. Research has been conducted by federal and state agencies, universities, private research organizations, and consultant engineers. Many reports have been published describing the development and application of the methods.

In October 1982, the U.S. Air Force Engineering and Services Center (AFESC) sponsored a study that was conducted by the U.S. Army Engineer Waterways Experiment Station (WES) to compare the results from several nondestructive testing (NDT) methods on selected Air Force airfield pavements (*1*). The purpose of the study was to provide AFESC with an assessment of the nondestructive approach to pavement evaluation so that the Air Force could make sound decisions as to the possible uses and benefits of NDT pavement evaluation schemes.

The scope of the project involved comparisons of selected NDT equipment and procedures on representative airfield pavements and a comparison of the NDT results to those obtained from the standard Air Force evaluation procedures based on test pit measurements. WES selected six leading firms with demonstrated NDT capabilities. These firms represented the state of the art in terms of commercial NDT equipment and available analytical evaluation methods. In addition, WES demonstrated three NDT schemes that it had developed, and AFESC demonstrated its NDT evaluation method. The field demonstrations were conducted within five selected test areas at MacDill Air Force Base (AFB), Tampa, Florida, during October and November 1982.

From the MacDill study, it was recommended that the comparison should be repeated at other sites to produce more conclusive results (*1*). These sites should cover more typical pavements over fine-grained soils (clays and silts), test pit data should be collected concurrently with the NDT data, and the pavements should be of such design that a range of allowable loads and overlay thicknesses would be anticipated so that a better comparison of results could be made. A set of test areas that require rehabilitation under common aircraft loads was also identified as a requirement. A standard evaluation procedure was also recommended.

The Navy, Air Force, Army, and FAA are in various stages of implementing a layered elastic design and evaluation procedure for airfield pavements. NDT offers a useful method for determining the modulus values for input into the design and evaluation. In order to specify the equipment requirements and also compare the results to conventional design and evaluation procedures, a field verification is required.

PURPOSE AND SCOPE

A layered elastic method of analysis was used to examine applicability of various NDT equipment to the structural evaluation of airfield pavements. All existing available NDT equipment (representative types) used for airfield testing were covered and predicted moduli from the various devices were compared.

NDT EQUIPMENT EVALUATED

Seven different NDT devices were evaluated. Three of the devices impart vibratory loads to the pavement, whereas four devices are impulse or falling-weight loading devices. The devices and specific characteristics of each are given in Table 1. Detailed descriptions of each device are given in the following paragraphs.

Kuab Model 50 Falling Weight Deflectometer (FWD)

The Kuab FWD is a trailer-mounted impulse loading device that produces its load using a unique two-mass system in which a falling weight is dropped onto a buffered second weight to

A. J. Bush III, Pavement Systems Division, U.S. Army Corps of Engineers, Waterways Experiment Station, 3909 Halls Ferry Road, Vicksburg, Miss. 39180. R. A. Bentsen, The Asphalt Institute, Research Park Drive, P.O. Box 14052, Lexington, Ky. 40512.

TABLE 1 NONDESTRUCTIVE TESTING DEVICE CHARACTERISTICS

Device Name	Dynamic Force Range, lbf	Load Transmitted by	Number and Type of Deflection Sensors	Deflection Sensor Spacing
Kuab FWD	3,000 to 15,100	Sectionalized circular plate 11.8 in. dia.	7 Seismometers	Fixed at 0, 8, 12, 18, 24, 36, 48 in.
Dynatest HWD	10,000 to 55,000	Circular plate 11.8 in. or	7 Geophones	Variable 12 to 96 in.
Dynaflect	1,000 peak to peak	Two 16 in. dia. x 2 in. width urethane-coated steel wheels	5 Geophones	Variable 0 to 48 in.
Dynatest FWD	1,500 to 27,000	Circular plate 11.8 in. or 17.7 in. dia.	7 Geophones	Variable 12 to 96 in.
Road Rater 2008	500 to 7,000 peak to peak	Circular plate 18 in. dia.	4 Geophones	Variable 24 to 48 in.
WES 16-Kip	500 to 30,000 peak to peak	Circular plate 18 in. dia.	4 Geophones	Variable 24 to 60 in.
Phonix FWD	2,300 to 23,000	Circular plate 11.8 in. dia.	6 Geophones	Variable 8.3 to 58 in.

produce pavement deflections. The load is transmitted to the pavement by an 11.8-in.-diameter plate that is segmented into quarters and cushioned with a corrugated rubber pad. The model tested has an impulse range of 2,600 to 14,000 lb. The testing system is powered by batteries on the trailer that are charged by a separate alternator on the towing vehicle. Deflections are measured by seven seismometers at fixed locations at and away from the loading plate. The Kuab FWD that was tested was able to perform loadings at distances up to 28 in. below the pavement surface and was equipped with a coring rig, but neither of these features was used or evaluated.

Pavement loadings can be produced at four adjustable drop levels. There is no limitation to the sequence or number of drops that can be run at a given location. Load and deflection data are produced with each drop and recorded with an MS DOS computer. The computer produces a paper copy as the data are collected and can also store the information to magnetic tape.

Dynatest Model 8081 Heavy Weight Deflectometer (HWD)

The Dynatest 8081 HWD is a trailer-mounted device capable of producing impulse loads from 8,000 to 55,000 lb. The single-pulse transient load is generated by a weight dropping on rubber pads that transmit the force to the pavement through either an 11.8- or 17.7-in.-diameter steel plate cushioned with a thin rubber pad. The testing system is powered by batteries on the trailer that are charged by a heavy-duty alternator on the towing vehicle. Deflections are recorded by seven geophones that are placed 1 ft apart starting at the center of the load plate, but the outer six can be varied from 12 to 96 in. away from the plate.

The falling weight system is controlled by an MS DOS computer and can produce up to five loadings selected from any combination of four adjustable drop heights. Load and deflection data are recorded on paper with each loading and can be automatically saved to a magnetic disk.

Dynaflect

The Dynaflect is a trailer-mounted electromechanical system for measuring the dynamic deflection of a pavement. Pavement deflection is produced by the counterrotation of two eccentrically loaded masses rotating at a fixed frequency of 8 Hz. A 1,000-lb, peak-to-peak sinusoidal load is transmitted to the pavement by two 4-in.-wide, 16-in. outside diameter polyurethane-coated steel wheels spaced 20 in. apart.

Once the mass rotation has been initiated and the loading wheels lowered, the Dynaflect produces constant pavement deflection and can be towed along the pavement in this manner. Pavement deflections at a test point are measured with five geophones that are aligned between the two wheels and lowered when deflection measurements are desired. One geophone is placed directly between the wheels, and the others are spaced at 1-ft intervals away from the loading wheels. Deflections readings are displayed on visual readouts by the electronic control system and can be produced on paper by the companion printer.

Dynatest Model 8003 FWD

The Dynatest Model 8003 FWD is a trailer-mounted, impact load device that can produce a load between 1,500 and 25,000 lb. The single-pulse transient load is generated by a weight dropping on rubber pads that transmit the force to the pavement through a 11.8-in.-diameter steel or dense rubber plate cushioned with a thin rubber pad. The testing system is powered by batteries on the trailer that are charged by a heavy-duty alternator on the towing vehicle. Deflections are recorded by seven geophones that are typically placed 1 ft apart from the center of the load, but the outer six can be varied from 12 to 96 in. away from the plate.

The falling weight system is controlled by a Hewlett-Packard IPC and can produce up to five loadings selected from any combination of four adjustable drop heights. Load and deflection data are recorded on paper with each loading and can be automatically saved to a magnetic disk.

Road Rater Model 2008

The Road Rater Model 2008 is an electrohydraulic vibratory loading system with an 8,000-lb reaction mass. The system is trailer mounted and has a self-contained power supply that supports the electronic and hydraulic systems. The vibratory load can be adjusted up to 7,000 lb peak-to-peak over a frequency range from 5 to 100 Hz and operates at a standard frequency of 20 Hz. The load is transmitted to the pavement through an 18-in.-diameter steel plate and is monitored by three load cells mounted on the plate.

Four geophones are used to measure deflection, with one measuring at the center of the plate and three at locations away from the plate. The deflection, load, and frequency data are recorded on a digital printer contained in the system controller box.

WES 16-kip Vibrator

The WES 16-kip vibrator is an electrohydraulic vibratory loading system with a 16,000-lb reaction mass. The system is contained in a 36-ft semitrailer along with supporting power supplies and automatic data recording equipment. The vibratory load can be varied up to 30,000 lb peak-to-peak over a frequency range of 5 to 100 Hz. The standard test frequency is 15 Hz, and the load is transmitted to the pavement through an 18-in.-diameter steel plate and measured by three load cells mounted on the plate. Up to five velocity transducers located at the plate and at points away from the plate are calibrated to measure deflections.

The load and deflection results are recorded on an x–y plotter and a digital printer. The x–y plotter records load versus the deflection of the velocity transducer on the plate as the vibratory load is increased from zero to maximum. The plot is used to calculate the dynamic stiffness modulus (DSM), which is the slope (load/deflection) of the plot between loads of 10 and 14 kips. Deflection results of all the sensors can be printed at any time as the load is swept from zero to the maximum of 30,000 lb.

Phonix ML10000 FWD

The Phonix FWD is a trailer-mounted device that can impart a dynamic impulse load of between 2,300 and 23,000 lb to the pavement surface. The load is produced by mechanically raising a circular mass to one of five set drop heights and then dropping it onto rubber pads that transmit the force to a padded 11.8-in.-diameter steel plate. The entire testing system operates from two 12-volt batteries that are contained in the trailer, and which in turn are charged by a small generator. Deflections are recorded by six geophones, five of which can be adjusted to any position from 8.3 to 58 in. from the loading plate.

Data produced by the Phonix FWD are recorded by an MS DOS system computer. The Phonix FWD is set up to produce three drops from the chosen height. The deflection of each sensor is recorded from each drop height; the load is recorded only on the third drop. The load and deflection data from the third drop are automatically recorded on magnetic media by the computer.

EXPERIMENTAL DESIGN AND DESCRIPTION OF TESTS

Two different phases of tests were performed in this study (*2*). First, calibration and repeatability experiments were performed to analyze the ability of each device to perform NDT consistently and reliably. All of these experiments were conducted over a 3-day period at WES. Then tests were performed at five different airfields for the collection of NDT and in situ pavement strength data. The NDT data were collected in a 2-week period immediately following the conclusion of the experiments performed at WES, whereas the in situ pavement strength tests were performed at each site following the completion of the NDT field tests.

Short-Term Repeatability

The experiment used to analyze the short-term repeatability of each machine involved having each device perform 25 tests at one test location in as short a period of time as the device would allow. The tests were performed at maximum load except for the Dynatest HWD, which would have overranged its deflection sensors in this experiment at maximum load, and each device performed this experiment on an asphalt concrete (AC) and a portland cement concrete (PCC) pavement. The vibratory devices and the Kuab FWD all performed the tests in one test sequence without lifting the loading plate. The Dynatest FWD and Dynatest HWD performed the tests in five series of five drops each. The Phonix FWD performed the tests in 25 series of three drops each with the recorded test data being the last drop of each series.

Field Testing

The field testing was performed on an array of airfield pavements. The pavement array is designed to include the three

TABLE 2 AIRFIELD AND PAVEMENT TYPES BY SITE

Site	Airport	Pavement Description
1	Brookley Airport Mobile, AL	17-in. PCC
2	Brookley Airport Mobile, AL	2-in. AC/10-in. PCC
3	NAS Pensacola, FL	10-in. PCC
4	NAS Pensacola, FL	2.5-in. AC
5	Robins AFB Warner-Robins, GA	8-in. AC
6	Robins AFB Warner-Robins, GA	8-in. AC/7-in. PCC
7	Birmingham ANG Birmingham Municipal, AL	7-in. PCC
8	Birmingham ANG Birmingham Municipal, AL	7-in. AC/7-in. PCC
9	Birmingham Army Guard Birmingham Municipal, AL	5-in. AC
10	Birmingham Municipal, AL	2-in. AC/7-in. PCC
11	Sheppard AFB Wichita Falls, TX	21-in. PCC
12	Sheppard AFB Wichita Falls, TX	6-in. AC

types of pavement surfaces—rigid, flexible, and composite; two relative strengths of pavements—thick and thin; and two types of subgrade—fine- and coarse-grained. Combining each pavement type, strength, and subgrade type yielded an array of 12 test sites. Five airfields were selected for the performance of this phase of testing. The airfields and the pavement types are presented by site in Table 2 and are shown in the pavement array in Figure 1.

NDT was performed to determine the effects of pavement type, thickness, and subgrade type on the deflections from each machine. In order to compare deflections between machines, the force outputs of each device were selected to maximize the number of devices operating at the same load level. These selected force outputs were called target loads, and each device operated at its maximum load level. The direct sampling tests will help characterize the in situ conditions of each site for comparison with the backcalculation data. The NDT and direct pavement sampling that are described were performed at each test site.

Nondestructive Testing: Replicate Tests

The purpose of these tests was to study the effects of the three variables in the pavement array on all the machines as well as to study the effect of load variation within the abilities of each device over the pavement array. In order to ensure that these effects could be identified, as many external noise variables as possible were blocked out of the experiment. To block out the variation due to change in thickness or material properties from one point to another, tests were performed on one point at each pavement site. This test point was designated the reference point at each test site. The effects of temperature were blocked out by performing the replicate tests either in the early morning or in midafternoon when the temperature would be fairly constant. The loading applied by the devices was also blocked. All loads 15,000 lb and less were conducted in Block 1 tests, whereas the loads heavier than 15,000 lb were conducted in Block 2 tests. Block 1 tests were conducted first at each pavement site to eliminate any effects that may have been caused by consolidation of the pavement layers under the heavier loads. There are 19 device and load combinations in Block 1 and 4 in Block 2. The devices and their respective target loads in each block are presented in Table 3.

All of the Block 1 and 2 tests were replicated three times at each pavement site. The order of testing for each replicate was randomized. Each replicate test consisted of bringing a device over the reference point and conducting three tests at the specified load. Therefore, for a given device and load,

NDT EQUIPMENT EVALUATION

EXPERIMENTAL DESIGN

SUBGRADE STRENGTH / TYPE	FINE		COARSE	
	THICK	THIN	THICK	THIN
AC	Site #12 Sheppard AFB 7" AC 20" Base 14 CBR Subgrade	Site #9 Birmingham 4" AC 4" Base 28" Subbase 16 CBR Subgrade	Site #5 Robins AFB 8" AC 8" Base 46 CBR Subgrade	Site #4 Pensacola NAS 5.5" AC 13.5" Base 16 CBR Subgrade
PCC	Site #11 Sheppard AFB 21" PCC 6" Base k = 81 pci	Site #7 Birmingham 7" PCC k = 82 pci	Site #1 Mobile Brookley Field 18" PCC k = 294 pci	Site #3 Pensacola NAS 10" PCC 4" Base k = 303 pci
COMPOSITE	Site #8 Birmingham 6.5" AC 7" PCC k = 27 pci	Site #10 Birmingham 2" AC 7" PCC 14" Base k = 192 pci	Site #6 Robins AFB 10" AC 7.5" PCC k = 476 pci	Site #2 Mobile Brookley Field 2" AC 10" PCC

FIGURE 1 Pavement array of field testing sites.

TABLE 3 TARGET LOAD LEVELS FOR REPLICATE TESTING

	Target Load, kips							
	Block 1					Block 2		
Device	1	5	7	10	15	20	25	50
Kuab FWD		X	X	X	X			
Dynatest HWD				X	X		X	X
Dynaflect	X							
Dynatest FWD				X	X		X	
Road Rater	X	X	X					
WES 16-kip	X	X	X	X	X			
Phonix FWD				X	X	X		

there were nine deflection basins collected. The 19 load and device combinations in Block 1 yielded 171 deflection basins at each site. Thirty-six deflection basins were collected for each site in Block 2 testing.

Direct Pavement Sampling

The tests in the direct pavement sampling investigation were performed in a test pit that was approximately 4 by 4 ft and located directly beneath the NDT reference point at each site. In-place testing was performed on each layer, and then an undisturbed sample was extracted from the subgrade at each test location. Bag samples were also collected from the granular base and subbase layers and from the subgrade materials for laboratory testing.

The in-place testing at the flexible pavement test sites consisted of determining the California bearing ratio (CBR), water content, and density of each pavement layer. For the PCC and composite pavement test sites, plate-bearing tests were conducted directly beneath the PCC slab. Density and water content were determined on each layer.

TEST RESULTS AND DATA ANALYSIS

Short-Term Repeatability

The analysis of the data for each device and both pavement types included determining coefficient of variation (COV) of each deflection sensor over all 25 tests, determining the variation in deflection and load over the 25 tests, and making notations on any significant changes or anomalies in the test data.

The deflections of the first sensor for each test from each of the devices on the AC and PCC pavements are shown in Figure 2. Note that the deflection data for the Dynaflect were multiplied by 15 for ease of illustration. Each first drop of the five-drop series for the Dynatest FWD on PCC showed consistently lower deflection than the other four drops. The deflection difference in the averages of the five first-drop readings and the other 20 readings was 11.2 percent. The 20 consistent readings had a COV of 0.36 percent. The Dynatest HWD exhibited this same phenomenon on the AC pavement on three of the five series of drops. Those three deflections varied 10.4 percent from the other 22 deflections, which had a COV of 0.89 percent. The seating load for both of these devices may not be high enough to settle the plate onto the pavement surface. However, this phenomenon was not exhibited on the other corresponding pavement surface by either of the Dynatest devices.

As the Dynatest FWD tests on AC in this experiment progressed, the deflections increased; and in particular, the second drop of each five-drop series showed consistently higher deflection, and the second drop of the last series of five tests overranged the sensor, which is rated up to 80 mils. A plot of the next four sensors away from the plate of the Dynatest FWD does not show this higher deflection on the second drop of the series but, in fact, shows slightly higher deflection on the first drop of the series. Note that except for the last series, when the deflection sensor was overranged, none of these deflection readings varied by more than 3 percent from the other readings. This variation is considered within the sensitivity of the sensors.

The Kuab FWD exhibited a higher deflection and corresponding lower stiffness value on the first drop of its 25-drop sequence on the asphalt surface. This is the same phenomenon exhibited by the Dynatest devices, noting that the Kuab FWD did not raise the plate during its operation for this test. The Phonix FWD displayed a higher load for its first recorded test; however, this is not a function of the seating load. Recall that the Phonix FWD only records the load on the third drop of its required three-drop test and then raises the plate before another test is performed.

The scale of Figure 2 flattens out the data, but the Road Rater had three distinct measuring periods in its deflection data on the asphalt pavement. During each of these measuring periods, the deflection of the sensor at the plate would consistently decrease to between 12 and 20 percent below the initial deflection in the period, then increase to the approximate level found at the beginning of the period, and then drop to about the same level. The shift was not evident in the loading from the Road Rater; the COV of load throughout the test was only 0.8 percent. The shift was also noticed in the other sensors, but the trend was less apparent as the distance from the load increased. A consistent, constant drop over the data might be expected with a vibratory device on AC pavement (as was evident with the WES 16-kip), but the large drops noticed in the data are suspect.

The COV of deflection for each of the device sensors on each of the pavement types is shown in Figure 3. Except for the Road Rater on the asphalt pavement, all of the devices showed an increase in COV of deflection as the sensor's distance from the plate increased, as expected. The Road Rater on the AC section showed a dramatic increase in COV of deflection of the sensors close to and at the loading plate. The Road Rater also showed the highest COV of deflection on the PCC pavement. The COV of deflection for the Road Rater on the PCC ranged from 3.2 to 7.4 percent depending on the sensor, whereas the other devices ranged from only 0.3 to 2.6 percent. The high COV for the last sensor of the Phonix FWD on the AC was due to a bad reading on one test.

Field Testing: Deflection Test Results

Deflections for each device at each of the 12 sites are presented in Table 4. These data are the average of the last two tests of three that were conducted during the three replicate tests. Therefore, these data are the average of six randomly collected deflection basins at the same location.

Direct Pavement Sampling

California Bearing Ratio Tests

CBR tests were conducted beneath the asphalt surface pavements in accordance with MIL-STD-621A (*3*), Method 101. CBR is a measure of the soil resistance to penetration of a

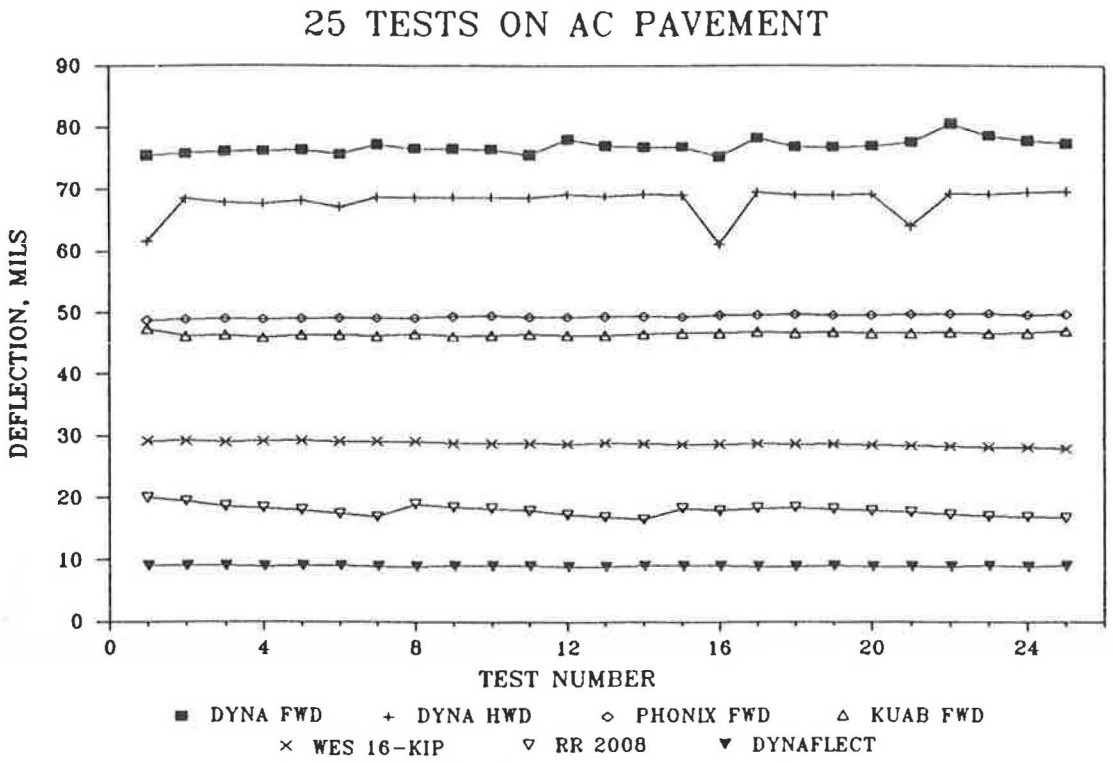

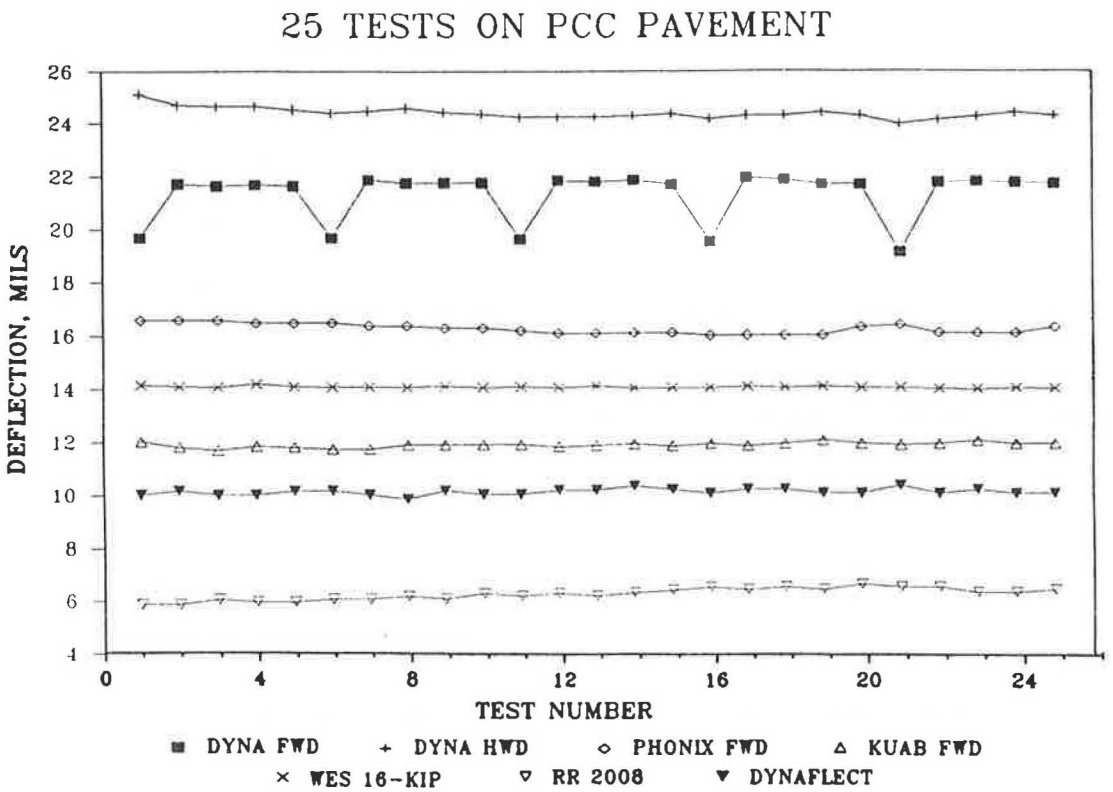

FIGURE 2 First sensor deflections from short-term repeatability experiment.

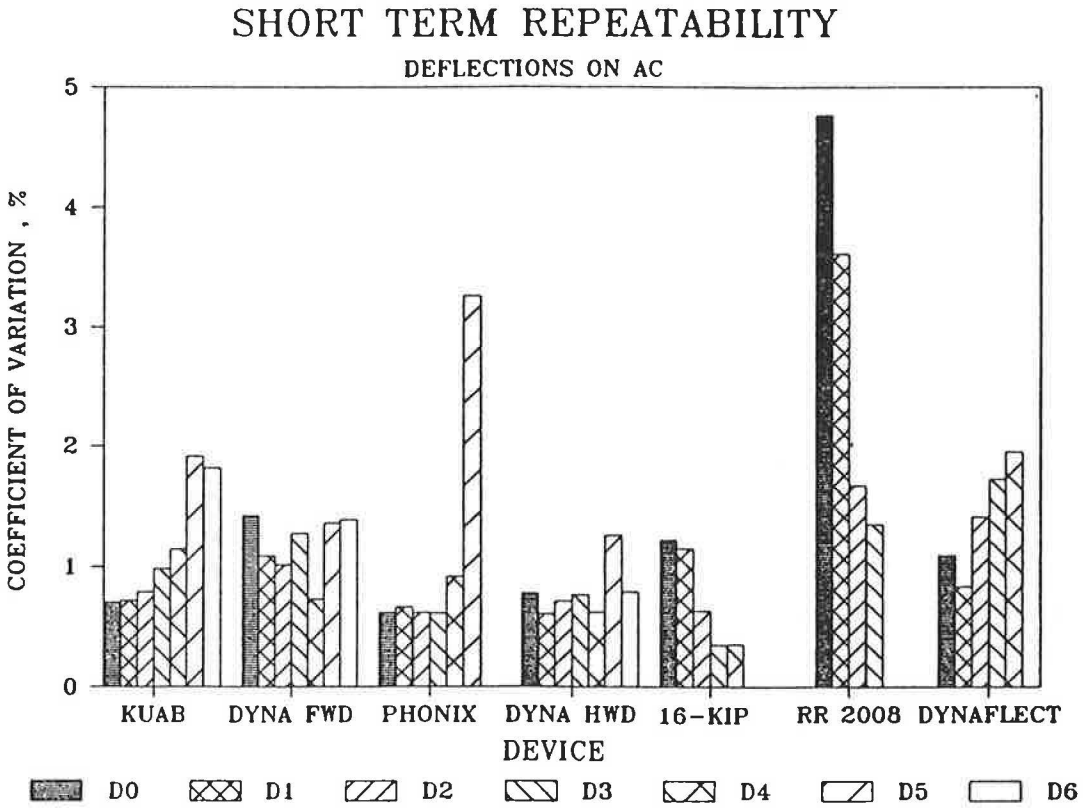

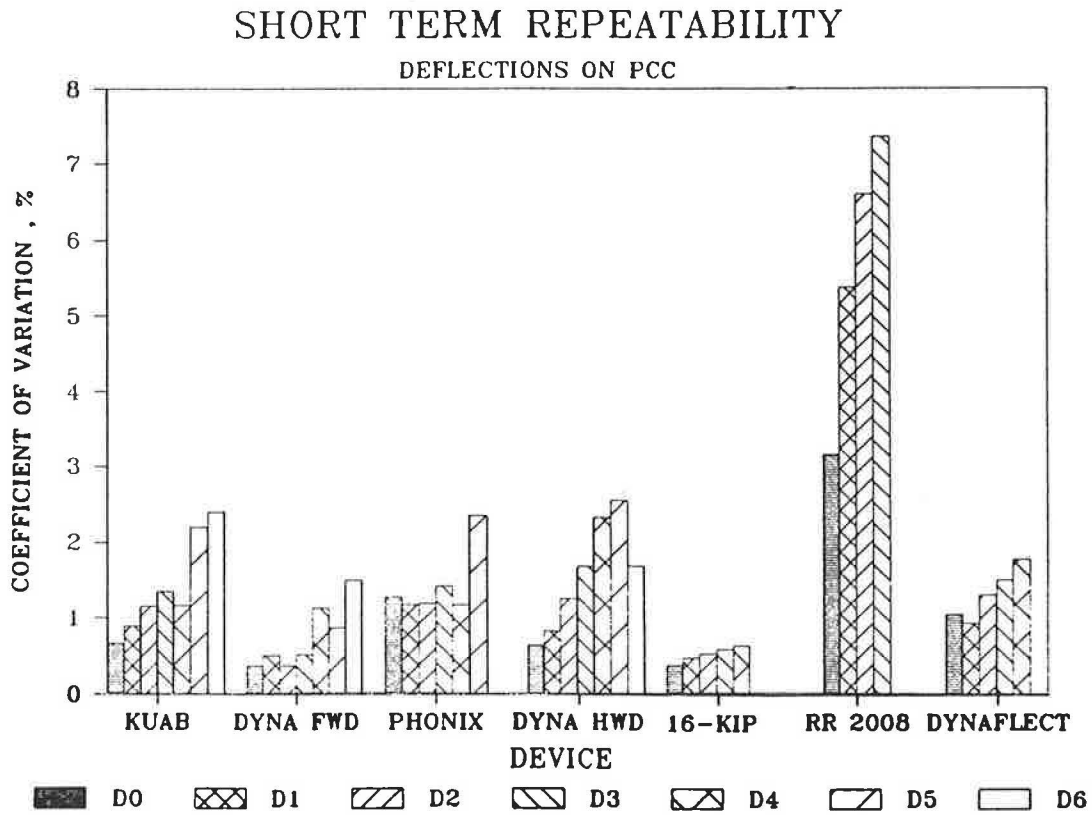

FIGURE 3 Coefficient of variation of deflections from short-term repeatability experiment.

TABLE 4 MEAN DEFLECTION BASINS

KUAB DEFLECTIONS, MILS

SITE	MEAN FORCE LBS	D0 MEAN	D1 MEAN	D2 MEAN	D3 MEAN	D4 MEAN	D5 MEAN	D6 MEAN
1	14116	2.67	2.55	2.43	2.50	2.40	2.23	2.11
2	14160	5.36	4.11	4.02	3.77	3.51	2.97	2.72
3	14151	3.70	3.54	3.40	3.16	3.03	2.62	2.20
4	14105	22.25	16.43	12.68	8.73	6.27	3.67	2.52
5	13928	11.73	8.45	6.44	4.40	3.05	1.49	0.88
6	14100	11.83	6.89	5.32	4.71	4.35	3.59	2.82
7	14241	10.15	9.72	9.41	8.69	7.99	6.29	4.67
8	14160	9.28	7.21	6.25	5.04	4.04	2.75	1.74
9	14126	24.98	13.83	7.99	3.45	1.80	1.48	1.42
10	14070	6.75	6.10	5.86	5.35	4.81	3.76	2.72
11	14403	2.15	2.01	1.88	1.82	1.80	1.71	1.62
12	14431	31.77	24.10	19.38	13.20	9.29	4.77	3.30

DYNA HWD DEFLECTIONS, MILS

SITE	MEAN FORCE LBS	D0 MEAN	D1 MEAN	D2 MEAN	D3 MEAN	D4 MEAN	D5 MEAN	D6 MEAN
1	50707	8.23	7.80	7.40	6.92	6.40	5.95	5.39
2	44303	15.14	12.95	11.72	10.12	8.49	7.14	5.80
3	50863	17.37	16.36	14.83	13.00	11.05	9.21	7.39
4	47110	70.62	47.33	24.08	13.81	9.17	6.70	5.13
5	50065	34.79	22.96	12.19	6.39	3.57	2.37	1.88
6	50292	26.98	18.96	15.25	12.51	10.15	8.24	6.60
7	50345	29.84	26.94	22.26	17.33	12.57	8.50	5.07
8	49885	29.77	24.46	17.76	12.64	8.37	5.97	4.03
9	49887	53.50	24.83	6.71	4.69	4.79	4.14	3.41
10	49820	26.02	23.71	19.94	15.73	11.59	8.48	6.00
11	50872	6.64	6.31	6.03	5.68	5.27	4.84	4.42
12	47063	83.49	61.13	34.41	19.34	12.38	9.62	8.04

(continued on next page)

TABLE 4 *(continued)*

	DYNAFLECT DEFLECTIONS, MILS					
SITE	MEAN FORCE LBS	D0 MEAN	D1 MEAN	D2 MEAN	D3 MEAN	D4 MEAN
1	1000	0.19	0.18	0.19	0.17	0.18
2	1000	0.25	0.24	0.23	0.18	0.18
3	1000	0.20	0.18	0.18	0.13	0.12
4	1000	0.64	0.45	0.30	0.19	0.14
5	1000	0.36	0.24	0.14	0.07	0.06
6	1000	0.32	0.27	0.25	0.19	0.16
7	1000	0.69	0.65	0.54	0.41	0.30
8	1000	0.34	0.32	0.23	0.14	0.10
9	1000	0.53	0.25	0.15	0.10	0.09
10	1000	0.38	0.36	0.29	0.20	0.15
11	1000	0.15	0.14	0.15	0.12	0.13
12	1000	1.11	0.83	0.54	0.34	0.27

	DYNA FWD DEFLECTIONS, MILS						
SITE	MEAN FORCE LBS	D0 MEAN	D1 MEAN	D2 MEAN	D3 MEAN	D4 MEAN	D5 MEAN	D6 MEAN
1	25485	4.43	3.48	3.53	3.02	3.34	2.73	2.99
2	25348	8.62	6.85	6.25	5.16	4.56	3.64	3.22
3	25093	8.68	8.05	7.46	6.43	5.66	4.57	3.85
4	24415	46.60	24.26	11.86	7.06	5.02	3.61	2.96
5	24870	19.76	10.90	5.30	2.53	1.53	1.01	0.99
6	25027	17.84	8.77	7.32	5.85	4.85	3.75	3.26
7	25347	13.17	11.93	9.87	7.57	5.53	3.54	2.19
8	25334	15.45	10.74	7.56	5.28	3.55	2.49	1.79
9	24632	38.43	12.69	2.76	2.24	2.37	1.85	1.79
10	25277	13.06	11.35	9.57	7.40	5.44	3.77	2.84
11	25763	3.15	2.92	2.85	2.63	2.55	2.17	2.13
12	24635	51.34	32.31	16.82	9.13	5.91	4.37	4.20

TABLE 4 *(continued on next page)*

TABLE 4 (*continued*)

ROAD RATER DEFLECTIONS, MILS

SITE	MEAN FORCE LBS	D0 MEAN	D1 MEAN	D2 MEAN	D3 MEAN
1	6740	0.95	0.67	0.73	0.58
2	6895	2.00	1.33	1.13	0.90
3	6925	2.63	1.63	1.33	1.20
4	6967	7.57	4.00	2.63	2.02
5	6965	3.38	1.00	0.50	0.35
6	6948	4.05	2.47	1.97	1.67
7	7003	5.62	3.82	2.87	2.10
8	6995	3.33	1.88	1.27	0.78
9	6935	5.00	1.13	0.75	0.67
10	6918	3.27	2.33	1.70	1.20
11	6985	1.42	0.90	0.82	0.77
12	6932	9.07	4.43	2.37	1.65

WES 16-KIP DEFLECTIONS, MILS

SITE	MEAN FORCE LBS	D0 MEAN	D1 MEAN	D2 MEAN	D3 MEAN
1	15013	2.13	1.17	1.61	1.46
2	14395	4.18	3.42	2.80	2.27
3	14494	4.24	3.35	2.67	2.19
4	15009	12.04	9.77	3.97	2.34
5	14474	6.31	5.07	1.84	1.07
6	15142	7.51	6.11	4.20	3.36
7	15093	10.07	8.46	6.07	4.35
8	14808	6.45	5.75	3.40	2.19
9	14827	10.02	7.08	2.49	2.13
10	14385	5.89	5.21	3.53	2.43
11	14535	2.69	1.97	1.84	1.69
12	14198	18.76	16.12	7.58	4.84

PHONIX DEFLECTIONS, MILS

SITE	MEAN FORCE LBS	D0 MEAN	D1 MEAN	D2 MEAN	D3 MEAN	D4 MEAN	D5 MEAN
1	19499	3.98	2.85	2.52	2.52	2.40	2.07
2	20392	6.93	5.35	4.77	4.10	3.47	2.95
3	20289	6.70	6.13	5.57	4.90	4.22	3.57
4	18881	35.88	19.13	9.35	5.37	3.73	2.87
5	19740	15.17	8.37	4.05	1.87	1.10	0.80
6	19808	14.17	6.85	5.57	4.60	3.72	3.07
7	19946	9.72	8.62	7.20	5.48	3.90	2.80
8	19190	11.35	7.80	5.38	3.72	2.45	1.88
9	18685	29.23	9.80	1.67	1.73	1.75	1.50
10	19877	9.13	7.80	6.45	5.00	3.65	2.77
11	19499	2.50	2.25	1.95	2.00	1.90	1.77
12	19156	40.03	25.47	13.25	6.58	4.37	3.53

TABLE 5 CBR TEST RESULTS

Location	Test Number	Measured CBR	Average CBR
	Site No. 4		
Top of base	1	90	88
	2	82	
	3	92	
Middle of base	1	93	100
	2	98	
	3	106	
	4	103	
Top of subgrade	1	15	16
	2	17	
	3	17	
	Site No. 5		
Top of base	1	60	77
	2	96	
	3	74	
Top of subgrade	1	44	46
	2	41	
	3	52	
16 in. into subgrade	1	20	25
	2	26	
	3	29	
	Site No. 9		
Top of base	1	47*	11
	2	11	
	3	10	
Top of subbase	1	50	40
	2	33	
	3	37	
Top of subgrade	1	14	16
	2	14	
	3	19	
14 in. into subgrade	1	29	32
	2	39	
	3	29	
	Site No. 12		
Top of base	1	111	117
	2	118	
	3	123	
Top of subgrade	1	15	13
	2	15	
	3	13	
14 in. into subgrade	1	3.9	4.3
	2	4.3	
	3	4.6	

* Test result discarded.

TABLE 6 MOISTURE AND DENSITY TEST RESULTS

Location	Nuclear Gage			Oven Dry
	Water Content	Dry Density	Wet Density	Water Content
Site No. 1				
Top of subgrade	*	*	*	10.9
Site No. 2				
Top of subgrade	*	*	*	**
Site No. 3				
Top of base	13.0	115	128	9.5
Top of subgrade	18.4	104	123	15.5
Site No. 4				
Top of base	11.2	128	138	8.2
Middle of base	10.1	125	135	6.4
Top of subgrade	18.3	108	126	14.5
Site No. 5				
Top of base	*	*	*	2.6
Top of subgrade	16.0	116	135	9.6
16 in. into subgrade	18.2	110	130	9.9
Site No. 6				
Top of subgrade	8.8	119	129	8.5
Site No. 7				
Top of subgrade	22.6	111	133	19.9
Site No. 8				
Top of subgrade	19.3	115	137	18.6
Site No. 9				
Top of base	8.7	130	134	3.0
Top of subbase	16.8	115	133	15.0
Top of subgrade	24.0	107	130	20.2
14 in. into subgrade	24.6	112	132	18.8
Site No. 10				
Top of base	13.8	111	131	17.9
Site No. 11				
Top of base	7.1	134	142	6.1
Site No. 12				
Top of base	3.8	143	147	3.1
Top of subgrade	18.2	109	127	15.7
14 in. into subgrade	*	96	*	21.6

* Test not conducted, or data inconsistent.

3-in.^{2} piston expressed as a percent of a standard. The standard is 1,000 psi at 0.1-in. penetration or 1,500 psi at 0.2-in. penetration. CBR tests are used to determine relative soil strengths. Tests were performed on each layer of the foundation below the asphalt surface. CBR values were also determined below the undisturbed sample that was extracted from the subgrade. CBR data for the asphalt surface sites are presented in Table 5.

Moisture and Density Tests

At each site location, moisture content and density tests were conducted. Density and moisture content data were collected on each layer of foundation material at each site. Densities were determined with the nuclear gauge on the granular materials and with drive cylinders of known volume on the fine-grained soils. Moisture contents were taken on all layers using the oven-dry sample method. Results of the moisture and density tests are presented in Table 6.

Plate Bearing Tests

Thirty-in.-diameter plate bearing tests were conducted on the surface of the subgrade beneath the slab at the PCC and composite pavement sites. A 40-ft-long flatbed trailer spanned the gap left by removing the 4- × 4-ft PCC surface. This trailer was loaded with 1-ton lead blocks against which the hydraulic ram would react to apply the necessary force to the 30-in.-diameter plate used in testing the subgrade. The plate bearing tests were conducted in accordance with MIL-STD-621A (*3*), Method 104. Plate bearing test results are presented in Table 7.

Laboratory Testing

The bag samples were tested to determine the soil classification using the Unified Soil Classification System. The results of these tests are presented in Table 8.

TABLE 7 PLATE BEARING TEST RESULTS

Site Number	Depth from Surface, in.	k* pci
1	18.0	294
3	10.0	303
6	17.5	476
7	7.0	82
8	13.5	27
10	9.0	192
11	21.0	82

* k = slope of average pressure versus deflection curve during loading.

TABLE 8 SUMMARY OF SOIL CLASSIFICATION TEST RESULTS

Site No.	Sample No.	Layer	Atterberg Limits LL	PL	PI	Specific Gravity	Percent Gravel	Percent Fines	Classification
1	1	Subgrade	NP	NP	NP	2.66	2	98	Silty sand (SM)
2	2	Subgrade	16	10	6	2.67	2	98	Clayey silty sand (SM-SC)
3	3	Base	NP	NP	NP	2.65	20	80	Gravelly silty sand (SP-SM)
3	4	Subgrade	NP	NP	NP	2.64	0	100	Silty sand (SP-SM)
4	5	Base	19	13	6	2.67	18	82	Gravelly silty sand (SM-SC)
4	6	Subgrade	NP	NP	NP	2.65	0	100	Silty sand (SP-SM)
5	7	Base	NP	NP	NP	2.65	76	24	Sandy gravel (GP)
5	8	Subgrade	44	16	28	2.68	1	99	Clayey sand (SC)
6	9	Subgrade	19	10	9	2.67	2	98	Clayey sand (SC)
7	10	Subgrade	33	15	18	2.72	8	92	Sandy clay (CL)
8	11	Subgrade	30	14	16	2.72	12	88	Gravelly sandy clay (CL)
9	12	Base	17	11	6	2.83	62	38	Sandy silty gravel (GP-GM)
9	13	Subgrade	35	16	19	2.73	32	68	Sandy clayey gravel (GC)
9	14	Subbase	35	15	20	2.74	26	74	Gravelly clayey sand (SC)
10	15	Base	33	15	18	2.69	--Sample contained asphalt--no tests--		
10	16	Subgrade	38	15	23	2.74	6	94	Sandy clay (CL)
11	17	Base	17	10	7	2.69	36	64	Gravelly silty sand (SP-SM)
11	18	Subgrade	23	11	12	2.69	2	98	Clayey sand (SC)
12	19	Base	15	10	5.	2.71	47	53	Sandy silty gravel (GP-GM)
12	20	Subgrade	35	22	13	2.68	0	100	Sandy clay (CL)

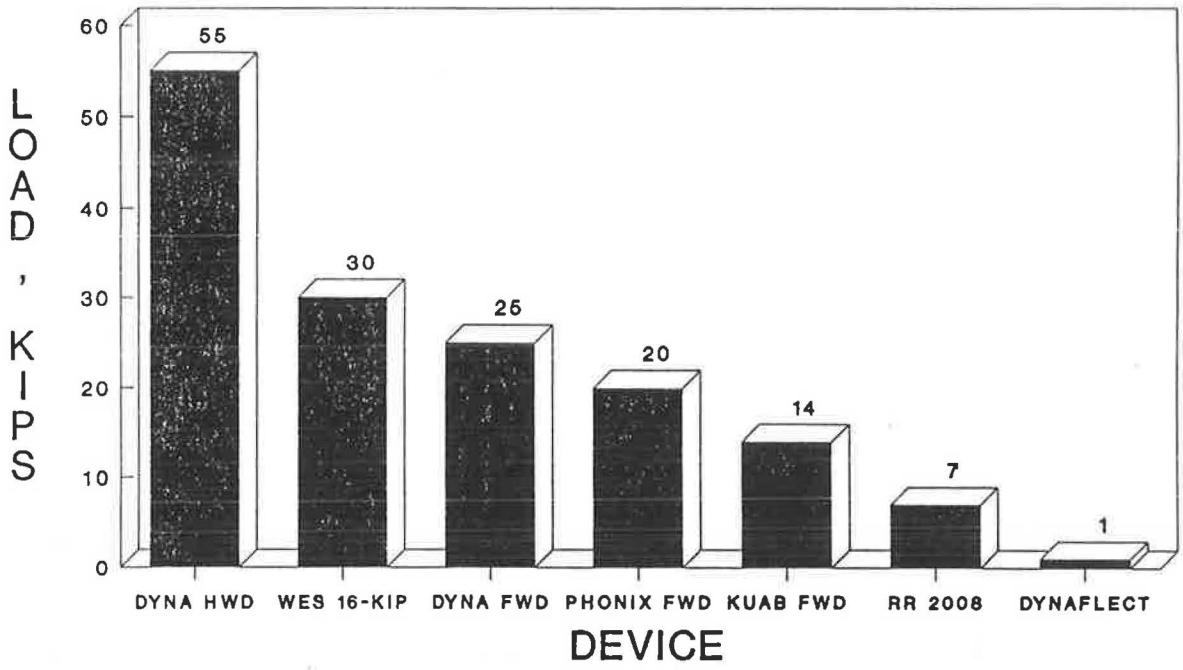

FIGURE 4 Maximum load output for NDT devices.

TABLE 9 SUMMARY OF INPUTS FOR BACKCALCULATION PROGRAM (BISDEF)

Site	No. of Layers	No. of Variable Layers	Layer 1, ksi			Layer 2, ksi			Layer 3, ksi		
			E min	E max	E in.	E min	E max	E in.	E min	E max	E in.
1	2	2	2500	7000	3500	1	75	20			
2	3	2			250*	2500	7000	3500	1	75	20
3	2	2	2500	7000	3500	1	75	20			
4	3	3	200	1000	350	5	150	30	1	75	20
5	3	2			250*	5	150	30	5	70	25
6	3	2			200*	2500	7000	3500	1	75	20
7	2	2	2500	7000	3500	1	75	20			
8	3	2			150*	1000	7000	2500	1	75	20
9	3	2			250*	5	150	30	1	75	20
10	3	2			200*	2500	7000	2500	1	75	20
11	2	2	2500	7000	3500	1	75	20			
12	3	3	100	1000	250	5	150	30	1	75	20

* Fixed modulus.

Backcalculation of Moduli

The BISDEF program (*4*) was used to backcalculate moduli values for each pavement using deflection basins from each device during the replicate testing. Deflection basins from the maximum loads (Table 3 and Figure 4) were selected for analysis. Because variability in the first drop was noted during the short-term repeatability tests, only the last two tests of each of the three replicates were analyzed. Therefore, a total of six tests for each device were used in the backcalculation. Results for subgrade modulus values are presented in Tables 8 through 10. Subgrade modulus is presented because for other pavement layers the moduli were either fixed or were calculated at a predetermined limit. The NDT equipment malfunctioned in some cases and only four basins were recorded.

The BISDEF program uses the BISAR (*5*) elastic layer program to calculate deflections. The pavement system is described by layers that can be of fixed or variable moduli. For variable layers, a minimum, a maximum, and an initial starting moduli are defined. For the analysis presented herein, the 12 pavement sites were described as shown in Table 8. The asphalt surface moduli were fixed on Sites 2, 5, 6, 8, 9, and 10. All other layers for each site were allowed to vary between the ranges given in Table 9.

A rigid layer was placed at 20 ft below the surface for these modulus calculations. The procedure is limited to knowing where a rigid layer exists. The elastic solution is best represented when reasonably accurate modulus values are selected for those layers that are held constant and the elastic solution for the variable layers is within the maximum and minimum values selected. The BISDEF program will accurately find the best elastic solution for up to three variable layers. This solution may not be acceptable because pavements are not linearly elastic mediums.

The SPSS statistical analysis program (*6*) was used for analysis of variance. For all 12 pavement sites, the differences in moduli were found to be significant.

To compare the differences, bar charts will be presented. Subgrade modulus results are shown in Figure 5 for the impulse load devices on AC sites. The devices are plotted in order of decreasing load magnitude. Generally, the modulus increases with load, indicating that the subgrade materials are stress dependent (i.e., the modulus decreases with increased stress).

Subgrade modulus values for vibrators on the AC sites are shown in Figure 6. Again, they are plotted in order of decreasing load magnitude. The increase in modulus with decrease in load applies for the WES 16-kip and the Dynaflect. The Road Rater values appear to be highly variable. All devices are shown in Figure 7. They are plotted in order of decreasing load magnitude. The WES 16-kip modulus values are significantly lower on the two pavements on the right in Figure 7. These sites are fine-grained soil that should be more stress

TABLE 10 BACKCALCULATED SUBGRADE MODULI FOR ASPHALT PAVEMENTS

	Site 5			Site 4		
	Count	Mean KSI	Standard Deviation	Count	Mean KSI	Standard Deviation
KUAB	6	58.3	1.454	6	23.3	0.668
DYNA HWD	6	54.1	0.203	6	20.7	0.075
DYNAFLECT	6	69.8	0.471	4	29.6	0.944
DYNA FWD	6	61.1	1.005	6	19.9	0.095
ROAD RATER	4	70.0	0.059	6	16.1	4.291
WES 16-KIP	6	55.3	0.863	4	26.9	0.606
PHONIX	6	67.7	0.824	6	20.9	0.478

	Site 12			Site 9		
	Count	Mean KSI	Standard Deviation	Count	Mean KSI	Standard Deviation
KUAB	6	18.6	0.151	6	58.4	2.310
DYNA HWD	6	14.5	0.049	6	58.4	0.613
DYNAFLECT	6	15.7	0.068	6	45.7	13.877
DYNA FWD	6	15.6	0.304	6	46.1	0.892
ROAD RATER	6	19.0	1.221	6	49.6	3.636
WES 16-KIP	6	11.9	0.196	6	26.1	2.900
PHONIX	6	17.5	0.412	6	54.5	0.454

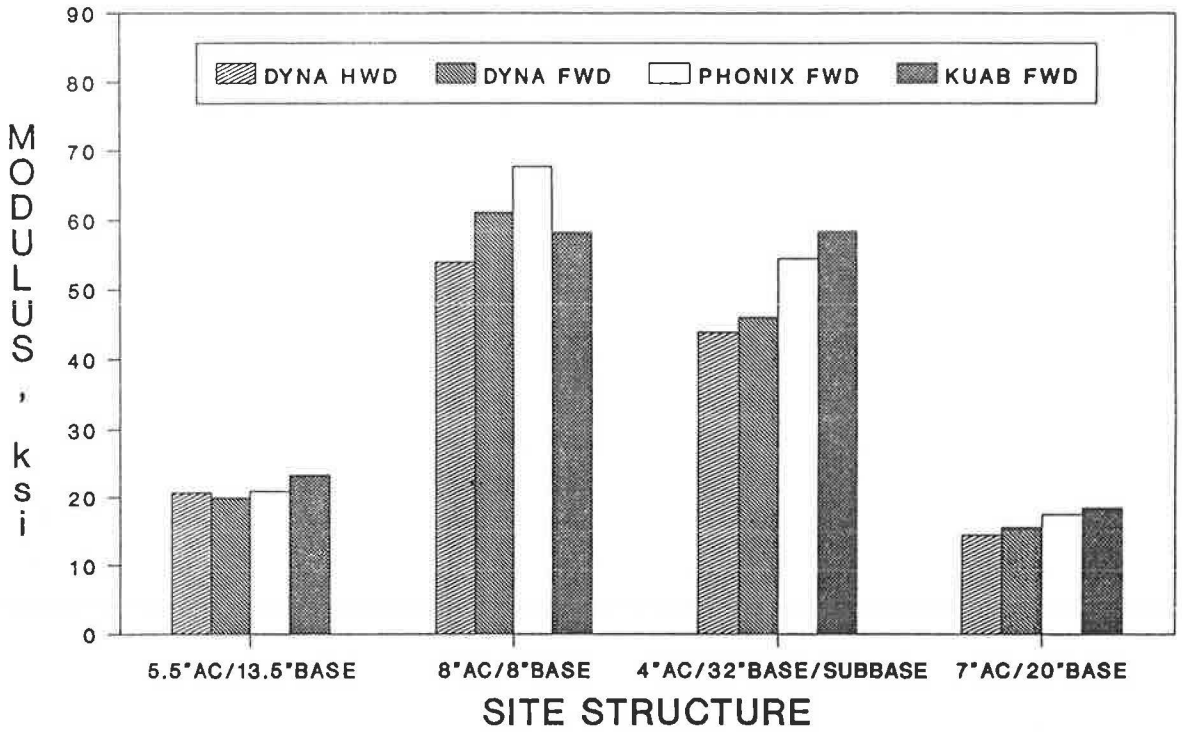

FIGURE 5 Backcalculated subgrade moduli for AC sites with FWDs.

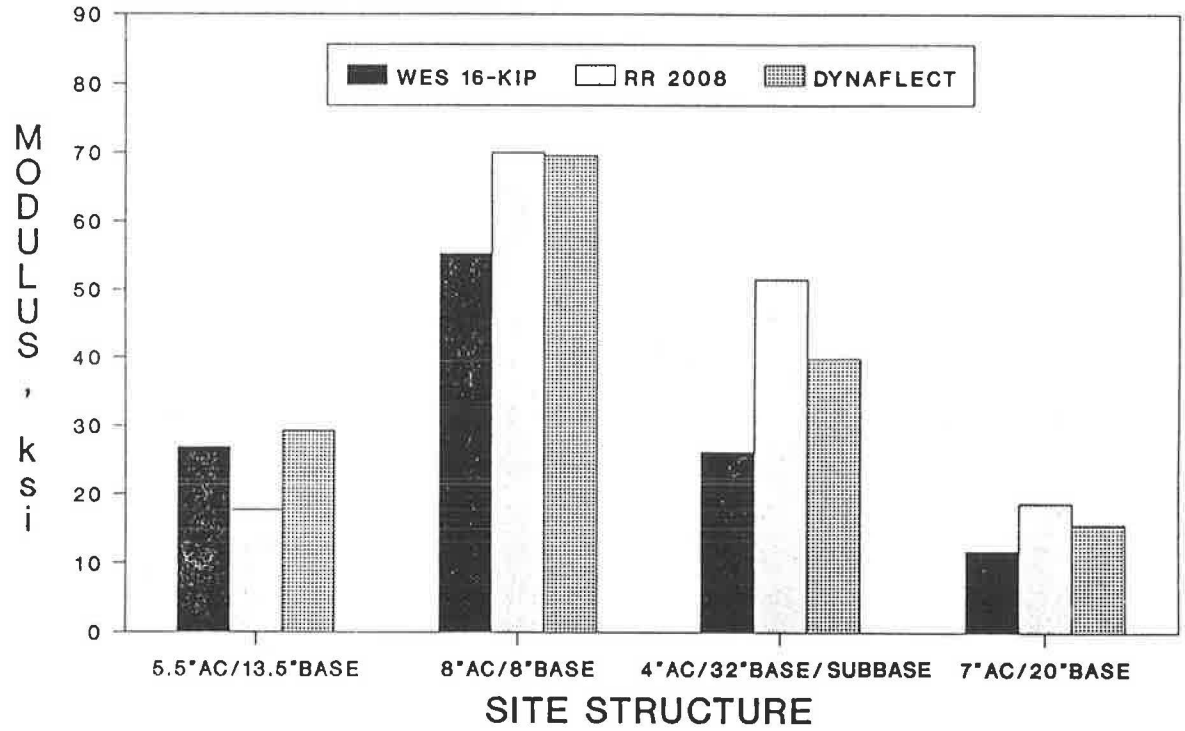

FIGURE 6 Backcalculated subgrade moduli for AC sites with vibrators.

sensitive than the coarse-grained sands of the other pavements. The WES 16-kip applies a 16,000-lb preload to the pavement. This preload on a stress-dependent subgrade may account for the lower modulus values.

The modulus values for the PCC sites from the impulse load devices data are shown in Figure 8. The modulus values generally increase with decreased load except for the lighter device, the Kuab. The Kuab modulus values appear to be variable.

The subgrade modulus values for the vibrators on PCC pavements are shown in Figure 9. On thick PCC pavement, the Dynaflect values are significantly lower than either the

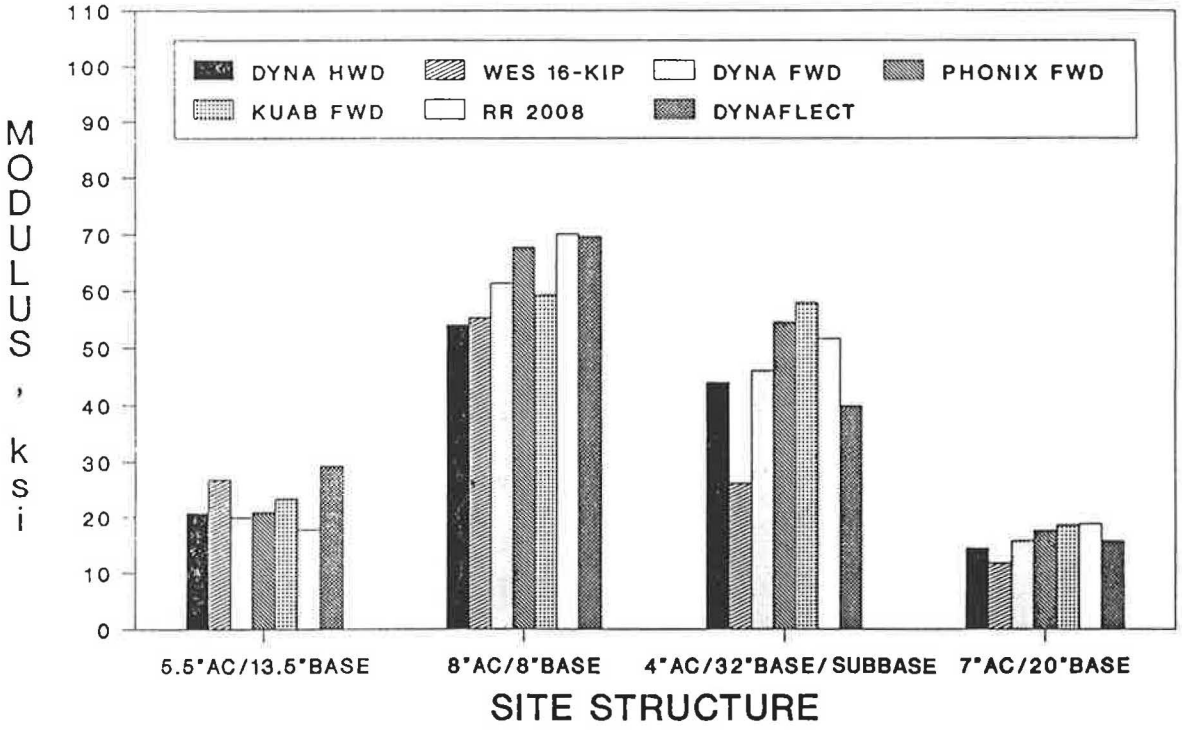

FIGURE 7 Backcalculated subgrade moduli for AC sites.

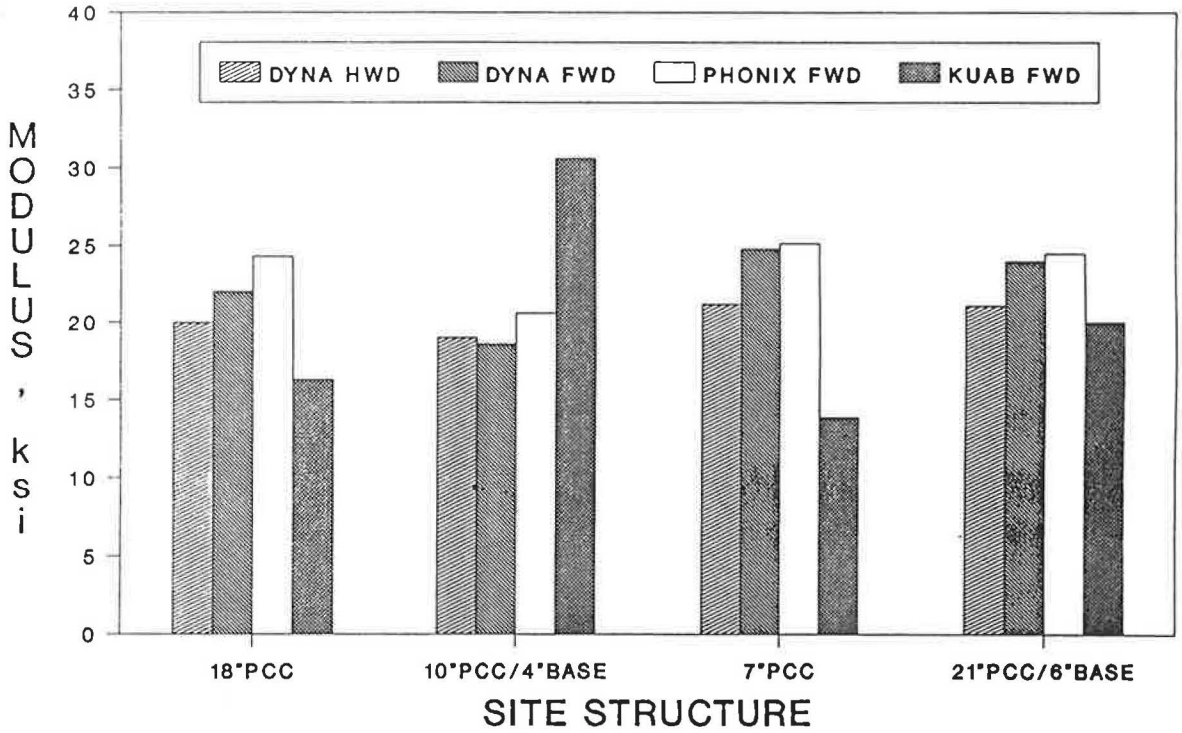

FIGURE 8 Backcalculated subgrade moduli for PCC sites with FWDs.

WES 16-kip or the Road Rater. The light load (1,000 lb_f) of the Dynaflect may not seat the thick PCC slabs and the deflections may be from only movement of the slab and not the pavement system. This stiffness reversal was also shown in the MacDill study (*1*).

Results from all devices on PCC pavements are shown in Figure 10. The Dynaflect values are significantly lower on the thick pavements. The WES 16-kip values are higher for the pavement plotted on the left of the figure that has a sand subgrade. Granular materials should increase in modulus with increase in confining stress. The confining stress would increase with the higher preload of the WES 16-kip.

Composite pavement subgrade moduli from the FWDs are shown in Figure 11. Again, the higher loads give lower moduli

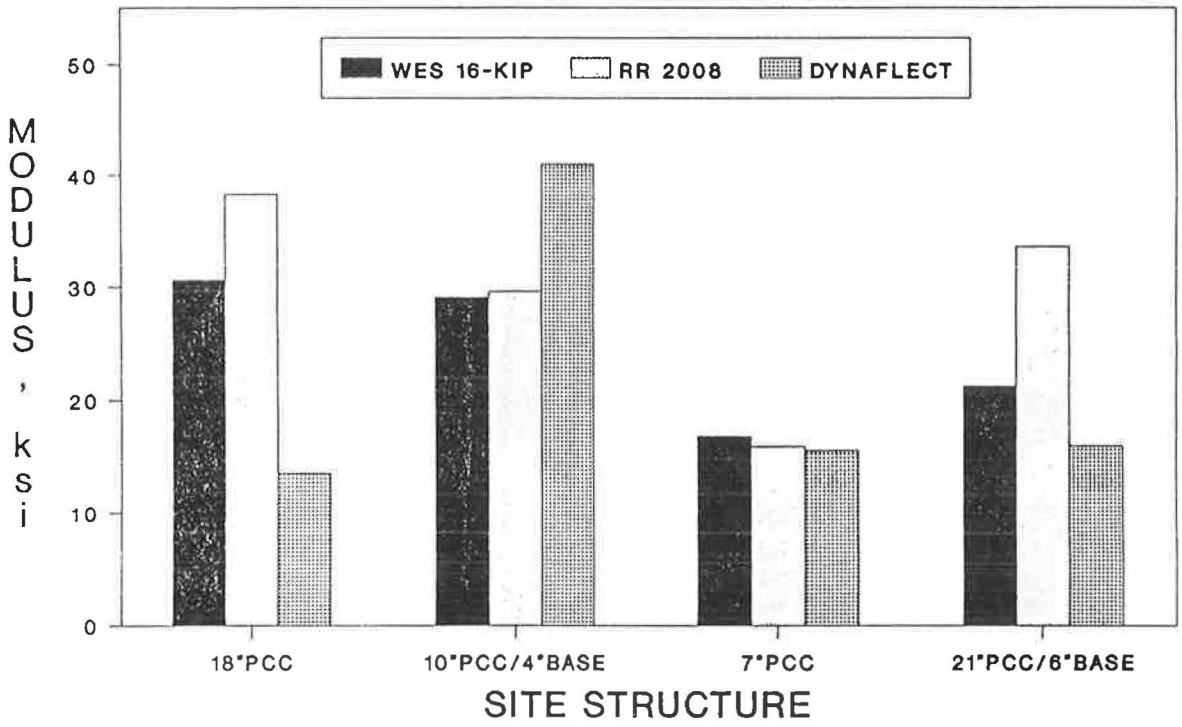

FIGURE 9 Backcalculated subgrade moduli for PCC sites with vibrators.

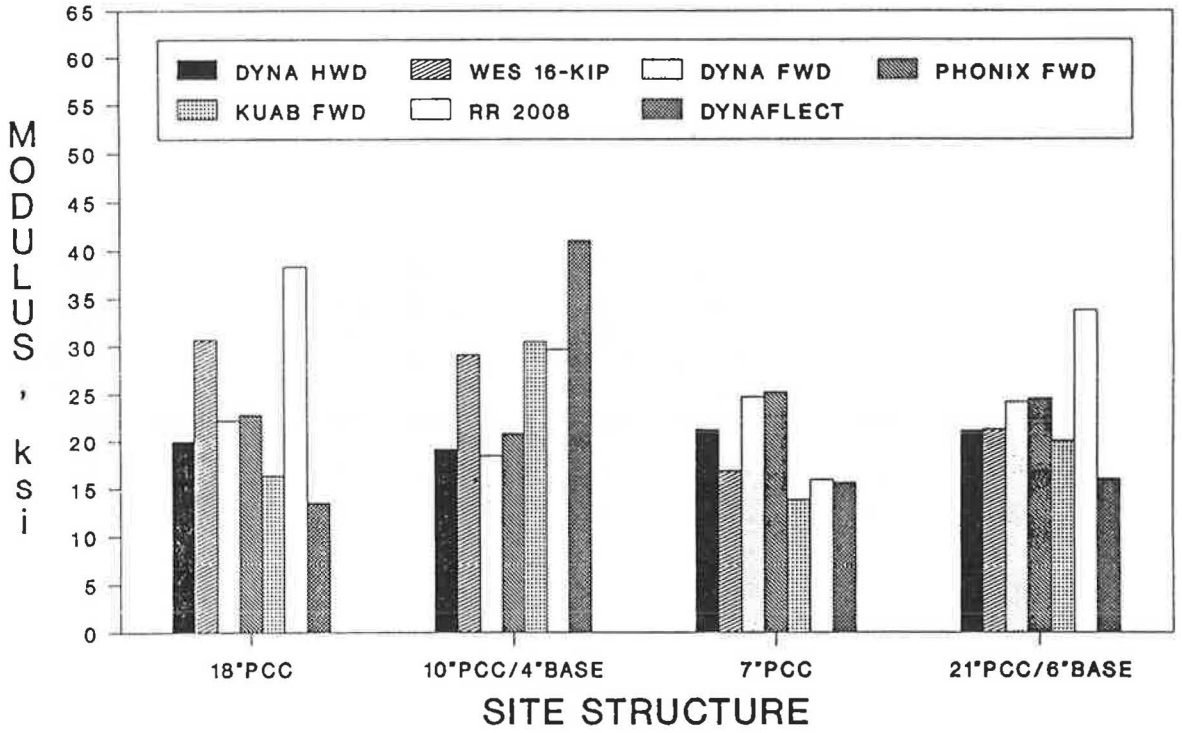

FIGURE 10 Backcalculated subgrade moduli for PCC sites.

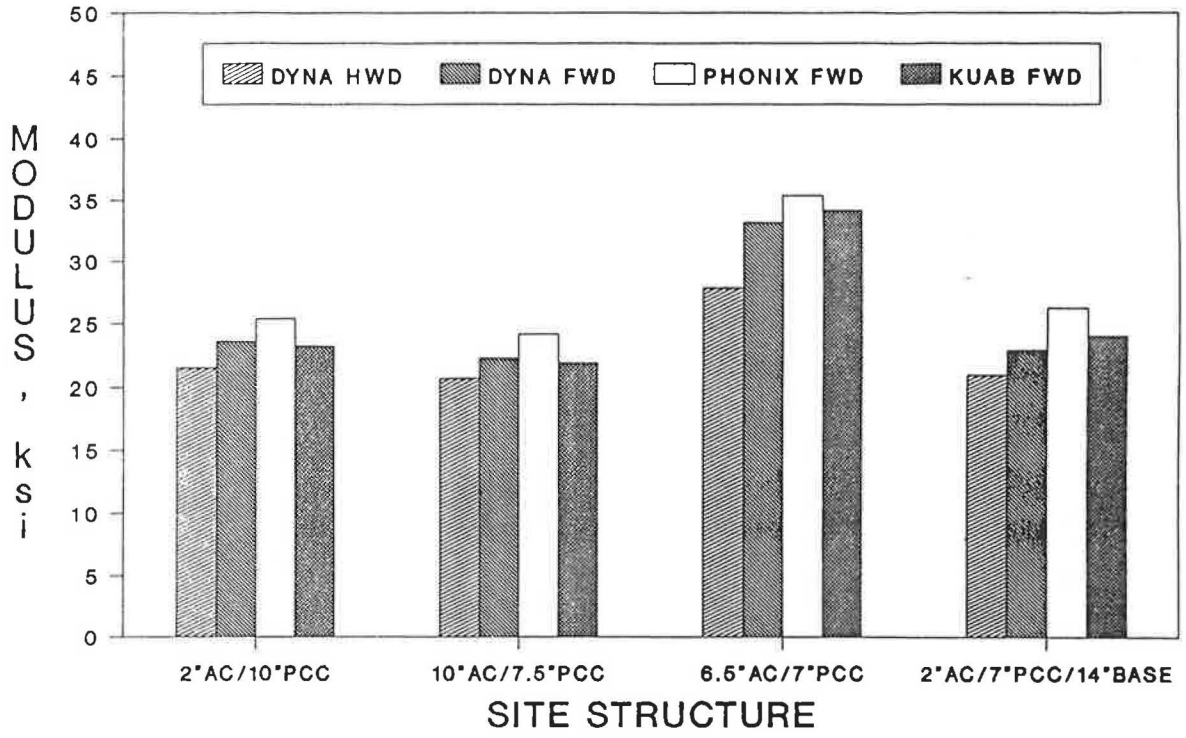

FIGURE 11 Backcalculated subgrade moduli for composite sites with FWDs.

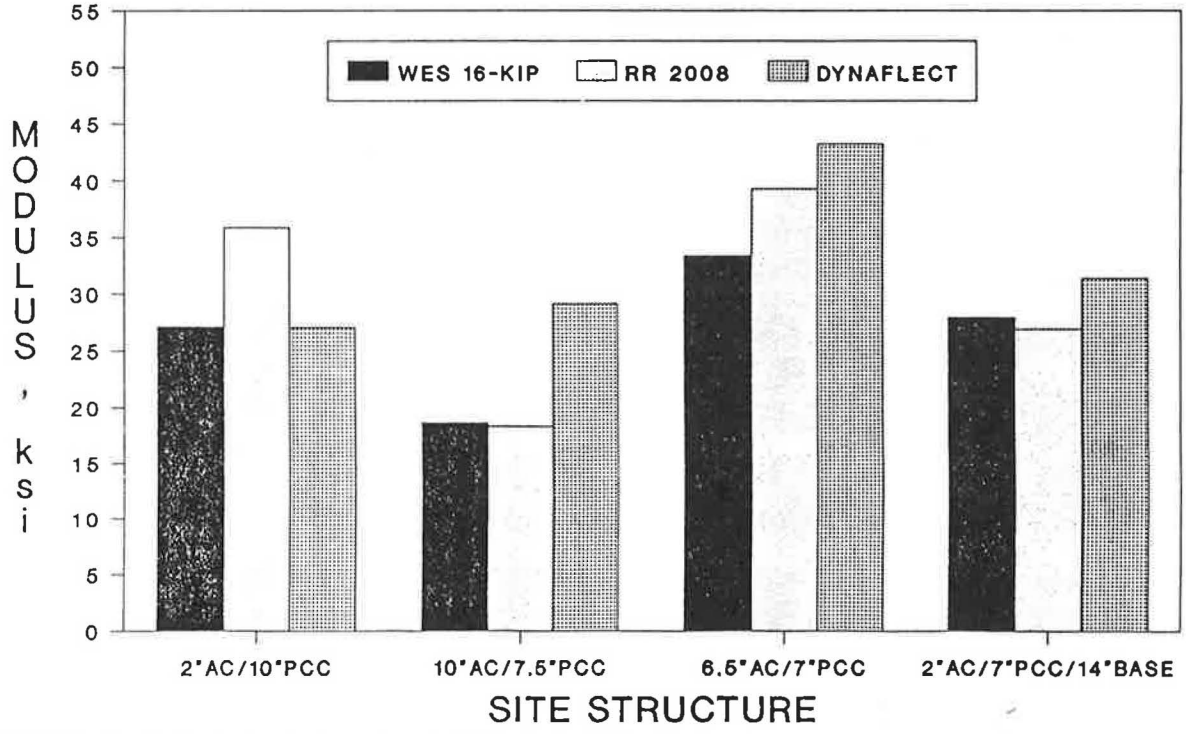

FIGURE 12 Backcalculated subgrade moduli for composite sites with vibrators.

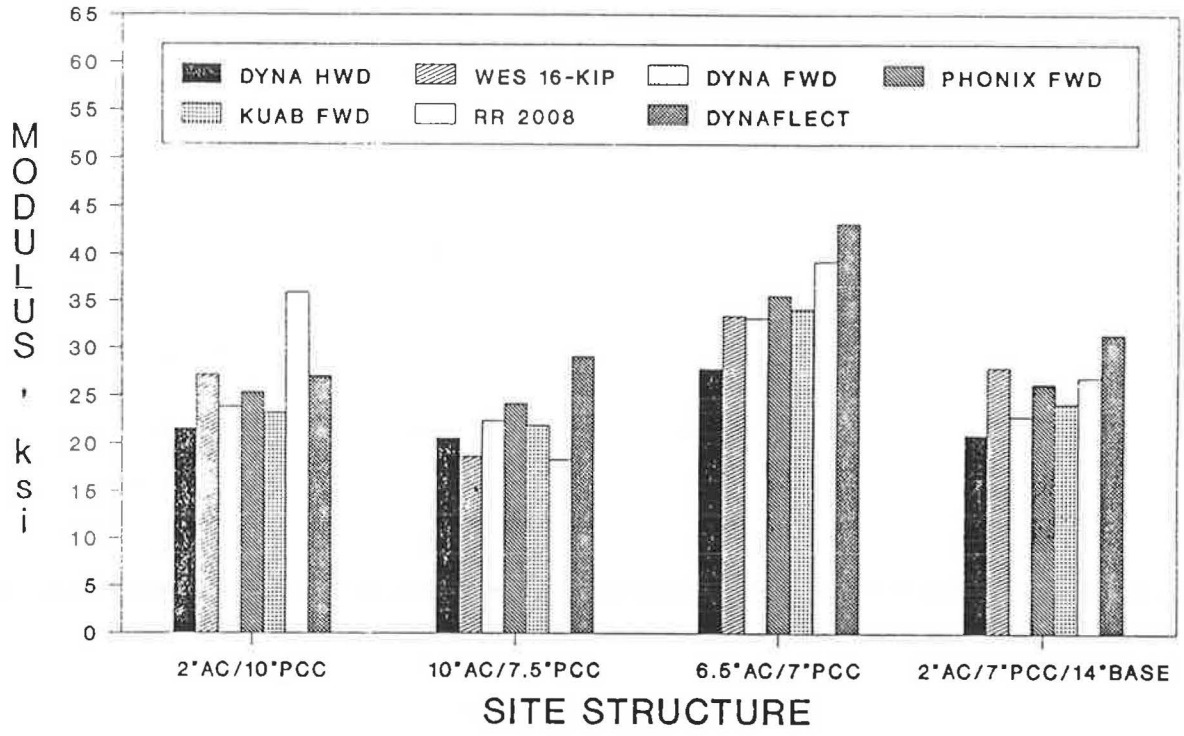

FIGURE 13 Backcalculated subgrade moduli for composite sites.

with the exception of the Kuab. Vibrator subgrade values on composite pavements are shown in Figure 12. Again the Road Rater appears to be highly variable. Modulus values for all devices are shown in Figure 13 for the composite pavements. For the composite pavements, the Dynaflect values are significantly larger than those for the other devices.

Allowable Load and Overlay Requirements

To define how the variability in subgrade moduli translates to allowable aircraft load and rehabilitation requirements, average pavement thicknesses were selected in a sensitivity analysis. The pavement parameters are as follows:

Design Aircraft: DC–10
Design Load: 590 kips
Design Passes: 100,000

	AC			*PCC*			*Composite*		
	E	μ	*H*	*E*	μ	*H*	*E*	μ	*H*
Layer 1	300	0.35	5	6000	0.15	10	300	0.35	5
Layer 2	40	0.35	12	Variable	0.4	—	6000	0.15	8
Layer 3	Variable	0.4	—				Variable	0.4	—

where

E = layer moduli (ksi),
μ = Poisson's ratio, and
H = layer thickness (in.).

The AIRPAVE program (*4*) was used to calculate the allowable aircraft loads and overlay thickness requirements for the DC–10 aircraft for these pavements with variations of the subgrade moduli. Results are shown in Figures 14 through 16 for each of the pavements. Overlay calculations are for AC overlays on AC and composite pavements and PCC overlays for PCC pavements. For the AC pavement, change in overlay thickness requirements and AGAL is very small when the subgrade modulus is greater than 20,000 psi. This is because the strain in the bottom of the AC layer controls on this pavement rather than the vertical strain in the subgrade.

Using the moduli data from Tables 10 through 12 and Figures 14 through 16, maximum variations in AGAL and overlay thicknesses for a single pavement site can be determined. These are as follows:

Pavement Type	*Range in AGAL for DC–10 (kips)*	*Range in Overlay Thickness (in.)*
AC	239 to 344	6.5 to 10.6
PCC	264 to 373	11.3 to 17.0
Composite	294 to 350	13.3 to 15.9

From this analysis, the maximum variation in overlay thickness requirement is about 4 in. of AC or 6 in. of PCC. These ranges are approximations but do indicate that different devices can give significant differences in rehabilitation requirements. These differences are significant in terms of construction costs.

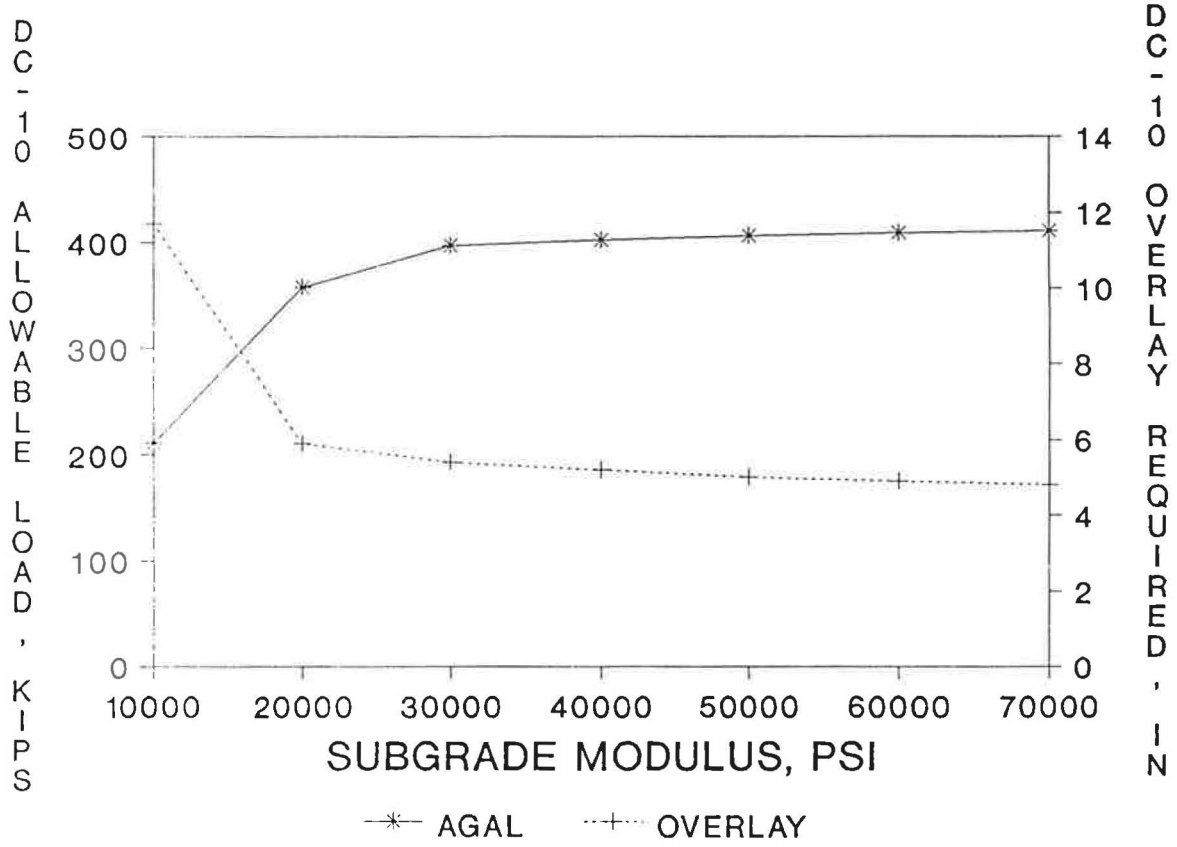

FIGURE 14 Allowable gross aircraft loads and overlay thickness requirements for asphalt pavements.

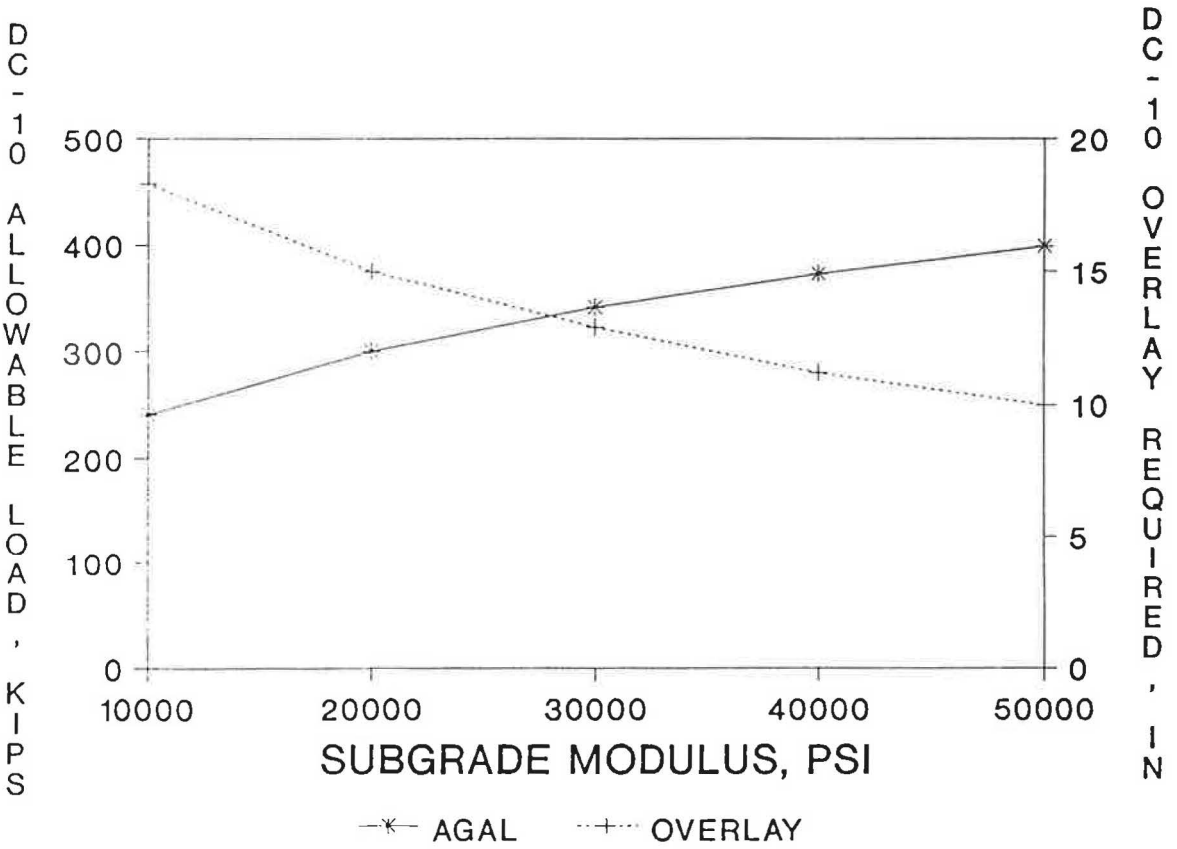

FIGURE 15 Allowable gross aircraft loads and overlay thickness requirements for PCC pavements.

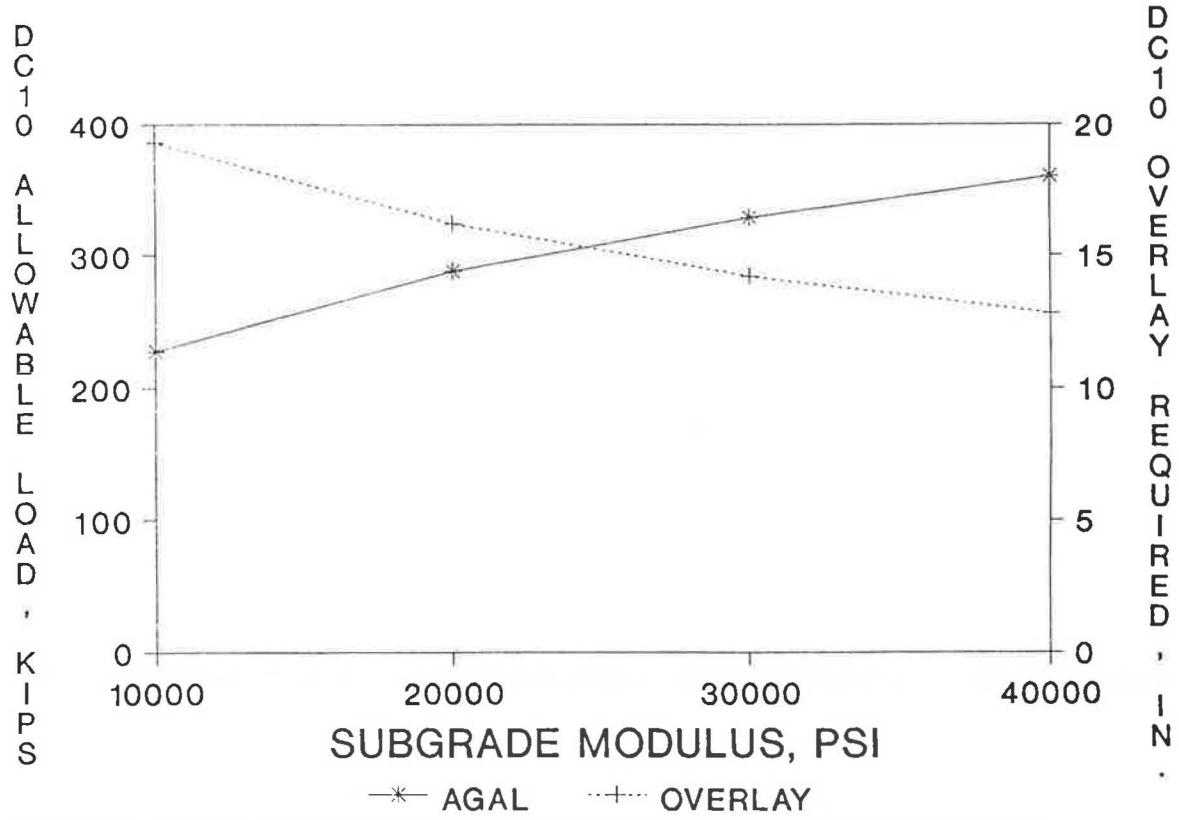

FIGURE 16 Allowable gross aircraft loads and overlay thickness requirements for composite pavements.

TABLE 11 BACKCALCULATED SUBGRADE MODULI FOR PORTLAND CEMENT CONCRETE PAVEMENTS

	Site 1			Site 3		
	Count	Mean KSI	Standard Deviation	Count	Mean KSI	Standard Deviation
KUAB	6	16.3	0.315	6	30.6	0.498
DYNA HWD	6	20.0	0.077	6	19.0	0.191
DYNAFLECT	6	13.7	0.384	6	40.8	1.651
DYNA FWD	6	22.0	1.467	6	18.6	0.640
ROAD RATER	6	39.1	6.264	6	29.6	0.559
WES 16-KIP	4	30.6	2.231	6	28.9	0.325
PHONIX	6	24.3	3.755	6	20.6	1.028
	Site 11			Site 7		
	Count	Mean KSI	Standard Deviation	Count	Mean KSI	Standard Deviation
KUAB	6	20.0	1.680	6	13.9	0.483
DYNA HWD	6	21.1	0.114	6	21.2	0.206
DYNAFLECT	6	16.1	0.923	6	15.5	0.403
DYNA FWD	6	24.0	0.528	6	24.8	0.660
ROAD RATER	6	33.1	8.849	6	15.9	1.198
WES 16-KIP	6	21.4	2.840	6	16.8	0.328
PHONIX	6	24.5	0.370	6	25.1	0.435

TABLE 12 BACKCALCULATED SUBGRADE MODULI FOR COMPOSITE PAVEMENTS

	Site 6			Site 2		
	Count	Mean KSI	Standard Deviation	Count	Mean KSI	Standard Deviation
KUAB	6	22.0	0.334	6	23.2	0.860
DYNA HWD	6	20.7	0.119	6	21.5	0.170
DYNAFLECT	6	28.8	0.890	6	27.1	0.546
DYNA FWD	6	22.3	0.400	6	23.6	0.412
ROAD RATER	6	18.4	0.837	6	35.9	2.658
WES 16-KIP	6	18.7	0.108	6	27.1	0.345
PHONIX	6	24.2	0.210	6	25.4	0.565
	Site 8			Site 10		
	Count	Mean KSI	Standard Deviation	Count	Mean KSI	Standard Deviation
KUAB	6	34.2	1.263	6	24.0	0.719
DYNA HWD	6	27.9	1.100	6	20.9	0.240
DYNAFLECT	6	43.1	0.977	6	31.2	0.744
DYNA FWD	6	33.1	0.936	6	22.9	0.146
ROAD RATER	6	39.3	5.064	6	27.0	0.388
WES 16-KIP	6	32.8	1.401	6	27.9	1.329
PHONIX	6	35.4	1.596	6	26.2	0.797

CONCLUSIONS

On the basis of preliminary analysis of data from seven NDT devices on 12 airfield pavements, the following conclusions are presented:

1. When conducting tests with an FWD, the first drop results are sometimes erroneous and should always be discarded.
2. The deflections and backcalculated moduli are highly variable from the Road Rater device.
3. The backcalculated moduli from the Kuab device does not follow the patterns of the other FWDs.
4. The variation in subgrade moduli from the seven devices results in significant differences in allowable aircraft load and overlay thickness requirements.

ACKNOWLEDGMENTS

The author gratefully acknowledges the support of the U.S. Army Engineer Waterways Experiment Station (WES) and the project sponsors, the U.S. Air Force Engineering and Services Center, the Naval Facilities Engineering Command, the FAA, and the Department of the Army, Office of Chief of Engineers. Permission was granted by the Chief of Engineers to publish this paper.

REFERENCES

1. J. W. Hall. *Comparative Study of Nondestructive Pavement Testing, MacDill Air Force Base, Florida.* Technical Report GL-87-15, U.S. Army Engineer Waterways Experiment Station, Vicksburg, Miss., 1987.
2. R. A. Bentsen, A. J. Bush, III, and J. A. Harrison. *Evaluation of Nondestructive Test Equipment for Airfield Pavements, Phase I, Calibration Test Results and Field Data Collection.* Technical Report GL-89-3, U.S. Army Engineer Waterways Experiment Station, Vicksburg, Miss., Jan. 1989.
3. Headquarters, Department of Defense. *Test Method for Pavement Subgrade, Subbase, and Base-Course Materials.* Military Standard MIL-STD-621A, Washington, D.C., 1964.
4. A. J. Bush, III, and D. R. Alexander. Pavement Evaluation Using Deflection Basin Measurements and Layered Theory. In *Transportation Research Record 1022,* TRB, National Research Council, Washington, D.C., 1985, pp. 16–29.
5. Koninilijke/Shell Laboritorium. *BISAR Users Manual: Layered Systems Under Normal and Tangential Loads.* Amsterdam, Holland, 1972.
6. SPSS, Inc. *SPSS/PC+ Advanced Statistics V2.0.* Marija J. Norusis, Chicago, Ill., 1988.

The views expressed in this paper are those of the author, who is responsible for the facts and accuracy of the data. The contents do not necessarily reflect the official views or policies of WES. The paper does not constitute a standard, specification, or regulation.

Publication of this paper sponsored by Committee on Strength and Deformation Characteristics of Pavement Sections.

Comparing Measured and Theoretical Depth Deflections Under a Falling Weight Deflectometer Using a Multidepth Deflectometer

J. I. YAZDANI AND T. SCULLION

Installation and use of the multidepth deflectometer (MDD) for monitoring pavement response are described. The MDD measures depth deflections in pavements. MDDs are installed in specially drilled holes and up to six modules may be placed in a single hole. This device measures the relative deflection of each layer with respect to an anchor point located approximately 7 ft below the surface. Three sections at the Texas Transportation Institute Research Annex have been instrumented with MDDs. These sections have the same materials but varying layer thicknesses. An effort was made to measure the movement of the anchor. Measuring the anchor movement permits calculation of the absolute depth deflection at each MDD sensor. Surface and depth deflections were measured under FWD loadings. The MODULUS computer program was used to backcalculate the layer moduli from surface deflections. These moduli values along with the layer thickness information were entered into the BISAR layered elastic program to predict the theoretical deflections at depths corresponding to the MDD sensor locations and at the anchor. The analysis was conducted for an infinite subgrade and for a 20-ft depth to bedrock. A comparison of measured versus calculated deflections revealed that a better match was obtained between the two with the bedrock at 20-ft depth.

The procedure used by several investigators to verify modulus backcalculation procedures is to compare the results obtained from an appropriate theoretical analysis of nondestructive test (NDT) data to those obtained from laboratory testing of the pavement materials. Resilient modulus tests are commonly performed on base course and subgrade materials using a triaxial test apparatus. For thin surfacing, repeated load diametral tests are performed. The problem with this approach is that it is difficult, if not impossible, to duplicate field loading conditions in the laboratory. The problem is particularly acute for granular base materials, where laboratory specimens have to be remolded to the same moisture and density as in the field, and then subjected to loading conditions as close as possible to those under moving vehicles. Despite the problems inherent in this approach, verification of modulus backcalculation procedures remains a crucial concern, particularly with the publication of the new *AASHTO Design Guide* (*1*), which advocates NDT evaluations for pavement maintenance and rehabilitation designs.

Three research pavement sections at the TTI Research Annex were instrumented with multidepth deflectometers (MDDs). These devices measure the transient deflection between a particular location in the pavement and an anchor located about 7 ft below the surface. By simultaneously measuring surface and depth deflections under FWD loadings, a procedure is presented to evaluate the effectiveness of modulus backcalculation procedures. The surface deflections are used to backcalculate layer modulus E values; these are then used to predict depth deflections. The error between measured and calculated deflections is defined.

A unique feature of this work is that the movement of the MDD anchor has been recorded using a geophone mounted on the center core. The analysis therefore uses absolute, rather than relative, deflections.

In the next section, the MDD system and the installation procedures are described. The experimental setup at the TTI Research Annex is then presented, followed by a description of the test procedure, results obtained, and details of the analysis.

Texas Transportation Institute, College Station, Tex. 77843.

THE MULTIDEPTH DEFLECTOMETER

The Texas Transportation Institute (TTI) has been evaluating multidepth deflectometers (MDDs) as pavement instrumentation tools since early 1988 (*2*). The system was developed in South Africa and has been used extensively as an integral part of their accelerated loading program (*3*). The MDD is typically installed at the layer interfaces and is used to measure both the transient relative depth deflection profile and the permanent deformations in each layer. Figure 1 shows a schematic of a typical MDD that consists of modules with linear variable differential transformers (LVDTs).

The LVDTs are positioned at different depths in the pavement to measure any movement in these layers. The modules are locked in position by turning the clamping nut, which forces the steel balls outward, clamping them against the sides of the hole. The interconnecting rod is adjustable and contains LVDT cores at spacings that coincide with the module placement. A typical MDD installation is shown in Figure 2. In practice, up to six modules may be placed in a single hole. The interconnecting rod is fixed to an anchor located at approximately 7 ft below the pavement surface. When data are being acquired, a connector cable is attached to the data capture system. When the MDD is not in use, a brass surface

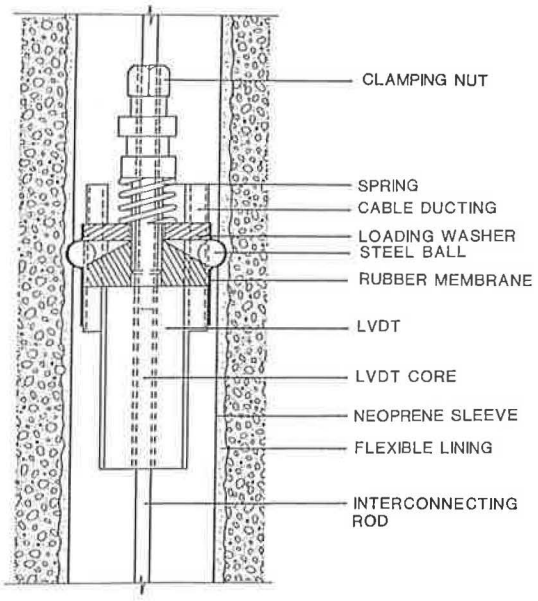

FIGURE 1 Components of MDD module.

cap, which is flush with the surface, completely seals the hole. The brass cap is lined with a rubber ring on the inside to prevent the intrusion of dirt and moisture.

Installation Procedure

In order for the MDD to operate effectively, special care has to be exercised in installing the MDD unit. The test hole for instrumentation of the pavement section has to be drilled vertically. Percussion drills and a specially designed drilling rig are used for the drilling procedure. A 1.5-in.-diameter hole is drilled to a depth of approximately 7 ft. The top 1 in. of the pavement is drilled with a special 2.5-in. drilling bit for installation of the top cap. The top cap is mounted flush with the surface. The top of the MDD has to be level with the pavement to avoid any point loading on it after installation.

The hole is then lined with a 0.1-in. rubber lining tube and the voids between the tube and the wall are filled with rubber grout. The lining prevents the adjacent material from dislodging when under stress and guides the MDD anchor pin and rod for correct installation. The rubber grout is asphalt based and is strong enough to hold back the layer material from protruding into the hole under load; at the same time, it should not affect the pavement material behavior.

The MDD anchor pin is then led through the hole and locked in place using a cement and sand paste. This procedure fixes the anchor pin, so that the LVDT movements are relative to the anchor pin. This is followed by installing a pilot rod, which is used to guide the MDD modules vertically and to the right position. The MDD modules are installed into the correct predetermined position using an installation tool specially made for the purpose. The module is guided to the correct position in the test hole and secured by turning the clamping nut at the top of the MDD module. This forces the steel balls against the wall, holding the module in place. Similarly all the other modules are installed. The modules are

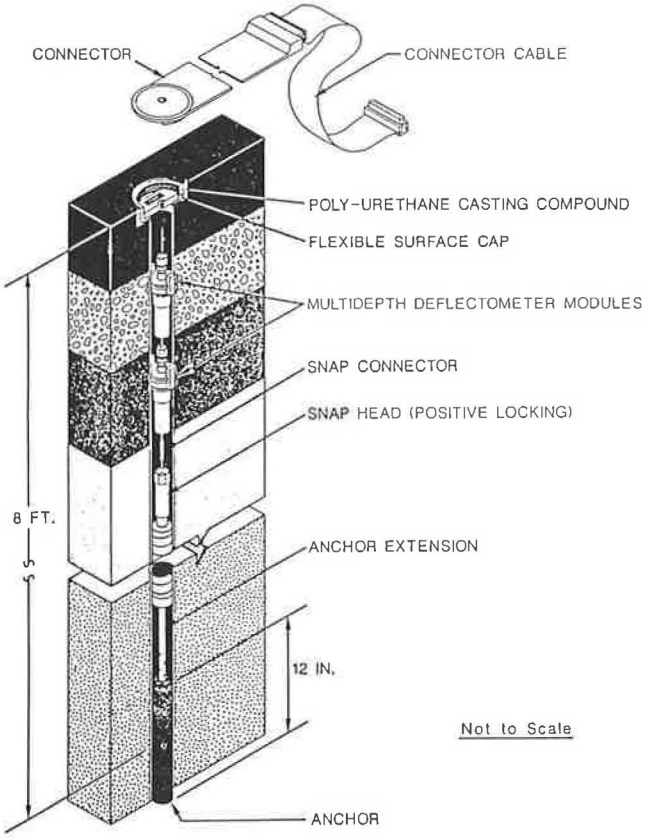

FIGURE 2 Typical cross section of MDD after installation.

numbered from the shallowest to the deepest in ascending order. The modules having been fixed in place, they must be calibrated before operation. The complete installation takes approximately 1½ days. The hole is drilled and lined, and the anchor is installed on the first day. The rubber grout takes approximately 12 hr to set, depending on the temperature. On the second day, the MDD modules are installed and calibrated.

Calibration

Before operation of the MDD, the LVDT modules have to be calibrated to remove any zero error. In order to calibrate the MDD unit, a signal conditioner box, and a calibrator unit fitted with a dial gage mounted on a screw adjusting mechanism, are used. The potentiometer settings on the signal conditioner are first adjusted to be the same as obtained from calibration in the laboratory. The MDD core is moved up and down against the modules manually to determine its mid-zero position. The calibrator unit is then placed above the MDD hole, and the core to one of the LVDTs is connected to it. The screw mechanism is turned until the module reads zero on the conditioner unit. The dial gage is set to a zero reading and the screw mechanism is turned until the dial gage reads 0.30 in. (maximum displacement range of a Schaevitz E300 LVDT). With the dial gage at 0.30 in., the conditioner unit should read 10 (volts). If not, it should be adjusted to read 10 (volts). As a check, the dial gage is reset to zero

displacement and the conditioner observed to see if it gives a zero reading. The procedure is repeated for each module installed in the MDD unit. With the calibration procedure over, the final potentiometer settings are noted.

After the MDD is calibrated, it is sealed off with a brass cap, which is screwed flush with the pavement surface. The surface cap is removed during a measuring operation to enable a cable to be connected from the MDD to a computerized data acquisition system (Figure 2).

MDD Recovery

One of the major advantages of the MDD is that the unit can be retrieved in case the test site has to be abandoned or the LVDTs are to be replaced. With reference to Figure 2, the only parts of the system that cannot be retrieved are the anchor and the rubber lining. The MDD modules, center core, snap head connector, and surface cap can be recovered for future use. Replacing MDD modules in an existing hole can be accomplished in 1 day.

LVDT Selection

There are several factors that must be considered when selecting the appropriate LVDT. These include range, sealed versus unsealed, and type of LVDT. To date, both the E300 (range ± 0.30 in.) and the E100 (range ± 0.10 in.) have been used. The E300 LVDTs are preferred for long-range testing over the E100 LVDTs, because they have a wider range.

If an LVDT is proposed to be used for long-term monitoring of pavements, the hermetically sealed LVDTs may be opted. In hermetically sealing the LVDT, it is enclosed in a heavy-wall, stainless steel housing with an integral stainless steel bore liner (*4*). The hermetic sealing provides air-tight protection to the LVDTs from the moist and corrosive environment. Unsealed LVDTs are in use at the Texas A&M Research Annex since the fall of 1987 without problems (*2*). At the Research Annex, the LVDT holes are sealed by a brass cap on top of the MDD. This procedure prevents excessive moisture from entering the hole; however, condensation buildup has occurred.

Before the present study at the Research Annex, only ac LVDTs have been used. This study will also investigate the dc LVDTs. The main difference between the two LVDT types is the signal conditioner box. The dc LVDT has an integrated signal conditioning feature, eliminating the need for a separate signal conditioner box as in the ac LVDT. As a result of built-in signal conditioning, the dc LVDT need only be calibrated once, after installation.

Data Logging System of the MDD

The MDD voltage output is first processed by a six-channel signal conditioner box. The signal conditioner box converts MDD output into computer form. The signal conditioner box has six channels because up to six LVDTs can be installed in each MDD unit. Each channel is set to give a calibrated output of ± 10 volts for the full range of the LVDT on 100 percent scale. The conditioner box has several features including a scaling switch that permits the user to select the full-range scale (2, 5, 10, 20, 40, 50, or 100 percent), a zero-offset potentiometer, and digital output. The range setting makes the system more sensitive and permits the monitoring of small displacements. For example, on 100 percent scaling, 10 volts is equal to a movement of 0.30 in. (Schaevitz E300 LVDT); on 10 percent scaling, 10 volts LVDT output would be equal to 0.030 in. Loads are applied to the system by either NDT equipment or truck. The LVDTs monitor the differential movement between the pavement layers and the fixed anchor. TTI has developed a specialized data acquisition system for logging MDD pulses under falling weight deflectometer (FWD) and truck loads. A Compaq 386/20 microcomputer is used with a Data Translation circuit board. A sampling rate of 5,000 readings per channel per second is used. Under FWD loading, a 60-ms recording interval is used. Triggering has been automated on the basis of a response of any sensor greater than a preset trigger level. The pretrigger information, 100 data points, is stored and is included in the output record. For recording truck data, the truck length and speed are input. The sampling rate is automatically calculated and the triggering is automated. For trucks, 1,000 data points per channel are stored. The files created are read directly into LOTUS for display and analysis.

Data Cleanup and Scaling

Figure 3a shows a typical MDD trace under an FWD loading. Along with the trace of the FWD drop, it also shows the 100 pretrigger points that the data acquisition system has stored. These pretrigger points are useful in calculating the average scaling factor. Figure 3a shows a high-frequency noise present in the signal. The source of the noise has not been detected. The noise has been reported in both truck loading as well as FWD testing. The noise was problematic in that it made it difficult to determine the true maximum deflection, particularly when low-magnitude (<2 mils) signals were being analyzed.

To clean up the signal, therefore, a filter program has been developed. This program performs a fast Fourier transform on the signal. The noise has been determined to have a frequency of 130 Hz. The spectrum of the signal was filtered and the frequency components that were over 120 Hz were attenuated. This procedure is followed by an inverse Fourier transform to return the signal to the time domain. The filtered signal is shown in Figure 3b. The whole trace has now come close to the horizontal axis, making it easier to reduce the actual deflection.

USES OF MDD

The MDD is used to monitor the pavement response under a single load or performance in repeated load tests. Under a single load, the MDD measures the relative deflection between its position and the anchor. When the MDD is installed, the no-load output voltage is recorded. After repeated load, changes in the no-load reading measure the permanent deformation that has occurred. By placing the MDDs at layer interfaces,

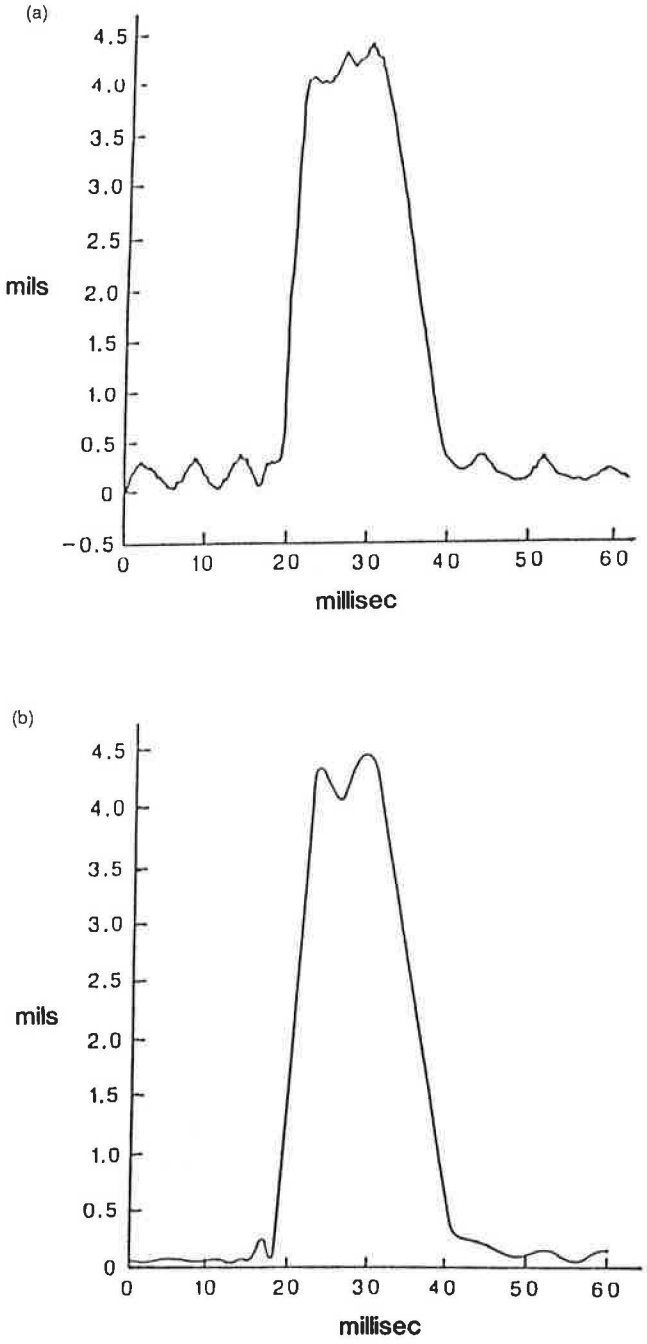

FIGURE 3 MDD response (a) before filtering and (b) after filtering.

it is possible to monitor the deformation that has occurred in each layer of the structure.

South African investigators have conducted numerous accelerated load tests over the past decade using their heavy vehicle simulators (HVSs) (*5*). The results of one of these investigations are shown in Figure 4 (*6*). This figure shows the performance of a lightly cemented granular base and thin surfacing under heavy loads. As shown, the induced rutting was measured to occur primarily in the cemented layer.

In the remainder of this paper, observations of pavement response under the FWD are presented.

MDD INSTALLATION AT TTI RESEARCH ANNEX

Three pavement test sections at the Texas Transportation Institute (TTI) Research Annex have been instrumented with MDDs. The MDD installation is shown in Figure 5. These sections have similar materials but varying layer thicknesses. Section 9 has thinner base and subbase than Section 12. Section 11 has a thin AC layer.

Figure 6 shows the setup used to measure the anchor movement. One of the geophones of the FWD is attached to a circular plate screwed on top of the core. When the FWD load was dropped, the seventh sensor would read the anchor movement, whereas the remaining six geophones would provide the surface deflection. The movement of the core thus obtained was added to the individual peak deflections to obtain total absolute deflection at the LVDT location.

The FWD was used as the loading device in the study. The FWD is an impulse loading machine capable of imparting a range of loads by varying the drop heights. The FWD sensors were located at 1-ft intervals for each test reported in this paper. The FWD load plate was placed as close as possible to the MDD hole, and surface and depth deflections were recorded. The load plate was then moved approximately 18 and 30 in. from the MDD hole and the drop sequence repeated. The electronics at Sections 11 and 12 prevented positioning the FWD on top of the MDD. At each location, the MDD anchor movement was recorded. The FWD positions at which the MDD responses were acquired are shown in Figure 7.

ANALYSIS PROCEDURE

The analysis procedure used consisted of the following steps:

1. From FWD surface deflections, the layer moduli were backcalculated using the MODULUS backcalculation program (*7*).
2. These backcalculated layer moduli, along with the layer thickness information, are entered in the BISAR layered elastic program to forward calculate the deflections and movements at the desired locations including the anchor positions.
3. The accuracy of the calculated movements is verified by calculating percent difference between measured and calculated movements at the anchor as well as at the MDD modules.

For this study, while performing the backcalculation, two depths to bedrock have been investigated. The first is an infinite depth, and the second is a depth to bedrock of 240 in. from the surface. The depth to bedrock of 240 in. was selected on the basis of seismic studies of the area, which indicate a stiff layer at about 20 ft. In the analysis, the test sections have been modeled as three-layered systems. Section 9 has been modeled as 5 in. of AC over 8 in. of crushed limestone (CLS) base over subgrade (infinite or 240-in. depth to bedrock from surface). Section 11 has been modeled as 1 in. of AC over 16 in. of CLS base over subgrade (infinite or 240-in. depth to bedrock from surface). Section 12 has been modeled as 5 in. of AC over 24 in. of CLS base over subgrade (infinite or 240-in. depth to bedrock from surface). The

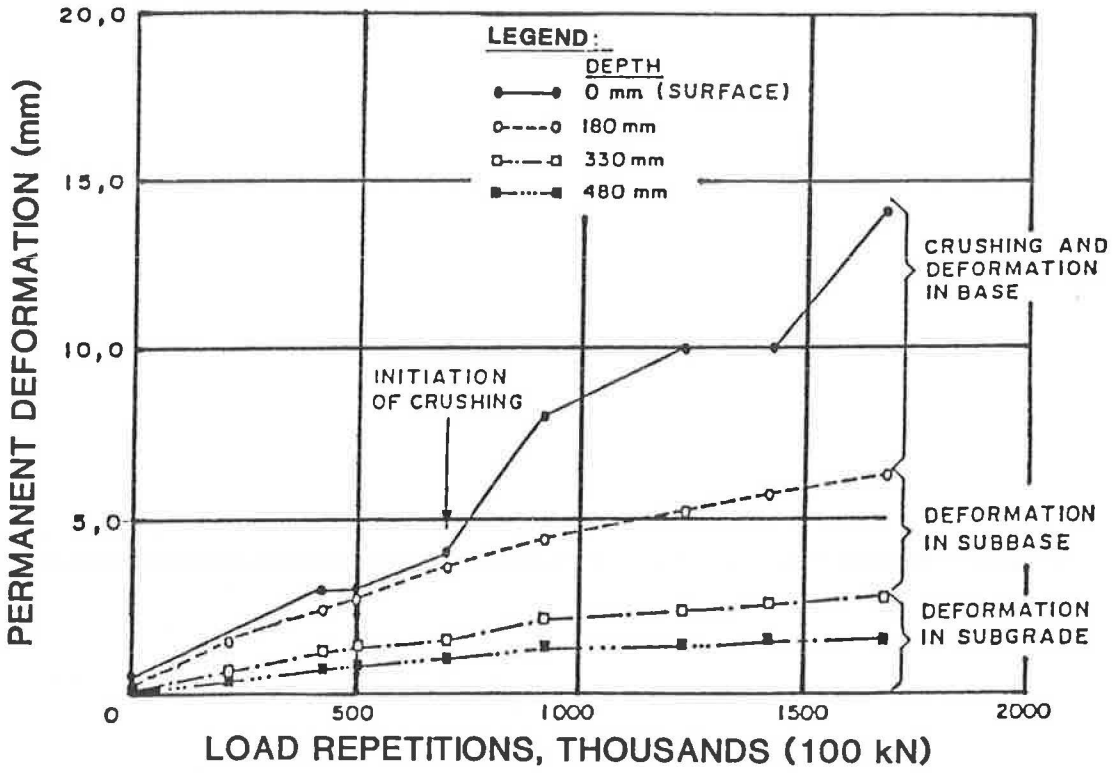

FIGURE 4 MDD results from accelerated road tests (*6*).

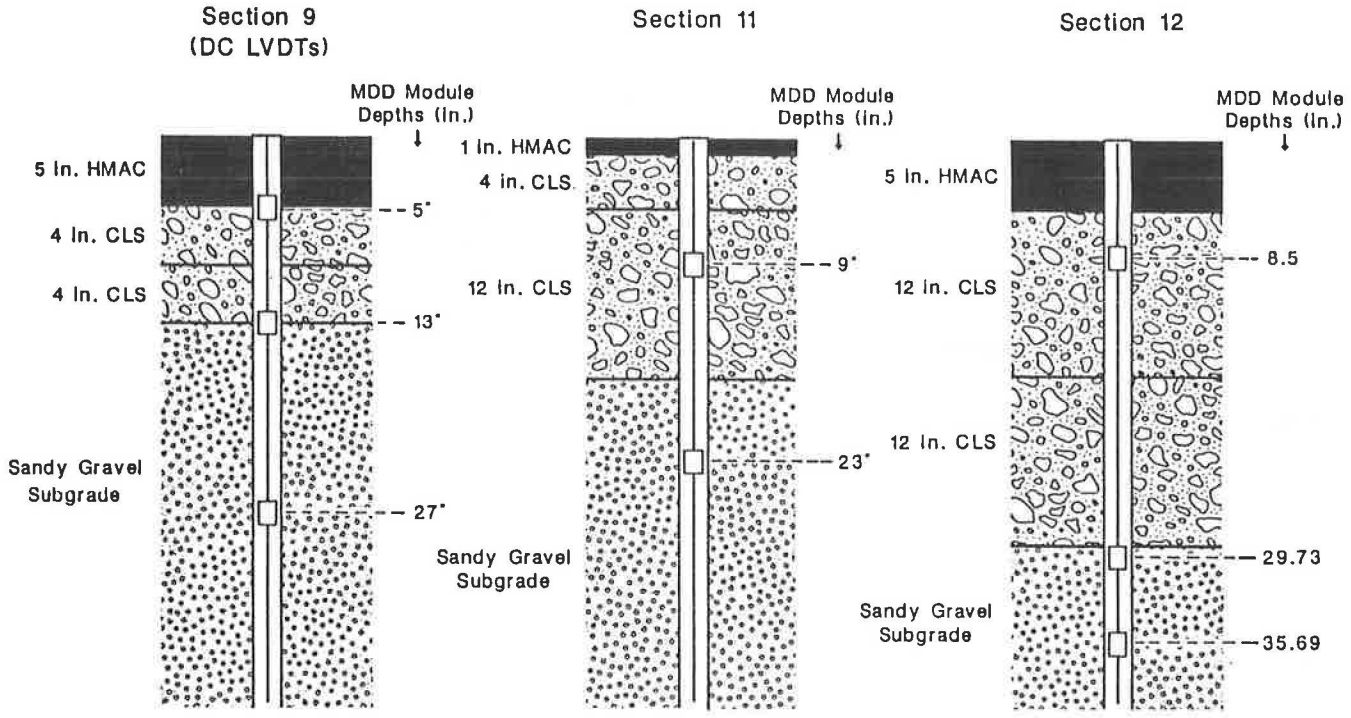

FIGURE 5 MDD installation at TTI Research Annex.

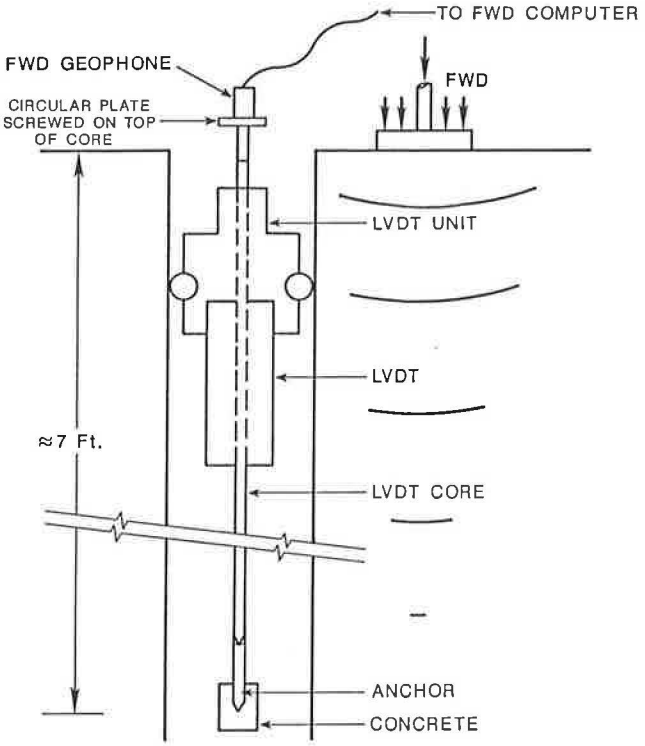

FIGURE 6 Setup to measure anchor movement.

FWD loads that have been considered are in the range of 9,000 lb, to resemble the response of an 18-kip, single-axle truck.

DISCUSSION OF RESULTS

Table 1 presents the surface deflections (W1–W6) and the depth deflections (D1–D3) measured under approximately a 9,000-lb-load FWD at different positions with respect to the MDD at Section 12. The distance from MDD is the distance measured from the center of the FWD loading plate to the center of the MDD hole. The FWD positions that are considered simulate a truck approaching the MDD. The anchor movements are also measured at the same time. Table 2 shows the moduli values backcalculated from the surface deflections (W1–W6) using the MODULUS backcalculation program. The moduli values have been backcalculated for an infinite subgrade (Table 2a) as well as assuming a bedrock at 240 in. from the surface (Table 2b). In both cases, the pavement section has been analyzed as a three-layered system (5 in. of AC over 24 in. of CLS base over subgrade). A lower percent error per sensor was observed in case of infinite subgrade than in the case of a 240-in. depth to bedrock.

Tables 3 and 4 show the depth deflections calculated at the MDD sensor locations and at the anchor. The differences in loads in Tables 2a and 2b and Tables 3 and 4 are attributed

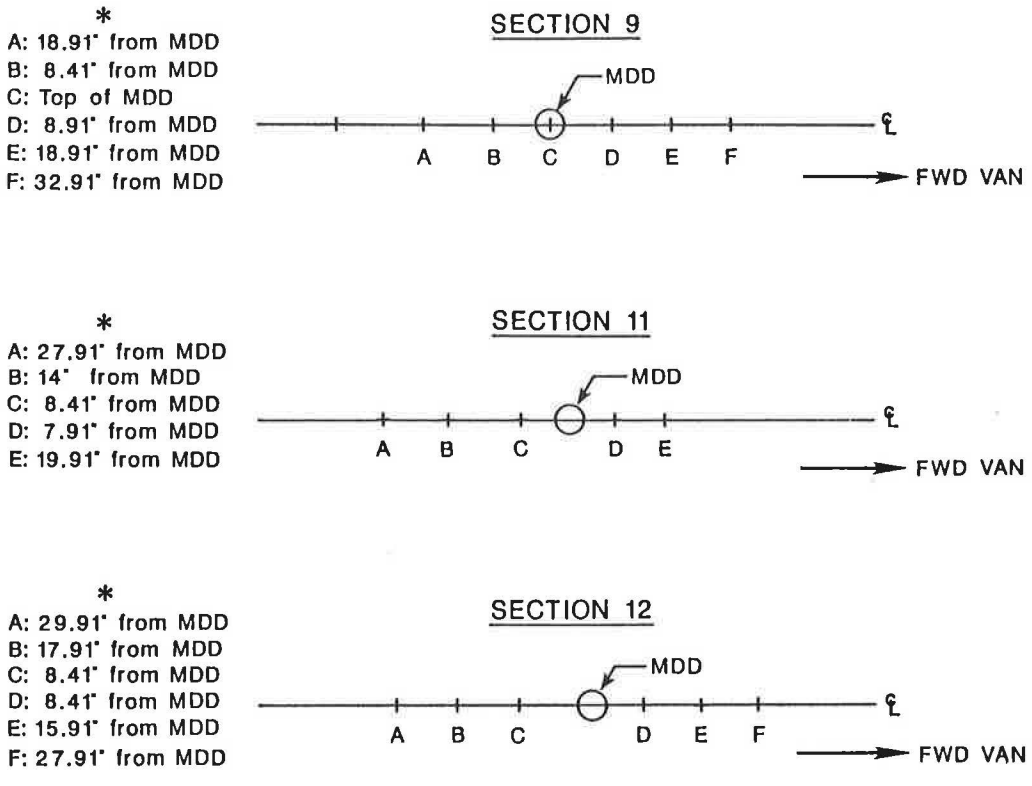

*All distances from center of FWD loading plate to MDD.

FIGURE 7 FWD positions from MDD.

TABLE 1 MEASURED DEFLECTIONS—SECTION 12[a]

Distance From MDD (in.)	Load (lbs)	Surface Deflections (mils)						Depth Deflections (mils)			Anchor (mils)
		W1	W2	W3	W4	W5	W6	D1	D2	D3	
29.91	8560	9.99	5.91	3.08	1.96	1.47	1.18	2.57	2.32	2.32	1.33
17.91	8816	9.46	5.99	3.15	2.04	1.55	1.30	4.43	3.16	2.97	1.46
8.41	8656	9.46	5.82	3.12	1.92	1.42	1.06	6.76	3.79	3.40	1.50

[a] Simultaneously measured surface and depth deflections:

(W1, W2, W3, W4, W5, W6): Surface deflections at 1 foot spacings

(D1, D2, D3): Absolute depth deflections (MDD value plus anchor movement)

Anchor movement measured using setup shown in Figure 6.

TABLE 2 MODULI VALUES BACKCALCULATED FROM MODULUS (7)—SECTION 12, INFINITE SUBGRADE AND 20-FT DEPTH TO BEDROCK

Section A[a]

Station	Load (lb)	Measured Deflection (mils)							Calculated Moduli Values (psi)				Absolute Percent Error/Sensor
		R1	R2	R3	R4	R5	R6	R7	Surface (E1)	Base (E2)	Subbase (E3)	Subgrade (E4)	
1.000	8,655	9.46	5.82	3.12	1.92	1.42	1.06	0.00	785,347	34,886	0	34,886	1.35
1.000	8,815	9.46	5.99	3.15	2.04	1.55	1.30	0.00	680,784	40,886	0	32,351	2.44
1.000	8,559	9.99	5.91	3.08	1.96	1.47	1.18	0.00	573,279	37,637	0	33,296	0.90
Mean		9.64	5.91	3.12	1.97	1.48	1.18	0.00	679,803	37,803	0	33,511	1.56
Std. dev.		0.31	0.09	0.04	0.06	0.07	0.12	0.00	106,037	3,003	0	1,281	0.79
Var. coeff. (%)		3.18	1.44	1.13	3.10	4.43	10.17	0.00	15.60	7.94	0.00	3.82	50.44

Section B[b]

Station	Load (lb)	Measured Deflection (mils)							Calculated Moduli Values (psi)				Absolute Percent Error/Sensor
		R1	R2	R3	R4	R5	R6	R7	Surface (E1)	Base (E2)	Subbase (E3)	Subgrade (E4)	
1.000	8,655	9.46	5.82	3.12	1.92	1.42	1.06	0.00	723,960	41,702	0	25,802	2.50
1.000	8,815	9.46	5.99	3.15	2.04	1.55	1.30	0.00	637,865	49,502	0	23,184	5.28
1.000	8,559	9.99	5.91	3.08	1.96	1.47	1.18	0.00	519,832	45,575	0	24,118	3.90
Mean		9.64	5.91	3.12	1.97	1.48	1.18	0.00	627,219	45,593	0	24,368	3.89
Std. dev.		0.31	0.09	0.04	0.06	0.07	0.12	0.00	102,480	3,900	0	1,327	1.39
Var. coeff. (%)		3.18	1.44	1.13	3.10	4.43	10.17	0.00	16.34	8.55	0.00	5.44	35.71

[a]District 17, County 23, Annex 12.

		Moduli Range (psi)	
	Thickness (in.)	*Minimum*	*Maximum*
Pavement	5.00	100,000	1,000,000
Base	24.00	15,000	250,000
Subbase	0.00	0	0
Subgrade	Infinity	10,000	10,000

[b]District 17, County 23, Annex 12.

		Moduli Range (psi)	
	Thickness (in.)	*Minimum*	*Maximum*
Pavement	5.00	100,000	1,000,000
Base	24.00	15,000	250,000
Subbase	0.00	0	0
Subgrade	211.00	10,000	10,000

TABLE 3 DEPTH DEFLECTIONS CALCULATED FROM BISAR—SECTION 12, INFINITE SUBGRADE

Distance From MDD (in.)	Load (lb)	MDD Depth Deflections (mils)			Anchor Movement[a] (mils)
		D1	D2	D3	
29.91	8,560	2.43	2.20	2.08	1.41
17.91	8,816	4.08	3.27	2.84	1.59
8.41	8,656	6.28	3.27	2.84	1.54

[a]Depth 72 in.

TABLE 4 DEPTH DEFLECTIONS CALCULATED FROM BISAR—SECTION 12, 20-FT DEPTH TO BEDROCK

Distance From MDD (in.)	Load (lb)	MDD Depth Deflections (mils)			Anchor Movement[a] (mils)
		D1	D2	D3	
29.91	8,560	2.52	2.30	2.14	1.27
17.91	8,816	4.11	3.20	2.83	1.47
8.41	8,656	6.15	3.51	3.00	1.42

[a]Depth 72 in.

TABLE 5 COMPARISON OF MEASURED AND CALCULATED DEPTH DEFLECTIONS—SECTION 12, FWD LOCATED 29.91 in. FROM MDD, LOAD 8,560 lb

MDD Sensor No.	MDD Deflections (mils)			Percent Difference (%)	
	Measured	Calculated		Infinite Subgrade	20-ft Bedrock
		Infinite S/G	20-ft Bedrock		
1 (at 8.5 in.)	2.57	2.43	2.52	5.45	1.95
2 (at 29.75 in.)	2.32	2.20	2.30	5.17	0.86
3 (at 35.69 in.)	2.32	2.08	2.14	10.34	7.76
Anchor (at 72 in.)	1.33	1.41	1.27	6.01	4.51
Average Difference/Sensor				6.74	3.77

TABLE 6 COMPARISON OF MEASURED AND CALCULATED DEPTH DEFLECTIONS—SECTION 12, FWD LOCATED 17.91 in. FROM MDD, LOAD 8,816 lb

MDD Sensor No.	MDD Deflections (mils)			Percent Difference (%)	
	Measured	Calculated		Infinite Subgrade	20-ft Bedrock
		Infinite S/G	20-ft Bedrock		
1 (at 8.5 in.)	4.43	4.08	4.11	7.90	7.22
2 (at 29.75 in.)	3.16	3.27	3.20	3.48	1.26
3 (at 35.69 in.)	2.97	2.84	2.83	4.38	4.71
Anchor (at 72 in.)	1.46	1.59	1.47	8.90	0.68
Average Difference/Sensor				6.17	3.47

to the rounding off that MODULUS performs in matching the deflection basins. These were calculated assuming both an infinite subgrade as well as a 240-in. depth of bedrock. The moduli values backcalculated from surface deflections and the layer thickness information were entered in the BISAR layered elastic program to calculate the deflections.

The deflections calculated at the three sensors and the anchor were then compared with those measured by the MDD for each of the three locations. The results are presented in Tables 5 through 7. Table 5 suggests that by using the backcalculated E values, the average error in predicting deflections within the pavement was 6.7 percent assuming an infinite subgrade and 3.8 percent assuming a depth to bedrock of 20 ft. The average percent difference per sensor was found to be less at each position of the FWD with the bedrock assumed to be 240 in. from the surface.

Tables 8 and 9 present a summary of this process for Sections 9 and 11. For both of these sections as well, a 240-in.

TABLE 7 COMPARISON OF MEASURED AND CALCULATED DEPTH DEFLECTIONS—SECTION 12, FWD LOCATED 8.41 in. FROM MDD, LOAD 8,856 lb

MDD Sensor No.	MDD Deflections (mils)			Percent Difference (%)	
		Calculated			
	Measured	Infinite S/G	20-ft Bedrock	Infinite Subgrade	20-ft Bedrock
1 (at 8.5 in.)	6.76	6.28	6.15	7.10	9.02
2 (at 29.75 in.)	3.79	3.27	3.51	13.72	7.39
3 (at 35.69 in.)	3.40	2.84	3.00	16.50	11.76
Anchor (at 72 in.)	1.50	1.54	1.42	2.67	5.33
Average Difference/Sensor				10.00	8.38

TABLE 8 COMPARISON OF MEASURED AND CALCULATED DEPTH DEFLECTION—SECTION 11, SUMMARY

Distance From MDD (in.)	Load (lbs)	Measured Depth Deflection (mils)			Calculated Depth Deflection (mils)						Avg. Diff/Sensor	
					Infinite Subgrade			Bedrock: 20' Deep				
		D1	D2	Anchor	D1	D2	Anchor	D1	D2	Anchor	Infinite S/Grade	Bedrock 20' Deep
27.91	8752	3.33	3.44	2.00	2.94	2.82	2.00	3.17	3.00	1.91	9.91	7.37
14.00	8656	8.07	6.44	2.33	5.50	4.31	2.33	5.97	4.68	2.29	21.64	18.36
8.41	8608	12.27	8.12	2.50	7.80	5.04	2.46	8.22	5.49	2.44	25.32	22.60

TABLE 9 COMPARISON OF MEASURED AND CALCULATED DEPTH DEFLECTION—SECTION 9, SUMMARY

Distance From MDD (in.)	Load (lbs)	Measured Depth Deflection (mils)				Calculated Depth Deflection (mils)								Avg. Diff/Sensor	
						Infinite Subgrade				Bedrock: 20' Deep					
		D1	D2	D3	Anchor	D1	D2	D3	Anchor	D1	D2	D3	Anchor	Infinite S/Grade	Bedrock 20' Deep
18.91	8760	5.08	5.17	3.87	1.54	4.76	4.48	3.56	1.83	4.96	4.77	3.68	1.62	11.34	4.76
8.41	8640	8.94	8.06	4.77	1.58	9.45	7.03	4.48	1.90	8.26	7.23	4.82	1.80	11.30	8.22

depth to bedrock results in a smaller average percent difference than for an infinite subgrade.

CONCLUSIONS

The following conclusions can be drawn:

1. Setting a depth to bedrock of 20 ft produced a better fit between measured and calculated depth deflections.
2. The average errors on the thicker sections (9 and 12) were acceptable (less than 9 percent per sensor), indicating that linear elasticity for backcalculating E values is reasonable for thick pavements.
3. The average errors on the thin pavement (1 in. asphalt over 16 in. granular base) were high. The errors were greater than 20 percent, indicating that linear elasticity does a relatively poor job at predicting deflections within these thin pavements. The theoretical deflection consistently underpredicted measured deflections. Difficulty of backcalculating layer moduli for thin pavements may result in a poor match.

Work is now under way to determine if, by making different assumptions in the modeling process, the percent error could

be reduced. The nonlinearity of the thin pavement is probably due to stiffening of the underlying granular layers. This makes it a candidate for analysis by other methods. Finite element techniques, for example, account for material stress sensitivity and use the Mohr-Coulomb failure criteria in analyzing pavement response. Work is under way to determine how the nonlinearity of the thin pavement may be accounted for.

The MDD appears to be an excellent tool for validating backcalculation procedures and its use is recommended over the traditional laboratory testing approach.

ACKNOWLEDGMENTS

This work is part of an ongoing research study sponsored by the Texas State Department of Highways and Public Transportation and the FHWA. The assistance of Paul Chan, who built the data capture and signal processing procedures, and of the instrumentation team comprising John Ragsdale, Brad Neal, and Stephen Phillips is gratefully acknowledged.

REFERENCES

1. *AASHTO Guide for Design of Pavement Structures*. AASHTO, Washington, D.C., 1986.
2. T. Scullion, J. Uzan, J. I. Yazdani, and P. Chan. *Field Evaluation of the Multi-Depth Deflectometers*. Research Report 1123-2, Texas Transportation Institute, Texas A&M University, College Station, Sept. 1988.
3. J. E. B. Basson, O. J. Wijnberger, and J. Skultety. *The Multidepth Deflectometer: A Multistage Sensor for the Measurement of Deflections and Permanent Deformations at Various Depths in Road Pavements*. Technical Report RP/3/81, Institute of Transportation and Road Research, South Africa, Feb. 1981.
4. *Handbook of Measurement and Control*. Schaevitz Engineering, Pennsauken, N.J., 1976.
5. C. R. Freeme, J. H. Maree, and A. W. Viljoen. Mechanistic Design of Asphalt Pavements and Verifications using the Heavy Vehicle Simulator. *Proc., 5th International Conference on Structural Design of Asphalt Pavements*, Vol. I, The Delft University of Technology, The Netherlands, Aug. 1982, pp. 156–173.
6. M. Debeer, E. Horak, and A. T. Visser. The Multidepth Deflectometer System for Determining the Effective Elastic Moduli of Pavement Layers. *Proc., 1st International Symposium on NDT and Backcalculation of Moduli*, ASTM, Philadelphia, Pa., 1988.
7. J. Uzan, T. Scullion, C. H. Michalek, M. Paredes, and R. L. Lytton. *A Microcomputer Based Procedure for Backcalculating Layer Moduli from FWD Data*. Research Report 1123-1, Texas Transportation Institute, Texas A&M University, College Station, Sept. 1988.

Publication of this paper sponsored by Committee on Strength and Deformation Characteristics of Pavement Sections.

Microcomputer Application To Determine the Load Zoning for Low-Volume Roads

B. LANKA SANTHA, W. YANG, AND ROBERT L. LYTTON

A computerized procedure, LOADRATE, Version 2.0, has been developed by the Texas Transportation Institute (TTI) for the Texas State Department of Highways and Public Transportation (SDHPT) to evaluate the structural adequacy of light pavement structures, specially for the purpose of load zoning. The LOADRATE program uses data obtained from the Dynaflect or the falling weight deflectometer (FWD) to evaluate pavement condition. A simple mechanistic procedure is used to calculate rut depth, given the number of passes of a wheel load or a multiple-axled vehicle, or vice versa. When supplied with estimated traffic, the procedure can be used to predict the remaining life of pavement sections and to provide an estimate of pavement condition. LOADRATE can make temperature and moisture corrections for the base course modulus. It can also estimate the effects of seasonal variations of the base course moduli on the life of the pavement. Significant improvements of Version 2.0 are the incorporation of a nonlinear relationship for modulus versus deviator stress for sandy subgrades and the reconstruction of the two data bases used in the program. The rut depth can be better determined from these improvements. In the case studies, the strength of the pavement at the edge is weaker than the strength of the pavement in the outer wheel path. A paved shoulder not only prevents water penetration into the road bed, but also provides some lateral support to maintain pavement strength.

Most of the pavements in the United States are light pavement structures on rural roads or, as they are commonly called, low-volume roads. In the state of Texas, these roads are farm-to-market (FM) roads, most of which are two-layer pavement systems consisting of a granular base layer covered with a thin asphalt surface treatment laid over in situ or improved subgrade. The surface treatment acts as a wearing course as well as a waterproofing course. As a result of heavier trucks and higher traffic volumes on these roads, various highway agencies have determined that there is a decisive need for a fast and efficient way to evaluate the structural integrity of these light pavement structures, specially for the purpose of load zoning. The agencies responsible must be able to evaluate the structural adequacy of any light pavement structure when considering load zoning. Therefore, an efficient, nondestructive testing (NDT) procedure is required to determine the traffic damage to pavements.

A mechanistic modeling approach developed for this purpose involves a computerized procedure to analyze data obtained from the Dynaflect or the falling weight deflectometer (FWD). With other information about pavement sections (e.g., traffic data, base course thickness, and subgrade material type), the elastic moduli of the base course and subgrade, number of passes to achieve a specified rut depth, and remaining life can be determined. The remaining life determination is based on a maximum specified rut depth that is the criterion of acceptability. Rut depths are caused by the accumulating pavement deformation under repeated load applications. Each time a load passes, the pavement rebounds less than it was deflected under the load. With repeated loading and unloading sequences, each layer accumulates a significant amount of permanent deformation. Rutting in the wheel path is not only uncomfortable to motorists, but also can cause hydroplaning of vehicles under wet conditions.

LOADRATE (Version 2.0) is the most recently improved version of a computerized procedure for evaluating light pavements. The flow chart of the LOADRATE program is shown in Figure 1. The following sections are organized similarly to the general flow of calculations shown in Figure 1.

The LOADRATE program, developed by The Texas Transportation Institute (TTI) (*1,2*), uses the deflection basin obtained from the Dynaflect or FWD to determine the nonlinear elastic properties of the base course and the subgrade (*3*). The LOADRATE program has been further revised to improve its capabilities and accuracy. A significant improvement of the new version of LOADRATE is the incorporation of a fifth curve to the ILLI-PAVE (*4,5*) subgrade model and the reconstruction of the data base of surface deflection basins used in the program. The nonlinear elastic properties of the base course and the subgrade can be better determined from these improvements. The capability for making seasonal temperature and moisture corrections for the base course modulus has also been added to the program (*6*). The temperature and moisture correction capability allows the user to evaluate seasonal variations of the base course moduli. Finally, the rut depth calculation is achieved using a new approach developed by Yapa and Lytton (*7*). The new rut depth prediction approach makes use of interpolation within a data base of three-dimensional rut depth calculations.

In addition to the theoretical improvements, the new LOADRATE program also provides better outputs. It calculates the number of load repetitions to cause a given rut depth and, using estimated traffic rates, computes the remaining life in years. It also provides several graphic capabilities such as plots of base moduli, subgrade moduli, number of passes, and remaining life for all points along a pavement section for which deflections were measured.

Texas Transportation Institute, Texas A&M University, College Station, Tex. 77843.

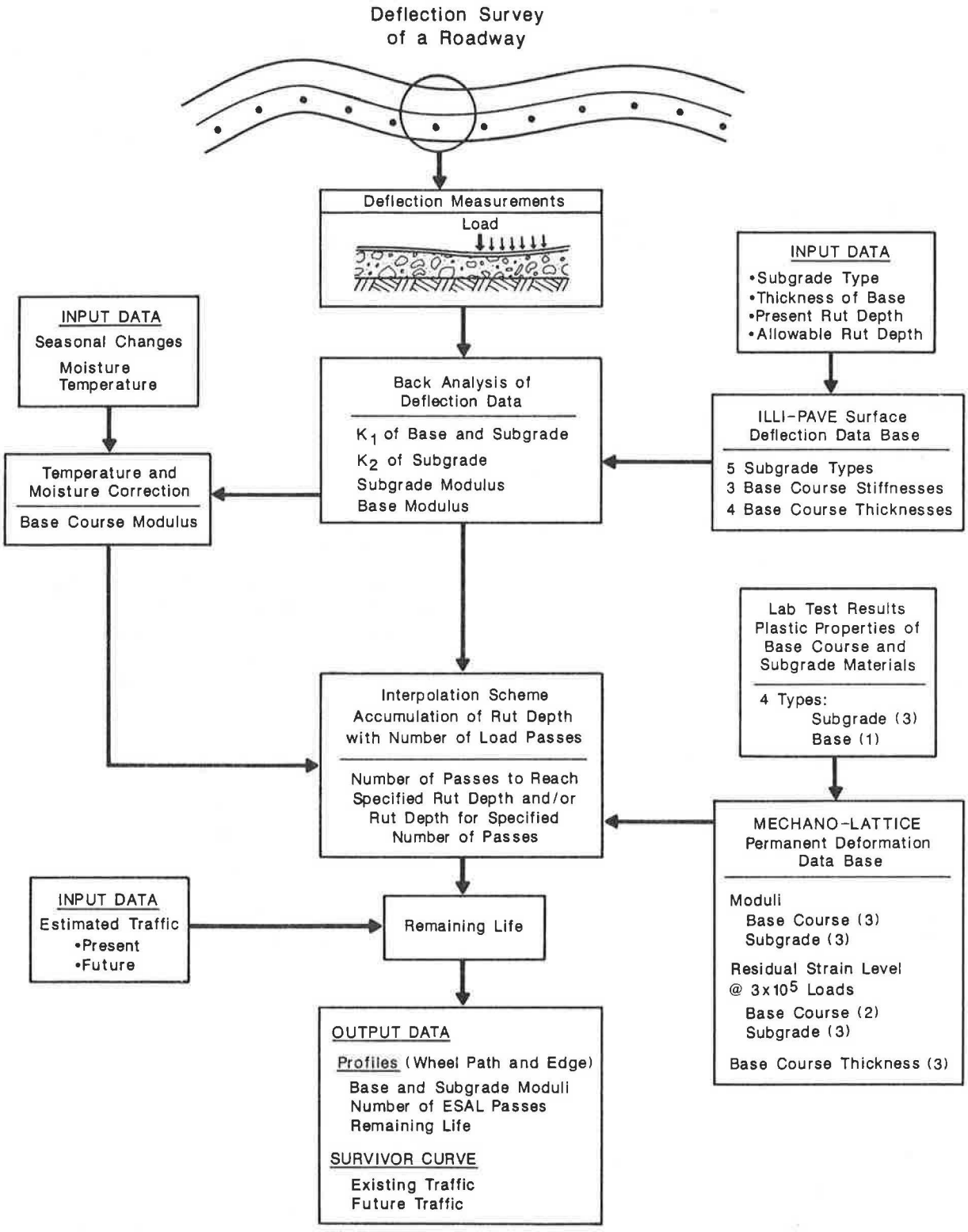

FIGURE 1 Flow chart of the LOADRATE program.

The LOADRATE program has been custom built into a system for the Texas State Department of Highways and Public Transportation (SDHPT). Dynaflect data analyses are made possible by the correlation between the readings of the two devices. LOADRATE is based on a Dynatest FWD and load level of 10,956 lb; therefore, the new version will usually yield better results from analyzing FWD data than Dynaflect data. In order to conduct the deflection survey, the FWD can be used to collect deflection basins along a section of pavement to be load rated. Each deflection basin is analyzed separately by LOADRATE to determine the nonlinear material properties, rut depth, and remaining life. The processes it uses are described in the following section.

LOADRATE PROGRAM

ILLI-PAVE Finite Element Analysis To Reconstruct the Surface Deflection Data Base

The load-deflection relationship of layered systems was investigated by Burmister (*8,9*) in the 1940s. He adapted Boussinesq's theory of distribution of stresses in an elastic half-space under the compressive action of a rigid body to include a layered system. Subsequently, many computerized systems of closed-form solutions were developed. Among them, the BISAR and CHEVRON programs have been widely used by pavement engineers. These solutions assume linearly elastic material properties.

More versatile numerical approaches such as the finite element method are able to simulate both linearly and nonlinearly elastic materials. ILLI-PAVE (*4,5*), a finite element program, was used by LOADRATE to model the load-deflection relationship. ILLI-PAVE considers an axisymmetrical solid of revolution and allows for linear as well as nonlinear stress-dependent elastic moduli for coarse- and fine-grained soil. This program can predict the flexible pavement response to load by comparing the results of computer modeling with field test data (*10*). The following paragraphs will describe the use of ILLI-PAVE in this study and the material models that were input.

Nonlinear Material Properties

The thin surface course of the pavement does not contribute much in terms of pavement rigidity. A representative modulus of 30,000 psi was used in the analysis for surface courses of 1-in. thickness or less. The elastic modulus of the base course material is expressed as

$$E = K_1\theta^{K_2} \tag{1}$$

where

θ = the bulk stress (or sum of the principal stresses),
K_1 = modulus coefficient, and
K_2 = modulus exponent, assumed to be 0.33 (*1*).

The subgrade properties are described by the five curves shown in Figure 2. These five nonlinear relationships represent very soft, soft, medium, stiff, and very stiff subgrades. The fifth curve, for a sandy subgrade, was developed because of the need to represent these stiff subgrades. A description of the development of the fifth curve will be discussed later.

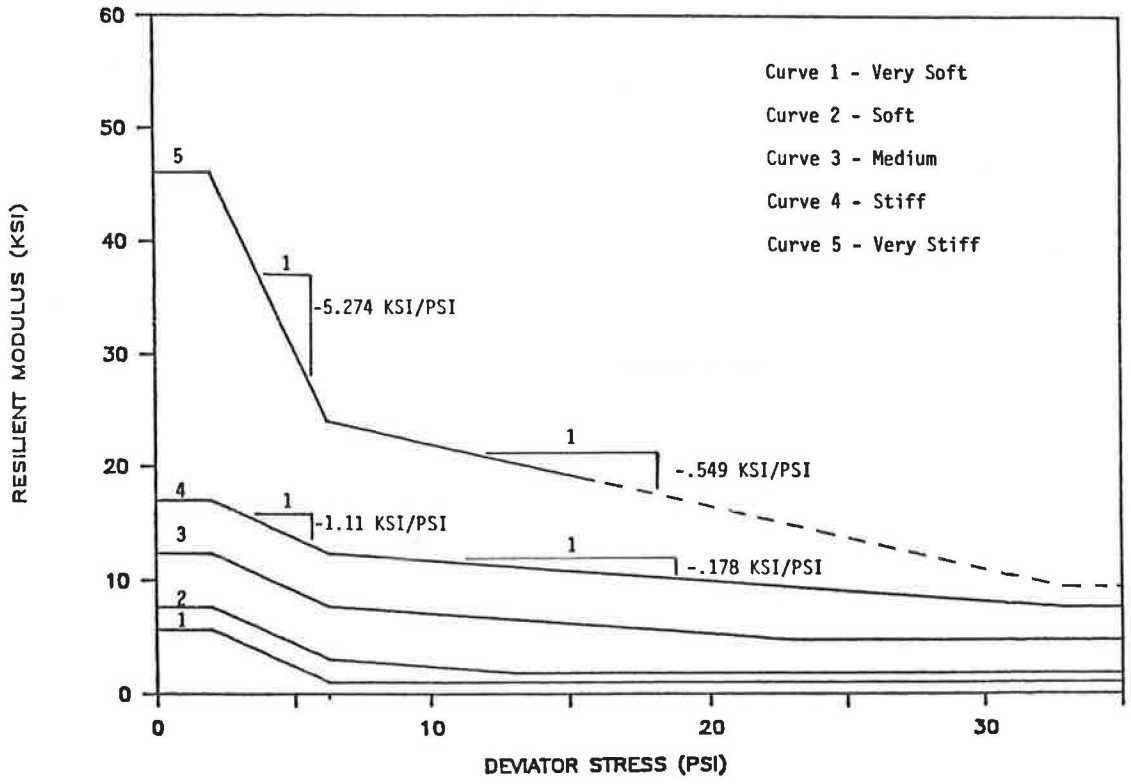

FIGURE 2 Subgrade soil material models.

The other four curves have been successfully used in the ILLI–PAVE program (*4,5*). A summary of the pavement material properties used in the analyses with ILLI–PAVE is presented in Table 1.

In recent and current research work (*11–13*), a comprehensive constitutive model has been developed to characterize the nonlinear material properties for all types of coarse- and fine-grained materials. The model has the form

$$E = K_1\theta^{K_2}\sigma_d^{K_3} \quad (2)$$

It can also be written as

$$E = f(\theta, J_2') \quad (3)$$

where

σ_d = deviator stress,
J_2' = second stress invariant, and
K_1, K_2, K_3 = material constants.

One of the findings of these investigations (*11–13*) is that all soils, both fine- and coarse-grained, have decreasing moduli with increasing deviator stress. The sandy subgrade model developed in this study demonstrates the same behavior, as shown in Figure 2.

Use of ILLI–PAVE Surface Deflection Data Base

The data base that was used to determine the nonlinear elastic properties of the base course and the subgrade in the earlier version of the LOADRATE program was based on the ILLI–PAVE subgrade model (first four curves in Figure 2). The ILLI–PAVE subgrade model basically represents a clay or silt subgrade. The earlier LOADRATE program performed poorly when the subgrade consisted of sandy material (*14*). It underpredicted the sandy subgrade moduli; therefore, as a remedial measure, a different curve was developed for the sandy subgrades that was similar to the ILLI–PAVE subgrade model. A new set of ILLI–PAVE runs and regressions was carried out to regenerate the data base used to determine the nonlinear elastic properties of the base course and subgrade. In order to obtain enough load-deflection data to cover a wide spectrum of light pavement structures with different materials, 60 ILLI–PAVE runs were made. These simulations included a combination of the five subgrade types and three base course materials, with K_1 values of 10,000, 100,000, and 200,000. In addition, four different base course thicknesses (1-, 6-, 12-, and 18-in.) were used. For all these combinations, an FWD loading of 100 psi was used, and the corresponding load was 10,956 lb. The regression analyses and correlations of the various parameters were performed according to the procedure used to develop the data base in the original version of LOADRATE (*1*).

The ILLI–PAVE subgrade model is based on the results of a series of laboratory tests (*15,16*). Specimens were tested for those models without lateral confining pressure (e.g., $\sigma_3 = 0$). Plots of resilient modulus versus repeated deviator stress were used to develop these four curves. The point at which a substantial change occurred in the slope of the resilient modulus and deviator stress relation was called the "break-point" deviator stress. Two linear regression analyses were conducted using the data for deviator stresses on either side of the break-point deviator stress. It was possible to find the point of intersection using the two regression lines. The resilient modulus and deviator stress corresponding to the intersection point and the slopes of the two regression lines were recorded.

Thompson and Robnett (*16*) studied the effects of the resilient modulus at the break point E_{Ri} and the slope of the regression line below the break-point deviator stress M_1 on the surface deflections of flexible pavements. It was found that E_{Ri} effects were most pronounced and primarily controlled the surface deflection. Variations of M_1 were fairly insensitive to surface deflections except at low E_{Ri} values. The data used to develop the fifth curve for the sandy subgrades were obtained from a separate TTI research project (*14*). In that project, triaxial tests were carried out as a part of the effort to develop a new rut depth model. During the triaxial testing, several steps were taken to ensure that the laboratory test procedure would closely simulate the actual field conditions. The subgrade material chosen for this study was a red-brown silty sand with a liquid limit of 19. Average density and moisture content of the samples tested were 110 lb/ft^3 and 14.0 percent, respectively. The fraction of soil passing through a 200 sieve was 11.5 percent. The tests were carried out at confining pressures of 1, 4, and 8 psi for four deviator stress levels ranging from 2 to 11.8 psi. The complete set of test data is presented in Table 2. The confining and deviator stress levels applied to the samples were chosen from the results of a series of CHEVDEF elastic layered program runs simulating a standard 9,000-lb load on a typical low-volume road.

A haversine load pulse with a load-unload period of 0.1 sec and a rest period of 0.9 sec was used to apply the deviator load. This pulse was applied by a Material Testing System's servocontrolled machine (the MTS). The deformations were measured by LVDTs mounted between the top and the bottom platens. Graphite powder was used between Teflon papers on the platens to reduce the errors due to end effects. The fifth curve developed from these data is shown in Figure 3. This curve was developed from two linear regression analyses for the data, one at less than and one at greater than the break-point deviator stress. These two straight lines were used to construct the new curve for the subgrade model, according to the method used to develop the ILLI–PAVE subgrade model (*16*). The break-point deviator stress of the new curve is 6.2 psi, which is exactly the same as for all other ILLI–PAVE subgrade curves. Figure 3 shows the new curve and data points highlighting the three confining pressures. Increasing the confining pressure increased the resilient moduli of the soils used for the test. The new subgrade model used in developing the new data base is shown in Figure 2. The five nonlinear elastic moduli curves represented the very soft, soft, medium, stiff, and very stiff subgrades.

MODEL FOR SEASONAL CHANGES OF MATERIAL PROPERTIES

The latest version of the LOADRATE program is able to correct the base modulus for temperature and moisture variation. The theoretical procedure was described by Chandra et al. (*6*). As stated earlier, the relationship between the

TABLE 1 MATERIAL PROPERTIES USED IN ILLI-PAVE RUNS

Property	Surface Course	Base Course	Subgrade				
			Very Stiff	Stiff	Medium	Soft	Very Soft
Unit Weight (pcf)	145.00	135.00	110.00	125.00	120.00	115.00	110.00
Lateral Pressure Coefficient at Rest	0.87	0.60	0.82	0.82	0.82	0.82	0.82
Poisson's Ratio		0.38	0.45	0.45	0.45	0.45	0.45
Unconfined Compressive Strength (psi)			32.80	32.80	22.85	12.90	6.21
Deviator Stress (psi)							
Upper Limit			32.80	32.80	22.85	12.90	6.21
Lower Limit			2.00	2.00	2.00	2.00	2.00
Deviator Stress at Break Point (psi)			6.20	6.20	6.20	6.20	6.20
Initial Elastic Modulus (ksi)			24.00	12.34	7.68	3.02	1.00
Elastic Modulus at Failure (ksi)			9.392	7.605	4.716	1.827	1.00
Constant Elastic Modulus (psi)	30,000						
Friction Angle (degrees)		40.0	30.0	0.0	0.0	0.0	0.0
Cohesion (psi)		0.0	0.0	16.4	11.425	6.45	3.105

TABLE 2 TRIAXIAL TEST DATA FOR SANDY SUBGRADE

Location	Sample	Confining Pressure (psi)	Deviator Stress (psi)	Resilient Modulus (ksi)
District 8	S1	1	2.2	32.75
FM 1983		1	5.2	22.21
# 7, 9, 10		1	8.1	17.43
		1	11.7	18.40
		4	2.2	49.80
		4	5.3	24.98
		4	8.1	21.08
		4	11.9	18.98
		8	2.2	52.57
		8	5.2	28.66
		8	8.1	24.14
		8	11.8	22.60
	S3	1	2.1	35.93
		1	5.3	22.90
		1	8.1	19.34
		1	11.6	16.30
		4	2.1	48.13
		4	5.2	29.74
		4	8.2	25.39
		4	11.8	21.92
		8	2.0	52.68
		8	5.2	46.31
		8	8.2	31.00
		8	11.8	26.87

resilient modulus and bulk stress for granular materials is given in Equation 1. The change of modulus ΔE with respect to a change of bulk stress $\Delta\theta$ is obtained by taking the derivative of Equation 1, which is

$$\Delta E = K_1 K_2 \theta^{K_2 - 1} \Delta\theta \quad (4)$$

Basically, the procedure has two models, namely, the thermal and moisture models. The thermal model requires material type, modulus, coefficient of thermal expansion, and Poisson's ratio at the reference temperature of the base course material as input. The moisture model requires reference suction values (in psi). Each model computes the change of modulus due to temperature and suction changes separately. Addition of the two modulus changes yields the net modulus change.

Thermal Model

The thermal model is based on the micromechanical approach, which treats the granular materials as elastic spheres in contact and subjected to temperature changes. In this model, the soil

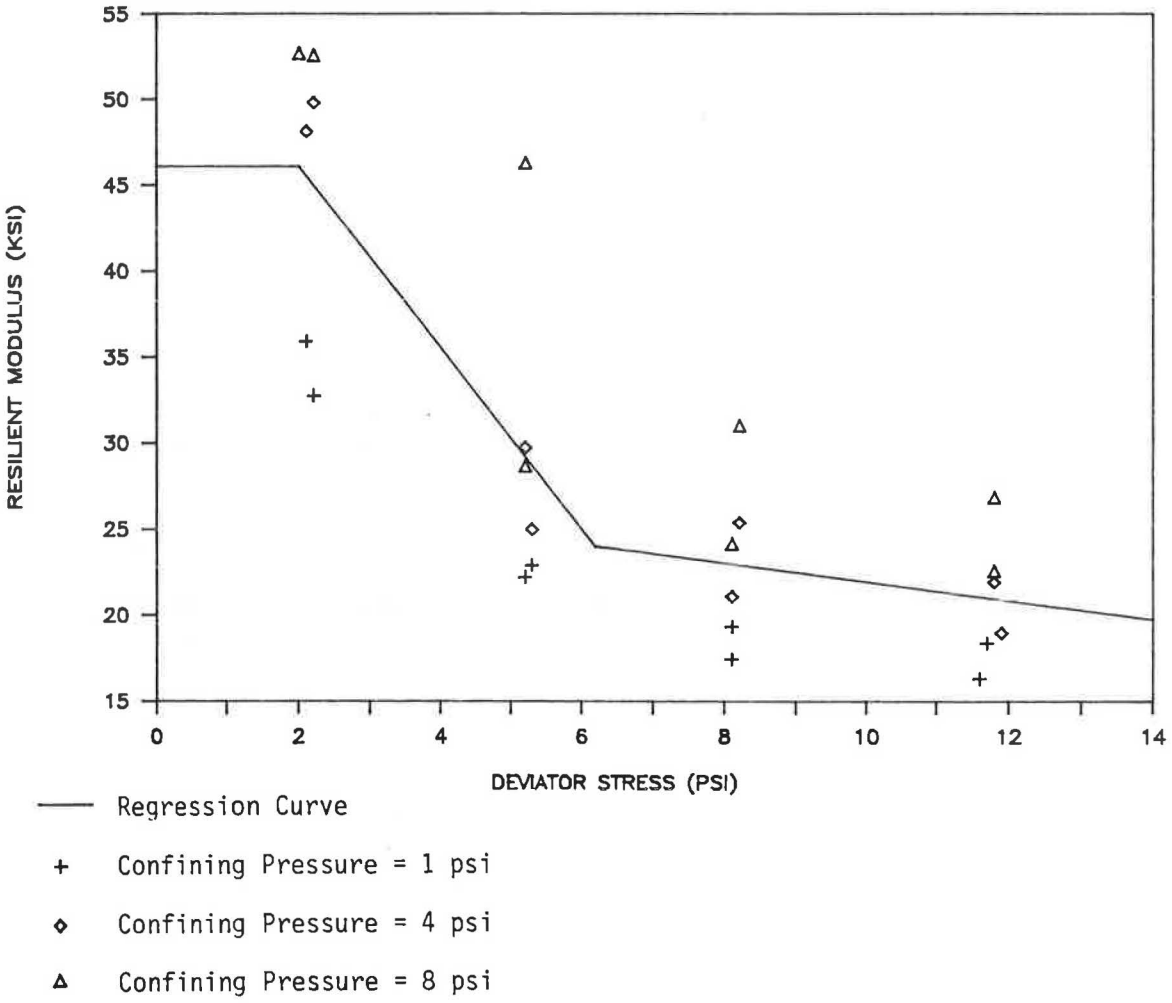

FIGURE 3 Nonlinear modulus versus deviator stress curve for sandy subgrade.

particles are assumed to be confined in all directions. An increase in temperature will cause an increase in the contact forces between particles, leading to an increase in stiffness of soil.

An increase in temperature also causes an increase in stiffness that depends on the initial level of confining pressure and on the material properties. Chandra et al. (*6*) derived the hydrostatic pressure p due to a change of temperature ΔT as

$$p = \left[\frac{x}{\sqrt{2}\omega} + \frac{(1 - x)}{4\omega}\right] (\tfrac{1}{3}\alpha_v \Delta T)^{3/2} \quad (5)$$

where

x = fraction of close-packed spheres;
α_v = volume thermal coefficient, which is approximately three times the linear thermal coefficient α;
$\omega = 3(1 - \nu^2)/4E$, a material property term; and
ν = Poisson's ratio.

If an initial bulk stress is θ, the change of bulk stress ($\Delta\theta_T$) because of a temperature change is given by the hydrostatic pressure p in Equation 5.

Moisture Model

The moisture model is also based on a micromechanical approach that represents the load-deformation behavior of a partially saturated soil following thermodynamic laws. The model consists of equal spheres in contact, surrounded by an air-water mixture, and each considered as a different phase. Both phases are modeled as homogeneous, isotopic, linear elastic materials.

Chandra et al. (*6*) derived a relationship for the change in the mean principal stress due to suction change $\Delta\theta_s$, which is defined as

$$\Delta\theta_s = C_w(\Delta P_w) \quad (6)$$

where

ΔP_w = change in mean principal stress of the water phase, which is the change in suction;
$C_w = V_w/V_T$;
V_w = volume of water; and
V_T = total volume.

Thus,

$$\Delta\theta_s = -\Delta(\text{Suction})(V_w/V_T) \quad (7)$$

Using Equations 5 and 7, Equation 4 can be rewritten as

$$\Delta E = K_1 K_2 \theta^{K_2-1} (\Delta\theta_T + \Delta\theta_s) \quad (8)$$

The temperature and moisture correction capability enables the user to represent the seasonal variations of the base moduli. As a result, the performance of a pavement under changing climatic conditions can also be analyzed.

RUT DEPTH PREDICTION MODEL

The new version of LOADRATE uses a simple mechanistic procedure (*7,14*) to calculate the rut depth and number of passes. There are a number of models to relate the plastic strain accumulation with the number of load repetitions. Yapa et al. (*7*) give a detailed description of these models. The rut depth model in the latest version of LOADRATE uses the following equation:

$$\varepsilon_p = aN^b \quad (9)$$

where

ε_p = total residual strain at the end of N cycles, and
a, b = material constants.

Yapa et al. (*7*) used the data obtained from a series of laboratory tests and published literature to develop typical values for the material constants a and b for various types of soils. The Unified Soil Classification is used to categorize the soil types for this purpose. The subgrade materials are divided into three groups. They include heavy clay (CH), silty clay and clayey silt (CL–ML), and clayey sand or uniform sand (SC–SM). All of the granular materials used for the base course were considered as one group. The average b values for CH, CL–ML group, SC–SM group, and base course material were 0.236, 0.162, 0.142, and 0.125, respectively. A curve-fitting technique was used to describe the behavior of the a values with respect to the resilient modulus for these four groups of materials. Table 3 presents the a and b values for these soil groups in the rut depth model.

RUT DEPTH DATA BASE

The Mechano-lattice program (*17,18*) was used to construct the rut depth data base. The program models the layered pavement system as a three-dimensional assembly of numerous cube-shaped units. Each unit has 28 spring-like elements that behave as energy-absorbing material under loading and unloading, corresponding to the permanent deformation behavior of the material layer it represents. A traveling wheel rolls over this assemblage and causes an elastic and a permanent deformation response in each unit. Beyond the influence of the wheel load, the elements recover most of the energy by rebounding, but the residual strains in each element are accumulated as residual deformation in the pavement. For the next pass of the wheel, the initial conditions of the elements will be reset to these latest residual stresses and strains. In this process, the permanent deformation behavior of each material layer affects the stress distribution and the total deflections of the pavement in an interactive manner. Yandell (*17,18*) pointed out that the method of superposition, which is commonly used in layered elastic and finite element approaches, ignores the interaction effects between elastic and plastic behavior in different material layers. The Mechano-lattice program has been verified using results from several

TABLE 3 RUTTING PARAMETERS FOR PAVEMENT MATERIALS

Material	Rutting Parameter	
	Intercept $a \times 10^4$	Slope b
Base Course	$174\ M_R^{-0.57}$	0.125
Subgrade		
Heavy Clay (CH-clay)	$933\ M_R^{-2.64}$	0.236
Clayey Silt/Silty Clay (CL-ML)	$10\ M_R^{-0.73}$	0.162
Clayey/Silty Sand (SC-SM)	$750\ M_R^{-1.62}$	0.142

* M_R - Resilient Modulus (in ksi)

TABLE 4 INPUT PARAMETERS FOR MECHANO-LATTICE RUNS

Parameter	Unit	Level 1	Level 2	Level 3
Resilient Modulus	psi			
- Base Course		100,000	70,000	40,000
- Subgrade		25,000	15,000	5,000
Accumulated Residual Strain	in/in			
- Base Course		0.0075	0.0025	
- Subgrade		0.0100	0.0060	0.0020
Base Thickness	in	18.0	12.0	6.0

test track experiments and has been shown to predict acceptable results (*19,20*).

Because in a low-volume road the effect of the surface treatment is negligible on the structural performance of the pavement as a whole, the surface-treated layer was not considered in the simulation (*14*). Input data for the Mechano-lattice program require three basic material parameters and the thickness of the pavement layers. Elastic modulus, accumulated residual strain after a specified number of load repetitions, and Poisson's ratio are the three material parameters. Because Poisson's ratio did not have a significant effect on the output over its possible range of variation, it was kept constant for both layers. This reduced the total number of input parameters to five, namely, the elastic modulus of both the base course and the subgrade, the accumulated residual strain of both the base course and the subgrade, and the thickness of the base layer. It was decided to use the resilient modulus in place of the elastic modulus for both layers because the difference was negligible for the type of materials under consideration. In order to include all possible types of low-volume pavements in the state of Texas, the input parameters were varied within a wide range of values, as presented in Table 4.

A total of 162 Mechano-lattice (*17*) runs were made to build the data base. The calculated rut depths represent the depressions caused by 300,000 load repetitions, measured under a 4-ft straightedge placed across the wheel path.

In the new LOADRATE program, the rut depth value for a particular road is predicted using base and subgrade material properties, Equation 9, and a multidimensional polynomial interpolation routine (*21*) with the data base developed by the Mechano-lattice runs.

CALCULATION OF THE REMAINING LIFE

The calculation of the remaining life requires as input the number of passes (ESALs) to cause a maximum acceptable rut depth and traffic information. As discussed previously, the number of passes of an 18-kip, single-axle load (ESAL) to cause a specified level of rut depth can be calculated using the rut depth prediction model. Allowable rut depth is a criterion provided by the user at which the pavement requires major rehabilitation. To determine remaining life of the test sections in years, traffic information must also be provided by the user.

PROGRAM LIMITATIONS

Thus, the LOADRATE program was developed for a two-layer system that consists of a base and the subgrade. The failure criterion used in the LOADRATE program is based on the allowable rut depth; fatigue cracking in the surface layer is not considered. As a result, the LOADRATE program has limitations. It can only be used

1. For FM roads with a surface treatment layer. (It cannot be used for asphalt concrete surface pavements.)
2. To predict rutting failure. (It cannot be used to predict fatigue cracking failure.)

CASE STUDY

The following case study demonstrates various applications of the latest version of the LOADRATE program in the structural evaluation of light pavements.

FM Road 3225 is located in Henderson County, Texas, and consists of a 15-in.-thick crushed-limestone base on sandy clay. The wearing surface is 1-in.-thick emulsion asphalt treatment layer. The Texas triaxial classification for the subgrade was 5.0. The existing load limit is 58,420 lb gross vehicle weight (GVW). There is a gravel pit close to this road. Due to the load limit in this road, trucks loaded with gravel must follow a longer path to reach the main road. Presently, an

TABLE 5 TRAFFIC DATA FOR FM 3225 ROAD

Traffic Data analysis for FM 3225, Henderson County

Estimated Vehicles/Day: 25 Date of Estimation: 11/23/88

Distribution of Truck Traffic: (Vehicles/day)		18-Kip Equivalent AASHTO 86(SN = 2, Pt = 2.0)	Daily 18-Kip Equivalent
2-axle Dumps:	5	3.18	15.9
3-axle Dumps:	5	2.66	13.3
3-S2 Dumps:	17	3.73	63.41
			92.61

Above traffic estimates are based on data provided by the Gravel Supplier for the last 3 months (August, September, October of 1988)

Traffic Estimates assuming no growth:

Yearly 18-Kip Equivalent: 33,802.65

10-Year 18-Kip Equivalent: 338,026.5

20-Year 18-Kip Equivalent: 676,053

Removal of load restrictions will increase the gravel business by 10%. This raises the 18-Kip Equivalent as follows:

Yearly 18-Kip Equivalent: 37,182.91

10-Year 18-Kip Equivalent: 37,1829.1

20-Year Kip Equivalent: 743,658.3

Assuming a uniform 5% increase/year in business the following traffic levels are expected:

Yearly 18-Kip equivalent: 37,182.91

10-Year 18-Kip Equivalent: 467,761

20-Year 18-Kip Equivalent: 1,229,267

Existing traffic on this road was taken as 50% of the above figures. This will give an existing yearly 18-Kip Equivalent of 18,592.

average of 25 gravel trucks are moving along the alternative route daily. An increase of its load limit to 80,000 lb would allow these trucks to use FM 3225. Thus, there was a request to increase the load limit of FM 3225. As a result of this request, Texas SDHPT officials decided to study the possibility of increasing the load limit of FM 3225. The calculation of the expected additional traffic data provided by the SDHPT is presented in Table 5. As shown, the present traffic was estimated to have an annual ESAL of 18,592 with a 5 percent growth rate. In order to meet the SDHPT requirements, the allowable rut depth value was taken as 0.5 in., and there was no existing rut depth as the surface course was new. All of this information was used to run the LOADRATE program.

In April 1989, a set of FWD tests was carried out on FM 3225 for a 2.5-mi section. The testing consisted of 23 FWD readings in the outer wheel path and another 23 FWD readings between the edge of the road and outer wheel path. A cross section of the test road is shown in Figure 4. The distance between test points was 0.1 mi. During the test, the air temperature was about 80°F. According to the information obtained from SDHPT officials, there was some rain in the pavement area about 1 to 4 weeks before the date of testing.

The FWD readings made for a load level of 10,956 lb were used for the LOADRATE analysis. The analysis was done in five steps. The first analysis was done with the data taken in the outer wheel path with existing traffic data. The results of this LOADRATE run are presented in Table 6. The second analysis was made of the outer wheel path data with future traffic; the output file is presented in Table 7. Results obtained from these two LOADRATE runs were used to compare the

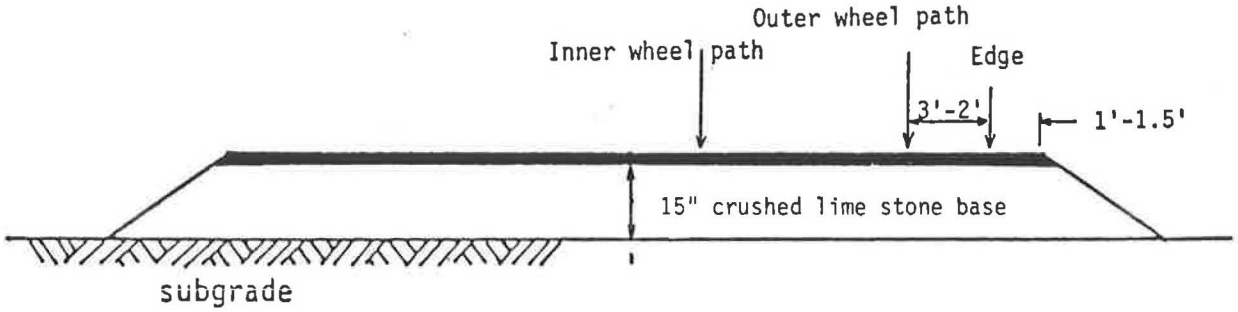

FIGURE 4 Cross section of the test road indicating outer wheel path and edge positions (FWD testing points).

performance of the pavement under two traffic conditions—one, the current traffic, and the second, the future expected traffic when a gravel hauling operation is under way.

The third LOADRATE analysis was made using FWD data taken at the edge of the road with existing traffic data. Results obtained from this analysis (Table 8) were used to compare the structural capabilities of the pavement in the outer wheel path and at the edge. As the fourth step, LOADRATE was used to compute the changes in the base moduli in the outer wheel path due to seasonal changes of moisture and temperature. For this purpose, the future condition was assumed to be during the summer when a typical base course temperature is 95°F and a typical suction value is −90 psi. The measured base course temperature and the suction values on the day of the FWD tests were 75°F and −40 psi, respectively. The revised moduli were used to predict the number of passes that the pavement could withstand under the different moisture and temperature conditions.

RESULTS

The results obtained from the LOADRATE analysis in the outer wheel path for existing traffic conditions are plotted in Figures 5 and 6. The subgrade modulus in Figure 5 varies within a close range when compared to the variation of the base moduli. Figure 6 shows the variation of the number of ESAL passes to cause a 0.5-in. rut depth. This number of passes is directly related to the modulus values of the base and subgrade. In these two figures, the higher the modulus values, the higher the number of ESAL passes, and vice versa. Figure 6 shows that the first 0.8 mi of the tested pavement section can carry a higher number of passes than the sections between the 0.9- to 1.2- and 1.7- to 2.2-mi marks.

Figure 7 shows the variation of predicted remaining life in the outer wheel path for both the existing and future traffic. From the two curves, there would be a minimum of 6.5 years of life reduction in all of the test sections due to the additional traffic. In some sections, this value would be as long as 12 years. This same information is shown in another way in Figure 8. In the curve for the existing traffic, all the sections tested have a remaining life of at least 11 years, whereas the future traffic curve has a minimum remaining life of only 4 years. Also, it can be seen that 50 percent of the sections tested have a remaining life of 16 years under the existing traffic, but only 6 years with future traffic. These results explain the effects of the increase in load limit for this road. On the basis of these analyses, the highway agency (considering that if the load limit is increased to 80,000 lb, the pavement would need major rehabilitation work by the end of 6 years) must decide whether they can afford the cost of repairs at that time. Under the existing traffic conditions, the road would not need major repair for 16 years.

The LOADRATE program results obtained by analyzing the FWD data taken at the edge of the pavement indicate that the pavement structure at the edge is weaker than the pavement structure in the outer wheel path. Figures 9–11 show this situation. The base modulus in the outer wheel path is higher than the base modulus at the edge for most of the locations tested (Figure 9). Figure 10 shows that the subgrade moduli in the outer wheel path are not always greater than those beneath the edge. The effect of weak base and subgrade at the edge results in a lower life span at the edge (Figure 11) if the traffic passes close to the edge. There is a tendency to have more truck traffic on the edge under conditions such as passing and meeting approaching traffic. The results obtained from the temperature and moisture corrections indicate that an increase of temperature and suction values will increase the base course modulus value (Table 9). Pavement performance for the seasonally adjusted base moduli can also be analyzed by LOADRATE (Table 10).

CONCLUSIONS

A computer program, LOADRATE Version 2.0, has several improvements. The program uses a new rut depth prediction model, and is able to make temperature and moisture corrections for the base modulus. A new nonlinear modulus versus deviator stress curve has been added to the subgrade model in the LOADRATE program to represent sandy subgrades. The new LOADRATE program analyzes FWD or Dynaflect data to calculate the remaining life to reach a given rut depth. The strength of the pavement at the edge is weaker than the strength of the pavement in the outer wheel path. A paved shoulder not only prevents water penetration into the road bed, but also provides some lateral support to maintain pavement strength. The LOADRATE program has been tested with several case studies and is ready for use in the structural evaluation of FM roads at the project level. As a recommendation for future improvements in the program, the temperature and moisture corrections should be extended

TABLE 6 RESULTS OF LOADRATE ANALYSIS OF THE FWD DATA TAKEN IN THE OUTER WHEEL PATH WITH EXISTING TRAFFIC

TEXAS TRANSPORTATION INSTITUTE
LOAD RATING OF LIGHT PAVEMENT

JOB : FWD TESTING(OWP) (INPUT FILE B:F3225A.LRD)

DISTRICT: 0 COUNTY:Cty ROAD:10108 fm3225
ALLOWABLE RUT(INS): .5 RECORDED RUT(INS): 0

TRUCK NO. 1
AXLE NUMBER SINGLE WHEEL/ESWL(LBS)
1 9000

ANNUAL TRAFFIC GROWTH RATE: .05 # OF YEARS: 10 FIRST YEAR TRAFFIC: 18592
TOTAL NUMBER OF PASSES DURING ABOVE PERIOD: 233848

DATE:4-25-89 FALLING WEIGHT DEFLECTOMETER

* SEC #	BASE (IN)	D1 (MILS)	D7 (MILS)	FWD LOAD (LBS)	E1-BASE (PSI)	E2-SUBG (PSI)	* NO. OF PASSES	REMAINING LIFE (YEARS)
0.000	15.0	39.90	1.77	10584	35357	9117	395093	14.8
0.100	15.0	35.42	1.53	11040	53529	11364	624657	20.2
0.200	15.0	32.91	1.73	11328	70569	10336	632379	20.4
0.300	15.0	36.09	1.53	11072	51030	11682	627737	20.3
0.400	15.0	37.89	1.73	11032	46229	9902	446626	16.2
0.500	15.0	29.33	1.61	11048	87063	10436	663672	21.0
0.600	15.0	40.48	1.41	10648	34270	11964	578970	19.2
0.700	15.0	31.14	1.09	11312	61642	15895	776165	23.1
0.800	15.0	39.39	1.37	10688	37385	11642	581866	19.3
0.900	15.0	41.55	2.17	11032	33684	7928	350894	13.6
1.000	15.0	41.00	2.89	10912	25188	6287	281085	11.5
1.100	15.0	37.58	1.81	11168	48233	9072	418612	15.5
1.200	15.0	84.98	2.45	10688	9555	6639	286230	11.7
1.300	15.0	38.21	1.25	11056	40941	13507	647850	20.7
1.400	15.0	33.81	1.85	11440	67741	9276	459234	16.5
1.500	15.0	43.74	2.01	10768	28590	8393	355715	13.8
1.600	15.0	29.10	1.37	11536	92670	12615	745707	22.6
1.700	15.0	42.53	2.61	10688	24102	6782	295516	12.0
1.800	15.0	61.10	1.53	11160	14675	10857	483601	17.1
1.900	15.0	40.25	1.97	10672	34504	8559	374035	14.3
2.000	15.0	34.75	2.01	11064	53449	8071	389147	14.7
2.100	15.0	50.03	3.05	10544	13525	6173	271495	11.2
2.200	15.0	36.60	1.65	10840	47677	9632	438994	16.0

* NUMBER OF PASSES AND REMAINING LIFE FOR SPECIFIED RUT DEPTH OF .5 in

Remaining Life(yrs)	Cumulative % Sections
1	100.0
2	100.0
3	100.0
4	100.0
5	100.0
6	100.0
7	100.0
8	100.0
9	100.0
10	100.0
11	100.0
12	82.6
13	82.6
14	73.9
15	60.9
16	52.2
17	43.5
18	39.1
19	39.1
20	30.4
21	8.7
22	8.7
23	4.3

TABLE 7 RESULTS OF LOADRATE ANALYSIS OF THE FWD DATA TAKEN IN THE OUTER WHEEL PATH WITH FUTURE TRAFFIC

TEXAS TRANSPORTATION INSTITUTE
LOAD RATING OF LIGHT PAVEMENT

JOB : FWD TESTING(OWP) (INPUT FILE a:f3225af.LRD)

DISTRICT: 0 COUNTY:Cty ROAD:10108 fm3225
ALLOWABLE RUT(INS): .5 RECORDED RUT(INS): 0

TRUCK NO. 1
AXLE NUMBER SINGLE WHEEL/ESWL(LBS)
1 9000

ANNUAL TRAFFIC GROWTH RATE: .05 # OF YEARS: 10 FIRST YEAR TRAFFIC: 55775
TOTAL NUMBER OF PASSES DURING ABOVE PERIOD: 701532

DATE:4-25-89 FALLING WEIGHT DEFLECTOMETER

* SEC #	BASE (IN)	D1 (MILS)	D7 (MILS)	FWD LOAD (LBS)	E1-BASE (PSI)	E2-SUBG (PSI)	* NO. OF PASSES	REMAINING LIFE (YEARS)
0.000	15.0	39.90	1.77	10584	35357	9117	395093	6.2
0.100	15.0	35.42	1.53	11040	53529	11364	624657	9.1
0.200	15.0	32.91	1.73	11328	70569	10336	632379	9.2
0.300	15.0	36.09	1.53	11072	51030	11682	627737	9.2
0.400	15.0	37.89	1.73	11032	46229	9902	446626	6.9
0.500	15.0	29.33	1.61	11048	87063	10436	663672	9.6
0.600	15.0	40.48	1.41	10648	34270	11964	578970	8.6
0.700	15.0	31.14	1.09	11312	61642	15895	776165	10.8
0.800	15.0	39.39	1.37	10688	37385	11642	581866	8.6
0.900	15.0	41.55	2.17	11032	33684	7928	350894	5.6
1.000	15.0	41.00	2.89	10912	25188	6287	281085	4.6
1.100	15.0	37.58	1.81	11168	48233	9072	418612	6.5
1.200	15.0	84.98	2.45	10688	9555	6639	286230	4.7
1.300	15.0	38.21	1.25	11056	40941	13507	647850	9.4
1.400	15.0	33.81	1.85	11440	67741	9276	459234	7.1
1.500	15.0	43.74	2.01	10768	28590	8393	355715	5.7
1.600	15.0	29.10	1.37	11536	92670	12615	745707	10.5
1.700	15.0	42.53	2.61	10688	24102	6782	295516	4.8
1.800	15.0	61.10	1.53	11160	14675	10857	483601	7.4
1.900	15.0	40.25	1.97	10672	34504	8559	374035	5.9
2.000	15.0	34.75	2.01	11064	53449	8071	389147	6.1
2.100	15.0	50.03	3.05	10544	13525	6173	271495	4.5
2.200	15.0	36.60	1.65	10840	47677	9632	438994	6.8

* NUMBER OF PASSES AND REMAINING LIFE FOR SPECIFIED RUT DEPTH OF .5 in

Remaining Life(yrs)	Cumulative % Sections
1	100.0
2	100.0
3	100.0
4	100.0
5	82.6
6	69.6
7	47.8
8	39.1
9	30.4
10	8.7

TABLE 8 RESULTS OF LOADRATE ANALYSIS OF THE FWD DATA TAKEN AT THE EDGE WITH EXISTING TRAFFIC

TEXAS TRANSPORTATION INSTITUTE
LOAD RATING OF LIGHT PAVEMENT

JOB : FWD TESTING(EDGE) (INPUT FILE a:f3225b.LRD)

DISTRICT: 0 COUNTY:Cty ROAD:10801 fm3225S
ALLOWABLE RUT(INS): .5 RECORDED RUT(INS): 0

TRUCK NO. 1
AXLE NUMBER SINGLE WHEEL/ESWL(LBS)
1 9000

ANNUAL TRAFFIC GROWTH RATE: .05 # OF YEARS: 10 FIRST YEAR TRAFFIC: 18592
TOTAL NUMBER OF PASSES DURING ABOVE PERIOD: 233848

DATE:4-25-89 FALLING WEIGHT DEFLECTOMETER

* SEC #	BASE (IN)	D1 (MILS)	D7 (MILS)	FWD LOAD (LBS)	E1-BASE (PSI)	E2-SUBG (PSI)	* NO. OF PASSES	REMAINING LIFE (YEARS)
0.000	15.0	64.24	1.37	10328	11647	10618	478650	17.0
0.100	15.0	72.57	1.89	10232	10743	8820	349105	13.6
0.200	15.0	76.49	2.33	10216	9683	7188	302373	12.2
0.300	15.0	52.89	2.05	10640	17079	8268	331920	13.1
0.400	15.0	54.50	2.05	10584	14983	7831	319960	12.7
0.500	15.0	69.11	1.57	10048	11342	10319	469889	16.7
0.600	15.0	55.68	1.61	10800	16796	10733	478841	17.0
0.700	15.0	76.89	1.33	10464	12427	12584	529794	18.2
0.800	15.0	61.53	1.97	10480	11430	8537	340793	13.3
0.900	15.0	55.92	2.93	10520	9629	5918	267080	11.1
1.000	15.0	61.61	1.85	10336	11215	9042	355418	13.7
1.100	15.0	61.34	2.93	10528	8866	6002	267338	11.1
1.200	15.0	59.96	1.65	10560	13129	10171	463398	16.6
1.300	15.0	51.13	1.65	10832	20843	9627	370665	14.2
1.400	15.0	61.22	2.21	10176	10006	7673	316335	12.6
1.500	15.0	58.78	1.61	10592	13888	9960	381854	14.5
1.600	15.0	56.62	2.73	10496	10644	6466	280868	11.5
1.700	15.0	55.17	1.73	10512	15758	9524	368266	14.1
1.800	15.0	60.35	2.21	10120	9746	7359	307319	12.3
1.900	15.0	56.19	2.37	10488	11557	6785	290286	11.8
2.000	15.0	74.88	3.30	10064	8202	5648	266818	11.1
2.100	15.0	74.61	1.97	10048	10303	8268	333318	13.1
2.200	15.0	58.82	2.41	10160	9465	6887	293608	11.9

* NUMBER OF PASSES AND REMAINING LIFE FOR SPECIFIED RUT DEPTH OF .5 in

Remaining Life(yrs)	Cumulative % Sections
1	100.0
2	100.0
3	100.0
4	100.0
5	100.0
6	100.0
7	100.0
8	100.0
9	100.0
10	100.0
11	100.0
12	73.9
13	56.5
14	34.8
15	21.7
16	21.7
17	4.3
18	4.3

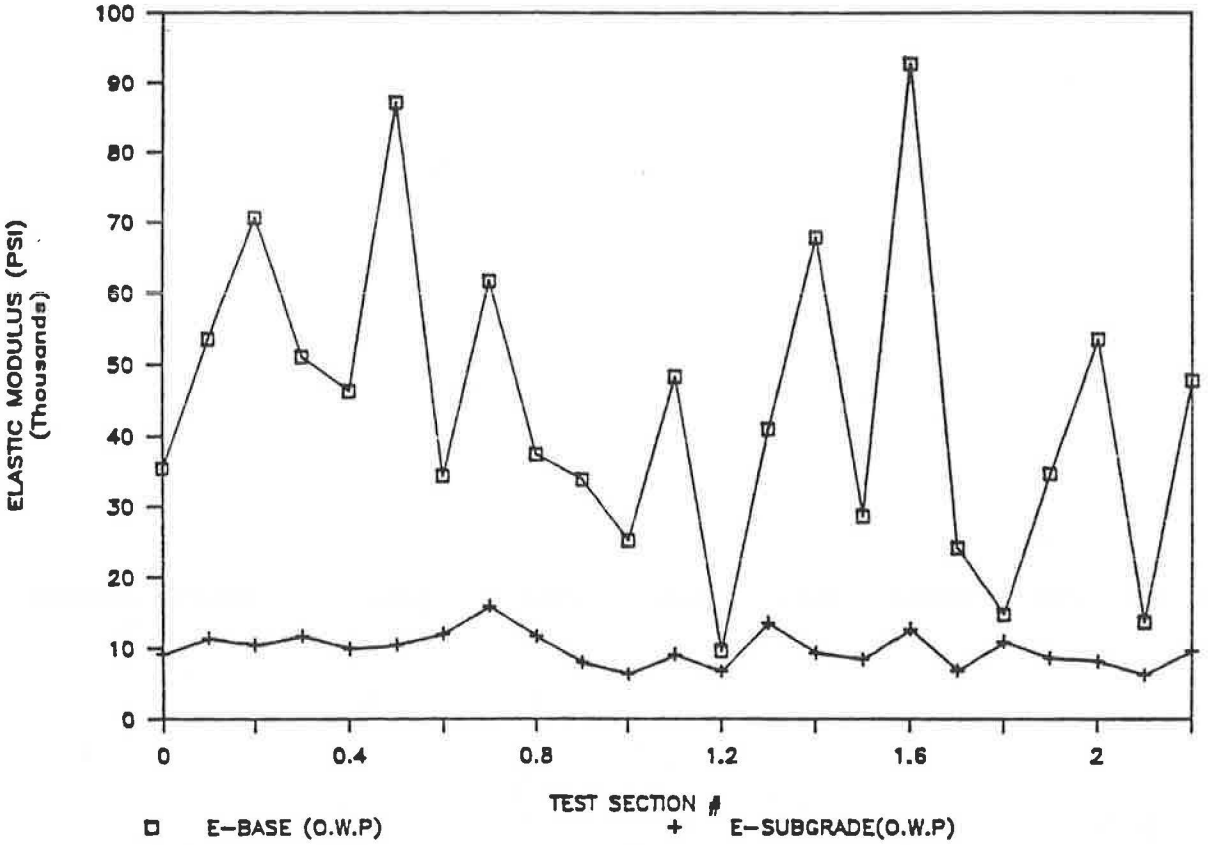

FIGURE 5 Subgrade and base moduli variation in outer wheel path.

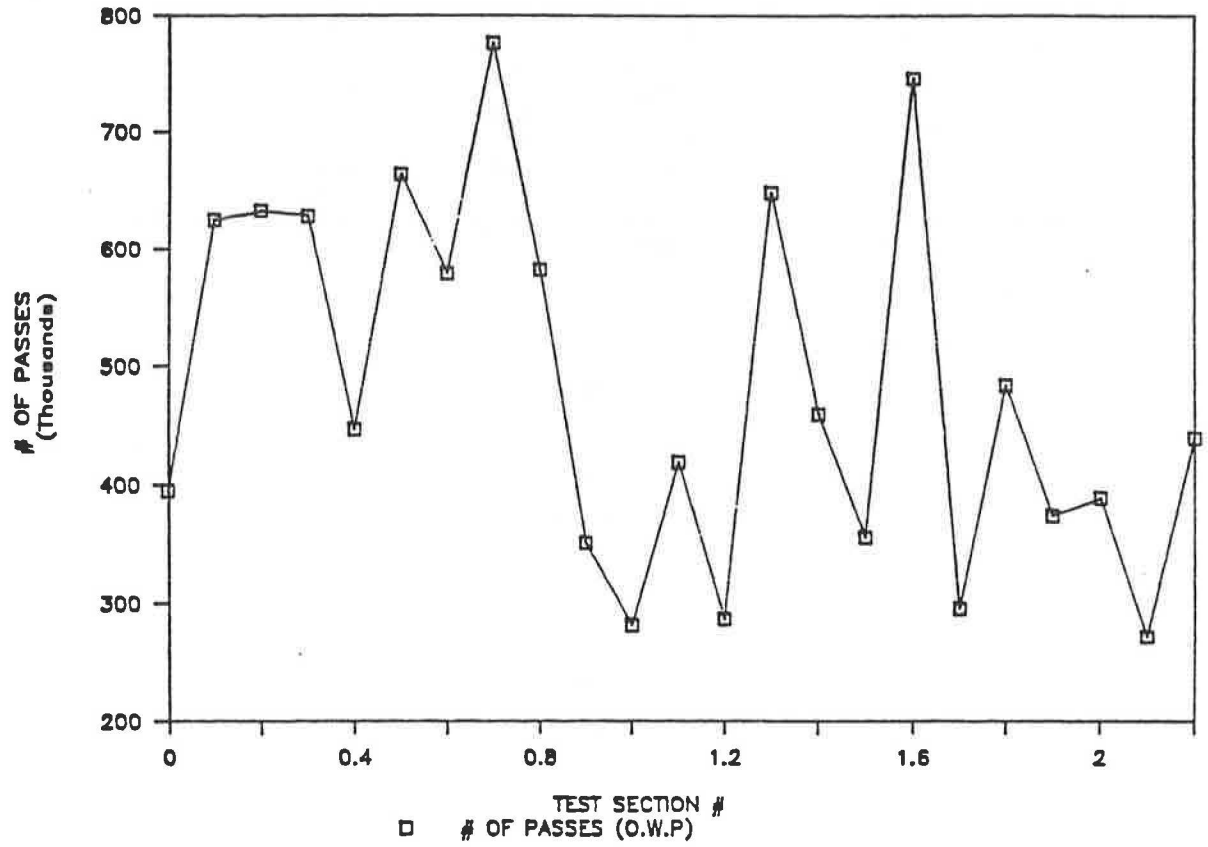

FIGURE 6 Variation of number of ESAL passes to cause 0.5-in. rut-depth along the project length.

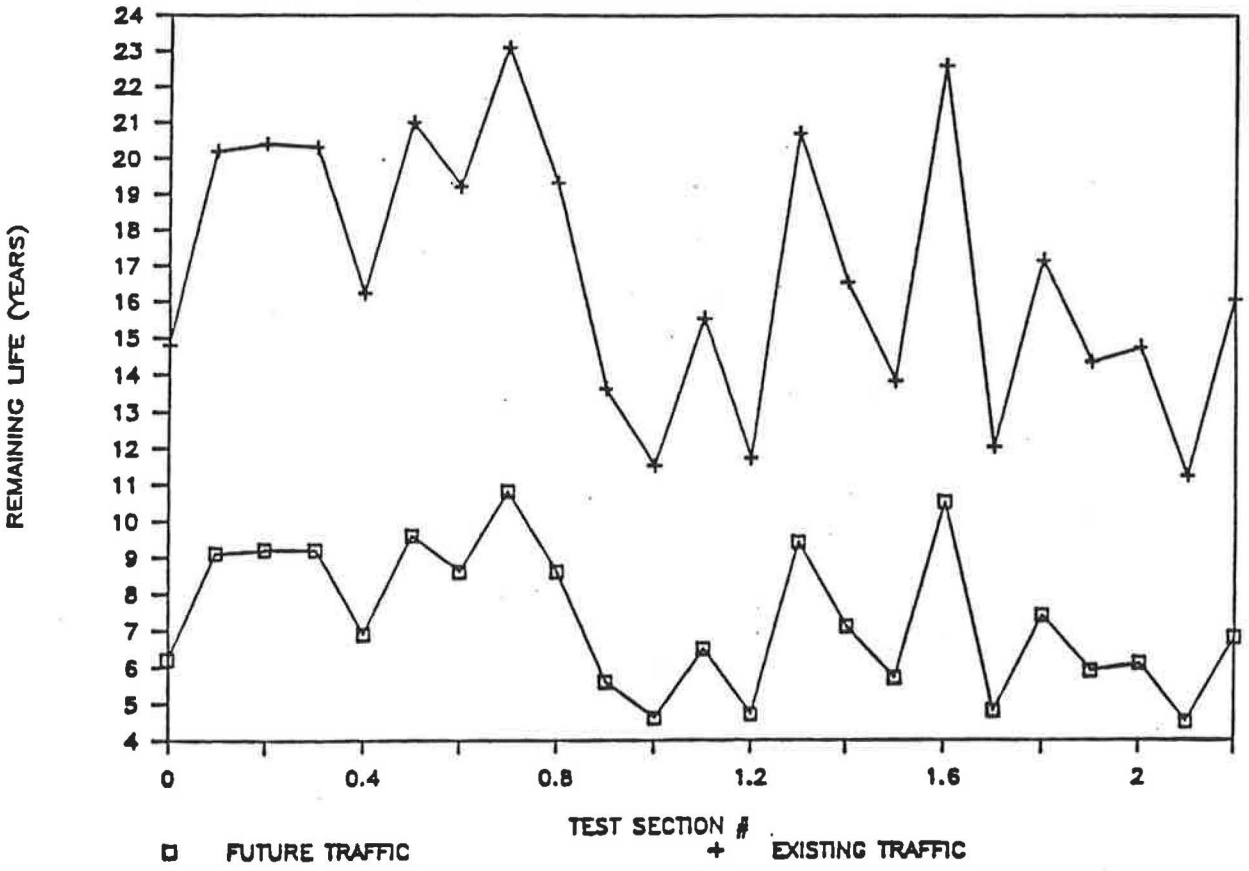

FIGURE 7 Variation of remaining life in the outer wheel path along the test pavement (for existing and future traffic).

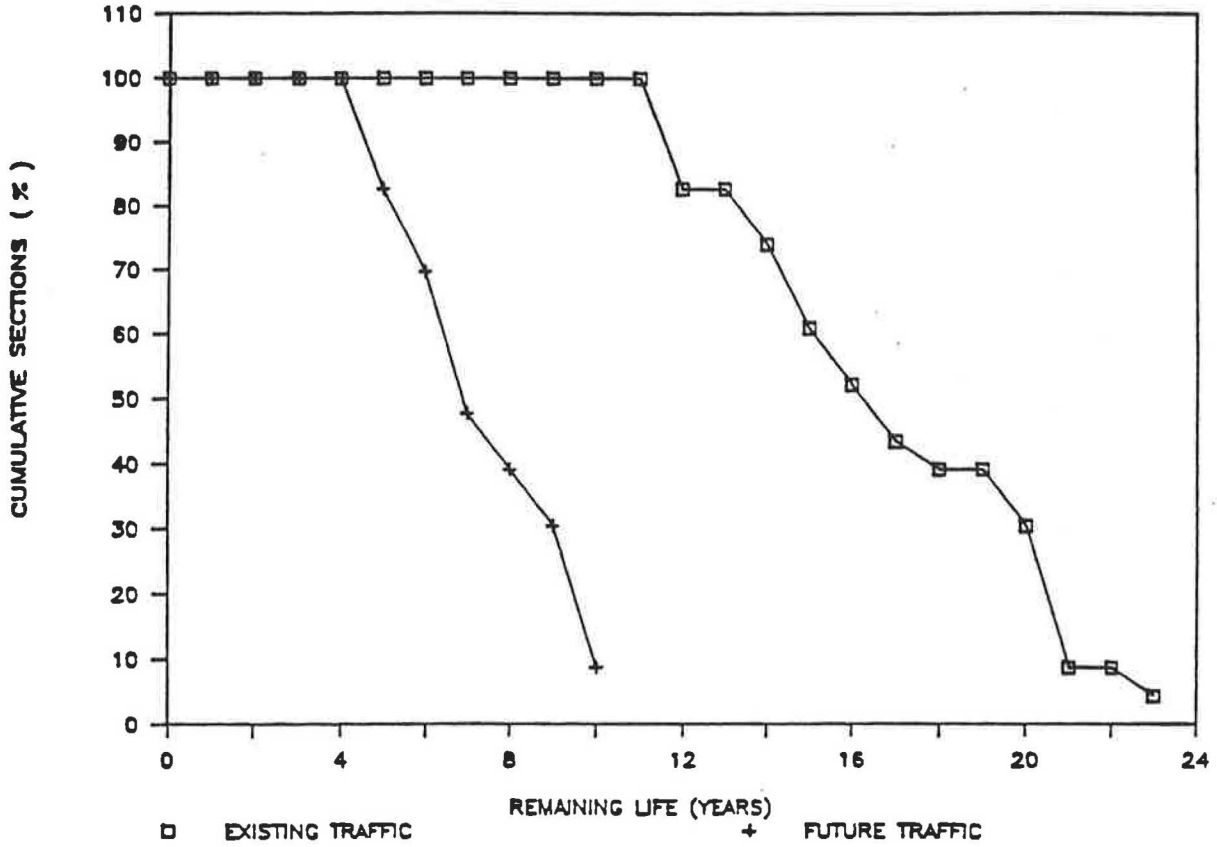

FIGURE 8 Remaining life of the cumulative sections (in percent) in the outer wheel path (for existing and future traffic).

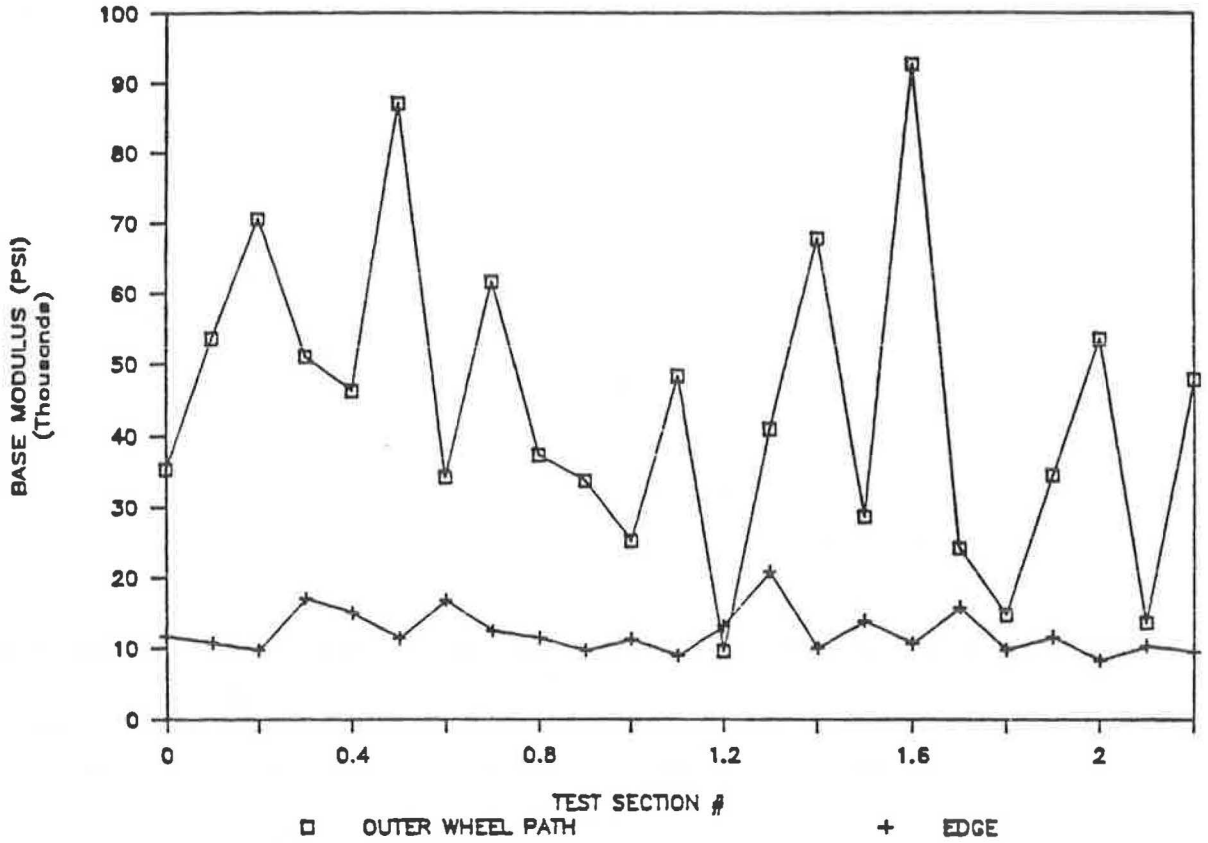

FIGURE 9 Variation of base moduli in outer wheel path and edge along the project length.

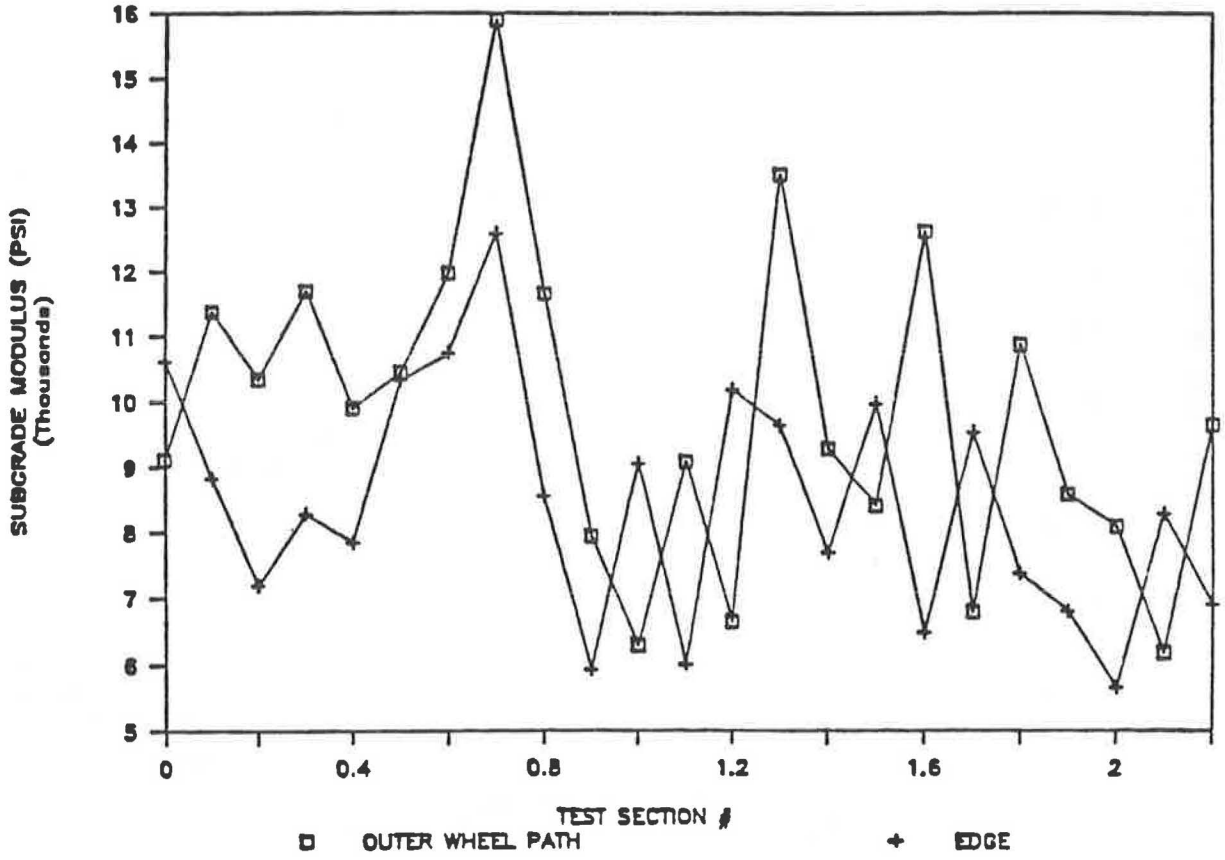

FIGURE 10 Variation of subgrade moduli in outer wheel path and edge along the project length.

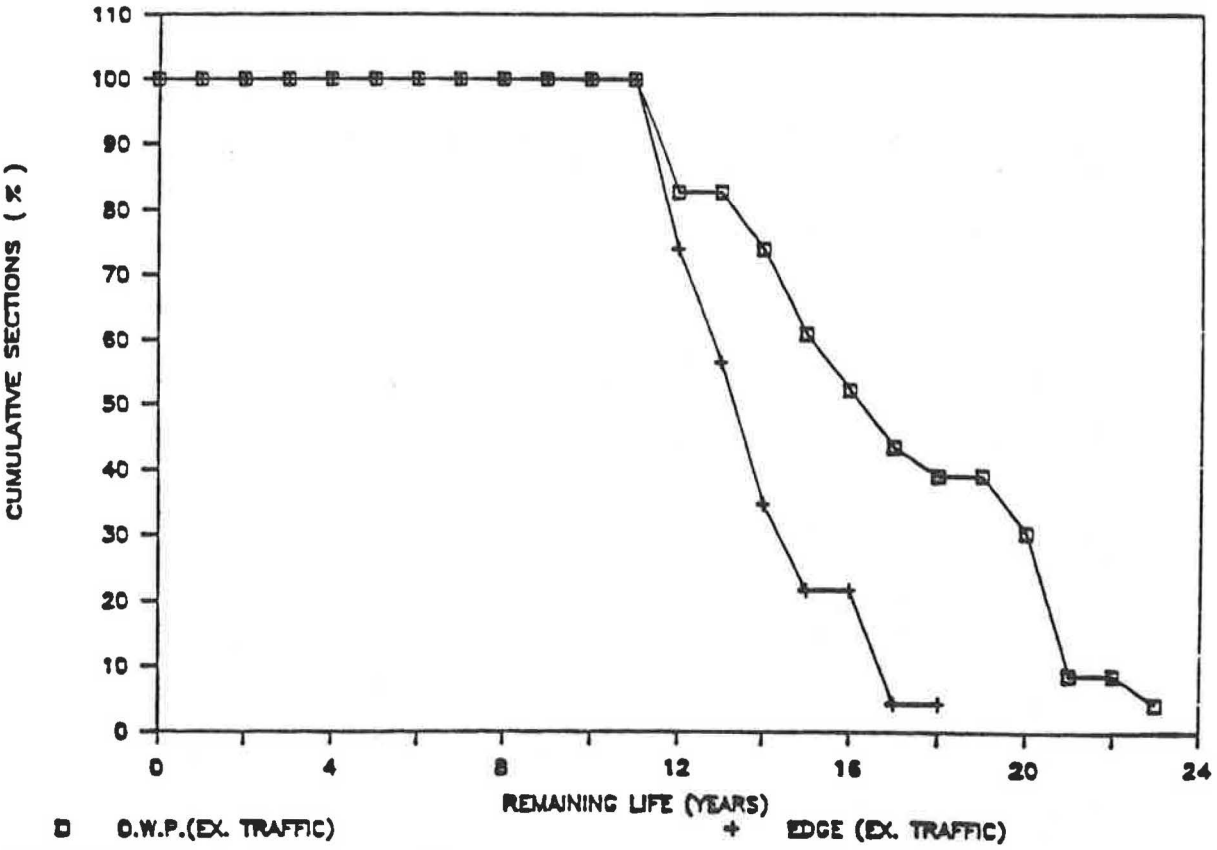

FIGURE 11 Remaining life of the cumulative sections (in percent) for existing traffic in the outer wheel path and edge.

TABLE 9 RESULTS OF TEMPERATURE AND MOISTURE CORRECTION FOR BASE MODULI AT OUTER WHEEL PATH

TEMPERATURE CORRECTION DATA

INPUT CONDITIONS:		WANTED CONDITIONS:	
TEMPERATURE =	75.0 deg. F	TEMPERATURE =	95.0 deg. F
SUCTION =	-40.0 psi	SUCTION =	-90.0 psi

SEC #	INPUT MODULUS (psi)	WANTED CONDITION MODULUS (psi)	MODULUS CHANGE DUE TO TEMPER. (psi)	MODULUS CHANGE DUE TO SUCTION (psi)
0.0	35357	38669	1618	1693
0.1	53529	57180	1784	1867
0.2	70569	75932	2621	2742
0.3	51030	54362	1628	1704
0.4	46229	49917	1803	1886
0.5	87063	94122	3450	3609
0.6	34270	36493	1087	1137
0.7	61642	64539	1416	1481
0.8	37385	39896	1227	1284
0.9	33684	37268	1752	1832
1.0	25188	29260	1990	2082
1.1	48233	52514	2092	2189
1.2	9555	10753	586	613
1.3	40941	43177	1093	1143
1.4	67741	73579	2853	2985
1.5	28590	31429	1387	1451
1.6	92670	98218	2711	2836
1.7	24102	27567	1693	1771
1.8	14675	15557	431	451
1.9	34504	37993	1705	1784
2.0	53449	59386	2902	3035
2.1	13525	15703	1064	1113
2.2	47677	51786	2008	2101

TABLE 10 RESULTS OF LOADRATE ANALYSIS OF THE FWD DATA FOR TEMPERATURE AND MOISTURE-CORRECTED BASE MODULI VALUES

```
 TEXAS TRANSPORTATION INSTITUTE
LOAD RATING OF LIGHT PAVEMENT

JOB : FWD TESTING(OWP)          (INPUT FILE B:TAB10F.LRD)

DISTRICT: 0      COUNTY:Cty     ROAD:10108 fm3225
ALLOWABLE RUT(INS): .5      RECORDED RUT(INS): 0

TRUCK NO. 1
AXLE NUMBER   SINGLE WHEEL/ESWL(LBS)
    1              9000

ANNUAL TRAFFIC GROWTH RATE: .05   # OF YEARS: 10   FIRST YEAR TRAFFIC: 55775
TOTAL NUMBER OF PASSES DURING ABOVE PERIOD: 701531

DATE:4-25-89   FALLING WEIGHT DEFLECTOMETER
                TEMP. CORRECTED                 *              **              *
 SEC    BASE       E1-BASE     E2-SUBGR    NO. OF       RUT DEPTH     REMAINING LIFE
 #     (IN)        (PSI)       (PSI)      PASSES         (IN)          (YEARS)
0.000   15.0        38669        9117      402098         0.87            6.3
0.100   15.0        57180       11364      636919         0.55            9.3
0.200   15.0        75932       10336      642202         0.55            9.3
0.300   15.0        54362       11682      637140         0.55            9.3
0.400   15.0        49917        9902      453799         0.77            7.0
0.500   15.0        94122       10436      673458         0.52            9.7
0.600   15.0        36493       11964      587898         0.60            8.7
0.700   15.0        64539       15895      784149         0.45           10.9
0.800   15.0        39896       11642      591024         0.59            8.7
0.900   15.0        37268        7928      357416         0.98            5.7
1.000   15.0        29260        6287      286794         1.22            4.7
1.100   15.0        52514        9072      426083         0.82            6.6
1.200   15.0        10753        6639      286062         1.23            4.7
1.300   15.0        43177       13507      656026         0.53            9.5
1.400   15.0        73579        9276      468293         0.75            7.2
1.500   15.0        31429        8393      362001         0.97            5.8
1.600   15.0        98218       12615      753690         0.47           10.6
1.700   15.0        27567        6782      301439         1.16            4.9
1.800   15.0        15557       10857      483038         0.73            7.4
1.900   15.0        37993        8559      380956         0.92            6.0
2.000   15.0        59386        8071      398687         0.88            6.3
2.100   15.0        15703        6173      271200         1.29            4.5
2.200   15.0        51786        9632      446620         0.79            6.9

*  NUMBER OF PASSES AND REMAINING LIFE FOR SPECIFIED RUT DEPTH OF  .5 in
** RUT DEPTH FOR SPECIFIED NUMBER OF PASSES OF  701531  IN  10 YEARS

     Remaining Life(yrs)          Cumulative % Sections
            1                            100.0
            2                            100.0
            3                            100.0
            4                            100.0
            5                             82.6
            6                             73.9
            7                             47.8
            8                             39.1
            9                             30.4
           10                              8.7
```

to the subgrade to study the complete seasonal variations in the pavement.

ACKNOWLEDGMENT

This paper presents partial results of a 3-year study on the effect of overweight vehicles on FM roads, sponsored by the Texas SDHPT. The authors are extremely grateful for this support. The authors also wish to thank K. M. Chua of the University of New Mexico for his help in developing the LOADRATE program.

REFERENCES

1. K. M. Chua and R. L. Lytton. Load Rating of Light Pavement Structures. In *Transportation Research Record 1043*, TRB, National Research Council, Washington, D.C., 1985.
2. K. M. Chua and R. L. Lytton. Structural Evaluation and Load Zoning Consideration of Light Pavements. Presented at the Transportation Research Board 66th Annual Meeting, TRB, National Research Council, Washington, D.C., Jan. 1987.
3. K. M. Chua. *Nondestructive Testing of Pavements and Backcalculation of Moduli*. STP 1026, ASTM, Philadelphia, Pa., 1989.
4. J. L. Figueroa and M. R. Thompson. Simplified Structural Analysis of Flexible Pavements for Secondary Roads Based on ILLI-PAVE. In *Transportation Research Record 766*, TRB, National Research Council, Washington, D.C., 1980, pp. 5–10.
5. *ILLI-PAVE User's Manual*. Transportation Facilities Group, Department of Civil Engineering, University of Illinois at Urbana-Champaign, May 1982.
6. D. Chandra, K. M. Chua, and R. L. Lytton. Effects of Temperature and Moisture on the Load Response of Granular Base Course Material in Thin Pavements. In *Transportation Research Record 1252*, TRB, National Research Council, Washington, D.C., 1989, pp. 33–41.
7. K. A. S. Yapa, K. M. Chua, and R. L. Lytton. A Simplified Mechanistic Rut Depth Prediction Procedure for Low-Volume Roads. Presented at the Transportation Research Board 68th Annual Meeting, Washington, D.C., Jan. 1989.
8. D. M. Burmister. The Theory of Stresses and Displacements in Layered Systems and Applications to Design of Airport Runways, Proc., HRB, National Research Council, Washington, D.C., Vol. 23, 1943, pp. 126–148.
9. D. M. Burmister. The General Theory of Stresses and Displacement in Layered System. *Journal of Applied Physics*, Vol. 16, 1945.
10. M. L. Taylor. *Characterization of Flexible Pavements by Non-Destructive Testing*. Civil Engineering Department, University of Illinois at Urbana-Champaign, Ph.D. dissertation, 1978.
11. J. Uzan. Characterization of Granular Material. In *Transportation Research Record 1022*, TRB, National Research Council, Washington, D.C., 1985, pp. 52–59.
12. P. V. Lade and R. B. Nelson. Modelling the Elastic Behavior of Granular Materials. *International Journal for Numerical and Analytical Method in Geomechanics*, Vol. 11, No. 5, Sept.–Oct. 1987, pp. 521–542.
13. W. W. Crockford, K. M. Chua, W. Yang, and S. K. Rhee. *Response and Performance of Thick Granular Layers*. Draft Interim Report, U.S. Air Force, Texas A&M University, College Station, May 1988.
14. K. A. S. Yapa. *A Simplified Mechanistic Rut Depth Prediction Procedure for Low-Volume Roads*. M.S. thesis, Texas A&M University, College Station, Dec. 1988.
15. M. R. Thompson and Q. L. Robnett. *Final Report—Resilient Properties of Subgrade Soils*. Transportation Engineering Series, No. 14, Civil Engineering Studies, Illinois Cooperative Highway and Transportation Series No. 160, University of Illinois at Urbana-Champaign, Urbana, Ill., June 1976.
16. M. R. Thompson and Q. L. Robnett. Resilient Properties of Subgrade Soil. *Transportation Engineering Journal*, ASCE, Jan. 1979, pp. 71–89.
17. W. O. Yandell. Mechano-Lattice Prediction of Pavement Performance. *Proc., 4th Conference on Asphaltic Pavements for Southern Africa*, Capetown, 1984, pp. 201–215.
18. W. O. Yandell and R. L. Lytton. The Effect of Residual Stress and Strain Build Up in a Flexible Pavement by the Repeated Rolling of a Tire. Interim Report RF 4087-1, Research Foundation, Texas A&M University, College Station, Oct. 1979.
19. W. O. Yandell. New Method of Simulating Layered Systems of Unbound Granular Material. In *Transportation Research Record 1022*, TRB, National Research Council, Washington, D.C., 1985, pp. 91–98.
20. W. O. Yandell. Measurement and Prediction of Foreward Movement and Rutting in Pavements Under Repetitive Wheel Loads. In *Transportation Research Record 888*, TRB, National Research Council, Washington, D.C., 1982, pp. 77–84.
21. W. H. Press, B. P. Flannery, S. A. Tenkolsky, and W. T. Vetterling. *Numerical Recipes: The Art of Scientific Computing*. Cambridge University Press, Cambridge, England, 1987, pp. 77–101.

Publication of this paper sponsored by Committee on Strength and Deformation Characteristics of Pavement Sections.

State-of-the-Art Pavement Instrumentation

NADER TABATABAEE AND PETER SEBAALY

Various types of strain gauges, pressure cells, deflection, temperature, and vehicle transverse position indicators have been used to instrument flexible pavements. Each sensor has its own design, operation, and installation techniques in addition to large variability in unit cost. The state of the art of these instruments is described in terms of their designs, performance, installation, and availability. Various types of strain gauges for the bonded and unbonded pavement layers are discussed. Different types of pressure cells are described, and some recommendations are given for the selection of the type and dimensions of these gauges. The principles of the acceleration, velocity, and deflection measuring devices are discussed. Temperature sensors are also described and the basic features of each element are presented. Finally, the various types of the transverse position indicators are discussed.

The structural responses of a pavement system under actual dynamic loads are of primary concern to design, management, and materials engineers. The design engineer's first objective is to design a pavement system that can withstand a specified number of loading cycles. Environmental effects such as temperature, which greatly affect the response of flexible pavements, have to be considered also. The pavement management engineer, who is primarily interested in how the performance of the pavement decays with the number of loading cycles, should always be aware of the rate of deterioration in order to implement an effective maintenance or rehabilitation strategy. The materials engineer, responsible for providing a rutting-and-cracking-resistant mix, must evaluate the effects of heavy loads, high tire pressures, and high and low temperatures on the responses of the asphalt concrete material. The goal is to minimize the rutting of asphalt concrete pavements under high temperatures and their cracking under low temperatures.

To accommodate the concerns and goals of the three groups of engineers, the structural responses of the pavement system must be known. The magnitude of the compressive stresses and strains and the vertical deflections of the pavement layers under dynamic loading are the primary components of the surface rutting problem. On the other hand, tensile stresses and strains in the asphalt concrete layer are the primary components of the cracking problem. In addition, the pavement temperature is a major component for both distresses. There are a number of theoretical models that predict rutting and cracking. But, each response model has its own assumptions regarding material properties, constitutive relationships, and load function characteristics. Models range from simple static linear elastic models to more complex dynamic viscoelastic models. Regardless of their complexity, these models must be validated and calibrated before they can be relied on in design, management, and material selection. The in situ instrumentation of pavement systems offers a reliable approach for calibration and validation of these models and contributes to a better understanding of the behavior of pavement materials.

Strain gauges, pressure cells, deflection gauges, and temperature sensors have been used since the early 1900s to monitor the in situ responses of pavement structures. Currently, there are many different versions of each of these sensors used by various researchers and investigators throughout the world. Each sensor type has its own advantages and disadvantages, which are based on the design of the gauge and the recommended method of installation. A review of the state of the art of flexible pavement instrumentation is presented in which the various gauges and their recommended methods of installation are discussed.

STRAIN MEASUREMENT

The magnitude and directions of the critical strains in pavement structures under dynamic loadings are of great concern to researchers in the areas of analysis and design of flexible pavements. Fatigue failure of flexible pavements results from high tensile strains at the bottom of the asphalt layer. Rutting and permanent deformations are related to high shear strains in the asphalt layer and high compressive strains throughout the other layers of the system.

The type of gauge used to measure strains in flexible pavements depends on the location of interest. Electrical resistance strain gauges are usually used in bonded layers, and linear variable differential transformers (LVDTs) are used in unbonded layers. The various types of gauges used in bonded and unbonded layers are discussed in the following paragraphs. A more detailed performance evaluation and cost and availability information are given by Sebaaly et al. (*1*).

Strain Gauges for Bonded Layers

The following is a review of the methods that have been used by various investigators to measure the strain in asphalt concrete pavement layers. These methods can be grouped into four categories:

- *H*-gauges and strip gauges.
- Foil strain gauges cemented to or embedded in carrier blocks prepared in the laboratory.
- Foil strain gauges cemented to a core extracted from the pavement.
- Strain coils.

Pennsylvania Transportation Institute, Pennsylvania State University, Research Building B, University Park, Pa. 16802.

H-Gauges

The *H*-gauge consists of a strip of a given material onto which a strain gauge is connected. The ends of the strip are connected to metal bars with rectangular cross sections that act as anchors, thus forming the letter *H*. These transducers are embedded at the bottom of the asphalt concrete layer. As the pavement experiences strains under the application of the load, the anchor bars move with the pavement, producing elongation in the strip. The strain registered by the strain gauge attached to the strip will be the same as the true strain in the asphalt concrete if the stiffness of the strip is the same or somewhat less than that of the asphalt concrete layer. Otherwise the strip tends to reinforce the pavement, thus leading the strain gauge to underregister. A large stiffness differential between the two materials results in the debonding of anchor bars from the pavement materials and failure of the instrumentation. Different investigators have used different materials and dimensions for the strip as well as the anchor bars to overcome the aforementioned problems.

The Transport and Road Research Laboratory (TRRL) in England designed the earliest type of *H*-gauge, an aluminum strip 0.5 in. (12.6 mm) wide by 0.010 in. (0.25 mm) thick onto which a 225-ohm resistive foil strain gauge, 4 in. (101 mm) long, was cemented (*2*). Two 0.06-in.^{2} (39.7-mm^2) steel bars were connected to the aluminum strip at right angles. The resistive foil gauge and aluminum strip were waterproofed and wrapped in polyvinylchloride (PVC) tape.

In the Nardo Road Test, a full-scale experiment conducted by the Organization for Economic Cooperation and Development (OECD), seven research teams used different types of strain gauge transducers grouped into three different categories as shown in Figure 1 (*3*).

In recent years, the Technical University of Denmark has modified *H*-gauges to improve their durability against moisture and fatigue and to better match the stiffnesses of the strip materials and asphalt concrete (*4,5*). The strain gauge is completely embedded in a strip of fiberglass-reinforced epoxy with low stiffness but high flexibility and strength. Each end of the epoxy strip is attached to a stainless steel anchor bar, and protection against mechanical and chemical deterioration is provided by several layers of coating, as shown in Figure 2. These gauges are commercially available through Dynatest (*6*).

Another commercially available strip gauge transducer is the Omega encapsulated strain gauge (*7*). These transducers have been designed for use in rough ambient conditions. Various types of these gauges have temperature-dependent characteristics similar to those of asphalt concrete materials. The gauge is made of a 350-ohm, wire strain gauge 3.5 in. (88 mm) long embedded between two layers of polycarbonate. According to the manufacturer of these gauges, their service temperature is from −60°F to +160°F (−50°C to +70°C). The maximum service temperature is less than the temperature of hot mix during paving operation [280°F (140°C)]. Therefore, this gauge may not survive after paving.

PRINCIPLE	MODEL	ACTIVE LENGTH OF WIRE/ANCHOR	RESISTANCE (Ω)	COST (US $)	TEAM	ASSEMBLY
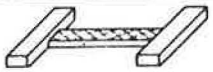	KYOWA KM-120-H2-11L 100-3	70 MM/104 MM	120 ± 1 %	40	3	- FIXATION OF ANCHOR BARS IN THE LABORATORY
	KYOWA KM-120-H2-11L 100-3	70 MM/106 MM	120 ± 1 %	35	5	
	KYOWA KM-120-H2-11L 100-3	70 MM/100 MM	120 ± 1 %	75	7	
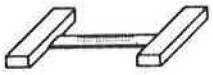	KYOWA KC-70-A1-11	67 MM/130 MM	120	35	2	- GAUGE GLUED TO SUPPORT AND FIXATION OF ANCHOR BARS IN THE LABORATORY
	PL 30 ou KYOWA KFC-30-C1-11	30 MM/100 MM	120	23	6	
	HBM DA 3	88 MM/140 MM	350	180	1	
	HBM LP 21 60-120	60 MM/60 MM	120	12	1	- GLUED ON MARSHALL SPECIMEN CUT TO 1/3 HEIGHT
	BLH FAE 2-300-35 PL	76 MM/76 MM	350	35	8	- GLUED ON LABORATORY SPECIMEN
	HBM 20/600 XA21	20 MM/20 MM	600 ± 0.25	10	9	- GLUED IN THE CENTER OF A LABORATORY SPECIMEN
	METAL FOIL GAUGE	13 MM/25 MM	120	15	4	- GLUED ON A BLOC OF SHEET ASPHALT
	HBM LP 21 60-120	60 MM/60 MM	120	12	1	- GLUED ON CORE TAKEN FROM THE PAVEMENT
	HBM 60/600 LP 21		600 ± 0.25	15	3	

FIGURE 1 Classification of Nardo gauges (*3*).

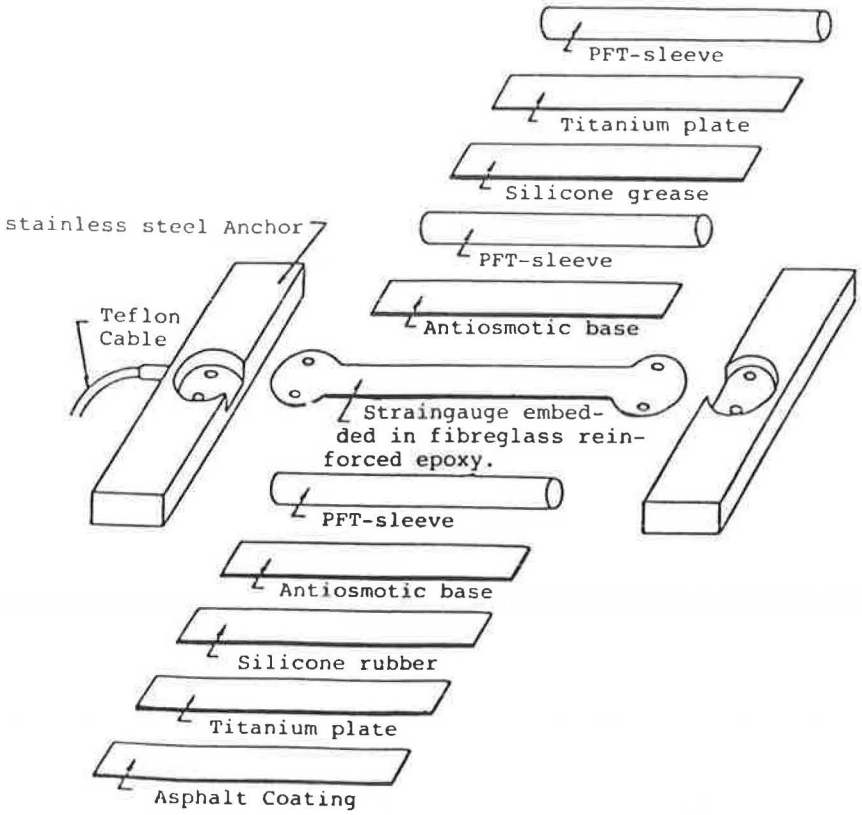

FIGURE 2 Different layers of modified Danish *H*-gauge (*6*).

Foil Strain Gauges on Carrier Block

The first technique for strain measurement at the bottom of the asphalt concrete layer was developed at Koninklyke Shell Laboratorium in Amsterdam (*8*). These gauges consisted of foil strain gauges 1.18 in. (30 mm) long cemented to a thin sand asphalt carrier block in both longitudinal and transverse directions. The block was then placed at the top of the base and covered by paving mix.

Researchers at the Alberta Research Council (ARC) in Canada embedded strain gauges in thin sheets of asphalt to measure longitudinal strain at the bottom of the asphalt concrete layer (*9*). The asphalt mastic and the strain gauges form a transducer that is approximately 6.5 × 6.5 × 0.8 in. (165 × 165 × 20 mm). These transducers were used in the Nardo Road Test, at FHWA's Accelerated Loading Facility (ALF) and at the Pennsylvania test track (*4,10*).

The principle behind this group of transducers is that the asphalt on the surface of the carrier block will soften when it comes into contact with the hot paving mix. Therefore, the carrier block and the paving mix will bond together and form a monolithic layer of asphalt concrete.

Foil Strain Gauges Cemented to Cores

This method is similar to the previous approach except that the carrier blocks are full-depth cores extracted from the actual pavement rather than laboratory-compacted carrier blocks.

The main concern with this approach is whether effective bonding is achieved between the instrumented core and the surrounding pavement. If the bonding agent, which is usually a type of epoxy, is too stiff relative to the pavement, then stress concentrations will be formed around the core. These stress concentrations may initiate cracks in the vicinity of the core. If the bonding agent is too soft relative to the pavement, the dynamic loading may cause the bond between the core and the surrounding pavement to fail, and the core will then act as a rigid body. Based on this discussion, the stiffness of the bonding agent should be very similar to that of the pavement to approach a monolithic layer behavior.

Researchers at the Technical Research Center of Finland have used this method at the Virttaa test field (*11*). They used 6-in. (150-mm) core samples retrofitted into a hole in the pavement with a tolerance of less than 0.04 in. (1 mm). The strain gauges were cemented on the cores, and the cores were glued back to the bituminous pavement. The strain gauges were dual-foil strain gauges with 350-ohm resistance, 3 in. (75 mm) long.

Researchers at FHWA have installed this type of transducer at the Pavement Testing Facility (PTF) to be tested with the Accelerated Loading Facility (ALF) machine. They used cores that were 4 in. (100 mm) in diameter and strain gauges 2 in. (50 mm) long with 120-ohm resistance. No sign of debonding or crack initiation was noticed in the area surrounding the cores for over 6 million repetitions of 18-kip ESALs.

The main advantage of this method is that the gauge can be retrofitted into an existing pavement and can be used for strain measurement in virtually any direction.

Strain Coils

Inductive coils (also known as Bison coils) produce an electromagnetic output proportional to the distance between two coils. The assembly consists of two coils—one acts as a transmitter and the other as receiver. A special electronic unit is needed for amplification, balancing, and recording of the output. The coils can be cemented to a carrier block. Due to electromagnetic coupling, these coils are affected by moving metals, e.g., wheels, and by the energy output from the ignition system of the vehicles; this limits their usefulness.

Strain Measurement in Unbonded Material

Soil strain measurement methods are very limited, comprising basically two types of devices:

- Inductive coils, and
- LVDT-type strain gauges.

Inductive Coils

The same coils that are used for bonded layers can be applied to unbonded materials. The size of the coils is selected so that the distance between the coils is within the range of 1 to 4 coil diameters.

An important advantage of inductive coils is that the coils (sensors) are not mechanically connected; therefore, they do not disturb the soil mass excessively, reinforce the soil mass, or impede its deformation. Their limitations were discussed in the previous section.

LVDT-Type Soil Strain Gauges

The most recent version consists of two aluminum alloy flanges 2.5 in. (63 mm) in diameter attached to the ends of an LVDT. The flanges anchor into the soil and the LVDT measures the differential displacements between flanges. TRRL and Dynatest manufacture these gauges.

PRESSURE MEASUREMENT

Basic Design Requirements

The main requirements in the design of pressure cells are the abilities

- To measure the stress in the free-field condition, that is, without changing the state of stress in the soil mass.
- To place the pressure cell in the soil mass without appreciably disturbing the existing state of stress in the soil mass.

These requirements are interrelated and cannot be fully satisfied because the introduction of a measuring instrument into a soil mass disturbs the stress distribution. The presence of the instrument will usually cause redistribution of free-field stress. This redistribution depends on the stiffness of the cell diaphragm as well as the ratio of cell thickness to its diameter (also called aspect ratio). Torry and Sparrow (*12*) performed a theoretical analysis for a pressure cell in a uniaxial stress field. They studied the effect of the flexibility factor on the pressure cell registration. The flexibility factor was defined by

$$\text{Flexibility Factor} = \frac{E_s d^3}{E_c t^3} \tag{3}$$

where

E_s = Young's modulus of the soil material,
E_c = Young's modulus of the cell material,
d = diameter of the cell diaphragm, and
t = thickness of the cell diaphragm.

Figure 3 shows the variation of pressure cell registration as a function of flexibility factor for different values of aspect ratio. The cell registration factor c represents the ratio of measured to actual stress values. According to this figure, cell registration remains nearly constant for a flexibility factor less than 1.0. In order to reduce the error in pressure measurements, cell registration close to 1 is desired. This condition occurs when the aspect ratio is as small as possible, less than 0.2, and the flexibility factor is less than 1.0.

Types of Pressure Cells

In the previous section, general design requirements for pressure cells were reviewed. In this section, the particular characteristics of some of the existing cells will be discussed. There are two basic types of embedded soil pressure cells: diaphragm cells and hydraulic cells.

The diaphragm cells consist of a stiff circular diaphragm supported by an integral stiff annular ring. This diaphragm is deflected by the applied external soil pressure. Electrical resistance strain gauges or some other type of strain measurement sensors are bonded to the interior face of the diaphragm (*13*). A diaphragm cell may have one or two independent active faces.

The hydraulic-type pressure cells consist of two circular (or in some cases, rectangular) steel plates welded together around their periphery to form a chamber or cavity. This chamber is filled with some type of de-aired liquid such as mercury. The total stress acting on the faceplates is balanced by an equal pressure induced in the internal liquid. This type of cell provides average soil pressure.

TRRL/LVDT Pressure Cell

The TRRL/LVDT pressure cell is a diaphragm-type pressure cell that uses an LVDT to measure deflection of the diaphragm under soil pressure. The LVDT core fitted to one diaphragm can be screwed to its null position in the LVDT body attached to the other diaphragm. The cell is then sealed and maintained at this position under zero pressure. A thick annular ring reduces the effect of lateral stress on the cell

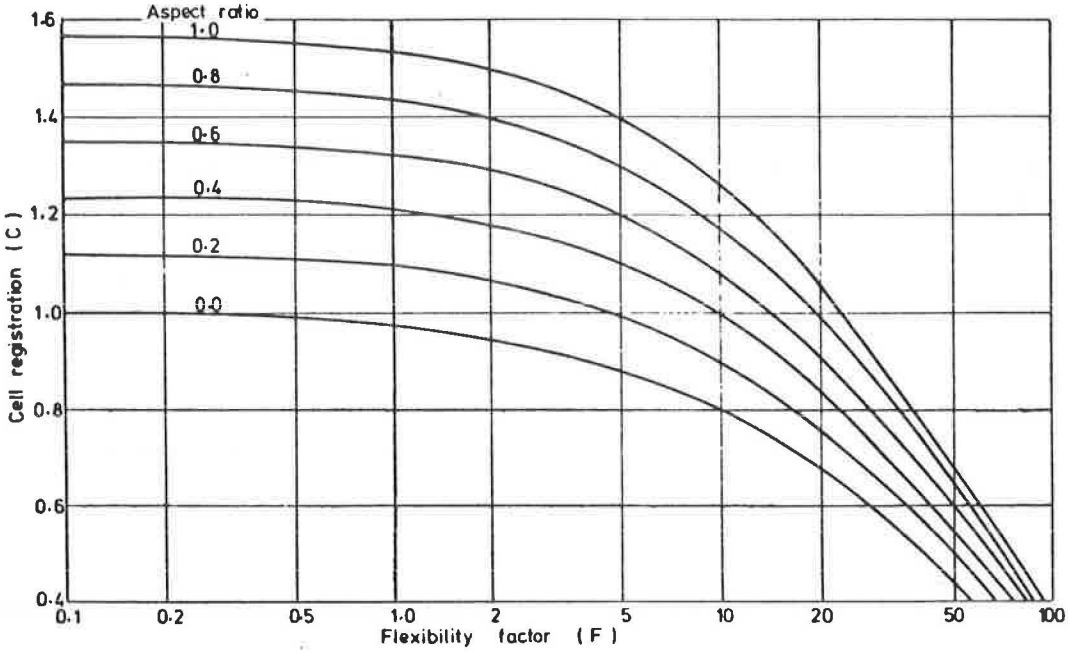

FIGURE 3 Variations of pressure cell registration with flexibility factor (*12*).

registration. This cell can be used for short-term static and dynamic loading conditions.

Nottingham Pressure Cells

The Nottingham pressure cell is a diaphragm-type pressure cell made of titanium. The sensing element is a four-arm active strain gauge bridge (full Wheatstone bridge) bonded to the inner side of the diaphragm. The strain gauges have a resistance of 350 ohms. The bridge is supplied with 10 volts of direct current. Potentiometric balance is provided across chosen arms of the Wheatstone bridge, and a 500-kohm calibration resistor can be switched across one arm to simulate a fixed stress input.

The diaphragm has a diameter of 1.5 in. (38 mm) and a thickness of 0.08 in. (2 mm). The cell has an overall diameter of 2.5 in. (64 mm) and a thickness of 0.43 in. (11 mm).

WES Soil Pressure Cells

This hydraulic pressure cell was developed by the U.S. Army Corps of Engineers at the Waterways Experiment Station (WES). It has a diameter of 6 in. (152 mm) and an overall thickness of 1 in. (25 mm). It is fabricated from stainless steel and consists of a circular faceplate that reacts on an internal mercury-filled chamber. Pressure on the faceplate is averaged and transmitted by the mercury to an internal membrane. Four strain gauges forming a full Wheatstone bridge are attached to the rear of the internal membrane. They undergo resistance change proportional to strains in the membrane that are induced by the pressure applied on the faceplate and transmitted through the mercury. This cell can be used for pressure measurement under short-term static and dynamic loading conditions.

SOPT Pressure Cells

These cells were developed at the Technical University of Denmark. They are of hydraulic type with an oil-filled cavity. The cells are made of pure titanium and their geometry has been improved by tapering the edges at 45 degrees. These cells have a thickness of 0.5 in. (13 mm) and are available in diameters of 2.68 and 3.86 in. (68 and 98 mm). The smaller cell is appropriate for use in clays and sands with fine aggregates, whereas the larger one is used in soils with large aggregates. The induced liquid pressure is measured with a full strain-gauge bridge. These pressure cells are commercially available and, according to the manufacturer, have a service life of more than 36 months and a fatigue life of more than 3×10^6 cycles (*6*).

DEFLECTION MEASUREMENT

Different types of instrumentation are available to measure vertical deflections in the pavement system. They can be grouped into the following categories:

- Acceleration-measuring devices,
- Velocity-measuring devices, and
- Deflection-measuring devices.

The following is a description of each category and their measuring elements.

Acceleration-Measuring Devices

The displacement of a point on the pavement can be evaluated by double-integrating the acceleration signal of that point.

Thus accelerometers can be used to measure pavement deflection. The output signal of an accelerometer can be integrated by electrical hardware or through software after digitization. Accelerometers can only measure dynamic instantaneous displacement because the point of measurement should experience a certain level of excitation. Accelerometers do not need any reference points; their reference is enclosed within the actual unit. Therefore, they can be used as a stand-alone unit on the surface or embedded into the pavement layers at any depth.

Velocity-Measuring Devices

The velocity signal of the pavement surface under a given dynamic load can be integrated once to generate the deflection time response. Therefore, geophones can be used to measure pavement deflections. A mass is attached to a spring with support to the pavement surface. A wire (or coil) attached to the mass becomes part of the total mass. When the pavement surfaces moves, the magnet and support also move. The geophone frequency is defined as the frequency of oscillation in the theoretical case of no damping. This frequency is controlled by the ratio of total mass to spring constant. When the measurement frequency becomes smaller, this ratio should be increased. Therefore, a larger mass should be used for low-frequency measurements. The use of a larger mass would also increase the overall dimensions and unit price of the geophone.

Geophones are very rugged and can withstand high temperatures of hot mix asphalt. Geophones can measure only dynamic transient deflections, but do not need any reference points.

Deflection-Measuring Devices

These devices measure the actual deflection, and hence the signal does not need to be integrated. The majority of these devices use a linear variable differential transformer (LVDT) to measure both the static and transient dynamic deflections. Some deflection devices, called single-layer deflectometers (SLDs), measure the deflection of a given layer of the pavement system. The most sophisticated type of deflection-measuring device, called multidepth deflectometer (MDD), can measure the deflection at various points throughout the pavement depth.

Single-Layer Deflectometer

The SLD consists of an LVDT or a strain gauge fixture that is connected to the surface of any layer of the pavement at one end and attached to a reference rod at the other end. Reference rods as long as 8 to 10 ft (2.5 to 3 m) have been used. The basic assumption is that the reference rod is anchored at a point deep enough so that the deflection at that point due to surface loading is at a minimum. When the upper part of the SLD deflects with the pavement, the reference rod will not move. Therefore, the relative movement of the upper part with regard to the reference rod is equal to the actual pavement movement. Figure 4 shows an LVDT SLD. One advantage of the SLD is that it can measure both static and dynamic deflections and also resilient and permanent deformations.

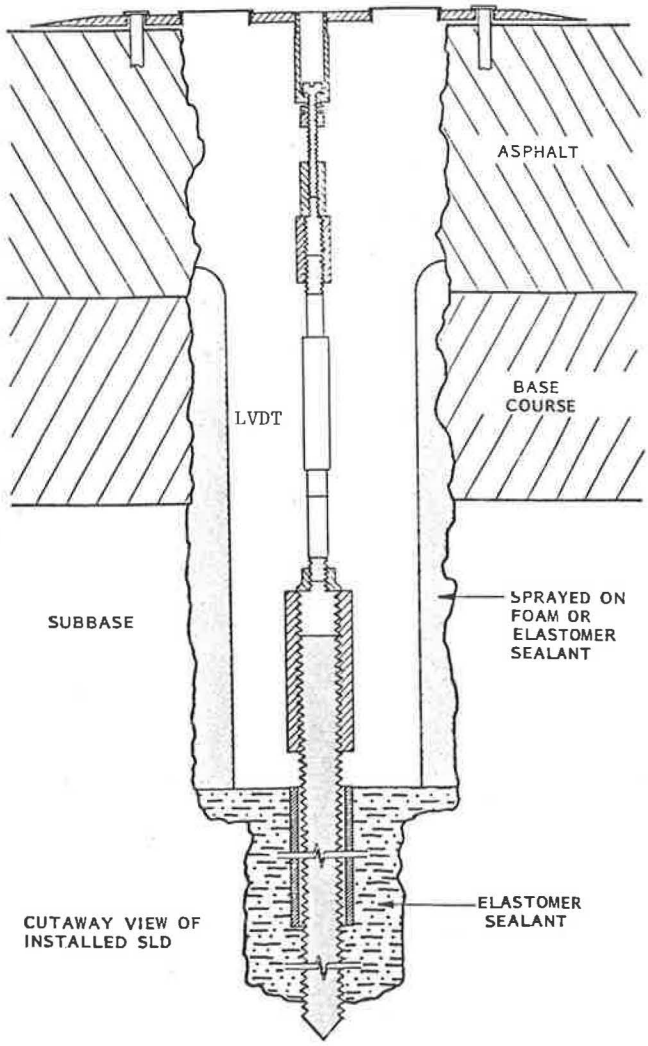

FIGURE 4 LVDT single-layer deflectometer.

Multidepth Deflectometer

The MDD is an LVDT-based instrument used in pavement research for measuring either the resilient or permanent deformations. In the schematic of an MDD installation shown in Figure 5, two MDD modules are installed within the pavement layers. The measuring unit is an LVDT mounted within a module that can expand laterally to clamp onto the sides of the hole. As many as six MDD modules may be placed in any hole. The minimum distance that modules can be placed apart is limited by the length of the module, which is approximately 6 in. (150 mm). The anchor for the LVDT cores is placed approximately 8 ft (2.5 m) below the pavement surface.

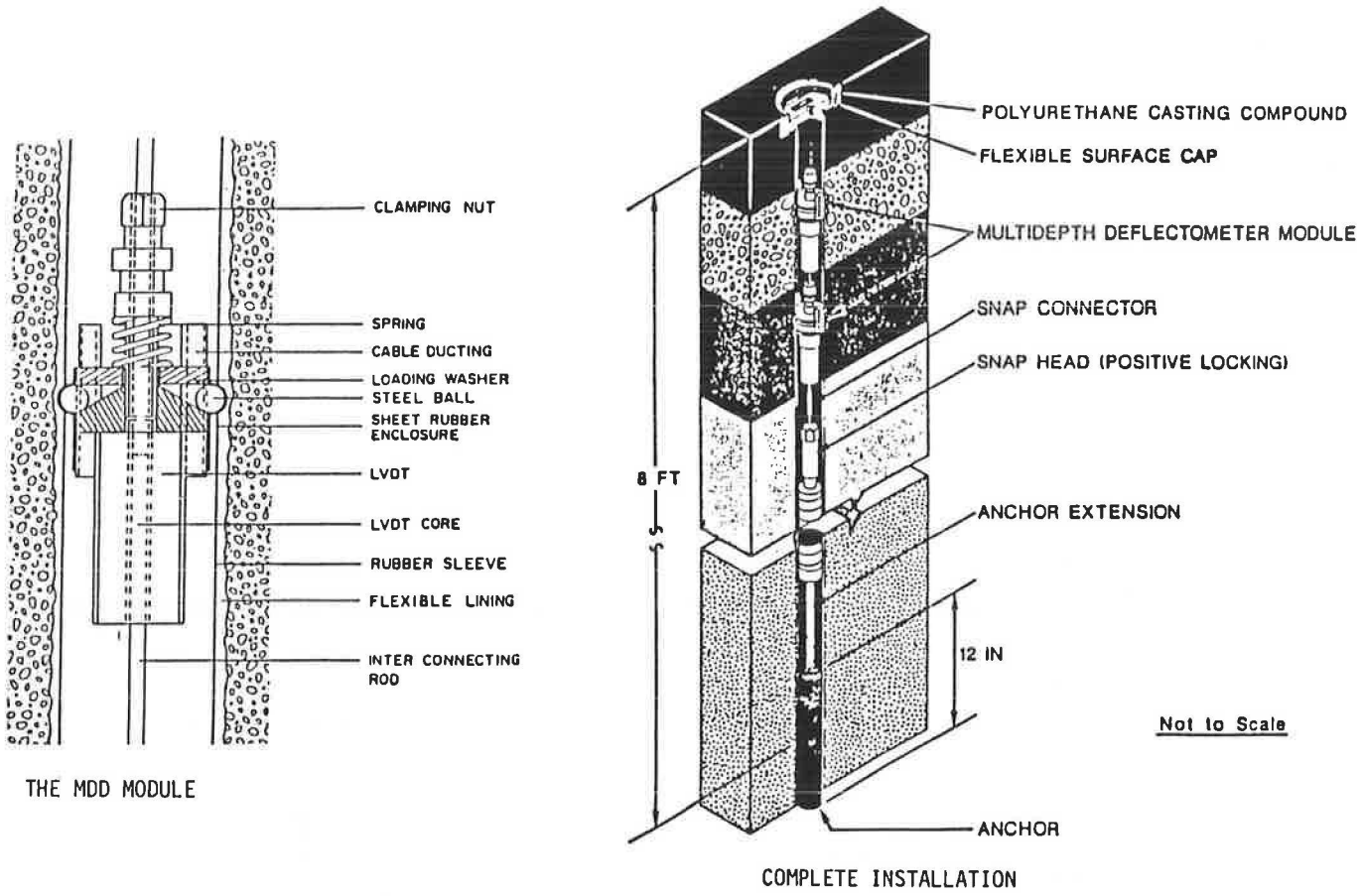

FIGURE 5 The multidepth deflectometer.

The deformation of each layer can be measured and its contribution to the overall deformation determined.

TEMPERATURE MEASUREMENT

The temperature throughout the pavement layer has a significant influence on the magnitude of deflections and strains. The temperature affects the stiffness of the asphalt concrete layers, which in turn affects the pavement response.

Thermocouples

Thermocouples are the most widely used temperature sensor. A thermocouple operates on the basis that, when two dissimilar metals are put in contact with each other, a small voltage is induced at their junction.

Thermocouples are suitable for point sensing only. To measure the temperature at several points relatively close to each other, a thermocouple tree should be formed. Thermocouples are rugged and can withstand shock and vibration. They have a very fast response time and are considered active gauges, which means there is no need to introduce a source of power into the circuit. An important point concerning the connection of a thermocouple is that all lead wires from the thermocouple junction to the readout device should be of the same alloy.

Type-*T* thermocouples, made of copper and constantan, are usually used in pavements, because they can be used from subzero temperatures to about 700°F (370°C). This type of thermocouple has an accuracy of about ±1.8°F (±1°C).

Metal Film RTDs

Resistance temperature detectors (RTDs) are temperature-sensitive resistors. The modern construction technique for RTDs involves depositing or screening a platinum or metal glass slurry film onto a small flat ceramic substrate, then etching with a laser trimming system, and sealing. The most common RTDs are made of either platinum-nickel or aluminum alloys. As the surrounding temperature increases, the resistance of the metal increases. The operating temperature for RTDs is from −328°F to +1,202°F (−200°C to +650°C), and their measurements are accurate and repeatable. An RTD element can be spread over a large area, providing a representative temperature of a member by averaging the temperature over the area.

Thermistor Probes

Thermistors are temperature-sensitive resistors, generally made of semiconductor materials. Different oxides of metals such

as nickel, manganese, iron, cobalt, copper, magnesium, and titanium are used in their construction. Thermistors exhibit a large change in resistance with temperature, which makes them very accurate devices, to ±0.18°F (±0.1°C). However, this increased sensitivity also causes them to be extremely nonlinear. Manufacturers have not standardized thermistor curves to the extent of RTD and thermocouple curves, so the performance and cost of these devices vary widely among manufacturers.

Thermistors are very susceptible to permanent decalibration at high temperatures. Their use is generally limited to temperatures from −58°F to +572°F (−50°C to +300°C). Extended exposure of thermistors to high temperatures will cause them to drift out of their specified tolerances.

Monolithic Integrated Circuits

Monolithic integrated circuits or solid-state transducers are a recent innovation in thermometry. These devices contain two-terminal integrated-circuit temperature transducers that produce output currents proportional to absolute temperature. These devices have linear and repeatable outputs; therefore, the devices need neither linearization circuitry nor calibration.

Due to their high-impedance current output, these transducers are not affected by voltage drops. Thus, the length of the lead wires will not affect the measurement. Any well-insulated twisted pair of wires is sufficient for operation long distances from the readout device. The transducers are available in hermetically sealed packages and can be used within a temperature range of −65°F to +300°F (−55°C to +150°C). These transducers can be very useful for embedment in pavements.

VEHICLE TRANSVERSE POSITION INDICATORS

In a field testing operation, to study pavement response under load, it is imperative to know the location of the loaded area relative to the measuring instrument. For a small number of measurements at low vehicle speed, visual observation of painted marks on the pavement or tire imprints left on a strip of flour may be adequate. However, for a large number of measurements at high speeds, faster and more accurate means of measurement must be utilized. The following paragraphs describe the common types of transverse position indicators.

Inductive Technique

This technique is used for determining the lateral position of wheels on flexible pavements. A drive coil is rigidly mounted on the rear axle and two detector loops are installed either on the pavement surface or at the interface between binder and wearing course (*14*). The device operates on the basis of the principle of mutual inductance between the coils and the loops. The loops are positioned on the road so that equal voltages are induced into each loop when the wheels are at the desired lateral offset. Deviations from the desired offset can be measured by means of summing and differential amplifiers. The device provides a continuous record of lateral displacement from a line within a range of ±4 in. (±100 mm) and with an accuracy of ±0.2 in. (±5 mm).

ARRB Device

This device consists of a 1.1-m length of nickel-chrome resistance wire mounted on a 1-in. (25-mm) strip of laminated plastic (*15*). When a wheel crosses the assembly, the spring steel makes contact with the resistance wire, hence reducing the series resistance and the voltage across the device. The voltage is proportional to the position at which the edge of the tires crossed the TPI. The device provides measurement with an accuracy of 0.2 in. (5 mm). The device has been reported to be operational after passage of 10,000 axle pairs.

Photoelectric System

The photoelectric locator system uses a high-intensity light attached to the test vehicle, which is directed onto an array of photocells or photodiodes mounted in the center of the vehicle travel path. The light activates one or more photo devices as it passes directly overhead, thus indicating a relative vehicle position.

The illumination source is normally constructed of a high-intensity 12-volt halogen bulb with a concentrating reflector similar to the type found in a common flashlight. This assembly is mounted under the test vehicle on a gimbal that permits the lamp to be manually adjusted in any direction. Power is supplied from the test vehicle battery. A photo array consisting of either photoelectric or photodiode cells is fixed to the center of the test lane just before the test section.

Laser-Guided System

The laser tracking system operates in exactly the same manner as the photoelectric system, except a laser is substituted for the halogen lamp and the sensor array is moved to the side of the road. The active guidance option is the only major difference between the two systems.

A 5- to 10-mW helium neon laser, operating in the 632.8-nm range, emits a visible red beam of randomly polarized light, and is used as a light source for this method. This beam is intercepted by an array of near-infrared photodiodes mounted on the side of the road adjacent to the test section. As the vehicle approaches the section, the highly coherent laser beam illuminates one or more sensors, indicating the relative offset from the target centerline. An illuminated sign board replaces the LED display used above and serves as a visual feedback device, instructing the vehicle driver to move to the right or left to properly track the centerline. Each light on the sign board represents one sensor in the array and thus provides an error magnitude measurement as well as a rate of correction measurement that helps to prevent excessive correction overshoot.

Ultrasonic System

This method uses ultrasonic waves to judge distance. In operation, a sound pulse is transmitted from the edge of the test section toward the targeted vehicle and the return echo is detected and timed. The elapsed time between the two pulses is proportional to the vehicle distance. A target-to-transmitter distance of 10 ft (3 m) translates into a period of approximately 17.55 ms with a resolution of 0.12 in. (3.05 mm) over this range. Measurements can be made as far as 33 ft (10 m) away and still be accurate to within 1 percent. A target board may be mounted on the test vehicle to obtain more accurate measurements.

SUMMARY AND RECOMMENDATIONS

It has been discussed that various types of strain gauges, pressure cells, deflection devices, temperature sensors, and vehicle transverse position indicators can be used to instrument flexible pavements. However, the individual design and operational characteristics of the gauges control the actual application of each gauge. The following represents a set of recommendations on the use of these gauges:

- The *H*-gauges can only be used in new constructions. If high temperatures and heavy loads are expected, the stiffness of the carrier strip may cause loosening of the anchor bars from the surrounding asphalt concrete materials. Therefore, under these circumstances, the strip material with the lowest modulus of elasticity should be selected (i.e., plastic strip should be used rather than aluminum).
- The laboratory compacted blocks and the asphalt mastic carrier blocks are only applicable for new construction. The major concern with this type of gauges is that when the carrier blocks softens due to high paving temperatures, the entire block might be deformed due to compaction forces. Therefore, it is not clear what kind of strains the deformed strain gauge will be recording.
- The instrumented core gauges can be installed in both new and old pavements. The process involves some disturbances of the aggregate and asphalt cement structure due to cutting and retrofitting of the instrumented core. The epoxy used to glue the gauges to the cores must be carefully selected with properties closely matching the asphalt concrete materials. The epoxy layer must be as thin as possible to avoid measuring the strains developed within the thick layer of epoxy. In addition, the strain gauges must be located over a representative range of aggregates and asphalt cement binder. Therefore, the length of the gauge must be at least three to four times the maximum size of aggregates. On the other hand, the longer the strain gauge the larger the area over which the strain is being averaged. Therefore, an optimum gauge length must be determined.
- The calibration of pressure cells presents a major drawback in using these gauges. It is almost impossible to replicate the field conditions in a laboratory set up. In situ calibration of the pressure cells may be a valid approach. This can be accomplished by loading the instrumented section with a nondestructive testing device such as the FWD, Dynaflect, or static truck load and monitoring the response of the pressure cell simultaneously. Use the surface deflections basin to backcalculate the layers moduli and use these moduli with an analysis model to predict the measured stresses at the location of the pressure cell. The relationship between the measured values and the calculated ones should provide the calibration curve for the embedded pressure cell. At the present time, there are no field performance data from either the hydraulic-type or the diaphragm-type of pressure cell. However, the best expected accuracy of any type of pressure cells is around ±20 percent.
- The LVDT-type strain gauges are the only type that can be used to measure strains in subgrade soils. They can be installed in both new and old pavements. However, it is recommended that they are installed during construction if feasible. A fairly experienced technician is needed to conduct a successful installation. It is also recommended that the complete data acquisition system be connected during installation to ensure that the gauge is not driven outside its active range.
- The signals from the acceleration and velocity measuring devices require double and single integration, respectively, to obtain the actual pavement deflection signal. The accuracy of the integrated signal is highly dependent on the cutoff points and the level of noise in the raw signal. It has also been noted that the time and frequency domain integrations could result in completely different results. The velocity measuring devices suffer from another problem that is related to their frequency range. As the frequency range of the geophones becomes smaller, their actual size becomes larger. Currently, the 1- and 2-Hz geophones have a 3-in. diameter and 5-in. height. In order to capture the entire deflection signal from a moving truck, it is necessary to use the low-frequency geophones, but their large physical size makes it impossible to embed them in the pavement layers.
- The deflection measuring devices can be installed into both new and old pavements. The SLD is simpler to design and install than the MDD. However, the use of the SLD involves greater disturbance of the pavement than the MDD. It will generally take three different SLDs at different locations to measure what a single MDD can measure at one location. Based on past experience with SLDs and MDDs, it is recommended that the LVDTs should be of the AC type and must be hermetically sealed to minimize the damage due to in situ moisture. The installation of an SLD can be accomplished by any competent technician, whereas the installation of the MDD requires a very well trained technician and special tools.
- All of the temperature sensors discussed in this paper have the required range for monitoring pavement temperatures. Thermocouples have been widely used in the area of pavement instrumentation. The solid state transducers provide a large linear range and may be used a lot easier than other sensors.
- All five different types of the vehicle transverse position indicators discussed in this paper are expected to provide adequate resolution for the purposes of pavement instrumentation activities. The best replicates of a loaded truck traveling at testing speeds between 20 and 50 mph are expected within ±3 in. The resolution of any one of the discussed devices exceeds that by a large margin. Basically the ultrasonic and the laser systems are similar, except the laser-guided system may be a little more expensive.

ACKNOWLEDGMENT

The authors would like to acknowledge the FHWA, which is providing the funds for the project.

REFERENCES

1. P. Sebaaly, N. Tabatabaee, and T. Scullion. *Instrumentation for Flexible Pavements*. Report FHWA-RD-89-084, FHWA, U.S. Department of Transportation, 1989.
2. J. F. Potter, H. C. Mayhew, and A. P. Mayo. *Instrumentation of the Full Scale Experiment on Al Trunk Road at Conington, Huntingdonshire*. Report LR 296, Road Research Laboratory, Crowthorne, Berkshire, England, 1969.
3. Organisation for Economic Cooperation and Development. *Full-Scale Pavement Tests*. Paris, 1985.
4. Organisation for Economic Cooperation and Development. *Strain Measurements in Bituminous Layers*. Paris, 1985.
5. P. Ulidtz. *Pavement Analysis*. Elsevier, 1987.
6. *Dynatest 8000 FWD Test System*. Dynatest Consulting, Inc., Ojai, Calif., undated.
7. *Pressure, Strain and Force Measurement Handbook and Encyclopedia*. Omega Engineering, Inc., Stamford, Conn., 1987.
8. A. J. G. Klomp and T. W. Niesman. Observed and Calculated Strains at Various Depths in Asphalt Pavements. *Proc., 2nd International Conference on the Structural Design of Asphalt Pavements*, University of Michigan, Ann Arbor, 1967, pp. 671–688.
9. J. T. Christison, K. O. Anderson, and B. P. Shields. In Situ Measurements of Strains and Deflections in a Full-Depth Asphaltic Concrete Pavement. *Proc., Association of Asphalt Paving Technologists*, Vol. 47, 1978, pp. 398–433.
10. D. A. Anderson, P. Sebaaly, N. Tabatabaee, R. Bonaquist, and C. Churilla. *Pavement Testing Facility-Pavement Performance of the Initial Two Test Sections*. Final Report FHWA/RD-88/060, FHWA, U.S. Department of Transportation, 1988.
11. M. Huhtala, J. Pihlajamäki, and M. Pienimäki. Effects of Tires and Tire Pressures on Road Pavements. In *Transportation Research Record* 1227, TRB, National Research Council, Washington, D.C., 1989.
12. A. C. Torry and R. W. Sparrow. The Influence of the Diaphragm Flexibility on the Performance of an Earth Pressure Cell. *Journal of Scientific Instruments*, Vol. 44, 1967, pp. 781–785.
13. J. Dunnicliff. *Geotechnical Instrumentation for Monitoring Field Performance*. John Wiley, New York, 1988.
14. A. R. Halliday. *An Inductive Technique for Determining the Lateral Position of Test Wheels on Roads*. Supplementary Report 306, Transport and Road Research Laboratory, Crowthorne, Berkshire, England, 1977.
15. K. G. Sharp, R. A. K. Hannay, and D. W. Potter. A Device to Measure the Transverse Position of a Vehicle in a Traffic Stream. *Proc., 14th Australian Road Research Board Conference*, Part 8, Melbourne, Australia, 1988, pp. 196–206.

Publication of this paper sponsored by Committee on Applications of Emerging Technology.